

# Investigating Multiscale Sedimentological Heterogeneity in Upper Cretaceous Carbonate Platforms, Tresp Basin, South- Central Pyrenees

---

*A thesis submitted to the University of Manchester for the degree of  
Doctor of Philosophy  
in the Faculty of Science and Engineering*

2017

Jonathan Josef Lavi

School of Earth and Environmental Sciences

Basin Analysis and Petroleum Geosciences Group

The University of Manchester

## CONTENTS

List of Figures .....	7
List of Plates .....	10
List of Tables .....	11
Abstract.....	13
Declarations .....	14
Copyright Statement.....	14
Dedication .....	15
Acknowledgements.....	16
1 Introduction.....	17
1.1 Rationale and Objectives.....	17
1.2 Thesis Structure and Author Contributions.....	18
1.3 Geological Background.....	19
1.3.1 Structural Setting.....	19
1.3.2 Palaeogeographic Evolution.....	21
1.3.3 Previous Studies .....	23
1.4 Sequence Stratigraphy of Carbonate Systems .....	23
1.5 Mixed Carbonate-Siliciclastic Systems .....	24
1.5.1 Controlling Mechanisms.....	24
1.5.2 Effects on Carbonate Production and Depositional Geometries .....	25
1.5.3 Sequence Stratigraphy of Mixed Carbonate-Siliciclastic Systems.....	27
1.5.4 Implications to petroleum exploration .....	27
1.6 Sedimentology and Geometry of Depositional Elements in Carbonate and Mixed Carbonate-Siliciclastic Settings .....	28
1.6.1 Hierarchy .....	28
1.6.2 Carbonate Shoal Bodies .....	29
1.6.3 Clinoforms and Clinothems .....	32
1.6.4 Infralittoral Prograding Wedges.....	32
1.6.5 Biogenic Build-Ups.....	33
1.6.6 Rudist Formations: Palaeoecology and Geometries .....	34
1.7 References.....	36
2 Methods and Materials .....	44

2.1	Sedimentological logging and sampling .....	44
2.2	Core logs .....	44
2.3	Thin Section Preparation and Microscopy .....	45
2.4	Modal Analysis .....	45
2.5	XRD Analysis .....	46
2.6	Construction of Cross-Sections .....	47
2.7	Digital Outcrop Modelling (DOM) .....	48
2.7.1	Lidar .....	48
2.7.2	Photogrammetry .....	49
2.7.3	Digital Outcrop Model Construction and Measurement of Geological Elements ...	51
2.8	References .....	52
3	Controls on Basin-Scale and Platform-Scale Architecture of Upper Cretaceous Carbonate Platforms.....	54
3.1	Abstract .....	54
3.2	Introduction and aims .....	55
3.3	Regional Geology.....	56
3.3.1	Tectonic History.....	57
3.4	Methods & Materials .....	57
3.5	Revision of the Chronostratigraphy within the Upper Cretaceous of the Tremp Basin .....	59
3.5.1	Chronostratigraphic Framework .....	59
3.5.2	Stratigraphic constraints .....	62
3.5.3	Revised stratigraphy for the Tremp Basin .....	63
3.6	Santa Fe and Pradina Platforms .....	66
3.6.1	Bounding Surfaces.....	66
3.6.2	Lithofacies and Depositional Environments.....	66
3.6.3	Architecture.....	68
3.7	Congost Platform.....	70
3.7.1	Bounding Surfaces.....	70
3.7.2	Lithofacies and Depositional Environments.....	71
3.7.3	Architecture.....	78
3.7.4	Distribution of Terrigenous Material.....	79
3.8	Sant Corneli Platform .....	79
3.8.1	Bounding Surfaces.....	79

3.8.2	Lithofacies and Depositional Environments.....	80
3.8.3	Architecture.....	87
3.8.4	Distribution of Terrigenous Material.....	87
3.9	Bastus Platform .....	88
3.9.1	Bounding Surfaces.....	88
3.9.2	Lithofacies and Depositional Environments.....	88
3.9.3	Architecture.....	98
3.9.4	Distribution of Terrigenous Material.....	98
3.10	Lower and Upper Terradets Platforms.....	99
3.11	Discussion.....	100
3.11.1	Global Sea Level Variations.....	100
3.11.2	Platform Architecture and Development.....	101
3.11.3	Main Controls on Basin Development .....	108
3.11.4	Source, Distribution, Mechanisms and Effect of Siliciclastic Input .....	110
3.12	Conclusions .....	112
3.13	References.....	114
4	Testing Controls on Facies Architecture Development and Sequence Stratigraphy within Upper Cretaceous Mixed Carbonate-Siliciclastic Platforms .....	120
4.1	Abstract .....	120
4.2	Introduction.....	121
4.2.1	Rationale and Aims.....	121
4.2.2	Geological Background.....	122
4.3	Methods and Materials .....	125
4.3.1	Fieldwork and Petrography.....	125
4.3.2	Construction of Platform Cross-Section .....	125
4.3.3	Construction of Sequence Stratigraphic Framework .....	126
4.3.4	Definition of Subsidence Rates and Plotting of Relative Sea-level .....	126
4.3.5	Stratigraphic Forward Modelling .....	126
4.4	Lithofacies and Depositional Environments.....	127
4.5	Platform Dimensions and Topography.....	137
4.6	Sequence Stratigraphic Interpretation .....	139
4.6.1	Surfaces .....	139
4.6.2	Stacking Patterns.....	141
4.6.3	Interpreted Sequences.....	142
4.6.4	Subsidence and Relative Sea-Level History.....	147

4.6.5	Evaluation of the Interpretation and Controls on Sequence Development .....	149
4.6.6	Key Characteristics of the Sequence Stratigraphic Interpretation.....	152
4.7	Stratigraphic Forward Modelling.....	153
4.7.1	Modelling Approach .....	153
4.7.2	CarboCAT Modelling Parameters .....	155
4.7.3	Qualitative Sensitivity Analysis.....	156
4.7.4	Forward Modelling Results and Interpretation.....	158
4.8	Discussion .....	164
4.8.1	Comparison of Sequence Stratigraphic Correlation with Forward Models .....	164
4.8.2	Implications for Sequence Stratigraphic Interpretations.....	168
4.9	Conclusions.....	171
4.10	References.....	172
5	Advances in Understanding the Internal and Outcrop-Scale Geometries of Shoal and Build-Up Bodies within Upper Cretaceous carbonate platforms.....	177
5.1	Abstract .....	177
5.2	Introduction.....	178
5.2.1	Rationale and aims .....	178
5.2.2	Sedimentology of Shoal and Build-up Geobodies.....	179
5.2.3	Dimensions of Shoal and Build-up Geobodies .....	181
5.2.4	Study Area .....	186
5.3	Methods and Materials .....	188
5.3.1	Fieldwork and Lithofacies Analysis.....	188
5.3.2	Digital Outcrop Data Acquisition and Processing.....	189
5.3.3	Digital Outcrop Model (DOM) Construction and Geobody Picking .....	189
5.3.4	Quantification Scheme for Sigmoidal Geometries.....	190
5.3.5	Mapping Regional-Scale Depositional Elements.....	191
5.4	Results .....	192
5.4.1	Platform Margin Shoal and Clinoform Bodies.....	192
5.4.2	Platform Interior Shoal Bodies .....	196
5.4.3	Platform Margin Build-ups .....	199
5.4.4	Platform Interior Build-ups.....	203
5.5	Discussion .....	204
5.5.1	Platform Margin Shoal and Clinoform Bodies.....	204
5.5.2	Platform Interior Shoal Bodies .....	207
5.5.3	Platform Margin Build-Ups.....	208
5.5.4	Platform Interior Build-Ups.....	211

5.5.5	Implications for Assessment and Prediction of Geobody Geometries .....	213
5.5.6	Limitations and Outlook .....	219
5.6	Conclusions.....	221
5.7	References.....	222
6	Synthesis.....	228
6.1	Summary of Main Results and Implications .....	228
6.2	Sequence Stratigraphy and Mixed Carbonate-Siliciclastic Systems.....	230
6.3	Geometrical Quantification and Classification of Carbonate Geobodies.....	231
6.4	Implication for Hydrocarbon Production and Exploration.....	233
6.5	Applicability of the Platforms of the Tremp Basin as Analogues for Middle Eastern Carbonate Systems .....	235
6.5.1	Rationale and Aims.....	235
6.5.2	Cenomanian-Turonian Rudist Platforms of the Arabian Shelf .....	235
6.5.3	Turonian-Santonian Rudist Platforms of the Tremp Basin.....	240
6.5.4	Discussion.....	241
6.5.5	Conclusions.....	247
6.6	Outlook.....	248
6.7	Conclusions.....	250
6.8	References.....	253
	Appendices.....	259
	Appendix A: Localities and Map Data .....	259
	Appendix B: Field Logs and Well Logs.....	260
	Appendix C: Sample and Thin Section Data .....	402
	Appendix D: Geobody Measurements.....	403

Word count: 79632

## LIST OF FIGURES

Figure 1.1: Structural overview of the South-Central Pyrenees and the Tremp Basin.....	21
Figure 1.2: Generalised palaeogeographic setting of Western Europe and the Northern Atlantic during Turonian-Campanian times .....	22
Figure 1.3: Palaeogeographic setting of north-eastern Spain and Southern France during the Santonian .....	22
Figure 1.4: Top: Proposed hierarchy scheme for build-ups and shoal bodies within carbonate platforms. Bottom: Schematic illustrating the hierarchy of sedimentological and geometrical elements within carbonate platforms .....	29
Figure 1.5: Conceptual sketch the internal geometrical hierarchy of shoal bodies of the modern Great Bahama Bank .....	31
Figure 1.6: Classification scheme of depositional shape established by Jung and Aigner (2012), modified .....	34
Figure 3.1: Simplified geological map of the Tremp Basin.....	58
Figure 3.2: Updated Chronostratigraphic framework for the Upper Cretaceous Platform Cycles proposed by Simó (1993).....	62
Figure 3.3: Revised chronostratigraphic correlations of the Cenomanian-Campanian carbonate platforms of the Tremp Basin .....	64
Figure 3.4: Combined Cross-Section of the Cenomanian-Santonian Platforms in the Tremp Basin .....	65
Figure 3.5: Cross-Plot of quartz, clay minerals and microcline contents within the localities of the Bastus Platform.....	99
Figure 4.1: Simplified geological map of the Tremp Basin.....	123
Figure 4.2: A: Cross section of the Bastus Platform.....	124
Figure 4.3: Sedimentary log key.....	125
Figure 4.4: Composite log of the nearshore sediments of the Bastus Platform exposed at Camarasa, scale 1:500.....	132
Figure 4.5: Composite log of the platform interior sediments of the Bastus Platform exposed at Oliana, scale 1:500 .....	133
Figure 4.6: Composite log of the platform margin sediments of the Bastus Platform exposed at Montagut Gully, scale 1:500 .....	134
Figure 4.7: Composite log of the platform margin sediments of the Bastus Platform exposed at Carreu River, scale 1:500 .....	135
Figure 4.8: Composite log of the basinal sediments of the Bastus Platform exposed at Tamurcia, scale 1:500 .....	136

Figure 4.9: Simplified sedimentary patterns of the Bastus Platform, used to construct the sequence stratigraphic interpretation .....	143
Figure 4.10: Sequence Stratigraphic interpretation of the Bastus Platform .....	146
Figure 4.11: Diagrams of eustasy, relative sea level, subsidence and relative sea-level fall magnitude for specific sections of the Bastus Platform .....	148
Figure 4.12: CarboCAT modelling parameters and lithofacies concept for the produced stratigraphic forward models .....	156
Figure 4.13: Comparison of the produced cross-section and cross-sections of the three-dimensional stratigraphic forward models created using variations in relative sea level .....	161
Figure 4.14: Comparison of the produced cross-section and cross-sections of the three-dimensional stratigraphic forward models created using variations in sediment productivity or tectonic tilt .....	163
Figure 5.1: Conceptual sketch of the different architectural elements and their scales within carbonate platforms .....	182
Figure 5.2: Geological Map of the study area within the Tremp Basin .....	188
Figure 5.3: Schematic concept of the quantification parameters for clinofolds, modified from the scheme established by Anell and Midtkandal (2015).....	190
Figure 5.4: Quantification concept and parameters for the clinofolds of the Bastus Platform margin grainstone shoals.....	191
Figure 5.5: Annotated screenshot of a Google Earth view with an overlay of the geological maps by Institut Cartogràfic i Geològic de Catalunya (2007), showing three possible scenarios occurring during geobody measurement .....	192
Figure 5.6: Outcrop photograph of the Congost A Sequence platform margin outcrop at Gallinove .....	193
Figure 5.7: Conceptual diagram of the grainstone shoal clinofolds of the Bastus Platform margin .....	195
Figure 5.8: Digital outcrop model of the Carreu River outcrop, showing the Bastus Platform margin deposits.....	195
Figure 5.9: Outcrop view showing the internal structure of the Sant Corneli Platform Interior shoals .....	197
Figure 5.10: The digital outcrop model produced for the Congost B Sequence exposure at Congost d'Erinyà, representing the platform margin .....	199
Figure 5.11: Digital outcrop model of the Montagut Gully outcrop, showing the Bastus Platform margin deposits.....	202
Figure 5.12: Conceptual sketch of the build-ups formed at the Bastus Platform Margin.....	202



Figure 5.13: Left: Outcrop view of the Bastus Platform interior build-ups. Right: detail view of the build-ups .....	204
Figure 5.14: Cross plot of average width against average length of shoal bodies gathered from the literature .....	217
Figure 5.15: Cross plot of maximum width against maximum thickness of shoal bodies gathered from current literature.....	217
Figure 5.16: Cross plot of average width against average length of Cretaceous aged build-ups with dimensions smaller than 1.2 km gathered from literature data .....	218
Figure 5.17: Cross plot of average width against average thickness from biogenic constructions from selected literature .....	218

## LIST OF PLATES

Plate 3.1: Photomicrographs of different variants of the platform top lithofacies of the Santa Fe and Pradina Limestones.....	70
Plate 3.2: Outcrop photographs illustrating the bedding relationships of the Congost A Sequence, as well as under- and overlying sequences.....	74
Plate 3.3: Photomicrographs of the Congost A Sequence.....	75
Plate 3.4: Overview and detail photographs of the Congost B Sequence (LFA CGB) and the basinal deposits of the Congost Platform (LFA RE).....	76
Plate 3.5: Photomicrographs of the Congost B Sequence (Lithofacies Association CGB) and the Congost Slope deposits (RE1).....	77
Plate 3.6: Outcrop and thin section images of lithofacies association NIT of the Sant Corneli Platform.....	83
Plate 3.7: Field photographs illustrating the various facies of the Sant Corneli Platform interior (LFA IR).....	84
Plate 3.8: Photomicrographs highlighting the details of the various lithofacies within the Sant Corneli Platform interior (LFA IR).....	85
Plate 3.9: Field photographs and photomicrographs of the slope and basin lithofacies of the Sant Corneli Platform.....	86
Plate 3.10: Outcrop photographs of the lithofacies association <i>Nearshore tidally influence delta</i> of the Bastus Platform.....	90
Plate 3.11: Photomicrographs of the <i>Nearshore tidally influence delta</i> lithofacies association of the Bastus Platform.....	91
Plate 3.12: Outcrop photographs of the platform interior lithofacies association (PI) of the Bastus Platform.....	93
Plate 3.13: Photomicrographs of selected samples from the platform interior lithofacies association (PI) of the Bastus Platform.....	94
Plate 3.14: Outcrop photographs of the Bastus Platform Margin (PM) and Upper Slope (US) lithofacies associations.....	95
Plate 3.15: Photomicrographs illustrating the Bastus Platform margin (PM) and upper slope (US) lithofacies association.....	96
Plate 3.16: Outcrop images and photomicrographs of the slope and basinal lithofacies of the Bastus Platform.....	97

## LIST OF TABLES

Table 2.1: Point counting classes used during modal analysis .....	47
Table 2.2: List of digital elevation model datasets used to georeference and scale Photogrammetry models.....	51
Table 3.1: Lithofacies scheme for the Santa Fe and Pradina Carbonate Platforms.....	69
Table 3.2: Lithofacies scheme for the Congost Carbonate Platform .....	73
Table 3.3: Siliciclastic contents in the Congost Platform as determined by modal analysis .....	79
Table 3.4: Siliciclastic contents in the Congost Platform as determined by XRD analysis.....	79
Table 3.5: Lithofacies scheme for the Sant Corneli Carbonate Platform.....	82
Table 3.6: Siliciclastic contents along the Sant Corneli Platform as determined by modal analysis .....	88
Table 3.7: Siliciclastic contents along the Sant Corneli Platform as determined by XRD analysis	88
Table 3.8: Lithofacies scheme for the Bastus Carbonate Platform.....	92
Table 3.9: Summary of platform characteristics and dimensions .....	102
Table 3.10: Overview of sediment thickness (calculated from the cross-section, Figure 3.4) and subsidence rates derived from these based on the duration of each platform (cf. Figure 3.3) along the data points from the cross-section .....	102
Table 4.1: Lithofacies scheme for the Bastus Carbonate Platform.....	131
Table 4.2: Overview of water depth indicators and estimated water depths for individual gross depositional environments (GDE), their lithofacies, and the respective locality .....	138
Table 4.3: Summary table of geometrical and stratigraphic parameters defined for the Bastus Platform from the field and sequence stratigraphic interpretation, and those shown by the results of the individual forward modelling.....	159
Table 5.1: Geometrical data of grainstone shoals throughout geological time, collected from a variety of literature sources.....	184
Table 5.2: Geometrical data of biogenic build-ups in Cretaceous times, collected from a variety of literature sources.....	185
Table 5.3: Quantification results of the clinofolds within the platform margin outcrop of the Congost A Sequence at Gallinove .....	193
Table 5.4: Average geometrical parameters for each grainstone shoal host unit of the Bastus Platform margin, measured at the Carreu River outcrop.....	196
Table 5.5: Dimensions of the platform interior shoals of the Sant Corneli Platform (Lithofacies NIT1).....	197
Table 5.6: Dimensions of the platform interior shoals of the Bastus Platform (Lithofacies PI1)	198
Table 5.7: Results of the measurements of sigmoids within the build-up unit of the Congost B sequence platform margin at Congost d’Erinyá .....	200

Table 5.8: Measured thicknesses and widths of individual lithofacies of the Bastus platform margin at Montagut Gully and Carreu River .....	203
Table 5.9: Dimensions of the platform interior rudist build-ups of the Bastus platform (Lithofacies PI3 and PI3).....	204
Table 5.10: Summary data for the depositional element and internal geometry of the Congost A and Bastus Platform margin shoal bodies .....	206
Table 5.11: Summary data for depositional element geometry of the Sant Corneli and Bastus Platform interior shoal bodies .....	208
Table 5.12: Summary Data for the depositional element geometry of the Congost B and Bastus Platform margin build-ups .....	209
Table 5.13: Summary data for the internal geometry of the Congost B and Bastus Platform margin build-ups .....	211
Table 5.14: Summary data for the depositional element geometry of the Bastus Platform interior build-ups .....	212
Table 6.1: Summary information of the Cretaceous Carbonate systems in the eastern Arabian Shelf and their geometry forming depositional elements.....	236
Table 6.2: Summary information of the Upper Cretaceous Carbonate Platforms of the Tresp Basin in the South-Central Pyrenees and their geometry forming depositional elements.....	241

## ABSTRACT

During the Upper Cretaceous, rudist-bivalve-dominated carbonate platforms formed within shallow water on the margins of the Tethys Ocean. These are characterised by diverse carbonate facies, often arranged complexly on a sub-seismic scale, and formed by biogenic build-ups, bioclastic shoal bodies and prograding margin clinofolds. Understanding the controls on this heterogeneity is necessary to accurately reconstruct the facies architecture. This thesis is an integrated multi-scale study, defining the geometry, development, and controls on platform architecture and facies distribution within the Upper Cretaceous of the Trepas Basin from platform- to outcrop scale.

The five investigated carbonate platforms (Cenomanian to Santonian) are separated by major flooding surfaces, each corresponding to a sea-level oscillation on the scale of ca. 3 My. Correlation of smaller-scale eustatic sea-level variations to changes in platform architecture was not possible, implying that regional processes pose a strong control on platform development on smaller time-scales. High-detail cross-sections of the basin show how the architecture of these platforms changed following a variety of controlling mechanisms. These include a fault-controlled margin in the early stages and a pelagic drape following the OAE2 at the Cenomanian-Turonian boundary. Subsequent global sea-level fall resulted in subaerial exposure and the deposition of a lowstand wedge, while later global sea-level rise resulted in successive retrogradation of the platform margins, and subsidence and increased sedimentation rates resulted in stepwise thickening of the younger platform successions. Here, local antiform growth also resulted in differential subsidence and laterally uneven thickness development.

Comparison of a detailed sequence stratigraphic interpretation of the Santonian Bastus Platform with stratigraphic forward models produced as part of a partner project at Royal Holloway University of London provided insight on possible controlling mechanisms on stratigraphic architecture and facies distribution. The architecture of the Bastus Platform could be modelled using variations in carbonate productivity or via introducing tectonic tilt, while keeping eustatic sea level constant. However, introducing variations in eustatic sea level did not result in fitting models. This demonstrates that changes in carbonate productivity and differential subsidence are possible controls on sequence stratigraphic development of carbonate systems, next to the commonly acknowledged sea-level variations.

Geobody dimensions and internal structure, gathered from digital outcrop data, show shoal complexes and infralittoral prograding wedges on the scale of several 10s by few kilometres, with thicknesses of few metres and several 10s of metres, respectively. Biogenic build-ups vary from few 100s metres to few kilometres in both width and length, and show either sigmoidal internal structure or are formed of composite bioherms and biostromes. Platform morphology and architecture, and hydrodynamic and ecological factors are interpreted to pose the underlying controls on geobody shape and size in these examples. Comparison with similar bodies in various Phanerozoic examples shows that unique width, length and thickness relationships may exist within each platform, but are not universal or directly transferrable to similar platforms.

The combined results of this study highlight how basin-scale reconstructions are necessary as a framework for understanding the multi-scale variety of controls on platform architecture. On platform scale, knowledge of controls on sequence formation is fundamental for prediction of facies architecture. Only with this information can adequate analogues be defined and comparisons of geobodies between different platforms be made confidently.

## DECLARATIONS

No portion of the work referred to in the thesis has been submitted in support of an application for another degree or qualification of this or any other university or other institute of learning.

## COPYRIGHT STATEMENT

- I. The author of this thesis (including any appendices and/or schedules to this thesis) owns certain copyright or related rights in it (the "Copyright") and s/he has given The University of Manchester certain rights to use such Copyright, including for administrative purposes.
- II. Copies of this thesis, either in full or in extracts and whether in hard or electronic copy, may be made only in accordance with the Copyright, Designs and Patents Act 1988 (as amended) and regulations issued under it or, where appropriate, in accordance with licensing agreements which the University has from time to time. This page must form part of any such copies made.
- III. The ownership of certain Copyright, patents, designs, trade marks and other intellectual property (the "Intellectual Property") and any reproductions of copyright works in the thesis, for example graphs and tables ("Reproductions"), which may be described in this thesis, may not be owned by the author and may be owned by third parties. Such Intellectual Property and Reproductions cannot and must not be made available for use without the prior written permission of the owner(s) of the relevant Intellectual Property and/or Reproductions.
- IV. Further information on the conditions under which disclosure, publication and commercialisation of this thesis, the Copyright and any Intellectual Property University IP Policy (see <http://documents.manchester.ac.uk/display.aspx?DocID=24420>), in any relevant Thesis restriction declarations deposited in the University Library, The University Library's regulations (see <http://www.library.manchester.ac.uk/about/regulations/>) and in The University's policy on Presentation of Theses.

*For my family*

## ACKNOWLEDGEMENTS

Completing this thesis would have not been possible without the help and support of my supervisors, colleagues, family and friends, and I would like to extend my thanks to anyone who has helped me throughout this endeavour.

First and foremost, I am grateful to Dr Cathy Hollis for the continuous support and supervision throughout the project. Further thanks are due to Dr Stefan Schröder, for the both productive and amusing discussions in a unique mixture of German and English geological terms.

BP plc. are greatly thanked for providing the financial support for this project. Dr Ian Billing, Dr James Gardner, Dr Christoph Lehman, Dr Anna Matthews and Dr Katherine Tutton of the BP Iraq Team and Prof Peter Burgess of the University of Liverpool are gratefully acknowledged for their tremendous effort in providing discussions and feedback on the geological concepts and interpretations.

Thanks are due to Dr John Waters from the School of Earth, Atmospheric and Environmental Sciences for conducting XRD measurements.

For their enthusiastic assistance during fieldwork, discussions at the outcrop, and help in keeping me motivated during long trips to rural Catalonia, I am eternally grateful to Dr Richard Newport, Dr Matthew Warke, Angel Arantegui, Lorenzo Valetti, Arne Schwab and Joseph Ward. Please also accept my apologies for the excessively long hikes, ridiculous working hours, lack of rest days, for making you carry large amounts of rocks and car batteries (and for the occasional dissolved jacket), and for the physical and mental toll taken by all these tasks!

For help with the acquisition and processing of the Lidar data, my thanks are due to Dr Brian Burnham, Dr Billy Head and Dr David Hodgetts. Furthermore, Dr Thomas Seers is gratefully acknowledged for his insights and advice on the acquisition of photogrammetry data, as well as providing and modifying his computer code for processing, and so making this part of the project a part of reality at all.

I thank my dear friends Vasily Alekseev, Harun Cakir, Dr Sebastian Hammerschmidt and Dr Alexander Petrovic for giving me geological, academic or personal advice on how to make it through the last 4 years and tackling the many aspects this project.

Kirstin, I thank you for all the encouragement and support, and for constantly reminding me that there is a world outside of research.

Finally, my greatest thanks go out to my parents and sister, without whom I would undoubtedly have not made it to where I am today.



# 1 INTRODUCTION

## 1.1 Rationale and Objectives

Carbonate systems are a frequent host to hydrocarbon reservoirs of major economic significance throughout the world (Roehl and Choquette, 1985). In the Cretaceous strata of the Arabian Shelf, these are often carbonate platforms with rudist bivalves as important sediment producers (Scott et al., 1993). These rudist systems often form highly complex internal architecture of facies with varying fluid-flow properties, leading to heterogeneity that can significantly impede reservoir characterisation and optimisation of production. These heterogeneities are often on sub-seismic scale and not correlateable between wells. Understanding the architecture of such systems is therefore important for the characterisation and prediction of such heterogeneity. Analogous outcrops are a fundamental source for data used to inform both reservoir models to improve understanding of the subsurface (Alexander, 1993; Grammer et al., 2004; Howell et al., 2014), as well as numerical forward models that help predict facies distribution and architecture (e.g. Burgess and Wright, 2003; Burgess, 2013).

The Upper Cretaceous carbonate platforms of the Tresp Basin in the South-Central Pyrenees offer a basin-wide exposure, allowing high-resolution stratigraphic studies and quantification of depositional elements such as rudist build-ups, grainstone shoals and clinofolds. These were chosen for their rudist-dominated facies as a potential analogue for the Cretaceous hydrocarbon systems of the Arabian Shelf. The presence of siliciclastic material on some areas of the Arabian Shelf and in the proximal areas of the Tresp Basin requires assessing the impact of the siliciclastic input on carbonate productivity in such “mixed systems”. To allow this, a review on the mechanisms and controls of carbonate and siliciclastic mixing will be presented during the introduction.

This study aims to present a multiscale investigation of the stratigraphic architecture and facies distribution of several rudist-dominated carbonate platform in the form of three papers:

1. Investigating how basin-scale and regional controls such as relative sea-level fluctuations, subsidence, tectonism, carbonate productivity and siliciclastic input affect development of a series of platforms over time and the architecture of each individual platform.
2. A study on the sequence stratigraphy of the Santonian Bastus Platform. Here, a conventional sequence stratigraphic interpretation is constructed based on field and map data. This is then tested against stratigraphic forward models that were produced in a parallel-running project at the Royal Hollow University of London. Through this, the

effects of relative sea-level variations, subsidence and carbonate productivity on the development of stacking patterns and facies distribution are investigated.

3. Quantification of rudist build-ups and grainstone clinoform geometries through the application of digital outcrop modelling, and investigating geometrical patterns and the controls on these.

The results and conclusions of these chapters are then compared with a selection of carbonate systems from the Arabian shelf (Chapter 6). This is done in order to evaluate the applicability of the Upper Cretaceous outcrops of the Tresp Basin as analogues for the rudist-dominated hydrocarbon reservoirs of the Arabian Shelf. Lastly, an outlook on the remaining issues and points of interest will be presented, with suggestions made on future studies that are expected to contribute towards the understanding of sedimentary architecture of carbonate systems.

## 1.2 Thesis Structure and Author Contributions

This thesis is submitted in alternative format. Three of the chapters are presented as research papers in journal format. Due to this structure, some repetition between the chapters is present. The structure of the thesis and corresponding authors are as follows:

### **Chapter 1:** *Introduction*

J. Lavi – Primary author

### **Chapter 2:** *Methods*

J. Lavi – Primary author

### **Chapter 3:** *Controls on Basin-Scale and Platform-Scale Architecture of Upper Cretaceous Carbonate Platforms*

J. Lavi – Data collection, interpretation and primary author

C. Hollis – Primary supervisor, manuscript co-author and reviewer

P. Burgess – Manuscript reviewer, co-supervisor

I. Billing, C. Lehmann, J. Gardner, A. Matthews, K. Tutton – Industry advisors

S. Schröder – Co-supervisor

### **Chapter 4:** *Testing controls on facies architecture development and sequence stratigraphy within Upper Cretaceous mixed carbonate-siliciclastic platforms*

J. Lavi – Data collection, interpretation and primary author

C. Hollis – Primary supervisor, manuscript co-author and reviewer

P. Burgess – Manuscript reviewer, co-supervisor

G. Antonatos – Production and quality control of stratigraphic forward models  
I. Billing, C. Lehmann, J. Gardner, A. Matthews, K. Tutton – Industry advisors  
S. Schröder – Co-supervisor

**Chapter 5:** *Advances in Understanding the Internal and Outcrop-Scale Geometries of Shoal and Build-Up Bodies within Upper Cretaceous carbonate platforms*

J. Lavi – Data collection, processing and interpretation and primary author  
C. Hollis – Primary supervisor, manuscript co-author and reviewer  
T. Seers – Development of code for photogrammetry data processing  
I. Billing, C. Lehmann, J. Gardner, A. Matthews, K. Tutton – Industry advisors  
S. Schröder – Co-supervisor

**Chapter 6:** *Synthesis*

J. Lavi – Primary author

### 1.3 Geological Background

The study area is situated in the Spanish South-Central Pyrenees, to its majority in the province of Lleida, Catalonia, with some western parts within the neighbouring province of Aragon. It spans between 41°30'00"N and 42°30'00"N, and 0°15'00"E and 2°00'00"E, measuring a total of ca. 7500 km<sup>2</sup> (Figure 1.1).

#### 1.3.1 Structural Setting

The Pyrenees are part of the Alpine mountain chain of western Europe, having formed during the Late-Cretaceous to Oligocene due to the convergence of the Iberian and European plates (Choukroune, 1992). They are situated between Spain and France, spanning from East to West across a length of approximately 300 km, and with a width of 140 km (Simó, 1986). The Pyrenees are divided into five main areas, which are separated by major faults (Souquet and Peybernes, 1977; Choukroune, 1992; Figure 1.1):

1. The Aquitaine foreland, which is characterised by concentric folds, and overthrust by,
2. The North Pyrenean Zone, featuring Hercynian basement exposures and locally highly metamorphosed Cretaceous flysch deposits
3. The Axial Zone, consisting predominantly Hercynian basement, with sporadic remnants of Mesozoic cover
4. The South Pyrenean Units, consisting of southward thrust Palaeozoic, Mesozoic and Cenozoic sheets

5. The Ebro foreland, dominated by Tertiary molasses which directly overlie the Hercynian basement

The North Pyrenean Fault (NPF) separates the North Pyrenean Zone from the Hercynian Basement further South, and is commonly interpreted as the boundary between the European and Iberian plates. In the Central Pyrenees it features a southward down-throw of ca. 15 kilometres and estimations are that the fault reaches down as far as the Moho (Simó, 1986).

Within the South Pyrenean Zone, three units of thrust sheets are identified (Muñoz et al., 1986). The lower thrust sheets feature pre-Hercynian basement. The middle thrust sheets display both basement, a partial Mesozoic succession as well as some Eocene flysch deposits. Finally, the upper thrust sheets feature a preserved Mesozoic sequence of substantial thickness (Figure 1.1).

The carbonate platforms investigated in this study are exposed within the upper thrust sheet group. From south to north, these thrust sheets are: the Serres Marginales, the Montsec and Bóixols thrust sheet (Villalba-Breva and Martín-Closas, 2012 after Muñoz, 1989). Together with the areas around Noguera, north of the town of La Pobla de Segur and Sopeira, they provide outcrops of a proximal-distal transect through the carbonate platforms investigated in this study. Within the Bóixols thrust sheet, the Sant Corneli anticline and Santa Fe Syncline (West of Organyá) pose the main structural elements (Figure 1.1).

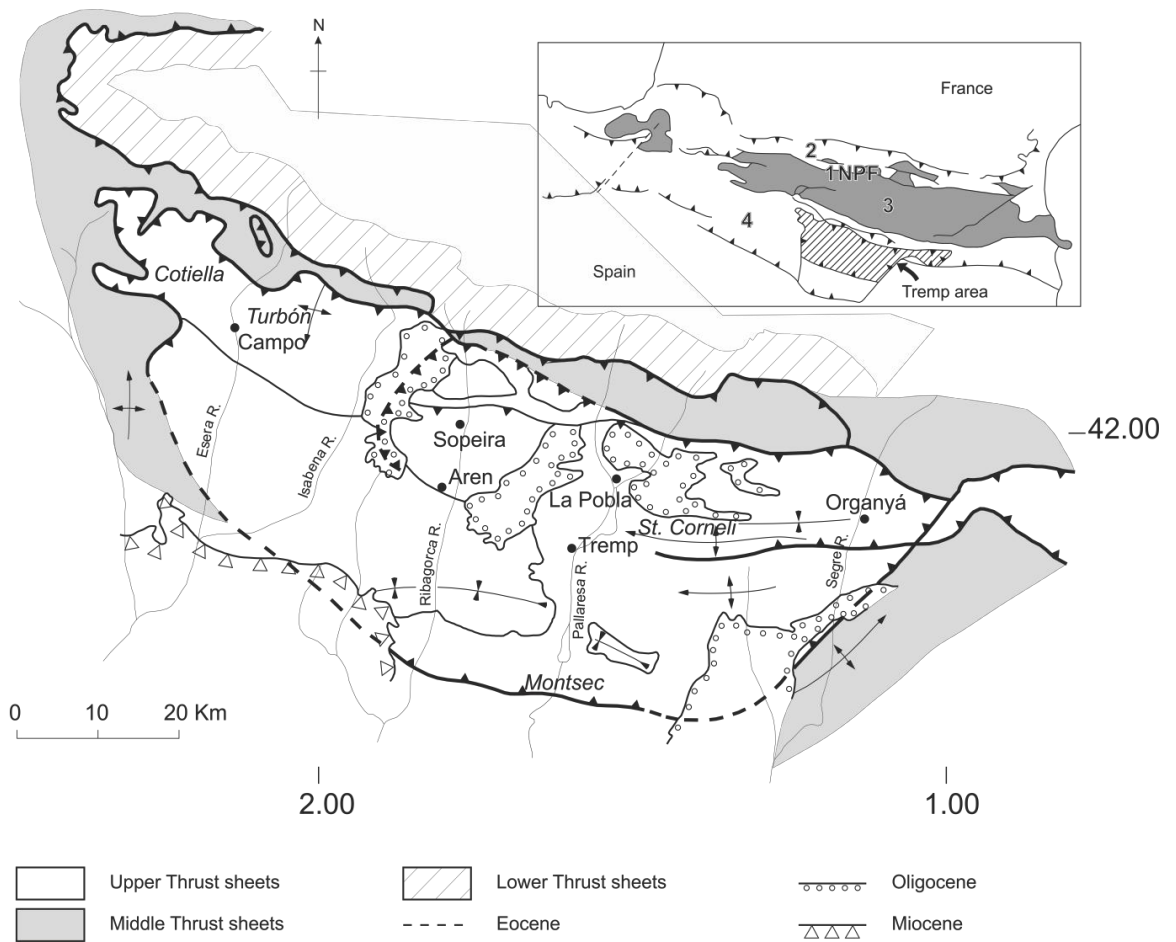


**Figure 1.1: Structural overview of the South-Central Pyrenees and the Tremp Basin.** The major tectonic elements indicated in the upper-right overview map are the North Pyrenean Fault (NPF), the North Pyrenean Zone (2), the Axial Zone (3), composed mainly of Hercynian Basement, and the South Pyrenean Zone (4). The detailed map of the Tremp Basin illustrated the three thrust sheet units within the South Pyrenean Zone together with the overlying Cenozoic sediments. Modified after Simó (1986).

### 1.3.2 Palaeogeographic Evolution

The palaeogeographic setting in the South-Central Pyrenees during the Upper Cretaceous is strongly affected by the convergence of the Iberian and European Plates. Due to the simultaneous anti-clockwise rotation of the Iberian plate, the repercussions of the convergence became apparent earlier in the Eastern Pyrenees, and slightly later in the West (Puigdefàbregas and Souquet, 1986). A narrow, approximately SSE-NNW orientated basin formed between the two plates, opening into the Bay of Biscay to the northwest, with shallow marine deposition occurring on both the Iberian and French side on narrow continental shelves (Ziegler, 1990). The Ebro Massif served as the most prominent source of clastic sediment, increasing in volume during the Upper Cretaceous, and smaller persistent clastic systems formed in the Eastern Pyrenees during terminal Cretaceous times (Plaziat, 1981; Figure 2). Subsequently, some of the later platforms are mixed carbonate-siliciclastic systems.

The palaeolatitude of the Tresp area during the Upper Cretaceous is interpreted to have been between 30° to 40° North (Owen, 1983; Simó, 1993). However, newer interpretations place it closer to 30° North (Philip and Floquet, 2000). Studies of clay minerals made by Nagtegaal (1972) in the area suggest that the climate varied from subtropical and semiarid in the Mid-Cretaceous into more arid in the Maastrichtian. Booler (1994) suggests humid climatic conditions throughout the Upper Cretaceous based on diagenetic features.

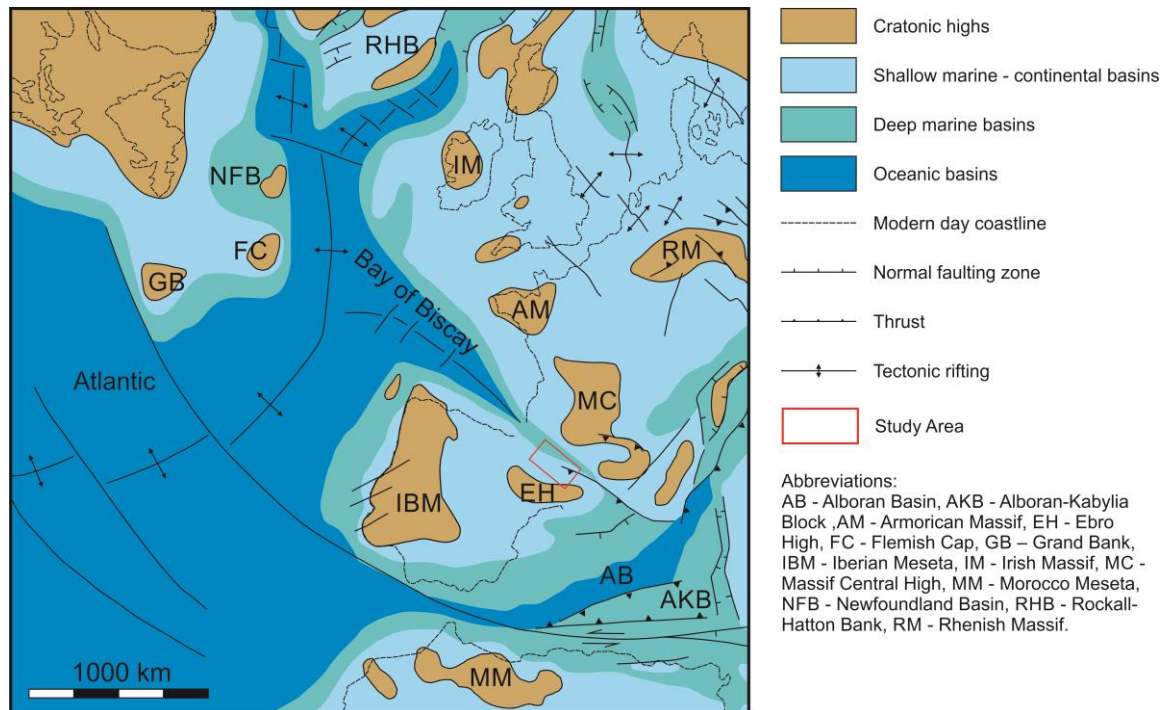


Figure 1.2: Generalised palaeogeographic setting of Western Europe and the Northern Atlantic during Turonian-Campanian times. Modified from (Ziegler, 1990).

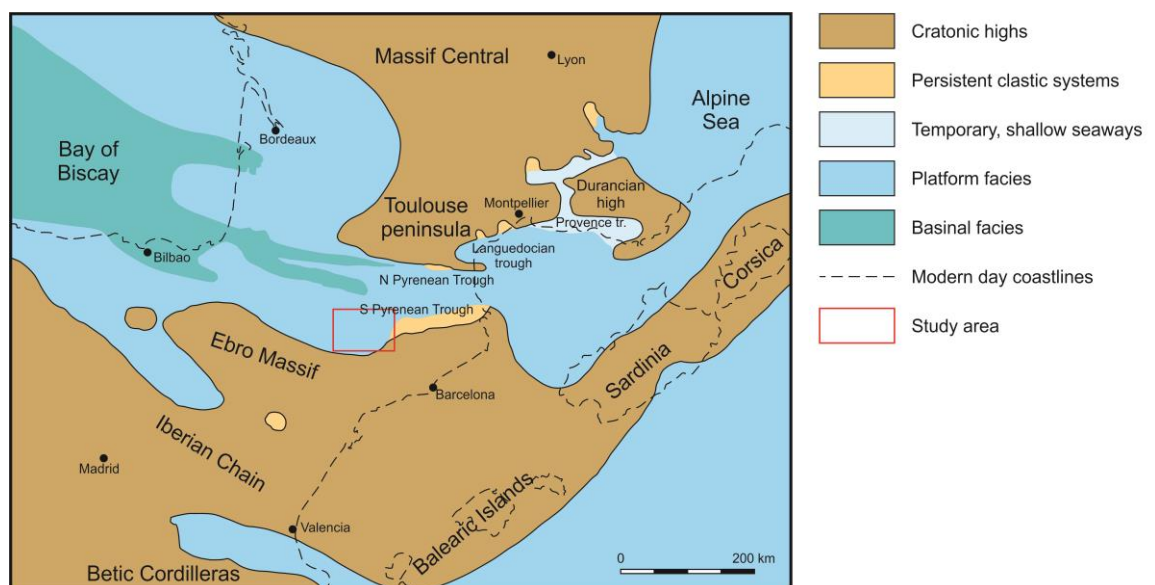


Figure 1.3: Palaeogeographic setting of north-eastern Spain and Southern France during the Santonian (modified from Plaziat, 1981).

### 1.3.3 Previous Studies

The Upper Cretaceous carbonate platforms of the Tremp Basin were previously the subject of a number of regional and outcrop-based studies. Mey et al. (1968), Gallemí et al. (1982, 1983), Hottinger et al. (1989), and Gallemí Paulet (1992) initially established the regional stratigraphy and correlated successions across the area. The regional-scale studies of Simó (1986, 1989, 1993) provide a detailed investigation of the carbonate platforms, including stratigraphy, sequence development, subsidence and an evaluation of the controls on deposition. For the Cenomanian to Coniacian Santa Fe, Pradina, Congost and Sant Corneli Platforms, these regional-scale studies were complemented by the work of Booler (1994) and Booler and Tucker (2002). On outcrop scale, Pascual et al. (1989), Caus et al. (1999), and Boix et al. (2011) published studies on the sedimentology and rudist and benthic foraminifer-based biostratigraphy of the Cenomanian to Santonian of the Montsec area. Gili (1993), Booler (1994), Skelton et al. (1995, 2003), Gili et al. (1996), Vicens et al. (1998), Sanders and Pons (2001), Pomar et al. (2005) and Caus et al. (2013) investigated the platform margin successions of the Turonian to Santonian platforms in the area of the Sant Corneli Anticline. These studies concentrate on the biostratigraphy and sedimentology of the rudist systems, with some lithostratigraphic correlations made across the basin. In the basinal areas around Sopeira, Caus et al. (1997) and Drzewiecki and Simó (1997) made contributions towards the biostratigraphy of the area, correlating some of the basinal deposits to the platform top, and defining sequence stratigraphic patterns according to the regional framework. Drzewiecki and Simó (2000, 2002) further investigate the nature of the slope and debris-flow sediments in line with the evolution of the specific platforms and sea-level variations.

### 1.4 Sequence Stratigraphy of Carbonate Systems

Sequence stratigraphic interpretations are a frequently used tool for understanding the development and controls on sedimentary systems over time. These are used widely in order to interpret facies distribution and sedimentary architecture in both siliciclastic and carbonate settings (Catuneanu et al., 2011). Part of this study addresses how a large number of these sequence stratigraphic concepts interpret temporal variations of relative sea-level as the fundamental mechanism for explaining the formation of stratal patterns and surfaces (e.g. Read, 1995; Lehrmann and Goldhammer, 1999), with processes such as carbonate productivity and differential subsidence only being considered more recently (e.g. Burgess, 2001; Burgess et al., 2001; Pomar and Kendall, 2011; Pomar et al., 2012; Burgess and Prince, 2015). The following section therefore provides an overview of the characteristics of the sequence stratigraphy of carbonate systems.

The concept of sequence stratigraphy has evolved significantly since its conception, and as a result, a number of approaches for defining depositional sequences and systems tracts were proposed (e.g. Mitchum et al., 1977; Vail et al., 1977; Haq et al., 1987; Van Wagoner et al., 1988, 1990; Hunt and Tucker, 1992; Catuneanu et al., 2011). Only some of these are designed to be applied to carbonate systems (Schlager, 2005). This is due to their intrinsic difference to siliciclastic systems in their mode of formation and the associated reaction to sea-level fluctuations (Handford and Loucks, 1993).

The key differentiation between siliciclastic and carbonate systems lies in how carbonate sediment is sourced locally through carbonate-producing organisms, as opposed to introduction of material into the shelf in siliciclastic systems (Catuneanu et al., 2009). Due to the ability of carbonate factories to produce rigid structures, these systems are different to siliciclastic systems in that they do not rely on the equilibrium between slope angle, sediment supply, grain size and wave energy to dictate the shape of the platform (Schlager, 2005). Furthermore, a large amount of possible controls on sedimentation in carbonate systems exist, including light penetration/water depth, nutrient levels, water temperature and ocean chemistry, wave energy, diagenesis, and biological factors such as binding, encrusting and bioerosion (Catuneanu et al., 2009). Also notable for carbonate systems are the common occurrence of *Type 3 sequence boundaries*, which are characterised by a flooding surface between a highstand systems tract and the respective overlying transgressive systems tract (Schlager, 1999). Moreover, the frequent absence of transgressive and maximum flooding surfaces and systems tracts is characteristic (Schlager, 2005).

Due to this diversity of controls and elements, no general sequence stratigraphic model can be applied universally to all carbonate systems (Catuneanu et al., 2009). Because of this, empirical studies of various systems and ages are a valuable addition to a repertoire of analogues used to support interpretations (Harris et al., 1999).

## 1.5 Mixed Carbonate-Siliciclastic Systems

Siliciclastic material was introduced Tresp Basin from the southern Ebro High in increasing amounts over the course of the Upper Cretaceous. The following section provides an overview of the mechanisms and effects of mixing of siliciclastics and carbonate sediments in order to highlight the possible effects on the carbonate systems and implications for interpretations.

### 1.5.1 Controlling Mechanisms

Mixed carbonate-siliciclastic systems typically form where carbonate platforms are in contact with a source of terrigenous material, such as fluviodeltaic areas or coastal mud flats (Catuneanu et al., 2011). Clastic input may be controlled by changes in sea level and base-level,



as well as fault related uplift, the formation of thrusts sheets – as often occurring in foreland basins – or via changes in climatic conditions. Alternatively, an axial supply of clastic material may occur into the basin through mechanisms such as long-shore drift, shoreline parallel currents, contour-flowing currents or through tide- and wind-induced circulation (Catuneanu et al., 2011). Mount (1984) suggested that mixing can occur through a variety of processes: (1) punctuated mixing, introducing material from one environment into the other via extreme, sporadic events such as storms. (2) facies mixing, which occurs along boundaries between two different facies. (3) in-situ mixing, where carbonate is produced on or within siliciclastic substrates. (4) source mixing, which occur via nearby uplift and erosion of lithified nearby carbonate strata. Budd and Harris (1990) consider mixtures between carbonate and siliciclastic facies as occurring spatially or temporally. In the smaller scaled spatial variability, the facies are mixed laterally through local processes, whereas temporal variability is controlled by large-scale variations in sea level and accommodation, occurring in the vertical stratigraphic succession through platform-wide introduction of siliciclastics into the carbonate system. Lastly, climatic effects will have a substantial effect on the nature of the siliciclastics which may be introduced into a carbonate system (Friedman, 1988): In warm and dry climates, coarse grained and clay-poor material is introduced periodically during flash flooding, allowing carbonate production during the intermittent periods. In humid climates, sediment is introduced more consistently and often dominated by fine-grained material, restricting carbonate production to further offshore areas.

These various concepts of mixing controls and mechanisms show that the interaction of siliciclastics and carbonates is very case-specific, presumably reliant on the scale of observation and the involved mechanisms of transport and carbonate production. The areas of particular interest are to which extent the introduction of siliciclastics affects carbonate productivity and in turn the geometry of geobodies. These two aspects are inherently difficult to constrain and quantify. In this study, a basin-scale example of a land-attached platform is presented and discussed. Using high-resolution sequence stratigraphic interpretations will allow addressing the effects of siliciclastic input, by attempting to identify the reaction of the carbonate factory. Additionally, quantification of geobody dimensions and investigation of their sedimentological characteristics will help unravel the influences of siliciclastic input on their geometries.

### **1.5.2 Effects on Carbonate Production and Depositional Geometries**

Terrigenous input can have negative impact on carbonate production in several ways (Catuneanu et al., 2011):

- Increased turbidity through suspended fine-grained material, which reduces the penetration depth of light in the water column and subsequently inhibits the growth of organisms reliant on photosynthesis.
- Both mud and sand grade terrigenous material may disrupt the feeding mechanisms of some organisms, or bury them completely.
- High influxes of nutrients associated with the clastics may lead to greater levels of microbial activity, and are detrimental to the carbonate production capacity of many organisms, as many of these are oligotrophic.

Foram-mollusc assemblages are generally more common in mixed systems than coralgal ones, due to the resistance of these organisms to the negative effects of siliciclastic influx (Mount, 1984). Various examples of carbonate production in clastically influenced systems show that at least some carbonate producing organisms have been able to adapt to these conditions, such as patch reefs on clastic shelves (Queensland shelf, Australia; Larcombe et al., 2001), reefs established on abandoned delta-front bars (Mahakan Delta, Indonesia, Wilson and Lokier, 2002), coral reefs sustaining periodic clastic shedding by neighbouring delta fans (Red Sea; Tucker, 2003) as well as growth on toe-of-slope (Eocene of the Great Australian Bight; Sharples et al., 2014).

The effects of siliciclastic input on Upper Cretaceous rudist formations was discussed by Sanders (1998). The interaction between siliciclastics and rudist formations results in several characteristic changes in fabric and lithology, and distinct stratigraphic contacts or transitions. Sanders (1998) concluded that moderate and/or infrequent influx of clastic material only has a subordinate effect on the growth of rudist formations. For both pure carbonate and mixed systems, Sanders (1998) has presented an idealised concept of the possible associations of rudists or corals depending on water-depth and energy. Overall, it is implied that rudists show a tolerance to a wider range of environmental conditions than colonial corals. Specifically, colonial corals are rare in mixed siliciclastic environments, and in pure carbonate environments are limited to a certain range of water depths and energies. Subsequently, the fact that mixed-Coral rudist bioherms are dominated by either corals or an association of corals and rudists in the lower parts of sequences, and to transition into almost exclusively rudists at their top is a direct result of a zonation based on bathymetry, with an upward-shallowing trend (Sanders, 1998). With respect to their distribution along a platform, a differentiation is observed in mixed systems. Rudists were able to proliferate in areas which were less favourable for coral and sponge growth, and they tend to dominate proximal platform zones which are more strongly influenced by direct siliciclastic input (Sanders, 1998).

The control of siliciclastic input on the depositional geometry of modern coral reef carbonates was investigated by Santisteban and Taberner (1988). They concluded that the siliciclastic sedimentary bodies generally controlled the geometry and positioning of the reefs, with rare case where the opposite occurs. However, McNeill et al. (2004) argued that the topographic highs formed by carbonate bodies generally tend to act as deflectors for siliciclastics, leading to channelization around the build-ups.

### 1.5.3 Sequence Stratigraphy of Mixed Carbonate-Siliciclastic Systems

Due to the combination of factors controlling the development of mixed carbonate-siliciclastic systems, there is an inherent lack of sequence stratigraphic approaches designed specifically for interpreting them. Early sequence stratigraphic concepts for mixed carbonate-siliciclastic systems were presented by Handford and Loucks (1993). Two end-members of sequence types are proposed more recently (Catuneanu et al., 2011): in *lower-carbonate upper-clastic sequences*, carbonates are deposited on the platform during a transgressive or highstand systems tract, while siliciclastics follow during the late highstand, forced regression and lowstand systems tracts, akin to the proposed mechanism of reciprocal sedimentation coined by Wilson (1967). In *lower-mudrock upper-carbonate sequences*, mudrocks deposit in the basinal and outer-shelf deposits, and are interpreted as transgressive systems tracts, while carbonates are deposited in shallower areas and represent prograding highstand facies. This sequence type is typically observed in carbonate ramp settings, and has also been interpreted by Catuneanu et al. (2011) into the previous descriptions of the Tremp Basin of Simó (1993).

The difficulty in interpreting these systems lies in how variations in siliciclastic volume and type may have various effects on the carbonate system and in turn on sequence formation. In this study, the investigation of the sequence stratigraphy, architecture and siliciclastic contents within a platform is expected to provide insight on how interpretations of these systems can be improved.

### 1.5.4 Implications to petroleum exploration

An extensive review of the implications of mixed carbonate-siliciclastic systems on petroleum exploration was presented by McNeill et al., (2004); On regional scale, key considerations are the abrupt lateral facies changes that may occur in mixed systems, and shallow burial and early diagenesis resulting in similar acoustic properties of laterally equivalent siliciclastics and carbonates, which makes differentiation in the subsurface difficult. However, it is noted that the palaeotopography of reefs may influence the channelling of siliciclastics within the basin, providing a degree of predictability of facies in reservoir modelling. Santisteban and Taberner (1988) suggested the opposite, in which the siliciclastics had a major control on the positioning

of reef bodies. This highlights how individual mixed systems may behave differently depending on the nature of the carbonate producers and the siliciclastic material.

On a local scale, siliciclastics do not entirely inhibit the in-situ production of carbonate, as demonstrated in Recent mixed systems (e.g. Larcombe et al., 2001; Wilson and Lokier, 2002; Tucker, 2003; Sharples et al., 2014). This results in a close juxtaposition of both lithologies, and highlights that vertical changes between the two are not necessarily the result of regional-scale processes, as suggested previously by Budd and Harris (1990). Furthermore, coarse-grained clastics (sand and gravel size) can be transported over long distance into the carbonate environment, introducing possible grain-size variations, which may affect petrophysical and fluid flow properties. Lastly, localised processes at the mixing zones of clastic and carbonate material, such as meeting of fluviodeltaic systems and ocean-currents, are able to sort the material by grain size and physical properties. As a result, local and compartmentalised deposits may form implying that these small scale processes and interfaces have as much potential in the appearance of depositional “sequences” as eustatic sea-level variations (McNeill et al., 2004).

## **1.6 Sedimentology and Geometry of Depositional Elements in Carbonate and Mixed Carbonate-Siliciclastic Settings**

### **1.6.1 Hierarchy**

In order to establish a concept of hierarchy within the different geological and geometrical terms used throughout this study, a classification scheme is presented (Figure 1.4). It defines the hierarchy within different geological elements (sedimentary systems, depositional environments, etc.) and the equivalent geometrical element (platform, geobody, etc.) that are discussed in this thesis, together with an approximate scale and an example. The high variability of many geological systems however may result in overlap of scales of different elements, as well as in more complex compartmentalisation or in fluid transitions between elements.

## Carbonate Platform Geobody Hierarchy

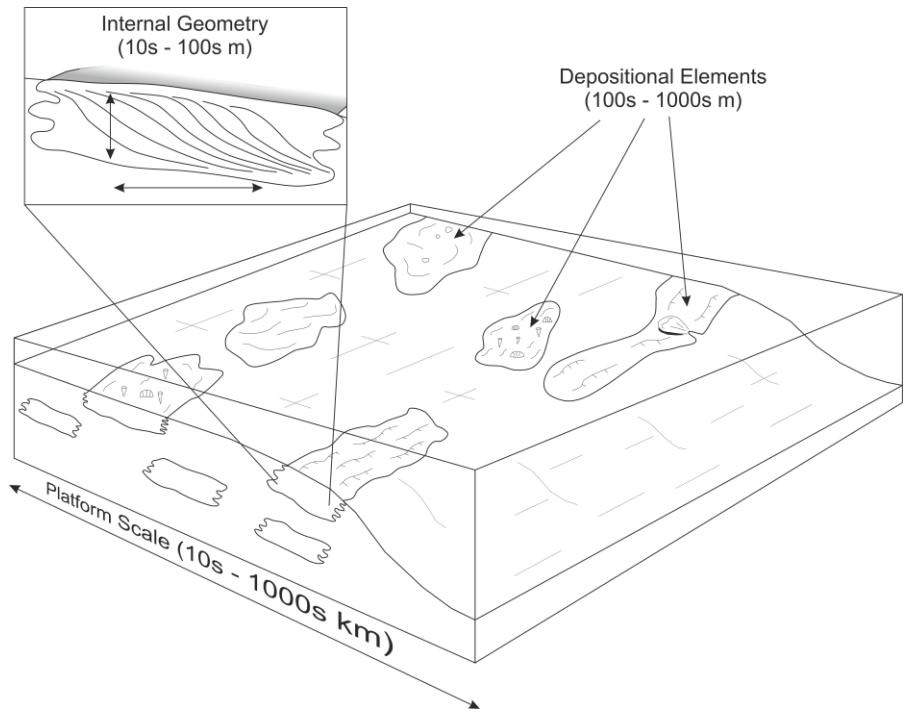


**Figure 1.4:** Top: Proposed hierarchy scheme for build-ups and shoal bodies within carbonate platforms. Bottom: Schematic illustrating the hierarchy of sedimentological and geometrical elements within carbonate platforms. Chapter 5 focuses on defining the scales of depositional elements and their internal geometry. Elements are not drawn to scale, and the depicted internal geometry is for illustration purposes only. For cliniforms, internal geometries include widths, heights, angles and bed thicknesses. For bedded/mounded geometries, these would include thickness, width and length of the feature, as well as slope angles. The platform scale architecture is investigated in Chapter 3.

### 1.6.2 Carbonate Shoal Bodies

The term grainstone shoal is generally attributed to depositional elements comprised of sand waves or subaqueous dunes as defined by Allen (1980), consisting of either bioclastic or ooidal/peloidal grains and a grainstone depositional texture as defined by Dunham (1962). The large-scale geometries of shoal bodies have been widely studied in the modern ooid shoals of

the Bahamas, where they occur along large areas of the platform margin (Ginsburg, 1956; Ball, 1967; Hine, 1977; Harris, 2009; Harris et al., 2011; Rankey and Reeder, 2011). The main types of sand bodies are marine sand belts, tidal bar belts, eolian ridges and platform interior sand blankets (Ball, 1967). Tidal-bar belts and marine sand belts are formed through the accumulation of grains by dominantly daily tidal flows and wave- and storm generated currents (Hine, 1977). These shoal bodies generally form in areas where waves or tidal currents are locally increased by changes in seafloor topography, providing a sorting mechanism, and where these coincide with high local carbonate production rates, providing a source of sand-grade grains (Harris, 2009). Platform interior sand blankets are characterised by obscured internal structure following intensive bioturbation. They are found in the areas between the high-energy platform edge and the low-energy zones leeward of islands (Harris, 2009). The orientation of the shoal bodies in regards to the platform margin is dictated by the local topography and wave energy, which is why they may vary within the platform (Harris, 2009).

Shoal bodies may vary widely in width and length, reaching up to several 10s of kilometres in strike. Smaller sand bars tend to be rounded, while larger ones (>1km) are generally elongated (Harris et al., 2011). They are constituted of several possible elements: longitudinal tidal sand ridges, transverse shoulder bars, parabolic bars, and intermediate sand flats (Rankey and Reeder, 2011). Not all elements are present within every shoal body, and their arrangement is unique for each case, and dictated by the surrounding geomorphology, bathymetry, wave energy and carbonate production rates (Rankey and Reeder, 2011). The vertical succession is generally described as a shallowing-upwards sequence, forming packages of few metres in thickness. In the example of the Joulter's Cay, Great Bahama Bank, this shows as a transition from peloidal wackestones, over fine-peloidal packstone to ooidal packstones at the top (Harris, 2009). In many examples, cross-section dip indicates transport of grains towards the platform interior. In the vertical succession, this leads to ooid shoals commonly overlying lagoonal sediments (Harris, 2009). However, when the shoal body occurs in the leeward side of an isolated bank, transport can be directed off-bank (Hine, 1977). However, in tidal bars, the cross-beds occurring at the top of the shallowing-up sequence dip perpendicularly to the bar trend (Harris, 2009). The cross-beds may vary in dip angles, reaching up to 24° (Gonzalez and Eberli, 1997).

Ancient carbonate sand shoal bodies are widely known from outcrop and subsurface examples, where they range from 1 km to 20 km. A well-known example includes the Triassic Muschelkalk in Germany (Aigner et al. 2007) and Oman (Koehrer et al., 2012). These formed laterally extensive bodies (10-20 km), with only gradual changes in facies due to very gentle dip of clinofolds (<0.01°; Palermo et al., 2010). Other well-studied shoal bodies are in the Cretaceous

of the Arabian Shelf (Grélaud et al., 2010; Adams et al., 2011) and the Permian Basin of Texas (Kerans and Harris, 2010).

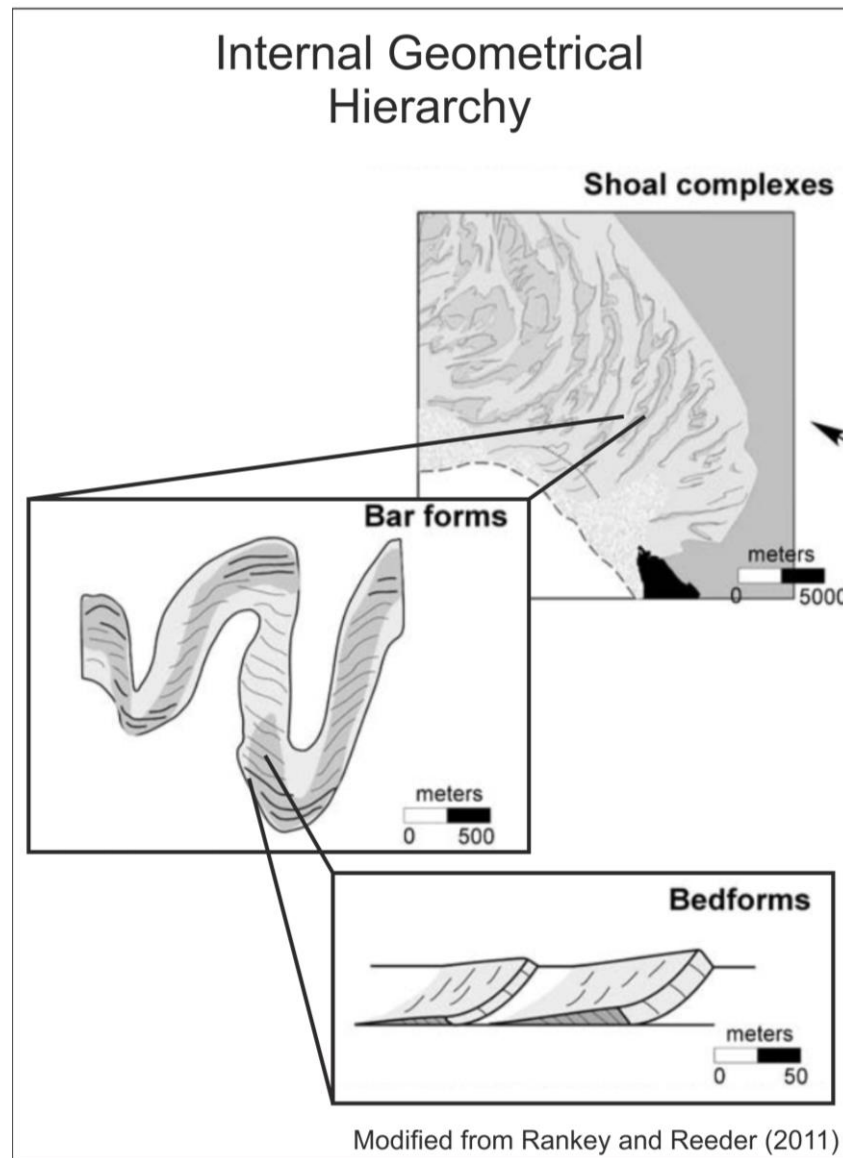


Figure 1.5: Conceptual sketch the internal geometrical hierarchy of shoal bodies of the modern Great Bahama Bank (modified from Rankey and Reeder, 2011).

Understanding the spatial distribution of shoal bodies within the carbonate system remains a challenge, as these systems prove highly variable both in lateral and vertical facies architecture. A general concept of the preferred location of shoal bodies is accepted since the establishment of the generalised facies models in carbonate platforms and ramps (Wilson, 1975; Burchette and Wright, 1992). Because shoals often form laterally discontinuous bodies of high permeability and present a complex internal structure, their presence can strongly influence fluid flow and hydrocarbon recovery in mature hydrocarbon reservoirs. Therefore, there has been renewed interest in their lateral and vertical scales in recent years. The study of modern shoal systems is often used to produce a statistical distribution of such bodies throughout a

platform (Harris et al., 2011, 2015; Purkis and Vlaswinkel, 2012; Purkis et al., 2015). This knowledge is later applied to subsurface systems through application of various modelling techniques, such as Multiple Point Statistics (Levy et al., 2008; Rankey et al., 2008; Carrillat et al., 2010; Jung et al., 2012), fuzzy logic algorithms (e.g. Demicco and Klir, 2001) or object-based modelling.

### **1.6.3 Clinoforms and Clinothems**

Next to parallel bedding, the dominant large-scale bedform in carbonate sediments is clinoformal cross-bedding. The term clinoform originally described the sigmoidally dipping sedimentary surfaces of shelf margins (Rich, 1951), but is now used to describe the topset, foreset and bottomset (defined by Gilbert, 1885). The term clinothem additionally refers to the whole rock unit, rather than just the bedding surface (Rich, 1951). Because petrophysical contrasts often occur on both sides of the sigmoidal bedding planes, or between the bottom and top of a clinothem, they pose an influence on reservoir properties. Furthermore, clinoforms can influence how bedforms are correlated within a reservoir, impacting reservoir sweep. Therefore, clinoform geometries have been widely studied in clastic sedimentary systems (e.g. Anell and Midtkandal, 2015; Graham et al., 2015). Examples of clinothems and large-scale cross-bedded foresets are also prevalent in bioclastic carbonates (e.g. Bosellini, 1984). Such clinoforms were quantified in the subsurface on seismic scale in rudist platform settings of the mid-Cretaceous Arabian Shelf (e.g. Droste, 2010), providing information on dimensions and angles. However, for carbonate settings, the attempts to quantify such geometries in outcrop is limited to only very few examples (e.g. Grélaud et al., 2010; Adams et al., 2011; Natih Formation, Oman). Most importantly, few attempts to introduce a uniform quantification system have been made (e.g. Anell and Midtkandal, 2015; Patruno et al., 2015).

### **1.6.4 Infralittoral Prograding Wedges**

Infralittoral prograding wedges (IPW) have been defined as large-scale sedimentary bodies with internal seaward-prograding inclined beds (Hernández-Molina et al., 2000). They are supplied with sediment that is mobilised from the upper shoreface environments during episodes of high water energy (storms), and resedimented seawards at depths where wave energy is reduced and no longer keeps grains in suspension (Hernández-Molina et al., 2000; Mitchell et al., 2012). It has been previously proposed that IPW are dependant on the existence of pre-existing seafloor physiography, for example in the form of shelf-indenting canyons, which concentrates storm energy in a narrow zone (Mateu-Vicens et al., 2008; Ortega-Sánchez et al., 2014).

A multitude of examples of IPW is described in Late Pleistocene and Holocene clastic settings. These are in the shelves of the western Mediterranean and the Gulf of Cadiz (Hernández-Molina et al., 2000; Ortega-Sánchez et al., 2014), southern California, southeast Australia and the



Manawatu Coast of New Zealand (Mitchell et al., 2012). Examples of IPW in carbonate settings are known in the prograding oolitic wedges of the Pliocene-lower Pleistocene of Italy (Pomar and Tropeano, 2001; Mateu-Vicens et al., 2008), and the Jurassic carbonate ramps of western France (Andrieu et al., 2017), the Iberian Basin (Pomar et al., 2015) and Morocco (Pierre et al., 2010; Amour et al., 2013). Lateral extents of IPW are commonly on the scale of several 10s of kilometres in strike, but may extend across 100s of kilometres across the continental shelf. In dip, these range from few 100s of metres to few kilometres, and thicknesses lie between 0.5 metres and several 10s of metres (Ortega-Sánchez et al., 2014; Pomar et al., 2015). Bedding angles of the internal surfaces span between 1.5° and 15°, and are thus smaller than those commonly observed in carbonate sand shoals (Pomar et al., 2015).

### 1.6.5 Biogenic Build-Ups

The terms bioherm and biostrome, coined by Cumings (1932), are some of the most frequent terms to describe the geometric characteristics of biogenic build-ups, while the terms reef and bank are used to discern their genetic origin (Klement, 1967). More recently, the terms skeletal reefs and reef mounds were introduced for these elements (Tucker and Wright, 1990). The differentiation between a biostrome and bioherm is clearly defined – based on whether the geobody forms significant topography in relation to the surrounding sediment and on the steepness of its flanks. However, terms such as bar, sheet, and mound are often used liberally and interchangeably between different studies, publications and authors. To address this, Jung and Aigner (2012) presented a classification scheme (Figure 1.6) which gives each descriptive term for a bioconstruction a specific – yet qualitative – geometrical outline and shape.

Numerous studies investigated the quantification of organic build-up shapes (e.g. Immenhauser et al., 2002; Loucks and Kerans, 2003; Adams et al., 2005; Janson et al., 2015). For an example of lenticular Albian rudist-coral-stromatoporoid patch reefs in the Mavericks Intraself Basin, Texas, Aconcha et al. (2008) defined their length to be 1.5-2.5 times greater than their width, and these build-ups show elongation perpendicular to palaeo-wind and -current directions. Phelps et al., (2008) were able to show that the relief of build-ups amounts to ca. 9.5% of their width, on the basis of an example from Permian fusulinid mounds in the mixed carbonate-siliciclastic system of the Permian Basin, Texas. From outcrop observation, they conclude that the build-ups were round to oblate in plan-view. However, these are generally isolated and unique examples of geometrical relationships, and testing the validity of these on either similar build-ups, or build-ups consisting of other organisms have not been done to date. Similarly, the spatial arrangement of build-ups and their distribution within carbonate systems was the subject of a number of studies. Examples from the Carboniferous (Janson and Madriz, 2012), Triassic and Jurassic (Amour et al., 2012) and the Cretaceous (Aconcha et al., 2008) illustrate

that capturing the spatial arrangement of build-ups and establishing overarching rules for their distribution is particularly difficult due to the nature of outcrop and the difficulties to differentiate many facies in the subsurface using seismic lines and wireline logs.

The internal architecture of different build-ups was also described in many publications (e.g. Ross and Skelton, 1993; Sanders and Pons, 2001; Kerans, 2002; Pomar et al., 2005). However, most studies are descriptive and only rare attempts are made at quantification and establishing geometrical rules. Pomar and Ward (1994) previously tied the internal sigmoidal structure of prograding reefs to their sequence stratigraphic development, showing the significance of internal structure and surfaces.

Type (Class)	Examples	Strike-section	Dip-section	Plan-view
<b>Mound</b>	<b>Mud Mounds, Rudist Mounds</b>			
<b>Bar</b>	<b>Shoals, Barrier Reefs, Tidal &amp; Channel Bars</b>			
<b>Bow</b>	<b>Atoll, Fringing Reefs, Tidal &amp; Channel Bars</b>			
<b>Pinnacle</b>	<b>Pinnacle Reef, Knob</b>			
<b>Wedge</b>	<b>Reef debris, Aprons, Wedges</b>			
<b>Fan</b>	<b>Fans, Reef Debris, Spill-Over Lobes</b>			
<b>Cliniform</b>	<b>Progradational debris, Aprons, Wedges</b>			
<b>Sheet</b>	<b>Biostromes, Temprestites, Mud Flats</b>			

Figure 1.6: Classification scheme of depositional shape established by Jung and Aigner (2012), modified. Highlighted in bold are geobody classes and examples that are characterised in this study. The scheme is purely geometrical, so that build-ups of various biogenic origins may be classified using the same shape.

### 1.6.6 Rudist Formations: Palaeoecology and Geometries

In the past, authors have proposed that rudists have actively displaced corals as the main reef builders during the Cretaceous (Kauffman and Johnson, 1988). However, Scott et al. (1990) later proposed that the decline of coral reefs occurred independently of rudist evolution, arguing that mixed communities of rudist and corals flourished on some late Cretaceous platforms. They therefore attribute the demise of corals to the sea-level rise and fluctuations in marine productivity occurring between the lower and upper Cretaceous. These environmental changes had less of an effect on rudist populations, which is why they were able to advance from the

inner-shelf and platform areas out onto the platform margin by occupying the open niche left behind by the corals.

Rudist formations and the sediments derived from them form many important hydrocarbon reservoirs in the Middle East, the Gulf of Mexico and parts of the Mediterranean Tethys. As with other hydrocarbon plays, the reservoir potential is dictated by the type and setting of the rudist formations, as well as by stratigraphic context and diagenetic history (Ross and Skelton, 1993).

### **Geometries Produced by Rudist Formations**

Rudists are known to have formed a variety of depositional geometries, each tied to the specific position of the build-up on the carbonate platform (Ross and Skelton, 1993). Several specific types of rudist build-ups were previously defined by Ross and Skelton (1993):

Steep margin complexes can establish on high angle slopes (>10 degrees), either at intraplatform basin margins caused by extensional faulting, or directly tied to syndepositional faulting at the margin. They tend to be aggradational, occasionally forming successions of up to several hundreds of metres thickness and showing abrupt lateral facies transitions (Ross and Skelton, 1993). Notable are the lack of coherent organic frameworks and of a resistant outer rim, as opposed to coralline build-ups. Since rudists acted to stabilise the surrounding substrate and contributed to sediment transport down slope, the resulting topography is described as a round-shouldered carbonate bank complex (Ross and Skelton, 1993). Furthermore, it was shown that early cementation and reworking played an important role in the build-up formation, and allowed lithified blocks to be transported into the slope (Borgomano and Philip, 1987).

Low-angle open shelf margin complexes include those established on slopes with less than 10° (often <3°) dip and facing open marine basins. They are commonly progradational in nature, composed of multiple shoaling-up sequences of up to tens of metres thickness (Ross and Skelton, 1993). In their lower parts, the sequences show common corals and sponges, with rudists becoming more dominant towards the top, as a direct expression of a bathymetrical faunal zonation (Scott, 1988; Sanders, 1998). The slopes are subjected only to low hydrodynamic energies, resulting in deposition of packstones and wackestones (Ross and Skelton, 1993).

Inner-shelf basin prograding margin complexes form extensive, tabular platforms with very low angles, in which sediment from the shoals is dispersed and fined towards the basin (Ross and Skelton, 1993). The main transport mechanisms are considered to be tidal currents, with some rare influences by storm action (Burchette and Britton, 1985; Mishrif Formation). Internally,

such successions consist of repeated coarsening up progradational units of few metres thickness, which are interpreted to represent migrating shoal banks (Ross and Skelton, 1993).

Isolated build-ups with rudists may establish themselves locally on sea-floor highs, for example upon biogenic mounds, structural highs, salt diapirs or volcanic intrusions. Such constructs known from the early Cretaceous are preceded by stacked coral mounds and mud mounds (Ross and Skelton, 1993).

Inner-shelf and platform rudist biostromes form laterally extensive (up to several hundreds of metres) and thin (rarely more than a metre or two) tabular bodies, lacking any significant topographical relief (Masse and Philip, 1981). Laterally, they pass into the host sediment without discrete flanking deposits. Internally, they show para-autochthonous floatstones which are characterised by a remarkably low rudist diversity, with one species commonly dominating (Sanders, 1996).

## 1.7 References

- Aconcha, E., C. Kerans, and H. Zeng, 2008, Seismic Geomorphology Applied to Lower Glen Rose Patch Reefs in the Maverick Basin, Southwest Texas: Gulf Coast Association of Geological Societies Transactions, v. 58, p. 3–23.
- Adams, E. W., C. Grelaud, M. Pal, A. E. Csoma, O. S. Al Ja'aidi, and R. A. Hinai, 2011, Improving reservoir models of Cretaceous carbonates with digital outcrop modelling (Jabal Madmar, Oman): static modelling and simulating clinoforms: Petroleum Geoscience, v. 17, no. 3, p. 309–332, doi:10.1144/1354-079310-031.
- Adams, E. W., J. P. Grotzinger, W. a. Watters, S. Schröder, D. S. McCormick, and H. a. Al-Siyabi, 2005, Digital characterization of thrombolite-stromatolite reef distribution in a carbonate ramp system (terminal Proterozoic, Nama Group, Namibia): AAPG Bulletin, v. 89, no. 10, p. 1293–1318, doi:10.1306/06160505005.
- Alexander, J., 1993, A discussion on the use of analogues for reservoir geology: Geological Society, London, Special Publications, v. 69, no. 1, p. 175–194, doi:10.1144/GSL.SP.1993.069.01.08.
- Allen, J. R. L., 1980, Sand waves: A model of origin and internal structure: Sedimentary Geology, v. 26, no. 4, p. 281–328, doi:10.1016/0037-0738(80)90022-6.
- Amour, F., M. Mutti, N. Christ, A. Immenhauser, S. M. Agar, G. S. Benson, S. Tomás, R. Alway, and L. Kabiri, 2012, Capturing and modelling metre-scale spatial facies heterogeneity in a Jurassic ramp setting (Central High Atlas, Morocco): Sedimentology, v. 59, no. 4, p. 1158–1189, doi:10.1111/j.1365-3091.2011.01299.x.
- Amour, F., M. Mutti, N. Christ, A. Immenhauser, G. S. Benson, S. M. Agar, S. Tomás, and L. Kabiri, 2013, Outcrop analog for an oolitic carbonate ramp reservoir: A scale-dependent geologic modeling approach based on stratigraphic hierarchy: AAPG Bulletin, v. 97, no. 5, p. 845–871, doi:10.1306/10231212039.
- Andrieu, S., B. Brigaud, J. Barbarand, and E. Lasseur, 2017, Linking early diagenesis and sedimentary facies to sequence stratigraphy on a prograding oolitic wedge: The Bathonian of western France (Aquitaine Basin): Marine and Petroleum Geology, v. 81, p. 169–195, doi:10.1016/j.marpetgeo.2017.01.005.
- Anell, I., and I. Midtkandal, 2015, The quantifiable clinothem - types, shapes and geometric relationships in the Plio-Pleistocene Giant Foresets Formation, Taranaki Basin, New Zealand: Basin Research, p. 1–21, doi:10.1111/bre.12149.
- Ball, M. M., 1967, Carbonate Sand Bodies of Florida and the Bahamas: SEPM Journal of

- Sedimentary Research, v. Vol. 37, no. 2, p. 556–591, doi:10.1306/74D7171C-2B21-11D7-8648000102C1865D.
- Boix, C., G. Frijia, V. Vicedo, J. M. Bernaus, M. Di Lucia, M. Parente, and E. Caus, 2011, Larger foraminifera distribution and strontium isotope stratigraphy of the La Cova limestones (Coniacian–Santonian, “Serra del Montsec”, Pyrenees, NE Spain): *Cretaceous Research*, v. 32, no. 6, p. 806–822, doi:10.1016/j.cretres.2011.05.009.
- Booler, J. P., 1994, Carbonate facies, sequences and associated diagenesis, Upper Cretaceous, Tremp Basin, Spanish Pyrenees: Durham University, 317 p.
- Booler, J., and M. E. Tucker, 2002, Distribution and geometry of facies and early diagenesis: the key to accommodation space variation and sequence stratigraphy: Upper Cretaceous Congost Carbonate platform, Spanish Pyrenees: *Sedimentary Geology*, v. 146, no. 3–4, p. 225–247, doi:10.1016/S0037-0738(01)00120-8.
- Borgomano, J., and J. Philip, 1987, The rudist carbonate build-ups and the gravitary carbonates of the Gargano-Apulian margin (Southern Italy, Upper Senonian): *Memoire Societ  Geologica Italiana*, v. 40, p. 125–132.
- Bosellini, A., 1984, Progradation geometries of carbonate platforms: examples from the Triassic of the Dolomites, northern Italy: *Sedimentology*, v. 31, no. 1, p. 1–24, doi:10.1111/j.1365-3091.1984.tb00720.x.
- Budd, D. A., and P. M. Harris, 1990, Carbonate-siliciclastic mixtures: SEPM Reprint Series No. 14: 272 p.
- Burchette, T. P., and S. R. Britton, 1985, Carbonate facies analysis in the exploration for hydrocarbons: a case-study from the Cretaceous of the Middle East: Geological Society, London, Special Publications, v. 18, no. 1, p. 311–338, doi:10.1144/GSL.SP.1985.018.01.13.
- Burchette, T. P., and V. P. Wright, 1992, Carbonate ramp depositional systems: *Sedimentary Geology*, v. 79, no. 1–4, p. 3–57, doi:10.1016/0037-0738(92)90003-A.
- Burgess, P. M., 2013, CarboCAT: A cellular automata model of heterogeneous carbonate strata: *Computers & Geosciences*, v. 53, p. 129–140, doi:10.1016/j.cageo.2011.08.026.
- Burgess, P. M., 2001, Modeling carbonate sequence development without relative sea-level oscillations: *Geology*, v. 29, no. 12, p. 1127–1130, doi:10.1130/0091-7613(2001)029<1127:MCSDWR>2.0.CO;2.
- Burgess, P. M., and G. D. Prince, 2015, Non-unique stratal geometries: implications for sequence stratigraphic interpretations: *Basin Research*, v. 27, no. 3, p. 351–365, doi:10.1111/bre.12082.
- Burgess, P. M., and V. P. Wright, 2003, Numerical Forward Modeling of Carbonate Platform Dynamics: An Evaluation of Complexity and Completeness in Carbonate Strata: *Journal of Sedimentary Research*, v. 73, no. 5, p. 637–652, doi:10.1306/020503730637.
- Burgess, P. M., V. P. Wright, and D. Emery, 2001, Numerical forward modelling of peritidal carbonate parasequence development: implications for outcrop interpretation: *Basin Research*, v. 13, no. 1, p. 1–16, doi:10.1046/j.1365-2117.2001.00130.x.
- Carrillat, A., S. K. Sharma, T. Grossmann, G. Iskenova, and T. Friedel, 2010, Geomodeling of Giant Carbonate Oilfields with a new Multipoint Statistics Workflow, *in* Abu Dhabi International Petroleum Exhibition and Conference: Society of Petroleum Engineers, doi:10.2118/137958-MS.
- Catuneanu, O. et al., 2009, Towards the standardization of sequence stratigraphy: *Earth-Science Reviews*, v. 92, no. 1–2, p. 1–33, doi:10.1016/j.earscirev.2008.10.003.
- Catuneanu, O., W. E. Galloway, C. G. S. C. Kendall, A. D. Miall, H. W. Posamentier, A. Strasser, and M. E. Tucker, 2011, Sequence Stratigraphy: Methodology and Nomenclature: *Newsletters on Stratigraphy*, v. 44, no. 3, p. 173–245, doi:10.1127/0078-0421/2011/0011.
- Caus, E., C. Llopart, J. Rosell, and J. M. Bernaus, 1999, El Coniacense superior-Santonense inferior de la Sierra del Montsec (Pirineos, NE de Espa a): *Revista Sociedad Geol gica de Espa a*, v. 12, p. 269–280.
- Caus, E., M. Parente, V. Vicedo, G. Frijia, and R. Mart nez, 2013, *Broeckina gassoensis* sp. nov., a larger foraminiferal index fossil for the middle Coniacian shallow-water deposits of the Pyrenean Basin (NE Spain): *Cretaceous Research*, v. 45, p. 76–90,

doi:10.1016/j.cretres.2013.08.002.

- Caus, E., A. Teixell, and J. M. Bernaus, 1997, Depositional model of a Cenomanian-Turonian extensional basin (Sopeira Basin, NE Spain): interplay between tectonics, eustasy and biological productivity: *Palaeogeography, Palaeoclimatology, Palaeoecology*, v. 129, no. 1–2, p. 23–36, doi:10.1016/S0031-0182(96)00051-X.
- Choukroune, P., 1992, Tectonic Evolution Of The Pyrenees: *Annual Review of Earth and Planetary Sciences*, v. 20, no. 1, p. 143–158, doi:10.1146/annurev.earth.20.1.143.
- Cumings, E. R., 1932, Reefs or Bioherms? *Geological Society of America Bulletin*, v. 43, no. 1, p. 331–352, doi:10.1130/GSAB-43-331.
- Demicco, R. V., and G. J. Klir, 2001, Stratigraphic simulations using fuzzy logic to model sediment dispersal: *Journal of Petroleum Science and Engineering*, v. 31, no. 2–4, p. 135–155, doi:10.1016/S0920-4105(01)00126-7.
- Droste, H., 2010, High-resolution seismic stratigraphy of the Shu'aiba and Natih formations in the Sultanate of Oman: implications for Cretaceous epeiric carbonate platform systems: *Geological Society, London, Special Publications*, v. 329, no. 1, p. 145–162, doi:10.1144/SP329.7.
- Drzewiecki, P. A., and J. A. Simó, 1997, Carbonate Platform Drowning and Oceanic Anoxic Events on a Mid-Cretaceous Carbonate Platform, South-Central Pyrenees, Spain: *Journal of Sedimentary Research*, v. Vol. 67, no. 4, p. 698–714, doi:10.1306/D426861C-2B26-11D7-8648000102C1865D.
- Drzewiecki, P. A., and J. A. Simó, 2002, Depositional processes, triggering mechanisms and sediment composition of carbonate gravity flow deposits: examples from the Late Cretaceous of the south-central Pyrenees, Spain: *Sedimentary Geology*, v. 146, no. 1–2, p. 155–189, doi:10.1016/S0037-0738(01)00171-3.
- Drzewiecki, P. A., and J. A. Simó, 2000, Tectonic, eustatic and environmental controls on mid-Cretaceous carbonate platform deposition, south-central Pyrenees, Spain: *Sedimentology*, v. 47, no. 3, p. 471–495, doi:10.1046/j.1365-3091.2000.00286.x.
- Dunham, R., 1962, Classification of carbonate rocks according to depositional texture, *in* W. E. Ham, ed., *Classification of Carbonate Rocks: AAPG Memoir 1: Tulsa, OK, AAPG*, p. 108–121.
- Friedman, G. M., 1988, Case Histories of Coexisting Reefs and Terrigenous Sediments: The Gulf of Elat (Red Sea), Java Sea, and Neogene Basin of the Negev, Israel, *in* L. J. Doyle, and H. H. Roberts, eds., *Developments in Sedimentology V42: Carbonate-Clastic Transitions*: p. 77–97, doi:10.1016/S0070-4571(08)70165-1.
- Gallémí, J., R. Martínez, and J. M. Pons, 1983, Coniacian - Maastrichtian of the Tremp Area (South Central Pyrenees): *Newsletters on Stratigraphy*, v. 12, no. 1, p. 1–17.
- Gallémí, J., R. Martínez, and J. M. J. Pons, 1982, Unidades del Cretácico superior en los alrededores de Sant Corneli (Provincia de Lleida): *Cuadernos de Geología Ibérica*, v. 8, p. 935–948.
- Gallémí Paulet, J., 1992, Los yacimientos con equínidos del Cretácico superior del Prepirineo de la provincia de Lleida.: *Universitat Autònoma de Barcelona*, 428 p.
- Gilbert, G. K., 1885, The Topographic features of lake shores: *U. S. Geological survey. 5th annual report*, p. 69–123.
- Gili, E., 1993, Facies and Geometry of les Collades de Basturs Carbonate Platform, Upper Cretaceous, South-Central Pyrenees, *in* J. Simo, R. W. Scott, and J.-P. Masse, eds., *Cretaceous Carbonate Platforms: AAPG Memoir 56: Tulsa, OK, AAPG*, p. 343–352.
- Gili, E., E. Vicens, A. Obrador, P. W. Skelton, and G. Lopez, 1996, Las formaciones de rudistas de la plataforma de sant corneli (cretacico superior, unidad central surpirenaica): *Revista Española de Paleontología*, p. 172–181.
- Ginsburg, R. N., 1956, Environmental relationships of grain size and constituent particles in some South Florida carbonate sediments: *Bulletin of the American Association of Petroleum Geologists*, v. 40, no. 10, p. 2384–2427, doi:10.1306/5CEAE598-16BB-11D7-8645000102C1865D.
- Gonzalez, R., and G. P. Eberli, 1997, Sediment transport and bedforms in a carbonate tidal inlet; Lee Stocking Island, Exumas, Bahamas: *Sedimentology*, v. 44, no. 6, p. 1015–1030,

- doi:10.1046/j.1365-3091.1997.d01-59.x.
- Graham, G. H., M. D. Jackson, and G. J. Hampson, 2015, Three-dimensional modeling of clinoforms in shallow-marine reservoirs: Part 2. Impact on fluid flow and hydrocarbon recovery in fluvial-dominated deltaic reservoirs: *AAPG Bulletin*, v. 99, no. 6, p. 1049–1080, doi:10.1306/01191513191.
- Grammer, G. M., P. M. Harris, and G. P. Eberli, 2004, Integration of Outcrop and Modern Analogs in Reservoir Modeling: Overview with Examples from the Bahamas, *in* G. M. Grammer, P. M. M. Harris, and G. P. Eberli, eds., *Integration of Outcrop and Modern Analogs in Reservoir Modeling*: AAPG Memoir 80: p. 1–22, doi:10.1306/M80924C1.
- Grélaud, C., P. Razin, and P. Homewood, 2010, Channelized systems in an inner carbonate platform setting: differentiation between incisions and tidal channels (Natih Formation, Late Cretaceous, Oman): *Geological Society, London, Special Publications*, v. 329, no. 1, p. 163–186, doi:10.1144/SP329.8.
- Handford, C., and R. G. Loucks, 1993, Carbonate Depositional Sequences and Systems Tracts—Responses of Carbonate Platforms to Relative Sea-Level Changes, *in* R. G. Loucks, and J. F. Sarg, eds., *Carbonate Sequence Stratigraphy: Recent Developments and Applications*: AAPG, p. 3–40, doi:10.1306/M57579C1.
- Haq, B. U., J. Hardenbol, and P. R. VAIL, 1987, Chronology of Fluctuating Sea Levels Since the Triassic: *Science*, v. 235, no. 4793, p. 1156–1167, doi:10.1126/science.235.4793.1156.
- Harris, P. M., 2009, Depositional environments of carbonate platforms: *Search and Discovery*, v. Article #6, p. 31–60.
- Harris, P. M., S. J. Purkis, and J. Ellis, 2011, Analyzing Spatial Patterns in Modern Carbonate Sand Bodies From Great Bahama Bank: *Journal of Sedimentary Research*, v. 81, no. 3, p. 185–206, doi:10.2110/jsr.2011.21.
- Harris, P. M., S. J. Purkis, J. Ellis, P. K. Swart, and J. J. G. Reijmer, 2015, Mapping bathymetry and depositional facies on Great Bahama Bank: *Sedimentology*, v. 62, no. 2, p. 566–589, doi:10.1111/sed.12159.
- Harris, P. M., A. H. Saller, and J. A. Simo, 1999, Advances in Carbonate Sequence Stratigraphy: *SEPM (Society for Sedimentary Geology)*, 1-10 p., doi:10.2110/pec.99.63.
- Hernández-Molina, F. J., L. M. Fernández-Salas, F. Lobo, L. Somoza, V. Díaz-del-Río, and J. M. Alveirinho Dias, 2000, The infralittoral prograding wedge: a new large-scale progradational sedimentary body in shallow marine environments: *Geo-Marine Letters*, v. 20, no. 2, p. 109–117, doi:10.1007/s003670000040.
- Hine, A. C., 1977, Lily Bank, Bahamas: History of an Active Oolite Sand Shoal: *Journal of Sedimentary Research*, v. 47, no. 4, p. 1554–1581, doi:10.1306/212F73B5-2B24-11D7-8648000102C1865D.
- Hottinger, L., K. Drobne, and E. Caus, 1989, Late cretaceous, larger, complex miliolids (foraminifera) endemic in the Pyrenean faunal province: *Facies*, v. 21, no. 1, p. 99–133, doi:10.1007/BF02536833.
- Howell, J. a., a. W. Martinius, and T. R. Good, 2014, The application of outcrop analogues in geological modelling: a review, present status and future outlook: *Geological Society, London, Special Publications*, v. 387, no. 1, p. 1–25, doi:10.1144/SP387.12.
- Hunt, D., and M. E. Tucker, 1992, Stranded parasequences and the forced regressive wedge systems tract: deposition during base-level fall: *Sedimentary Geology*, v. 81, no. 1–2, p. 1–9, doi:10.1016/0037-0738(92)90052-S.
- Immenhauser, A., B. Van Der Kooij, A. Van Vliet, W. Schlager, and R. W. Scott, 2002, An ocean-facing Aptian-Albian carbonate margin, Oman: *Sedimentology*, v. 48, no. 6, p. 1187–1207, doi:10.1046/j.1365-3091.2001.00416.x.
- Janson, X., K. Lee, C. Zahm, and C. Kerans, 2015, Ground-penetrating radar imaging of Albian rudist buildups, central Texas: *Interpretation*, v. 3, no. 3, p. SY67-SY81, doi:10.1190/INT-2014-0273.1.
- Janson, X., and D. D. Madriz, 2012, Geomodelling of carbonate mounds using two-point and multipoint statistics: *Geological Society, London, Special Publications*, v. 370, no. 1, p. 229–246, doi:10.1144/SP370.5.

- Jung, A., and T. Aigner, 2012, Carbonate Geobodies: Hierarchical Classification and Database - A New Workflow for 3D Reservoir Modelling: *Journal of Petroleum Geology*, v. 35, no. 1, p. 49–65, doi:10.1111/j.1747-5457.2012.00518.x.
- Jung, A., T. Aigner, D. Palermo, S. Nardon, and M. Pontiggia, 2012, A new workflow for carbonate reservoir modelling based on MPS: shoal bodies in outcrop analogues (Triassic, SW Germany): *Geological Society, London, Special Publications*, v. 370, no. 1, p. 277–293, doi:10.1144/SP370.13.
- Kauffman, E. G., and C. C. Johnson, 1988, The Morphological and Ecological Evolution of Middle and Upper Cretaceous Reef-Building Rudistids: *PALAIOS*, v. 3, no. 2, p. 194, doi:10.2307/3514530.
- Kerans, C., 2002, Styles of Rudist Buildup Development along the Northern Margin of the Maverick Basin, Pecos River Canyon, Southwest Texas: *Gulf Coast Association of Geological Societies Transactions*, v. 52, p. 501–516.
- Kerans, C., and P. M. Harris, 2010, Shelf Physiography and Accommodation as Controls on Permian Grainstone Bodies: *Search and Discovery*, v. Article #5.
- Klement, K. W., 1967, Practical classification of reefs and banks, bioherms and biostromes: *AAPG Bulletin*, v. 51, p. 167–168.
- Koehrer, B., T. Aigner, H. Forke, and M. Pöppelreiter, 2012, Middle to upper khuff (Sequences KS1 to KS4) outcrop-equivalents in the Oman Mountains: Grainstone architecture on a subregional scale: *GeoArabia*, v. 17, no. 4, p. 59–104.
- Larcombe, P., A. Costen, and K. J. Woolfe, 2001, The hydrodynamic and sedimentary setting of nearshore coral reefs, Central Great Barrier Reef shelf, Australia: Paluma Shoals, a case study: *Sedimentology*, v. 48, no. 4, p. 811–835, doi:10.1046/j.1365-3091.2001.00396.x.
- Lehrmann, D. J. D. J., and R. K. GOLDHAMMER, 1999, Secular Variation in Parasequence and Facies Stacking Patterns of Platform Carbonates: A Guide to Application of Stacking-Patterns Analysis in Strata of Diverse Ages and Settings, *in Advances in Carbonate Sequence Stratigraphy: SEPM (Society for Sedimentary Geology)*, p. 187–225, doi:10.2110/pec.99.11.0187.
- Levy, M., P. M. Harris, and S. Strebelle, 2008, Multiple-Point Statistics ( MPS )/ Facies Distribution Modeling ( FDM ) of Carbonates – an Isolated Platform Example: v. 40292.
- Loucks, R. G., and C. Kerans, 2003, Lower Cretaceous Glen Rose “Patch Reef” Reservoir in the Chittim Field, Maverick County, South Texas: *Gulf Coast Association of Geological Societies Transactions*, v. 53, p. 490–503.
- Masse, J., and J. Philip, 1981, European Fossil Reef Models: *SEPM (Society for Sedimentary Geology)*, 399-426 p., doi:10.2110/pec.81.30.
- Mateu-Vicens, G., L. Pomar, and M. Tropeano, 2008, Architectural complexity of a carbonate transgressive systems tract induced by basement physiography: *Sedimentology*, v. 55, no. 6, p. 1815–1848, doi:10.1111/j.1365-3091.2008.00968.x.
- McNeill, D. F., K. J. Cunningham, L. a Guertin, and F. S. Anselmetti, 2004, Depositional themes of mixed carbonate-siliciclastics in the South Florida Neogene; application to ancient deposits: Integration of outcrop and modern analogs in reservoir modeling: *AAPG Memoir 80*, p. 23–43.
- Mey, P. H. W. H. W., P. J. C. Nagtegaal, K. J. Roberti, and J. J. A. Hartevelt, 1968, Lithostratigraphic subdivision of post-hercynian deposits in the south-central Pyrenees, Spain: *Leidse Geologische Mededelingen*, v. 41, p. 221–228.
- Mitchell, N. C., G. Masselink, J. M. Huthnance, L. M. Fernandez-Salas, and F. J. Lobo, 2012, Depths of Modern Coastal Sand Clinofolds: *Journal of Sedimentary Research*, v. 82, no. 7, p. 469–481, doi:10.2110/jsr.2012.40.
- Mitchum, R. M., P. R. Vail, and S. Thompson, 1977, Seismic Stratigraphy and Global Changes of Sea Level, Part 2: The Depositional Sequence as a Basic Unit for Stratigraphic Analysis: Section 2. Application of Seismic Reflection Configuration to Stratigraphic Interpretation, *in J. B. S. P. R. Vail, R. G. Tod, ed., Seismic Stratigraphy--Applications to Hydrocarbon Exploration: AAPG Memoir 26: AAPG*, p. 53–62.
- Mount, J. F., 1984, Mixing of siliciclastic and carbonate sediments in shallow shelf environments:



- Geology, v. 12, no. 7, p. 432, doi:10.1130/0091-7613(1984)12<432:MOSACS>2.0.CO;2.
- Muñoz, J. A., 1989, The structure of the Pyrenees, *in* M. Marzo, and C. Puigdefàbregas, eds., Alluvial deposits of the successive foreland basing stages and their relation to the Pyrenean thrust sequences. 4th international conference on fluvial sedimentology, guidbook series, Excursion num. 10: Servei Geològic de Catalunya, p. 7–13.
- Muñoz, J. A., A. Martínez, and J. Verges, 1986, Thrust sequences in the eastern Spanish Pyrenees: *Journal of Structural Geology*, v. 8, no. 3–4, p. 399–405, doi:10.1016/0191-8141(86)90058-1.
- Nagtegaal, P., 1972, Depositional history and clay minerals of the Upper Cretaceous basin in the south-central Pyrenees, Spain: *Leidse Geologische Mededelingen*, v. 47, no. 2, p. 251–275.
- Ortega-Sánchez, M., F. J. Lobo, A. López-Ruiz, M. A. Losada, and L. M. Fernández-Salas, 2014, The influence of shelf-indenting canyons and infralittoral prograding wedges on coastal morphology: The Carchuna system in Southern Spain: *Marine Geology*, v. 347, p. 107–122, doi:10.1016/j.margeo.2013.11.006.
- Owen, H. G., 1983, Atlas of continental displacement, 200 million years to the present: CUP Archive.
- Pascual, O., J. M. J. Pons, and E. Vicens, 1989, Rudist horizons in the Montsec (South Central Pyrenees), *in* Cretaceous of the Western Tethys. Proceedings 3rd International Cretaceous Symposium, Tübingen 1987: p. 215–230.
- Patrino, S., G. J. Hampson, and C. a-L. Jackson, 2015, Quantitative characterisation of deltaic and subaqueous clinofolds, *in* Millennium Atlas: Elsevier B.V., p. 79–119, doi:10.1016/j.earscirev.2015.01.004.
- Phelps, R. M., C. Kerans, S. Z. Scott, X. Janson, and J. A. Bellian, 2008, Three-dimensional modelling and sequence stratigraphy of a carbonate ramp-to-shelf transition, Permian Upper San Andres Formation: *Sedimentology*, v. 55, no. 6, p. 1777–1813, doi:10.1111/j.1365-3091.2008.00967.x.
- Philip, J., and M. Floquet, 2000, Late Cenomanian; Map 14, *in* J. Dercourt, M. Gaetani, B. Vrielynck, E. Barrier, B. Biju-Duval, M. F. Brunet, J. P. Cadet, S. Crasquin, and M. Sandulescu, eds., Peri-Tethys Atlas, Paleogeographical Maps, Explanatory Notes: Paris, France, CVGM/CGMV, p. 129–136.
- Pierre, A., C. Durllet, P. Razin, and E. H. Chellai, 2010, Spatial and temporal distribution of ooids along a Jurassic carbonate ramp: Amellago outcrop transect, High-Atlas, Morocco: Geological Society, London, Special Publications, v. 329, no. 1, p. 65–88, doi:10.1144/SP329.4.
- Plaziat, J.-C., 1981, Late Cretaceous to Late Eocene palaeogeographic evolution of Southwest Europe: *Palaeogeography, Palaeoclimatology, Palaeoecology*, v. 36, no. 3–4, p. 263–320, doi:10.1016/0031-0182(81)90110-3.
- Pomar, L., M. Aurell, B. Bádenas, M. Morsilli, and S. F. Al-Awwad, 2015, Depositional model for a prograding oolitic wedge, Upper Jurassic, Iberian basin: *Marine and Petroleum Geology*, v. 67, p. 556–582, doi:10.1016/j.marpetgeo.2015.05.025.
- Pomar, L., P. Bassant, M. Brandano, C. Ruchonnet, and X. Janson, 2012, Impact of carbonate producing biota on platform architecture: Insights from Miocene examples of the Mediterranean region: *Earth-Science Reviews*, v. 113, no. 3–4, p. 186–211, doi:10.1016/j.earscirev.2012.03.007.
- Pomar, L., E. Gili, A. Obrador, and W. C. Ward, 2005, Facies architecture and high-resolution sequence stratigraphy of an Upper Cretaceous platform margin succession, southern central Pyrenees, Spain: *Sedimentary Geology*, v. 175, no. 1–4, p. 339–365, doi:10.1016/j.sedgeo.2004.11.009.
- Pomar, L., and C. G. S. C. Kendall, 2011, Architecture of Carbonate Platforms: A Response to Hydrodynamics and Evolving Ecology, *in* Controls on Carbonate Platform and Reef Development: SEPM (Society for Sedimentary Geology), p. 187–216, doi:10.2110/pec.08.89.0187.
- Pomar, L., and M. Tropeano, 2001, Formation in Matera ( southern Italy ): New insights offshore deposits: *AAPG bulletin*, v. 85, no. 4, p. 661–690.

- Pomar, L., and W. C. Ward, 1994, Response of a late Miocene Mediterranean reef platform to high-frequency eustasy: *Geology*, v. 22, no. 2, p. 131, doi:10.1130/0091-7613(1994)022<0131:ROALMM>2.3.CO;2.
- Puigdefàbregas, C., and P. Souquet, 1986, Tecto-sedimentary cycles and depositional sequences of the Mesozoic and Tertiary from the Pyrenees: *Tectonophysics*, v. 129, no. 1–4, p. 173–203, doi:10.1016/0040-1951(86)90251-9.
- Purkis, S., G. Casini, D. Hunt, and A. Colpaert, 2015, Morphometric patterns in Modern carbonate platforms can be applied to the ancient rock record: Similarities between Modern Alacranes Reef and Upper Palaeozoic platforms of the Barents Sea: *Sedimentary Geology*, v. 321, p. 49–69, doi:10.1016/j.sedgeo.2015.03.001.
- Purkis, S. J., and B. Vlaswinkel, 2012, Visualizing lateral anisotropy in modern carbonates: *AAPG Bulletin*, v. 96, no. 9, p. 1665–1685, doi:10.1306/02211211173.
- Rankey, E. C., P. M. Harris, C. Energy, T. Company, B. C. Road, and S. Ramon, 2008, Remote Sensing and Comparative Geomorphology of Holocene Carbonate Depositional Systems, *in* J. Lukasik, and J. A. (Toni) Simo, eds., *Controls on Carbonate Platform and Reef Development*, SEPM Special Publication: p. 317–322.
- Rankey, E. C., and S. L. Reeder, 2011, Holocene Oolitic Marine Sand Complexes of the Bahamas: *Journal of Sedimentary Research*, v. 81, no. 2, p. 97–117, doi:10.2110/jsr.2011.10.
- Read, J. F., 1995, Overview of carbonate platform stratigraphy and reservoirs in green-house and ice-house worlds, *in* J. . Read, ed., *Milankovitch Sea-level Changes, Cycles, and Reservoirs on Carbonate Platforms in Greenhouse and Ice-House Worlds*: SEPM (Society for Sedimentary Geology), p. 1–102, doi:10.2110/scn.95.35.0001.
- Rich, J. L., 1951, Three Critical Environments of Deposition, and Criteria for Recognition of Rocks Deposited in each of them: *Geological Society of America Bulletin*, v. 62, no. 1, p. 1, doi:10.1130/0016-7606(1951)62[1:TCEODA]2.0.CO;2.
- Roehl, P. O., and P. W. Choquette, 1985, Introduction, *in* P. O. Roehl, and P. W. Choquette, eds., *Carbonate Petroleum Reservoirs*: New York, NY, Springer New York, p. 1–15, doi:10.1007/978-1-4612-5040-1\_1.
- Ross, D., and P. Skelton, 1993, Rudist formations of the Cretaceous: a palaeoecological, sedimentological and stratigraphical review, *in* V. P. Wright, ed., *Sedimentology Review/1*: Oxford, UK, Blackwell Publishing Ltd., doi:10.1002/9781444304534.
- Sanders, D., 1996, Rudist biostromes on the margin of an isolated carbonate platform: The Upper Cretaceous of Montagna della Maiella, Italy: *Eclogae Geologicae Helvetiae*, v. 89, no. 2, p. 845–871.
- Sanders, D., 1998, Upper Cretaceous “Rudist” formations: *Geologisch-Palaeontologische Mitteilungen Innsbruck*, v. 23, p. 37–59.
- Sanders, D., and J. M. Pons, 2001, Stratigraphic architecture of a Santonian mixed siliciclastic-carbonate succession (Catalonian Pyrenees, Spain): *Facies*, v. 44, no. 1, p. 105–135, doi:10.1007/BF02668170.
- Santisteban, G., and C. Taberner, 1988, Sedimentary Models of Siliciclastic Deposits and Coral Reefs Interrelation, *in* L. J. Doyle, and H. H. Roberts, eds., *Developments in Sedimentology V42: Carbonate-Clastic Transitions*: p. 35–76, doi:10.1016/S0070-4571(08)70164-X.
- Schlager, W., 2005, Sequence stratigraphy of the T factory, *in* *Carbonate Sedimentology and Sequence Stratigraphy*: p. 105–146.
- Schlager, W., 1999, Type 3 Sequence Boundaries, *in* *Advances in Carbonate Sequence Stratigraphy*: SEPM (Society for Sedimentary Geology), p. 35–45, doi:10.2110/pec.99.11.0035.
- Scott, R. W., 1988, Evolution of Late Jurassic and Early Cretaceous Reef Biotas: *PALAIOS*, v. 3, no. 2, p. 184, doi:10.2307/3514529.
- Scott, R. W., P. A. Fernandez-Mendiola, E. Gili, and A. Simo, 1990, Persistence of Coral-Rudist Reefs into the Late Cretaceous: *PALAIOS*, v. 5, no. 2, p. 98, doi:10.2307/3514807.
- Scott, R. W., J. A. T. Simo, and J.-P. Masse, 1993, Economic Resources in Cretaceous Carbonate Platforms: An Overview, *in* J. Simo, R. W. Scott, and J.-P. Masse, eds., *Cretaceous carbonate platforms*: AAPG Memoir 56: Tulsa, OK, AAPG, p. 15–23.

- Sharples, A. G. W. D., M. Huuse, C. Hollis, J. M. Totterdell, and P. D. Taylor, 2014, Giant middle Eocene bryozoan reef mounds in the Great Australian Bight: *Geology*, v. 42, no. 8, p. 683–686, doi:10.1130/G35704.1.
- Simó, A., 1986, Carbonate platform depositional sequences, Upper Cretaceous, south-central Pyrenees (Spain): *Tectonophysics*, v. 129, no. 1–4, p. 205–231, doi:10.1016/0040-1951(86)90252-0.
- Simó, A., 1989, Controls on Carbonate Platforms and Basin Development: *SEPM (Society for Sedimentary Geology)*, 365-378 p., doi:10.2110/pec.89.44.
- Simó, A., 1993, Cretaceous carbonate platforms and stratigraphic sequences; south-central Pyrenees; Spain., *in* J. Simo, R. W. Scott, and J.-P. Masse, eds., *Cretaceous carbonate platforms: AAPG Memoir 56*: Tulsa, OK, AAPG, p. 325–342, doi:10.1306/M56578C1.
- Skelton, P. W., E. Gili, E. Vicens, and A. Obrador, 1995, The growth fabric of gregarious rudist elevators (hippuritids) in a Santonian carbonate platform in the southern Central Pyrenees: *Palaeogeography, Palaeoclimatology, Palaeoecology*, v. 119, no. 1–2, p. 107–126, doi:10.1016/0031-0182(95)00063-1.
- Skelton, P. W., E. Gili, E. Vicens, A. Obrador, and G. López, 2003, Revised lithostratigraphy of the Upper Cretaceous (Santonian) carbonate platform succession on the northern flank of Sant Corneli, southern Central Pyrenees: *Journal of Iberian Geology*, v. 29, p. 73–87.
- Souquet, P., and B. Peybernes, 1977, La chaîne alpine des Pyrénées: *Géologie Alpine*, v. 53, p. 193–216.
- Tucker, M. E., 2003, Mixed clastic-carbonate cycles and sequences; Quaternary of Egypt and Carboniferous of England: *Geologia Croatica*, v. 56, no. 1, p. 19–37.
- Tucker, M. E., and V. P. Wright, 1990, *Carbonate Sedimentology*: Oxford, UK, Blackwell Publishing Ltd., doi:10.1002/9781444314175.
- Vail, P. R., R. M. Mitchum, and S. Thompson, 1977, Seismic Stratigraphy and Global Changes of Sea Level, Part 3: Relative Changes of Sea Level from Coastal Onlap, *in* J. B. S. P. R. Vail, R. G. Tod, ed., *Seismic Stratigraphy--Applications to Hydrocarbon Exploration: AAPG Memoir 26*: AAPG, p. 63–81, doi:10.1306/M26490C5.
- Vicens, E., G. López, and A. Obrador, 1998, Facies succession, biostratigraphy and rudist faunas of Coniacian to Santonian platform deposits in the Sant Corneli anticline (Southern Central Pyrenees): *Geobios*, v. 31, p. 403–427, doi:10.1016/S0016-6995(98)80089-2.
- Villalba-Breva, S., and C. Martín-Closas, 2013, Upper Cretaceous paleogeography of the Central Southern Pyrenean Basins (Catalonia, Spain) from microfacies analysis and charophyte biostratigraphy: *Facies*, v. 59, no. 2, p. 319–345, doi:10.1007/s10347-012-0317-1.
- Van Wagoner, J. C., R. M. Mitchum, K. M. Campion, and V. D. Rahmanian, 1990, Siliciclastic Sequence Stratigraphy in Well Logs, Cores, and Outcrops: Concepts for High-Resolution Correlation of Time and Facies: *Siliciclastic Sequence Stratigraphy in Well Logs, Cores, and Outcrops: Concepts for High-Resolution Correlation of Time and Facies: AAPG Methods in Exploration Series 7*, no. 7, p. 1–55, doi:0-89181-657-7.
- Van Wagoner, J. C., H. W. Posamentier, R. M. Mitchum, P. R. Vail, J. F. Sarg, T. S. Loutit, and J. Hardenbol, 1988, An overview of the fundamentals of sequence stratigraphy and key definitions, *in* *Sea-Level Changes - An Integrated Approach*, *SEPM Special Publication: SEPM (Society for Sedimentary Geology)*, p. 39–45, doi:10.2110/pec.88.01.0039.
- Wilson, J. L., 1975, *Carbonate Facies in Geologic History*: New York, NY, Springer New York, 472 p., doi:10.1007/978-1-4612-6383-8.
- Wilson, J. L., 1967, Cyclic and Reciprocal Sedimentation in Virgilian Strata of Southern New Mexico: *Geological Society of America Bulletin*, v. 78, no. 7, p. 805, doi:10.1130/0016-7606(1967)78[805:CARSIV]2.0.CO;2.
- Wilson, M. E. J., and S. W. Lokier, 2002, Siliciclastic and volcanoclastic influences on equatorial carbonates: Insights from the Neogene of Indonesia: *Sedimentology*, v. 49, no. 3, p. 583–601, doi:10.1046/j.1365-3091.2002.00463.x.
- Ziegler, P., 1990, *Geological Atlas of Western and Central Europe*, Shell Internationale Petroleum Maatschappij BV/Geological Society of London: Amsterdam, Elsevier.

## 2 METHODS AND MATERIALS

### 2.1 Sedimentological logging and sampling

Sedimentary logging of 42 selected sections was conducted at 13 localities throughout the study area in order to define and quantify the exposed lithologies. A list of investigated localities is given in Appendix A, Table A.1.1. Traditional methods were used in logging; individual beds were recorded on a scale of 1:50, with a series of parameters being logged. These were: thickness, lithology, depositional textures after the classification of Dunham (1962) and of Embry and Klovan (1971), sedimentary structures, fossil assemblages, grain sizes and sorting, colour and weathering behaviour, the nature of bedding surfaces and transitions between beds, as well as cleaning/dirtying upwards trends. A key for all sedimentary logs is given in Appendix B, Figure B.1.1. The positions of individual logs were selected to provide maximal coverage of the sedimentary succession exposed across the outcrop. Where sedimentary logs were interrupted by faults, beds were correlated along these and logging continued normally, while the position of the fault being noted. The logs recorded on 1:50 scale are presented in Appendix B.2, with a complete list presented in Table B.2.1.

Where possible, composite sedimentary logs were produced by combining overlapping sections or by defining the gap between two stratigraphically successive logs. Furthermore, selected sections were redrawn at a 1:500 scale to allow integration into platform-scale cross-sections and sequence stratigraphic interpretations (cf. section 2.6). A total of 6 of these composite logs at 1:500 scale was created, which are presented in Appendix B.3. For a list of these logs refer to Appendix B.3, Table B.3.1.

Samples were taken systematically along the majority of recorded logs. The selection of beds to be sampled was made to ensure unique lithologies were always sampled, whereas recurring lithologies are sampled at semi-regular intervals along the length of each log. For each sample, the bed of origin was marked on the corresponding log, and GPS coordinates noted where of interest. In some instances beds were sampled laterally in order to investigate continuity in texture in this direction. For these samples, GPS coordinates and a short lithological description were noted, and the position of the sampling location marked on a photograph of the outcrop. A list of samples is presented in Appendix C (enclosed CD).

### 2.2 Core logs

During the regional exploration campaigns by several oil companies in the 1960's and 1970's, a number of wells were previously drilled and partially cored in the South-Central Pyrenees. As a

large amount of the Upper Cretaceous sediments between the Montsec range and the Sant Corneli anticline are covered by Paleogene deposits, these well logs and cores provide a valuable insight into the subsurface and allow for better correlations and interpretations of the platform-scale architecture. A total of 6 cores were logged at 1:10 scale, with the following parameters being recorded: lithology, colour, depositional textures after the classification of Dunham (1962) and the expansion Embry and Klovan (1971), sedimentary structures, skeletal assemblages, cements, fractures, stylolites, grain sizes, sorting, rounding, as well as trends within these parameters and major surfaces. The data from these wells was used to confirm facies in outcrop, and to improve correlations between localities and adjacent lithofacies. A list of these logs is given in Appendix B.4, Table B.4.1, accompanied by the digitised logs.

### 2.3 Thin Section Preparation and Microscopy

Preparation of thin sections analysed in this study was done externally by Independent Petrographic Services Ltd., Aberdeen, and by Keele University. The process followed in these laboratories is closely similar to the thin section preparation procedure described by Tucker (1996); samples are cut to appropriate size, polished, and then fixed onto a 76x26 mm glass slide using blue-dyed epoxy. The blue epoxy serves to easily recognise porosity during microscopy. The samples are then cut and polished down to a thickness of 30  $\mu\text{m}$ , after which the complete samples are stained with Alizarin Red S and potassium ferricyanide to enable differentiating between ferroan carbonate phases, as well as between calcite, aragonite and dolomite. All thin sections are then covered with another thin glass slide. Staining of the entire sample surface and covering with glass allows a maximal area to be analysed during point counting, which in turns provides a higher accuracy for modal analysis data.

In thin section analysis, the following parameters were logged and described:

- Carbonate textures according to Dunham (1962) and Embry and Klovan (1971)
- Porosity after Choquette and Pray (1970)
- Present allochems and skeletal assemblage, grain size, rounding and sorting
- Siliciclastic contents, grain size, rounding and sorting
- Sedimentary structures, bioturbation and imbrication (if present)
- Cement mineralogy and crystal morphology
- Diagenetic effects: Precipitation, compaction and dissolution

Thin section descriptions are presented in Appendix C.2.

### 2.4 Modal Analysis

Modal analysis of a subset of thin sections was performed in order to gain compositional and grain size data. A subset of 89 samples was selected so that for each relevant lithofacies 3-5 thin

sections were analysed. This was in order to provide better statistical relevance and an overview of the heterogeneity within each lithofacies. The analysis was performed using a computer-supported point-counting setup controlled by the software *PETROG 3*, provided by *Conwy Valley Systems Limited*. Modal analysis results are presented in Appendix C.3.

A review of the application and discussion of the accuracy of point counting methods for geological studies was previously presented in numerous studies (Chayes, 1956; van der Plas and Tobi, 1965; Solomon and Green, 1966; Ingersol et al., 1984). Following the results of these studies, 300 points were counted for each sample, as this amount was shown to provide the highest statistical significance in relation to analysis time. As many of the samples are mud-dominated, the sizes of only up to 100 grains were determined to ensure an equal sample-size for grain size data across all samples. In all cases, the whole area of the thin section was analysed, while the software defined 300 equally spaced points within the defined area. In cases where the same grain was captured by several points (e.g. exceptionally large rudist fragments), the modal composition was logged for all points, whereas the grain size was only recorded once. This provides a bulk-rock mineralogical/bioclastic composition, while not skewing the grain size distribution. A bulk-rock quantification of the composition is later favourable when using modal analysis data to calculate petrophysical parameters in various diagenetic scenarios.

The categories into which logged grains were allocated can be summarised into six classes: detrital grains, bioclasts, carbonate grains, authigenic minerals, porosity, matrix and artefacts. The individual categories comprising each of these classes are presented in Table 2.1. Grain size is defined via major and minor axis of the grain. Grain-size parameters were automatically calculated following the method of Folk and Ward (1957): Mean grain size, sorting, skewness, kurtosis. These are presented in  $\mu\text{m}$ ,  $\phi$ , and descriptively. For the results of grain size analysis refer to Appendix C.3.

## 2.5 XRD Analysis

For mineral phase recognition and quantification, bulk-rock XRD analysis was conducted on a subset of 65 samples. Preparation for this method included choosing an ideally homogeneous sub-sample of the desired rock to be analysed, avoiding any unusually large shells and crystallised fractures. Weathered surfaces were removed mechanically using a rotary drill to avoid sample contamination by mineral products of weathering. The cleaned sub-sample was then milled to a powder using an agate mill, which was analysed at The University of Manchester using a Bruker D8 Advance diffractometer by Dr John Waters. Values of present mineral phases are given in %. Results of the XRD analysis are presented in Appendix C.4.

**Table 2.1: Point counting classes used during modal analysis.**

Class/Constituent Group	Tier 1 Differentiation	Tier 2 Differentiation
Detrital Grains	Biotite, Extrabasinal – Extrusive, Extrabasinal-Igneous, Feldspar Group, Intrabasinal – Mudstone, Pyrite, Quartz – monocrystalline, Quartz - Polycrystalline	
Bioclastic grains	Bivalve (Non-Rudist) or Brachiopod	
	Bryozoans	
	Calcareous Sponges	
	Coral	Transported Fragment, Skeleton
	Echinoids	
	Foraminifera	Praealveolina, Miliolids, Lacazina, Undefined small benthic, Uniserial, Biserial, Fusulinids, Globorotaliids, Undefined Planktonic
	Gastropods	
	Green Algae	Charophytes Dasyclads
	Red algae	Branching Encrusting
	Rudist	
Siliceous sponge spicules		
Carbonate Grains	Ooids	Concentric Radial
	Peloids	
Authigenic Minerals	Calcite	Non-Ferroan Ferroan
	Dolomite	Non-Ferroan Ferroan
	Quartz	Idiomorphic Amorphous
	Pyrite	
Matrix	Micrite	
	Detrital optically non-resolvable clay	
	Undifferentiated	
Porosity	Fracture	
	Interparticle	
	Intraparticle	
	Mould	
	Vug	
Artefacts	Preparation fracture	
	Grain plucking	

## 2.6 Construction of Cross-Sections

The cross-sections presented in Chapters 3 and 4 were constructed from a combination of map and subsurface data, literature sources, as well as field observations and interpretations. Map data points were chosen where a complete or partial and relevant section of the Upper Cretaceous is exposed and mapped. The data points and relevant map sheets are listed in Appendix A.2, Table A.2.1. Since these data points did not necessarily lie in-line on a south-north – and thus proximal-distal – transect of the basin, data points were projected onto a central idealised cross-section line. This provides direct distances between extrapolated facies belts. These distances are marked on the top part of the cross-section, between each data-point pair. Relative proximal-distal distances between data points within each of the main platform areas (proximal, interior, margin and basin) were preserved by projecting the data points of each area

onto the central line uniformly at 90 degrees. This inevitably leads to the projected position of the platform margin data points (Collades, Montagut and Carreu), as well as the Isona data point, to be more landward than the current geographical position of the outcrops implies. This solution was chosen over projecting these data points in a way that artificially brings them closer to the basinal data points (Barranc d'Esplugafreda, Tamurcia, Barranc de Miralles, Serra de Sant Grevas), as platform topography is more uniform within the interior areas, and a more realistic representation of the platform margin and slope is preferential. Following the results of (Puigdefàbregas et al., 1992), the tectonic compression that led to the Pyrenean orogeny has previously reduced the length of the basin from ca. 375 km to about 225 km, resulting in a decompression factor of 1.66. This factor is applied to all north-south measurements of length done on current geographic exposures to restore the palaeo-position of individual facies and depositional environments.

For each platform, lithofacies are displayed in their respective colour noted the respective facies tables. The cumulative thickness of each lithofacies and their vertical relationships at a respective data point is presented. The vertical exaggeration is of a factor of 25. Implied retrogradational and progradational trends, as they are drawn between data points in the correlation panel, are either carried over from literature sources, or based on interpretations made within this study.

Based on the interpretations of depositional environments, water depth and energy, individual data points within each platform are cascaded downwards, so that they are aligned to an interpreted palaeo-sea level. This serves to give the platform sketch a more realistic appearance and facilitate recognising depositional topography and various platform areas. Note that the vertical distance from the top of a unit to the interpreted palaeo-sea level does not correspond with the vertical scale of the sediment package, as this is for visualisation purposes only.

## **2.7 Digital Outcrop Modelling (DOM)**

### **2.7.1 Lidar**

The application of Light Detection and Ranging (Lidar) has become widespread for quantitative studies of geometrical data in outcrop. Many reviews have been published, presenting the application, advantages and disadvantages (e.g. Bellian et al., 2005; Pringle et al., 2006; Hodgetts, 2013). Lidar datasets allow generating realistic, high-resolution digital outcrop models (DOM) that can be supplemented with stratigraphic, lithological and petrophysical data. These can be used to inform both subsurface reservoir models and stratigraphic forward models (Hodgetts, 2013). Digital outcrop model studies were predominantly performed in clastic depositional systems (e.g. Schuppers, 1993; Pringle et al., 2004; Fabuel-Perez et al., 2010),



although an increasing number on carbonate systems are made more recently (e.g. Adams et al., 2005, 2011; Reijnders et al., 2008; Verwer et al., 2009).

Lidar functions by releasing laser pulses toward the measured object in a rapid succession. By determining the travel time of the returning signal, the distance towards the object can be calculated (Pringle et al., 2006). Hundreds to hundred thousands of measured points with x-y-z-coordinates together are referred to as point-clouds (Bellian et al., 2005). Outcrops are commonly scanned from multiple different positions to reduce occlusion and to achieve maximum detail on rugose surfaces (Bellian et al., 2005). The intensity of the reflected signal varies based on the properties of the scanned object, and may be used to visualise the points in greyscale. Furthermore, digital photographs of the outcrop may be draped onto the dataset to achieve photorealistic digital outcrop models. These are useful for visual interpretation of geological features (Hodgetts, 2013). However, distortion of draped photographs may occur where outcrop surfaces are very uneven.

In this study, a RIEGL LMS-Z420i scanner was used. Outcrops were typically scanned from a distance of 200-500 metres and from several positions in order to increase resolution and fill gaps in the point cloud caused by protruding features. First, a low-resolution 360° scan of the environment was performed. This is combined with wide-angle photographs using a Nikon D100 digital SLR camera mounted on top of the scanner. In a second step, the desired outcrop face was targeted and scanned in high resolution (typically >10 cm point distance), and photographs of the outcrop taken with a 50 mm lens for later colouring of the model. This was typically done in several smaller overlapping subsections for each outcrop face. The RIEGL RiSCAN Pro software was used for point cloud cleaning, including removal of noise and undesired parts of the point cloud (scree slope, vegetation) and draping of photographs to produce realistic colouring of the model. Point clouds from individual scan positions were combined and exported to Virtual Reality Geological Studio for further interpretation (Section 2.7.3).

### 2.7.2 Photogrammetry

The workflow for producing a digital outcrop model using photogrammetry and extracting quantitative data on geobody geometries can be divided into three stages; data acquisition, construction and scaling of the model, and the extraction of features. This workflow is elaborated and briefly discussed in the following.

#### **Acquisition of Images**

The images used to construct the photogrammetry models in this study were acquired using a Nikon D100 digital SLR camera with a 50 mm set focal length lens. The images were taken from distances between 70 m (Carreu River locality) and 450 m (Congost d'Erinyá) from the outcrop

surface. While lenses with higher focal lengths would have allowed higher resolution texture mapping of the resulting models, and thus tracing of smaller features, using such a lens has proved to produce high levels of noise and generally poor quality point clouds (field tests in this study and James and Robson, 2012).

Where possible, images for photogrammetry based models were acquired by continuously taking images perpendicular to the outcrop, with an overlap of 20-30%. Due to rough terrain, this was not always possible, and so several images were often taken from the same position and the camera view-point moved along the outcrop in a fan-like motion. While this acquisition technique typically produces a much larger number of images than required for model construction, it ensures sufficient overlap between images and images of each feature from several angles, thereby ensuring a high-resolution model.

### **Construction of Point Cloud**

In this study, the VisualSFM and bundler software packages (Wu, 2011; Wu et al., 2011) were used to create 3D digital outcrop models for sedimentary and stratigraphic analysis. The algorithm applied is similar to the one described in Westoby et al. (2012); pairs of images from the digital photographs acquired in the field were matched by the software using reference points between the two images. Through triangulation of the matched image features, initially a sparse, and then a dense 3D point cloud of the matching features can be reconstructed.

Post-processing of the data included removal of noise and undesired areas (vegetation, slopes) using Meshlab 1.3.3 (2014). This was followed by a Poisson surface reconstruction to create a mesh that represents the surface between points in the cloud (Kazhdan et al., 2006). For visualisation purposes, the resulting mesh was textured using a subset of the images that were used for the construction of the point cloud.

### **Scaling and Georeferencing**

The point cloud produced with the method described above is initially placed in an arbitrary coordinate system and thus not to scale. It is necessary, however, to use a reference model to ensure that any measurements are within a reasonable error from the real-world geological features. The reference model used for this study was a digital elevation model (DEM) based on aerial lidar surveys available from the Spanish National Centre for Geographical Information (Instituto Geográfico Nacional and Centro Nacional de Información Geográfica, 2011; Table 2.2). This DEM has a reported point-distance of <1.4 m.

The point clouds produced in this study were initially roughly aligned to the DEM using the software CloudCompare (version 2.6.2; 2016), by picking matching point pairs on both datasets.

This was followed by fine alignment using the Iterative Closest Point (ICP) algorithm of the software, allowing the position and scale of the point cloud to be adjusted to the DEM.

**Table 2.2: List of digital elevation model datasets used to georeference and scale Photogrammetry models.**

Dataset	Applied DOM
PNOA_2009_Lote_CAT_336-4674_ORT-CLA-COL	Carreu River and Montagut Gully
PNOA_2009_Lote_CAT_338-4672_ORT-CLA-COL	Carreu River and Montagut Gully
PNOA_2009_Lote_CAT_338-4674_ORT-CLA-COL	Carreu River and Montagut Gully
PNOA_2009_Lote_CAT_328-4684_ORT-CLA-COL	Congost d'Erinyá
PNOA_2009_Lote_CAT_328-4686_ORT-CLA-COL	Congost d'Erinyá
PNOA_2009_Lote_CAT_330-4684_ORT-CLA-COL	Congost d'Erinyá
PNOA_2009_Lote_CAT_330-4686_ORT-CLA-COL	Congost d'Erinyá
PNOA_2009_Lote_CAT_340-4672_ORT-CLA-COL	Gallinove North and Gallinove North
PNOA_2009_Lote_CAT_340-4674_ORT-CLA-COL	Gallinove North and Gallinove North
PNOA_2009_Lote_CAT_342-4672_ORT-CLA-COL	Gallinove North and Gallinove North
PNOA_2009_Lote_CAT_342-4674_ORT-CLA-COL	Gallinove North and Gallinove North

### Tracing of Features

Extraction of geological features such as bedding planes or fractures from digital outcrop model in this study follows a method developed by Seers (2015). The method relies on the source photographs of the 3D model as a base for tracing visible bedding surfaces on the photographs, and projecting the according pixels are onto the point cloud as lines in the coordinate system of the model. The main advantage of this method is that it can pick desired features below the resolution of the point cloud, which are still registered and projected onto the model at the appropriate resolution. Overlapping lines can be combined to produce continuous lines on the basis of interpretation.

### 2.7.3 Digital Outcrop Model Construction and Measurement of Geological Elements

Digital outcrop models were constructed from the lidar and photogrammetry point clouds in Virtual Reality Geological Studio 2016. Point clouds and parts of the outcrop covered by vegetation or unnecessary scree slopes were removed to reduce model complexity. Tectonic dip was removed by aligning the point cloud to a stratigraphic horizon. This ensured that measured angles were relative to a horizontal stratigraphic surface. In the case of lidar data, point clouds were meshed in VRGS, whereas photogrammetry point clouds were meshed in previous stages. Lithofacies and stratigraphic horizons were then defined along the DOM using the “Geobody” tool, consulting previously constructed photo-panels from the field for reference. Geological elements such as reef bodies and clinothem bodies were also picked using the “Geobody” tool, providing basic measurements. More specific measurements for each geobody are then made

using the measuring tool. The results of geobody measurements are presented in Chapter 5. For some outcrops, a processed subset of the data are presented here, whereas the complete data is presented in Appendix E.2.

## 2.8 References

- Adams, E. W., C. Grelaud, M. Pal, A. E. Csoma, O. S. Al Ja'aidi, and R. A. Hinai, 2011, Improving reservoir models of Cretaceous carbonates with digital outcrop modelling (Jabal Madmar, Oman): static modelling and simulating clinofolds: *Petroleum Geoscience*, v. 17, no. 3, p. 309–332, doi:10.1144/1354-079310-031.
- Adams, E. W., J. P. Grotzinger, W. a. Watters, S. Schröder, D. S. McCormick, and H. a. Al-Siyabi, 2005, Digital characterization of thrombolite-stromatolite reef distribution in a carbonate ramp system (terminal Proterozoic, Nama Group, Namibia): *AAPG Bulletin*, v. 89, no. 10, p. 1293–1318, doi:10.1306/06160505005.
- Bellian, J. A., C. Kerans, and D. C. Jennette, 2005, Digital Outcrop Models: Applications of Terrestrial Scanning Lidar Technology in Stratigraphic Modeling: *Journal of Sedimentary Research*, v. 75, no. 2, p. 166–176, doi:10.2110/jsr.2005.013.
- Chayes, F., 1956, *Petrographic Modal Analysis – An elementary statistical appraisal*: New York, John Wiley & Sons Inc., 113 p.
- Choquette, P. W., and L. C. Pray, 1970, Geologic Nomenclature and Classification of Porosity in Sedimentary Carbonates: *AAPG Bulletin*, v. 54, no. 2, p. 207–250.
- CloudCompare (version 2.6.2) [GPL software], 2016, Retrieved from <http://www.cloudcompare.org/>.
- Dunham, R., 1962, Classification of carbonate rocks according to depositional texture, *in* W. E. Ham, ed., *Classification of Carbonate Rocks*: AAPG Memoir 1: Tulsa, OK, AAPG, p. 108–121.
- Embry, A. F., and J. E. Klovan, 1971, A Late Devonian reef tract on northeastern Banks Island, NWT: *Bulletin of Canadian Petroleum Geology*, v. 19, no. 4, p. 730–781.
- Fabuel-Perez, I., D. Hodgetts, and J. Redfern, 2010, Integration of digital outcrop models (DOMs) and high resolution sedimentology - workflow and implications for geological modelling: Oukaimeden Sandstone Formation, High Atlas (Morocco): *Petroleum Geoscience*, v. 16, no. 2, p. 133–154, doi:10.1144/1354-079309-820.
- Folk, R. L., and W. C. Ward, 1957, Brazos River Bar: A study in the significance of grain size parameters: *SEPM Journal of Sedimentary Research*, v. 27, no. 1, p. 3–26, doi:10.1306/74D70646-2B21-11D7-8648000102C1865D.
- Hodgetts, D., 2013, Laser scanning and digital outcrop geology in the petroleum industry: A review: *Marine and Petroleum Geology*, v. 46, p. 335–354, doi:10.1016/j.marpetgeo.2013.02.014.
- Ingersoll, R. V., T. F. Bullard, R. L. Ford, J. P. Grimm, J. D. Pickle, and S. W. Sares, 1984, The Effect of Grain Size on Detrital Modes: a Test of the Gazzi-Dickson Point Counting Method: *Journal of Sedimentary Petrology*, v. 54, no. 1, p. 103–116, doi:10.1306/212F83B9-2B24-11D7-8648000102C1865D.
- Instituto Geográfico Nacional, and Centro Nacional de Información Geográfica, 2011, VUELO FOTOGRAFÉTRICO DIGITAL con VUELO LIDAR.
- James, M. R., and S. Robson, 2012, Straightforward reconstruction of 3D surfaces and topography with a camera: Accuracy and geoscience application: *Journal of Geophysical Research: Earth Surface*, v. 117, no. F3, p. n/a-n/a, doi:10.1029/2011JF002289.
- Kazhdan, M., M. Bolitho, and H. Hoppe, 2006, Poisson Surface Reconstruction, *in* Proceedings of the Fourth Eurographics Symposium on Geometry Processing: Eurographics Association, SGP '06, p. 61–70.
- Meshlab 1.3.3, 2014, 1.3.3: Visual Computing Lab - ISTI - CNR, Retrieved from <http://meshlab.sourceforge.net/>.
- van der Plas, L. V. D., and A. C. Tobi, 1965, A chart for judging the reliability of point counting results: *American Journal of Science*, v. 263, no. 1, p. 87–90, doi:10.2475/ajs.263.1.87.

- Pringle, J., A. Gardiner, and R. Westerman, 2004, Topics: Virtual geological outcrops - fieldwork and analysis made less exhaustive? *Geology Today*, v. 20, no. 2, p. 67–71, doi:10.1111/j.1365-2451.2004.00450.x.
- Pringle, J. K., J. A. Howell, D. Hodgetts, A. R. Westerman, and D. M. Hodgson, 2006, Virtual outcrop models of petroleum reservoir analogues: a review of the current state-of-the-art: *First Break*, v. 24, no. 1093, p. 33–42, doi:10.3997/1365-2397.2006005.
- Puigdefàbregas, C., J. A. Muñoz, and J. Vergés, 1992, Thrusting and foreland basin evolution in the Southern Pyrenees, *in* K. R. McClay, ed., *Thrust Tectonics*: Dordrecht, Springer Netherlands, p. 247–254, doi:10.1007/978-94-011-3066-0\_22.
- Reijnders, G. et al., 2008, Simulating the Outcrop: Surface To Subsurface Integration of a Carbonate Reservoir, Khuff Formation, Oman, *in* Proceedings of Abu Dhabi International Petroleum Exhibition and Conference: Society of Petroleum Engineers, p. 1–5, doi:10.2118/118332-MS.
- Schuppers, J. D., 1993, Quantification of turbidite facies in a reservoir-analogous submarine-fan channel sandbody, south-central Pyrenees, Spain, *in* S. S. Flint, and I. D. Bryant, eds., *The Geological Modelling of Hydrocarbon Reservoirs and Outcrop Analogues*. International Association of Sedimentologists Special Publication 15: Oxford, UK, Blackwell Publishing Ltd., p. 99–112, doi:10.1002/9781444303957.ch3.
- Seers, T. D., 2015, Image Based Characterisation of Structural Heterogeneity within Clastic Reservoir Analogues: University of Manchester, 248 p.
- Solomon, M., and R. Green, 1966, A chart for designing modal analysis by point counting: *Geologische Rundschau*, v. 55, no. 3, p. 844–848, doi:10.1007/BF02029658.
- Tucker, M., 1996, *Methoden der Sedimentologie*: Stuttgart, Enke, 366 p.
- Verwer, K., O. Merino-Tome, J. a. M. Kenter, and G. Della Porta, 2009, Evolution of a High-Relief Carbonate Platform Slope Using 3D Digital Outcrop Models: Lower Jurassic Djebel Bou Dahar, High Atlas, Morocco: *Journal of Sedimentary Research*, v. 79, no. 6, p. 416–439, doi:10.2110/jsr.2009.045.
- Virtual Reality Geological Studio, 2016: Retrieved from <http://www.vrgeoscience.com/>.
- Westoby, M. J., J. Brasington, N. F. Glasser, M. J. Hambrey, and J. M. Reynolds, 2012, “Structure-from-Motion” photogrammetry: A low-cost, effective tool for geoscience applications: *Geomorphology*, v. 179, p. 300–314, doi:10.1016/j.geomorph.2012.08.021.
- Wu, C., 2011, VisualSFM: A Visual Structure from Motion System: <<http://ccwu.me/vsfm/>>.
- Wu, C., S. Agarwal, B. Curless, and S. M. Seitz, 2011, Multicore Bundle Adjustment: CVPR.

### 3 CONTROLS ON BASIN-SCALE AND PLATFORM-SCALE ARCHITECTURE OF UPPER CRETACEOUS CARBONATE PLATFORMS

Jonathan Lavi<sup>1</sup>, Cathy Hollis<sup>1</sup>, Peter Burgess<sup>2\*</sup>, Ian Billing<sup>3+</sup>, James Gardner<sup>3</sup>, Christoph Lehmann<sup>3</sup>, Anna Matthews<sup>3</sup>, Katherine Tutton<sup>3</sup>, Stefan Schröder<sup>1</sup>

Contact: [jonathan.lavi@manchester.ac.uk](mailto:jonathan.lavi@manchester.ac.uk)

<sup>1</sup>School of Earth, Atmospheric and Environmental Sciences, The University of Manchester, Manchester, M13 9PL, UK

<sup>2</sup>Department of Earth Sciences, Royal Holloway University of London, London, TW20 0EX, UK

<sup>3</sup>BP Exploration, Chertsey Road, Sunbury-On-Thames, Middlesex TW16 7LN.

\*Now at School of Environmental Sciences, University of Liverpool, Liverpool L69 3GP, UK

+Now at School of Science, University of Derby, Kedleston Road, Derby DE22 1GB, UK

#### 3.1 Abstract

Relative sea-level variations are the basis of sequence stratigraphic interpretations of carbonate systems, and thus are regarded to pose the main control on platform development. In structurally active settings, such as foreland basins, tectonic controls likely exert strong controls on relative sea level, in the form of local subsidence, formation of structural highs and faulting. The Tresp basin in the South-Central Pyrenees exhibits continuous exposure of Upper Cretaceous carbonate platforms, allowing an in-depth study of the effects of various mechanisms on their evolution. Through a detailed comparison of the sedimentary record with global eustasy, large- and small-scale tectonic events, as well as the introduction of siliciclastic material, it is possible to evaluate to what degree these mechanisms control carbonate deposition over time. This further allows determining and quantifying the effects of the various processes on platform architecture. Measurable features of carbonate platform morphology and architecture include the topography and extent of the platform, position and form of the platform margin, the dominant organism types and width of facies belts. Global sea level variations played a role in basin-scale platform evolution, as recognised in major subaerial unconformities formed during sea-level fall and the successive retrogradation of platform margins during net sea level rise. A reinterpretation of the chronostratigraphy of the platform indicates that individual platforms were deposited during 3<sup>rd</sup> order sea level oscillations (ca. 2-3 Ma). However, the tectonic development of the basin leads to a variety of regional and small-

scale variations within each platform. This includes extensional faulting shaping the margins of earlier platforms, successive back-stepping of younger margins as a response to relative sea-level rise, as well as local subsidence and anticline formation resulting in varying sediment thicknesses across the platform.

### 3.2 Introduction and aims

Correlation of carbonate strata between outcrop localities or using discrete subsurface datasets is often challenged by the heterogeneity and small scale of depositional elements within these systems. The traditional tools for subsurface surveying only offer limited insight into the architecture of these sedimentary systems. Sequence stratigraphy is an interpretative tool that can be used to predict the facies architecture within carbonate systems (Catuneanu et al., 2011). These interpretations are based on the assumption that fluctuations in relative sea level are the main driving mechanism of carbonate sedimentation and thus the formation of sedimentary sequences (e.g. Goldhammer et al., 1990; Southgate et al., 1993; Pomar and Ward, 1994). Carbonate systems however, may react to a variety of external and internal factors inherent to relative sea-level changes including influx of siliciclastic material, variations in environmental conditions and the associated change in the dominant carbonate factory (Schlager, 2005). Moreover, uncertainty is introduced through the differential response of platforms to subaerial exposure depending on exposure length and dominating climate (e.g. Sattler et al., 2005; Hollis, 2011). Understanding the variable effects of these mechanisms across the carbonate platform, as well as incorporating the basin-scale evolution proves a key interest. These are important for improving both the correlation of carbonate successions and the prediction of facies distribution and stratigraphic architecture within carbonate platform systems in both 2D and 3D, and for ensuring sequence stratigraphic interpretations are correct.

The area of Tresp in the South-Central Pyrenees shows excellent exposure of Upper Cretaceous carbonate platforms. They are dominated by skeletal wackestones and packstones, deposited in a moderate to low energy lagoon, which was influenced by influxes of coarse-grained siliciclastic sediment. Rudist build-ups, with corals, formed within the platform interior and on the platform margin. The Upper Cretaceous successions investigated in this study have been the focus of many regional and local publications. Earlier regional studies have described the individual formations exposed around the area of Tresp and made initial correlations between them (Mey et al., 1968; Gallemí et al., 1982, 1983; Hottinger et al., 1989; Gallemí Paulet, 1992). Simó (1986, 1989, 1993) conducted an in-depth study on a regional scale and investigated platform evolution. Numerous studies were published on a more local scale or on single outcrops on the platform interior (Pascual et al., 1989; Caus et al., 1999; Boix et al., 2011), the platform margin

areas (Skelton et al., 1995, 2003; Gili et al., 1996; Vicens et al., 1998; Booler and Tucker, 2002; Pomar et al., 2005), and the basinal areas (Caus et al., 1997, Drzewiecki and Simo, 1997, 2000, 2002).

While many regional studies on the Tremp basin investigated sedimentary successions, their internal architecture and biostratigraphy, they often do not set the new insight into a regional context. This limits the value of each individual study within a larger setting, and may lead to potential flaws in interpretation, as the basin-scale evolution is not integrated to full extent. The aim of this study is to refine the interpretation of architecture of these mixed carbonate-siliciclastic platforms, based on both data from older studies and new field observations. It will then discuss and determine the dominant control mechanisms on the architecture and facies distribution, and evaluate to which extent each of the carbonate platforms were affected by these, and how the platforms evolved through time. This will show the criticality of considering global, regional and local processes when interpreting the development of carbonate systems over time.

### 3.3 Regional Geology

The study area is in the south-central Pyrenees, in the western part of the Lleida province of Catalonia, and partially in the eastern areas of the province of Aragon, Spain. The basin itself is named after the town of Tremp, which lies in the centre of the study area. Structurally, it lies in the upper of three thrust sheet groups defined by Muñoz et al. (1986), which encompasses a well preserved Mesozoic succession. These thrust sheets are the Serres Marginales in the South, followed by the Montsec and Bóixols thrust sheets further to the north (Villalba-Breva and Martín-Closas, 2012 after Muñoz, 1989). The Sant Corneli Anticline and the Santa Fe Syncline are important structural elements within the Bóixols thrust sheet, and provide many of the investigated outcrops.

The Tremp basin was established in the foreland of the converging Iberian and European plates, following a rifting phase during the Jurassic (Choukroune, 1992). Deposition of carbonates occurred in a roughly SSE-NNW trending trough, which was open to the west towards the Bay of Biscay, and to the east towards the Tethys Ocean (Plaziat, 1981). Starting in the late Cretaceous, siliciclastic sedimentation became increasingly prevalent. Initially this occurred from the southerly located Ebro Massif (Gómez-Gras et al., 2016), but during the latest Cretaceous and early Cenozoic also in form of conglomerates and flysch from the rising Pyrenees in the North (Muñoz et al., 1986).



The palaeolatitude of the Tremp basin is interpreted between 30° to 40° North (Owen, 1983; Simó, 1993), although later studies suggest a latitude closer to 30° North (Philip and Floquet, 2000). Simulations of wind direction indicate an Eastward direction (Poulsen et al., 1998). Clay mineral studies suggest the climate was subtropical and semiarid during the middle Cretaceous and transitioned towards arid conditions by the end of the Cretaceous (Nagtegaal, 1972). However, on the base of diagenetic studies, Booler (1994) suggests climatic conditions were humid throughout these times.

### 3.3.1 Tectonic History

The tectonic history of the Pyrenean foreland is complex, and therefore a large number of mechanisms may have affected sedimentation. The drifting of the Iberian plate towards the European plate (Puigdefàbregas and Souquet, 1986) resulted in an initially passive margin during the lower and mid-Cretaceous. The sinistral rotation of the Iberian plate resulted in extensional movement and normal faulting in the Sopeira area starting Cenomanian times (Puigdefàbregas and Souquet, 1986; Caus et al., 1997). The effects are reported at least until the Santonian, and it potentially had a large influence on shaping the margins of the earlier platforms, creating shallow platform tops adjacent to deep basins, and frequently caused mass-transport into the basinal realm (Drzewiecki and Simó, 2000, 2002). Furthermore, the transition into a compressional regime is evident in the emergence of the Sant Corneli Anticline, that is interpreted to have started forming during Santonian times (Drzewiecki et al., 2014; Markley et al., 2014), or Campanian at the latest (Shackleton et al., 2011). It represents a precursor of the imminent development of the Montsec and Bóixols Thrusts sheets in the area, that are reported to have been active by Maastrichtian times (Teixell and Muñoz, 2000).

## 3.4 Methods & Materials

Sedimentary logs on a scale of 1:50 were recorded at 11 localities, using to the methodology described in Chapter 2, in order to define lithologies and interpret depositional environments and stratigraphic evolution. Textures were described using the nomenclatures by Dunham (1962), Embry and Klovan (1971). Samples were taken systematically along these logged sections (cf. Chapter 2). From these, thin sections were prepared and analysed according to the methodology described in Chapter 2, in order to define grain assemblages and interpret depositional environments. XRD analysis was performed on a subset of samples from each lithofacies using the methodology described in Chapter 2.1.4 to obtain information about the mineralogical composition. These data are presented in the respective section of the appendix.

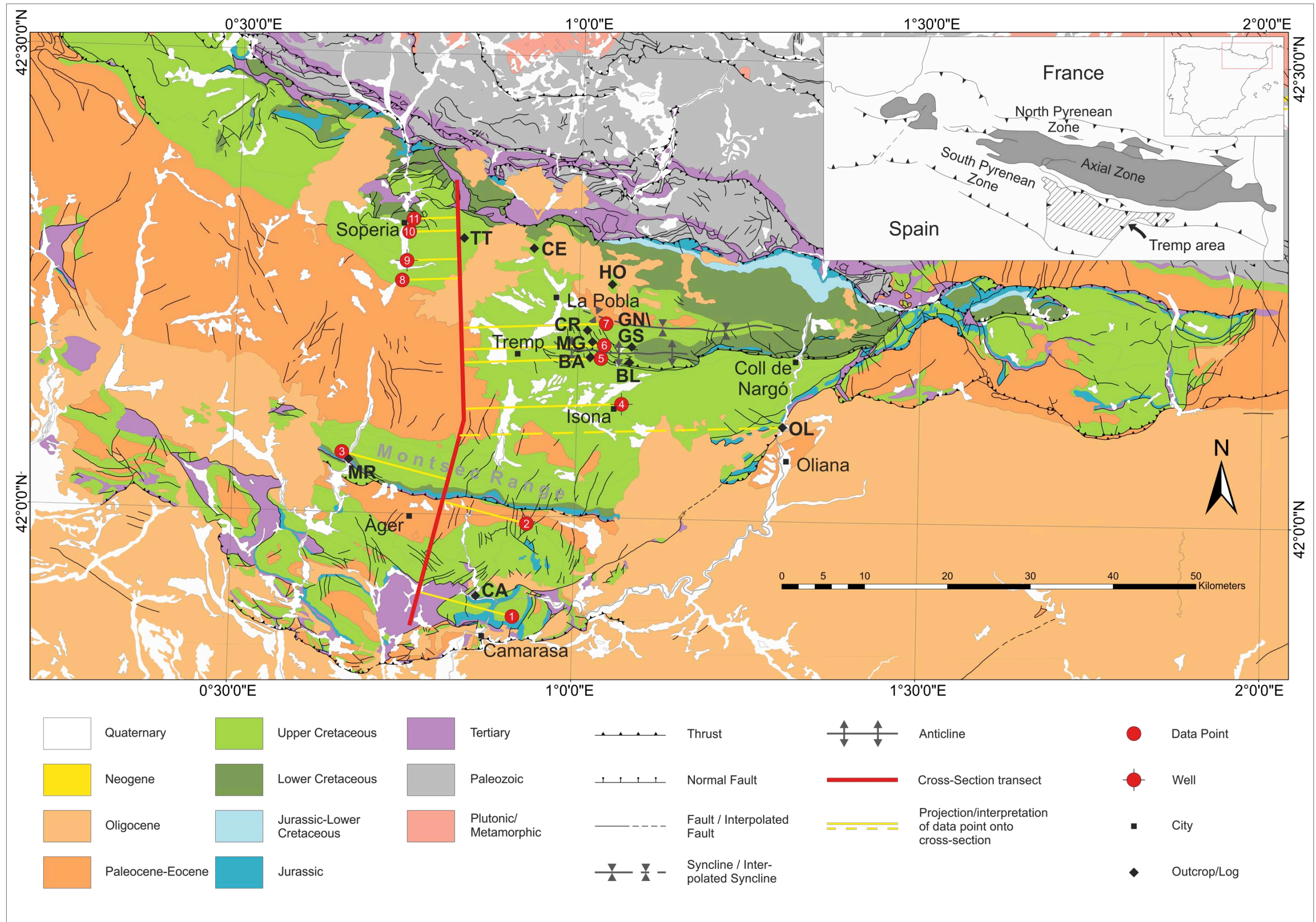


Figure 3.1: Simplified geological map of the Tremp Basin (Modified from Institut Cartogràfic i Geològic de Catalunya, 2015). Numbers in data points refer to the ones used in Figure 3.4. BA = Collades de Basturs, BL = Borrell, CA = Camarasa, CE = Congost d'Erinyà, CR = Carreu River, GN/GS = Gallinove North/South, HO = Hortonedà, MG = Montagut Gully, MR = Mont Rebei, OL = Oliana, TT = Torre de Tamurcia. Upper right corner: generalised structural map of the Pyrenees (Modified after Simó, 1986).

For each defined depositional environment, the present lithofacies were interpreted with respect to their relative position to fair weather wave base (FWWB) and storm wave base (SWB). This was done using the water-depth indicators of Flügel (2010), as well as specific water-depth indications given by Sanders, (1998), Sanders and Höfling (2000), and Sanders and Baron-Szabo (2008) for Cretaceous rudist-bearing carbonate platforms. The relative position to FWWB and SWB was then used to estimate palaeobathymetry, under the assumption that the narrow seaway between the Iberian and European plate, in which the Tremp basin formed (Plaziat, 1981), posed a restricted basin with similar fair-weather wave base of the Mediterranean in recent times. The FWWB and SWB of the Plio-Pleistocene Mediterranean were previously estimated at <10 m and 15 metres, respectively (Messina et al., 2007).

Cross-sections were constructed using a combination of field data, publically available maps and subsurface data (cf. Chapter 2 for detailed method, and Appendices A and B for a list of maps used and log data). Based on the calculated compression factor of 1.66 experienced by the sediments across the area (Puigdefàbregas et al., 1992), the original lateral extent of facies were interpreted.

The dimensions of the platforms and the individual architectural elements were determined from the produced cross sections. The inclination of specific platform segments (platform top and slope) is calculated based on the distance between the two corresponding reference points (i.e. shoreline, platform break, toe of slope), and the interpreted water depth range for the lithofacies at that locality. The platform trajectory is determined via dip-directions of sedimentary structures (i.e. clinoform dip directions and orientation of build-ups).

## **3.5 Revision of the Chronostratigraphy within the Upper Cretaceous of the Tremp Basin**

### **3.5.1 Chronostratigraphic Framework**

The chronostratigraphic framework of the study area was previously interpreted on a regional scale by Simó (1986, 1989, 1993) as well as in more local studies by numerous authors (e.g. Caus et al., 1993; Drzewiecki and Simo, 2000; Sanders and Pons, 2001; Drzewiecki and Simó, 2002; Skelton et al., 2003; Boix et al., 2011; Albrich et al., 2014). To constrain the numerical ages of the individual platform cycles, and understand the effects of sea level fluctuations, subsidence and tectonics on the sedimentary systems, a revised chronostratigraphic framework was constructed for this study using a variety of more recent sources (Figure 3.2A-C). The geological time-scale by Gradstein et al., (2012), together with the foraminiferal biozones of Hardenbol et al. (1998) were used for this framework (Figure 3.2A), with all datasets adapted to these

numerical ages. The carbonate platform cycles previously defined by Simó (1993) were adjusted to the new time-scale (Figure 3.2B) on the basis of foraminiferal-biozone constraints, previously established stratigraphic constraints or termination of geological stages, relative sea level trends, and interpretations made in this study. For reference, the previous interpretation of Simó (1993), adapted to the time scale used in this study, is presented Figure 3.2F.

For the revised interpretations of the platform cycles, the previous correlations of Simó (1993) with the foraminiferal biozones of Haq et al. (1987) were retained, with the most up-to date biozones by Hardenbol et al. (1998) used to substitute the out-dated ones. Specifically, there are 4 changes to the biozones:

- *Rotalipora reicheli* was substituted with *Thalmaninella reicheli*
- *Whiteinella archaeocretacea* was added between *Rotalipora cushmani* and *Helvetoglobotruncana helvetica*.
- *Dyocibicides primitiva* / *Marginotruncana sigali* were substituted with *Marginotruncana schneegansi*
- *Globotruncana ventricosa* was substituted with *Contusotruncana plummerae*
- 

These changes merely affect the nomenclature of the biozones. However, the changes made to the numerical-ages of the biozones in Gradstein et al. (2012) and Hardenbol et al. (1998) since the interpretations of Simó (1993) result in different absolute ages and time-spans for each platform sequence.

The eustatic sea level curve presented by Kominz et al. (2008) is plotted in Figure 3.2C, with the adjusted platform cycle time-spans highlighted in grey shading. Given that the platform cycles were interpreted to each represent a 3<sup>rd</sup> order sea level cycle (Simó, 1993), the boundaries of the adjusted cycles were matched to events of abrupt sea level rise where possible, however priority is given to maintaining allocation to the respective biozone.

The main tectonic events in the study area are summarised in Figure 3.2E (from Puigdefàbregas and Souquet, 1986). The rifting phase that dominated sedimentation in the Jurassic waned in the Lower Cretaceous. With the onset of the convergence of the Iberian and European plates in the upper Cretaceous, the rotation of the Iberian plate continued until the Santonian. Prior to the initial collision, from the mid-Turonian, increased subsidence rates are observed in the centre and northern part of the study area (Simó, 1993; Figure 1D).

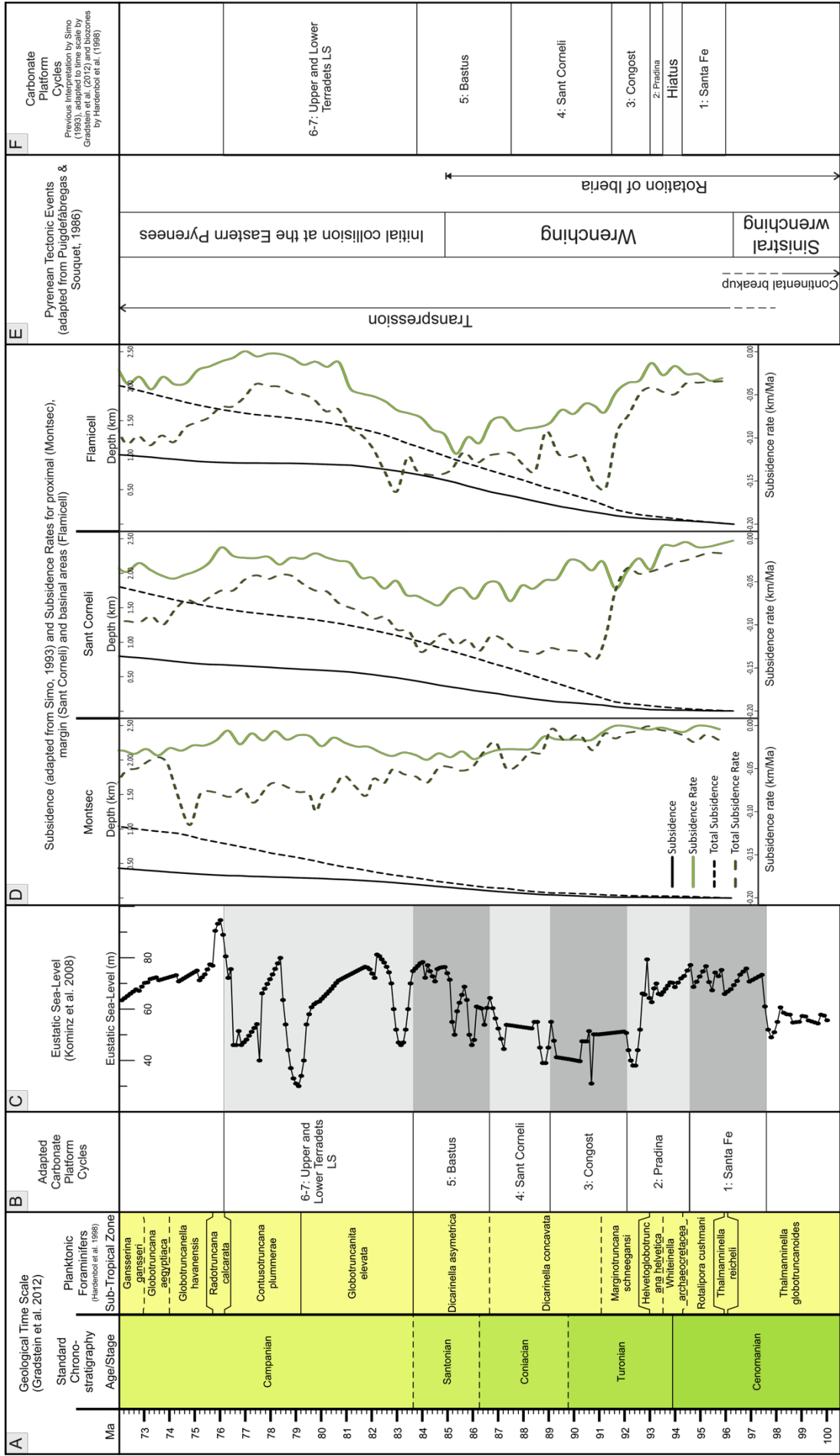


Figure 3.2: Updated Chronostratigraphic framework for the Upper Cretaceous Platform Cycles proposed by Simó (1993). A) Geological time scale (Gradstein et al., 2012) and planktonic foraminiferal zones (Hardenbol et al., 1998). B) The carbonate platform cycles of Simó (1993), recalibrated to the modern time scale. C) Eustatic sea-level curve (Kominz et al., 2008) with corresponding platform intervals highlighted in grey shades. D) Thermal and total subsidence defined by Simó (1993) for the proximal (Montsec), margin (Sant Corneli) and basinal sections (Flamicell), adapted to the revised time scale. E) Tectonic events in the Pyrenees (Puigdefàbregas and Souquet, 1986). F) Historic, unchanged platform cycles as defined by Simó (1993), highlighting the difference between the past interpretation and the interpretation presented here (B).

### 3.5.2 Stratigraphic constraints

Few studies have attempted to correlate the lithostratigraphy of the South-North transect of the Tresp area (e.g. Pons and Caus, 1996; Caus et al., 2013), and a large variation in stratigraphic nomenclature exists throughout the basin as a result. The strontium isotope stratigraphy (SIS) studies presented by Boix et al. (2011) and Caus et al. (2013) successfully correlated platform interior deposits of the Sant Corneli Platform and the Bastus Platform in the Montsec area to the platform margin facies in the northward Sant Corneli anticline. Furthermore, Gili et al. (2008) correlated several outcrops within the Sant Corneli Anticline itself on the basis of SIS. Since these studies used an older geological time scale (Gradstein et al., 2004), the absolute ages implied by these SIS studies were not carried over to this study. The remaining correlations within the basin are made using ammonoids and planktonic foraminiferal biozones (Pons and Caus, 1996; Hardenbol et al., 1998), characteristic large benthic foraminifera (genus *Lacazina*; Hottinger et al., 1989, genus *Orbitoides*; Albrich et al., 2014), and rudist associations (Pascual et al., 1989; Gili, 1993; Hardenbol et al., 1998; Vicens et al., 1998; Skelton et al., 2003; Boix et al., 2011), and a combination of the above with lithostratigraphic correlations (Mey et al., 1968; Nagtegaal, 1972; Gallemí et al., 1982; Simó, 1986, 1989, 1993; Hottinger et al., 1989). A revised stratigraphic framework has been created through a review, comparison and unification of these past studies, in corroboration with the original field observations made during this study.

The applicability of rudist associations as biostratigraphic markers was investigated in more detail in an attempt to refine the regional stratigraphy. The rudist associations observed by Vicens et al. (1998) in the Carreu area and those by Gili (1993) in the Collades de Basturs area imply that both localities are age-equivalent. This interpretation was later confirmed by SIS in a study by Gili et al. (2008). The rudist associations in the Montsec area (Pascual et al., 1989; Boix et al., 2011) show a large overlap with those reported in the area of the Sant Corneli anticline (Gili, 1993; Vicens et al., 1998). The age-allocation of some rudists (e.g. *Hippurites praecessor* and *H. socialis*), differs between studies, but these species are not considered age-indicative by Hardenbol et al. (1998). Also notable is the absence of the age-indicative *Vaccinites giganteus Major* from the Montsec section. Overall, the large variations in age-allocation of different rudist associations throughout the study area and the difficulty of correlating individual

outcrops amongst each other over distances of tens of kilometres, together with the absence of age-indicative species across the platform suggests that a large-scale rudist biostratigraphic framework is not feasible, although small-scale correlations can be made.

### 3.5.3 Revised stratigraphy for the Tremp Basin

A revised stratigraphy that implements the chronostratigraphic framework used in this study (Figure 3.2) is presented in Figure 3.3. This is based on the framework presented by Simó (1993) and later updated by Sanders and Pons (2001) and Booler and Tucker (2002). Furthermore, it includes revised regional classification of formations as presented by Caus et al. (1999), Drzewiecki and Simó (2000), Caus et al. (2009), and re-evaluation of ages from the geological maps of the Catalan Institute of Geology. The key changes incorporated into the chronostratigraphic diagram presented in Figure 3.3 are:

- Temporal separation of the Congost A and Congost B sequences (Booler, 1994; Booler and Tucker, 2002; and as observed in this study).
- The Montsec Sandstones have been re-allocated to the Santonian Sant Corneli Cycle. Sanders and Pons (2001) previously correlated these with the Bastus Cycle, but most recent maps attribute them to the previous cycle (Institut Cartogràfic i Geològic de Catalunya, 2002).
- Separation of the intermediate areas of the Sant Corneli Platform into the Collada Gassó Formation and the Montagut Limestones (Nomenclature and correlation based on Gallemi et al., 1983; Caus et al., 2013; Institut Cartogràfic i Geològic de Catalunya, 2015).
- Addition of the La Cova Limestones to the interior areas of the Sant Corneli Platform and of the Font de Bagasses Marls to the Bastus Platform, including indications of internal geobodies in the latter (Stratigraphic names by Caus et al., 1999; correlation based on rudist associations by Pascual et al., 1989, Boix et al., 2011, Gili, 1993, and Vicens et al., 1998; and SIS by Caus et al., 2013).
- Addition of the Camarasa Sandstones to the Bastus Cycle. Simó (1993) originally did not correlate them with this cycle, but they were attributed to it in the most recent maps (Institut Cartogràfic i Geològic de Catalunya, 2014).
- The Aramunt Vell Member, which represents the platform margin deposits of the Bastus Cycle in the Montagut Gully and Carreu outcrops (Sanders and Pons, 2001), has been adjusted to terminate at the top surface of the platform cycle (Gili et al., 2008, and as observed in Carreu; this study). It is also adjusted to be in contact with the underlying Montagut Limestones (Skelton et al., 2003; Institut Cartogràfic i Geològic de Catalunya, 2010; and field observations in this study).
- Lateral correlation of the Aramunt Vell Member with the Collades de Basturs member is implied (based on similar rudist associations in Gili, 1993, and Vicens et al., 1998, SIS by Gili et al., 2008, and correlations in this study).
- Addition of the debris flows in the topmost parts of the basinal Bastus Cycle (observed during this study).
- Addition of the debris flows in the basinal areas of the Sant Corneli Cycle (Described by Caus et al., 1993 and Booler, 1994).

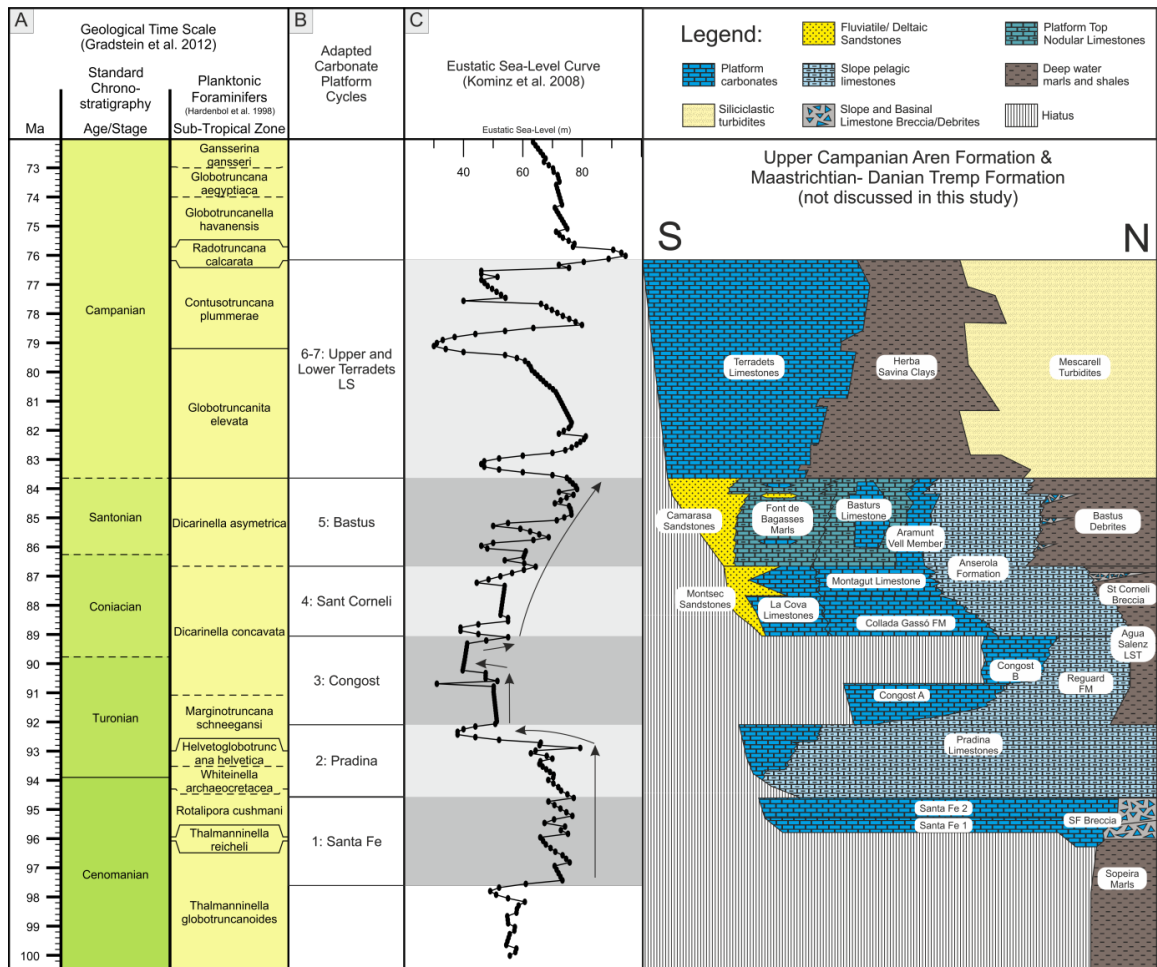


**Figure 3.3: Revised chronostratigraphic correlations of the Cenomanian-Campanian carbonate platforms of the Tremp Basin.** The age-spans of Simó (1993; B) are adapted to the Gradstein et al. (2012; A) geological time scale, and correlated to the relative sea level curve of Kominz et al. (2008; C) as outlined in Section 3.5.1. The revised chronostratigraphy is based on data from previous authors (cf. Sections 3.5.2 and 3.5.3), as well as original work conducted in this study. Stratigraphic nomenclature used by previous authors is noted for reference, but are not used further in this study due to their inconsistent nature.



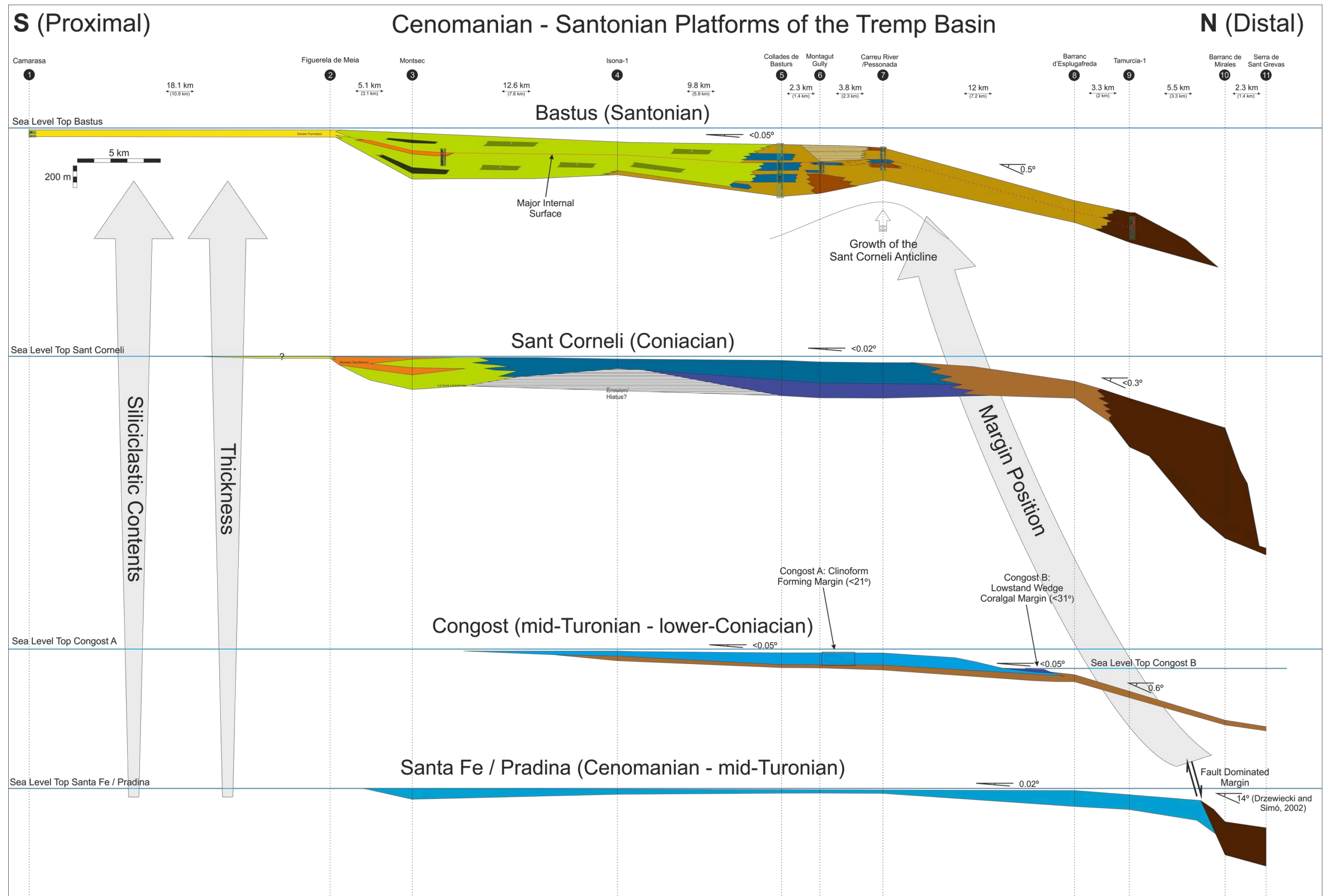


Figure 3.4: Combined Cross-Section of the Cenomanian-Santonian Platforms in the Tremp Basin. The maps used to construct these cross-sections are listed in the appendix. The colour key is represented in the lithofacies tables for each platform: Table 3.1, Table 3.2, Table 3.5, and Table 3.8. The numbers indicating the locations of data points are noted in Figure 3.1. Estimated angles for platform top and slope are presented. The angles are exaggerated in this figure. Blue horizontal lines represent interpreted palaeo-sea levels at the top of each platform. Note that the resulting palaeo-water depth is not drawn to scale. In the Bastus Platform, a major surface of possible sequence stratigraphic significance is highlighted. This is further discussed in Chapter 4. The position of the platform margin grainstone clinoforms of the Congost A and the margin coralgial build-ups of the Congost B are highlighted with respective angles. Detailed quantification of these elements is presented in Chapter 5. Also highlighted is the area of faulting that dominated the margin of the Santa Fe platform (Booler, 1994; Drzewiecki and Simó, 2000, 2002).

### 3.6 Santa Fe and Pradina Platforms

The following description of the Santa Fe and Pradina Platforms is dominantly based on literature review. During this study, some of the reported features were confirmed in the field, but no in-depth study of the platforms was conducted. Sources are cited where the information stems from literature, and observations made during this study are left without citation.

#### 3.6.1 Bounding Surfaces

The Santa Fe platform unconformably overlies the Jurassic Dogger, Portlandian or Lower Cretaceous Aptian/Albian in the south of the study area. Towards the Montsec area, it shows a conformable contact with the Aptian/Albian. In the Sant Corneli Anticline, it unconformably overlies the Albian bioclastic limestones of the Coll d'Abella Member. In the basal section, the lower contact is concordant and sharp against underlying Aulet Formation (Mey et al., 1968).

The boundary between the Santa Fe and Pradina platforms is conformable and sharp across the platform top, while being transitional in the basin and is interpreted as a drowning unconformity (Drzewiecki and Simó, 1997). The upper boundary of the Pradina platform is generally sharp across the platform top. In the Montsec area, it forms an erosional unconformity with the Sant Corneli Platform, with the intermediate Congost Platform sediments missing. Other authors have described a palaeosol in several locations at this surface (Soriano, 1992; Drzewiecki and Simó, 1997). In the basal section, the upper contact is sharp and conformable with the slope nodular limestones of the Congost Platform ("Reguard Formation"; Institut Cartogràfic i Geològic de Catalunya, 2015), which is interpreted as a marine flooding surface (Drzewiecki and Simó, 1997). No distinct transgressive or maximum flooding surfaces were observed in the field both in the Santa Fe or Pradina Platforms, but several systems tracts are described to occur in the basal sections by previous authors (Caus et al., 1993; Booler, 1994; Drzewiecki and Simó, 1997, 2000, 2002).

#### 3.6.2 Lithofacies and Depositional Environments

Three depositional environments are differentiated in the Santa Fe platform; platform interior (lagoonal), platform margin, and slope facies assemblages (Table 3.1 and Plate 3.1). In the platform interior, foraminiferal and molluscan wackestones and packstones (Plate 3.1a;b) are marly, wavy bedded and nodular at the base, and more bedded to massive at the top. The siliciclastic fraction is limited to very rare and very fine grained, angular monocrystalline quartz grains. Overall, these sediments were interpreted to represent a fairly low-productivity lagoonal environment (Simó, 1993; Booler, 1994). The abundance of benthic foraminifera implies shallow water depths during deposition. Poor sorting and angular bioclastic material shows that energy levels were predominantly low. The diverse but rudist-dominated fauna implies that

environmental conditions were restricted to some degree (Booler, 1994). The Santa Fe platform top typically has a comparably thin and uniform thickness of 10-20 metres throughout the study area (Simó, 1993).

The platform margin succession has a cumulative thickness of 150 metres, consisting of coarsening- and cleaning- upward packages of wackestone to packstone to grainstone with fragments of rudists and echinoids, as well as large benthic foraminifera (*Praealveolina*; Booler, 1994). Several metre-wide patch reefs of caprinid rudists (Booler, 1994) and coral boundstones (Caus et al., 1993) are described in the upper parts. These lithofacies are interpreted as a narrow platform margin belt of rudist and coral patch reefs, closely associated with skeletal grainstone and packstone shoals (Caus et al., 1993; Booler, 1994). Moreover, Caus et al. (1993) described karstic fissures and cavities, filled with wackestones dominated by calcispheres and pelagic foraminifera. These are interpreted by Booler (1994) to represent a period of subaerial exposure of the platform margin succession before repeated flooding and infilling of the fissures with sediment deposited during the later Pradina cycle.

The basinal and slope deposits of the Santa Fe are divided into two units; the Sopeira Marls and the overlying Santa Fe Breccia (Caus et al., 1993). The Sopeira marls show up to 350 metres of alternating pelagic nodular bioturbated wackestones and marls with planktonic and small benthic foraminifera, calcispheres and rare shell fragments (Caus et al., 1993). The Santa Fe breccia shows pelagic calcisphere mudstones and wackestones, intercalated with several types of debris-flow deposits consisting of various sized clasts from the platform margin, showing skeletal grainstones, rudist and coral boundstones, and packstones with large rudist and coral fragments, and common *Praealveolina* (Caus et al., 1993; Booler, 1994; Drzewiecki and Simó, 2000). Slumping and soft sediment deformation features are also common. The slope itself is interpreted to have an angle of between 12 and 15 degrees (Caus et al., 1993; Drzewiecki and Simó, 2002). The debrites are interpreted to have resulted from fault activity that dominated the shape of the margin (Drzewiecki and Simó, 2002).

The Pradina Platform shows massive to bedded, well- to medium-sorted wackestones to packstones dominated by calcispheres (Plate 3.1c;d). Further allochems are occasional large rudist fragments and fine to very fine grained bivalve and echinoid fragments, rare planktonic and small benthic foraminifera, as well as bryozoan fragments. The thickness gradually increases from 10 metres in the south to 90 metres in the northernmost part of the study area (Booler, 1994). Siliciclastic components are limited to very rare silt grade angular quartz grains. Occasional glauconite grains and bed-bound ferrous concretions of up to 2 cm in size are concentrated in discreet beds. Booler (1994; after Soriano 1992) noted that in the southernmost exposure along the Montsec, the Pradina formation also displays a progradational package of

grainstones with an upward-increase in the amount of skeletal fragments. The sedimentary characteristics of the Pradina Limestones are interpreted to represent deposition on a low energy slope to basin (Caus et al., 1993). Only the progradational grainstones at the top of the south most exposures described by Soriano (1992) are allocated to shallow-water platform deposition. The calcispheres and echinoderm dominated fauna is interpreted to be a result of a platform-wide eutrophication that was unfavourable for rudists and corals (Caus et al., 1993), coinciding with a  $\delta^{13}\text{C}$  excursion (Drzewiecki and Simó, 2000).

### 3.6.3 Architecture

The platform top deposits of the Santa Fe and Pradina show a remarkably consistent and thin succession across the platform top (10-20 m thickness each). Sediment packages are interpreted to be thicker at the margins and within the basin because of the strong influence of early post-rift extensional faulting in the Sopeira area (Caus et al., 1997; Drzewiecki and Simó, 2000, 2002). Consequently, the Santa Fe platform shows a wide, shallow platform interior, ca. 26.5 km in width, followed by a  $\leq 4.5$  km wide margin with a steep slope towards the basin. Because of their low cumulative thickness along the majority of the platform top, the Santa Fe and Pradina platform are mapped as one unit in the cross sections and figures presented in this study. Furthermore, the margin and basinal deposits are not differentiated in the geological maps used to create the cross sections (list of maps given in the Appendix). On the basis of the estimated water depths (Table 3.1) and the distances between shoreline and platform break (Figure 3.4) the angle of the platform top was determined to be  $0.02^\circ$ . The angle of the margin was previously interpreted to be up to  $14^\circ$  (Drzewiecki and Simó, 2002).

The interpretation of stratigraphic architecture applies only to the Santa Fe platform, as only on this platform are gross depositional environments mapped. This is because the Pradina Platform comprises sediments that were deposited as a pelagic drape across the shelf (Soriano, 1992; Caus et al., 1993; Simó, 1993; Booter, 1994), inheriting the previous topography, with no distinct facies change across the platform.

**Table 3.1: Lithofacies scheme for the Santa Fe and Pradina Carbonate Platforms.**

Lithofacies Code / log colour	Lithofacies	Geometries and bedding character	Characteristic sedimentary structures / organisms	Observed Section	Interpretation	Gross Depositional Environment	Water Depth Indicators	Estimated Water Depths
SF1	Rudist fragment wackestones with Praealveolina and other bioclasts	Tabular	Praealveolina as a characteristic organism. Common rudist fragments. Other fauna includes bryozoans, echinoid fragments, small benthic foraminifera, and red algae.	Montsec, Gallinove, Congost d'Erinyá	Platform interior wackestones with abundant and diverse fauna	Platform Top	<ul style="list-style-type: none"> <li>Wackestones with large bioclasts</li> <li>Diverse phototrophic benthic fauna</li> </ul>	Above FWWB 0-5 m
SF2	Wackestones, packstones, grainstones and floatstones as well as rudist and coral patch reefs	Several metre-wide rudist and coral patch reefs	Skeletal fragments, mainly of rudists and echinoids, as well as the large benthic foraminifera Praealveolina.	Montsec, Gallinove, Congost d'Erinyá	Platform margin patch reefs, debris and shoal complexes	Platform Margin	<ul style="list-style-type: none"> <li>Rudist patch reefs</li> <li>Common bioclastic fauna</li> </ul>	Above FFWB, lower than SF1 5-10 m
SF3	Marls, transitioning upwards into nodular wackestones	Tabular (?)	Planar bedding. Pelagic fauna; benthonic and planktonic foraminifera in the bottom parts. Predominantly calcispheres at the top parts. Fine grained shell debris	Sant Grevas (Caus et al., 1993; Booler, 1994; Drzewiecki and Simó, 2000, 2002)	Basinal/Pelagic deposits	Basin	<ul style="list-style-type: none"> <li>Pelagic, fine-grained marls and wackestones.</li> </ul>	Well below SWB >50 m
SF4	Pelagic mudstones and debris flows with clasts from the platform margin/interior	Westward thinning wedges.	Clasts within the matrix originate from the platform margin facies (SF2) and from the slope. May exceed 10 metres in diameter. Matrix: wackestones and packstones with calcispheres and rare foraminifera	Sopeira (Caus et al., 1993; Booler, 1994; Drzewiecki and Simó, 2002)	Pelagic background sedimentation and tectonically triggered debris flows from the platform margin.	Basin	<ul style="list-style-type: none"> <li>Pelagic, fine grained mudstones</li> </ul>	Considerably below SWB >50 m
PR1	Calcisphere dominated wackestone to packstones	Tabular	Abundant calcispheres. Other small planktonic organisms, including foraminifera and ostracods. Rare echinoid, bryozoan and rudist fragments. Glauconite in discreet beds.	Montsec, Gallinove, Congost d'Erinyá	Platform slope to basin deposits in a low-nutrient and low-productivity platform (Booler 1994)	Pelagic Drape	<ul style="list-style-type: none"> <li>Pelagic Fauna</li> <li>Glauconite</li> </ul>	Considerably below FWWB >50 m
Lithofacies Association / Correlation Panel Unit Colour	Santa Fe Platform	Santa Fe Platform	Sopeira Marls	Santa Fe Breccia	Pradina Platform			

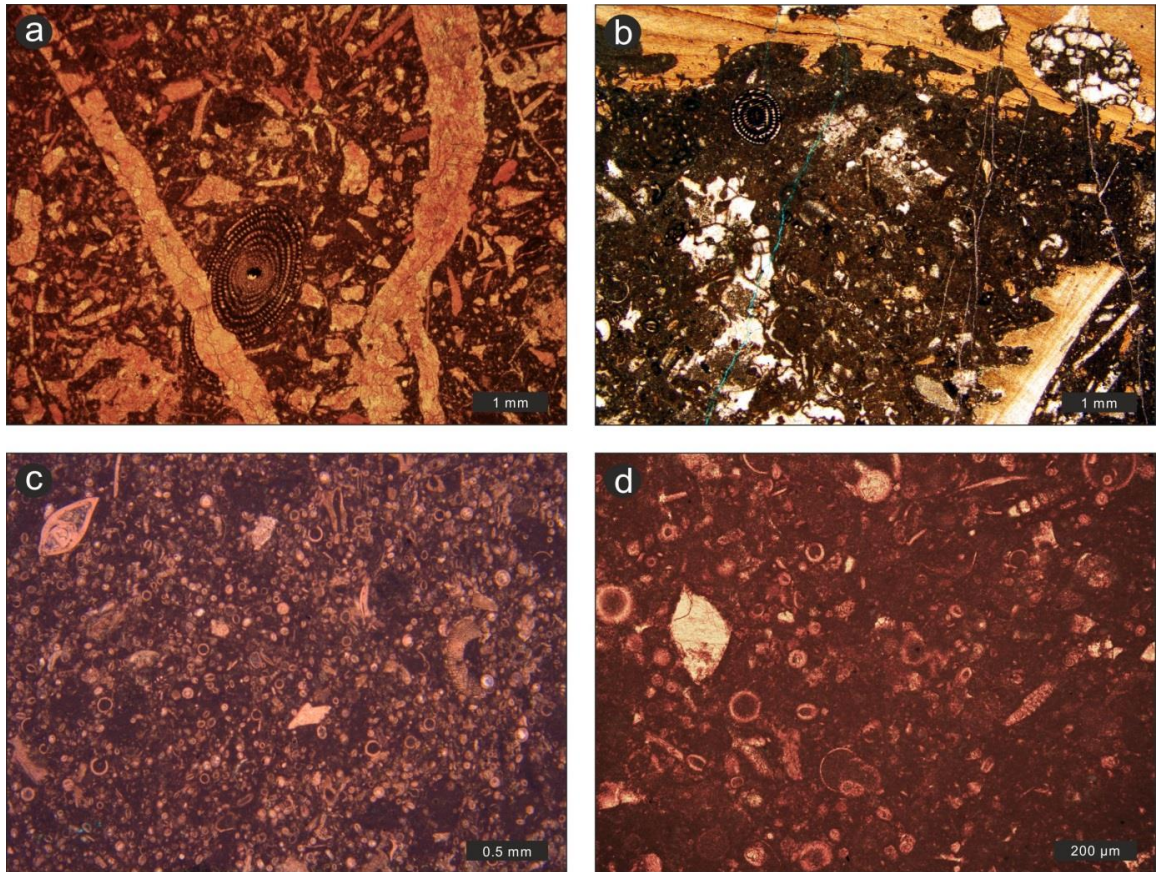


Plate 3.1: Photomicrographs of different variants of the platform top lithofacies of the Santa Fe and Pradina Limestones.

a and b: bioclast dominated and mud dominated variants of the Santa Fe platform top lithofacies (SF1), respectively. Note angular rudist shell fragments are omnipresent. Furthermore, the age-diagnostic large benthic foraminifera *Praealveolina* is recognisable in both images.

c and d: grain dominated and mud dominated variants of the platform top lithofacies of the Pradina platform (lithofacies PR1). Calcispheres are the most common components. Furthermore, small shell fragments of bivalves and echinoids are recognisable.

## 3.7 Congost Platform

### 3.7.1 Bounding Surfaces

The Congost Platform sediments are missing in the Montsec area, where an erosional unconformity separates the older Pradina Platform deposits from the younger Sant Corneli Platform sediments. The lower boundary is conformable to the Pradina in the former platform margin areas (Gallinove, Congost d'Erinyá), and sharp in the basinal areas (Tamurcia). The top boundary is sharp in the platform top areas (Borrell; Plate 3.2), and shows minor evidence of karstification at the margin (Congost d'Erinyá; Plate 3.4b), the location of the platform margin at later stages. In the basinal areas, the upper boundary with the overlying Sant Corneli Platform is gradational.

### 3.7.2 Lithofacies and Depositional Environments

The Congost Platform is divided into two subunits, the Congost A and the Congost B, each showing unique platform top and platform margin lithofacies, and both sharing a common slope lithofacies. In total, these are grouped into 7 lithofacies associations (Table 3.2, Plates 3.2-3.5), which are interpreted to represent 3 gross depositional environments.

In the southern area, the Congost A subunit shows alternations of nodular wackestones and packstones to floatstones and rudstones with skeletal fragments and small benthic foraminifera (CGA1; Plate 3.2; Plate 3.3a). Small clusters of in-situ rudists and corals are also common. These beds are intercalated with metre-thick units of massive, well-sorted bioclastic grainstones (Plate 3.2; Plate 3.3b). Together, these lithofacies represent a diverse platform top faunal association produced in a shallow water lagoon, with occasional intercalations of beds of well-sorted reworked bioclastic material.

The margin shows a 50-90 metre thick unit, thickening to the north. It is formed of well-sorted and fine-grained bioclastic packstones and grainstones, with glauconite enriched in discrete beds (CGA2; Plate 3.3c;d). These form several metre-thick and 10s of metres wide clinofolds dipping up to 20° towards the North (Plate 3.2). This lithofacies extends over at least 3.7 km in width and 19.4 km in length (cf. Chapter 5). The bedforms are interpreted to have formed in a mechanism corresponding with that of the infralittoral prograding wedge (Hernández-Molina et al., 2000), where grains were mobilised from the platform top by storm events and deposited further seawards when current energy was reduced. This is supported by the wholly well-sorted bioclastic content, indicating transport of the material away from the production zone, and the presence of sparse planktonic foraminifera and calcispheres, indicating a partial marine influence. Intermittent periods of low sedimentation resulted in formation of glauconite rich beds. The scale of the bedforms as well as the lateral distribution of this facies across the study area further agrees with the dimensions of infralittoral prograding wedges presented by Pomar et al. (2015).

As a whole, the Congost A is interpreted to represent a shallow-water platform with an up to 20° steep margin formed by packstone/grainstone clinofolds. Overall, the Congost A deposits are correlated over least 23 km in width, across the Sant Corneli anticline. In the Montsec Area, an erosional unconformity lies between the previous Pradina Platform and the younger Sant Corneli Platform, implying the Congost was not deposited this far south. The southward reach of the lagoonal facies may therefore lie between the Sant Corneli Anticline and the Montsec Area. Furthermore, the exact differentiation of lagoonal and margin facies not possible in the cross sections or maps.

The Congost B phase is exposed northwards of the Congost A phase. Bedded skeletal boundstones, floatstones and rudstones with a diverse community of in-situ rudists and corals, as well as abundant skeletal fragments and benthic foraminifera (Plate 3.5a;b). Occasionally intercalated into these are beds of well-sorted and rounded bioclastic grainstones and packstones (CGB1; Plate 3.5c). Together, these lithofacies are interpreted to have deposited in shallow water lagoonal environments, due to the abundance of phototrophic benthic organisms and large amounts of micrite, representing low energy water depths and energy. The bioclastic intercalations represent periodic reworking in high-energy conditions due to the improved sorting and rounding, and lack of micrite mud. The margin is characterised by coral and red algae boundstones (CGB2) forming northward-verging, sigmoidal build-ups with a steep slope angle (up to 31°) and a relief of up to 28 metres (Plate 3.4a). They are interpreted to represent reefs forming at the platform margin, which aggraded and prograded basinwards. The absence of age-equivalent strata to the south, the stratigraphic architecture and northward (basinwards) position of this unit in relation to the Congost A phase suggests deposition after a fall in relative sea level, and it is interpreted to have formed as a lowstand wedge. This interpretation was previously made by (Booler, 1994) and is agreed with following the observations made here. This wedge is estimated to be just less than 2 kilometres long based on exposure.

For both the Congost A and Congost B, the slope sediments (RE1) show as nodular wackestones and packstones (Plate 3.4c). They are commonly wavy bedded, but occasionally appear bedded with occasional nodules. Common constituents are fine-grained shell fragments, as well as planktonic foraminifera and calcispheres (Plate 3.5d). Distinct beds are rich in glauconite. This lithofacies is interpreted as a pelagic slope sediment, with occasional periods of low sedimentation leading to glauconite precipitation.



Table 3.2: Lithofacies scheme for the Congost Carbonate Platform

Stratigraphic Unit / Correlation Panel Colour	Lithofacies Association / log colour	Lithofacies Association	Geometries and bedding character	Characteristic sedimentary structures / organisms	Observed Section	Interpretation	Gross depositional environment	Water Depth Indicators	Estimated water depth
Congost A Sequence	CGA1	Coral and Rudist Float/Rudstones and wackestones with intercalations of bioclastic grainstones	Laterally extensive beds, intercalations of grainstones	Diverse biota: mainly rudist and coral fragments, but also abundant miliolids and various other foraminifera, echinoids, bivalves, bryozoans and algae	Borrell	Shallow platform-top carbonate factory dominated by corals and rudists	Platform Top	<ul style="list-style-type: none"> <li>Abundant shallow water phototrophic organisms</li> <li>Green algae</li> <li>Pervasive encrustation and micritisation of bioclasts</li> </ul>	Above FWWB 0-5 m
		Large-scale cross-bedded packstones and grainstones	Large-scale cross bedding (several 10s metres wide), internally coarsening up over 3 sequences formed of metre to decimetre thick beds	Majority of the grains are finely fragmented bivalve shells and rare calcispheres. Textures grading from packstones to grainstones within the internal coarsening up sequences. Glauconite enriched in distinct horizons	Gallinove	Large-scale clinofolds of well-sorted bioclastic material being transported off-platform	Platform Edge	<ul style="list-style-type: none"> <li>Occasional planktonic organisms</li> <li>Horizons enriched in glauconite grains</li> <li>Relief of clinofolds observed in outcrop: Up to 21 m</li> </ul>	10-20 m (?)
Congost B Sequence	CGB1	Coral and rudist wacke/pack/float/rudstones and sheet-like coral-rudist-sponge beds with intercalations of bioclastic grainstones	Decimetre to metre-bedded, laterally extensive. Decimetre thick, few metre wide bioclastic lenses (?)	Diverse biota dominated by in-situ corals and rudists. Includes benthic foraminifera, gastropods, brachiopods, peloids and rare calcispheres. Intercalations of well sorted grainstones: rudist and coral fragments, foraminifera and peloids	Congost d'Erinyá, Hortonedá	Platform Top facies. Backreef lagoon forming behind build-ups (CGB2) at the margin of a lowstand wedge	Platform Top	<ul style="list-style-type: none"> <li>Abundant shallow water phototrophic organisms</li> <li>Green algae</li> <li>Pervasive encrustation and micritisation of bioclasts</li> </ul>	Above FWWB 0-5 m
		Internally massive coralline floatstones/boundstones	Laterally (dip) limited units of ca. 4-5 m thickness and few 10s m width. Aggradational to slightly progradational character	Relief forming build-ups dominated by micrite and in-situ corals, and abundant coralline red algae.	Congost d'Erinyá	Coralline Build-ups forming at the margin of a lowstand wedge	Platform Margin	<ul style="list-style-type: none"> <li>Abundant encrusting coralline algae</li> <li>Relief of margin observed in outcrop: up to 28 m</li> </ul>	Ranging from above FWWB to well below SWB 5-30 m
Congost Slope ("Reguard Formation")	RE1	Nodular marly limestones and marl with glauconite	Decimetre to few metre thick units grading upwards in texture from wackestone to packstone. Horizons of thinly bedded marls with limestone nodules. Laterally extensive	Fine grained bioclasts, grains of quartz and locally glauconite. Thoroughly bioturbated. Planktonic foraminifera, calcispheres, hyaline foraminifera, sponge spicules, ostracods, echinoderms, some bivalves. Large oyster fragments locally.	Gallinove, Congost d'Erinyá, Hortonedá	Bioturbated slope deposits with pelagic fauna and periods of low sedimentation (glauconite formation)	Slope	<ul style="list-style-type: none"> <li>Fine grain size,</li> <li>Abundance of pelagic organisms</li> <li>Glauconite rich horizons</li> </ul>	20-30 and more m

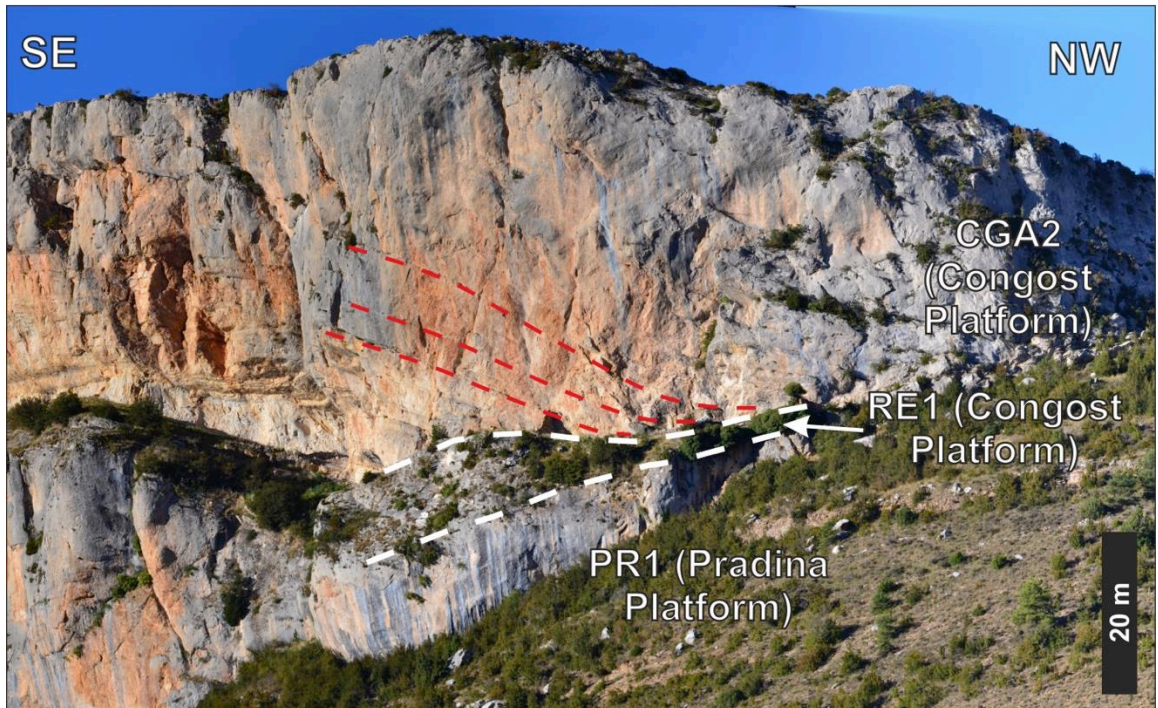
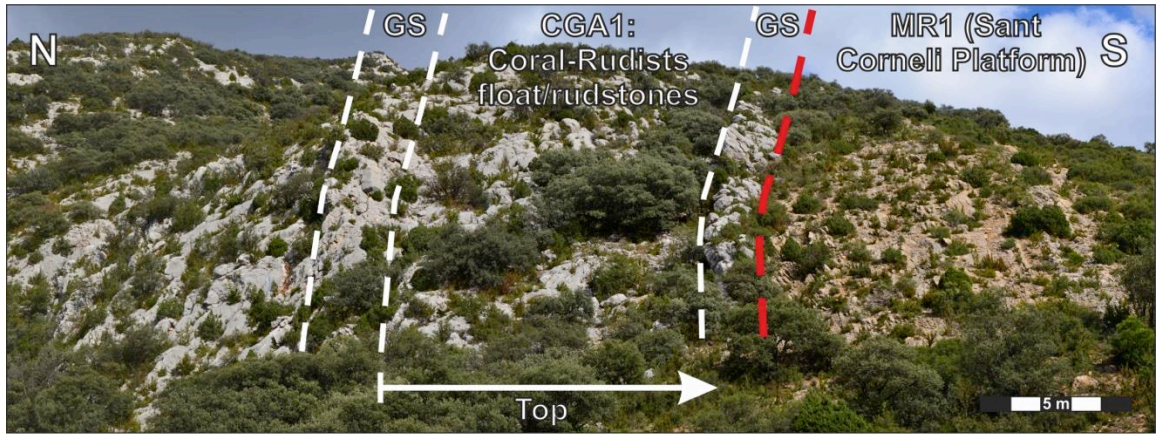
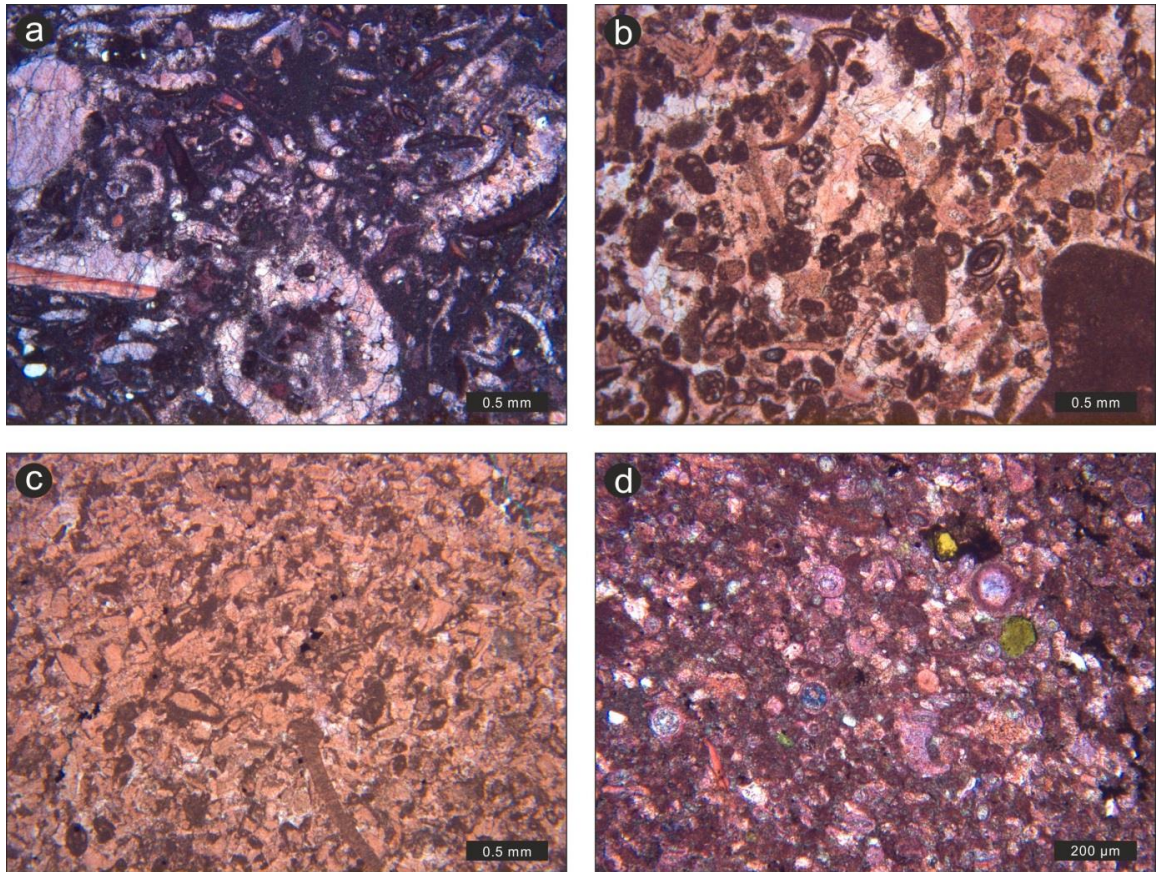


Plate 3.2: Outcrop photographs illustrating the bedding relationships of the Congost A Sequence, as well as under- and overlying sequences.

Top image: view of the Congost platform top lithofacies at Casa Borell, in the south of the Sant Corneli Anticline. The the boundary to the overlying lithofacies MR1 of the Sant Corneli Platform is clearly distinguishable due to the reddish colouring of these sediments and marked with a dashed red line. Marked with white dashed lines are the two grainstone horizons at the bottom and top of the coral-rudist floatstone and rudstone lithofacies (both CGA1) of the Congost A.

Bottom image: view of the cliff south of the mountain pass at Gallinove, showing the succssion of the Pradina to Congost Formations. Large-scale cross-bedding within the Congost A formation is highlighted with dashed lines.



**Plate 3.3: Photomicrographs of the Congost A Sequence.**

**a:** Example of a lagoonal floatstone from the top of the Congost A sequence, exposed at Borrell (Lithofacies CGA1). Large rudist debris were dissolved and the moulds cemented with ferroan calcite spar. Some benthic foraminifera and small amounts of quartz can be recognised.

**b:** Grainstones from one of the benches intercalating into the lagoonal deposits at Borrell (Lithofacies CGA1). Micrite is mostly absent, and sorting is slightly better than in the floatstones. Most of the components are small benthic foraminifera, as well as some shell fragments and peloids.

**c:** Coarse grainstone variant from the Congost A margin exposed at Gallinove (Lithofacies CGA2). Most components are recognised as highly fragmented shell debris, with some foraminifera and peloids also occurring. The grainstone is densely packed, leaving only little intergranular cement.

**d:** Fine grained packstone from the Congost A margin exposed at Gallinove (Lithofacies CGA2). Most common are highly fragmented bivalve shells, calcispheres, and echinoid fragments. Also visible are some small quartz grains as well as grains of glauconite.

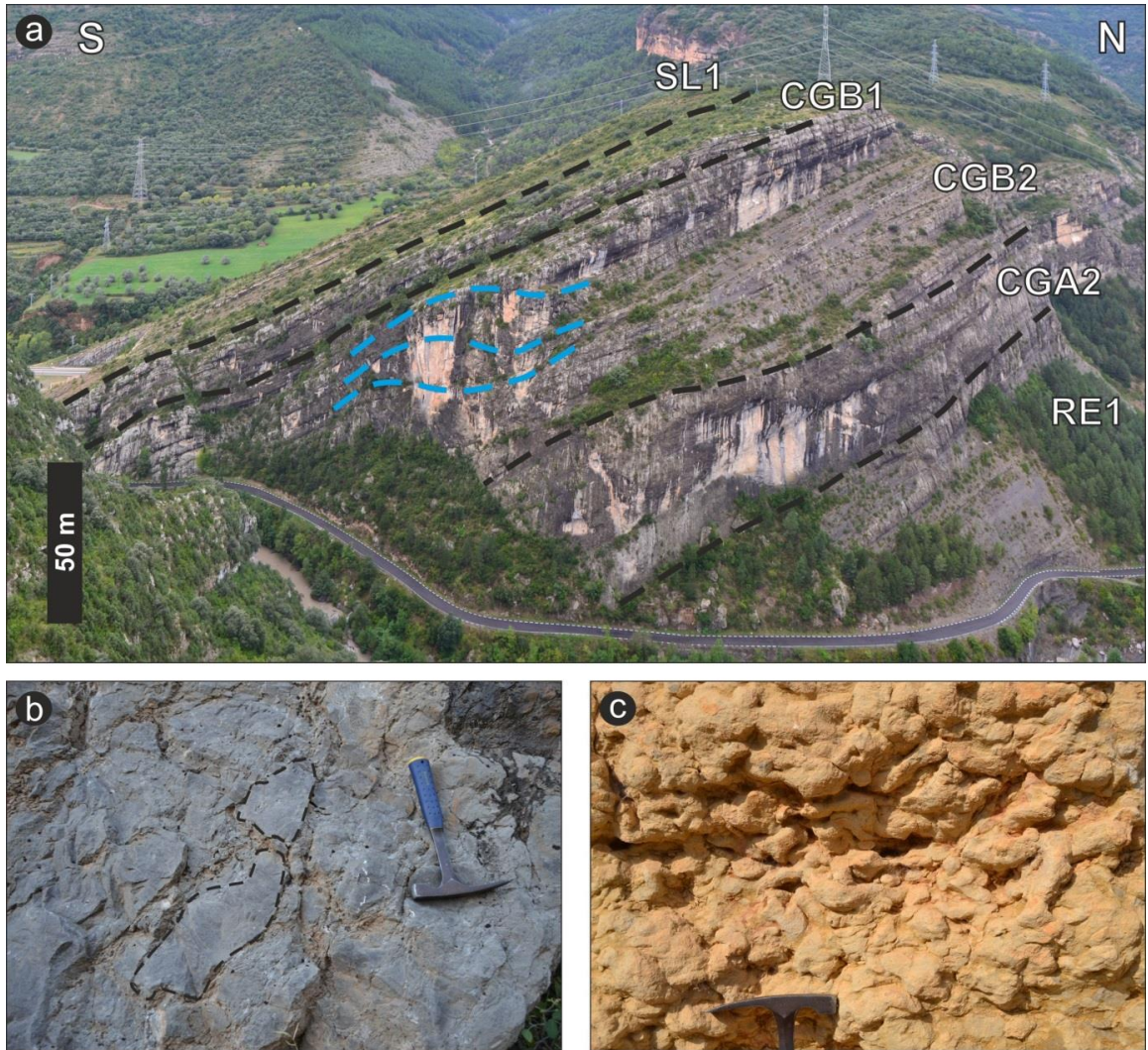


**Plate 3.4: Overview and detail photographs of the Congost B Sequence (LFA CGB) and the basal deposits of the Congost Platform (LFA RE).**

**a:** overview image of the platform margin succession at Congost d'Erinyá. The individual stratigraphic units are marked with their lithofacies codes on the image: RE1 = Slope nodular marly limestones and marl with glauconite; CGA2 = Congost Sequence A platform edge. Large-scale cross-bedded packstones and grainstones; CGB2 = Congost Sequence B platform margin. Internally massive coralline floatstones/boundstones; CGB1= Congost Sequence B lagoonal facies. Coral and rudist wacke/pack/float/rudstones with intercalations of grainstones; SL1= Sant Corneli Sequence, Upper slope nodular limestones and marls.

**b:** Detail photograph of brecciated limestones at the top of the Congost B Platform (lithofacies CGB1). Marked in dashed lines are the outlines of two prominent clasts. The brecciating is interpreted to be the result of subaerial exposure of the platform top.

**c:** Detail photograph of abundant bioturbation traces in the slope lithofacies (RE1) of the Congost B at the Hortonedá locality. Hammer head for scale.

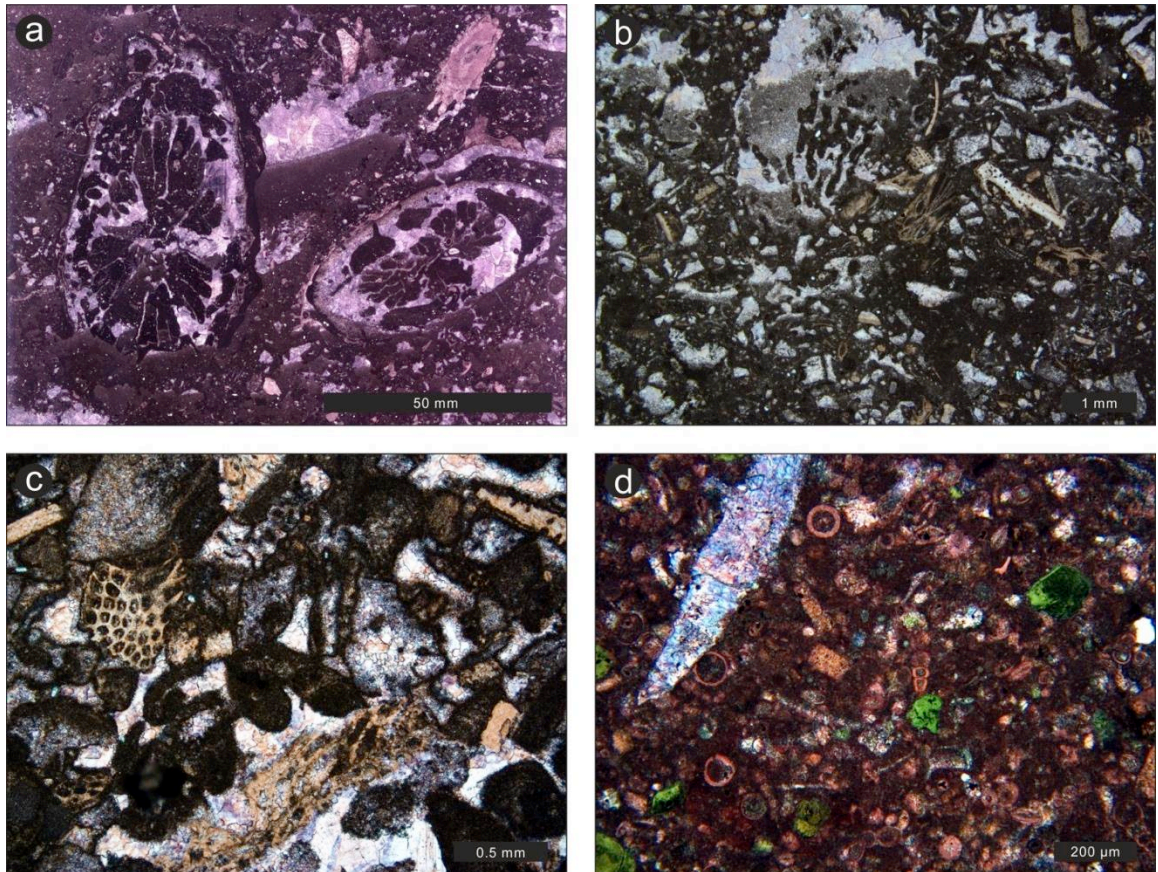


**Plate 3.5: Photomicrographs of the Congost B Sequence (Lithofacies Association CGB) and the Congost Slope deposits (RE1).**

**a:** Coralline boundstone from the build-up interval of the Congost B sequence (Lithofacies CGB2). Clearly visible are two coral heads filled with micrite, and the skeleton replaced by ferroan calcite cement. In the upper right corner, a section through an echinoid stem is observable.

**b:** Lagoonal floatstone from the backreef interval of the Congost B sequence (Lithofacies CGB1). Many moulds remaining after the selective dissolution of bioclasts are present. A geopetal feature is seen in the top of the image, indicating that some of the dissolution may have occurred during early phases.

**c:** Coarse lagoonal grainstone from the backreef interval of the Congost B sequence (Lithofacies CGB1). A variety of carbonate allochems can be distinguished, including rudist and bryozoan fragments, as well as peloids. The rounding and sorting of these rocks varies.

**d:** Example of the slope deposits of the Congost Platform (Lithofacies RE1) as it is exposed in the area of Gallinove. The wackestone to packstone texture is dominated by small shell fragments, calcispheres and planktonic foraminifera. Larger shell fragments are rare, and may leave moulds filled by calicispar. Glauconite grains as shown here are also common, although only in distinct horizons.

### 3.7.3 Architecture

The platform top of the Congost A is estimated to have been <23 km wide on the basis of the produced cross-sections (Figure 3.4). The clinoform-dominated margin prograded over at least 5 km, interpreted via the continuous exposure of these facies in S-N direction along the Sant Corneli anticline (Figure 3.1). Individual clinoforms showed lengths of at least 64 metres (Chapter 5). From the margin position at Gallinove, the slope facies are correlatable over an area of at least 8 km (Figure 3.1). For the Congost B, the lowstand wedge is estimated to have been <2 km wide on the basis of map data (Institut Cartogràfic i Geològic de Catalunya, 2015). Outcrop measurements show that the width of the corallgal margin build-ups was at least 80-100 m in width. The slope deposits are correlated across a distance of 8 km (Figure 3.1).

Estimations of water depths were made for each gross-depositional environment and the corresponding lithofacies association (Table 3.2). Using the established width of platform elements (top, margin, and slope) from the cross-section, estimated slope angles were calculated. For the platform top of the Congost A, the angle is <0.05°. The margin angle is taken from the measurements of clinoforms on outcrop (cf. Chapter 5), where an angle of <21° was measured. Furthermore, estimations of the slope angle were previously made by Booler (1994) on the basis of the increase in thickness of the prograding Congost A margin clinoform sediment package basinwards (north). It was concluded that the seafloor on which the clinoforms prograded showed an angle of 0.6° (Booler, 1994). For the Congost B, a platform top angle of <0.15° was calculated. However, similarity of facies with that of the Congost A platform top allows interpreting that the angle may have been lower than 0.05°. The measurements of the relief of the corallgal build-ups at the Congost d'Erinyá outcrop show that the angle here was up to 31° (Chapter 5). As the slope of the Congost B is interpreted to have remained unchanged since the Congost A, the angle of 0.6° defined by Booler (1994) is also applied here.

Both the large-scale cross-bedding in the Congost A sequence and the prograding coralline build-ups in the Congost B sequence show a northward trajectory. Subsequently, the platform axis is interpreted to be northwards directed. Nodular wackestones and packstones with a pelagic fauna and occasional glauconite beds, as well as more marl-rich intervals (lithofacies RE1), which are interpreted as slope sediments, are present northwards of the platform interior and platform margin facies, supporting this interpretation. These slope sediments underlie the Congost A in the area of Gallinove, where they reach about 15 metres in thickness. At the area of Congost d'Erinyá, they reach up to 240 metres below the Congost B (Booler and Tucker, 2002).

### 3.7.4 Distribution of Terrigenous Material

Overall, terrigenous content is low within the Congost Platform (Table 3.3; modal analysis, and Table 3.4; XRD analysis). The modal analysis shows a maximum content of 3.68% in the Congost A sequence, with the remainder of the stratigraphic units showing lower amounts. XRD analysis shows similar trends in terms of quartz contents.

**Table 3.3: Siliciclastic contents in the Congost Platform as determined by modal analysis.**

Lithofacies / Locality	CGA1 (Borrell)	CGA2 (Gallinove)	CGB2 (Congost d'Erinyá)	RE1 (Gallinove)
Siliciclastic contents: Average [%]	0.21	1.75	0.28	1.34
Siliciclastic contents: Min-Max [%]	0-1.00	0-3.68	0-1.00	0-2.33
n	8	17	6	4

**Table 3.4: Siliciclastic contents in the Congost Platform as determined by XRD analysis.**

Lithofacies / Locality		CGA2 (Gallinove)	CGB2 (Congost d'Erinyá)	RE1 (Gallinove)
Quartz [%]	Average	2.81	1.29	7.32
	Min-Max	0.78-4.4	0.95-2.07	N/A
Muscovite [%]	Average	0.66	1.32	2.68
	Min-Max	0-1.97	0-1.95	N/A
Kaolinite [%]	Average	0.51	0	0
	Min-Max	0-1.54	N/A	N/A
Clinocllore [%]	Average	N/A	N/A	0.84
	Min-Max	N/A	N/A	N/A
n		3	5	1

## 3.8 Sant Corneli Platform

### 3.8.1 Bounding Surfaces

In the area of the Montsec range, in the south of the study area, the Sant Corneli Platform unconformably overlies the Turonian Pradina Platform. Further north, in the areas of the Sant Corneli Anticline and Congost d'Erinyá, the lower boundary with the Congost Platform is sharp (Plate 3.9), with minor evidence of karstification in the latter (Plate 3.4b). Further north, the boundary is gradational. The upper boundary of the Sant Corneli Platform is sharp in the Montsec area, and gradational throughout the northern parts of the study area.

### 3.8.2 Lithofacies and Depositional Environments

There are 18 lithofacies defined within the Sant Corneli Platform deposits. They are grouped into 10 lithofacies associations, which represent 4 gross depositional environments (Table 3.5; Plate 3.6-Plate 3.9). These are outlined in the following.

South of the Montsec Range, over a transect of less than 3 km, poorly consolidated, decimetre-scale cross-bedded and well sorted sandstones are observed (NIT1; Plate 3.6c), intercalated with coarse grained, metre-scale cross-bedded grainstones and packstones with abundant rudist debris, benthic foraminifera and quartz-rich horizons (NIT2; Plate 3.6a,b,d,e). They may be 0.3 – 13.5 km long (average 3.8 km), and reach thicknesses of ca. 30 metres (cf. Chapter 5). This lithofacies association is interpreted to be dominated by deltaic sand, with periodic intercalations of bioclastic material reworked from the platform interior. A more extensive siliciclastic system may have persisted further to the south, but has either been lost to erosion or amalgamated with the nearshore sediments of the overlying Bastus Platform.

A complex facies mosaic is exposed laterally along the south side of the Montsec Range, interpreted to have extended over about 10 km in width (LFA IR; Plate 3.7; Plate 3.8). Dark, bituminous charophyte wackestones (IR1; Plate 3.8a) appear at the base and become less frequent up-section. The main sediments are nodular bioclastic wackestones and packstones with miliolinids, rudist debris and *Lacazina*, as well as horizons of rudist biostromes (IR2; Plate 3.7a,d; Plate 3.8b). Lens-shaped bodies of cross-bedded bioclastic grainstones with horizons of rhodoliths are periodically intercalated (IR3; Plate 3.7b,c; Plate 3.8c,d). Towards the top of the section, a thick succession of bedded bioclastic packstones and grainstones with abundant foraminifera and quartz-horizons are observed (IR4; Plate 3.8e). Together, this lithofacies association is interpreted to represent a partially restricted interior environment. The charophyte wackestone facies could have been deposited in brackish tidal pools whilst fine-grained, bioclastic limestones were deposited in fully marine conditions, with rudist build-ups occurring in discreet horizons. Quartz-rich horizons could represent periodic intercalations by tidal deltas or spillover lobes and washover bars, supporting the interpretations of Caus et al., (1997) and Boix et al. (2011).

Northwards, for ca. 25 km, marl-rich and fine-grained nodular wackestones and packstones with fine shell fragments and small benthic and planktonic foraminifera dominate (MR1). These represent deposition under low energies at water depths below fair-weather wave-base. They are frequently intercalated with wavy bedded, medium-grained bioclastic grainstones and packstones showing load-casts protruding into the underlying beds. They are interpreted to represent periodic events of coarser sediment influx and reworking during high-energy events, due to the larger grain sizes and smaller amounts of micrite. At the top of the section, the



sediments transition into alternations of fine-grained nodular wackestones with floatstones and rudstones with in-situ coral and rudist (MR2). Bioclasts include rudist fragments, miliolids, and *Lacazina*, amongst others. Further basinwards, these are replaced by thick, bedded units of medium to coarse bioclastic grainstones with abundant rudist debris (MR3). These lithofacies are interpreted to have been deposited above fair-weather wave-base, representing in-situ carbonate production and reworking in the form of platform margin build-ups and shoals.

Northwards, for approximately 25 km, marly limestones with few bioclasts and abundant intact echinoids (OR1) dominate, passing even further north into nodular wackestones and packstones with pelagic microfossils, small shell fragments and glauconite (SL1; Plate 3.9a,b). Eventually, these pass into grey calcareous marls and nodular wackestones with a pelagic fauna and minor amounts of silt (SL2; Plate 3.9c,d,e), showing slumping features and periodic intercalations of brecciated limestones consisting of material from the older platforms (SL3). Based on the absence of shallow water fauna, fine grain size, and increase in volume of marl, these lithofacies are interpreted as deep-water deposits. Slumping and intercalations of breccia suggest deposition on a low-angle slope. Occasional debris-flow deposits have been described and interpreted by previous authors to have been triggered by the fault activity in the area of Sopeira (Caus et al., 1993; Booler, 1994)

Lithofacies Association / Correlation Panel Colour	Lithofacies Code / log colour	Lithofacies	Geometries	Characteristic sedimentary structures / allochems	Observed Sections	Interpretation	Gross Depositional Environment	Water depth indicators	Estimated water depth
Nearshore Deltaic Sandstones (NS)	NS1	<i>Not exposed, only presumed. Either eroded or amalgamated with the Bastus Nearshore tidally influenced delta lithofacies association (cf. Table 3.8, p92)</i>			Camarasa (?)	Tidally influenced delta deposits	Near-shore		
Cross-bedded sandstones and intercalating bioclastic grainstones and packstones	NIT1	Poorly consolidated and partially cross-stratified sandstones		dm-scale cross-bedding, largely bioclast free. Medium to well sorted, medium to coarse grained	Vilanova de Meià	Multipisodic deltaic channels	Nearshore- Inner Ramp Transition	<ul style="list-style-type: none"> <li>Cross bedding</li> <li>Reddish horizons possibly representing exposure surfaces (NIT2, cf. log VMs, Appendix)</li> </ul>	Above FWWB ~0-10 m
	NIT2	Cross-bedded, quartz bearing bioclastic grainstones and packstones	Up to 30 m thick, and 0.3 - 13.5 km wide (mean = 3.9 km). No dip control	Grainstones and packstones with metre-scale cross-bedding. Occasional enrichment of rudist debris in some beds. Other components include echinoids, as well as miliolids and Lacazina in discreet beds	Vilanova de Meià	Nearshore bioclastic shoals and sand bars			
Dark charophyte limestones, nodular limestones with rudists and bedded bioclastic limestones	IR1	Micritic charophyte limestones with small benthic foraminifera		Wackestones and rare packstones with abundant charophytes, rare small benthic foraminifera and gastropods	Montsec	Restricted tidal pools	Inner Ramp/ Lagoon	<ul style="list-style-type: none"> <li>Charophyte limestones interpreted as tidal pools (very low water depth)</li> <li>Abundant micritic envelopes</li> <li>Possible exposure surfaces with rhodoliths (IR3)</li> </ul>	Above FWWB ~0-10 m
	IR2	Nodular marly limestones with rudists and large benthic foraminifera, rudist build-ups		Wackestones and packstones. Rudist debris, miliolinids, Lacazina, peloids. Intercalating horizons of in-situ rudists.	Montsec	Lagoon deposits			
	IR3	Cross-bedded bioclastic limestones intercalated into IR2	Several-metre scale cross-bedding	Well sorted and rounded grainstones and packstones. Rudist debris, miliolinids, peloids. Mud-rich reddish horizons with disc-shaped rhodoliths.	Montsec	Tidal delta deposits			
	IR4	Massive to bedded packstones and grainstones with rudists, large benthic foraminifera, encrusting red algae. Bar forming		Medium to fine grained, rounded packstones and grainstones. Rudist debris, miliolinids, Lacazina, encrusting coralline algae, peloids	Montsec	Bar deposits			
Mid-Ramp Phase A (Collada Gassó Formation)	MR1	Bioclastic packstones and grainstones interbedded into marly nodular limestones.		Wackestones with interbeds of orange-brownish packstones and grainstones. Decimetre-thick wavy bedding and load-casts at bottom surfaces of interbeds. Foraminifera, algae, some codiacean algae and red algae. Bivalves, gastropods, echinoderms, bryozoans, sponge spicules and rudist fragments.	Montagut Gully, Santa Fe Anticline	Fine grained mid-ramp deposits with storm beds	Inner- to Mid-Ramp	<ul style="list-style-type: none"> <li>Cross-bedding, sharp lower boundaries on well-sorted and micrite (interpreted as storm-beds in MR1)</li> <li>Loosely packed coral-rudist clusters (MR2)</li> <li>Common micritic envelopes (MR3)</li> <li>Enrichment and sorting of rudist shells in bedding surfaces (possible storm activity; MR3)</li> </ul>	Ranging between above FWWB (MR3) and below SWB (MR1) ~5-15+ m
Mid-Ramp Phase B (Montagut Limestones)	MR2	Bioturbated foraminiferal nodular marls alternating with well-bedded packstones and wackestones with in-situ corals and rudists		Wackestones, packstones, floatstones and rudstones with common corals and rudists (fragments and in-situ), echinoderms, miliolids, pecten, gastropods and brachiopods. Early Lacazina. Fe oxides and chert nodules	Montagut Gully	low-angle distal inner ramp deposit with occasional rudist and coral patch reefs			
Mid-Ramp Shoals	MR3	Bedded rudist grainstones	3-4 m cycles of 20-40 cm thick beds.	Bedded grainstones with rounded and well sorted rudist shell fragments, miliolid foraminifera, and peloids. Enrichments of larger rudist shells in discreet horizons. Quartz grains.	Carreu River	Distal inner-ramp shoals			
Marly limestones with echinoids	OR1	Echinoid rich nodular wacke/packstones and wavy bedded packstones.		Wackestone/packstone with fine-grained bioclasts and rare benthic foraminifera. Common wholly preserved echinoids.	Santa Fe Anticline	Outer Ramp deposits	Outer-Ramp	<ul style="list-style-type: none"> <li>Fine grain size</li> <li>Absence of cross-bedding</li> <li>Intercalations of sorted and bedded bioclastic packstones interpreted as storm beds</li> </ul>	Around to slightly below SWB >15 m
Pelagic nodular limestones and marls (Anserola FM)	SL1	Nodular calcareous marls and marls with pelagic fauna and glauconite		Strong bioturbation. Oysters, echinoderms, pecten, bryozoans, many bivalve fragments. Common glauconite grains and iron oxides.	Congost d'Erinyà	Upper Slope deposits	Upper Slope	<ul style="list-style-type: none"> <li>Glauconite</li> <li>Absence of phototrophic benthic organisms</li> </ul>	Considerably below SWB ~50 m
Pelagic marls and calcareous marls (Agua Salenz Formation)	SL2	Nodular calcareous marls with intercalations of grey marls, Mudstones and wackestones, rare packstones with pelagic fauna	Forming metre to 10s metre thick units.	Sponge spicules, calcispheres, small benthic foraminifera and echinoid and bryozoan fragments	Tamurcia	Pelagic slope deposits	Lower Slope	<ul style="list-style-type: none"> <li>Sponge spicules</li> <li>Dominant pelagic fauna</li> </ul>	Considerably below SWB ~100 m
Marls, calcareous marls and debris flows	SL3	Nodular calcareous marls similar to SL1 with intercalations of debris flow deposits and slumps	Ca. 10 m thick sheets of up to 700 metres in length. Westward thinning out (Booler, 1994). No strike control.	Common slumping structures and debris flow deposits. Clasts originating from the Santa Fe and Pradina platforms (Booler, 1994).	Sopeira (Booler, 1994)	Slope deposits with debris flows and slumps			

Table 3.5: Lithofacies scheme for the Sant Corneli Carbonate Platform

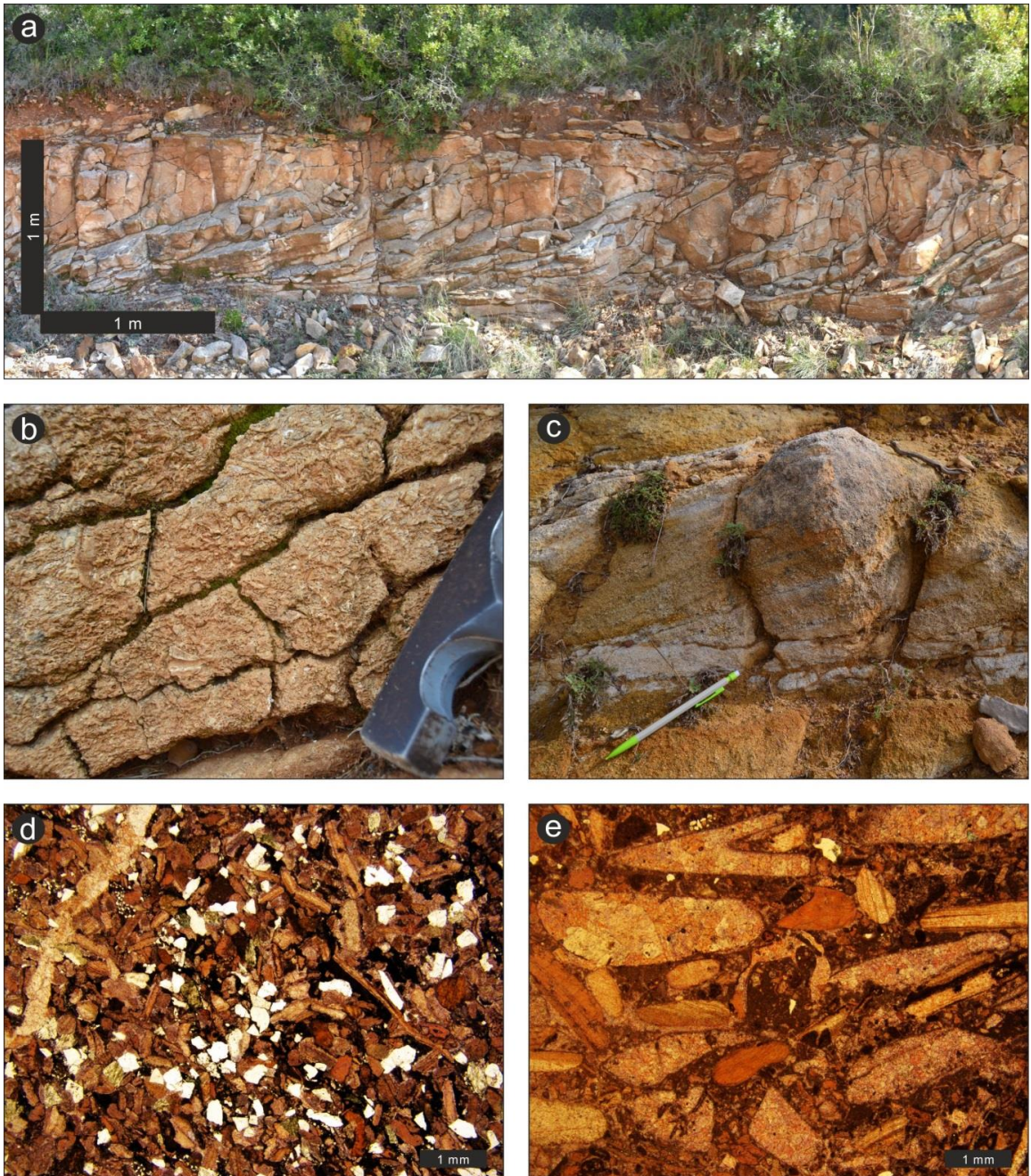


**Plate 3.6: Outcrop and thin section images of lithofacies association NIT of the Sant Corneli Platform.**  
**a:** overview of the sigmoidal, metre-scale cross-bedding within the limestone intercalations within lithofacies NIT2. The sandstones themselves are overgrown (upper part of the image).  
**b:** detailed image of a rudist debris rudstone/grainstone within lithofacies NIT2. Visible are the large amounts of cm-scale rudist fragments. Hammer head for scale.  
**c:** detailed view of dm-scale cross-bedding within lithofacies NIT1. Pencil for scale.  
**d:** photomicrograph of a quartz rich bed of lithofacies NIT2. Note angular quartz grains and partially rounded bioclastic components.  
**e:** photomicrograph of rudist rudstone bed from lithofacies NIT2. Note large relative size of rudist debris and their rounded edges.

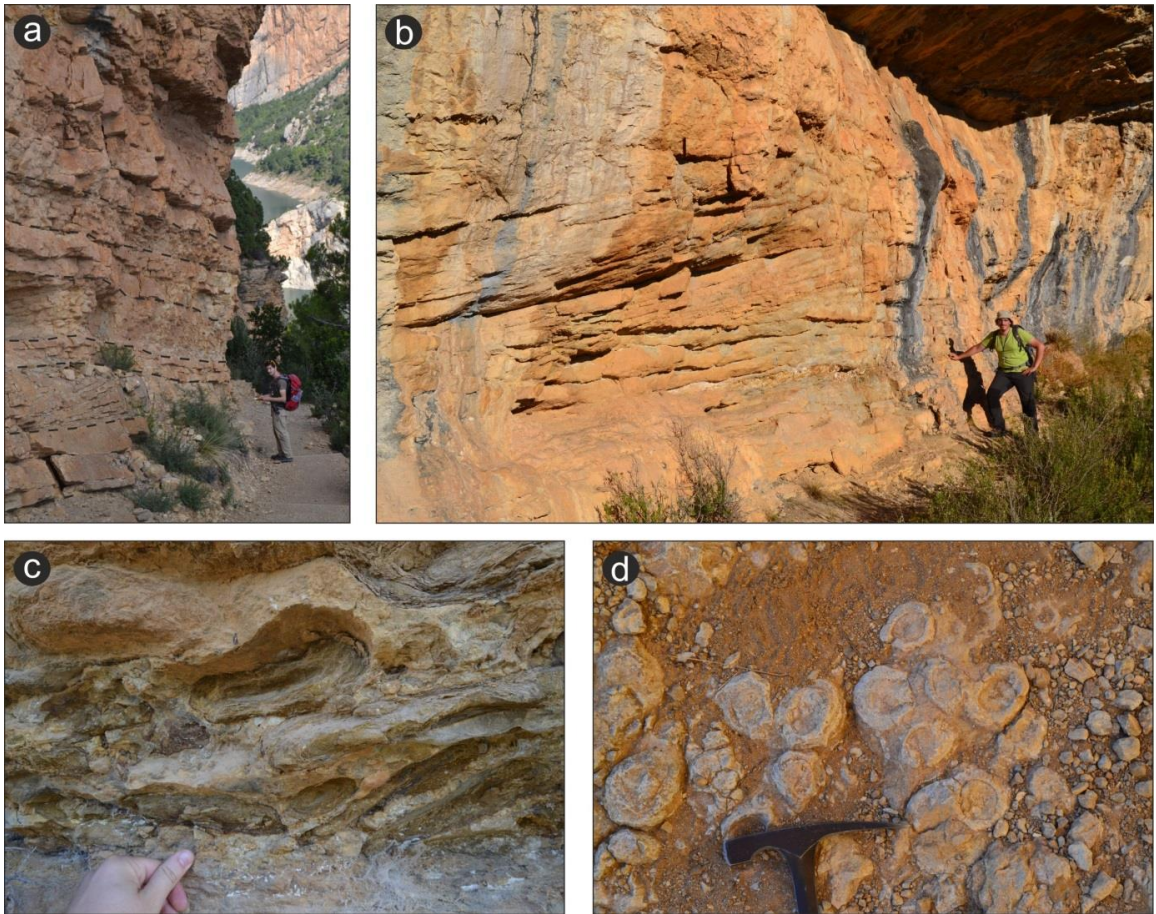


**Plate 3.7:** Field photographs illustrating the various facies of the Sant Corneli Platform interior (LFA IR).

**a:** intercalations of nodular and wavy bedded limestones within lithofacies IR2.

**b:** large scale cross-bedding within lithofacies IR3. Foresets are ca. 2.5 m thick and up to 20 metres wide. The sediments themselves are bioclastic grainstones dominated by rudist shell fragments.

**c:** detail image of rhodolite bearing bed at the base of lithofacies IR3. The rhodoliths are disc-shaped and show a concentric layering and are prone to weathering.

**d:** plan-view of rudist build-up within lithofacies IR2. Individual specimen are several cm large and colonies are densely clustered.

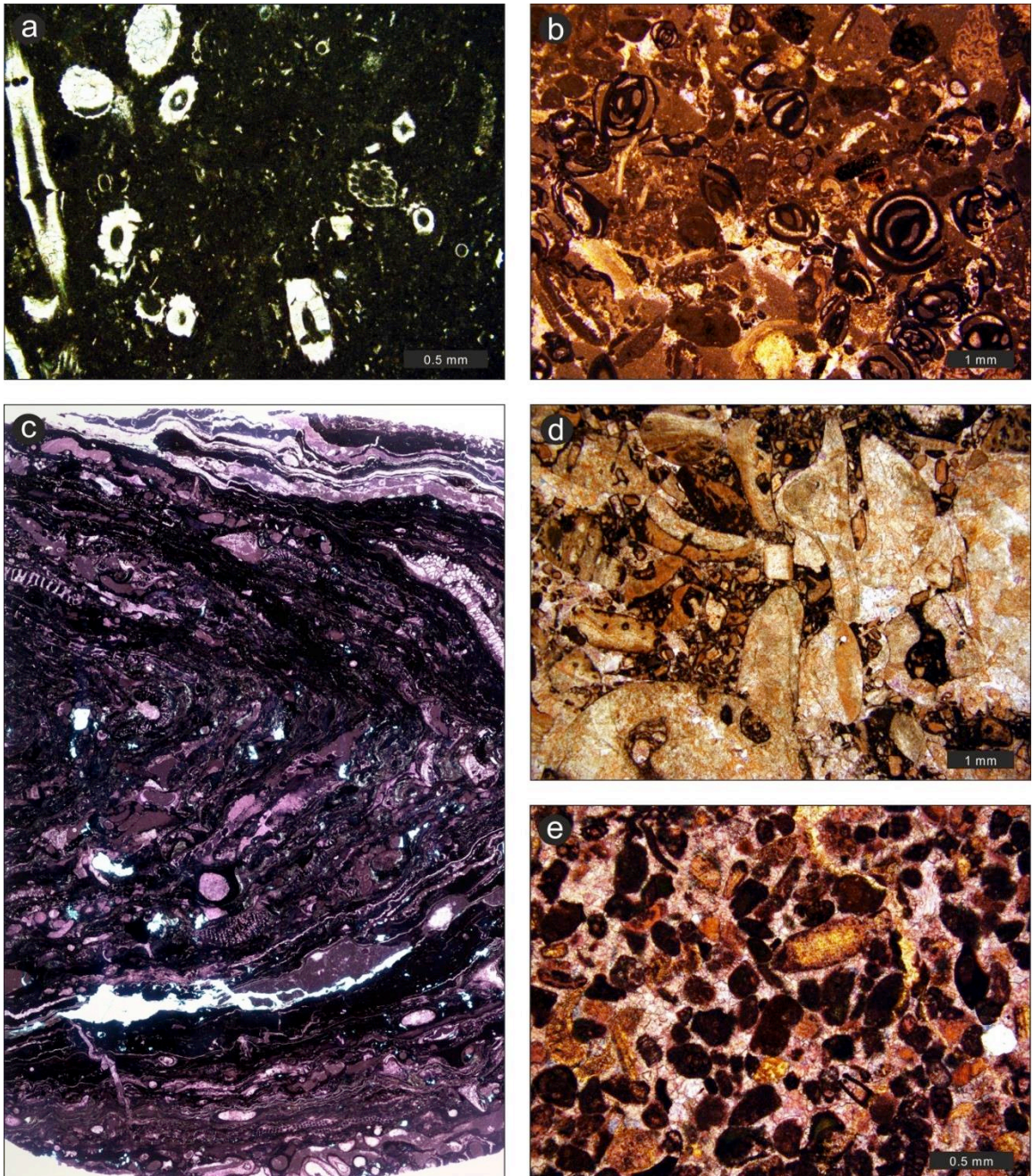


Plate 3.8: Photomicrographs highlighting the details of the various lithofacies within the Sant Corneli Platform interior (LFA IR).

a: Charophyte rich wackestone of lithofacies IR1. Note the abundant charophyte stems and oogon (right of image centre), as well as the dark micritic matrix.

b: Miliolid dominated packstones of lithofacies IR 2.

c: cross-section of a rhodolite found within lithofacies IR3. Note the various bioclasts bound into the laminae, as well as circular serpulid tubes. The dark laminae are formed by encrusting red algae.

d: rudstone from lithofacies IR3. Note the abundant and coarse grained rudist debris, as well as the smaller bioclasts filling the gaps between them. The rounding of the larger rudist fragments is advanced.

e: peloidal grainstone found within lithofacies IR4. Note common, well rounded bioclasts and rare angular quartz grains.

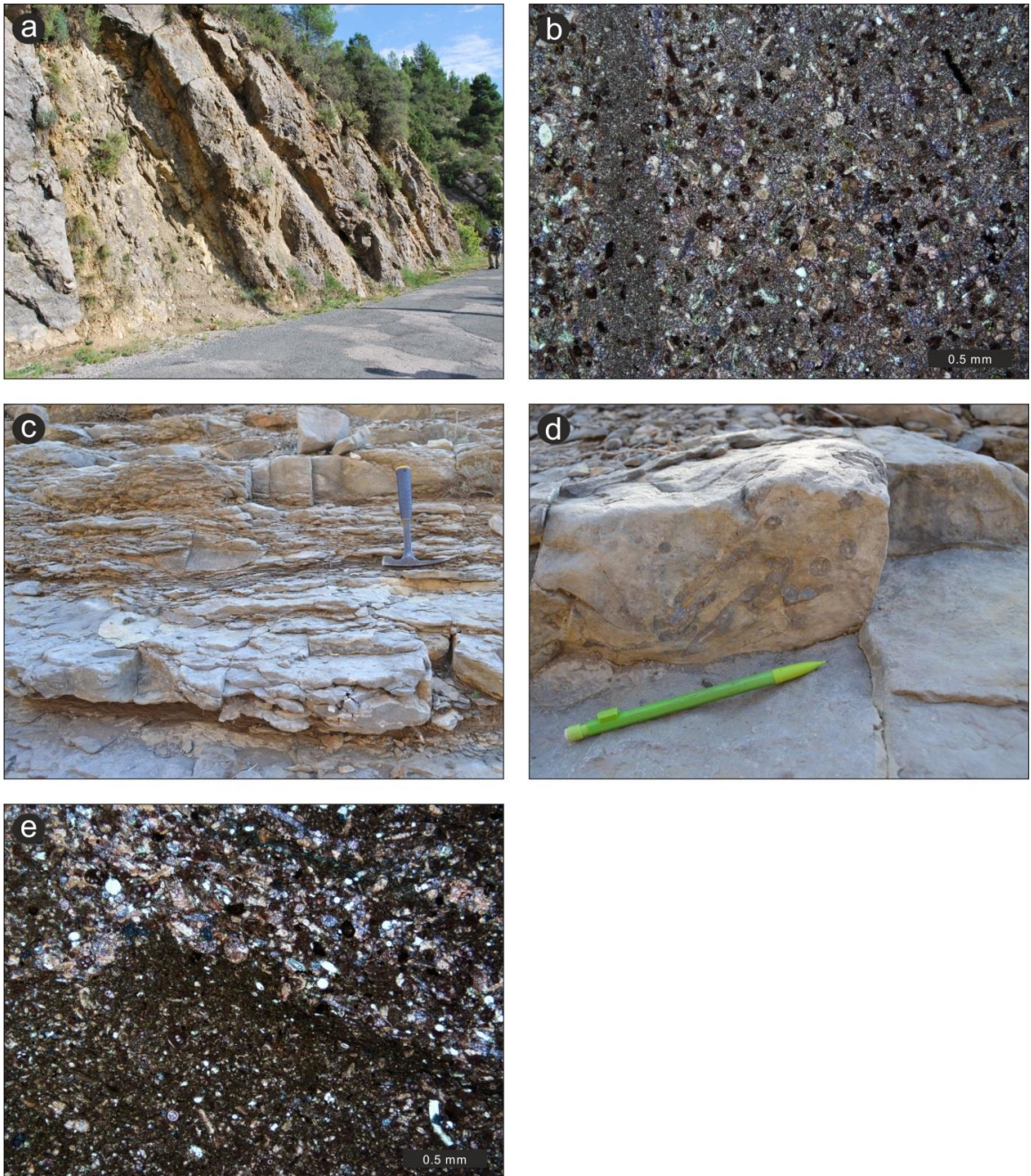


**Plate 3.9:** Field photographs and photomicrographs of the slope and basin lithofacies of the Sant Corneli Platform.

**a:** outcrop photograph of the lower boundary of the Sant Corneli in the slope area. The massive limestones at the left border of the image belong to the Congost Platform, and the transition to pelagic nodular limestones and marls of the Sant Corneli Platform (Lithofacies SL1) is an extraordinarily sharp boundary. Lithofacies SL1 continues in cyclic alternations between marly limestones and noular limestones, both with different degrees of resistance to weathering.

**b:** Photomicrograph of a packstone from lithofacies SL1. Peloids and very fine grained shell fragments are abundant, as well as small foraminifera. Some glauconite grains can be recognised. On the left side of the image, a bioturbation trace shows texture variation, being filled with mud-dominated sediment.

**c:** Outcrop photograph of the pelagic marls and calcareous marls lithofacies of the Sant Corneli platform slope (SL2). Alternations between bedded limestones and laminated marls are clearly visible. Hammer for scale.

**d:** detail photograph of bioturbation traces within lithofacies SL2. Pencil for scale.

**e:** Photomicrograph of Lithofacies SL2. Note the texture variation from wackestone (bottom left) to packstone (top right). Small shell fragments and silt grade quartz grains are dominant.

### 3.8.3 Architecture

Despite the clear transition from shallow to deep-water sediments northwards, a distinct slope break cannot be defined, whilst the facies transitions are gradual in the platform top and upper slope environments. Combined with the rapid transition to deeper water facies in the lower slopes, and the presence of slumping features and debrites, the Sant Corneli Platform is interpreted as a distally steepened ramp.

Following this, the inner ramp, which includes the lithofacies associations NIT and IR, extended over at least 13 km in width. The mid-ramp deposits of lithofacies MR1 extended over 25 km, whereas the distal inner ramp (lithofacies MR2 and MR3) covered the same area in the second half of the platform duration. The outer ramp and slope (lithofacies associations OR and SL) extended over at least another 25 km. Based on the water-depth indicators defined in the facies analysis (Table 3.5), and the estimated distances between shoreline, margin and slope, the platform shows an overall very low topography on the top ( $<0.02^\circ$ ), and a slightly steeper slope ( $0.15\text{-}0.3^\circ$ ).

The thickness of the sediments is roughly similar throughout the platform, showing ca. 200 metres. However, it varies somewhat across key points of the cross-section. The section penetrated by the well at Isona only presents about a third of the thickness when compared to the more northward areas of the mid-ramp. Moreover, the deep slope and basinal succession show a far greater thickness than the remainder of the platform ( $>600\text{ m}$ ).

The studies by Caus et al. (1993) and Boix et al. (2011) of the Montsec area show a westward to northwestwardly oriented direction of sediment transport and minor progradation. Furthermore, Bover (1994) describes westward thinning out of debrite beds in the area of Sopena. Facies transitions in the north of the Sant Corneli Anticline however show a northward to northeastwardly trajectory (Institut Cartogràfic i Geològic de Catalunya, 2010).

### 3.8.4 Distribution of Terrigenous Material

Modal analysis (Table 3.6) shows that quartz is the most common siliciclastic mineral in lithofacies association NIT (maximum 35%), followed by specific horizons within lithofacies association IR (maximum 14.33%, average 3.19%). Lithofacies MR1 and MR2 show generally less than 1% of quartz. On the slope, Lithofacies SL1 shows a slight increase in quartz contents with 3.03% on average. XRD analysis (Table 3.7) has shown a similar trend for quartz, with the highest concentration occurring in the lithofacies association NIT, after which concentrations fall again, and finally increase again in the slope and basin. Muscovite is found in traces in the platform interior (Lithofacies association IR; 0.47% at maximum), and is more common in the

slope and basin (maximum 2.79% in lithofacies SL2). Microcline is limited to the proximal environments (lithofacies association NIT; maximum 5.93%).

Lithofacies Association / Lithofacies	NIT	IR	MR1	MR2	SL1	SL2
<b>Average</b>	<b>20.33</b>	<b>3.19</b>	<b>0.67</b>	<b>0.33</b>	<b>3.03</b>	-
<b>Min- Max</b>	5.67-35.00	0-14.33	0.33-1	0-0.67	1.01-5.05	-
<b>n</b>	2	9	2	3	2	0

Table 3.6: Siliciclastic contents along the Sant Corneli Platform as determined by modal analysis

Lithofacies Association / Lithofacies		NIT	IR	MR1	MR2	SL1	SL2
n		2	2	0	0	1	1
Quartz	<b>Average</b>	<b>20.77</b>	<b>0.66</b>			<b>10.43</b>	<b>12.55</b>
	Min-Max	9.25-32.28	0.52-0.80				
Muscovite	<b>Average</b>	<b>0</b>	<b>0.24</b>			<b>1.36</b>	<b>2.79</b>
	Min-Max		0-0.47				
<b>Kaolinite</b>		<b>0</b>	<b>0</b>			<b>0</b>	<b>0</b>
<b>Clinochlore</b>		<b>0</b>	<b>0</b>			<b>0</b>	<b>0</b>
Microcline	<b>Average</b>	<b>3.12</b>	<b>0</b>			<b>0</b>	<b>0</b>
	Min	0.30-5.93					

Table 3.7: Siliciclastic contents along the Sant Corneli Platform as determined by XRD analysis

## 3.9 Bastus Platform

### 3.9.1 Bounding Surfaces

The lower bounding surface of this platform is unconformable to the Jurassic and Lower Cretaceous to the south (Camarasa area). It shows a sharp boundary with the underlying Sant Corneli Platform in Montsec area, and a gradational boundary in the Sant Corneli Anticline area and to the north (Tamurcia area). The upper boundary of the Bastus Platform with the Terradets Platform is sharp in the south and becomes more gradational northwards.

### 3.9.2 Lithofacies and Depositional Environments

The sediments of the Bastus Platform were allocated to 18 different lithofacies, which are grouped into 8 lithofacies associations (Table 3.8 and Plate 3.10 Plate 3.16). These associations are interpreted to represent 4 gross depositional environments.

The most southerly parts, which extend laterally for at least 18 km, comprise massive, well-cemented sandstones (NS1), and bedded poorly consolidated sandstones (NS2), as well as wavy



marls (NS3) with intercalations of quartz-rich grainstones (NS4; Plate 3.10; Plate 3.11). On the basis of the coarse grain size of siliciclastic components, small amount of marine fossils, presence of clay, and bedding characteristics these are interpreted to represent a system of stacked deltaic channels and mouth bars, as well as prodelta marls, with only few carbonate allochems sporadically introduced from seaward areas (cf. Elliott, 1986). Oppositely directed cross-bedding with clay-drapes likely indicate a tidal influence (Tucker, 2011).

In the Montsec area, dark grey foraminiferal wackestones (PI2; Plate 3.11b) dominate, interpreted as lagoonal background sedimentation. Lens-shaped intercalations of bioclast bearing sandstones and quartz-rich bioclastic grainstones (PI1; Plate 3.10a,b; Plate 3.11a) occur here, interpreted to represent reworked siliciclastic and skeletal material. Occasional beds of fine grained and well-sorted peloidal grainstones (PI3; Plate 3.11d) are interpreted as platform interior shoals, as they exhibit better sorting and rounding than the surrounding sediment. Rudist framestones and rudist debris floatstones and rudstones are also observed (PI4; Plate 3.10a,c,d; Plate 3.11c), and are interpreted as rudist biostromes with their associated debris forming within the lagoon. These lithofacies associations are interpreted to extend over an area of 27 km in width.

In the Sant Corneli Anticline area, a series of composite build-ups, comprising of northward-facing bioherms of massive rudist-coral boundstones (PM1) with debris aprons of bioclastic packstones (PM2; Plate 3.14a,b; Plate 3.15a), and frameworks of elevator rudist biostromes in the southern (backreef) areas (PM3&4; Plate 3.14c; Plate 3.15b) are observed in an area measuring 5-6 km (north-south). Occasionally quartz bearing, bioclastic grainstone and packstone beds with 10s metre scale cross-bedding dipping towards NNE (PM5; Plate 3.14d; Plate 3.15c,d) are found over- and underlying the build-ups. These grainstone units may reach up to few kilometres in width and length (cf. Chapter 5), and are interpreted as platform margin grainstone shoals due to their bedding nature and juxtaposition with the margin build-ups.

The platform margin build-ups and grainstones intercalate frequently with fine-grained, bioclastic wackestones and packstones with common benthic foraminifera (US1) and occasional metre-scale clusters of in-situ rudist and coral communities (US1b; Plate 3.14e; Plate 3.15e). The wackestones may occasionally also appear as thinly bedded marls (US2). These lithofacies are interpreted as upper slope deposits between FWB and SWB due to the general lack of shallow-water characteristics, with small patch reefs establishing locally. Decimetre thick beds of fine-grained bioclastic packstones and grainstones (US3; Plate 3.15f) are sporadically intercalated into the wackestone and marl intervals, representing reworked sediment beds formed during high-energy events, as they are composed of grain-rich accumulations within the slope sediment. Together, these lithofacies are interpreted to extend over an area measuring

ca. 14 km from south to north and records the transition from the platform margin into the basin.

In the northernmost part of the field area, thinly bedded pelagic calcareous wackestones and calcisiltites (LS1), representing deep-water sedimentation, are intercalated with beds featuring clasts sourced from the platform margin composite build-ups and shoals and erosive lower boundaries (LS2; Plate 3.16a-d). The latter are interpreted as debris flow deposits. These facies indicate periodic margin failure and resedimentation of material in the basinal realm. They are exposed for about 6 km, but are expected to continue further northwards.

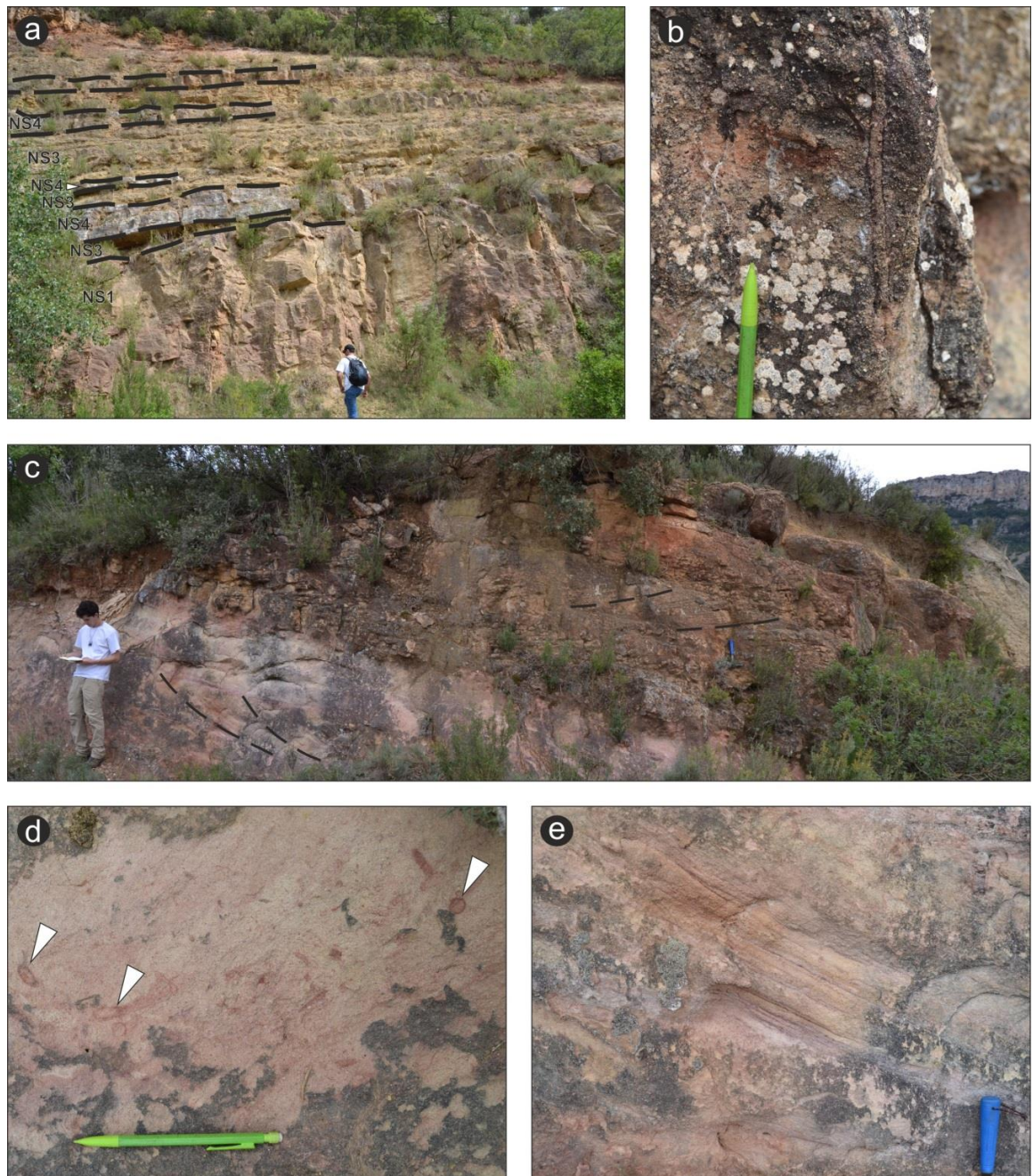


Plate 3.10: Outcrop photographs of the lithofacies association *Nearshore tidally influence delta* of the Bastus Platform

a: Overview photograph showing massive, well cemented sandstones at the bottom (lithofacies NS1), followed by

marls at the top (lithofacies NS3) with intercalations of quartz-rich bioclastic grainstones and packstones (lithofacies NS4) bedding surfaces marked with dashed lines. Person for scale.

b: Bioturbation structure of the ichnogenus *Skolithos*. Pencil for scale.

c: View of outcrop showing change from poorly cemented sandstones (lithofacies NS2; bottom left) into well cemented sandstones (top right). Dashed lines indicate cross-bedding surfaces in opposite directions between the two facies. Person for scale.

d: *Ophiomorpha*-type bioturbation traces in the poorly cemented sandstones of lithofacies NS2 (few complete burrows marked with arrows). Pencil for scale.

e: detail photograph of cross-bedding in the poorly cemented sandstones of lithofacies NS2. Hammer handle for scale.

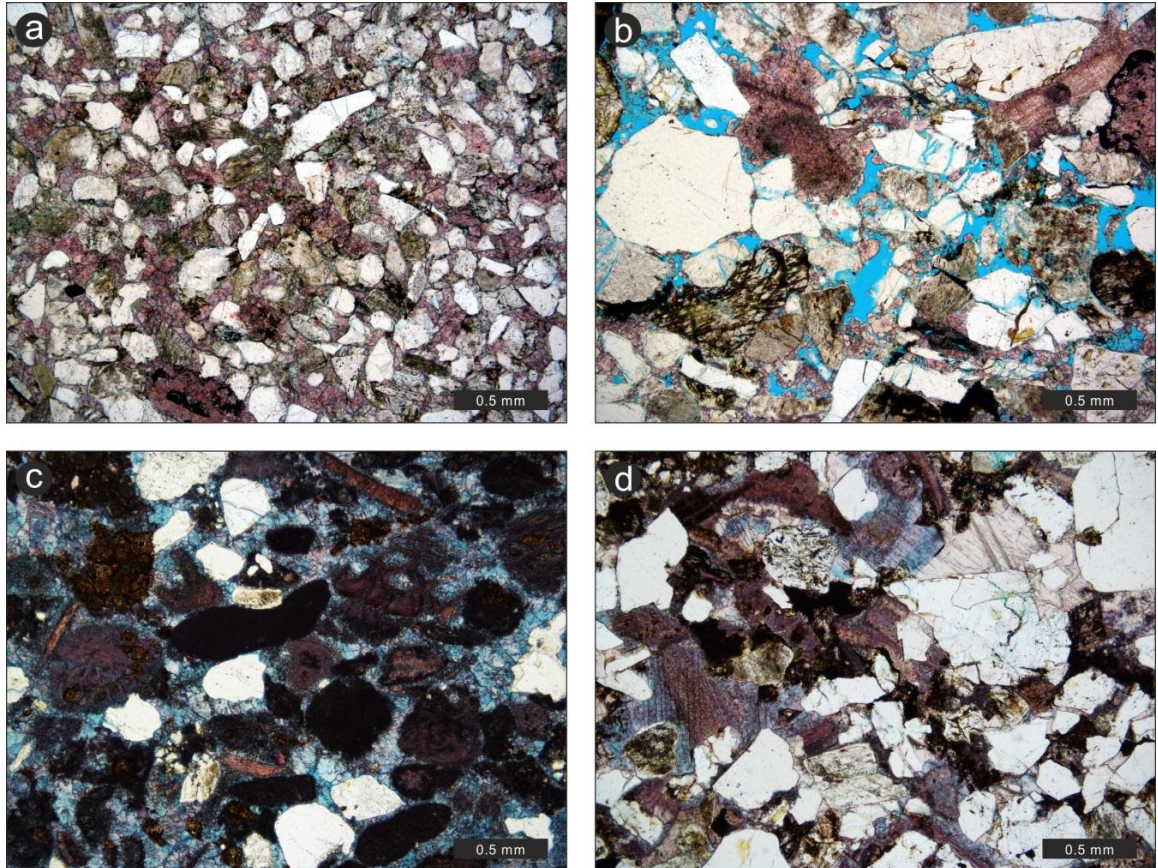


Plate 3.11: Photomicrographs of the *Nearshore tidally influence delta* lithofacies association of the Bastus Platform.

a: Lithofacies NS1. Note abundant angular monocrystalline quartz grains and thorough cementation with calcite spar cement.

b: Lithofacies NS2. Note poor cementation with calcite spar. Common siliciclastic grains are monocrystalline quartz grains, as well as some volcanic rock fragments (bottom left and centre right). Few bioclastic fragments are recognised. In the upper left part, an echinoid grain displays syntaxial overgrowth with calcite spar cement.

c and d: lithofacies NS4. Note the variation between contents of siliciclastics and carbonate components between the two samples. The sample depicted in c shows abundant peloids, as well as few angular quartz grains and several rounded bioclasts, as well as intact foraminifera. The sample depicted in d displays abundant siliciclastic components and few bioclastic grains.

Lithofacies Association / Correlation Panel Colour	Lithofacies Code / log colour	Lithofacies	Geometries and bedding	Characteristic sedimentary structures / organisms	Observed Sections	Interpretation	GDE	Water depth indicators	Estimated water depth	
Sandstones, marls and quartz-rich grainstones	NS1	Massive to banked, well sorted sandstones	Massive beds, 5-10 m thick	Well cemented, brown-yellowish sorted sandstones (mU-cU) with bioturbation (Skolithos). Internally massive with sharp lower and upper boundaries	Camarasa	Distributary Channels	Deltaic Nearshore Environment	<ul style="list-style-type: none"> <li>Potential palaeosols (cf. Chapter 3 and logs CAa/CAb, Appendix)</li> <li>dm-m scale cross-bedding</li> </ul>	Above FWWB ~0-10 m	
	NS2	Bedded, poorly consolidated sandstones with internal cross-bedding	Bedded, Few cm to dm in thickness	Internal metre-scale cross-bedding with clay drapes, pebble stringers, rip-up clasts, bioturbation (Ophiomorpha).	Camarasa	Mouth Bars				
	NS3	Wavy bedded marls and calcareous marls with angular quartz pebbles	Structureless, up to few metres in thickness	Mostly wavy bedded, 10s metre thick units. Occasional intercalations of NS4. Moderately common coarse and angular quartz pebbles. Rare shell fragments	Camarasa	Delta Front				
	NS4	Quartz-rich bioclastic grainstones and packstones	Decimetre-thick beds intercalated into NS3	Poorly sorted and poorly rounded grainstones and packstones, with quartz grains up to pebble in size. Allochems include shell fragments, miliolid foraminifera and peloids	Camarasa	Prodelta? Carbonate-Siliciclastic Mixing Zone				
Coarse grained sandstones and grainstones with rudist debris	PI1	Coarse grained bioclastic sandstones and quartz-rich grainstones with coarse rudist debris	200 m to 2.1 km wide bodies (mean = 1 km). Control on dip dimensions unavailable.	Sharp lower and upper boundaries, poor sorting. Coarse rudist debris amongst other bioclasts. Bioturbation (Skolithos and Thalassinoides)	Oliana	Reworking of lagoonal sediments and introduction of clastic material	Platform Interior	<ul style="list-style-type: none"> <li>Rare cross-bedding in siliciclastic dominated lithologies</li> <li>Abundant small benthic foraminifera</li> <li>Micritic envelopes in grain-dominated facies</li> </ul>	Above FWWB ~0-10 m	
Dark nodular wackestones with foraminifera and rudist biostromes	PI2	Nodular wackestones/packstones with abundant benthic foraminifera		Dark nodular limestones, abundant benthic foraminifera, occasional small shell fragments. Rare silt-grade quartz.	Oliana	Lagoonal background sedimentation				
	PI2b	Thin in-situ rudist bafflestone sheets		20-30cm thick sheets of densely packed small in-situ rudists	Oliana	Thin rudist patch reefs within lagoon				
Rudist biostromes, coarse rudist limestones, and fine peloidal and bioclastic limestones	PI3	Quartz-free peloidal grainstones and packstones	No data; outcrop limits <200m. Potentially similar dimensions to PI4	Sharp lower boundary, gradational upper boundary, exceptionally well sorted, fine grained bioclasts	Oliana	Platform interior shoals/bars				
	PI4	Rudist wacke/pack/float/rud/boundstones	1.5 km to 4.1 km wide bodies (mean = 2.59 km). Control on dip dimensions unavailable.	Nodular to wavy appearance. Coarse rudist debris and in-situ rudists. Occasional in-situ corals. Few fine grained angular quartz grains. Benthic foraminifera.	Oliana	Large-scale lagoonal patch reefs				
Rudist and coral bioherms, biostromes and bedded bioclastic limestones	PM1	Massive mixed coral-rudist boundstones	Forming bioherms of up to 6m thickness, 10s of metres wide	In situ corals and rudists. Wackestone matrix with fine shell fragments, planktonic foraminifera and rare calcispheres. Small amounts of silt-grade quartz.	Collades de Basturs, Montagut Gully, Carreu River	Barrier-type bioherms	Platform Margin	<ul style="list-style-type: none"> <li>Rudist-Coral bioherms (estimated up to 20m depth depending on wave energy; Sanders, 1998)</li> <li>Abundant micritic envelopes</li> <li>Large-scale cross-bedding</li> </ul>	Mostly above FWWB, possibly reaching to below FWWB ~5-15 m	
	PM2	Bedded, rudist-debris dominated grainstones and packstones	Dm-scale beds shedding off the bioherms of PM1.	Bedding on dm-scale. Mostly rudist and coral debris, peloids. Various degrees of rounding.	Collades de Basturs, Montagut Gully, Carreu River	Reef Talus of PM1				
	PM3	Sheet-like coral-rudist-sponge beds	Up to 3-4 m thickness and large lateral extent (<100 m)	Decimetre-scale beds of in-situ corals rudists, and sponges	Montagut Gully	Initial colonisation of bioconstructing organisms				
	PM4	Slender hippuritid frameworks	Up to 5-6 m thickness and large lateral extent (<100 m)	Elongated hippuritid rudists forming dense frameworks. Wackestone matrix with small shell fragments and rare silt-grade quartz.	Collades de Basturs, Montagut Gully, Carreu River	Biostromes in protected backreef environment				
Cross-bedded, quartz bearing bioclastic grainstones and packstones	PM5	Quartz-bearing grainstones and packstones, few 10s metres-scale cross-bedded	Laterally extensive units, few m thick, with internally few 10s of metre wide clinofolds	Well sorted, clean, peloid and foraminifera bearing grainstones with quartz grains at the topsets of clinofolds. Poorly sorted bioclastic packstones with abundant quartz at the bottomsets of clinofolds	Collades de Basturs, Montagut Gully, Carreu River	Platform margin grain/packstone shoal complexes				
Nodular wackestones, marls, patch reefs and packstone intercalations	(eroded deposits of this lithofacies)	US1	Nodular wackestones with foraminifera and shell fragments	Up to several 10s metres thick packages, uncommon foraminifera and shell fragments	Collades de Basturs, Montagut Gully, Carreu River	Upper slope background sedimentation	Upper Slope	<ul style="list-style-type: none"> <li>Frequent presence of solitary cunolites corals, interpreted as living as deep as 20-25 m (Sanders and Höfling, 2000; Sanders and Baron-Szabo, 2008)</li> <li>Periodic intercalations interpreted as storm deposits due to increased sorting and reduced micrite contents, (implying above SWB; Sanders and Pons, 2001)</li> </ul>	Below FWWB, Periodic influence of SWB given ~15-25 m	
		US1b	Rudist and coral boundstones within nodular wackestones (PM5)	<2 metres in diameter, up to 1 m thick.	In-situ corals and rudists	Collades de Basturs, Montagut Gully				Small-scale patch reefs on the upper slope
		US2	Thinly-bedded silty marls with solitary cunolites corals		Thinly bedded, common solitary cunolites corals	Carreu River				Siliciclastic-influenced upper slope
	US3	Foraminifera dominated packstones		Up to few metre thick packages intercalating into PM5. Decimetre-scale internal bedding. Small benthic foraminifera	Montagut Gully, Carreu River	Storm-beds below FWWB				
Pelagic wackestones and debris flows	SL1	Pelagic calcareous wackestones and calcisiltites		Thinly to platy bedded. Featuring sponge spicules and planktonic foraminifera	Tamurcia	Lower slope deposits	Lower Slope	<ul style="list-style-type: none"> <li>Sponge spicules</li> <li>Dominance of planktonic foraminifera</li> </ul>	Considerably below SWB ~100 m	
	SL2	Debris flow deposits with clasts originating from the platform margin	Width estimated at few 100 s metres. No control on length.	Pelagic mud-supported debris flow deposits with clasts up to metre in size. Erosive lower boundaries and gradational or sharp top boundaries	Tamurcia	Debrites from platform margin failure				

Table 3.8: Lithofacies scheme for the Bastus Carbonate Platform. White dashes in lithofacies US1-US3 indicate presumed eroded strata. The two far right columns provide an overview of water depth indicators and estimated water depths for individual gross depositional environments, their facies, and the respective locality. References for water-depth indicators are given in the appropriate case. Where no reference is given, the estimates given by Flügel (2010) are applied. GDE = Gross Depositional Environment.

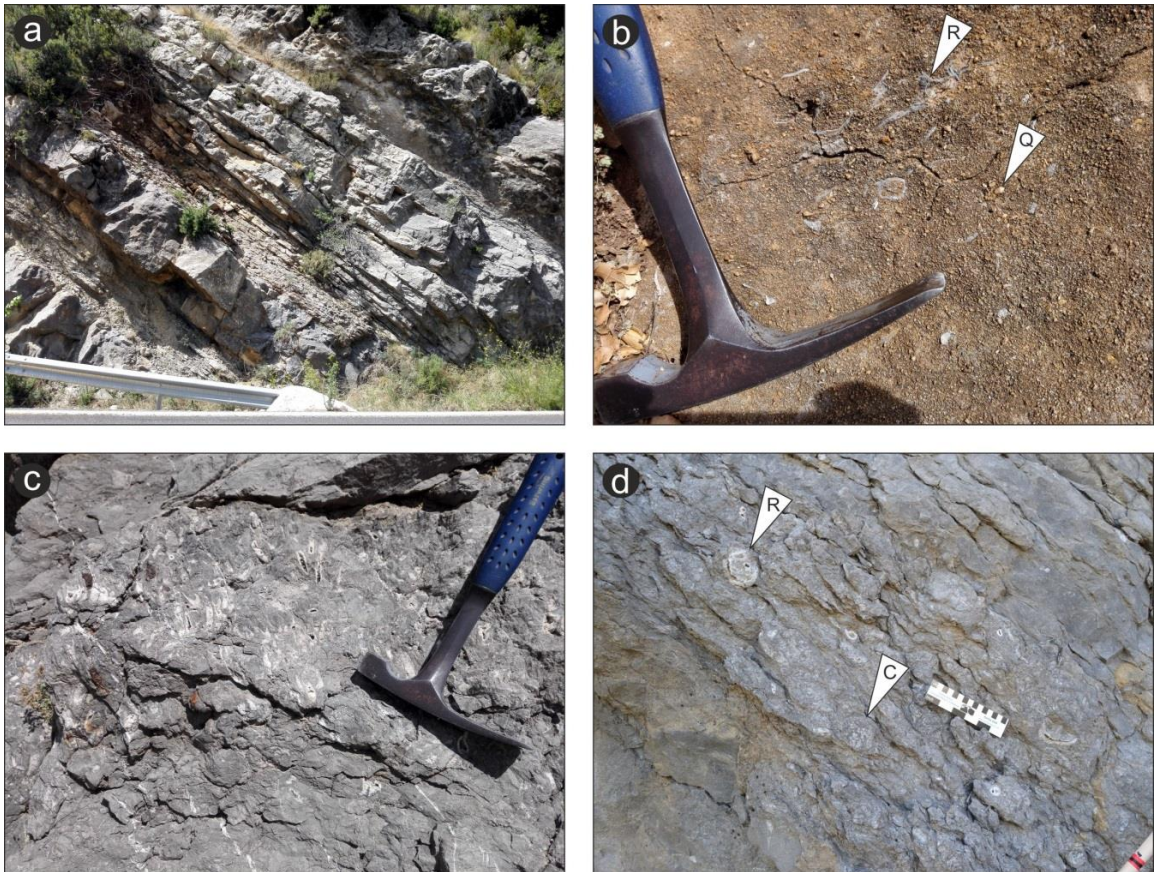


**Plate 3.12: Outcrop photographs of the platform interior lithofacies association (PI) of the Bastus Platform.**

**a:** overview photograph showing intercalations of prominent, massive to banked sandstone of the lithofacies PI1 and grainstone beds intercalated into recessive and bedded to nodular wackestone beds of the lithofacies PI2, PI3 and PI4. Note the gradational transitions from the limestone beds into the sandstone and grainstone units and the sharp upper boundaries of the sandstones and grainstones. Width of the image: ca. 9 metres.

**b:** detail photograph showing coarse quartz pebbles (Q) and rudist debris (R) within the quartz rich grainstones of lithofacies PI2. Hammer head for scale.

**c:** detailed view of the rudist bafflestone sheets of lithofacies PI2b.

**d:** rudist floatstone and rudstone bed of lithofacies PI4. Note large and intact rudists (R) and corals (C). Scale bar in cm and inches.

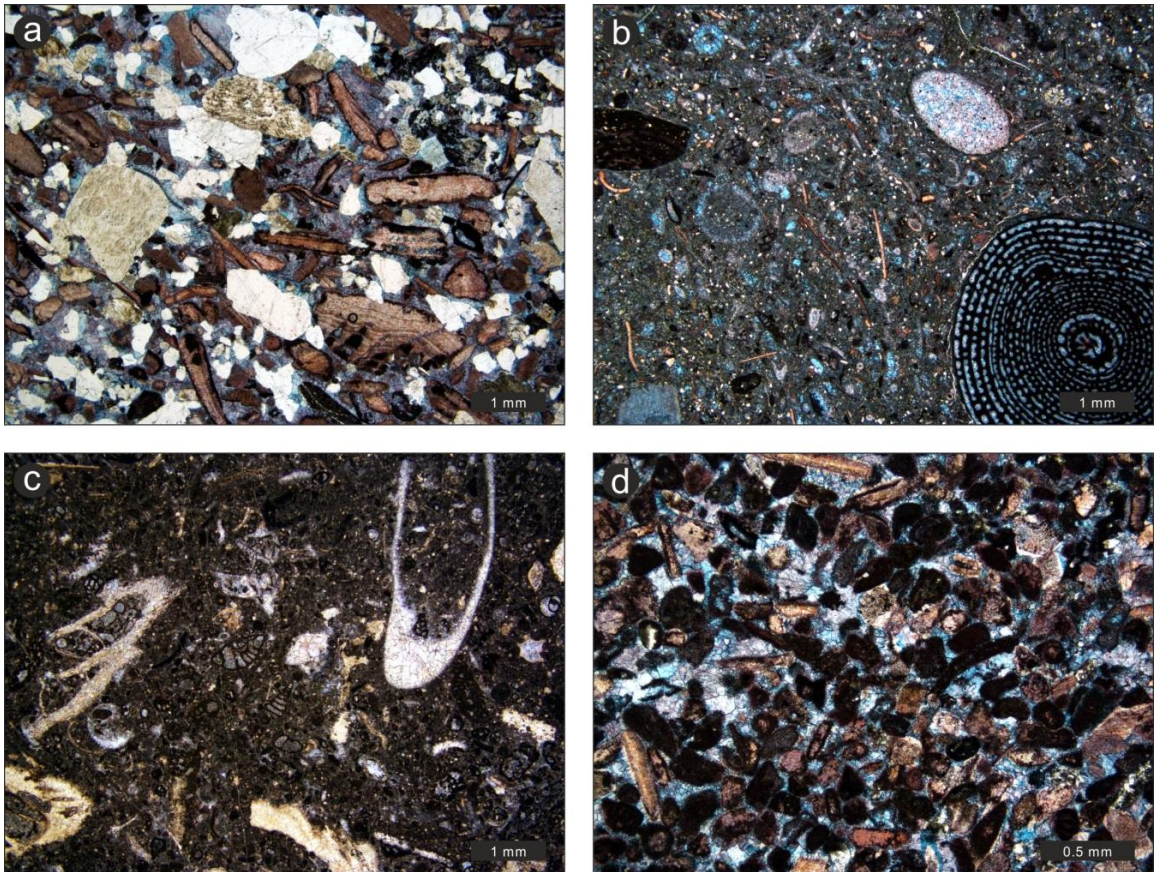


**Plate 3.13: Photomicrographs of selected samples from the platform interior lithofacies association (PI) of the Bastus Platform.**

**a: lithofacies PI1. Quartz rich bioclastic grainstone. Note cementation by calcite spar, poor sorting, and slight rounding on carbonate allochems. Quartz grains are mostly angular, while other siliciclastic grains may be sub-angular to sub-rounded.**

**b: lithofacies PI2. Abundant fine grained shell fragments, as well as occasional peloids and very fine grained quartz grains. Selective mouldic dissolution resulted in minimal amounts of porosity. Note the large benthic foraminifera of the genus *Lacazina* in the bottom right corner.**

**c: Rudist floatstone to rudstone of lithofacies PI4. Large rudist shell fragments are partially selectively dissolved and cemented by calcite spar (upper right), whereas others are preserved. Other components include small benthic foraminifera and other shell fragments.**

**d: lithofacies PI3. Well sorted peloidal grainstone showing ferroan cement in the intergranular spaces. Other grains include moderately rounded rudist shell fragments and echinoid fragments. Note the good sorting and the very low amount of quartz grains.**

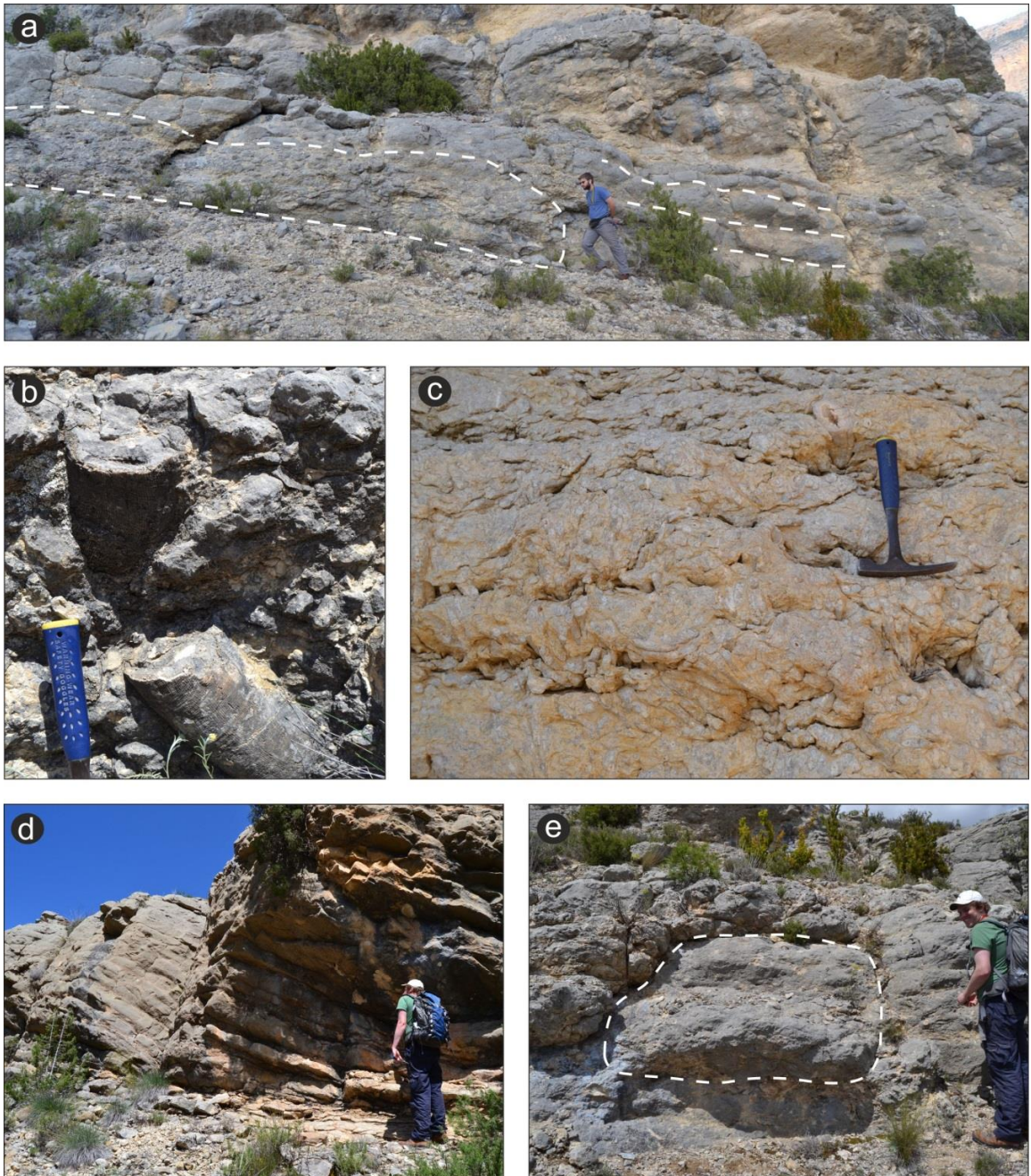


**Plate 3.14: Outcrop photographs of the Bastus Platform Margin (PM) and Upper Slope (US) lithofacies associations.**  
**a:** overview image of rudist-coral boundstone buildup (lithofacies PM1) and onlapping bedded rudist grainstones (lithofacies PM2). Outlines of the buildup and bedding surfaces are highlighted with dashed lines.  
**b:** detailed view of rudist-coral boundstone (Lithofacies PM1). Two large rudists are clearly visible, protruding out of the easily weathered micritic matrix. Hammer handle for scale.  
**c:** detailed view of the slender hippuritid frameworks of lithofacies PM4. Note the large amount of delicate rudists and the preferential orientation of individuals in a uniform direction.  
**d:** large-scale cross-bedding within lithofacies PM5. Note the bedding surfaces highlighted through differential weathering  
**e:** Small-scale patch reef found within lithofacies US1, highlighted with dashed lines.

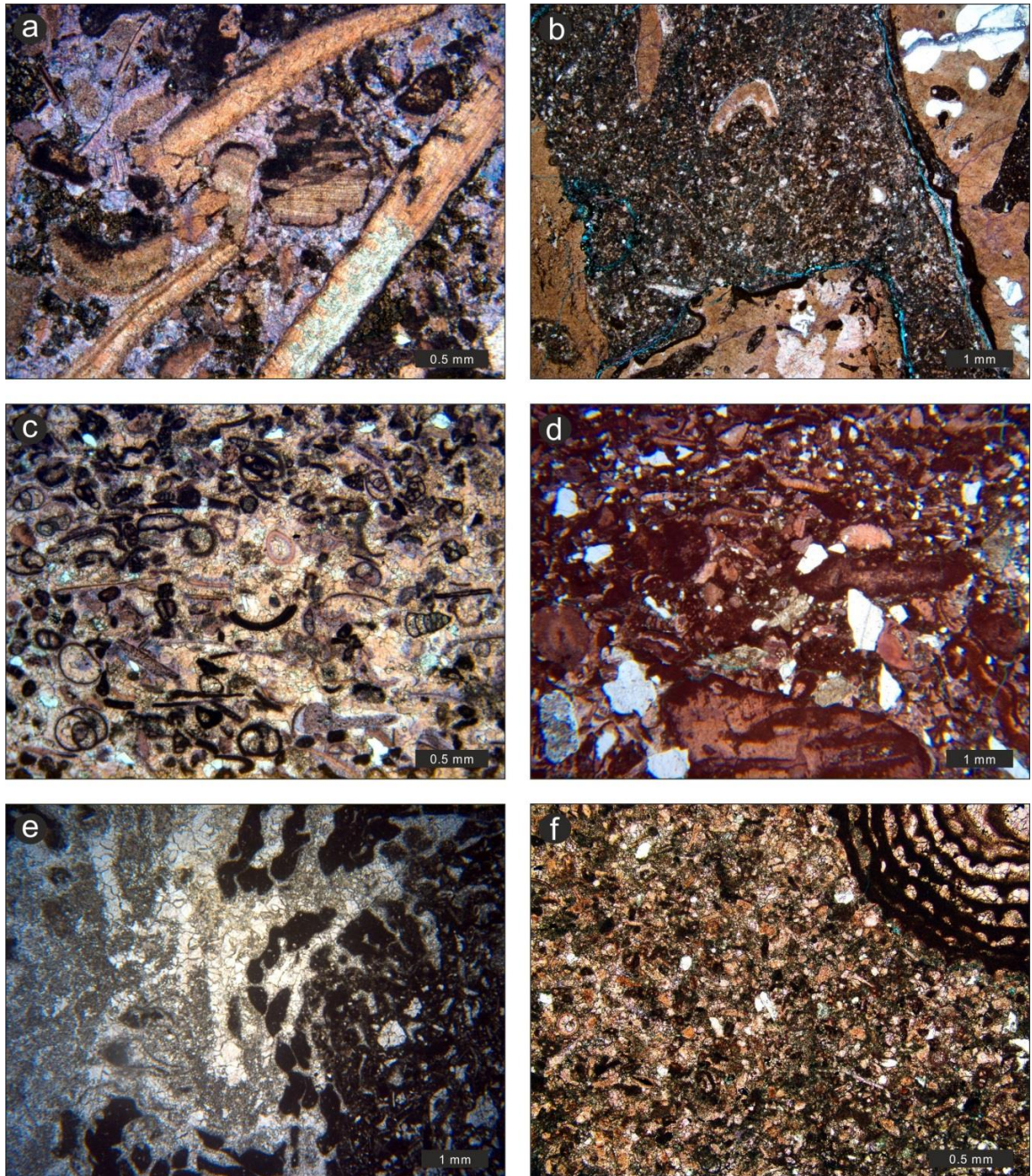


Plate 3.15: Photomicrographs illustrating the Bastus Platform margin (PM) and upper slope (US) lithofacies association.

a: Example of a rudist dominated grainstone of Lithofacies PM2. Note large rudist shell fragments with rounded edges. The intergranular space is cemented by ferroan calcite spar. Silification of a rudist shell can be observed in the bottom right of the image.

b: Rudist framework and filling matrix of Lithofacies PM4. The matrix filling the spaces between rudists is mostly fine grained, and shows few larger shell fragments. It also contains a small amount of silt-grade quartz. Silification of the rudist skeletons is apparent in the right side of the image.

c: Example from the topsets of a grainstone clinof orm of Lithofacies PM5. The rocks show a grainstone texture and are dominated by well sorted shell fragments, small benthic foraminifera and peloids. Fine grained quartz grains are rare.

d: Example from the bottomsets of a grainstone clinof orm of Lithofacies PM5. The packstones are dominated by poorly sorted and well-rounded rudist shell fragments, as well as poorly sorted and angular quartz grains.

e: View of a coral skeleton from a patch reef within lithofacies US1b. The coral skeleton (left side of the image) is surrounded by fine grained wackestone matrix with fine grained shell fragments (right, equivalent to lithofacies PM5).

f: Fine grained packstone from Lithofacies US3. The fine grained components include small skeletal fragments, peloids and occasional small benthonic foraminifera. Small amounts of quartz are also present. In the top right part of the image, a partial section of a large benthic foraminifera from the genus *Lacazina* is seen.



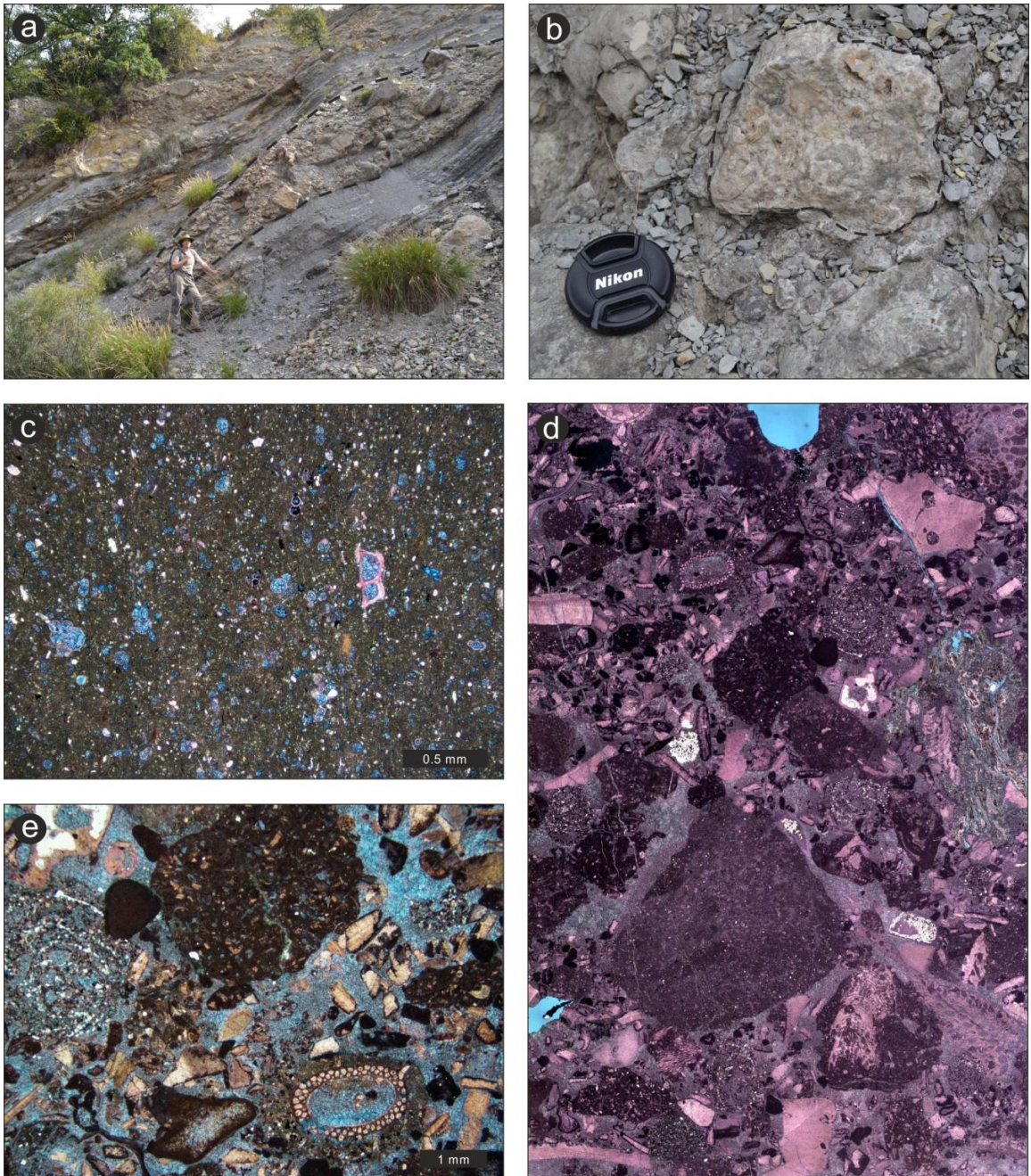


**Plate 3.16: Outcrop images and photomicrographs of the slope and basal lithofacies of the Bastus Platform.**

**a:** incising debrite bed (lithofacies SL3) into the thinly bedded mudstones of SL2. Note the outcrop is overturned. Bedding surfaces are highlighted with dashed lines. The lower boundary of the debrite bed is erosive and cuts into the stratigraphically underlying mudstones, whereas the upper boundary is conformable. Person for scale.

**b:** platform margin clast located within one of the debrite horizons of lithofacies SL3 (outlined with dashed lines). Note the tightly clustered hippuritid rudists similar to lithofacies PM4 (slender hippuritid frameworks). Lens cap for scale.

**c:** basal wackestone from lithofacies SL2. Most common organisms are calcispheres and planktonic foraminifera, as well as some small sponge spicules. Silt grade quartz grains are common. Note the intragranular pore space within pelagic organisms is cemented with ferroan calcite spar.

**d:** Debrite (lithofacies SL3) with matrix (SL2). Note the mixture of angular and rounded debrite clasts, as well as their varied sorting and lithological nature. Width of image 2.5 cm.

**e:** Detailed view of grainstone debrite clast found in lithofacies SL3. The grainstone is cemented with ferroan calcite spar. Note the high variety of organisms, as well as predominantly good rounding. A large extraclast consisting of fine grained bioclastic packstone is found in the top centre of the image. Bioclasts include slightly rounded rudist shell fragments, small and large foraminifera, with the latter being an agglutinating form, as well as bryozoans.

### 3.9.3 Architecture

Through the cross-section and study of lithofacies, the Bastus Platform is interpreted as a rimmed platform with a low angle slope. The platform top measures ca. 45-50 km, with a platform margin zone of ca. 5 km in width that marks the platform break. The slope then extends over at least 14 km, but total length is unknown due to limited exposure. Based on the exposure of the Upper Cretaceous in the area (Figure 3.1), a length of more than 115 km is presumed. Using the water depth estimates (Table 3.8) and the distances between these platform elements, a platform top angle of  $<0.05^\circ$  and a slope angle of  $<0.5^\circ$  are determined.

As with the previous platform cycle, there are some non-linear variations in thickness observed along the cross-section transect. The proximal sandstones are much thinner (ca. 60 m) than the lagoonal packstones (300-400 m). Moreover, there is a slight decrease in thickness of the platform margin succession at the northern Sant Corneli Anticline (Carreu river, 296 m) when compared to the south of the Anticline, further palaeo-landward (Collades de Basturs, 478 m; and Montagut Gully, 435 m). The thickness of the basinal deposits is 378 m (Tamurcia).

There are a number of indicators for platform trajectory in the Bastus sediments. The dip-section at Montagut shows a rough northward direction of the margin. The rudist biostromes in the back-margin at Collades and Carreu are interpreted to be oriented away from the northward margin (Gili, 1993; Vicens et al., 1998). In Collades, Sanders and Pons (2001) interpret several directions of slope dip, with a combined northward direction. At Carreu, the grainstone shoal clinoforms are dipping towards the north-northeast.

### 3.9.4 Distribution of Terrigenous Material

A general reduction of siliciclastic content is seen from the platform top towards the basin (Figure 3.5). Variability of siliciclastic content is high, within the platform interior (Montsec/Oliana; 0.33% and 53.00%). Quartz content is the highest in the nearshore environments (Modal Analysis: average 49.52%, XRD: 41.08%), but remains present in small percentages throughout the rest of the platform (between 16.22% and 2.91% on average), with a slight increase occurring again in the basin (average 9.50%; XRD data). Muscovite shows similar distribution throughout the platform, but also slightly higher concentrations in the basin. Kaolinite and Microcline are found almost exclusively in the nearshore and platform interior, with minor amounts of microcline also found in the margin. Clinocllore is restricted solely to the basinal areas.

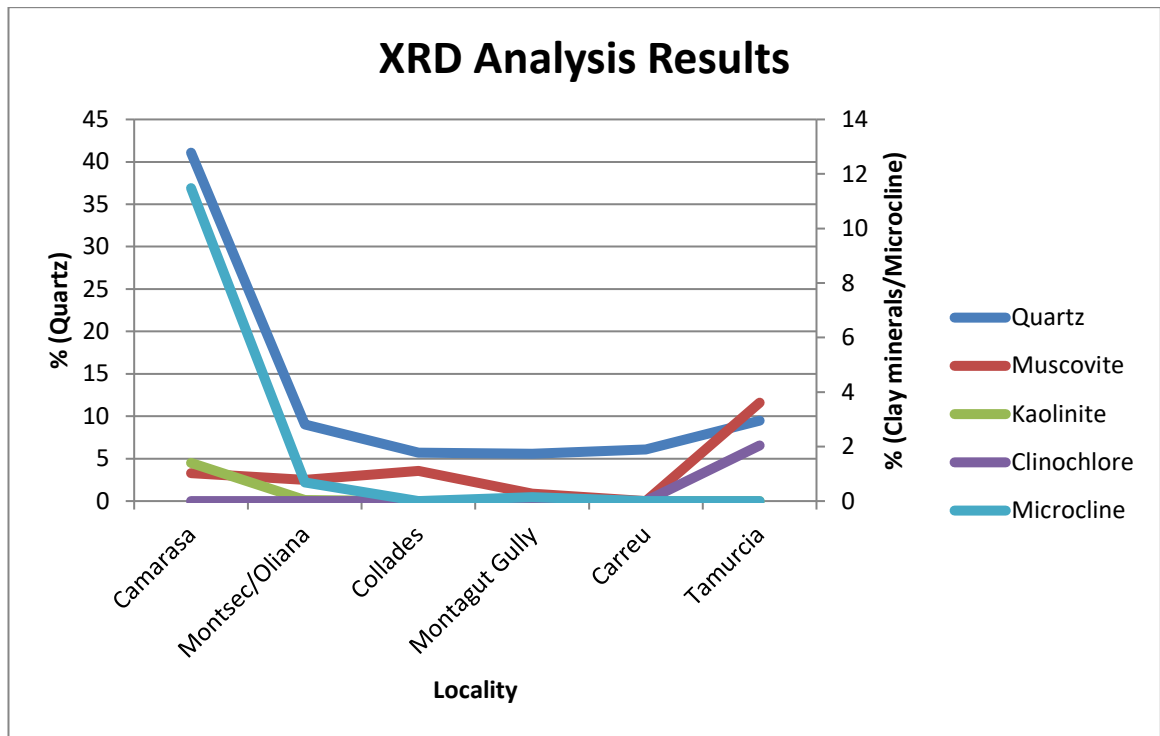


Figure 3.5: Cross-Plot of quartz, clay minerals and microcline contents within the localities of the Bastus Platform. The localities represent a transect of the platform from the proximal environments (Camarasa), over the platform interior (Montsec/Oliana), the platform margin (Collades, Montagut Gully, Carreu), and into the basin (Tamurcia).

### 3.10 Lower and Upper Terradets Platforms

The Terradets Platforms (referred to as Vallcarga-6 and Vallcarga-7 by Simó, 1993, and others) are of early to mid-Campanian age. They are interpreted to represent the maximum marine transgression during the Cretaceous and have a complex internal progradation pattern (Simó, 1993). The lower boundary of the Lower Terradets Platform is a prominent flooding surface in the platform interior, which also shows minor siliciclastic influx and dolomitisation. On the shelf, shallow water platform deposits are prominent. The platform interior limestones represent a lagoonal environment, with mudstone textures and rudists, and bioturbated fine grained wackestones-packstones interbedded with quartz-rich beds. In the platform margin, the facies exhibit very thick bedded to massive bioclastic grainstones-floatstones with rudist reefs, showing abundant rudists, coral fragments, and peloids. Molluscs, bryozoans, red-algae and echinoderm fragments are common. The upper slope is characterised by fine-grained calcareous marls and clays, and deep-water mudstones in the basin with siliciclastic turbidites.

An exposure surface forms the lower boundary of the Upper Terradets Limestones. The upper boundary is characterised by siliciclastic influx and angular unconformities near anticlines on the platform top, which are interpreted to be the result as the beginning of the Alpine thrusting (Simó, 1986, 1989). The platform top shows lacustrine mudstones with abundant charophytes (Pocovi, 1978), lagoonal, well-bedded to massive mudstone with rudists, bioturbated nodular wackestones and packstones with quartz-rich interbeds. The margin is characterised by bedded

to massive bioclastic grainstones and floatstones with rudist reefs and quartz grains define the platform margin facies.

### 3.11 Discussion

The review of stratigraphy and architecture of the Cenomanian to Santonian carbonate platforms of the Tremp area allows defining the main controls acting during their development. This discussion will first review the variations of the eustatic sea level during that time, in order to assess how this may have impacted the development of the carbonate platforms in the area. Following this, the platforms will be discussed chronologically, and the main controls on the basin development will be framed. Lastly, a discussion of carbonate productivity and transport and siliciclastic influx will be presented in light of the evolution of the basin.

#### 3.11.1 Global Sea Level Variations

Global sea level fluctuated significantly over the course of the Upper Cretaceous (Kominz et al., 2008). It rose to a highstand during the mid-Cenomanian to early Turonian, after which it fell sharply in the late Turonian and reached a low-point at the base of the Coniacian. From here, it rose gradually to the top of the Santonian, reaching a second highstand in the Campanian. Assuming sea level fluctuations to be the only control on platform evolution, a pattern of progradation (highstand), subaerial exposure (rapid sea level drop) and repeated gradual progradation or later aggradation (transgression and highstand) is expected.

Comparing the stacking patterns and key surfaces between platforms and within each platform yields mixed results. On a regional scale, the platforms clearly react to the changes in eustatic sea level in several ways: The unconformable surface between the uppermost Jurassic and the Cenomanian Santa Fe platform in the south of the Study area provides evidence of an abrupt rise in relative sea level to the highstand during Cenomanian and Turonian. The erosional hiatus occurring in the Montsec area between the Pradina and the Sant Corneli Platforms is clear evidence of the sharp eustatic sea-level drop at end-Turonian times. Later sea level fluctuations at platform boundaries are far less radical, leading to conformable and generally sharp contacts throughout the platform interiors and margins, and more transitional boundaries in basinal areas. The successive retrogradation of the Congost, Sant Corneli and Bastus platforms can be seen as a result of the net sea level rise between the Cenomanian and Santonian. Exceptions of the conformable contacts may exist, as seen in the lower boundary of the Sant Corneli basinal deposits, which show an angular unconformity (Institut Cartogràfic i Geològic de Catalunya, 2012), that is however attributed to fault-related margin failure (Drzewiecki and Simó, 2000, 2002).

The reviewed chronostratigraphic time scale shows a large amount of small-scale (<1 My) sea level oscillations within each platform. Assigning these small-scale oscillations to distinct developments within each platform cycle proves difficult. In this new correlation, at least 4 sea level oscillations are present within both the Santa Fe and Pradina Platforms. These cannot be clearly attributed to the lower and upper Santa Fe limestones, although these two are interpreted by Drzewiecki and Simó (2000) as the result of relative sea-level variations. Furthermore, Drzewiecki and Simó (2000) interpret a drowning of the Pradina platform as a result of a relative rise in sea level following the Santa Fe platform. Again, no distinct sea-level rise is recognisable in the revised chronostratigraphic framework at that time. Similarly, the interpretation of Simó (1993) of the Santa Fe and Pradina each representing a 3<sup>rd</sup> order sea level cycle is not immediately evident in the revised time scale, although it was proposed as such on the basis of field observations and in isotopic signatures (Soriano, 1992; Caus et al., 1993; Booler, 1994).

Within the late Turonian to early Coniacian, two phases of relative stillstand are observed, with the first at a higher sea level than the second. These can be allocated to the A and B sequences of the Congost Platform, respectively. During the first phase, stability in eustatic sea level and low accommodation space have led to progradation of the Congost A margin, resulting in the clinoform geometries observed in Gallinove. The sea level drop after this is represented by the deposition of the Congost B sequence as a lowstand wedge farther to the North. During this period, sea level was again stable, leading to internal prograding sigmoidal architecture of the coral boundstones. As such, the large-scale eustatic sea level trends are well preserved within the basin, in form of erosional unconformities, a lowstand wedge, and gradual backstepping of the platforms.

### **3.11.2 Platform Architecture and Development**

The combination of field observations, facies analysis and cross-sections (Figure 3.4) allow interpreting the broad architecture and trajectory of each platform (Table 3.9) and evaluating the subsidence experienced by each platform across the proximal-basinal transect (Table 3.10). Furthermore, the results allow defining the controls exerted by eustatic sea-level fluctuations, regional and local tectonic processes, carbonate productivity and siliciclastic input on platform development and resulting architecture. These are discussed for each platform in the following.

**Table 3.9: Summary of platform characteristics and dimensions.** Presented in brackets are references for specific values. The inclination of specific platform segments is calculated based on the distance between the two reference points (i.e. shoreline, platform break, toe of slope), and the interpreted water depth range for the lithofacies at that locality. The platform trajectory is determined via dip-directions of sedimentary structures (i.e. clinoform dip directions and orientation of build-ups).

Platform/Sequence	Architecture	Platform top Width	Platform Top inclination	Platform Margin Zone width	Margin inclination	Slope width	Slope inclination	Trajectory
Santa Fe	Rimmed platform	> 26.5 km	0.02°	4.5 km	14° (Drzewiecki and Simó, 2002)	?	?	Northwest/West (Soriano, 1993; Caus et al., 1993; Simó, 1993)
Pradina	Pelagic drape	-	-	-	-	-	-	?
Congost A	Rimmed platform	<23 km	<0.05°?	> 500 m?	Up to 21°	> 8 km	0.6° (Booler, 1994)	North-Northwest
Congost B	Rimmed lowstand wedge	<2 km?	<0.05°?	< 200 m	Up to 31°	> 8 km	0.6° (Booler, 1994)	North
Sant Corneli	Distally steepened ramp	> 36.6 km	<0.02°?	-	-	> 25 km	0.15-0.3°	Northwest?
Bastus	Rimmed platform	> 27.7 km	<0.05°	5-6 km	-	> 14.1 km	<0.5°	Northeast?

**Table 3.10: Overview of sediment thickness (calculated from the cross-section, Figure 3.4) and subsidence rates derived from these based on the duration of each platform (cf. Figure 3.3) along the data points from the cross-section (Left: proximal, right: distal. Numbers refer to Figure 3.1 and Figure 3.4). Cells shaded in grey represent the approximate area of the platform margin. Subsequently localities to the left are more proximal (platform top) and localities to the right of this are more distal (slope). For the Santa Fe, notable are the low thicknesses and subsidence rates on the platform top, and increased values at the margin and basin. Note that the Pradina Formation (duration of 3 My) was not included, however the thicknesses reported for the Santa Fe may include this formation as well, resulting in possible overestimation of subsidence rates. For the Congost, notable is a gradual increase of values between Isona and Barranc d'Espugafreda, followed by a drastic drop from Tamurcia northwards. Notable for the Sant Corneli is a gradual increase towards the basin, with a slight drop in Isona, and a substantial increase of values in Tamurcia. In the Bastus platform, a non-linear profile is observable. Notable is the intermittent decrease in values in Isona (platform top) and Carreu River (far platform margin).**

Platform name and duration	Value	1) Camarasa	2) Figuerola	3) Montsec	4) Isona	5) Collades de Basturs	6) Montagut Gully	7) Carreu River	8) Barranc d'Espugafreda	9) Tamurcia	10) Barranc de Miralles	11) Serra de Sant Grevas
Santa Fe (3 My)	Sediment thickness (m)	0	0	98	47	33	31	31	145	135	300	349
	Subsidence rate (m/My)	0	0	33	16	11	10	10	48	45	100	116
Congost (3 My)	Sediment thickness (m)	0	0	0	89	135	138	155	65	59	43	38
	Subsidence rate (m/My)	0	0	0	30	45	46	52	22	20	14	13
Sant Corneli (2.4 My)	Sediment thickness (m)	0	17	294	88	321	327	323	443	1005	62	-
	Subsidence rate (m/My)	0	7	123	37	134	136	135	185	419	26	-
Bastus (3 My)	Sediment thickness (m)	62	65	420	298	473	438	296	200	271	-	-
	Subsidence rate (m/My)	21	22	140	99	158	146	99	67	90	-	-

### **Santa Fe Platform**

The Santa Fe platform developed a flat platform top with bioclastic wackestones and abundant foraminifera, terminating at a margin dominated by rudist and coral-build-ups that showed a steep slope (up to 14°). Next to nodular wackestones, the slope is further characterised by periodic debris flow deposits. The steep slope and debris flow are accepted to be the result of fault activity in the area of Sopeira (Caus et al., 1993; Simó, 1993; Booter, 1994). Reactivation during the later stages of the Pyrenean orogeny has led to a thrust in this area showing overturned strata (Institut Cartogràfic i Geològic de Catalunya, 2015).

Eustatic sea level was at a high, and remained fairly stable for the duration of this platform. Together with the low sediment thickness on the platform top it is possible to conclude that rate of sedimentation in this area was low compared to the margin. Progradational features described by Simó (1993) at the platform margin and basin imply that sedimentation rates were higher in this area. This is also evident in the sediment reaching higher thickness than in the platform interior. Furthermore, siliciclastic contents are negligible and do not show discernible effects on carbonate productivity.

In the Platform Interior, the deposits of the Santa Fe platform show a twofold character: the bottom half of the succession is bedded and nodular, whereas the top half is predominantly massive with faint bedding surfaces on metre scale. Sediment composition remains similar, with textures showing as rudist fragment wackestones and packstones with occasional *Praealveolina*. The two facies are reported to be separated by a sharp bored surface across the platform interior (Drzewiecki and Simó, 2000), and previous authors have correlated this surface with a negative carbonate  $\delta^{13}\text{C}$  anomaly of ca. 4‰ across the basin (Caus et al., 1997; Drzewiecki and Simó, 1997). This indicates that a pronounced change in carbonate productivity occurred. There is no evidence in the eustatic sea-level curve of Kominz et al. (2008) for a significant eustatic event, which implies that a different mechanism may have led to this change in productivity. No distinct tectonic event is known during the duration of the Santa Fe Platform, and no distinct increase in siliciclastic contents is observed, which is why an oceanographic control on the change in productivity is suggested.

### **Pradina Platform**

Throughout the majority of the study area, the Pradina Platform shows nodular and massive wackestones and rare packstones, interpreted to have been deposited on a slope. These are dominated by calcispheres, and show small amounts of echinoid and rudist shell fragments. Only in the very south are skeletal grainstones reported (Caus et al., 1993).

The pelagic-dominated lithology and the uniform thickness of the Pradina Platform throughout the study area leads to these deposits being interpreted as a pelagic drape, deposited onto the previous topography during a significant change to carbonate productivity. This interpretation was previously suggested by several authors (Caus et al., 1993; Simó, 1993; Boole, 1994; Drzewiecki and Simó, 2000) and is agreed with here. Drzewiecki and Simó (1997, 2000) show that this coincides with a positive organic  $\delta^{13}\text{C}$  anomaly of 3‰ and suggest this change is the result of a cessation of benthonic productivity and deposition of pelagic carbonate following the Turonian Oceanic Anoxic Even (OAE). As eustatic sea level remains largely unchanged since the previous Santa Fe platform (Kominz et al., 2008), this is most likely triggered by a change in ocean circulation at the time. In the basin, the fault that controlled the Santa Fe margin continued to shape the seafloor, where frequent slumping features are reported (Drzewiecki and Simó, 2002). Apart from this, no major tectonic influence is observed.

### **Congost Platform**

The Congost A formed a flat-topped platform with margin formed by large-scale, steeply dipping (up to 21°) packstone and grainstone clinofolds. It follows a eustatic sea-level drop at the beginning of the Coniacian. Despite this eustatic sea-level drop, which is expected to result in a basinward migration of the margin, the margin is located further south (palaeo-landwards) than the margin of the older Santa Fe platform. This implies an underlying control of regional subsidence, triggered by the increasing compression of the basin. This confirms the differential subsidence as a controlling mechanism as previously proposed by Simó (1993). The eustatic sea-level drop, however, does manifest itself in subaerial exposure in the most southern parts of the field area, which lead to an unconformity in the area of the Montsec Range, where the Coniacian strata are missing. Overall, the sediment thickness is greater than in previous platforms, and a progradational nature is clearly observed in the margin packstone/grainstone clinofolds. These are attributed to high productivity on the platform top, with bioclastic material being periodically transported outwards by high energy events to form an infralittoral prograding wedge (cf. Hernández-Molina et al., 2000).

The Congost B is interpreted to form a lowstand wedge further basinward of the previous Congost A margin, which is limited to a few kilometres in width and exhibits a flat top with a steeply inclined margin (up to 31°). This is interpreted to be the result of the eustatic sea-level drop occurring in the late Coniacian (Kominz et al., 2008), forcing the margin basinwards. A change in the nature of the margin can be observed: It is no longer formed by packstone/grainstone clinofolds, but is shaped by sigmoidal and progradational/aggradational corallgal build-ups. This development may be linked to possible environmental changes following the eustatic sea-level drop. This may include changes in oceanic current patterns,



oxygen levels or nutrient levels. It is unlikely that net carbonate productivity rates were significantly reduced during the Congost B as opposed to the Congost A, as a similar thickness of sediment was deposited during a roughly similar period of time (cf. Figure 3.4). However, it is likely that less sediment was produced on the platform top, so that sediment transport off-platform and the formation of prograding clinofolds did not take place in the Congost B. Furthermore, total sediment thickness of ca. 70 metres at the margin of the Congost B indicates generation of accommodation space, while the corallgal build-ups and lagoonal factories were able to keep up, as recognised by the aggradational-progradation trends in the margin build-ups (Chapter 5). Lastly, siliciclastic contents are still restricted to minor amounts of silt-grade quartz, which show little to no effect on carbonate productivity or the platform architecture as a whole.

### **Sant Corneli Platform**

The proximal areas of the Sant Corneli Platform are characterised by siliciclastic input, whereas the platform interior shows a complex facies mosaic of lagoonal sediments. The margin areas show bedded coral and rudist rudstones and floatstones with some in-situ producers, as well as some reworked and well-sorted grainstones. Further basinwards, fine-grained wackestones and packstones dominate, transitioning into marls with debris flow deposits in the basin-most parts. The platform shows no distinct shelf break, and is thus interpreted to represent either a distally steepened ramp or a flat-topped platform with a shallow dipping slope. The inner and intermediate areas of the ramp are situated further southwards in relation to the older Congost A and B margins.

The backstepping of the platform is attributed to the net rise in eustatic sea level during this platform phase in relation to the previous Congost A. As the margin now rests on the flat lagoonal deposits of the Congost A, the lack of underlying topography leads to the lack of a pronounced platform break. In the mid-ramp areas, there is an upward facies change from nodular wackestones and packstones with intercalations of packstones and grainstones (lithofacies MR1), interpreted to be deposited below FWFB and above SWB, towards bedded coral and rudist rudstones, floatstones and boundstones (lithofacies MR2), interpreted as margin facies above FWFB. This change can be interpreted as a modest progradation of the platform. As eustatic sea level is on a modest rise during this time (Kominz et al., 2008), the mechanism is expected to lie either in keep-up of sediment productivity or localised tectonic processes. The effects of local subsidence are evident in the uneven increase in sediment thickness along the proximal-distal transect (Table 3.10). In the area of Isona, the sediment column is thinner than in the more proximal Montsec area, implying more accommodation was available in the latter.

A notable change in dominant carbonate factory is present between the underlying Congost B and the Sant Corneli Platform, with a community of rudists and corals returning to be the main producers at the platform margin during this phase. However, this development cannot be directly tied to the observed changes in sea level, regional, or local tectonics. Additionally, while siliciclastics are much more common in the proximal parts of the platform, these do not appear to have a significant influence on carbonate productivity, with total sediment thicknesses being higher than in the previous platform stages. Lastly, the debris flows described in the most basinal areas by Booler (1994) imply a local steepening of the slope. The previous mechanism proposed by this is a reactivation of the fault in the area of Sopeira (Booler, 1994; Drzewiecki and Simó, 2002).

In the basinal environment, the triggering of the Sant Corneli breccia (described by Booler, 1994; and Drzewiecki and Simó, 2002) seems likely to be in response to local tectonic processes, as opposed to eustatic sea level control, due to the general stability of eustatic sea level during that time. This would be caused by continuation of the fault activity that dominated the shape of the margin during the previous Santa Fe and Pradina Platforms (Drzewiecki and Simó, 2002), which is interpreted by Booler (1994) to be the main driving mechanism here, and fits such processes through the lithological descriptions of the breccia.

### **Bastus Platform**

The Bastus Platform is interpreted to have exhibited a flat platform top ( $<0.05^\circ$ ) with a gently dipping margin ( $<1^\circ$ ). The proximal parts are characterised by deltaic siliciclastic sequences, followed by nodular foraminiferal wackestones, reworked bioclastic-rich sandstones, quartz-bearing grainstones, and rudist biostromes in the platform interior. The margin shows composite rudist and coral build-ups, whilst the upper slope is dominated by fine-grained nodular wackestones deposited below FWWB. In the lower slope and basin, thinly bedded calcisiltites are intercalated with debris flow deposits that are composed of remobilised material from the margin.

The continuing rise of eustatic sea level during the Santonian (Kominz et al., 2008) has pushed the margin further south relatively to the older platforms. Overall, the platform margin is interpreted here to exhibit an aggradational behaviour, which was also previously suggested by Simó (1993). This aggradation is seen as the consequence of the net eustatic sea-level rise during the duration of this platform. Despite this aggradational trend, the platform margin sediments in the area of the Sant Corneli anticline are interpreted to be internally composed of several shallowing-upward successions, each between 50 and 100 metres in thickness. These begin with nodular, fine grained wackestones at the bottom, interpreted as upper slope deposits (US1 and US2), and transitioning upwards into massive and bedded coral and rudist

build-ups, rudist biostromes and bedded bioclastic grainstones and packstones (PM1-4), interpreted to represent composite margin build-ups. These small progradational successions cannot be tied into the smaller-scale fluctuations of eustatic sea level during the duration of this platform (Chapter 4). The control therefore may lie in self-organisation of the carbonate factory, rather than an underlying control of sea level on productivity (for example as demonstrated by Burgess and Wright, 2003).

The cross-section of the Bastus Platform shows that the margin area originally exhibited the quartz-bearing grainstones and packstones (PM5), possibly forming shoal bodies. The platform margin build-up lithofacies association (PM1-4) only established later in the platform lifespan (Figure 3.4). The mechanism for this development is discussed in detail in Chapter 4. It is suggested that the later occurrence of the composite build-ups is the result of a catch-up of carbonate productivity and proper establishment of a margin. In the earlier stages, however, the low-angle inherited underlying topography from the Sant Corneli Platform was the control for the development of platform margin shoals and lack of margin build-ups. With the increase in relative sea level later during the Santonian, more favourable conditions for the formation of a rudist-dominated margin were given, and the platform break became more pronounced with the establishment of these rudist build-ups.

The Bastus Platform shows the thickest sediment accumulation of all studied platforms, while maintaining an aggradational to retrogradational behaviour. This indicates that sediment productivity has reached a peak, and the rise of eustatic sea level was key in generating the required accommodation space for the deposition of these sediment volumes in an aggradational/retrogradational fashion. The nonlinear thickness profile across the proximal-distal transect is interpreted to be the result local differential subsidence (cf. Table 3.10). In the area of the northern Sant Corneli Anticline (Carreu River), the platform margin succession is thinner than in the south of the Anticline (Collades de Bastus and Montagut). This is interpreted to be the result of the syndepositional growth of the Sant Corneli Anticline (cf. Figure 3.4), which was shown to have initiated in early Santonian times (Drzewiecki et al., 2014; Markley et al., 2014).

The Bastus Platform shows a clear differentiation of carbonate factories along its profile. The platform interior shows thick successions of dark nodular wackestones dominated by benthic foraminifera, with occasional intercalations of rudist biostromes. At the margin, composite build-ups show an architecture defined by wave energy: massive coral-rudist bioherms act as a seaward barrier, with monospecific rudist biostromes forming in the protected backreef environment. These variations of the carbonate producing communities along the platform is interpreted as the result of environmental conditions favouring different organisms; rudist

biostromes and benthic foraminifera thrived in the low energy and shallow platform interior, whereas corals formed a rigid framework in the high-energy and slightly deeper platform margin. With the development of the Bastus Platform, this differentiation led to modest variation of the platform topography, forming a flat platform top ( $<0.05^\circ$ ) and a gentle platform break leading to a low-inclination slope ( $<1^\circ$ ). The cross-section of the Bastus Platform however shows that initially no distinct margin build-up facies were present. This implies that the final shape of the platform only developed later during the Santonian, and that the initial inherited topography from the Sant Corneli platform led to no pronounced margin break being present.

Of the platforms studied, the Bastus Platform shows the highest amounts of siliciclastic sediment. The long-term effects of siliciclastic input are considered minimal. As observed in the field, the rudist biostromes of the platform interior are quick to recover after the short and periodic events of sand influx. The overall increase in siliciclastic contents is attributed to the increasingly compressional nature of the basin, and the associated rise of the hinterland resulting in higher amounts of hinterland erosion. The dominant palaeoclimatic conditions may have also contributed to this episodic nature of siliciclastic input, mechanisms such as flash-flooding are known to frequently occur in dry arid climates and periodically introduce large amounts of siliciclastics into marine settings (Friedman, 1988). A correlation of individual periods of high siliciclastic influx with fluctuations of the eustatic sea level is unlikely. This is due to the unpredictable lateral migration of delta lobes, which may not necessarily be triggered by sea-level changes, but may be autogenic (Patrino et al., 2015).

Furthermore, since no exposure surfaces are observed on the platform margin successions, the debris beds introducing platform margin material into the basin are recognised to be controlled by a mechanism other than sea-level variation. Instead, the debris flows are either the result of oversteepening and instability of the margin, or triggered by the fault activity in the area of Sopeira, which was active until Campanian times (Drzewiecki and Simó, 2002).

### **3.11.3 Main Controls on Basin Development**

The observation of mechanisms controlling the development of the individual carbonate platforms allows defining to which extent they affected the development of the whole basin over the investigated time-span. The recalibration of platform intervals to the geological time scale (Gradstein et al., 2012) and eustatic sea-level fluctuations (Kominz et al., 2008) shows that each platform was on the order of 2-4 Ma. This coincides with the interpretation of Simó (1993), who proposed that each platform represents a 3<sup>rd</sup> order sea level cycle. However, key correlatable surfaces within each platform are difficult to define. It is possible to recognise higher order cyclicity affected by eustatic sea level in some cases, such as within the lowstand

wedge of the Congost B. This can be interpreted into the eustatic sea level curve of Kominz et al. (2008), as demonstrated in Section 3.11.2. Yet, it becomes clear that there are a number of additional possible controls on sedimentation. In the following, the developments evident in the stratigraphic record over the investigated time-span are used to interpret the controls basin evolution.

The slope breaks of younger platforms are observed to have moved southwards (palaeo-landwards) successively. This development is attributed mainly to the net eustatic sea-level rise between the Coniacian and Campanian, and is also influenced by the increasing subsidence rates in the area starting late Turonian-early Coniacian times that follow the oncoming compression of the basin. Additionally, the platform deposits thicken and the margin relief becomes less pronounced with each successive platform phase. This is interpreted to be the results of both net eustatic sea-level rise and increased local subsidence, as well as the stepwise retrogradation of the margins away from the fault system in the area of Sopeira, which dominated the margin shape of the previous platforms. Furthermore, productivity in the platform interior areas increases in later platform stages, as opposed to the productivity being concentrated around the margin in the older platforms. As a result, the more equal sediment productivity along the platform profile reduced the slope break.

It is observed that the platform deposits thicken with each successive cycle (Figure 3.4), particularly in the interior and margin areas. As with the stepwise regression of the margin, this is thought to have resulted from increased accommodation space due to increased subsidence rate. The net rise in eustatic sea level may also have had a significant contribution to this development. This development coincides with the platform margin relief becoming less pronounced during the course of the platform cycles. While the Santa Fe to Congost platforms shows a pronounced margin, later platform margins have a more gentle relief. This development is linked to the stepwise regression of the shelf with each platform cycle, thus lying on the flat previous platform top and inheriting less topography to form a more pronounced margin. Additionally, the platforms move further away from the fault system in the area of Sopeira that dominated the Santa Fe platform margin, but persisted into the early Santonian (Drzewiecki and Simó, 2002). Subsequently, this fault system shows less influence on the margin shape, but maintains an effect on the basinal sedimentation, as shown by the frequent fault-related debrites, reworking of older sediment through an escarpment, next to debrites resulting from margin failure through oversteepening, as defined by Drzewiecki and Simó (2002) on the basis of the textures of the debrites.

Observation of facies changes throughout the field area, in combination with reported sediment transport directions by other authors suggests that platform margins were often not linear lines.

Abundance of debris flows of both concurrent platform margin material and resedimented older strata, directed towards the northwest in the area of Sopeira (Caus et al., 1993; Boler, 1994; Drzewiecki and Simó, 2000, 2002) indicate that from Cenomanian and Santonian a localised depocentre may have formed here. This is possibly due to a normal fault that was active in the area between the Cenomanian and Campanian (Drzewiecki and Simó, 2000), and later inverted, leading to extensive overturning of the strata (Institut Cartogràfic i Geològic de Catalunya, 2015). In the east, northwards of the Sant Corneli anticline, facies transitions imply lack of a prominent margin breaks, and debrites are absent (Institut Cartogràfic i Geològic de Catalunya, 2010).

It is further observed that the trajectory of the platform margins changes over the course of the Upper Cretaceous. In the Santa Fe platform, it is roughly northwestwardly directed, and rotates towards the northeast during Coniacian-Santonian time. Afterwards, it possibly returns to a westward orientation. This change is most likely attributed to localised tectonics controlled by the counter clockwise rotation of Iberia and the convergence with the European plate (Puigdefàbregas and Souquet, 1986). However, it was found that some trajectory indicators are not necessarily indicative of the overall platform axis, such as with the grainstone shoal clinofolds formed at the Bastus Platform Margin, oriented slightly obliquely to the margin due to parallel currents (Chapter 5). Similarly, the localised depocentre in the area of Sopeira may have added significant bias to the definition of the platform trajectory. Therefore, it is suggested that a more comprehensive investigation of slope direction indicators would be necessary to properly identify the evolution of the platform trajectories over time.

#### **3.11.4 Source, Distribution, Mechanisms and Effect of Siliciclastic Input**

An increase in siliciclastic contents is observed over the studied time-span. Only traces of siliciclastics are noted in the Santa Fe, Pradina and Congost Platforms, whilst there are evidence of persistent siliciclastic systems in the nearshore environments of the Sant Corneli and Bastus Platforms. Furthermore, siliciclastic material is introduced in larger amounts onto the platform tops of these platforms. The large-scale mechanism for this is presumed to lie in the rise of the hinterland and the larger amounts of erosion that are associated with the increasing compression of the basin and the onset of the Pyrenean orogeny. Nevertheless, the platform top factories seem largely unaffected, as displayed by the presence of platform interior rudist build-ups. These could establish as the siliciclastics were only introduced further into the platforms in rare events (cf. Chapter 4).

While the provenance of the siliciclastic material was not studied in detail, the prevalence of angular, monocrystalline quartz grains, as well as the presence of microcline implies a possible

granitic source. Palaeogeographic reconstructions (Plaziat, 1981) show the major landmass south of the basin being the Ebro Massif, which has previously been suggested to be the source of siliciclastics at that time (Hoorn, 1970; Evans and Arche, 2002). Siliciclastic sources located in the east and north of the basin are also suggested between the terminal Cretaceous and the mid Eocene (Roige et al., 2014; Gómez-Gras et al., 2016). Subsequently, an axial supply of clastics into the basin during earlier times cannot be ruled out without more detailed provenance studies.

Overall, terrigenous material becomes more abundant in the younger platform stages; quartz grains are rare on the platform tops of the Santa Fe, Pradina and Congost platforms, and clay minerals occur to some extents in their basins. In the Sant Corneli and Bastus Platforms, quartz is abundant in the most proximal areas, and appears concentrated locally in bioclastic facies along the platform interior and margin. Clay minerals are found on both the platform top and in the basin. This upward increase in siliciclastic material is unlikely triggered by an eustatic sea-level fall, as eustatic sea level is rising towards the end of the Cretaceous (Kominz et al., 2008). Instead, it is interpreted to be directly linked to increased uplift in the hinterland, and progressing reduced proximity to the main southern sediment source – the Ebro Massif – via the convergence of the Iberian and European plate (Puigdefàbregas and Souquet, 1986; Evans and Arche, 2002; Roige et al., 2014). The continuation of this trend is evident in sedimentary environments turning to coastal plains during the Maastrichtian and finally to fluvial-dominated in the Danian (Gómez-Gras et al., 2016).

In the Sant Corneli and Bastus Platforms, where the siliciclastics are most common, they are not distributed equally throughout the platform. Siliciclastics dominate the proximal parts, implying input occurs persistently through deltaic systems. In the platform interior it is enriched in discrete horizons with erosive or sharp lower boundaries in the platform interior, showing coarse grain sizes, varying sorting, and exclusively angular grains. These indicate sudden and fast input of sediment, which was not transported over long periods of time. Clastics are introduced into the platform interior on a periodic basis, after which carbonate production resumes rapidly. Periodic flash floods are proposed mechanisms for such siliciclastic transport in the recent carbonate systems of the Red Sea, where corals persist to thrive despite periodic introduction of sand-grade quartz (Friedman, 1988).

Siliciclastics are found in small concentrations in the platform margin and basin, concentrated preferentially in the bioclastic packstone and grainstone facies, where they only account to 5-10% of the sediment. The drastic decrease of terrigenous contents towards the platform margins indicates that siliciclastic sediment transport was not strong enough to move a large amount of grains offshore. Only small quantities of fine-grained material were moved gradually.

This is further suggested by a reduction in grain size of clastics at the platform margin, causing and enrichment of sand-grade material on the platform top.

In the platform interior, siliciclastic dominated sediments often sharply overly rudist biostromes. Up-section, the siliciclastic dominated sediments transition once more into rudist biostromes and floatstones. This implies that the introduction of siliciclastic beds did not inhibit carbonate productivity for prolonged periods. At the margins, siliciclastics are restricted to the bioclastic facies altogether, where they only occur in minor amounts, while rudist and coral build-ups do not interact with them directly. This implies that the introduction of siliciclastics did not have a long-term impact on carbonate productivity. Rudist bivalves, which are the dominant carbonate producing macrofauna in these systems, have a high tolerance to terrigenous input of both fine and coarse grain sizes (Friedman, 1988). In the margin, it is suggested that terrigenous material followed the topography of the carbonate build-ups and had little direct effect on their development, as has been previously described by Santisteban and Taberner (1988).

The proposed mechanism of siliciclastic input through flash-flooding is typical for arid climatic conditions (Friedman, 1988), and thus agreed with the previously interpreted subtropical and semiarid to arid palaeoclimate (Nagtegaal, 1972). However, Booler (1994) argued arid to humid conditions through stable oxygen and carbon isotope signatures and diagenetic features. The association of clay minerals found in this study does not allow a decisive interpretation of palaeoclimate. Kaolinite was found in the proximal areas, which may be associated to weathering of aluminosilicates under semi-humid to humid conditions (Emery et al., 1990). However, the presence of chlorite and absence of kaolinite shown in the basinal areas was previously attributed to arid conditions by Nagtegaal (1972). With the diagenetic study of Booler (1994) not being tested, it would require a more extensive study of both clay minerals and isotopic signatures to accurately reconstruct palaeoclimate.

### 3.12 Conclusions

- The Cenomanian-Santonian carbonate Platforms of the Tresp area established in a partially restricted seaway between the Iberian and European plate over a period of ca. 14 My.
- The platforms are interpreted to coincide with 3<sup>rd</sup> order cycles of eustatic sea level (on the order of 2-4 Ma) after a recalibration of the regional chronostratigraphy to the revised time-scales of Gradstein et al. (2012) and the eustatic sea-level curve of Kominz et al. (2008). While it is possible to recognise higher order cyclicity affected by eustatic sea level in some cases, such as within the lowstand wedge of the Congost B, it becomes clear that there are a number of additional possible controls on sedimentation



- Boundaries between platforms can be tied to the eustatic sea level fluctuations described by Kominz et al. (2008), which are on the order of 2-4 Ma. These were interpreted as 3<sup>rd</sup> order sea level fluctuations by Simó (1993), and are shown here to be of appropriate duration and magnitude.
- The slope breaks of younger platforms moved successively further south. This is predominantly due to rise in eustatic sea level between the Coniacian and Campanian (Kominz et al., 2008) and subsidence starting in the late Turonian/early Coniacian, following the increasingly compressional nature of the basin (Simó, 1993).
- The platform deposits thicken and the margin relief becomes less pronounced with each successive platform phase. This is attributed to net eustatic sea level rise and increasing local subsidence, as well as retrogradation of the margin away from the fault system near Sopeira that dominated the margin shape of the older platforms.
- Siliciclastic contents increase gradually throughout the studied time-interval. This is associated with the rise of the hinterland and increased erosion.
- The trajectory of the Platform margins begins as roughly north-westward, rotating to north and north-eastward during Coniacian-Santonian times, and then possibly returns to westwards from the Campanian. This is attributed to localised tectonics resulting from the shift towards a compressional basin.
- Several tectonic and structural elements have had a significant effect on the evolution of the basin. This includes persistent fault activity in the basinal areas, as well as variable subsidence rates across the platforms leading to effects such as subaerial exposure of proximal environments and differential thickness.
- The dominant organisms changed several times over the course of the Upper Cretaceous in the area. Corals and rudist generally coexisted on the platform top, while the margin associations changed as a direct reaction of the organisms to the architecture of the shelf, rather than carbonate production actively shaping the large-scale topography of the platform. Global environmental conditions retained a large control on the dominant organism type, as seen in the Pradina Platform.

Internally, the architecture and development of each platform was affected to different degrees by eustatic sea-level variations, by regional subsidence, tectonic interactions and by environmental influences:

- The Santa Fe platform shows a thin platform top and a rimmed margin with a steep slope. It is the result of low sedimentation on the platform top, with faulting exerting a strong control on the margin shape.

- The Pradina Platform forms a comparably thin and mostly evenly thick layer of pelagic sediment across throughout all but the southernmost parts of the study area. It is interpreted as a pelagic drape following the OAE between the Cenomanian and Turonian, leading to a stop in shallow water carbonate production.
- The Congost Platform is split into an early progradational phase with a pronounced margin, followed by the formation of a lowstand wedge in a second phase. Former is the result of initial eustatic sea-level lowstand, with low accommodation space leading to progradation, and followed by another sea-level drop and an increase in local subsidence.
- The Sant Corneli Platform shows little topography and no substantial shifts in facies belts. A slightly thicker platform interior succession implies regional subsidence has occurred.
- The Bastus Platform shows a thicker succession in the platform interior than in the margin. This is once more attributed to increased subsidence in that area. Furthermore, thickness variations around the platform margin area are the effect of syndepositional growth of the Sant Corneli anticline. The presence of multiple internal sequences is possible, but could not be tied to eustatic sea-level fluctuations. Similarly, no eustatic control on siliciclastic input is suggested.

The sedimentary evolution of the Tremp Basin provides an excellent example to the multitude of complex regional and local controls on carbonate systems. Elements of sea level fluctuation, large-scale and localised tectonic processes, and the interlinked subsidence and changes in both carbonate productivity and siliciclastic input all contributed towards the architecture of the platforms. This complexity highlights the importance of considering various control mechanisms during interpretation of sedimentary systems in foreland basins such as this, but also in other settings where only some of the discussed controls may occur. It particularly shows that the application of sequence stratigraphic models based on only on relative sea-level fluctuations in such settings should be done with caution.

### 3.13 References

- Albrich, S., G. Frijia, M. Parente, and E. Caus, 2014, The evolution of the earliest representatives of the genus *Orbitoides*: Implications for Upper Cretaceous biostratigraphy: *Cretaceous Research*, v. 51, p. 22–34, doi:10.1016/j.cretres.2014.04.013.
- Boix, C., G. Frijia, V. Vicedo, J. M. Bernaus, M. Di Lucia, M. Parente, and E. Caus, 2011, Larger foraminifera distribution and strontium isotope stratigraphy of the La Cova limestones (Coniacian–Santonian, “Serra del Montsec”, Pyrenees, NE Spain): *Cretaceous Research*, v. 32, no. 6, p. 806–822, doi:10.1016/j.cretres.2011.05.009.
- Booler, J. P., 1994, Carbonate facies, sequences and associated diagenesis, Upper Cretaceous, Tremp Basin, Spanish Pyrenees: Durham University, 317 p.
- Booler, J., and M. E. Tucker, 2002, Distribution and geometry of facies and early diagenesis: the key to accommodation space variation and sequence stratigraphy: Upper Cretaceous Congost Carbonate platform, Spanish Pyrenees: *Sedimentary Geology*, v. 146, no. 3–4, p. 225–247, doi:10.1016/S0037-0738(01)00120-8.

- Burgess, P. M., and V. P. Wright, 2003, Numerical Forward Modeling of Carbonate Platform Dynamics: An Evaluation of Complexity and Completeness in Carbonate Strata: *Journal of Sedimentary Research*, v. 73, no. 5, p. 637–652, doi:10.1306/020503730637.
- Catuneanu, O., W. E. Galloway, C. G. S. C. Kendall, A. D. Miall, H. W. Posamentier, A. Strasser, and M. E. Tucker, 2011, Sequence Stratigraphy: Methodology and Nomenclature: *Newsletters on Stratigraphy*, v. 44, no. 3, p. 173–245, doi:10.1127/0078-0421/2011/0011.
- Caus, E., J. M. Bernaus, E. Calonge, and J. Martín-Chivelet, 2009, Mid-Cenomanian separation of Atlantic and Tethyan domains in Iberia by a land-bridge: The origin of larger foraminifera provinces? *Palaeogeography, Palaeoclimatology, Palaeoecology*, v. 283, no. 3–4, p. 172–181, doi:10.1016/j.palaeo.2009.09.019.
- Caus, E., A. Gómez-Garrido, A. Simó, and K. Sofiano, 1993, Cenomanian-Turonian platform to basin integrated stratigraphy in the South Pyrenees (Spain): *Cretaceous Research*, v. 14, no. 4–5, p. 531–551, doi:10.1006/cres.1993.1038.
- Caus, E., C. Llompart, J. Rosell, and J. M. Bernaus, 1999, El Coniacense superior-Santonense inferior de la Sierra del Montsec (Pirineos, NE de España): *Revista Sociedad Geológica de España*, v. 12, p. 269–280.
- Caus, E., M. Parente, V. Vicedo, G. Frijia, and R. Martínez, 2013, *Broeckina gassoensis* sp. nov., a larger foraminiferal index fossil for the middle Coniacian shallow-water deposits of the Pyrenean Basin (NE Spain): *Cretaceous Research*, v. 45, p. 76–90, doi:10.1016/j.cretres.2013.08.002.
- Caus, E., A. Teixell, and J. M. Bernaus, 1997, Depositional model of a Cenomanian-Turonian extensional basin (Sopeira Basin, NE Spain): interplay between tectonics, eustasy and biological productivity: *Palaeogeography, Palaeoclimatology, Palaeoecology*, v. 129, no. 1–2, p. 23–36, doi:10.1016/S0031-0182(96)00051-X.
- Choukroune, P., 1992, Tectonic Evolution Of The Pyrenees: *Annual Review of Earth and Planetary Sciences*, v. 20, no. 1, p. 143–158, doi:10.1146/annurev.earth.20.1.143.
- Drzewiecki, P. A., and J. A. Simó, 1997, Carbonate Platform Drowning and Oceanic Anoxic Events on a Mid-Cretaceous Carbonate Platform, South-Central Pyrenees, Spain: *Journal of Sedimentary Research*, v. Vol. 67, no. 4, p. 698–714, doi:10.1306/D426861C-2B26-11D7-8648000102C1865D.
- Drzewiecki, P. A., and J. A. Simó, 2002, Depositional processes, triggering mechanisms and sediment composition of carbonate gravity flow deposits: examples from the Late Cretaceous of the south-central Pyrenees, Spain: *Sedimentary Geology*, v. 146, no. 1–2, p. 155–189, doi:10.1016/S0037-0738(01)00171-3.
- Drzewiecki, P. A., and J. A. Simó, 2000, Tectonic, eustatic and environmental controls on mid-Cretaceous carbonate platform deposition, south-central Pyrenees, Spain: *Sedimentology*, v. 47, no. 3, p. 471–495, doi:10.1046/j.1365-3091.2000.00286.x.
- Drzewiecki, P. A., J. Vergés, L. Markley, and J. Olandt, 2014, Evidence for Syntectonic Growth of a Santonian Carbonate Platform on the Sant Corneli Anticline, South-Central Pyrenees, Spain, *in* 49th Annual Meeting of the Geological Society of America.
- Dunham, R., 1962, Classification of carbonate rocks according to depositional texture, *in* W. E. Ham, ed., *Classification of Carbonate Rocks: AAPG Memoir 1: Tulsa, OK, AAPG*, p. 108–121.
- Elliott, T., 1986, Deltas, *in* H. G. Reading, ed., *Sedimentary Environments and Facies: Oxford, Blackwell*, p. 615.
- Embry, A. F., and J. E. Klovan, 1971, A Late Devonian reef tract on northeastern Banks Island, NWT: *Bulletin of Canadian Petroleum Geology*, v. 19, no. 4, p. 730–781.
- Emery, D., K. J. Myers, and R. Young, 1990, Ancient subaerial exposure and freshwater leaching in sandstones: *Geology*, v. 18, no. 12, p. 1178, doi:10.1130/0091-7613(1990)018<1178:ASEAFL>2.3.CO;2.
- Evans, G., and A. Arche, 2002, The flux of siliciclastic sediment from the Iberian Peninsula, with particular reference to the Ebro: *Geological Society, London, Special Publications*, v. 191, no. 1, p. 199–208, doi:10.1144/GSL.SP.2002.191.01.14.
- Flügel, E., 2010, Recognizing Paleoenvironmental Conditions, *in* *Microfacies of Carbonate Rocks: Berlin, Heidelberg, Springer Berlin Heidelberg*, p. 587–640, doi:10.1007/978-3-642-03796-

- Friedman, G. M., 1988, Case Histories of Coexisting Reefs and Terrigenous Sediments: The Gulf of Elat (Red Sea), Java Sea, and Neogene Basin of the Negev, Israel, *in* L. J. Doyle, and H. H. Roberts, eds., *Developments in Sedimentology V42: Carbonate-Clastic Transitions*: p. 77–97, doi:10.1016/S0070-4571(08)70165-1.
- Gallemí, J., R. Martínez, and J. M. Pons, 1983, Coniacian - Maastrichtian of the Tresp Area (South Central Pyrenees): *Newsletters on Stratigraphy*, v. 12, no. 1, p. 1–17.
- Gallemí, J., R. Martínez, and J. M. J. Pons, 1982, Unidades del Cretácico superior en los alrededores de Sant Corneli (Provincia de Lleida): *Cuadernos de Geología Ibérica*, v. 8, p. 935–948.
- Gallemí Paulet, J., 1992, Los yacimientos con equínidos del Cretácico superior del Prepirineo de la provincia de Lleida.: *Universitat Autònoma de Barcelona*, 428 p.
- Gili, E., 1993, Facies and Geometry of les Collades de Basturs Carbonate Platform, Upper Cretaceous, South-Central Pyrenees, *in* J. Simo, R. W. Scott, and J.-P. Masse, eds., *Cretaceous Carbonate Platforms: AAPG Memoir 56*: Tulsa, OK, AAPG, p. 343–352.
- Gili, E., E. Vicens, A. Obrador, P. W. Skelton, and G. Lopez, 1996, Las formaciones de rudistas de la plataforma de sant corneli (cretacico superior, unidad central surpirenaica): *Revista Española de Paleontología*, p. 172–181.
- Gili, E., E. Vicens, and T. Steuber, 2008, The stratigraphical position of the rudist formations of the Sant Corneli anticline, southern central Pyrenees, based on strontium isotope analysis of the hippuritid rudist shells, *in* *Eighth International Congress on Rudists*, June 23-25, 2008, Izmir, Turkey: p. 22.
- Goldhammer, R. K., P. A. Dunn, and L. A. Hardie, 1990, Depositional cycles, composite sea-level changes, cycle stacking patterns, and the hierarchy of stratigraphic forcing: Examples from Alpine Triassic platform carbonates: *Geological Society of America Bulletin*, v. 102, no. 5, p. 535–562, doi:10.1130/0016-7606(1990)102<0535:DCCSLC>2.3.CO;2.
- Gómez-Gras, D., M. Roigé, V. Fondevilla, O. Oms, S. Boya, and E. Remacha, 2016, Provenance constraints on the Tresp Formation paleogeography (southern Pyrenees): *Ebro Massif VS Pyrenees sources: Cretaceous Research*, v. 57, p. 414–427, doi:10.1016/j.cretres.2015.09.010.
- Gradstein, F. M., G. Ogg, and M. Schmitz, 2012, *The Geologic Time Scale 2012 2-Volume Set*: elsevier.
- Gradstein, F. M., J. G. Ogg, and A. G. Smith, 2004, *A geologic time scale 2004*: Cambridge University Press.
- Haq, B. U., J. Hardenbol, and P. R. VAIL, 1987, Chronology of Fluctuating Sea Levels Since the Triassic: *Science*, v. 235, no. 4793, p. 1156–1167, doi:10.1126/science.235.4793.1156.
- Hardenbol, J., J. Thierry, M. B. Farley, T. Jacquin, P.-C. De Graciansky, and P. R. Vail, 1998, Mesozoic and Cenozoic Sequence Chronostratigraphic Framework of European Basins, *in* P.-C. de Graciansky, J. Hardenbol, T. Jacquin, and P. R. Vail, eds., *Mesozoic and Cenozoic Sequence Stratigraphy of European Basins: SEPM (Society for Sedimentary Geology)*, p. 3–13, doi:10.2110/pec.98.02.0003.
- Hernández-Molina, F. J., L. M. Fernández-Salas, F. Lobo, L. Somoza, V. Díaz-del-Río, and J. M. Alveirinho Dias, 2000, The infralittoral prograding wedge: a new large-scale progradational sedimentary body in shallow marine environments: *Geo-Marine Letters*, v. 20, no. 2, p. 109–117, doi:10.1007/s003670000040.
- Hollis, C., 2011, Diagenetic controls on reservoir properties of carbonate successions within the Albian-Turonian of the Arabian Plate: *Petroleum Geoscience*, v. 17, no. 3, p. 223–241, doi:10.1144/1354-079310-032.
- Hoorn, V., 1970, Sedimentology and paleogeography of an Upper Cretaceous turbidite basin in the south-central Pyrenees, Spain: v. 45.
- Hottinger, L., K. Drobne, and E. Caus, 1989, Late cretaceous, larger, complex miliolids (foraminifera) endemic in the Pyrenean faunal province: *Facies*, v. 21, no. 1, p. 99–133, doi:10.1007/BF02536833.
- Institut Cartogràfic i Geològic de Catalunya, 2010, *Mapa geològic de Catalunya (1:25 000)* -

- Aramunt 252-2-2 (66-22).
- Institut Cartogràfic i Geològic de Catalunya, 2014, Mapa geològic de Catalunya (1:25 000) - Camarasa 228-1-2 (65-26).
- Institut Cartogràfic i Geològic de Catalunya, 2012, Mapa geològic de Catalunya (1:25 000) - El Pont de Suert 213-2-2 (64-20).
- Institut Cartogràfic i Geològic de Catalunya, 2002, Mapa geològic de Catalunya (1:25 000) - San Salvador de Toló 290-2-2 (66-24).
- Institut Cartogràfic i Geològic de Catalunya, 2015, Mapa geològic de Catalunya 1:50.000 (mgc50Mv01\_etr89).
- Kominz, M. A., J. V. Browning, K. G. Miller, P. J. Sugarman, S. Mizintseva, and C. R. Scotese, 2008, Late Cretaceous to Miocene sea-level estimates from the New Jersey and Delaware coastal plain coreholes: an error analysis: *Basin Research*, v. 20, no. 2, p. 211–226, doi:10.1111/j.1365-2117.2008.00354.x.
- Markley, L., P. A. Drzewiecki, and J. Olandt, 2014, Sea Level and Tectonic Controls on the Development of the Santonian Collades de Basturs Carbonate Platform, South-Central Pyrenees, Spain, *in* 49th Annual Meeting of the Geological Society of America.
- Messina, C., M. A. Rosso, F. Sciuto, I. Di Geronimo, W. Nemeč, T. Di Dio, R. Di Geronimo, R. Maniscalco, and R. Sanfilippo, 2007, Anatomy of a Transgressive Systems Tract Revealed by Integrated Sedimentological and Palaeoecological Study: The Barcellona Pozzo Di Gotto Basin, Northeastern Sicily, Italy, *in* C. P. Gary Nichols, Ed Williams, ed., *Sedimentary Processes, Environments and Basins*: Oxford, UK, Blackwell Publishing Ltd., p. 367–400, doi:10.1002/9781444304411.ch17.
- Mey, P. H. W. H. W., P. J. C. Nagtegaal, K. J. Roberti, and J. J. A. Hartevelt, 1968, Lithostratigraphic subdivision of post-hercynian deposits in the south-central Pyrenees, Spain: *Leidse Geologische Mededelingen*, v. 41, p. 221–228.
- Muñoz, J. A., 1989, The structure of the Pyrenees, *in* M. Marzo, and C. Puigdefàbregas, eds., *Alluvial deposits of the successive foreland basing stages and their relation to the Pyrenean thrust sequences*. 4th international conference on fluvial sedimentology, *guidbook series*, Excursion num. 10: Servei Geològic de Catalunya, p. 7–13.
- Muñoz, J. A., A. Martínez, and J. Verges, 1986, Thrust sequences in the eastern Spanish Pyrenees: *Journal of Structural Geology*, v. 8, no. 3–4, p. 399–405, doi:10.1016/0191-8141(86)90058-1.
- Nagtegaal, P., 1972, Depositional history and clay minerals of the Upper Cretaceous basin in the south-central Pyrenees, Spain: *Leidse Geologische Mededelingen*, v. 47, no. 2, p. 251–275.
- Owen, H. G., 1983, *Atlas of continental displacement, 200 million years to the present*: CUP Archive.
- Pascual, O., J. M. J. Pons, and E. Vicens, 1989, Rudist horizons in the Montsec (South Central Pyrenees), *in* *Cretaceous of the Western Tethys*. Proceedings 3rd International Cretaceous Symposium, Tübingen 1987: p. 215–230.
- Patrino, S., G. J. Hampson, and C. a-L. Jackson, 2015, Quantitative characterisation of deltaic and subaqueous clinoforms: *Earth-Science Reviews*, v. 142, p. 79–119, doi:10.1016/j.earscirev.2015.01.004.
- Philip, J., and M. Floquet, 2000, Late Cenomanian; Map 14, *in* J. Dercourt, M. Gaetani, B. Vrielynck, E. Barrier, B. Biju-Duval, M. F. Brunet, J. P. Cadet, S. Crasquin, and M. Sandulescu, eds., *Peri-Tethys Atlas, Paleogeographical Maps, Explanatory Notes*: Paris, France, CVGM/CGMV, p. 129–136.
- Plaziat, J.-C., 1981, Late Cretaceous to Late Eocene palaeogeographic evolution of Southwest Europe: *Palaeogeography, Palaeoclimatology, Palaeoecology*, v. 36, no. 3–4, p. 263–320, doi:10.1016/0031-0182(81)90110-3.
- Pocovi, J., 1978, Estudio geológico de las Sierras Marginales Catalanas (Prepirineo de Lérida): *Acta Geològica Hispànica*, v. 13, no. 3, p. 73–79.
- Pomar, L., M. Aurell, B. Bádenas, M. Morsilli, and S. F. Al-Awwad, 2015, Depositional model for a prograding oolitic wedge, Upper Jurassic, Iberian basin: *Marine and Petroleum Geology*, v. 67, p. 556–582, doi:10.1016/j.marpetgeo.2015.05.025.

- Pomar, L., E. Gili, A. Obrador, and W. C. Ward, 2005, Facies architecture and high-resolution sequence stratigraphy of an Upper Cretaceous platform margin succession, southern central Pyrenees, Spain: *Sedimentary Geology*, v. 175, no. 1–4, p. 339–365, doi:10.1016/j.sedgeo.2004.11.009.
- Pomar, L., and W. C. Ward, 1994, Response of a late Miocene Mediterranean reef platform to high-frequency eustasy: *Geology*, v. 22, no. 2, p. 131, doi:10.1130/0091-7613(1994)022<0131:ROALMM>2.3.CO;2.
- Pons, J. M., and E. Caus, 1996, El Cretácico Superior en el Pirineo. *Paleontología: Revista Española de Paleontología*, 1996, v. N° EXTRAOR, p. 182–189.
- Poulsen, C. J., D. Seidov, E. J. Barron, and W. H. Peterson, 1998, The impact of paleogeographic evolution on the surface oceanic circulation and the marine environment within the Mid-Cretaceous tethys: *Paleoceanography*, v. 13, no. 5, p. 546–559, doi:10.1029/98PA01789.
- Puigdefàbregas, C., J. A. Muñoz, and J. Vergés, 1992, Thrusting and foreland basin evolution in the Southern Pyrenees, *in* K. R. McClay, ed., *Thrust Tectonics*: Dordrecht, Springer Netherlands, p. 247–254, doi:10.1007/978-94-011-3066-0\_22.
- Puigdefàbregas, C., and P. Souquet, 1986, Tecto-sedimentary cycles and depositional sequences of the Mesozoic and Tertiary from the Pyrenees: *Tectonophysics*, v. 129, no. 1–4, p. 173–203, doi:10.1016/0040-1951(86)90251-9.
- Roige, M., D. Gómez-gras, and E. R. Grau, 2014, The role of the Ebro Massif as a source area for the clastic systems of the southcentral Pyrenean Basin: no. October.
- Sanders, D., 1998, Upper Cretaceous “Rudist” formations: *Geologisch-Palaeontologische Mitteilungen Innsbruck*, v. 23, p. 37–59.
- Sanders, D., and R. Baron-Szabo, 2008, Palaeoecology of solitary corals in soft-substrate habitats: the example of *Cunulites* (upper Santonian, Eastern Alps): *Lethaia*, v. 41, no. 1, p. 1–14, doi:10.1111/j.1502-3931.2007.00039.x.
- Sanders, D., and R. Höfling, 2000, Carbonate deposition in mixed siliciclastic–carbonate environments on top of an orogenic wedge (Late Cretaceous, Northern Calcareous Alps, Austria): *Sedimentary Geology*, v. 137, no. 3–4, p. 127–146, doi:10.1016/S0037-0738(00)00084-1.
- Sanders, D., and J. M. Pons, 2001, Stratigraphic architecture of a Santonian mixed siliciclastic-carbonate succession (Catalonian Pyrenees, Spain): *Facies*, v. 44, no. 1, p. 105–135, doi:10.1007/BF02668170.
- Santisteban, G., and C. Taberner, 1988, Sedimentary Models of Siliciclastic Deposits and Coral Reefs Interrelation, *in* L. J. Doyle, and H. H. Roberts, eds., *Developments in Sedimentology V42: Carbonate-Clastic Transitions*: p. 35–76, doi:10.1016/S0070-4571(08)70164-X.
- Sattler, U., A. Immenhauser, H. Hillgärtner, and M. Esteban, 2005, Characterization, lateral variability and lateral extent of discontinuity surfaces on a Carbonate Platform (Barremian to Lower Aptian, Oman): *Sedimentology*, v. 52, no. 2, p. 339–361, doi:10.1111/j.1365-3091.2005.00701.x.
- Schlager, W., 2005, Carbonate facies models, *in* *Carbonate Sedimentology and Sequence Stratigraphy*: SEPM (Society for Sedimentary Geology), p. 55–71, doi:10.2110/csp.05.08.0055.
- Shackleton, J. R., M. L. Cooke, J. Vergés, and T. Simó, 2011, Temporal constraints on fracturing associated with fault-related folding at Sant Corneli anticline, Spanish Pyrenees: *Journal of Structural Geology*, v. 33, no. 1, p. 5–19, doi:10.1016/j.jsg.2010.11.003.
- Simó, A., 1986, Carbonate platform depositional sequences, Upper Cretaceous, south-central Pyrenees (Spain): *Tectonophysics*, v. 129, no. 1–4, p. 205–231, doi:10.1016/0040-1951(86)90252-0.
- Simó, A., 1989, Controls on Carbonate Platforms and Basin Development: SEPM (Society for Sedimentary Geology), 365-378 p., doi:10.2110/pec.89.44.
- Simó, A., 1993, Cretaceous carbonate platforms and stratigraphic sequences; south-central Pyrenees; Spain., *in* J. Simo, R. W. Scott, and J.-P. Masse, eds., *Cretaceous carbonate platforms*: AAPG Memoir 56: Tulsa, OK, AAPG, p. 325–342, doi:10.1306/M56578C1.
- Skelton, P. W., E. Gili, E. Vicens, and A. Obrador, 1995, The growth fabric of gregarious rudist

- elevators (hippuritids) in a Santonian carbonate platform in the southern Central Pyrenees: *Palaeogeography, Palaeoclimatology, Palaeoecology*, v. 119, no. 1–2, p. 107–126, doi:10.1016/0031-0182(95)00063-1.
- Skelton, P. W., E. Gili, E. Vicens, A. Obrador, and G. López, 2003, Revised lithostratigraphy of the Upper Cretaceous (Santonian) carbonate platform succession on the northern flank of Sant Corneli, southern Central Pyrenees: *Journal of Iberian Geology*, v. 29, p. 73–87.
- Soriano, K. A., 1992, Stratigraphy and sedimentology of Cenomanian-Santonian carbonate platforms, Montsec Mountains, south-central Pyrenees, Spain: University of Wisconsin - Madison, 320 p.
- Southgate, P., J. Kennard, and M. Jackson, 1993, Reciprocal Lowstand Clastic and Highstand Carbonate Sedimentation, Subsurface Devonian Reef Complex, Canning Basin, Western Australia: Chapter 6: Carbonate Sequence Stratigraphy: Recent Developments and Applications, no. M57, p. 157–179.
- Teixell, A., and J. A. Muñoz, 2000, Evolución tectonosedimentaria del Pirineo meridional durante el Terciario: una síntesis basada en la transversal del río Noguera Ribagorçana: *Revista de la Sociedad Geológica de España*, v. 13, no. 2, p. 251–264.
- Tucker, M. E., 2011, *Sedimentary Rocks in the Field: A Practical Guide*: Wiley-Blackwell, 288 p.
- Vicens, E., G. López, and A. Obrador, 1998, Facies succession, biostratigraphy and rudist faunas of Coniacian to Santonian platform deposits in the Sant Corneli anticline (Southern Central Pyrenees): *Geobios*, v. 31, p. 403–427, doi:10.1016/S0016-6995(98)80089-2.
- Villalba-Breva, S., and C. Martín-Closas, 2013, Upper Cretaceous paleogeography of the Central Southern Pyrenean Basins (Catalonia, Spain) from microfacies analysis and charophyte biostratigraphy: *Facies*, v. 59, no. 2, p. 319–345, doi:10.1007/s10347-012-0317-1.

## 4 TESTING CONTROLS ON FACIES ARCHITECTURE DEVELOPMENT AND SEQUENCE STRATIGRAPHY WITHIN UPPER CRETACEOUS MIXED CARBONATE-SILICICLASTIC PLATFORMS

Authors: Jonathan Lavi<sup>1</sup>, Cathy Hollis<sup>1</sup>, Peter Burgess<sup>2\*</sup>, Georgios Antonatos<sup>2</sup>, Ian Billing<sup>3+</sup>, James Gardner<sup>3</sup>, Christoph Lehmann<sup>3</sup>, Anna Matthews<sup>3</sup>, Katherine Tutton<sup>3</sup>, Stefan Schröder<sup>1</sup>

Contact: [jonathan.lavi@manchester.ac.uk](mailto:jonathan.lavi@manchester.ac.uk)

<sup>1</sup>School of Earth, Atmospheric and Environmental Sciences, The University of Manchester, Manchester, M13 9PL, UK

<sup>2</sup>Department of Earth Sciences, Royal Holloway University of London, London, TW20 0EX, UK

<sup>3</sup>BP Exploration, Chertsey Road, Sunbury-On-Thames, Middlesex TW16 7LN.

\*Now at School of Environmental Sciences, University of Liverpool, Liverpool L69 3GP, UK

+Now at School of Science, University of Derby, Kedleston Road, Derby DE22 1GB, UK

### 4.1 Abstract

Sequence stratigraphic principles are fundamental to the prediction of facies architecture within carbonate platforms, particularly from subsurface datasets. The early concepts of sequence stratigraphy interpret sedimentary stacking patterns on the basis of allochthonous controls (relative sea-level). In more recent work, possible autochthonous controls (carbonate productivity, sediment transport) on sedimentary architecture are considered equally important. In this study, the Upper Santonian Bastus Platform of the South-Central Pyrenees, which shows a complex facies architecture, is used to demonstrate the importance of a large number of controlling factors on facies architecture by comparing outcrop-based correlations using sequence stratigraphic principles to numerical stratigraphic forward models.

A conventional sequence stratigraphic framework was constructed using a combination of sedimentary logs, map and borehole data, interpreting possible 4<sup>th</sup> order and 5<sup>th</sup> order cyclicity. Four forward stratigraphic models were constructed to attempt to reproduce this cyclicity by varying potential controlling parameters. The first two models attempted to reproduce the interpreted stacking patterns through eustatic sea-level variations. A third model modified carbonate productivity over time whilst a fourth model introduced tectonic tilt half way through the model runtime. The models show that eustasy and the resulting relative sea-level variation only have a marginal effect on the generation of sedimentary cycles. Conversely, by varying carbonate productivity or introducing tectonic tilt it is possible to reproduce sedimentary



stacking patterns that were interpreted as 4<sup>th</sup> order sea-level cycles using the traditional sequence stratigraphic methods.

These results demonstrate how stacking patterns that apparently conform to sequence stratigraphic principles may not necessarily occur as a result of simple relative sea-level fluctuations. As such, they may lead to a misidentification of the mechanisms controlling platform architecture, reducing confidence in our ability to predict facies variability in time and space through lateral correlation of strata. Additionally, the presented sequence stratigraphic correlation further encountered a lack of platform-wide correlateable surfaces. The driving mechanism behind this is presumed in either non-uniform preservation of platform-wide events, or these having result from localised processes only affecting specific areas. Backed by stratigraphic forward modelling, these results can help to explain why correlation of carbonate successions are often difficult, and how modelling can be adapted to test various scenarios and produce unique solutions.

## 4.2 Introduction

### 4.2.1 Rationale and Aims

Sequence stratigraphy has become an accepted rule-base for understanding the development of sedimentary systems over time. It is widely used as a standard tool to facilitate prediction of sedimentary architectures in the subsurface (Catuneanu et al., 2011). The original concepts of sequence stratigraphy interpret sedimentary successions to reflect the temporal variations of relative sea-level during deposition (Mitchum et al., 1977; Vail et al., 1977; Haq et al., 1987; Sarg, 1988; Van Wagoner et al., 1988, 1990), usually through the correlation of prominent surfaces that result from variations in relative sea level (maximum flooding surfaces, flooding surfaces and sequence boundaries e.g. Read, 1995; Lehrmann and Goldhammer, 1999). Nevertheless, sediment productivity and transport have been shown to form stacking patterns similar to the sequences commonly interpreted as sea-level controlled (e.g. Burgess, 2001; Burgess et al., 2001; Burgess and Prince, 2015). Alternatively, such patterns are discussed to be formed by combinations of basin morphology, hydrodynamics and ecological developments (Pomar and Kendall, 2011; Pomar et al., 2012). This implies that both autochthonous and allochthonous controls on sedimentation need to be taken into account when making sequence-stratigraphic interpretations, rather than basing them on relative sea-level fluctuations alone.

This paper aims to take a well-understood carbonate succession and to identify the possible control mechanisms on its sedimentary architecture by comparing a correlation of outcrops based on sequence stratigraphic principles to a series of three-dimensional numerical forward

models. The forward models are designed to variably modify eustatic and relative sea level, sediment transport and productivity. The goal is to show to what extent these controls affect facies architecture through comparison of the modelling outputs to the platform geometries interpreted from field data.

#### 4.2.2 Geological Background

The structural setting of the Tremp basin, located in the South-Central Pyrenees (Figure 4.1), is heavily influenced by the convergence of the Iberian and European plates that began in the Santonian and lasted until the initial collision during the early stages of the Palaeogene (Puigdefàbregas and Souquet, 1986; Puigdefàbregas et al., 1992). The Mesozoic succession is preserved in the upper of three northward-directed thrust sheet groups (Muñoz et al., 1986). The relevant thrusts in the basin are the Serres Marginales, the Montsec and the Bóixols thrusts (Muñoz et al., 1986).

During the Upper Cretaceous, the south-north trending Tremp Basin formed on the southern side of a narrow trough between the Neo-Tethys and the Bay of Biscay (Plaziat, 1981), 30°N and 40°N of the equator (Simó, 1993). The palaeoclimate was transitioning from arid to semiarid (Nagtegaal, 1972; Booler, 1994). The Ebro High, situated to the south of the basin, is interpreted to have provided a source of siliciclastics that were shed onto the carbonate platforms (Roige et al., 2014; Gómez-Gras et al., 2016), with an increase in siliciclastic sediment supply occurring over the course of the Upper Cretaceous (Chapter 3).

The Bastus Platform is Santonian in age, the second youngest of multiple carbonate platforms that were established during the Upper Cretaceous in the Tremp Basin (Simó, 1993, and Chapter 3). It overlies the Coniacian Sant Corneli Platform, and is succeeded by the Terradets platform. Whilst pelagic sediments provide a good biostratigraphic control from foraminiferal and ammonoid assemblages, only a limited basin-scale biostratigraphic framework has been established in the area as most previous studies are only on outcrop scale (cf. Chapter 3). Chemostratigraphic studies are restricted to specific platforms (e.g. Caus et al., 1993, Santa Fe Platform; Caus et al., 2013, Sant Corneli Platform), or only correlate between neighbouring localities. Sedimentary correlations on a regional scale are supported by comparison of age-indicative rudist species within individual localities for local scale correlations and placed in the context of a revised chronostratigraphic framework based on compiled biostratigraphic data (Figure 4.2 and Chapter 3).

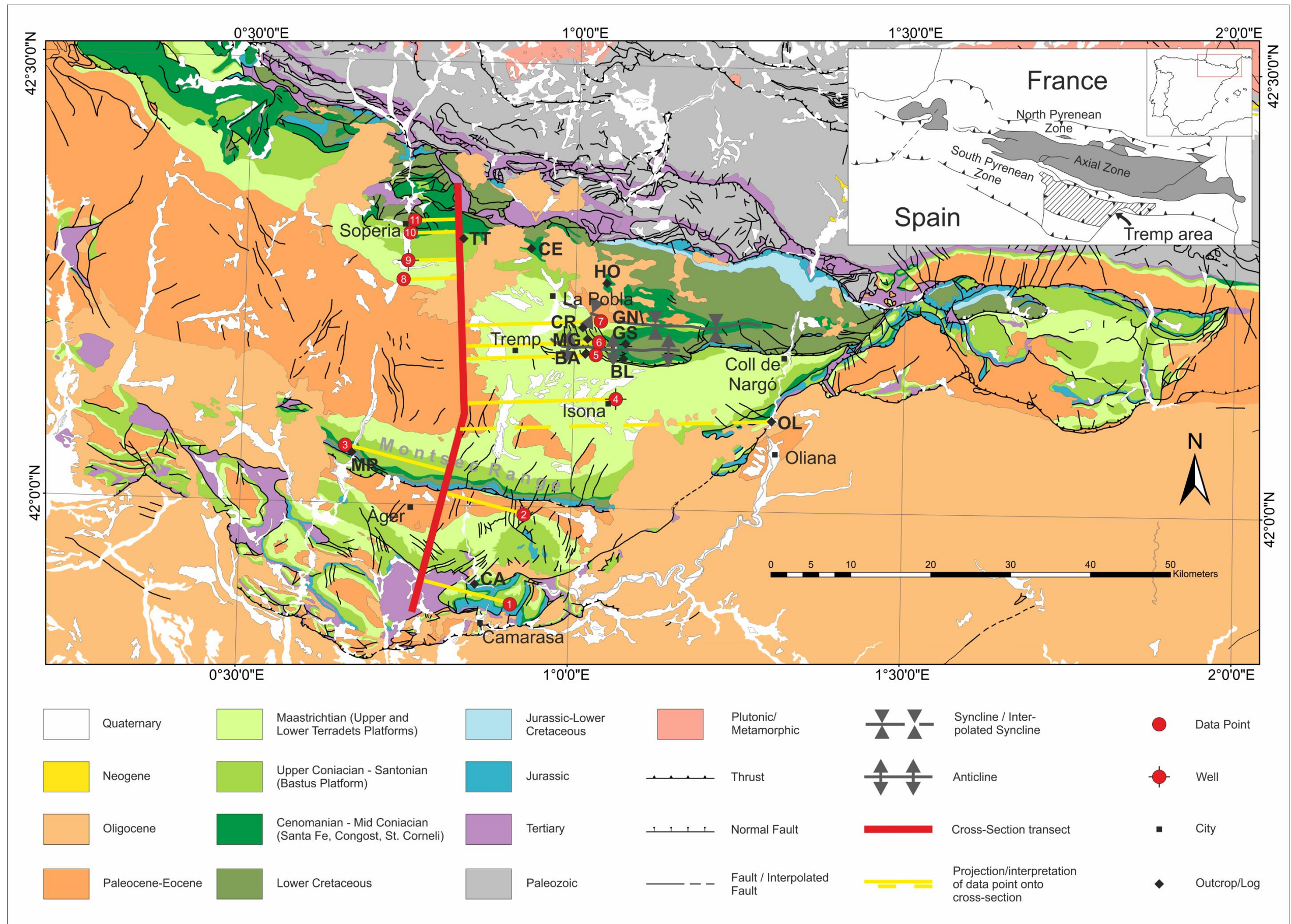


Figure 4.1: Simplified geological map of the Tremp Basin (Modified from Institut Cartogràfic i Geològic de Catalunya, 2015). Numbers in data points refer to the ones used in Figure 4.4. BA = Collades de Basturs, BL = Borrell, CA = Camarasa, CE = Congost d'Erinyà, CR = Carreu River, GN/GS = Gallinove North/South, HO = Hortonedà, MG = Montagut Gully, MR = Mont Rebei, OL = Oliana, TT = Torre de Tamurcia. Upper right corner: generalised structural map of the Pyrenees (Modified after Simó, 1986).

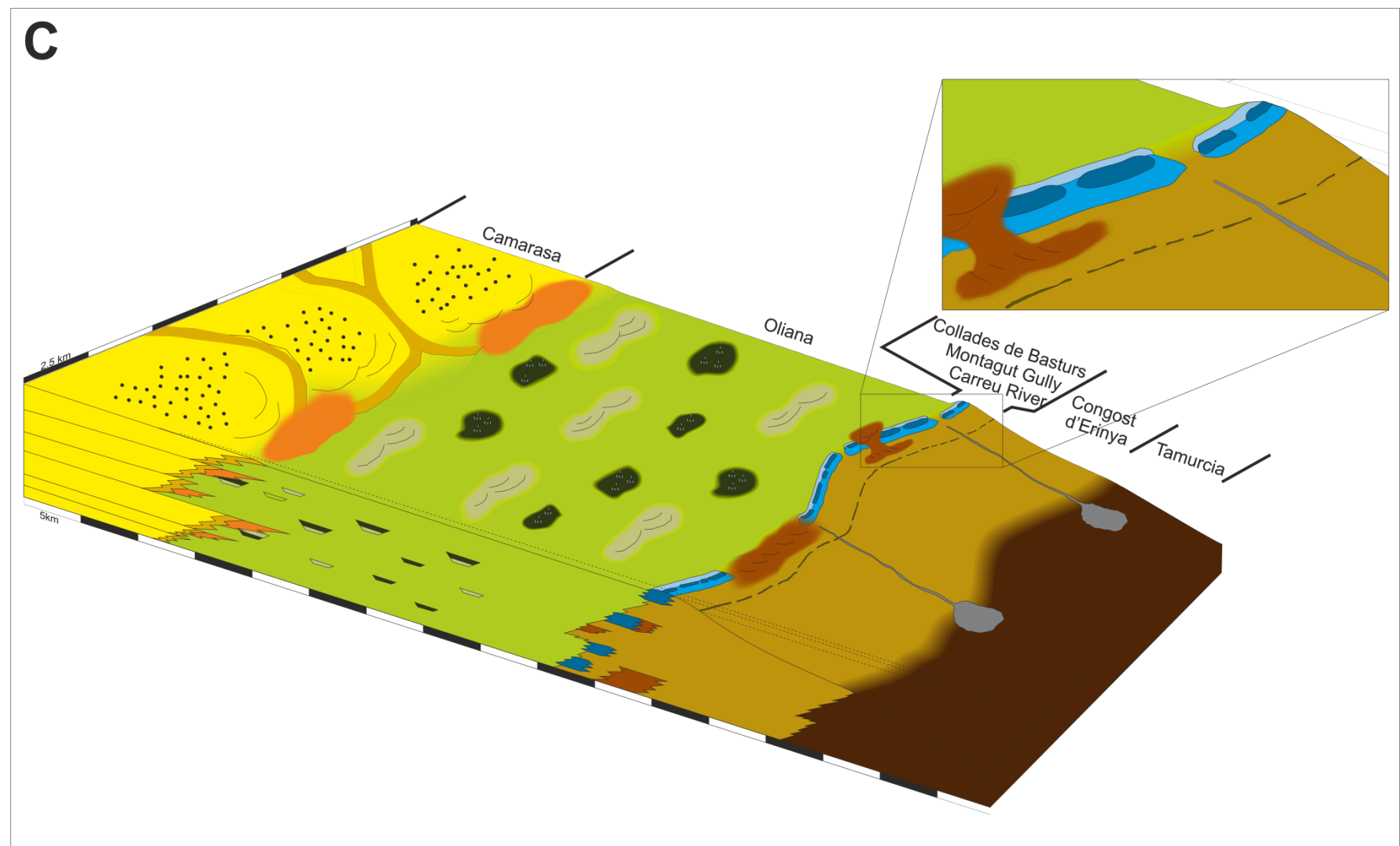
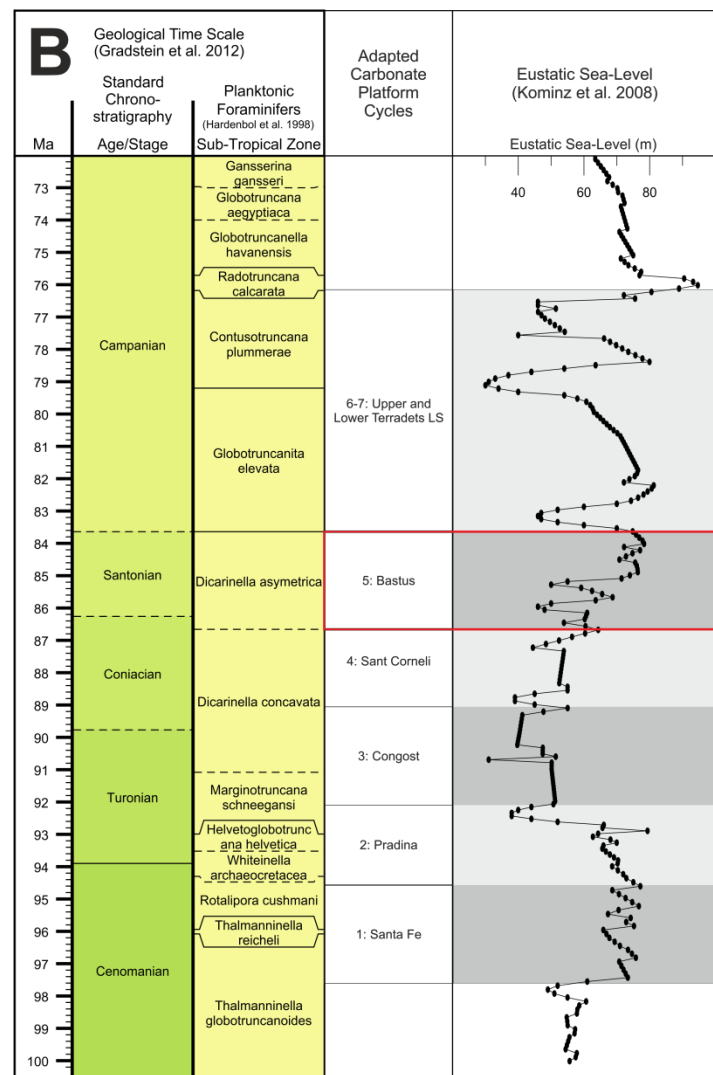
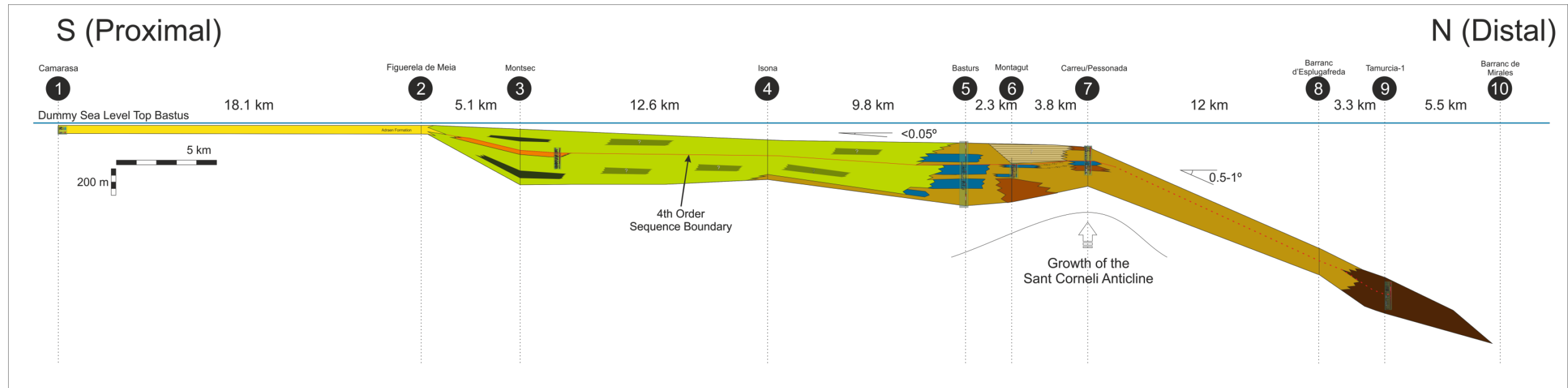


Figure 4.2: A: Cross section of the Bastus Platform. Numbers in circles above each data point refer to the numbers used for localities in Figure 4.1. Distances between data points are marked in kilometres above the cross-section. Marked are estimated angles for platform top and slope (cf. section 4.5), and presence of the major surface described in section 4.6.1. B: Geological time scale. This is composed of the geological time scale of Gradstein et al. (2012), the planktonic foraminiferal zones of Hardenbol et al. (1998), the carbonate platform cycles previously defined by Simó (1993), adjusted to the revised time-scale following a review of the biostratigraphic and lithostratigraphic framework (Chapter 3), and the eustatic sea-level curve of Kominz et al. (2008). The study interval is outlined in red C: Schematic depositional model of the Bastus Platform. Colours represent the lithofacies associations defined in table 4.1. Names on the top right indicate the field localities in which the lithofacies associations were observed and logged. The cut-out box highlights the lateral relationships of facies at the platform margin, particularly the leeward-windward differentiation of rudist facies in the composite build-ups, the discontinuity of build-ups in strike, and the juxtaposition and intercalation of the shoal facies (brown) and composite build-up facies (blue). The cross-section in this schematically figure does not represent true stacking patterns, but highlights potential bedding relationships between facies as they were observed in the field.

## 4.3 Methods and Materials

### 4.3.1 Fieldwork and Petrography

14 Stratigraphic logs were made at 5 localities on the scale of 1:50 (see Appendix B.2). These were later either directly scaled to 1:500 or composite logs created from several logs on that scale (see Appendix B.3). Lithofacies were sampled and 81 thin sections prepared in order to define depositional textures (Dunham, 1962; Embry and Klovan, 1971) and faunal assemblages, and interpret depositional environments and trends on the basis of these (see Appendices C.2 and D.4). Siliciclastic-dominated lithologies are plotted using the siliciclastic grain-size scale by Wentworth (1922).

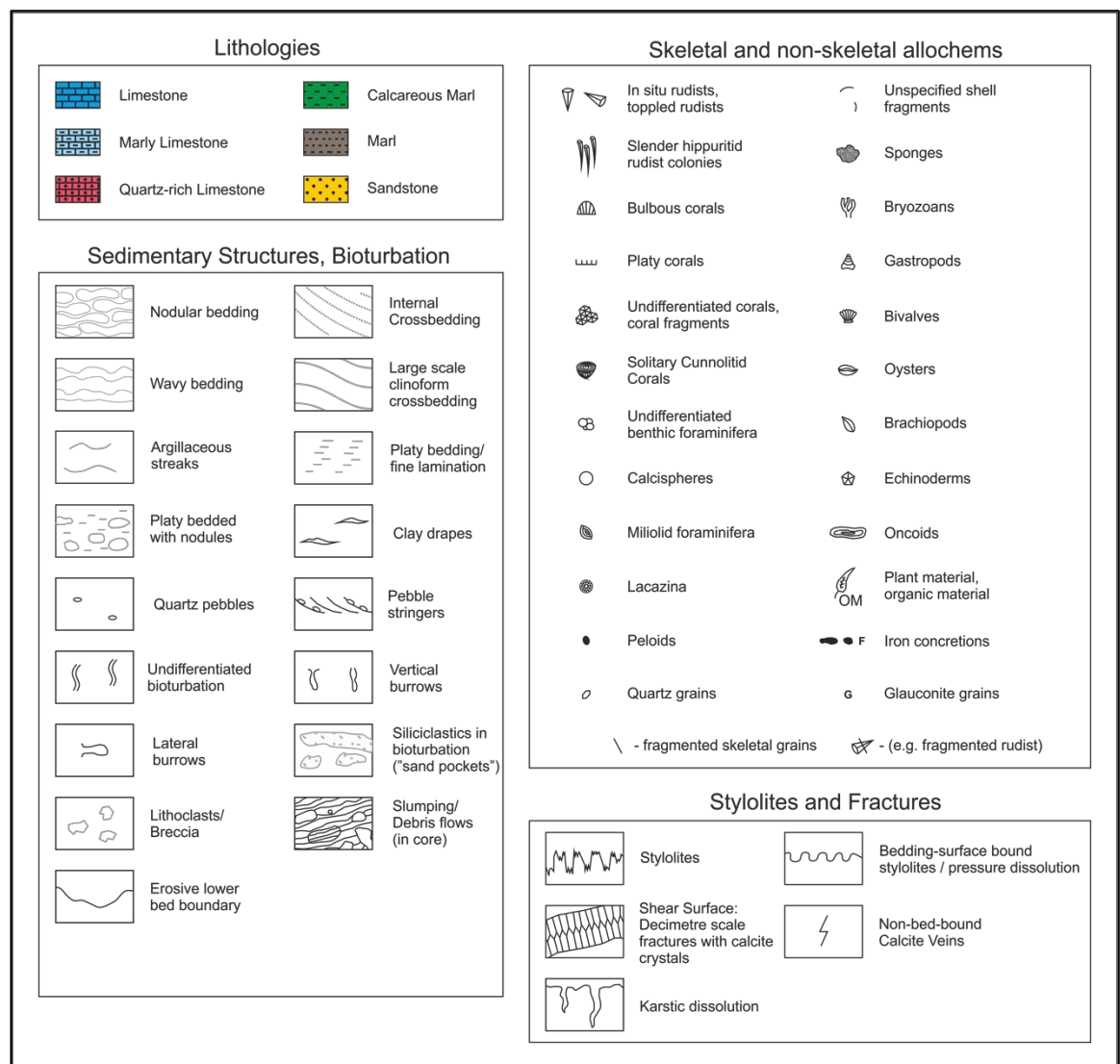


Figure 4.3: Sedimentary log key.

### 4.3.2 Construction of Platform Cross-Section

A cross-section was produced via publically available maps. Data points were selected based on exposure of the relevant stratigraphic flows section (see Appendix A.2, Table A.2.1). The position of

each data point was projected onto a central cross-section line to determine the distance between localities on a proximal-basinal transect, and to determine the pure dip-extent of stratigraphic elements. Lateral correlation between logs was made using prominent surfaces and lithofacies stacking patterns. This was supplemented by published data from boreholes, geological maps and by applying known biostratigraphic constraints (cf. Chapter 3). If it was not possible to log part of the sedimentary succession at a specific locality (e.g. because of inaccessible sections), the total thickness of the succession and expected lithofacies association was reconstructed using the maps, and the logged section was placed in the appropriate stratigraphic position. The previously established compression factor of 1.66 (Choukroune et al., 1990) was applied to the distances between data points on the projected cross-section lines to compensate for tectonic compression of the modern day localities.

### **4.3.3 Construction of Sequence Stratigraphic Framework**

On the basis of depositional environments interpreted from the defined lithofacies, the logs were subdivided into stacking patterns representing gradual upwards changes in depositional environments, and capped by surfaces which show a sudden change of depositional environment towards the following stacking pattern. These patterns are further interpreted as systems tracts following the depositional sequence approach of Van Wagoner et al. (1988, 1990) and Christie-Blick (1991). These systems tracts and key surfaces were correlated across logs to form a sequence-stratigraphic correlation panel.

### **4.3.4 Definition of Subsidence Rates and Plotting of Relative Sea-level**

Subsidence rates (m/My) were defined for relevant localities of the cross-section by dividing the total thickness of the platform deposits at that location with the time-span of the platform (3 My, cf. section 4.2.2). The eustatic sea-level curve presented by Kominz et al. (2008) for the platform interval (83.7-36.7 Ma, cf. Figure 4.2B) was used to delineate a eustatic sea-level curve with two components:

- A low-order oscillation with a period of 3 Ma and an amplitude of 23 m
- A high-order oscillation with a period of 0.6 Ma and an amplitude of 13 m

The combination of eustatic sea-level and subsidence during the investigated time interval allowed plotting relative sea-level curves for specific sections across the platform. Also plotted are magnitudes of relative sea-level fall.

### **4.3.5 Stratigraphic Forward Modelling**

Three-dimensional stratigraphic forward models of the Bastus Platform were constructed at Royal Holloway University of London using a modified version of CarboCAT (Burgess, 2013) as part of a parallel study. The model uses cellular automata to simulate a number of carbonate

factories with varying productivity rates based on water depth. Modelled processes also include a transported fraction, tectonic subsidence and eustatic sea-level oscillations. The model grid is defined by width, length and cell size, and is set to run for a pre-defined time, with a chosen time-step (Burgess, 2013). For this study, the input of siliciclastics and the effects of these on carbonate productivity have been integrated into the model, during work conducted as a part of a parallel study (Antonatos, *in prep.*).

The modelling parameters are divided into static parameters and variable parameters. The former are defined via the bounding parameters of the field example and do not change between modelling approaches or iterations. They include the dimensions, cell size, elapsed time and time-step of the model, the initial bathymetry, subsidence and euphotic zone depth. Furthermore, this includes the number of carbonate factories (on the basis of field interpretations) and the fraction of transported sediment they produce (on the basis of in-situ vs. bioclastic sediment thickness in logged sections). The variable parameters are modified between modelling approaches and model runs in an attempt to reconstruct the platform architecture that was observed from the field example. These include sea-level oscillation and amplitude, and the individual productivity of each carbonate factory (optionally varying over time).

The variable parameters (sea-level fluctuations, carbonate productivity over time) were changed with each model run to achieve a best fit to the reconstructed architecture of the Bastus Platform. The outputs were quality controlled by comparing slope and margin inclinations, platform top, margin and slope dimensions and the distribution of gross depositional environments. Additionally, total sediment column thicknesses and bed thickness distribution are compared with those from cross sections and numerical thickness distribution data sourced from field logs.

#### **4.4 Lithofacies and Depositional Environments**

The Bastus Platform is of Santonian age and is has been interpreted as a flat-topped platform with a gently inclined slope (Figure 4.2 and Chapter 3). Eight lithofacies associations (LFA) were defined (Table 3.8), with each association representing deposition under a specific mechanism within a gross depositional environment (GDE).

The proximal environment (Lithofacies NS1-4, exposed at Camarasa, cf. Figure 4.1 and 4.2A. Field photographs and photomicrographs are presented in Chapter 3) is dominated by siliciclastic lithofacies. It shows intercalations of massive and cross-bedded sandstones with escape structures (NS1) and poorly consolidated and decimetre-thick bedded sandstones with cross-bedding, bioturbation, pebble stringers and clay-drapes (NS2). Thick intervals of poorly

consolidated, wavy bedded marls with occasional quartz pebbles and rare shell fragments (NS3) are occasionally intercalated with decimetre-thick beds of quartz-rich grainstones (NS4). Based on observed dominance of moderately-matured siliciclastic material, as well as specific associations of sedimentary structures, these lithofacies are interpreted to represent a shallow-marine deltaic environment. The sandstones of NS1 are interpreted as deltaic distributary channels, based on the absence of matrix, massive bedding and presence of escape structures. NS2 is interpreted to represent deltaic mouth bars, due to the bedded character and the presence of cross bedding, pebble stringers and clay-drapes. NS3 shows an overall much finer grain size and more common marine fossils, and is thus interpreted as a delta-front or pro-delta environment. Minor amounts of carbonate bioclasts were probably introduced from the distal carbonate platform, and concentrated in horizons of reworked material (NS4).

The platform interior sediments are exposed north of Oliana and on the southern Montsec Range (Figure 4.1 and 4.2A). These consist mainly of intercalations of limestones and siliciclastic dominated beds (Lithofacies PI1-4; Figure 4.5). Wavy bedded, dark grey wackestones with abundant benthic foraminifera and occasional shell fragments (PI2) are ubiquitous and are interpreted to represent the background sedimentation in a restricted lagoon. The micrite-dominated texture, fine grain size and abundance of benthic foraminifera imply deposition under low energy and limited water depths (< few metres). Furthermore, the dark colour indicates high amounts of organic material, which is interpreted to be the result of deposition in restricted conditions.

Embedded within PI2 are massive-to-bedded bioclast-bearing sandstones and quartz-rich bioclastic grainstones with bioturbation, escape structures and occasional cross-bedding (PI1; Figure 4.5). These are interpreted to form lens-shaped bodies of reworked lagoonal and siliciclastic material. Poor sorting and rounding and very coarse maximum grain sizes, as well as the often sharp lower bed boundaries indicate sudden deposition under high energy conditions, with limited transport distances. Mixing of siliciclastic and carbonate material implies reworking of lagoonal deposits under deltaic influence. This suggests connectivity to the deltaic environment, with these sediments possibly acting as an extension of the delta lobes.

Rudist framestones and rudist debris floatstones and rudstones (PI4; Figure 4.5) show in-situ rudists and very coarse grained and angular rudist fragments in a micritic lime matrix. Due to the abundance of in-situ rudists and their interbedded position into the nodular lagoonal wackestones, they are interpreted to represent rudist biostromes and debris that formed sporadically as isolated patches in the lagoon. They internally bedded on up to 1.5 metre scale, adding to intervals of up to 50 metres thickness and interpreted to be ca. 1.5 kilometres long and ca. 2.7 kilometres wide (Chapter 5). Bedded, well-sorted and rounded peloidal grainstones



(PI3), comprise sorted and rounded peloids, shell fragments and foraminifera. The superb rounding and sorting, cross-bedding, and the absence of matrix indicate they have been formed under consistent wave agitation. They are therefore interpreted as lagoonal sand shoals.

The deposits of the platform margin area were investigated at Collades de Basturs, Montagut Gully, and Carreu River (Figures 4.1, 4.2A, Figure 4.6, and Figure 4.7). These sections are dominated by massive rudist-coral boundstones (PM1), up to 10 metres thick and at least 250 metres wide and 3.8 kilometres long (Chapter 5). They are interpreted as bioherms, as they show an organised, massive internal structure with abundant in-situ organisms. PM1 is commonly overlapped by bedded bioclastic packstones and grainstones comprising rounded, variably sorted rudist and coral debris and small benthic foraminifera (PM2). The close association with the bioherms, and the fragmented and rounded texture of the grains suggests that they formed as debris aprons to the bioherms. Landward of the boundstones are sheet-like beds of corals, rudist and sponges (PM3) as well as frameworks of elevator rudist boundstones with a micritic matrix (PM4). The delicate and organised nature of these facies and the abundance of fine-grained matrix indicate they formed in a protected environment. Together with their landward position of the bioherms this leads to interpreting them as biostromes forming in the protected back-reef areas. Together, this lithofacies association is interpreted to form a narrow zone of high faunal diversity, with textures varying substantially across a landward-seaward trend. It shows a slightly mounded geometry, and grades into muddier facies both proximally and distally.

Sigmoidally cross-bedded and quartz bearing bioclastic grainstone and packstones (PM5) comprising variably sorted and rounded shell fragments, peloids and small foraminifera occasionally laterally pass into the debris aprons (PM2), fringe the build-ups (PM1-4), or are found to over- and underlie them. They are interpreted as platform margin shoals on the basis of their clean texture, diverse skeletal composition and margin-parallel-directed cross-bed sets. They form continuous units (1-5 metres thick, at least 250 metres wide; Chapter 5), with no evidence of tidal channels.

Both build-ups and shoals (PM1-5) intercalate into thick successions of fine-grained wavy or nodular wackestones or silts (US1-2), featuring shell fragments, small benthonic foraminifera and occasional *Lacazina*, as well as bioturbation (at Collades de Basturs, Montagut Gully, Carreu River, cf. Figure 4.1 and 4.2A). The fine grain sizes and low abundance of benthic phototrophic fauna suggests deposition in a lower energy, deeper water environment than PM1-5, most likely the upper slope. Occasional metre-scale in-situ rudist and coral boundstones (US1b) and beds of packstones with common shell fragments and benthic foraminifera (US3) are intercalated into these. The former are interpreted as small upper slope patch reefs due to the organised internal

nature and 1-2 metres limited lateral extent. The latter are interpreted to represent reworked storm-beds, as the grain association is identical to the surrounding wackestones (US1/2), only a higher presence of grains and a lower amount of matrix is observed.

In the basinal deposits are exposed in the area of Tamurcia (Figure 4.1 and 4.2A). These are dominated of thinly bedded marls with small amounts of silt-grade quartz, common planktonic foraminifera, sponge spicules and rare small shell fragments occur (SL1; Figure 4.8). These are interpreted as pelagic sediments in a basinal environment based on the abundance of mud and dominance of pelagic organisms. Locally, SL1 facies are cut by channelized beds that are between few decimetres and several metres thick, and comprised of a breccia with clasts of rudists and coral boundstones or bioclastic grainstones (SL2; Figure 4.8). The clasts range between few millimetres to few metres in size. The abundance of shallow water organisms in these clasts, the angular, poorly sorted and very coarse maximum grain sizes, and the poorly organised texture suggest that these are debris flows resulting from periodic margin failure and resedimentation of material in the basinal realm.

Lithofacies Association / Correlation Panel Colour	Lithofacies Code / log colour	Lithofacies	Geometries and bedding	Characteristic sedimentary structures / organisms	Observed Sections	Interpretation	GDE	Water depth indicators	Estimated water depth	
Sandstones, marls and quartz-rich grainstones	NS1	Massive to banked, well sorted sandstones	Massive beds, 5-10 m thick	Well cemented, brown-yellowish sorted sandstones (mU-cU) with bioturbation (Skolithos). Internally massive with sharp lower and upper boundaries	Camarasa	Distributary Channels	Deltaic Nearshore Environment	<ul style="list-style-type: none"> <li>Potential palaeosols (cf. Chapter 3 and logs CAa/CAb, Appendix)</li> <li>dm-m scale cross-bedding</li> </ul>	Above FWWB ~0-10 m	
	NS2	Bedded, poorly consolidated sandstones with internal cross-bedding	Bedded, Few cm to dm in thickness	Internal metre-scale cross-bedding with clay drapes, pebble stringers, rip-up clasts, bioturbation (Ophiomorpha).	Camarasa	Mouth Bars				
	NS3	Wavy bedded marls and calcareous marls with angular quartz pebbles	Structureless, up to few metres in thickness	Mostly wavy bedded, 10s metre thick units. Occasional intercalations of NS4. Moderately common coarse and angular quartz pebbles. Rare shell fragments	Camarasa	Delta Front				
	NS4	Quartz-rich bioclastic grainstones and packstones	Decimetre-thick beds intercalated into NS3	Poorly sorted and poorly rounded grainstones and packstones, with quartz grains up to pebble in size. Allochems include shell fragments, miliolid foraminifera and peloids	Camarasa	Prodelta? Carbonate-Siliciclastic Mixing Zone				
Coarse grained sandstones and grainstones with rudist debris	PI1	Coarse grained bioclastic sandstones and quartz-rich grainstones with coarse rudist debris	200 m to 2.1 km wide bodies (mean = 1 km). Control on dip dimensions unavailable.	Sharp lower and upper boundaries, poor sorting. Coarse rudist debris amongst other bioclasts. Bioturbation (Skolithos and thalassinoides)	Oliana	Reworking of lagoonal sediments and introduction of clastic material	Platform Interior	<ul style="list-style-type: none"> <li>Rare cross-bedding in siliciclastic dominated lithologies</li> <li>Abundant small benthic foraminifera</li> <li>Micritic envelopes in grain-dominated facies</li> </ul>	Above FWWB ~0-10 m	
Dark nodular wackestones with foraminifera and rudist biostromes	PI2	Nodular wackestones/packstones with abundant benthic foraminifera		Dark nodular limestones, abundant benthic foraminifera, occasional small shell fragments. Rare silt-grade quartz.	Oliana	Lagoonal background sedimentation				
Rudist biostromes, coarse rudist limestones, and fine peloidal and bioclastic limestones	PI2b	Thin in-situ rudist bafflestone sheets		20-30cm thick sheets of densely packed small in-situ rudists	Oliana	Thin rudist patch reefs within lagoon				
	PI3	Quartz-free peloidal grainstones and packstones	No data; outcrop limits <200m. Potentially similar dimensions to PI4	Sharp lower boundary, gradational upper boundary, exceptionally well sorted, fine grained bioclasts	Oliana	Platform interior shoals/bars				
Rudist and coral bioherms, biostromes and bedded bioclastic limestones	PI4	Rudist wacke/pack/float/rud/boundstones	1.5 km to 4.1 km wide bodies (mean = 2.59 km). Control on dip dimensions unavailable.	Nodular to wavy appearance. Coarse rudist debris and in-situ rudists. Occasional in-situ corals. Few fine grained angular quartz grains. Benthic foraminifera.	Oliana	Large-scale lagoonal patch reefs	Platform Margin	<ul style="list-style-type: none"> <li>Rudist-Coral bioherms (estimated up to 20m depth depending on wave energy; Sanders, 1998)</li> <li>Abundant micritic envelopes</li> <li>Large-scale cross-bedding</li> </ul>	Mostly above FWWB, possibly reaching to below FWWB ~5-15 m	
	PM1	Massive mixed coral-rudist boundstones	Forming bioherms of up to 6m thickness, 10s of metres wide	In situ corals and rudists. Wackestone matrix with fine shell fragments, planktonic foraminifera and rare calcispheres. Small amounts of silt-grade quartz.	Collades de Basturs, Montagut Gully, Carreu River	Barrier-type bioherms				
	PM2	Bedded, rudist-debris dominated grainstones and packstones	Dm-scale beds shedding off the bioherms of PM1.	Bedding on dm-scale. Mostly rudist and coral debris, peloids. Various degrees of rounding.	Collades de Basturs, Montagut Gully, Carreu River	Reef Talus of PM1				
	PM3	Sheet-like coral-rudist-sponge beds	Up to 3-4 m thickness and large lateral extent (<100 m)	Decimetre-scale beds of in-situ corals rudists, and sponges	Montagut Gully	Initial colonisation of bioconstructing organisms				
Cross-bedded, quartz bearing bioclastic grainstones and packstones	PM4	Slender hippuritid frameworks	Up to 5-6 m thickness and large lateral extent (<100 m)	Elongated hippuritid rudists forming dense frameworks. Wackestone matrix with small shell fragments and rare silt-grade quartz.	Collades de Basturs, Montagut Gully, Carreu River	Biostromes in protected backreef environment	Platform Margin	<ul style="list-style-type: none"> <li>Rudist-Coral bioherms (estimated up to 20m depth depending on wave energy; Sanders, 1998)</li> <li>Abundant micritic envelopes</li> <li>Large-scale cross-bedding</li> </ul>	Mostly above FWWB, possibly reaching to below FWWB ~5-15 m	
	PM5	Quartz-bearing grainstones and packstones, few 10s metres-scale cross-bedded	Laterally extensive units, few m thick, with internally few 10s of metre wide clinofolds	Well sorted, clean, peloid and foraminifera bearing grainstones with quartz grains at the topsets of clinofolds. Poorly sorted bioclastic packstones with abundant quartz at the bottomsets of clinofolds	Collades de Basturs, Montagut Gully, Carreu River	Platform margin grain/packstone shoal complexes				
Nodular wackestones, marls, patch reefs and packstone intercalations	(eroded deposits of this lithofacies)	US1	Nodular wackestones with foraminifera and shell fragments		Up to several 10s metres thick packages, uncommon foraminifera and shell fragments	Collades de Basturs, Montagut Gully, Carreu River	Upper Slope	<ul style="list-style-type: none"> <li>Frequent presence of solitary cunolites corals, interpreted as living as deep as 20-25 m (Sanders and Höfling, 2000; Sanders and Baron-Szabo, 2008)</li> <li>Periodic intercalations interpreted as storm deposits due to increased sorting and reduced micrite contents, (implying above SWB; Sanders and Pons, 2001)</li> </ul>	Below FWWB, Periodic influence of SWB given ~15-25 m	
		US1b	Rudist and coral boundstones within nodular wackestones (PM5)	<2 metres in diameter, up to 1 m thick.	In-situ corals and rudists	Collades de Basturs, Montagut Gully	Small-scale patch reefs on the upper slope			
		US2	Thinly-bedded silty marls with solitary cunolites corals		Thinly bedded, common solitary cunolites corals	Carreu River	Siliciclastic-influenced upper slope			
Pelagic wackestones and debris flows		US3	Foraminifera dominated packstones		Up to few metre thick packages intercalating into PM5. Decimetre-scale internal bedding. Small benthic foraminifera	Montagut Gully, Carreu River	Storm-beds below FWWB	Lower Slope	<ul style="list-style-type: none"> <li>Sponge spicules</li> <li>Dominance of planktonic foraminifera</li> </ul>	Considerably below SWB ~100 m
		SL1	Pelagic calcareous wackestones and calcisiltites		Thinly to platy bedded. Featuring sponge spicules and planktonic foraminifera	Tamurcia	Lower slope deposits			
		SL2	Debris flow deposits with clasts originating from the platform margin	Width estimated at few 100 s metres. No control on length.	Pelagic mud-supported debris flow deposits with clasts up to metre in size. Erosive lower boundaries and gradational or sharp top boundaries	Tamurcia	Debrites from platform margin failure			

Table 4.1: Lithofacies scheme for the Bastus Carbonate Platform. White dashes in lithofacies US1-US3 indicate presumed eroded strata. The two far right columns provide an overview of water depth indicators and estimated water depths for individual gross depositional environments, their facies, and the respective locality. References for water-depth indicators are given in the appropriate case. Where no reference is given, the estimates given by Flügel (2010) are applied. GDE = Gross Depositional Environment.

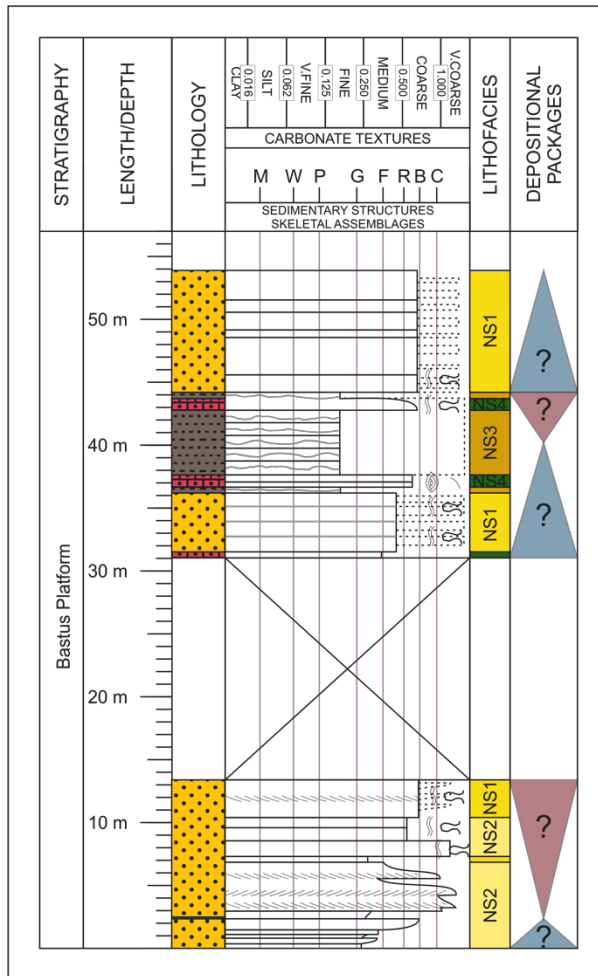


Figure 4.4: Composite log of the nearshore sediments of the Bastus Platform exposed at Camarasa, scale 1:500. A key for sedimentary logs is given in Figure 4.3. Lithofacies colours and codes are presented in Table 4.1. For locality see Figure 4.1. Original logs are at 1:50 scale, and are presented in Appendix B.

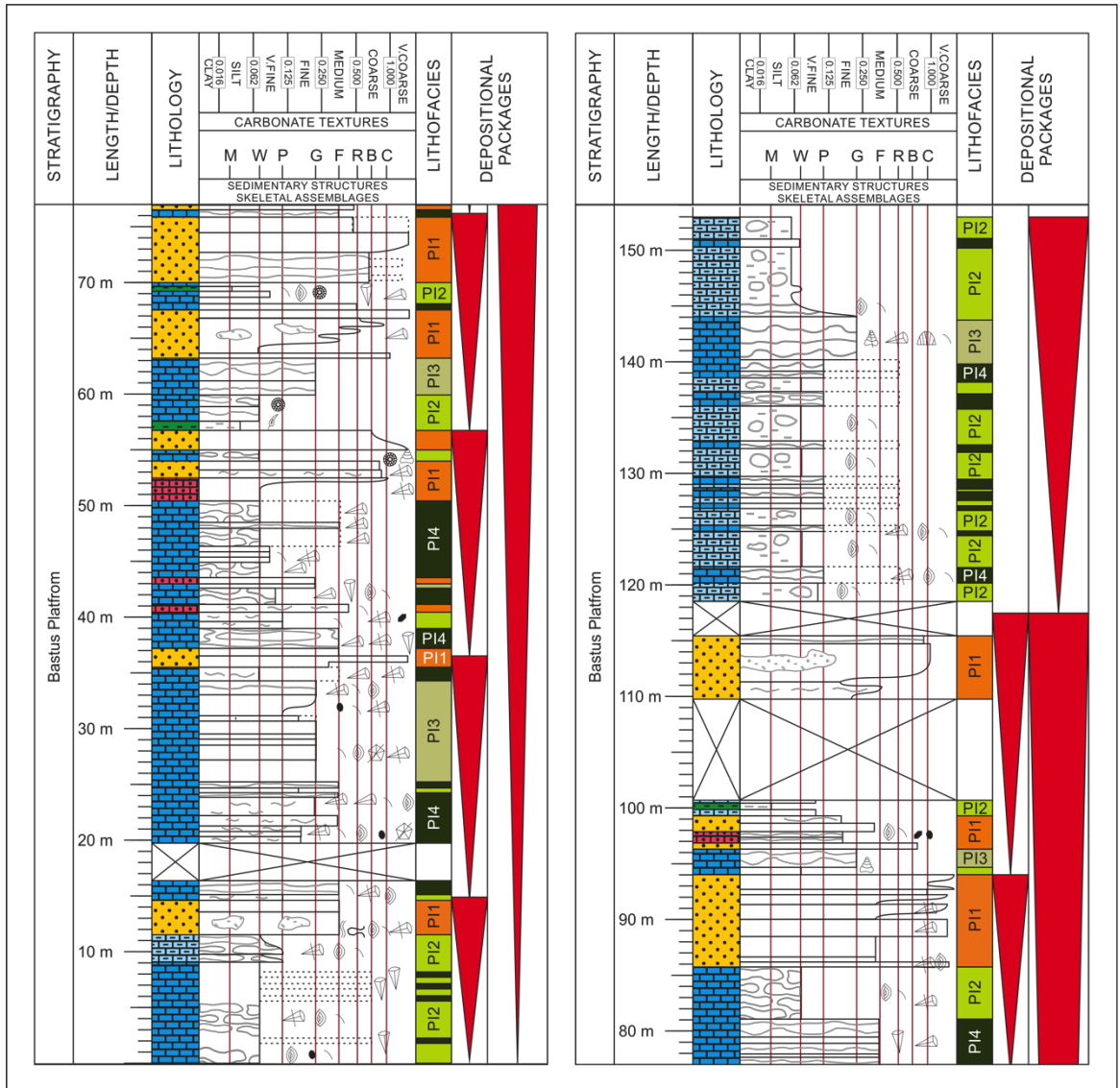


Figure 4.5: Composite log of the platform interior sediments of the Bastus Platform exposed at Oliana, scale 1:500. A key for sedimentary logs is given in Figure 4.3. Lithofacies colours and codes are presented in Table 4.1. For locality see Figure 4.1. Original logs are at 1:50 scale, and are presented in Appendix B.

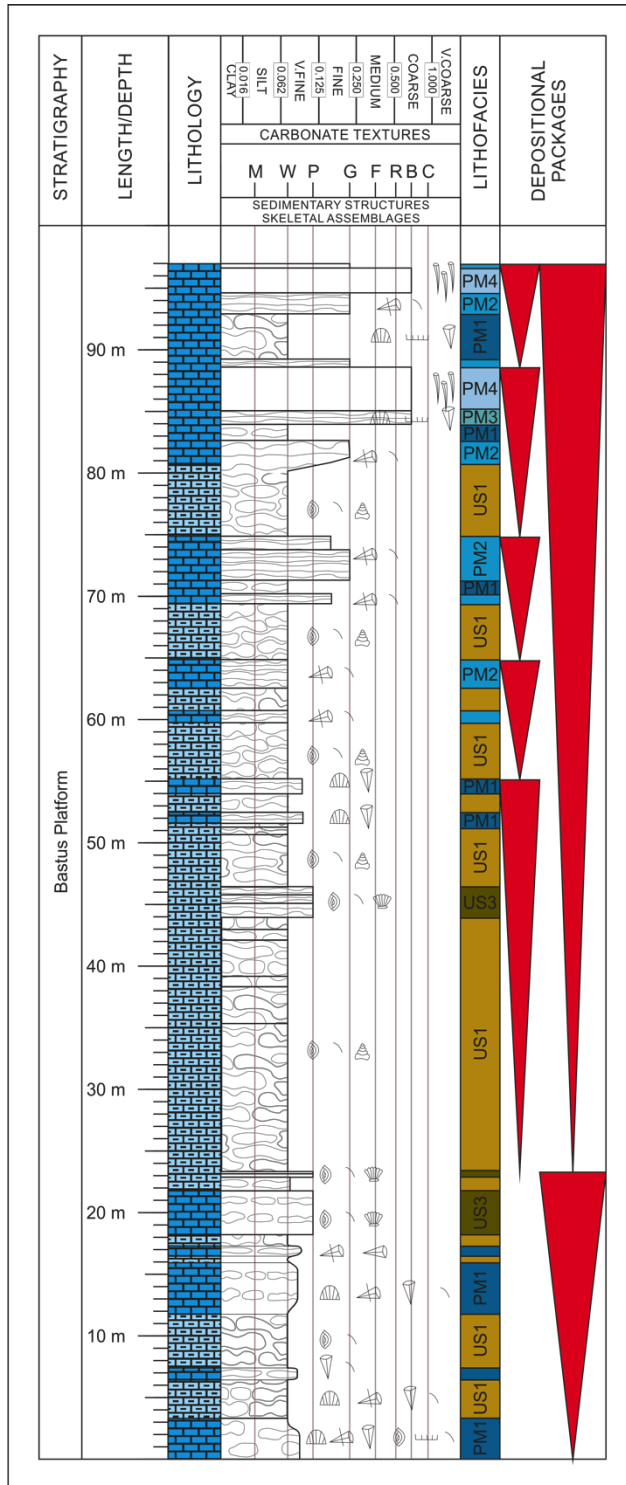


Figure 4.6: Composite log of the platform margin sediments of the Bastus Platform exposed at Montagut Gully, scale 1:500. A key for sedimentary logs is given in Figure 4.3. Lithofacies colours and codes are presented in Table 4.1. For locality see Figure 4.1. Original logs are at 1:50 scale, and are presented in Appendix B.

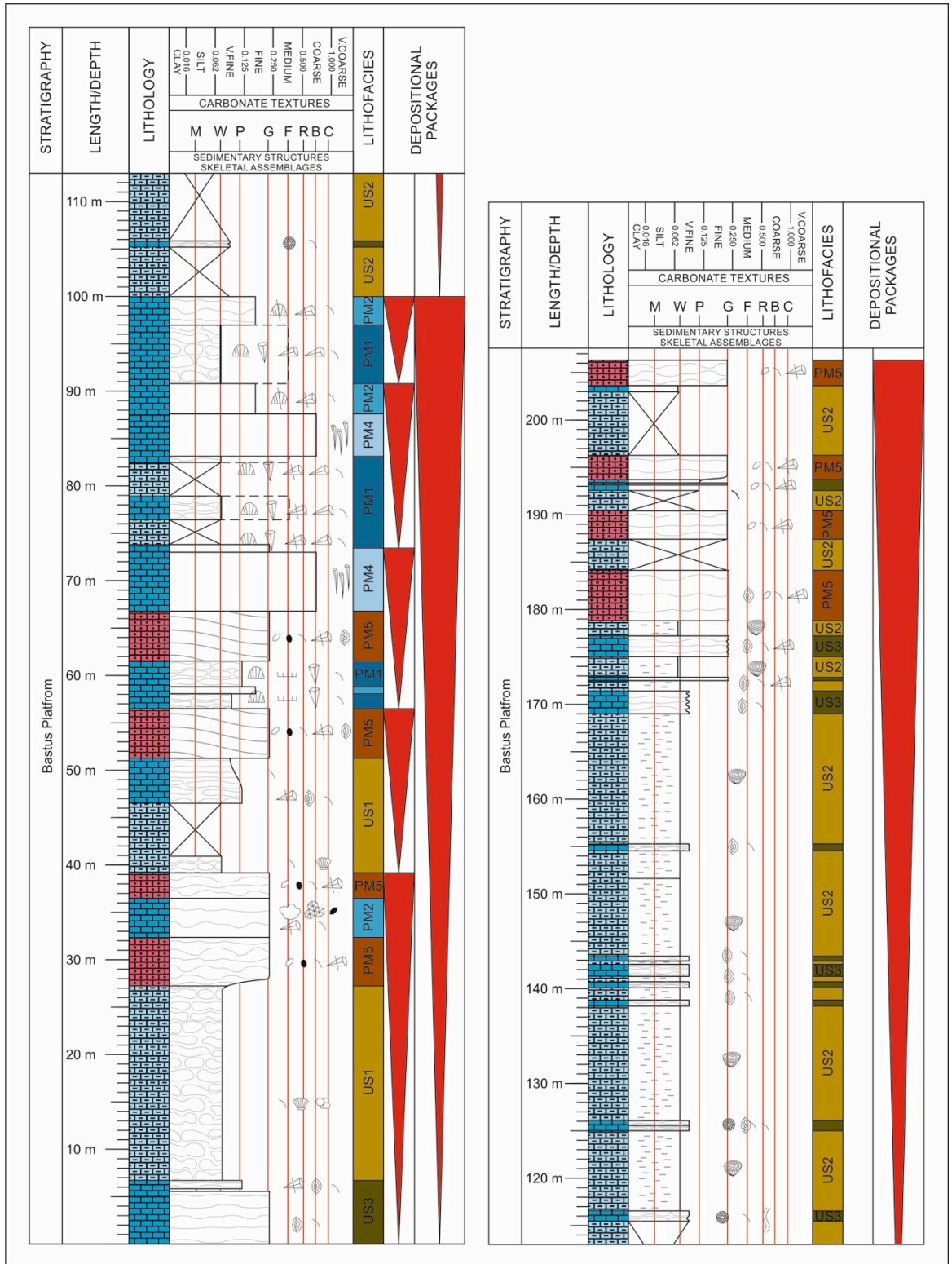


Figure 4.7: Composite log of the platform margin sediments of the Bastus Platform exposed at Carreu River, scale 1:500. A key for sedimentary logs is given in Figure 4.3. Lithofacies colours and codes are presented in Table 4.1. For locality see Figure 4.1. Original logs are at 1:50 scale, and are presented in Appendix B.

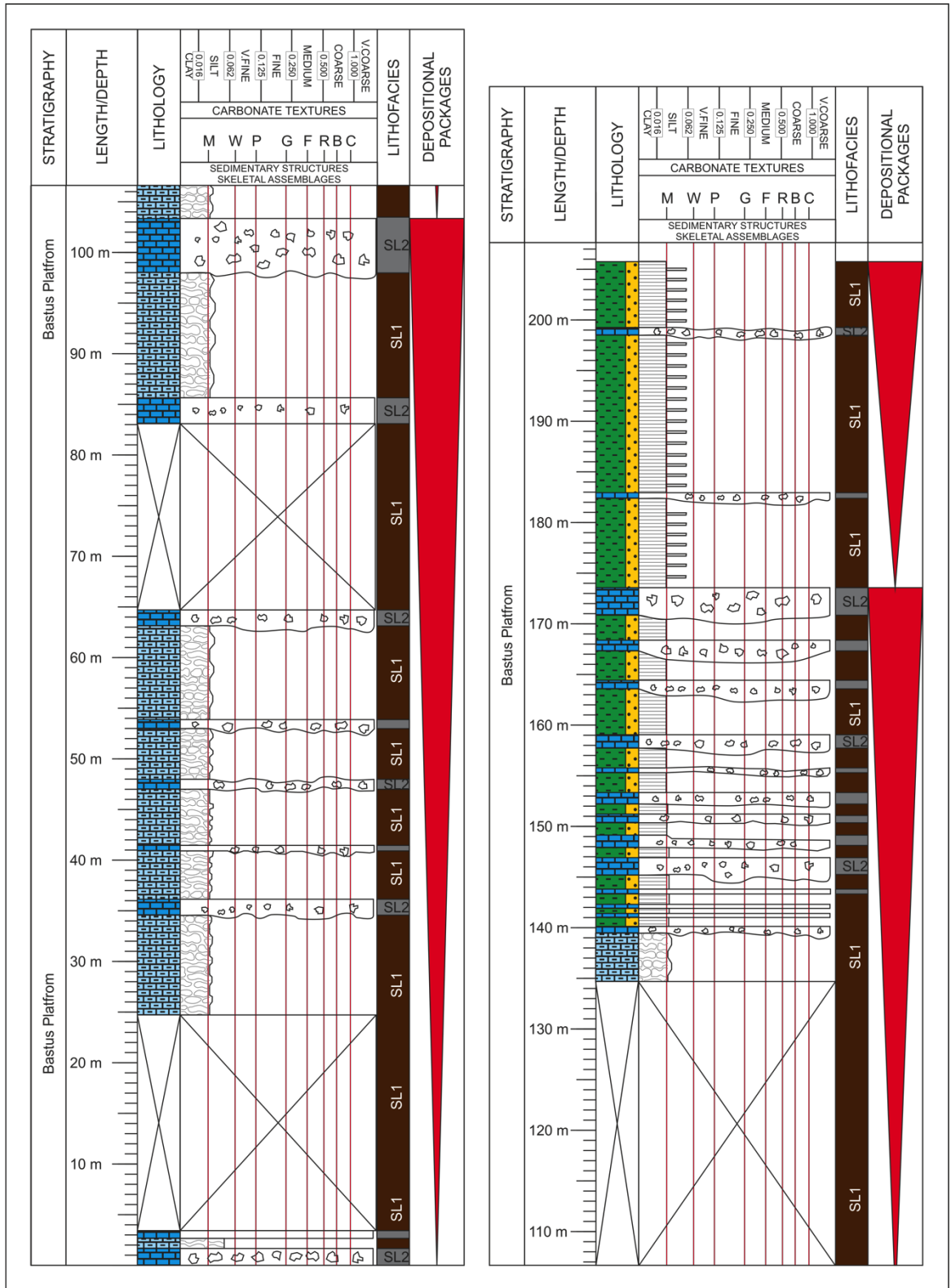


Figure 4.8: Composite log of the basal sediments of the Bastus Platform exposed at Tamurcia, scale 1:500. A key for sedimentary logs is given in Figure 4.3. Lithofacies colours and codes are presented in Table 4.1. For locality see Figure 4.1. Original logs are at 1:50 scale, and are presented in Appendix B.



## 4.5 Platform Dimensions and Topography

It was previously determined that the Bastus Platform comprised a platform top, approximately 52 kilometres wide and more than 115 kilometres in length, with a slope that was at least 23 kilometres wide and a NNE-trending basin axis (Chapter 3 and Figure 4.2). Total sediment thicknesses are derived from map data and logged sections (Chapter 3). The proximal, siliciclastic-rich marginal marine succession was only ca. 60 metres thick, whilst the platform interior and margin successions are up to 470 metres thick, decreasing to a maximum of 225 metres thickness on the slope (Figure 4.2). Widths and lengths of individual depositional elements, such as shoals or margin reefs, are further quantified in Chapter 5.

The relationship to fair-weather wave base (FWWB) was interpreted for each GDE and the respective LFA on the basis of microfacies, faunal composition and sedimentary features (Table 4.2), including the water-depth indicators presented by Flügel (2010). The position relative to FWWB was then translated into estimated water depths, assuming that the Tresp basin was partially restricted and showed low wave energy, based on its position in the seaway between the Iberian and European plate (Plaziat, 1981), similar to the modern day Mediterranean. The FWWB of the Plio-Pleistocene Mediterranean is defined as <10 m, and a storm wave base of 15 m (Messina et al., 2007). Estimations were further supported by the water depths defined for rudist and coral communities in both carbonate and mixed carbonate–siliciclastic systems by Sanders, (1998), Sanders and Höfling (2000), and Sanders and Baron-Szabo (2008). The resulting depth ranges were used to estimate the dip angles of the platform top and margin, using the relationship between lateral distance and the change in water-depth between respective localities. Resulting from the estimated water depths is an angle of the platform top of less than 0.05°, and a slope angle of 0.5° (Table 4.2).

**Table 4.2: Overview of water depth indicators and estimated water depths for individual gross depositional environments (GDE), their lithofacies, and the respective locality. References for water-depth indicators are given in the appropriate case. Where no reference is given, the estimates given by Flügel (2010) are applied. The rightmost column presents lengths of platform geometrical elements and the calculated angle. Numbers are rounded upwards.**

GDE	Lithofacies	Locality	Water depth indicators	Estimated water depth	Distance and angle
Proximal environment	<ul style="list-style-type: none"> <li>Sandstones, marls and quartz-rich grainstones</li> </ul>	<ul style="list-style-type: none"> <li>Camarasa</li> </ul>	<ul style="list-style-type: none"> <li>Potential palaeosols (cf. Chapter 3 and logs CAa/CAb, Appendix B)</li> <li>dm-m scale cross-bedding.</li> </ul>	Above FWWB ~0-10 m	<p>Platform Top:</p> <p>Distance from shoreline to platform break: 55 km</p> <p>Difference in water depth: 15 m</p> <p>Resulting inclination: &lt;0.05°</p>
Platform interior	<ul style="list-style-type: none"> <li>Coarse grained sandstones and grainstones with rudist debris (PI1)</li> <li>Dark nodular wackestones with foraminifera and rudist biostromes (PI2)</li> <li>Rudist biostromes, coarse rudist limestones, and fine peloidal and bioclastic limestones (PI3 and 4)</li> </ul>	<ul style="list-style-type: none"> <li>Oliana, Montsec</li> </ul>	<ul style="list-style-type: none"> <li>Rare cross-bedding in siliciclastic dominated lithologies</li> <li>Abundant small benthic foraminifera</li> <li>Micritic envelopes in grain-dominated facies</li> </ul>	Above FWWB ~0-10 m	
Platform Margin	<ul style="list-style-type: none"> <li>Rudist and coral bioherms, biostromes and bedded bioclastic limestones (PM1-4)</li> <li>Cross-bedded, quartz bearing bioclastic grainstones and packstones (PM5)</li> </ul>	<ul style="list-style-type: none"> <li>Collades de Basturs</li> <li>Montagut Gully</li> <li>Carreu River</li> </ul>	<ul style="list-style-type: none"> <li>Rudist-Coral bioherms (estimated up to 20m depth depending on wave energy; Sanders, 1998)</li> <li>Abundant micritic envelopes</li> <li>Large-scale cross-bedding</li> </ul>	To parts above FWWB and between FWWB and SWB ~5-15 m	
Upper Slope	<ul style="list-style-type: none"> <li>Nodular wackestones, marls, patch reefs and packstone intercalations (US1-3)</li> </ul>	<ul style="list-style-type: none"> <li>Carreu River</li> </ul>	<ul style="list-style-type: none"> <li>Frequent presence of solitary cunolites corals, interpreted as living as deep as 20-25 m (Sanders and Höfling, 2000; Sanders and Baron-Szabo, 2008)</li> <li>Periodic intercalations interpreted as storm deposits due to increased sorting and reduced micrite contents, (implying above SWB; Sanders and Pons, 2001)</li> </ul>	Below FWWB, Periodic influence of SWB given ~15-25 m	
Basin	<ul style="list-style-type: none"> <li>Pelagic wackestones and debris flow deposits (LS1-2)</li> </ul>	<ul style="list-style-type: none"> <li>Tamurcia</li> </ul>	<ul style="list-style-type: none"> <li>Sponge spicules</li> <li>Dominance of planktonic foraminifera</li> </ul>	Considerably below SWB ~100 m	

## 4.6 Sequence Stratigraphic Interpretation

### 4.6.1 Surfaces

#### **Bounding Surfaces**

The lower boundary of the Bastus Platform in the landward area is an erosional unconformity, where the Santonian sediments of the Bastus Platform overly Jurassic to lower Cretaceous bioclastic limestones or a karstified and bauxite-bearing Aptian succession (Institut Cartogràfic i Geològic de Catalunya, 2014). In the platform Interior, the lower boundary is a sharp, irregular contact, interpreted to be erosional with the underlying Sant Corneli Platform. The lower boundary in the vicinity of the platform margin and in the basin are mostly transitional (Sanders and Pons, 2001; Institut Geològic de Catalunya and Institut Cartogràfic de Catalunya, 2010).

The upper boundary of the Bastus Platform Cycle is gradational in the proximal areas (Institut Cartogràfic i Geològic de Catalunya, 2014), where the sandstones grade into the overlying limestones of the Terradets Platform. In the platform interior, the boundary between the nodular foraminiferal wackestones of the Bastus Platform and the massive to bedded limestones of the Terradets Platform is sharp. The boundary is gradational to the south of the platform margin (in the area of Collades de Basturs; Gallemí et al., 1982; Sanders and Pons, 2001), and sharp at the northern platform margin (Carreu River locality). The alterations of nodular wackestones and quartz bearing grainstones and packstones of the upper slope either transition into, or display a sharp boundary with, the overlying basinal shales of the Terradets platform. In the basinal areas, the top boundary is gradational as the mudstones, calcisiltites and debrites of the Bastus platform grade into the basinal succession of the Terradets platform, which shows intercalations of thin sandstone turbidite beds into dark grey marly mudstones and silts.

#### **Major Internal Surface**

A surface showing an abrupt change from shallow-water lithofacies to deeper lithofacies is observed across the southern half of the study area. In the proximal, Oliana section, there is an abrupt disappearance of the poorly sorted, bioclastic bearing sandstones and quartz-rich bioclastic limestones (lithofacies P13), and the succession continues as foraminiferal nodular wackestones, rudist bearing floatstones/rudstones and quartz-free peloidal grainstones. On the platform margin, in the Carreu River, a sharp boundary separates a succession of bioclastic limestones and rudist and coral bioherms and biostromes (lithofacies PM1-PM4) from overlying nodular wackestones of lithofacies US1. Strong erosion of these wackestones in the field means sedimentary features at this transition cannot be observed.

At the Montagut Gully locality, this surface is interpreted to lie at the top of the logged section. The section logged at Montagut comprises bioclastic limestones (lithofacies PM2) overlying coralline and rudist build-ups (lithofacies PM1 and PM4). Structural and stratigraphic correlations from the geological maps (Institut Cartogràfic i Geològic de Catalunya, 2010) show that these limestone beds are time-equivalent to those described below the sequence boundary at the Carreu River section (being mid-Santonian in age). This is further supported by similar of rudist-communities reported in the Carreu area (Vicens et al., 1998) and in the Collades de Basturs area (Gili et al., 1994).

At the Collades de Basturs section there are a total of three stacked successions of slope nodular wackestones (US1) to margin build-ups (PM1). Based on the thickness of the section above the major surface at the Carreu section, the surface is correlated to lie at the top of the last set of stacked beds at Basturs. This results in similar ratios of total sediment thickness above and below the major surface between the two localities.

In the basinal section at Tamurcia the surface is correlated with the top of the most prominent debrite beds roughly halfway through the section, where a transition from a section with frequent debrite beds to a sudden lack of debrite beds is evident. However, large gaps in exposure present a large uncertainty for this correlation.

It was not possible to recognise the surface within either the most proximal section at Camarasa, or at the basinal transect of Tamurcia. In Camarasa (cf. Figure 4.4; and logs CAa and CAb in the Appendix), a progradational trend is recognised in the lower parts of the section. Following a large unexposed section, the succession is interpreted to continue with a retrogradational trend from massive sandstones into marly limestones, which is followed by a progradation, with the sandstones returning to the top of the section. Because of the substantial gaps in this section and the possible amalgamation with the underlying Sant Corneli Platform Cycle, the major surface cannot be correlated confidently to this section.

The entire Bastus Platform is interpreted as a 3<sup>rd</sup> order cycle (cf. Chapter 3). The surface described here subdivides the platform deposits into two 100-300 m thick subunits with generally consistent, upward shallowing facies changes. The conventional sequence stratigraphic interpretation would assume that the subdivision of the platform therefore corresponds to 4<sup>th</sup> order cycles. Subsequently, the described surface would be interpreted as a 4<sup>th</sup> order sequence boundary and flooding surface. However, the conventional time-span of 4<sup>th</sup> order cycles lies within the range of few 100s ky (Vail et al., 1977; Van Wagoner et al., 1990). With approximately 1.5 My for each of the 4<sup>th</sup> order cycles defined here, these lie well above

this time-span. Therefore the two sequences are therefore referred to as Sequence 1 and Sequence 2, respectively.

No transgressive systems tracts, showing upward deepening trends of facies prior to shallowing, or maximum flooding surfaces are identified. The sections are mostly characterised by monotonous sections of fine grained facies with little change, prior to upward-shallowing. The sequence boundary is interpreted to coincide with this flooding event, as evident by the sharp transition from shallow-water to deep-water facies.

#### 4.6.2 Stacking Patterns

The lithofacies show consistent stacking patterns across the platform, which were used as a basis for the correlation and identification of key surfaces (Figure 4.9). These stacking patterns are not separated by diagenetically overprinted surfaces, but are defined by abrupt facies changes, mostly from relatively shallow-water facies to relatively deeper-water facies.

In the platform interior, interpreted typical stacking pattern comprise basal nodular wackestone (PI2) interbedded with rudist boundstones and peloidal grainstones (lithofacies PI3&4). These facies decrease in abundance upwards, whilst coarse-grained quartz-bearing grainstones and bioclastic sandstones (PI1) become increasingly common. The top bounding surface and the bottom bounding surface of the following stacking pattern are defined by a sudden facies change from coarse grainstones and sandstones (PI1) to thick successions of fine-grained nodular and foraminiferal wackestones (PI2). Overall, the succession is approximately 120 metres thick and is interpreted to represent an upward-shallowing trend from platform interior to proximal, marginal facies.

At the platform margin, the basal beds in each succession are fine-grained nodular wackestones of the upper slope (US1), with occasional, intercalated metre-scale rudist-coral patch reefs or larger bioherms (US1b and PM1, respectively). Towards the top, the platform margin lithofacies become more frequent, first in the form of mixed-rudist bioherms (PM1) and bioclastic grainstones (PM2), and later more frequent slender rudist biostromes and associated sheet-like coral-rudist-sponge beds (PM3&4) typical of the backreef environments. The bounding surfaces are defined by an abrupt change from either bioclastic grainstones (PM2) or biostromes and sheet-like coral-rudist-sponge beds (PM3&4) to nodular wackestones of the upper slope (US1). These successions are ca. 100 metres thick.

On the upper slope, successions are thinner (~60 metres thick) and comprise nodular or thinly bedded marly wackestones (US1/US2) at the base, with sporadic intercalations of wavy bedded bioclastic packstones with foraminifera (US3). Towards the top, large-scale cross-bedded bioclastic and quartz bearing grainstones and packstones become more common (PM5),

representing platform margin grainstone and packstone shoals. There is a sharp boundary with the overlying US1/2 of the next sequence.

In the lower slope, stacking patterns are ca. 100 metres thick and dominated by thinly bedded pelagic mudstones and calcisiltites at the base (LS1). Towards the top, debris-flow deposits with erosional lower boundaries become more frequent, showing both an upward increase in thickness as well as in the size of components (LS2). The stacking patterns end at a sudden facies change from frequent and thickly bedded debrites of lithofacies SL2 into thick successions of mudstones and calcisiltites (SL1).

### 4.6.3 Interpreted Sequences

The sequence stratigraphic correlation established for the Bastus Platform is presented in Figure 4.10. The interpretation uses the internal surface separating Sequence 1 from Sequence 2 as a datum (cf. Section 4.6.1), since this is the most prominent time-equivalent surface across the platform. On the basis of the stacking patterns described in Section 4.6.2, these can be further subdivided into internal cycles (S1.1 – S1.3 and S2.1 – S2.2, respectively). The sequences are described using Figure 4.4; platform interior facies refer to the section at Oliana, platform margin at Collades des Bastus and Montagut Gully, platform margin and slope successions at Carreu River and basinal facies from Tamurcia. Notable for both large-scale sequences and most of the smaller-scale sequences is that the thickness at the Carreu section is thinner than at the other platform margin section (Collades de Basturs and Montagut).

The first cycle, S1.1, is in most parts hypothetical. The presence of this cycle at Oliana is insinuated by the abrupt change from nodular wackestones (PM2) to rudist boundstones and floatstones (PI4) in the lower part of the section, which is interpreted as the boundary of a platform interior sedimentary stacking pattern as defined in Section 4.6.2 (Figure 4.9). In all localities, this cycle is interpreted to begin at the base of the Bastus platform. At Collades de Basturs, it is interpreted to terminate at the top of a thin bed of quartz-bearing grainstones and packstones (PM5). In Montagut, Carreu and Tamurcia, the lack of exposure or control on lithofacies only allows estimation of the presence of the sequence. It shows a thickness between 40 and 90 metres. At this point, platform interior did not show rudist build-ups, and comprised a thick succession of platform margin shoals. In the basin, no resedimented margin limestones were present.

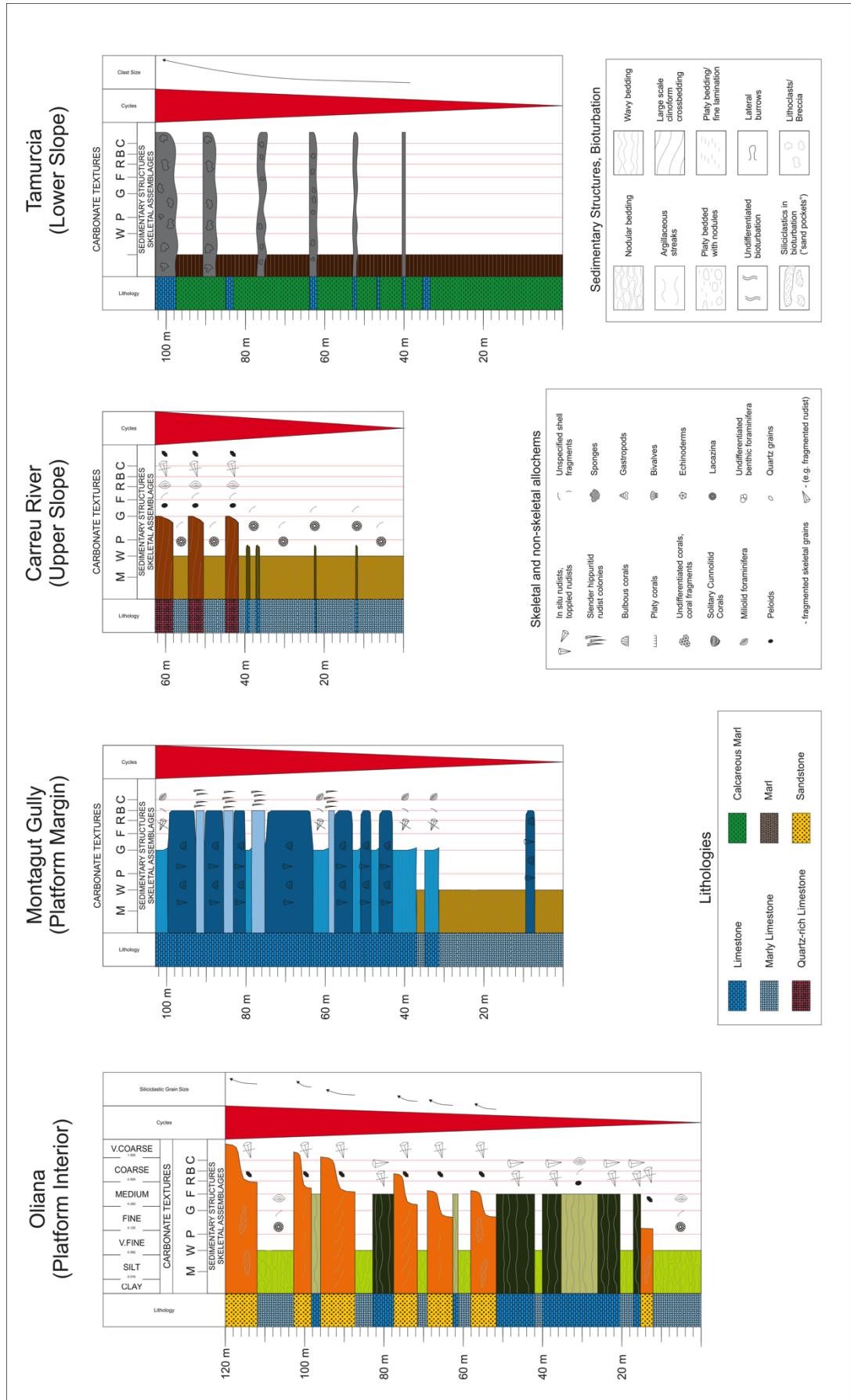


Figure 4.9: Simplified sedimentary patterns of the Bastus Platform, used to construct the sequence stratigraphic interpretation. Colours in the in the grain-size column represent the lithofacies noted in Table 3.8. Note that siliciclastics dominated lithologies (lithofacies P11; orange) are plotted using the siliciclastic grain size scale.

S1.2 is interpreted from outcrops in the platform interior, platform margin and basin, and is ~50-100 metres thick in total. The basal surface was not observed in the field, but is interpreted to occur at the base of the rudist boundstones and rudstone interval at the lower parts of the Oliana section, and at the top of the thin platform margin grainstone shoal interval at the bottom of the Collades de Carreu section. Both facies transitions are interpreted as bounding surfaces of the sedimentary stacking patterns (Section 4.6.2; Figure 4.9). The upper surface is also defined by the transition from shallow to deeper water facies. The platform interior is dominated by rudist-coral bioherms, which pass offshore via platform margin build-ups and grainstone shoals into basinal wackestones with, widely spaced, upward-thickening debrites.

S1.3 is defined at the base by a sharp transition from nodular platform interior wackestones into rudist dominated carbonates in the platform interior, and from grainstone shoals or platform margin build-ups into nodular slope wackestones in the platform margin areas. In the basinal areas, it commences with an abrupt disappearance of the lower slope debrites and dominance of pelagic wackestones. In the platform interior areas, the rudist build-ups give way to the first influx of siliciclastics, which is noted by the presence of coarse grained sandstones and quartz-dominated grainstones (PI1) which form a thick (~80 m) interval of stacked beds. In the platform margin, the slope wackestones are replaced by rudist composite build-ups and occasional margin grainstone shoals. The basinal succession shows an upward increase in debrite beds. Internally, a number of smaller scale stacking patterns (“parasequences”) can be interpreted in to this sequence (Figure 4.10), based on abrupt facies transitions from shallow to deep environments – similar to those used to define the sequences of higher orders.

Overall, the development of Sequence 1 is characterised by grainstone shoals occupying the margin initially, with the composite rudist-coral margin build-up becoming established towards the end of the sequence. Simultaneously, a large influx of siliciclastics occurs in the proximal parts, and frequent and increasingly thick debrite beds appear in the basin.

Sequence 2 is subdivided into two smaller sequences by assuming that the basal surfaces of lagoonal patch reef intervals within the Oliana section represent flooding events (As defined in Section 4.6.2, similar to sequence S1.2). Therefore, sequence S2.1 initiates at the defined major flooding surface (cf. Section 4.6.1) and terminates at the base of the patch reef interval at the uppermost parts of the Oliana log (Dark-green lithofacies PI4; lagoonal patch reefs). This top surface is interpreted onto the top of the last platform-margin facies interval within the Collades de Basturs log (blue lithofacies, PM1-4). In Montagut, this part of the section is presumed to be eroded on the top of the modern-day Sant Corneli anticline, as a structural reconstruction shows that a significant part of the section is missing. In Carreu, the top of this sequence is not well-pronounced, and is interpreted to lie within the small cluster of foraminiferal packstone



beds (lithofacies US3). In Tamurcia, this interpretation is based on the assumption that a large part of the section is missing above the recorded log (shaded and crossed area of Figure 4.10), so that the interpretation of the surface is purely hypothetical.

S2.2 initiates at the base of the lagoonal patch reef interval in the uppermost parts of Oliana (similarly to S1.2), and includes the interval of nodular wackestones at the top of the Collades de Basturs section. Again, this section is presumed to be eroded at Montagut Gully. In Carreu, it is represented by the topmost part of the log, where quartz-bearing grainstones and packstones (lithofacies PM5) become more frequent within the thinly bedded silty marls (lithofacies SL1). As with S1.2, there is no control on the thickness or facies variations within the section at Tamurcia.

Subsequently, Sequence 2 is characterised by a lack of platform margin build-ups, and by the presence of some platform margin grainstone and packstone shoals. In the platform interior, siliciclastics are absent and platform interior rudist build-ups are less common.

Overall, the transition from Sequence 1 to Sequence 2 is associated with a shift from progradational to aggradational stacking patterns to a sudden backstepping of the margin above the boundary between the sequences. This is most evident where the slope wackestones overlie the former platform margin build-ups at the boundary between the sequences (cf. Figure 4.2A and Figure 4.10, most prominently in the Carreu section). Furthermore, platform margin facies in the second sequence only occur in the southernmost (more proximal) areas of the Sant Corneli Anticline area in the area between Oliana and Collades de Basturs. Similarly, the frequent siliciclastic beds occurring in the platform interior during the later parts of the Sequence 1 retreat above the sequence boundary. They were not observed in platform interior during the upper sequence, but are interpreted have backstepped further to the south. This is supported by the consistent presence of siliciclastics throughout the platform time-span in the most proximal areas (Camarasa; Chapter 3).

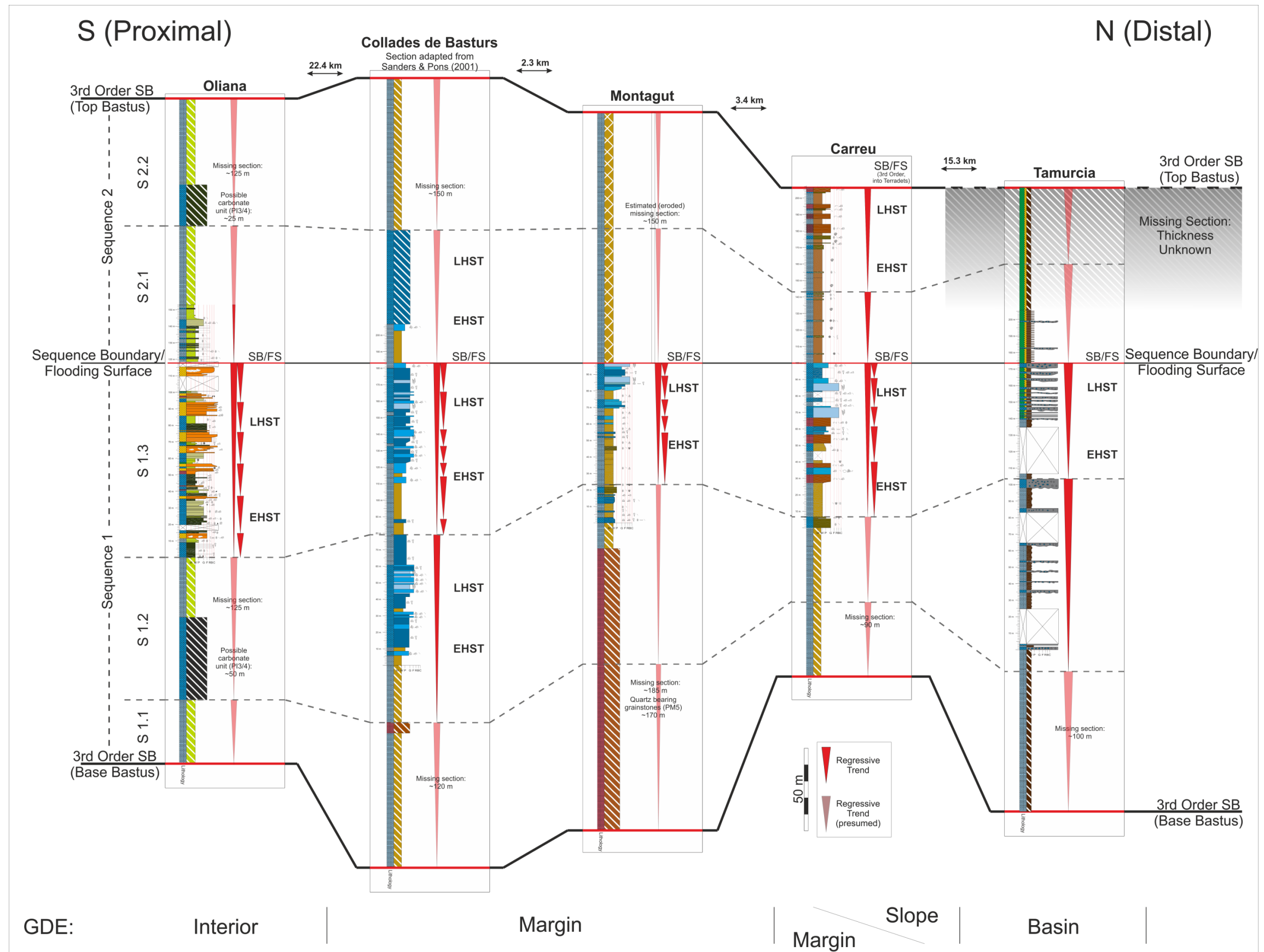


Figure 4.10: Sequence Stratigraphic interpretation of the Bastus Platform. The internal surface described in 4.4.3 is used as a datum. For lithofacies colour codes refer to Table 3.8. High-resolution versions of the logs are given in Figure 4.4-Figure 4.8. The section of Collades de Basturs is adapted from Sanders & Pons (2001). Noted at the bottom are the respective Gross Depositional Environments (GDE) represented by each section. The determined missing section and expected lithofacies association above and below each log is supplemented from map data and is denoted with bars with dashed colours. Interpreted low frequency sequences are numbered on the left-hand side of the figure (Sequence 1 and Sequence 2), as well as potential higher frequency sequences within these (1.1, 1.2; 2.1, 2.2 and 2.3). The base and top of the Bastus Platform are marked with bold lines, low frequency sequence boundaries with solid lines, and high frequency sequence boundaries with dashed lines. Symbols refer to the key presented in Figure 4.9. For localities refer to Figure 4.1 and Figure 4.2. EHST = Early Highstand; LHST = Late Highstand; GDE = Gross Depositional Environment.

#### 4.6.4 Subsidence and Relative Sea-Level History

The subsidence history for key points along the cross-section of the Bastus Platform was reconstructed (Figure 4.11). This subsidence model assumes that the sediment thickness deposited over the duration of the Bastus Platform (3 My) corresponds to the subsidence rate at specific locations along the platform. As compaction was not quantified in microfacies analysis, this calculation does not account for any post-depositional compaction of the sediment and calculated subsidence rates represent a minimum value.

Figure 4.11 illustrates that subsidence rates vary from a minimum of 21 m/My in the platform interior to >100 m/My at both Collades des Basturs and in the basin, at Tamurcia. Overall the rate of subsidence varies substantially across the platform. Most notably, there is a decrease in subsidence rate at the outer platform margin section at Carreu River, reflected by the reduced thickness of the sediment compared to other platform interior and platform margin sections (Figure 4.11).

Since these subsidence rates change substantially over relatively short distances, they are interpreted to be the direct result of tectonism in this area. It has been suggested that the Sant Corneli Anticline began to grow in the Santonian (Drzewiecki et al., 2014; Markley et al., 2014) and could explain why sediments are thinner within the Carreu River Section. Alternatively, differential compaction has resulted in a thinner sediment pile in the Carreu River section. This might occur if the sediments were more mud-rich than at nearby localities with a thicker succession, but this is not the case; the sediments at the Carreu River show similar overall sediment composition to the remaining platform margin sections (cf. Figure 4.10).

For the reconstruction of a relative sea-level curve, the global sea-level curve of Kominz et al. (2008; Figure 4.2B) was simplified to consist of a low-frequency oscillation (3 My period, 23 m amplitude), and a high-frequency oscillation (0.6 My period, 13 m amplitude; Figure 4.11). For the majority of localities the resulting curve shows an overall rise in relative sea-level, with slight variations in the rate of relative sea-level rise occurring as a result of the global sea-level fluctuations. Substantial periods of relative sea-level fall only occur in the most proximal sections (Camarasa), and to a very small extent in the platform interior (Montsec, Isona), the outer platform margin (Carreu River) and the basinal section (Tamura). In the platform margin, the sections of Collades de Basturs and Montagut Gully do not experience a net fall in relative sea level throughout the platform interval (Figure 4.11).

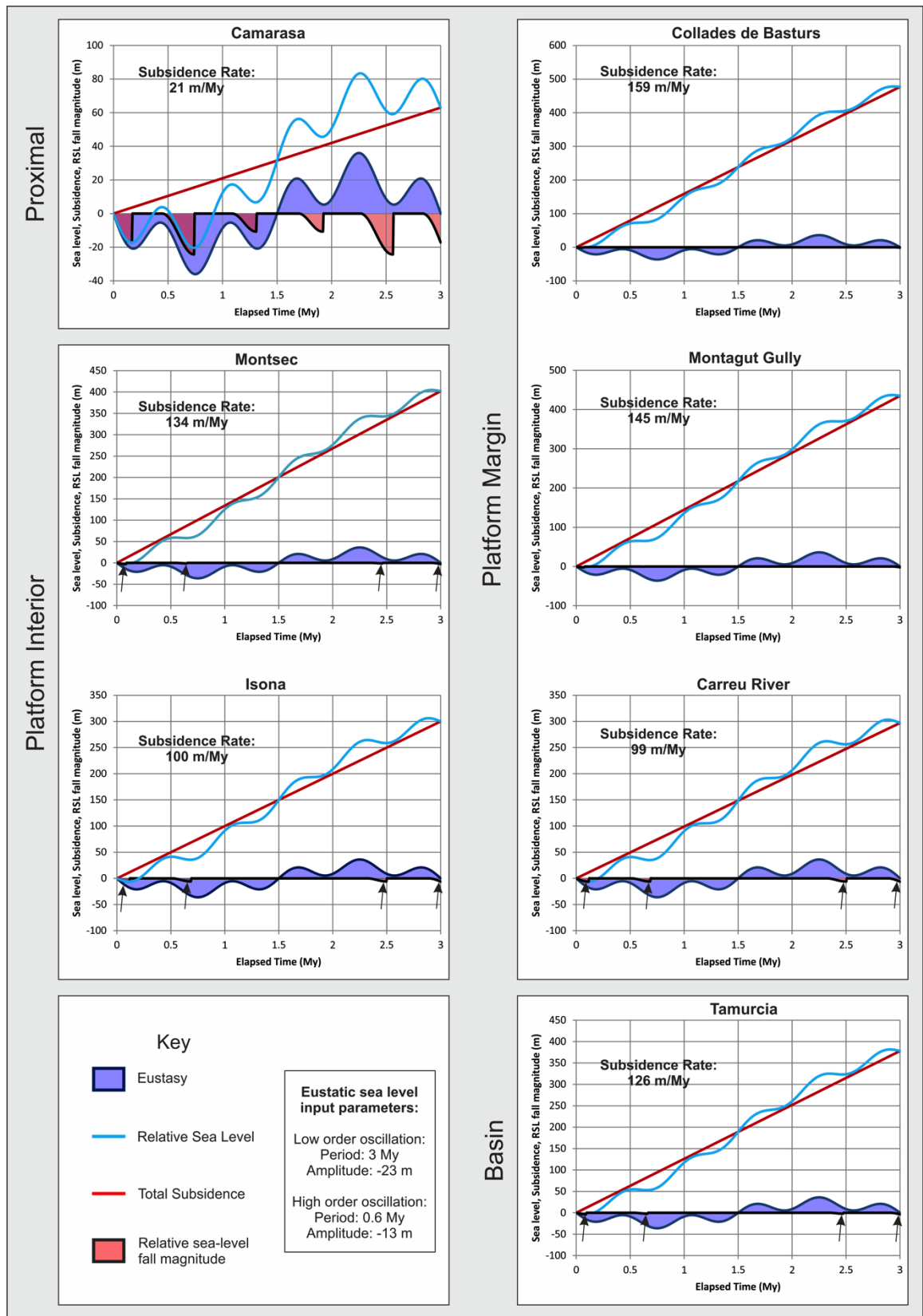


Figure 4.11: Diagrams of eustasy, relative sea level, subsidence and relative sea-level fall magnitude for specific sections of the Bastus Platform. Subsidence rate was determined through the time interval of the Bastus Platform (83.7-36.7 Ma = 3 My), and the total thickness of the sediment at the specific position. Compaction was not accounted for, resulting in minimum subsidence rates. The eustatic sea-level curve was simplified from the curve presented by Kominz et al. (2008; cf. Figure 4.2B). Notable is the general low amplitude to complete lack of relative sea-level fall periods throughout most of the platform, with the exception of the most proximal strata. Arrows in each graph highlight smaller periods of relative sea-level fall. Furthermore, it is notable that the Carreu River section presents the margin transect with the lowest subsidence rate (due to the thinner total sediment package),

and is the only one here to show periods of sea-level fall. This highlights how possible syntectonic growth of the Sant Corneli Anticline during this time, as proposed by Drzewiecki et al. (2015) and Markley et al. (2015), may have led to reduced subsidence here and different development of stacking patterns.

#### 4.6.5 Evaluation of the Interpretation and Controls on Sequence Development

The sedimentary architecture of the Santonian Bastus Platform has been reconstructed in cross section (Figure 4.2A), using a conventional sequence stratigraphic interpretation (Figure 4.10) based on field data. This provides the most realistic correlation of beds and surfaces. The Bastus Platform established during the flooding above the 3<sup>rd</sup> order sequence boundary at the top of the Sant Corneli Platform, a low angle, distally steepened ramp (Chapter 3). Within the Bastus Platform, two large sequences have been defined (Section 4.6.3):

- Sequence 1, which shows establishment, progradation and aggradation of rudist-coral build-ups and grainstone shoals along the platform margin. This resulted in a steepening of the platform margin and differentiation of the platform top from the slope and basin. At this time, siliciclastic influx extended into the platform interior.
- Sequence 2, which shows marked backstepping directly following the boundary, with a landward migration of the platform margin rudist-coral build-ups, and the retreat of clastic sediments from the platform interior.

Each sequence is further divided into smaller, high frequency shallowing-up sequences (Figure 4.9), defined by a sharp change from proximal to more distal facies, and an absence of diagenetically modified bounding surfaces.

Water depths on the platform top are interpreted to have been shallow (<10 m in the interior, ca. 5-15 m at the margin), on the basis of facies analysis showing abundant shallow-water indicators such as abundant benthic foraminifera, corals, and micritic envelopes (Table 4.2). The slope is only moderately deeper (~15-25 m), as seen by the frequent occurrence of large benthic foraminifera, whereas the basin only shows evidence of pelagic carbonate production and is therefore interpreted to be below the photic zone (~100 m). Moreover, wave and tidal energy on the platform top are thought to have generally been low, as indicated by the extensive presence of fine grained nodular wackestones in this area, with occasional localised higher energy indicated by accumulations of grainstone shoals and reworking of bioclasts and siliciclastics. Furthermore, the influence of siliciclastics on carbonate production appears to be minimal since rudist biostromes and rudstones in the platform interior quickly recover after periodic influxes of sandstones and siliciclastic rich grainstones (cf. Oliana section; Figure 4.5, and log OLa, Appendix B). There is also only a limited occurrence of siliciclastics in the allochthonous facies of the platform margin (cf. Collades de Basturs, Montagut Gully, and

Carreu Rivers sections; Figure 4.6, Figure 4.7, and Figure 4.10, and the respective 1:50 scale logs, Appendix B).

### **Controls on the Evolution of Sequence 1 and 2**

In Sequence 1, the composite rudist build-ups establish halfway through the sequence (S1.2), and are observed to prograde and finally aggrade (S1.3). In the platform interior, occasional biostromes and grainstone beds occur. A gradual increase in reworked quartz-bearing beds towards the top of the sequence is noted. In the basin, an increase in the frequency of debrite beds occurs towards the top of the sequence.

The initial progradation and then aggradation of the platform margin build-ups within Sequence 1 can be interpreted as a reaction of the carbonate factory to the rates of relative sea-level rise. Assuming consistent productivity, the margin was first able to prograde during times of low rate of relative sea-level rise. Later, an increase in rate of relative sea-level rise led to carbonate productivity aggrading. It is interpreted that this aggradation led to the oversteepening of the margin, and subsequently to the frequent deposition of resedimented margin material in debrite beds in the basin. Furthermore, the progradation and later aggradation of the platform allows the siliciclastic delta system in the most proximal areas to shed into the platform interior in the later stages of the platform (S1.3), as evident in the frequent occurrence of coarse reworked siliciclastics in Oliana.

The substantial variation of thickness across the platform, and particularly between the platform margin transects (Collades de Basturs, Montagut Gully, and Carreu River; Figure 4.10) was associated with different rates of subsidence in these localities (Section 4.6.4, Figure 4.11). This is associated here with the occurrence of localised growth of the Sant Corneli Anticline suggested by Drzewiecki et al. (2014) and Markley et al. (2014).

The boundary between Sequence 1 and Sequence 2 is defined as a flooding surface without signs of subaerial exposure, and is marked by an abrupt backstepping of facies. As the reconstructed sea-level curves (Figure 4.11) do not include possible variations in sedimentation rates (and thus in subsidence rates) over time, they show no marked change in the rate of relative sea-level rise half-way through the lifespan of the platform that may coincide with the backstepping. It is therefore not possible to evaluate on the basis of the reconstructed relative sea-level curves whether a distinct rise in relative sea level occurred at this time and led to the backstepping.

An alternative mechanism for the backstepping of facies following the sequence boundary may be a periodic reduction of carbonate productivity, during which productivity could not keep up with the rise in relative sea level and the platform subsequently stepped back. This could have

resulted from either a significant change in oceanic conditions such as change in levels of nutrients (Hallock and Schlager, 1986) or oxygen levels (Schlanger and Jenkyns, 1976), or via poisoning of the platform through siliciclastic input (Mount, 1984). The higher amount of clay and silt-grade marl above the sequence boundary at the Carreu River locality (lithofacies US2) may indicate that this was the case. However, no clear indications of a cessation/reduction of productivity in the sediments, such as hardgrounds or condensed sections, are observed. Alternatively, a rapid tectonic tilting event may have resulted in a backwards shift of facies following the sequence boundary. Such scenarios were previously discussed by Schlager (2005b) to lead to sudden backstepping of platform margins. However, it is expected that such tilting should coincide with significant indicators of slope instability, which were not observed here. The debris flow beds consisting of resedimented margin limestones are correlated to occur below the sequence boundary and not above it.

Sequence 2 follows the backstepping after the sequence boundary, with platform margin build-ups occurring in late S2.1 in Collades de Basturs (proximal platform margin). Later in the sequence, cross-bedded platform margin grainstone shoals are observed in Carreu River (distal platform margin). This indicates that the platform margin prograded towards this position later in the sequence. The absence of platform margin composite build-ups in the platform margin area of S2.2 may be explained with the discontinuity of these in strike (several km in length, cf. Chapter 5), leading to no build-up being noted in the cross-section. The discontinuity is indicated by the frequent interbedding with the quartz bearing grainstones in the platform margin sections and by map data (further discussed in Chapter 5). Alternatively, it is possible that no platform margin build-ups established here due to the higher occurrence of marl, as discussed for the absence of these above the sequence boundary.

The top of Sequence 2 marks the termination of the Bastus platform. After this, the prior platform margin areas are overlain with dark, fine grained pelagic calcareous shales and marls ("Herba-Savina Clays"; Gallemí et al., 1982; Sanders and Pons, 2001). This boundary is described as gradational in Collades de Basturs (Gallemí et al., 1982; Sanders and Pons, 2001) and was observed to be sharp in Carreu River. Furthermore, the boundary towards the overlying Terradets limestones is sharp in the platform interior area (Oliana; Institut Cartogràfic i Geològic de Catalunya, 2015). Throughout the study area, there are no indications of subaerial exposure at this boundary. This indicates that the Bastus Platform terminated as a result of rapid flooding and drowning.

### **Controls on High Frequency Cyclicity**

The five high-frequency sequences interpreted in the Bastus platform show thicknesses of ca. 50-120 m. Similarly to Sequence 1 and 2, their thickness may vary substantially across the

platform. They are characterised by the stacking patterns defined in Section 4.6.2, and generally display a shallowing-up trend. In the interior, this is reflected by a transition from foraminiferal nodular wackestones (PI2), fine grained peloidal grainstones (PI3) and rudist biostromes (PI4) towards reworked bioclastic sandstones and quartz-rich grainstones (PI1). At the platform margin localities, it is reflected by transition from upper slope nodular wackestones (US1/2) towards the composite build-ups of the margin (PM1-4), with transition from margin biostromes (PM1) and debris apron packstones (PM2) to backreef bioherms (PM3/4). In the basin, this is noted by an upward increase in frequency and thickness of the debris flows introducing remobilised platform margin material (SL2) into the basinal fine grained pelagic wackestones (SL1).

In this interpretation, the stacking patterns roughly correspond to a duration of 0.6 My. This time span compares to that defined for 4<sup>th</sup> order sea-level cycles by Vail et al. (1977) and Van Wagoner et al. (1990). This may lead to common interpretation of these as such 4<sup>th</sup> order cycles. The subsidence curves reconstructed in Section 4.6.4 indicate that these high-frequency cycles are the result of the periods of reduced rate of relative sea-level rise. However, the occurrence of differential subsidence that is recognised in the varying thickness of the sequences across the basin introduces uncertainty to this interpretation.

#### **4.6.6 Key Characteristics of the Sequence Stratigraphic Interpretation**

The key criteria defining the sequence stratigraphic framework are the backstepping of facies at the defined boundary between the lower and upper sequence, and the sedimentary stacking patterns within each sequence, interpreted as possible higher order sequences. A main challenge during this interpretation is posed by the absence of bio- and chemostratigraphic constraints. As a result, sequences are interpreted based on abrupt facies changes from shallow to deeper water facies. Additionally, it was shown via the varying thicknesses of sequences that differential subsidence occurred across the platform (Section 4.6.4). This complicates recognising the control on the formation of Sequences 1 and 2 and the smaller scale sequences within these, as discussed in Section 4.6.5.

The differential development of thickness across the proximal-basinal transect is a unique feature of this interpretation. Thickness does not solely increase towards the basin, but is found to decrease at key points in the platform interior and margin. This development is interpreted as the result of the syndepositional growth of the Sant Corneli Anticline through the duration of the Bastus Platform. By proposing that sediment thickness directly translates to subsidence, it can be concluded that subsidence rates varied locally across the platform (cf. Section 4.6.4). The locally varying subsidence can also be used to interpret the different number of smaller scale stacking patterns interpreted into S1.3 at Montagut Gully and Carreu River (5 for each locality),



compared to Collades de Bastus (7 stacking patterns; Figure 4.10). The reduced rates of accommodation on the rising Sant Corneli Anticline led to formation of smaller numbers of these “parasequences”.

Also characteristic is the lack of interpreted transgressive systems tracts, with all intervals of the logs interpreted as highstand systems tracts. The reconstructed relative sea-level curves (Figure 4.11) show that throughout the majority of the platform, relative sea level is in a constant state of rise. Lower rates of relative sea-level rise are observed during the eustatic regressions and lowstand, but no substantial amounts of relative sea-level drop are achieved due to the high rates of subsidence outpacing eustatic sea-level fall. This results in no stages of negative accommodation occurring, which in turn can lead to the absence of pronounced sequence boundaries and transgressive systems tracts (Catuneanu et al., 2011). Alternatively, the manifestation of transgressive deposits is not characteristic enough to allow distinguishing these from the sediments of the early highstand systems tracts.

Overall, this interpretation shows the importance of basin-scale correlations when attempting a sequence stratigraphic interpretation of such carbonate successions. There is a marked difference between the interpretation achieved on a basin-scale study here compared to those of Pomar et al. (2005) and Sanders and Pons (2001) for single sections. These authors have previously interpreted the sequence stratigraphic character of the Bastus Platform on outcrop scale. However, their interpretations are incompatible and cannot be tied into the basin-wide sequence stratigraphic framework presented in this study. Pomar et al. (2005) interpreted a series of progradational patterns into the Montagut Gully and Carreu River localities, and suggested the facies variation between rudist/coral-dominated limestones and benthic foraminiferal nodular wackestones was the result of a distinct change of carbonate factory. Sanders and Pons (2001) interpreted the exposure at Collades de Basturs as a series of shallowing-to-deepening successions with a general progradational trend. These are not compatible with the interpretation presented here, in which the Bastus Platform is separated into two large-scale progradational to aggradational sequences and five smaller, progradational sequences.

## **4.7 Stratigraphic Forward Modelling**

### **4.7.1 Modelling Approach**

The sequence stratigraphic interpretation of the Bastus Platform raises a number of issues that are attempted to be addressed and solved with three-dimensional stratigraphic forward modelling. One of the key aims is to test whether the two lower-hierarchy sequences and the five higher-hierarchy sequences of the Bastus Platform pose a plausible sequence stratigraphic

interpretation on the basis of relative sea-level fluctuations. This includes the stratigraphic development of each sequence, the width and migration of facies belts, and the facies transitions that are interpreted as boundaries between these sequences. Additionally, these models aim to test whether controls other than sea-level fluctuations, such as temporal variations in carbonate productivity or tectonic tilt are able to produce the observed stacking patterns and facies distribution.

To address these issues, four models were produced:

- 1) a model which assumes 2 cycles of relative sea-level oscillation and consistent carbonate productivity.

This model was conceived to reconstruct the two progradational 4<sup>th</sup> order cycles, separated by a sequence boundary/flooding surface, interpreted into the Bastus Platform (cf. Section 4.6.3). Therefore, the period of the relative sea level was defined as 2 My and the amplitude was set to 10 metres.

- 2) a model which assumes 5 cycles of relative sea-level oscillation and consistent
  - carbonate productivity.

This model was conceived to reconstruct the five small-scale shallowing sedimentary cycles interpreted into the Bastus Platform (cf. Section 4.6.3). The frequency of the relative sea level was defined as 0.5 My with an amplitude of 10 m to coincide with those proposed during the duration of the Bastus Platform (cf. Section 4.6.4).

- 3) a model which assumes stable eustatic sea level and variable carbonate productivity over time.

This model varies carbonate productivity in times of stable eustatic sea level to assess whether the interpreted 4<sup>th</sup> order cycles and sedimentary stacking patterns can form without eustatically controlled sea-level fluctuations. A hypothetical reduction of carbonate productivity rates is introduced: Production rates are at 100% between 0 and 1.5 My, then reduced to 10% of the original value for a period of 150 ky, after which they return to 100% for the remaining duration of the model.

- 4) a model which assumes stable eustatic sea level and productivity, but introduces a tectonic tilt of the platform of 0.08° tilt at 1.5 My.

This model keeps eustatic sea level and carbonate productivity constant. At 1.5 My, it introduces a rotation of the platform of 0.08° in a counter-clockwise motion, with the hinge point located at 0 km length to simulate hypothetical tectonic tilt and the resulting increase in

relative sea level. This aims to recreate the two progradational 4<sup>th</sup> order cycles interpreted into the Bastus Platform.

#### 4.7.2 CarboCAT Modelling Parameters

The model grid was defined by the size of the study area, and set to 100x50 km (Figure 4.12). The cell size was defined by the smallest depositional element to be modelled, and was set to 1x1 km. The elapsed run time was set to 3 My, following the time-span of the platform (83.7-36.7 Ma) according to the established chronostratigraphic time scale (cf. Section 4.2.2 and Figure 4.2B). The time-step was set to 3 ky to provide high vertical resolution while allowing quick computation time. The initial basement topography was defined by the interpreted low-inclined platform morphology with a gradient of 2.1m/km of the underlying Sant Corneli Platform (cf. Chapter 3). To provide the necessary accommodation for the total sediment thicknesses along the platform, differential subsidence set to 20m/My between 0-18 kilometres (from south to north). It then increases linearly between 19 and 50 km to a rate of 140 m/My, and remains at this value from 50 km onward. Siliciclastic material was introduced as a boundary condition, then transported via diffusion on the southern boundary of the model, and the introduced amount set to increase gradually over the model run time. The initial facies distribution was interpreted to be pre-defined by the basement topography, and matched to fit the distribution described at the base of the cross-sections from field data (Figure 4.2). Input for eustatic sea-level is given in amplitude (m) and frequency (1/My), and was defined by published data (Kominz et al. 2008).

Four principal carbonate factories are defined in the models (Figure 4.12) on the basis of the lithofacies interpretations (Section 4.4): 1) lagoonal background sedimentation, 2) lagoonal rudist patch reefs, 3) platform margin composite build-ups, 4) pelagic slope sedimentation. The production rate (m/My) for each factory was limited to values that produced the observed sediment thickness over the time-span of the model. Accumulation rate of sediment had to be high enough for the system to keep up with the subsidence, but was limited to a maximum that is considered non-physical (Enos, 1991; Bosscher and Schlager, 1992; Steuber, 2000). Factories 2 and 3 each may produce a set fraction of transported material, defined from the ratio of in-situ lithofacies to transported lithofacies from the relevant sedimentary logs. The maximum water depth for productivity for factories 2 and 3 (euphotic depth) was set to 40 m, as lower or higher values result in narrower or wider platform tops than that observed from the field example, respectively (Figure 4.12). A transported fraction of 0.5 was determined for factory 2, and 0.8 for factory 3. These fractions were defined based on the ratio between the thickness of *in-situ* strata (i.e. biostromes/bioherms; lithofacies PI4, PM1, PM3, PM4) and bioclastic strata (grainstones and packstones; lithofacies PI3, PM2) in the platform interior and margin sections.

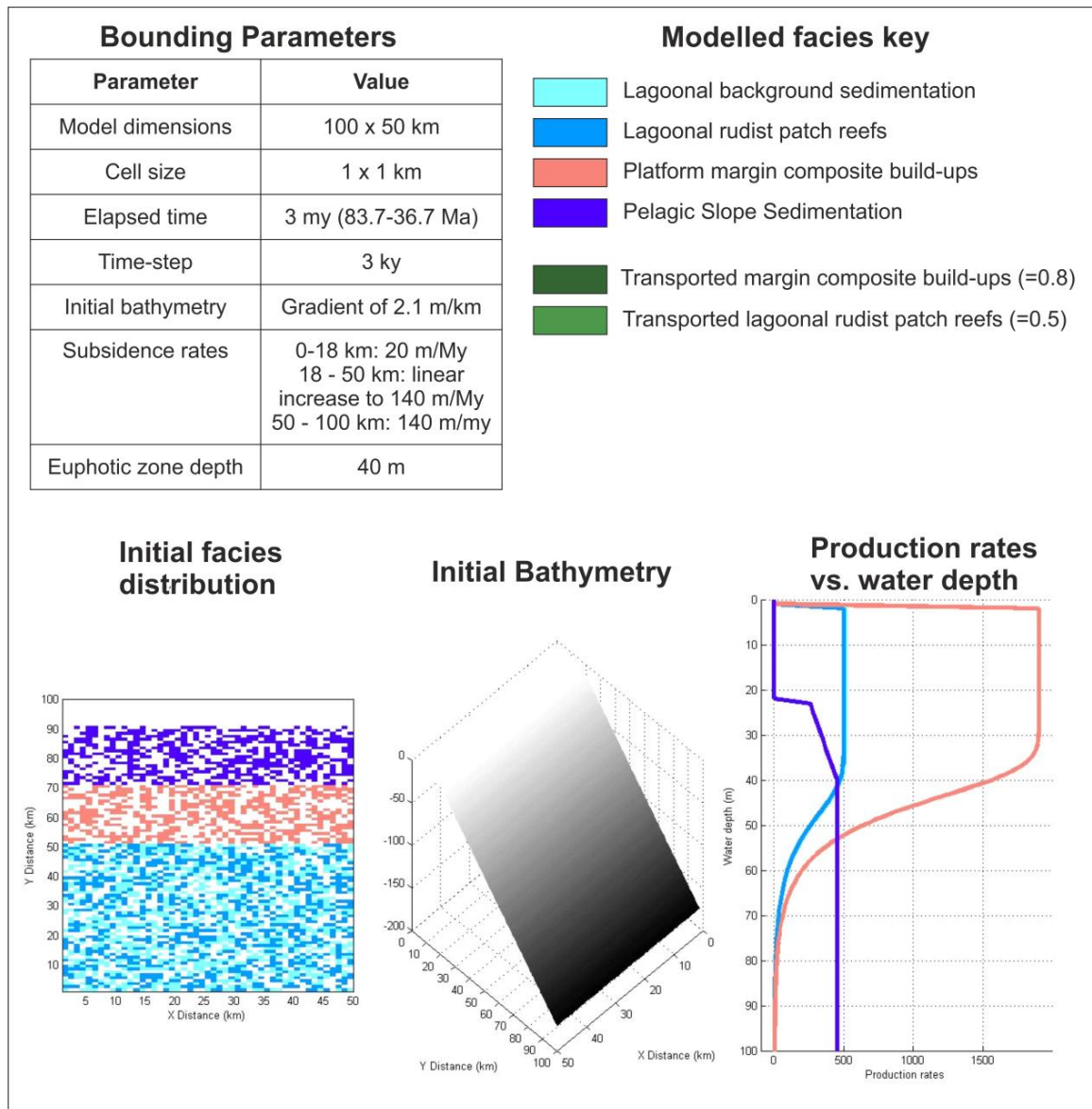


Figure 4.12: CarboCAT modelling parameters and lithofacies concept for the produced stratigraphic forward models. The table shows the numerical values for the bounding parameters defined in the model. The modelled facies key applies to all models in Figures 4.7 and 4.7. The transported fractions are noted in parentheses after the respective facies. The initial facies distribution is defined by the interpreted widths of facies belts at the bottom surface of the cross section of the Bastus Platform (cf. Figure 4.2A). The initial bathymetry was defined by the interpretation of the underlying Sant Corneli Platform as a ramp (cf. Chapter 3) and therefore shows a linear gradient. The water depth dependant production rates for each factory were derived using iterative testing, and are designed to achieve the lateral distribution of facies and the required sediment thickness across the platform (cf. Section 4.7.3).

### 4.7.3 Qualitative Sensitivity Analysis

#### Bounding Parameters and Productivity Rates

Quality control was made iteratively for each of the produced modelling approaches. The flexible base modelling parameters (productivity rates, subsidence rates, initial bathymetry, photic zone depth) were modified with each model run until the platform topography and width of facies belts observed in the cross-section were reproduced. The effects of changing some of these values are outlined below, and detailed descriptions are given by Antonatos (*in prep.*).

It was found that productivity values of 500 m/My are optimal for the platform interior background sedimentation and the platform interior rudist patch reefs. For the platform margin, rates of 1200 m/My were used. These values produce total modelled thicknesses that match well to field data. Lower values lead to failure of productivity to keep up with relative sea-level rise and eventual drowning, whereas higher values lead to margin breaks and slopes that are steeper than those interpreted from the field example. The productivity rates of the pelagic factory were set to 550 m/My. Lower values led to the platform developing a slope that was deemed too steep, whereas higher values were found to lead to stronger overall progradation of the platform. Subsidence rates were required to be changed according to the productivity rate to allow the platform to accumulate the observed sediment thickness without leading to subaerial exposure, which was not observed in the field.

Steeper initial bathymetry values or shallower euphotic zones lead to a shorter distance until the platform break, and less margin progradation. Sediment thickness and water depth along the platform are controlled by the combination of individual factory production profiles and subsidence rates.

### **Variable Parameters in Each Model**

For each individual modelling approach, the respective variable parameter (eustatic sea-level period and amplitude, productivity reduction and duration, and degree of tectonic tilt) was modified between model runs to replicate the sediment thickness, width of facies belts, and where possible to replicate internal stacking patterns. Some limitations are set by the features observed in the field and the presumed eustatic sea-level curve of Kominz et al. (2008).

For both models with oscillations in eustatic sea level, the period of the oscillation influences the point in time at which a change between systems tracts occurs (e.g. change from progradational behaviour during late highstand to aggradation during transgression). In the model based on 5 relative sea-level fluctuations, the period of the oscillation is clearly linked to small scale lateral shifting of the platform margin (ca. 5km) which occurs during transgression.

The amplitude of eustatic sea-level oscillations also shows an effect on the produced strata. In the model based on two eustatic oscillations, an amplitude higher than 20 m resulted in subaerial exposure, which was not observed in the field, whereas an amplitude between 0 and 10 m resulted in no effect of the sea-level fluctuation on the platform development, and the platform aggrading. In the model based on five oscillations, an amplitude higher than 10 metres resulted in extensive subaerial platform exposure during the lowstands, and a lower amplitude resulted in no pronounced progradation of the platform margin taking place.

In the model varying carbonate productivity rates for a specific time-span, the percentage of the original productivity rates to which it is reduced affects the distance of backstepping of the margin occurring at this time interval. Values between 10% and 0% of original productivity were tested. Smaller values show slightly further backstepping, but throughout this range of values resulting geometries are very similar. This is because the entire range of values poses a significant reduction of the original productivity. Furthermore, modifying the duration of productivity reduction has a slightly stronger effect, with longer durations leading to slightly stronger backstepping of the platform. Lastly, the point of time during which the reduction of productivity takes place directly affects the time at which the backstepping occurs, with earlier times of reduction leading to earlier backstepping and vice versa.

In the model that introduced tectonic tilt, a higher angle of tilt leads to stronger backstepping of the platform margin, and a lower angle to a less distinct backstepping. The duration of the tilting directly affects the time span in which tilting occurs, with higher values resulting in fast retrogradation rather than sharp backstepping. The point of time during which the rotation takes place directly affects the time at which the backstepping occurs, with earlier times of tilting leading to earlier backstepping and vice versa.

#### **4.7.4 Forward Modelling Results and Interpretation**

All models produced thickness profiles along the platform that are comparable with those determined from the field (Table 4.3, Figures 4.11 and 4.12). The position of the margin relative to the shoreline and the widths of facies belts (proximal, platform interior, margin, and slope) are similar to those established from the produced platform cross sections (Table 4.3). Furthermore, the inclination of the platform top and slope are comparable to those established for the Tremp Basin from field data.

For all models, the thickness of the proximal section (Camarasa), that of the platform margin (Collades the Bastus, Montagut Gully and Carreu River) and of the slope (Tamurcia) are comparable to those defined by the cross-section. However, the thickness variation observed in the platform interior (reduction of thickness between the sections Montsec and Isona) area was not recreated in the stratigraphic forward models.

Internally, all models tend to show sharp retrogradation of the margin from 0 My to ca. 0.6 My. This is interpreted as the result of the initial facies distribution set for the model putting the initial platform margin further basinwards than where it would naturally rest on the predefined underlying topography. Following this, key differences between the models are found in the internal facies patterns and stratigraphic development (Table 4.3, Figures 4.11 and 4.12). These are outlined and evaluated below.

Table 4.3: Summary table of geometrical and stratigraphic parameters defined for the Bastus Platform from the field and sequence stratigraphic interpretation, and those shown by the results of the individual forward modelling. The models generally match the thickness and rough facies distribution of the field example, but only models X and Y also produced the internal separation into two progradational sequences, separated by a surface defined by marked transition from shallow to deeper water facies. Shaded grey are the field example and the model inducing tectonic tilt, the latter being interpreted to represent the best-fit model on the basis of showing similarity in most parameters.

Scenario		Field example	1	2	3	4
Variable:		Presumed: Relative sea level	Relative Sea level (2 Ma oscillation)	Relative Sea level (5 Ma oscillation)	Decrease in productivity (reduction to 10% for 150 ky at 1.5 My)	Tectonic tilt (clockwise of 0.08° around hinge point at 0 km)
Thicknesses (m)	Proximal thickness	61	60	60	60	60
	Interior thickness	402	421	438	421	412
	Margin thickness	478-314	312	305	302	294
	Slope thickness	200				
	Basin thickness	377				
Position of margin relative to shoreline (km)		55	51	55	51	43
Width of facies belts (km)	Proximal	18.3-20.7	18	18	18	18
	Interior	15.9-26.3	28	32	28	20
	Margin	5-14.7	5	5	5	5
	Slope	>23	-			
Platform top inclination		<0.05°	<0.05°	<0.05°	<0.05°	<0.05°
Slope inclination		<0.5°	0.97	0.86	1.43	0.57
Low-order cyclicity	Number of sequences, duration	2 (ca. 1.5 My)	1 (3 My)	1 (3 My)	2 (ca. 1.5 My)	2 (ca. 1.5 My)
	Surfaces	Abrupt transition from shallow to deep facies	None	None	Abrupt transition from shallow to deep facies	Abrupt transition from shallow to deep facies
	Nature of sequences	Progradational to aggradational	0My-0.6My: retrogrades 0.6My-1.5My: progrades 1.5My-3My: aggrades	Progradational to aggradational	Progradation (ca. 2km) at begin of sequence. Continuing to aggradational, separated by ca. 10 km backstepping	Progradational (total ca. 20 km) to aggradational sequences, separated by ca. 25 km backstepping
High-order cyclicity	Number of sequences, duration	5 (ca 0.6 My duration)		5 (0.5 My duration) 10 m amplitude		
	Surfaces	Abrupt transition from shallow to deep facies	Not modelled	Exposure in proximal parts, facies transitions at margin	Not modelled	Not modelled
	Nature of sequences	Progradational		Progradational (Sequence 1) to aggradational (Sequences 2-5)		

### **Forward Model Assuming Two Cycles of Relative Sea-Level Fluctuations**

This model introduces an eustatic sea-level oscillation with a period of 2 My and an amplitude of 10 metres. In this model, the platform margin is observed to retrograde sharply between 0 My and 0.6 My. This is interpreted as the establishment phase of the platform, where the platform margin stabilises from the original facies distribution defined in Figure 4.13. After this, it progrades until ca. 1.5 My for ca. 17 km. This corresponds to the regressive part of the eustatic sea-level curve until the lowstand. Simultaneously, the most proximal parts experience subaerial exposure. At the beginning of the transgression, the platform margin aggrades until the end of the model runtime.

The progradational to aggradational trend that dominated the platform margin development in this model is not agreeable with the two progradational trends separated by backstepping that are proposed by the sequence stratigraphic interpretation of the Bastus Platform.

### **Forward Model Assuming Five Cycles of Relative Sea-Level Fluctuations**

This model introduces an eustatic sea-level oscillation with a period of 0.5 My and an amplitude of 10 metres. The result shows export of the proximal areas and platform interior (up to ca. 35 km) during eustatic regression and lowstand. The platform margin retrogrades from 0 My until ca. 0.25 My. After this, the platform margin shows a net progradation of ca. 15 km until 3.0 My, with small intervals of rapid lateral back and forth movements (ca. 5 km) of the margin during eustatic transgression (ca. every 0.5 My).

Overall, there are abrupt vertical facies transitions between margin and slope facies recognised at the platform margin area, but no clear separation in the cross-section into 5 smaller sequences as suggested by the sequence stratigraphic interpretation. Therefore, the resulting model, while achieving similar large-scale platform topography and width of facies belts, shows a different stratigraphic development than that interpreted in the sequence stratigraphic reconstruction.

To achieve a clear separation of 5 sequences, as proposed by the sequence stratigraphic interpretation, a sea-level amplitude of at least 30 metres is required (Antonatos, *pers. comm.*). This however results in extensive subaerial exposure of the platform interior and margin. As no subaerial exposure was described in the field, such a high amplitude of eustatic sea-level fluctuation is not considered a realistic parameter and cannot be used in the forward stratigraphic model.



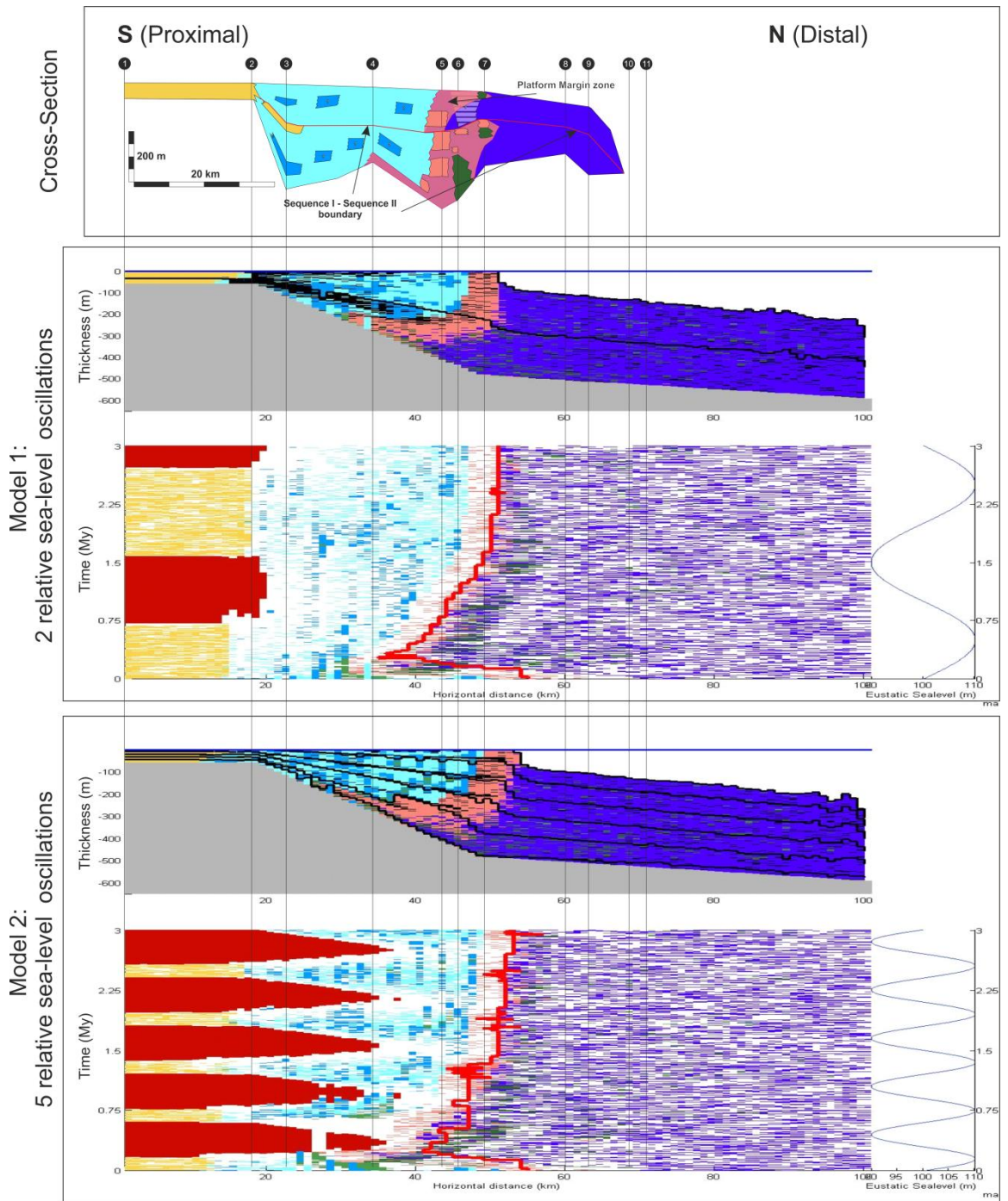


Figure 4.13: Comparison of the produced cross-section and cross-sections of the three-dimensional stratigraphic forward models created using variations in relative sea level. Top: cross-section of the Bastus Platform, drawn with scale and colour-coding of the stratigraphic forward models. Numbers at the top represent the cross-section data points (cf. Figure 4.2A). Lines are extended downwards from these to allow comparison with the model. Highlighted in pink is the interpreted area of the platform margin zone, in which platform margin build-ups may occur.

Middle: result of the stratigraphic forward model introducing two oscillations of eustatic sea level. The upper image represents a cross-section, the lower image a chronostratigraphic diagram (wheeler plot). To the right is the eustatic sea-level curve used in the model. Black lines in the cross-sections represent the top of eustatic sea-level sequences. Red intervals in the chronostratigraphic diagram represent subaerial exposure. The red line marks the lateral movement of the platform margin over time. Cells remaining white indicate no deposition took place during this time-step. It can be observed that the platform margin first retrogrades sharply during the initial 0.25 My. This is interpreted as the establishment phase of the platform. The margin then continues to prograde until ca. 1.5 Ma, after which it aggrades until 3 Ma. Subaerial exposure is present in the most proximal areas between ca. 0.7 and 1.6 Ma (regressive section of the eustatic sea-level curve).

Bottom: result of the stratigraphic forward model introducing five oscillations of eustatic sea level. Structure of the figure is identical to that above. It is observed that the platform margin retrogrades sharply for the first 0.25 Ma,

after which it progrades gradually for a total of ca. 15 km over the remainder of the time-span, with small-scale variations (ca. 5 km in both directions) occurring during eustatic sea-level rise. Subaerial exposure is extensive during the lowstands and reaches far into the platform interior (ca. up to 35 km).

### **Forward Model Assuming Stable Eustatic Sea Level and Variable Productivity**

This model introduces a reduction of productivity to 10% of the original values at 1.5 My, over a duration of 150 ky. After this, the productivity rates are restored to 100% until the end of the model runtime. The internal facies patterns show a sharp retrogradation of the margin during the first 0.25 My. In the cross-section, the platform margin then shows slight progradation to about 48 km. Following the reduction of the productivity rates, at ca. 2. My, the platform margin facies reach a further proximal position, and the facies belt is considerably wider than during the rest of the model (ca. 18 km). The margin trajectory is therefore only 5 km further landwards than before the reduction of productivity. At about 2.25 My, the platform margin returns to the position and width it had prior to the reduction of productivity rates.

Overall, the facies pattern produced in the cross-section is comparable with that of the sequence stratigraphic interpretation, while the chronostratigraphic chart suggests slightly different development than the one interpreted into the sequence stratigraphic panel. The model is lacking a clear differentiation of two progradational sequences, separated by a backstepping of the margin, after which the margin of the first sequence is overlain by the slope of the second sequence.

### **Forward Model Assuming Stable Sea Level and Sudden Tectonic Tilting**

This model introduced a clockwise tilt of  $0.08^\circ$  of the platform around a hinge point at 0 km at 1.5 My elapsed time. As with the previous models, the chronostratigraphic chart indicates that the platform margin retrogrades for ca. 8 km during the first 0.25 My of the model run time. After this, the platform margin mostly aggrades with the margin break located at ca. 48 km, and small lateral migration occurring on the scale of ca. 5 km. At 1.5 My, when the rotation takes place, the platform margin sharply backsteps over ca. 8 km. After this, it continues to aggrade for the remaining duration of the model.

The model cross-section can be interpreted slightly differently than the chronostratigraphic chart: an initial progradation of the margin, transitioning to an aggradational trend. This is followed by a distinct boundary at 1.5 My, after which the platform margin build-ups are sharply overlain by slope sediment, and the margin steps back a total of ca. 25 km. The margin then progrades again over ca. 0.25 My, until the platform margin reaches a position ca. 5 km more proximal than the margin of the previous sequence. Following this, the margin continues to aggrade at ca. 43 km. The two resulting sequences separated by a distinct flooding surface comply with the previously constructed sequence stratigraphic interpretation.

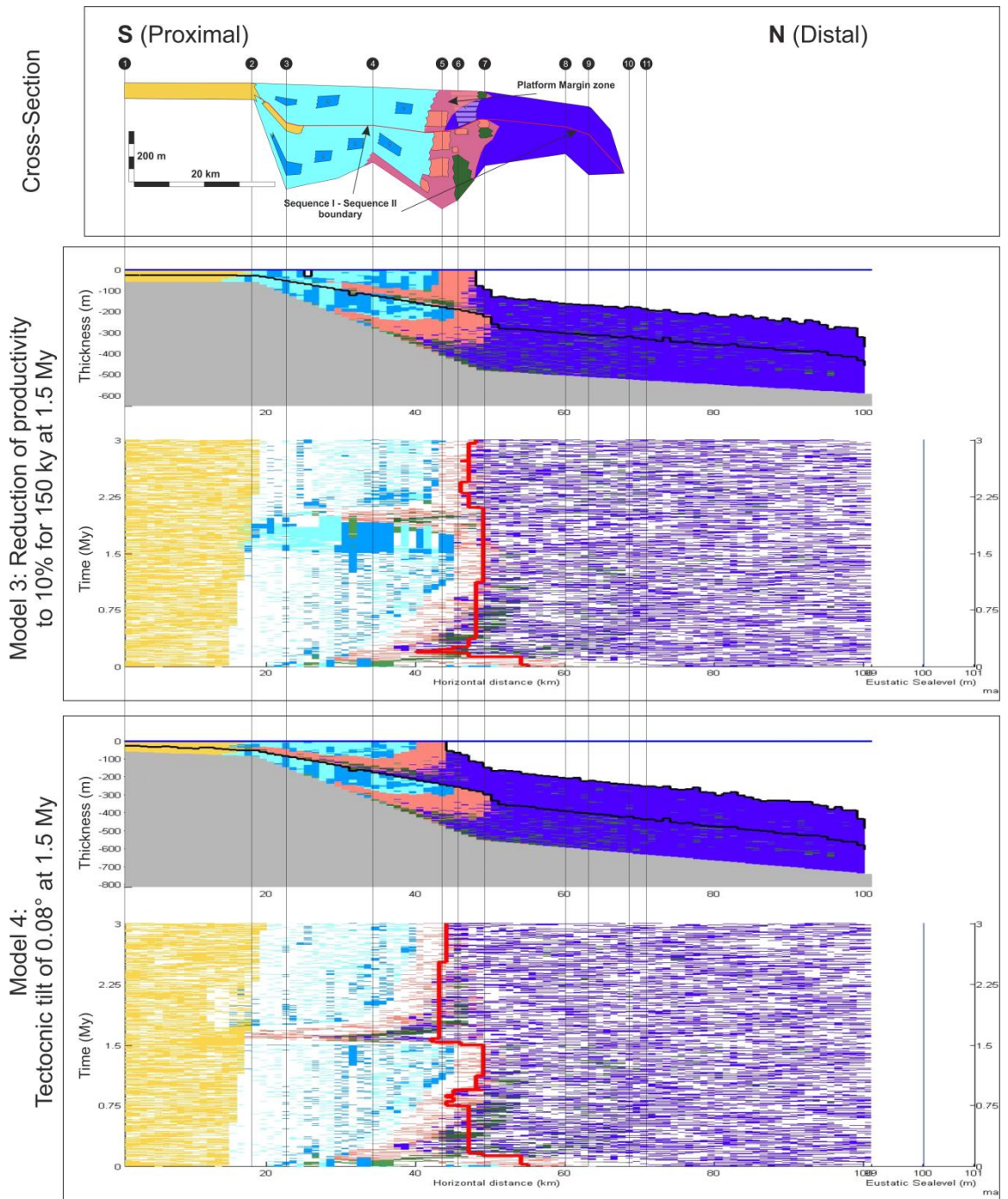


Figure 4.14: Comparison of the produced cross-section and cross-sections of the three-dimensional stratigraphic forward models created using variations in sediment productivity or tectonic tilt. Colour coding and structure of the figure are similar to that described for Figure 4.7. Top: cross-section of the Bastus Platform. Middle: result of the stratigraphic forward model introducing a reduction of productivity to 10% of the original value for a duration of 150 ky at 1.5 Ma run time. The cross-section shows two progradational to aggradational sequences separated by a sharp backstepping of the margin. The chronostratigraphic diagram shows that the platform margin retrogrades sharply during the first 0.25 Ma, after which it stabilises at ca. 48 km. A sharp landward migration (ca. 20 km) of the platform margin facies is observed at ca. 2 Ma. However, the margin trajectory only moves backwards by ca. 5 km. Bottom: result of the stratigraphic forward model introducing a clockwise tilt of  $0.08^\circ$  around a hinge point at 0 km. The cross-section shows two progradational to aggradational sequences, separated by a substantial backstepping of the margin facies. Here, former platform margin facies are sharply overlain by slope facies. As with the previous models the chronostratigraphic diagram shows that the platform margin first retrogrades strongly during the first 0.25 Ma. After this, the margin moves slightly between 45 and 50 km. At 1.5 Ma, there is a sharp backstepping (ca. 8 km), after which the margin trajectory continues to remain stable at ca. 43 km.

## 4.8 Discussion

### 4.8.1 Comparison of Sequence Stratigraphic Correlation with Forward Models

The sequence stratigraphic correlation of the Bastus Platform proposes platform growth is recorded by Sequence 1 and Sequence 2 (up to 300 m and 175 m thick, respectively), separated by a surface that shows an abrupt backstepping of the platform margin facies. The two large-scale sequences in turn comprise a total of five smaller scale sequences (high frequency cycles) with thicknesses of 50 – 120 metres – three in the lower sequence and two in the upper sequence.

To constrain the controls on the development of Sequence 1 and 2, stratigraphic forward modelling was used to attempt to replicate the stratigraphic architecture. Different models varied different parameters:

- A model introducing a fluctuation of relative sea level
- A model introducing a period of 150 ky during which the carbonate productivity is reduced to 10% of its original value
- A model introducing a clockwise tectonic rotation of  $0.08^\circ$  around a hinge point a 0 km.

Additionally, one model was produced to test whether variations in relative sea level could have produced the smaller-scale stacking patterns interpreted as high frequency cycles. This model introduced five fluctuations of relative sea level with an amplitude of 20 m.

The observed stacking patterns of both Sequences 1 and 2 or the high frequency cycles could not be replicated in forward modelling using variations in eustatic sea level (Figure 4.13), unless the amplitude was higher than 30 m. In this case, prolonged subaerial exposure of the platform top would have occurred. However, this feature was not observed in the field, and substantial relative sea-level drop on the platform interior and margin is not suggested by the relative sea-level curves constructed in Figure 4.11.

The models introducing either a reduction of productivity or a tectonic tilt resulted in stratal geometries similar to those interpreted into the Bastus Platform using conventional sequence stratigraphic correlation (Figure 4.14). This supports that a change in productivity or a tectonic influence might create similar, perhaps indistinguishable, stratal geometries than those typically interpreted as the result of a fluctuation of relative sea level.

The probability of the modelled scenarios occurring, and how they possibly address the key issues presented by the sequence stratigraphic interpretation (Section 4.6.6) are discussed in the following.

### **Mechanisms Affecting Low Frequency Cyclicity (Sequences 1 and 2)**

The stratal patterns interpreted into the sequence stratigraphic interpretation (Figure 4.10), particularly the separation into Sequence 1 and 2, and the backstepping of facies between them, were successfully reconstructed using a stratigraphic forward model that varies carbonate productivity (Figure 4.14). At 1.5 My run-time, the carbonate productivity of all four factories was reduced to 10% of the original value for a duration of 150 ky. After this it returned to the original value for the remaining run-time of the model. The original productivity rates are chosen to produce the final thickness of the Bastus Platform over the life-span of the platform, while confined to realistic ranges (Enos, 1991; Bosscher and Schlager, 1992; Steuber, 2000). However, the driving mechanism behind changes in carbonate productivity is generally poorly understood (Burgess, 2001), making quantification of productivity reduction within such a short time-span particularly difficult. This is additionally complicated by the fact that carbonate productivity and transport rates may be influenced by localised factors such as nutrient levels and wind patterns (Burgess, 2001).

The implications of a potential reduction of productivity onto local sedimentary features in the field were addressed in Section 4.6.5. As no sedimentary evidence for a platform-wide reduction in productivity, such as condensed horizons or hardgrounds were found, this scenario is unlikely. With the increased amount of silt in the slope nodular wackestones (US2) above the boundary between Sequence 1 and 2 at the Carreu River section, it is likely that fine-grained, suspended siliciclastic material reduced light penetration and led to cessation of platform margin rudist build-up development here. Since platform-margin build-ups are observed above the sequence boundary in Collades de Basturs (i.e. further to the South; Figure 4.10), and the platform interior does not show an increase in fine-grained siliciclastics, it is possible that the siliciclastic material was introduced axially onto the outer platform margin. With axial siliciclastic input pushing the margin build-ups southwards, this scenario would not involve a platform-wide reduction of productivity, but rather a landward shift of productivity zones. A similar model was previously discussed by Yancey (1991), only with direct input of siliciclastics from the shoreline resulting in a basinward shift of the carbonate production zone.

Changes in productivity resulting from oceanic conditions (nutrient levels) are known to often lead to replacement of one factory with another factory that can withstand the environmental change. This has been reported in the Turonian of the Tresp Basin (Pradina Limestones, Drzewiecki and Simó, 2000), where eutrophication resulted in platform-wide deposition of pelagic calcisphere wackestones. Furthermore, this is widely observed in the Mid-Cretaceous of the Arabian shelf, where periodic events lead to *Lithocodium-Bacinella* communities replacing the previous rudist- coral assemblages (Immenhauser et al., 2002; Rameil et al., 2010). Similarly

to the absence of hardgrounds or condensed horizons, such intervals during which the carbonate factory is completely replaced by another are not observed in the field. For this reason, the replacement of the factory by another was not considered in the forward model. For future models, it would therefore be of interest to model the axial input of siliciclastic material, as suggested by field evidence, in order to examine whether this may cause the observed back-stepping of margin facies after the sequence boundary. Confirming this scenario would require detailed investigation of slope angle indicators in the slope and basin sections.

The second forward modelling scenario simulated tectonic tilting of the platform. A tilt of  $0.08^\circ$  degrees around a hinge point at 0 km was introduced to the model at 1.5 My run time, successfully reproducing the interpreted stratal patterns (Figure 4.14). As discussed in Section 4.6.5, no evidence for an abrupt steepening of the slope, such as slumping features or an upward increase in the frequency of occurrence of debrite beds, is observed directly above the boundary between Sequence 1 and 2. Although rapid tectonic tilting is not unlikely in the Tresp Basin, considering the active nature of the foreland basin (Vergés et al., 2002), this absence of sedimentary evidence makes recognising such an event difficult.

Overall, the results of stratigraphic forward modelling show that both changes in carbonate productivity and tectonic tiling are mechanisms that may form stratal patterns commonly interpreted as the result of relative sea-level fluctuations. Sedimentary evidence for tectonic tilting related to the sequence boundary could not be found in the field, thus not allowing confident interpretation of this mechanism occurring. Increased marl contents above the sequence boundary in the outer platform margin imply localised reduction of productivity due to axial input of siliciclastics is possible. Other mechanisms of productivity reduction such as changes in nutrient levels may be possible, but are difficult to determine or quantify.

### **Mechanisms Affecting High Frequency Cyclicity**

The stratigraphic forward model attempting to reproduce the five high-frequency cycles interpreted into the Bastus Platform was not successful in doing so using the introduced eustatic oscillation with a period of 0.5 My and an amplitude of 10 metres (Figure 4.13). Iterative testing (Antonatos, *in prep.*) has shown that separation into five clear sequences is possible by increasing the amplitude to above 20 metres. However, this introduced subaerial exposure across the platform top. No evidence of subaerial exposure was found in the margin and platform interior in the field, as the sequences are only bound by abrupt facies changes from shallow to deeper water. Therefore, the model implies that relative sea-level oscillations are likely not the control on the establishment of these sequences.

While it was beyond the scope of this study to test in forward modelling, it is of interest to discuss other possible controls (productivity, sediment transport and tectonics) on their capability to produce high-frequency stratal patterns similar to those interpreted into the Bastus Platform. Such controls on small-scale stacking patterns have been discussed previously, and although quantification of these processes from field data is difficult, it was shown that these mechanisms can lead to formation of sequence-like sedimentary stacking patterns in the absence of relative sea-level fluctuations using forward modelling (Burgess, 2001).

For the Bastus Platform, it was previously suggested that rhythmic changes of the dominant carbonate factory led to the stacking patterns observed in Montagut Gully and Carreu River (Pomar et al., 2005). However, since these authors based their study only on a restricted section of the platform margin, their interpretations are not correlatable to those made on a further landward platform margin section (Collades de Basturs; Sanders and Pons, 2001), nor are they compatible with the interpretations made in this study for the platform interior or basal sections. Additionally, it was shown by Burgess (2016) that the section at Carreu River, interpreted by Pomar et al. (2005) to reflect high-frequency stratigraphic sequences, does not in fact show ordered bedding sequences. It is therefore interpreted here that no platform-wide evidence for significant change in carbonate factories exists. Rather, the stratal patterns observed in the platform margin reflect movements of neighbouring build-up (PM1-4) and shoal facies (PM5) within the area.

An alternative scenario is possible in a reduction of productivity rates, rather than complete switching of carbonate factories. Since this was shown to possibly affect the backstepping of the larger-scale Sequences 1 and 2, it is suggested that smaller-scale, higher-frequency variations in productivity may have led to the observed stacking patterns and the abrupt facies changes to deeper water facies – reflecting backstepping of the factories due to reduced productivity and inability to keep up with relative sea-level rise. Hallock and Schlager (1986) discussed how nutrients in terrestrial runoff lead to eutrophication and cessation of carbonate production before the arrival of the siliciclastic sediments themselves. In the Bastus Platform, this may occur to a less extreme degree, with productivity being strongly reduced instead of stopped completely. However, this scenario would imply a sequence stratigraphic relationship of the non-productivity phases with siliciclastic sediments, which could not be shown to exist in this study.

A third possible interpretation to the sequences is tectonic control. As the proposed high-frequency sequences are comparable in thickness/duration, suggesting a tectonic control on their formation would require a repetitive tectonic event to occur every 600 ky. Previous authors have suggested repetitive effects of tectonic activity on carbonate platforms on much

smaller scales. This includes fault controlled margins recording activity on a scale of 40 ky (Cisne, 1986; Benedictis et al., 2007) and tectonic activity cycles of 10-100 ky which are suggested as an alternative mechanism of sequence formation to the commonly used relative sea-level fluctuations (Hardie et al., 1991). As discussed for the separation of the low frequency Sequence 1 and 2, a tectonic influence is likely in the Tremp Basin. However, no repetitive tectonic activity on similar time-scale has been suggested so far, and evidence for tectonic influence at each sequence boundary, bar abrupt deepening of facies, was not found in the field.

#### **4.8.2 Implications for Sequence Stratigraphic Interpretations**

The comparison of sequence stratigraphic interpretations with stratigraphic forward modelling presented in this study can be used to challenge whether relative sea-level fluctuations are the dominant control on the formation of stacking patterns. It allows addressing:

- Identification of the main controls on sequence development. Particularly since sequence stratigraphic interpretations often invoke relative sea-level changes as the main mechanism for generation of sedimentary stacking patterns.
- Identification of key surfaces which are correlatable across the investigated platform where bio- and chemostratigraphic constraints are not available.

#### **Controls on Sequence Development**

Stacking patterns within carbonate platforms were previously often interpreted to be controlled by variations of relative sea level (e.g. Mitchum et al., 1977; Vail et al., 1977; Haq et al., 1987; Sarg, 1988; Van Wagoner et al., 1988, 1990). More recently, Burgess (2001), Burgess et al. (2001), Pomar and Kendall (2011), Pomar et al. (2012), and Burgess and Prince (2015) all discuss the importance of changes in carbonate productivity and self-organisation of the carbonate factories to produce stratal patterns that might be interpreted as being controlled by relative sea level. This project provides one of the few calibrations of stratigraphic forward modelling with outcrop data. This comparison allows testing the impact of processes that cannot be assessed from outcrop data alone, particularly carbonate productivity. Doing this is expected to help delineate a rule-set that allows better constraining of facies distribution, which in turn improves interpretation of facies architecture from subsurface dataset.

The reconstructed relative sea-level curves for the Tremp Basin show a gradual rise during the period of growth of the Bastus Platform (Figure 4.11). This may not be solely responsible for the landward shift in facies occurring between Sequences 1 and 2 interpreted by the sequence stratigraphic correlation. The stratigraphic forward models that introduce a variation of relative sea-level suggest this, as they did not result in comparable stratal patterns to those observed in



the field. Subsequent models then demonstrate that the marked backstepping between the sequences is more likely the result of changes in carbonate productivity or tectonic tilting.

The role of carbonate productivity on shaping the platform topography was demonstrated using stratigraphic forward modelling in this study. In the presented stratigraphic forward model, a distinct but short-lived reduction in platform-wide productivity led to a drastic backstepping of the platform. Additionally, it was shown in sensitivity analysis that the equilibrium between platform top, margin and pelagic productivity is decisive for the development and final shape of the platform (Antonatos, *in prep.*). A shallow euphotic zone (i.e. higher turbidity) leads to a more landward positioned platform break and slower progradation. If productivity rates are not high enough, no distinct platform break is formed, and the platform may drown if it cannot keep up with relative sea-level rise. While these concepts are well known (e.g. Pomar, 2001; Schlager, 2005), stratigraphic forward modelling provides a means of testing possible scenarios in a custom framework for each geological example. Moreover, stratigraphic forward modelling can be used in future studies to address other possible mechanisms for sequence generation that were beyond the scope of this study. Such mechanisms may include temporal variation of sediment transport and diffusion rates, as discussed by (Pomar and Kendall, 2011; Burgess and Prince, 2015).

Two aspects of the sequence stratigraphic interpretation were not addressed via stratigraphic forward modelling in this study. These are the differential thickness development across the platform, and the lack of interpreted transgressive systems tracts. Stratigraphic forward modelling offers a tool for investigating the controls on these two characteristics. Previously discussed was how the differential thickness development was the result of variations in subsidence and syndimentary growth of the Sant Corneli anticline in the basin (Section 4.6.4). Introducing this aspect into future forward models will allow more precise recognition of their effects on sedimentary architecture and sequence development. The lack of transgressive systems tracts was attributed to the high subsidence rates and variations in rates of relative sea-level rise (Section 4.6.4). While this was reproduced in the stratigraphic forward models based on relative sea-level fluctuations, and the absence of subaerial exposure surfaces in these indicates a similar development of sequences, these models did not reproduce the large-scale stratal patterns of the Bastus Platform. The lack of transgressive systems tracts should therefore be investigated in more detail in forward stratigraphic models with higher vertical resolution.

### **Identification of Key Surfaces**

One of the reoccurring hurdles with the conventional sequence stratigraphic interpretation presented for the Bastus Platform was the basin-wide recognition of surfaces. When isolated sections are observed, potential surfaces are easily recognised and interpreted as sequence

boundaries or flooding surfaces. However, lateral correlation of these surfaces to other parts of the platform is difficult. This was shown via comparison of the work of Sanders and Pons (2001) and Pomar et al. (2005) to the correlation presented in this study. This applies both to the major surface subdividing the Bastus Platform into two sequences, and the further separation of smaller sequences within these. This difficulty in correlating surfaces between localities can be caused by these surfaces being either the result of entirely local processes, or the subtle expression of a platform-wide event.

The advantage of comparing the sequence stratigraphic interpretation made in this study with stratigraphic forward models allows not only to test controlling mechanisms, but enables to simultaneously test whether surfaces can form resulting from these, and whether these form locally or platform-wide. This is evident in successfully separating Sequences 1 and 2 via variations in productivity or tectonic tilt, thus allowing interpreting the major boundary across the platform. Subsequently, implementing stratigraphic forward modelling allows defining whether surfaces have sequence stratigraphic relevance and improve interpretations. Potentially, this may allow to compensate for the lack of bio- and chemostratigraphic control, both via directly considering different controls on sequence formation, and via testing scenarios in stratigraphic forward modelling.

In stratigraphic forward modelling, the high frequency cycles on the scale of up to 100 metres (equivalent to a duration of ca. 0.6 Ma) interpreted by the sequence stratigraphic correlation could not be reproduced without inducing subaerial exposure in the models, and using amplitudes of sea-level fluctuation that are higher than those suggested by the reconstructed relative sea-level curves (Figure 4.11). However, such exposure was not recognised in the field. This implies either that the recognised sequences and surfaces are not controlled by the processes used for forward modelling (relative sea-level fluctuations), or that the subaerial exposure indicated by the models was not preserved or emergence was not long enough to form a distinct exposure surface. This appears to be the case for the Turonian-Coniacian Congost Platform of the Tremp Basin (Chapter 3), which subjected to prolonged subaerial exposure during its later stages, with little evidence for emergence (Selem, 2016). Both semiarid climates (Nagtegaal, 1972) and humid climates (Booler, 1994) were suggested for this time, adding uncertainty to the preservation potential of emergent surfaces.

Similar examples for the differential development of emergent surfaces are known from the Aptian Shu'aiba Formation of the Arabian Plate (e.g. Sattler et al., 2005; Hollis and Sharp, 2011; Rameil et al., 2012). Here, karst is recognised to appear only locally on structural highs, whereas other surfaces show a polygenetic character. Notable is the absence of deep-cutting karst features despite the long-term exposure in a tropical climate zone (Rameil et al., 2012). Such

examples indicate that it is likely that subaerial exposure may have taken place in sequences where relative sea-level fluctuations were the dominant control, but the emergence was not preserved. This is an important consideration for the sequence stratigraphic interpretations in systems where distinct surfaces are missing. Particularly the comparison with stratigraphic forward models provides a tool to simulate and test the effects of the controlling processes on exposure and the formation of surfaces or facies transitions.

#### 4.9 Conclusions

- The Santonian Bastus platform was a relatively low energy, flat-topped ( $<0.05^\circ$ ) platform dominated by foraminiferal wackestones with occasional rudist patch reefs, that was intercalated with sandstones deposited within a delta lobe of the coastal environment. Laterally discontinuous composite build-ups of coral-rudist boundstone define the platform margin, interbedded with bioclastic grainstone and packstone shoals. A low angle slope ( $<1^\circ$ ) dipped basinward and accumulated skeletal wackestones that pass offshore into skeletal wackestones and mudstones.
- The Bastus Platform is interpreted to have been deposited within a single 3<sup>rd</sup> order sea-level cycle over a period of  $\sim 3$  My, consistent with the interpretation of Simó (1993). It comprises two sequences, separated by a composite sequence boundary/flooding surface. The lowermost sequence shows progradation and aggradation as the platform margin is constructed. Within the uppermost sequence, there is a marked back-stepping of the platform and retreat of the platform margin, with gradual progradation towards the end of the platform duration. Each sequence comprises 2-3 higher frequency successions that can be correlated less confidently across the platform.
- Overall, the succession is 475 m thick (300 m in the lower and 175 m in the upper sequence). There are marked local thickness variations, however, with the thinnest succession occurring on the platform margin. Based on reconstructed relative sea-level curves, high rates of subsidence occurred across much of the platform during deposition of the Bastus Platform, but subsidence rates were lower where the platform margin is observed, suggesting reduced accommodation space led to a thinner sediment pile.
- It is proposed that this reduction in accommodation at the platform margin occurred because of the onset of growth of the Sant Corneli anticline, an indication that the basin had moved into a compressional regime with the onset of the Alpine Orogeny.
- No evidence of emergence of the carbonate platform was seen anywhere in the succession, interpreted to be indicative of high rates of subsidence leading to high relative sea level throughout the Santonian in the Tremp Basin.

- Absence of any evidence of relative sea-level fall and subaerial exposure implies that relative sea-level oscillations may have not been the dominant control on sequence formation in the Bastus Platform strata. Impact of various possible controls was investigated via comparison between outcrop data and numerical stratigraphic forward models. The key purpose is to determine whether the two defined sequences were more likely formed as a result of simple relative sea-level oscillations, as commonly interpreted in sequence stratigraphic correlations, or were more likely the result of either tectonic tilting or temporal changes in carbonate production rate.
- Stratigraphic forward models show that the separation of the Bastus Platform into two or five sequences was likely not caused by relative sea-level oscillations because the platform architecture could not be reproduced with simple relative sea-level oscillations. With high subsidence rates, control by eustatic sea-level fluctuations is unlikely.
- Stratigraphic forward models with either time-variable productivity or sudden tectonic tilting successfully reproduced interpreted stratal geometries. This indicates that these two mechanisms were a possible control on the formation of the two interpreted sequences. Possible mechanisms for tectonic tilting in foreland basins are well understood, but quantification of the effect of oceanographic changes on carbonate production rates through time remain difficult to quantify.
- Combined outcrop analysis and stratigraphic forward modelling highlights how sequence stratigraphic interpretations can be improved by testing the effects of mechanisms other than changes in relative sea level as the predominant control on stratal geometries.

#### 4.10 References

- Benedictis, D. De, D. Bosence, and D. Waltham, 2007, Tectonic control on peritidal carbonate parasequence formation: An investigation using forward tectono-stratigraphic modelling: *Sedimentology*, v. 54, no. 3, p. 587–605, doi:10.1111/j.1365-3091.2006.00851.x.
- Booler, J. P., 1994, Carbonate facies, sequences and associated diagenesis, Upper Cretaceous, Tremp Basin, Spanish Pyrenees: Durham University, 317 p.
- Bosscher, H., and W. Schlager, 1992, Computer simulation of reef growth: *Sedimentology*, v. 39, no. 3, p. 503–512, doi:10.1111/j.1365-3091.1992.tb02130.x.
- Burgess, P. M., 2013, CarboCAT: A cellular automata model of heterogeneous carbonate strata: *Computers & Geosciences*, v. 53, p. 129–140, doi:10.1016/j.cageo.2011.08.026.
- Burgess, P. M., 2016, Identifying Ordered Strata: Evidence, Methods, and Meaning: *Journal of Sedimentary Research*, v. 86, no. 3, p. 148–167, doi:10.2110/jsr.2016.10.
- Burgess, P. M., 2001, Modeling carbonate sequence development without relative sea-level oscillations: *Geology*, v. 29, no. 12, p. 1127–1130, doi:10.1130/0091-7613(2001)029<1127:MCSDWR>2.0.CO;2.
- Burgess, P. M., and G. D. Prince, 2015, Non-unique stratal geometries: implications for sequence stratigraphic interpretations: *Basin Research*, v. 27, no. 3, p. 351–365, doi:10.1111/bre.12082.

- Burgess, P. M., V. P. Wright, and D. Emery, 2001, Numerical forward modelling of peritidal carbonate parasequence development: implications for outcrop interpretation: *Basin Research*, v. 13, no. 1, p. 1–16, doi:10.1046/j.1365-2117.2001.00130.x.
- Catuneanu, O., W. E. Galloway, C. G. S. C. Kendall, A. D. Miall, H. W. Posamentier, A. Strasser, and M. E. Tucker, 2011, Sequence Stratigraphy: Methodology and Nomenclature: *Newsletters on Stratigraphy*, v. 44, no. 3, p. 173–245, doi:10.1127/0078-0421/2011/0011.
- Caus, E., A. Gómez-Garrido, A. Simó, and K. Sofiano, 1993, Cenomanian-Turonian platform to basin integrated stratigraphy in the South Pyrenees (Spain): *Cretaceous Research*, v. 14, no. 4–5, p. 531–551, doi:10.1006/cres.1993.1038.
- Caus, E., M. Parente, V. Vicedo, G. Frijia, and R. Martínez, 2013, *Broeckina gassoensis* sp. nov., a larger foraminiferal index fossil for the middle Coniacian shallow-water deposits of the Pyrenean Basin (NE Spain): *Cretaceous Research*, v. 45, p. 76–90, doi:10.1016/j.cretres.2013.08.002.
- Choukroune, P., F. Roure, and B. Pinet, 1990, Main results of the ECORS Pyrenees profile: *Tectonophysics*, v. 173, no. 1–4, p. 411–423, doi:10.1016/0040-1951(90)90234-Y.
- Christie-Blick, N., 1991, Onlap, offlap, and the origin of unconformity-bounded depositional sequences: *Marine Geology*, v. 97, no. 1–2, p. 35–56, doi:10.1016/0025-3227(91)90018-Y.
- Cisne, J. L., 1986, Earthquakes recorded stratigraphically on carbonate platforms: *Nature*, v. 323, p. 320–322, doi:10.1038/323320a0.
- Drzewiecki, P. A., and J. A. Simó, 2000, Tectonic, eustatic and environmental controls on mid-Cretaceous carbonate platform deposition, south-central Pyrenees, Spain: *Sedimentology*, v. 47, no. 3, p. 471–495, doi:10.1046/j.1365-3091.2000.00286.x.
- Drzewiecki, P. A., J. Vergés, L. Markley, and J. Olandt, 2014, Evidence for Syntectonic Growth of a Santonian Carbonate Platform on the Sant Corneli Anticline, South-Central Pyrenees, Spain, *in* 49th Annual Meeting of the Geological Society of America.
- Dunham, R., 1962, Classification of carbonate rocks according to depositional texture, *in* W. E. Ham, ed., *Classification of Carbonate Rocks: AAPG Memoir 1: Tulsa, OK, AAPG*, p. 108–121.
- Embry, A. F., and J. E. Klovan, 1971, A Late Devonian reef tract on northeastern Banks Island, NWT: *Bulletin of Canadian Petroleum Geology*, v. 19, no. 4, p. 730–781.
- Enos, P., 1991, Sedimentary parameters for computer modeling, *in* E. K. Franseen, W. L. Watney, C. G. St. Kendall, and W. Ross, eds., *Sedimentary Modeling: Computer simulations and methods for improved parameter definition: Kansas Geological Survey Bulletin 233*: p. 63–99.
- Flügel, E., 2010, Recognizing Paleoenvironmental Conditions, *in* *Microfacies of Carbonate Rocks: Berlin, Heidelberg, Springer Berlin Heidelberg*, p. 587–640, doi:10.1007/978-3-642-03796-2\_12.
- Gallémí, J., R. Martínez, and J. M. J. Pons, 1982, Unidades del Cretácico superior en los alrededores de Sant Corneli (Provincia de Lleida): *Cuadernos de Geología Ibérica*, v. 8, p. 935–948.
- Gili, E., G. López, A. Obrador, P. Skelton, and E. Vicens, 1994, Observaciones sobre la posición estratigráfica de las formaciones de rudistas de Sant Corneli (cuenca cretácica surpirenaica central): *Geogaceta*, v. 15, p. 34–36.
- Gómez-Gras, D., M. Roigé, V. Fondevilla, O. Oms, S. Boya, and E. Remacha, 2016, Provenance constraints on the Tremp Formation paleogeography (southern Pyrenees): Ebro Massif VS Pyrenees sources: *Cretaceous Research*, v. 57, p. 414–427, doi:10.1016/j.cretres.2015.09.010.
- Hallock, P., and W. Schlager, 1986, Nutrient Excess and the Demise of Coral Reefs and Carbonate Platforms: *PALAIOS*, v. 1, no. 4, p. 389, doi:10.2307/3514476.
- Haq, B. U., J. Hardenbol, and P. R. VAIL, 1987, Chronology of Fluctuating Sea Levels Since the Triassic: *Science*, v. 235, no. 4793, p. 1156–1167, doi:10.1126/science.235.4793.1156.
- Hardie, L. A., P. A. Dunn, and R. K. Goldhammer, 1991, Field and Modelling Studies of Cambrian Carbonate Cycles, Virginia Appalachians: *DISCUSSION: Journal of Sedimentary Research*, v. 61, no. 4, p. 636–646, doi:10.1306/D42677A3-2B26-11D7-8648000102C1865D.
- Hollis, C., and I. Sharp, 2011, Albian-Cenomanian-Turonian carbonate-siliciclastic systems of the

- Arabian Plate: advances in diagenesis, structure and reservoir modelling: introduction: *Petroleum Geoscience*, v. 17, no. 3, p. 207–209, doi:10.1144/1354-079310-060.
- Immenhauser, A., B. Van Der Kooij, A. Van Vliet, W. Schlager, and R. W. Scott, 2002, An ocean-facing Aptian-Albian carbonate margin, Oman: *Sedimentology*, v. 48, no. 6, p. 1187–1207, doi:10.1046/j.1365-3091.2001.00416.x.
- Institut Cartogràfic i Geològic de Catalunya, 2010, Mapa geològic de Catalunya (1:25 000) - Aramunt 252-2-2 (66-22).
- Institut Cartogràfic i Geològic de Catalunya, 2014, Mapa geològic de Catalunya (1:25 000) - Camarasa 228-1-2 (65-26).
- Institut Cartogràfic i Geològic de Catalunya, 2015, Mapa geològic de Catalunya 1:50.000 (mgc50Mv01\_etr89).
- Lehrmann, D. J. D. J., and R. K. GOLDHAMMER, 1999, Secular Variation in Parasequence and Facies Stacking Patterns of Platform Carbonates: A Guide to Application of Stacking-Patterns Analysis in Strata of Diverse Ages and Settings, *in* *Advances in Carbonate Sequence Stratigraphy: SEPM (Society for Sedimentary Geology)*, p. 187–225, doi:10.2110/pec.99.11.0187.
- Markley, L., P. A. Drzewiecki, and J. Olandt, 2014, Sea Level and Tectonic Controls on the Development of the Santonian Collades de Basturs Carbonate Platform, South-Central Pyrenees, Spain, *in* 49th Annual Meeting of the Geological Society of America.
- Messina, C., M. A. Rosso, F. Sciuto, I. Di Geronimo, W. Nemeč, T. Di Dio, R. Di Geronimo, R. Maniscalco, and R. Sanfilippo, 2007, Anatomy of a Transgressive Systems Tract Revealed by Integrated Sedimentological and Palaeoecological Study: The Barcellona Pozzo Di Gotto Basin, Northeastern Sicily, Italy, *in* C. P. Gary Nichols, Ed Williams, ed., *Sedimentary Processes, Environments and Basins: Oxford, UK, Blackwell Publishing Ltd.*, p. 367–400, doi:10.1002/9781444304411.ch17.
- Mitchum, R. M., P. R. Vail, and S. Thompson, 1977, Seismic Stratigraphy and Global Changes of Sea Level, Part 2: The Depositional Sequence as a Basic Unit for Stratigraphic Analysis: Section 2. Application of Seismic Reflection Configuration to Stratigraphic Interpretation, *in* J. B. S. P. R. Vail, R. G. Tod, ed., *Seismic Stratigraphy--Applications to Hydrocarbon Exploration: AAPG Memoir 26: AAPG*, p. 53–62.
- Mount, J. F., 1984, Mixing of siliciclastic and carbonate sediments in shallow shelf environments: *Geology*, v. 12, no. 7, p. 432, doi:10.1130/0091-7613(1984)12<432:MOSACS>2.0.CO;2.
- Muñoz, J. A., A. Martínez, and J. Verges, 1986, Thrust sequences in the eastern Spanish Pyrenees: *Journal of Structural Geology*, v. 8, no. 3–4, p. 399–405, doi:10.1016/0191-8141(86)90058-1.
- Nagtegaal, P., 1972, Depositional history and clay minerals of the Upper Cretaceous basin in the south-central Pyrenees, Spain: *Leidse Geologische Mededelingen*, v. 47, no. 2, p. 251–275.
- Plaziat, J.-C., 1981, Late Cretaceous to Late Eocene palaeogeographic evolution of Southwest Europe: *Palaeogeography, Palaeoclimatology, Palaeoecology*, v. 36, no. 3–4, p. 263–320, doi:10.1016/0031-0182(81)90110-3.
- Pomar, L., 2001, Types of carbonate platforms: a genetic approach: *Basin Research*, v. 13, no. 3, p. 313–334, doi:10.1046/j.0950-091x.2001.00152.x.
- Pomar, L., P. Bassant, M. Brandano, C. Ruchonnet, and X. Janson, 2012, Impact of carbonate producing biota on platform architecture: Insights from Miocene examples of the Mediterranean region: *Earth-Science Reviews*, v. 113, no. 3–4, p. 186–211, doi:10.1016/j.earscirev.2012.03.007.
- Pomar, L., E. Gili, A. Obrador, and W. C. Ward, 2005, Facies architecture and high-resolution sequence stratigraphy of an Upper Cretaceous platform margin succession, southern central Pyrenees, Spain: *Sedimentary Geology*, v. 175, no. 1–4, p. 339–365, doi:10.1016/j.sedgeo.2004.11.009.
- Pomar, L., and C. G. S. C. Kendall, 2011, Architecture of Carbonate Platforms: A Response to Hydrodynamics and Evolving Ecology, *in* *Controls on Carbonate Platform and Reef Development: SEPM (Society for Sedimentary Geology)*, p. 187–216, doi:10.2110/pec.08.89.0187.

- Puigdefàbregas, C., J. A. Muñoz, and J. Vergés, 1992, Thrusting and foreland basin evolution in the Southern Pyrenees, *in* K. R. McClay, ed., *Thrust Tectonics*: Dordrecht, Springer Netherlands, p. 247–254, doi:10.1007/978-94-011-3066-0\_22.
- Puigdefàbregas, C., and P. Souquet, 1986, Tecto-sedimentary cycles and depositional sequences of the Mesozoic and Tertiary from the Pyrenees: *Tectonophysics*, v. 129, no. 1–4, p. 173–203, doi:10.1016/0040-1951(86)90251-9.
- Rameil, N., A. Immenhauser, A. É. Csoma, and G. Warrlich, 2012, Surfaces with a long history: the Aptian top Shu'aiba Formation unconformity, Sultanate of Oman: *Sedimentology*, v. 59, no. 1, p. 212–248, doi:10.1111/j.1365-3091.2011.01279.x.
- Rameil, N., A. Immenhauser, G. Warrlich, H. Hillgärtner, and H. J. Droste, 2010, Morphological patterns of Aptian Lithocodium-Bacinella geobodies: relation to environment and scale: *Sedimentology*, v. 57, no. 3, p. 883–911, doi:10.1111/j.1365-3091.2009.01124.x.
- Read, J. F., 1995, Overview of carbonate platform stratigraphy and reservoirs in green-house and ice-house worlds, *in* J. . Read, ed., *Milankovitch Sea-level Changes, Cycles, and Reservoirs on Carbonate Platforms in Greenhouse and Ice-House Worlds*: SEPM (Society for Sedimentary Geology), p. 1–102, doi:10.2110/scn.95.35.0001.
- Roige, M., D. Gómez-gras, and E. R. Grau, 2014, The role of the Ebro Massif as a source area for the clastic systems of the southcentral Pyrenean Basin: no. October.
- Sanders, D., 1998, Upper Cretaceous "Rudist" formations: *Geologisch-Palaeontologische Mitteilungen Innsbruck*, v. 23, p. 37–59.
- Sanders, D., and R. Baron-Szabo, 2008, Palaeoecology of solitary corals in soft-substrate habitats: the example of *Cunulites* (upper Santonian, Eastern Alps): *Lethaia*, v. 41, no. 1, p. 1–14, doi:10.1111/j.1502-3931.2007.00039.x.
- Sanders, D., and R. Höfling, 2000, Carbonate deposition in mixed siliciclastic–carbonate environments on top of an orogenic wedge (Late Cretaceous, Northern Calcareous Alps, Austria): *Sedimentary Geology*, v. 137, no. 3–4, p. 127–146, doi:10.1016/S0037-0738(00)00084-1.
- Sanders, D., and J. M. Pons, 2001, Stratigraphic architecture of a Santonian mixed siliciclastic-carbonate succession (Catalonian Pyrenees, Spain): *Facies*, v. 44, no. 1, p. 105–135, doi:10.1007/BF02668170.
- Sarg, J. F., 1988, Carbonate Sequence Stratigraphy, *in* *Sea-Level Changes*: SEPM (Society for Sedimentary Geology), p. 155–181, doi:10.2110/pec.88.01.0155.
- Sattler, U., A. Immenhauser, H. Hillgärtner, and M. Esteban, 2005, Characterization, lateral variability and lateral extent of discontinuity surfaces on a Carbonate Platform (Barremian to Lower Aptian, Oman): *Sedimentology*, v. 52, no. 2, p. 339–361, doi:10.1111/j.1365-3091.2005.00701.x.
- Schlager, W., 2005a, Geometry of carbonate accumulations, *in* *Carbonate Sedimentology and Sequence Stratigraphy*: p. 39–54.
- Schlager, W., 2005b, Sequence stratigraphy of the T factory, *in* *Carbonate Sedimentology and Sequence Stratigraphy*: p. 105–146.
- Schlanger, S. O., and H. C. Jenkyns, 1976, Cretaceous Oceanic Anoxic Events: Causes and Consequences: *Geologie en Mijnbouw*, v. 55, no. 3–4, p. 179–184.
- Selem, A., 2016, Evidence of Exposure at a Third Order Sequence Boundary, Upper Cretaceous Congost Carbonate Platform, Spanish Pyrenees: The University of Manchester, 41 p.
- Simó, A., 1986, Carbonate platform depositional sequences, Upper Cretaceous, south-central Pyrenees (Spain): *Tectonophysics*, v. 129, no. 1–4, p. 205–231, doi:10.1016/0040-1951(86)90252-0.
- Simó, A., 1993, Cretaceous carbonate platforms and stratigraphic sequences; south-central Pyrenees; Spain., *in* J. Simo, R. W. Scott, and J.-P. Masse, eds., *Cretaceous carbonate platforms*: AAPG Memoir 56: Tulsa, OK, AAPG, p. 325–342, doi:10.1306/M56578C1.
- Steuber, T., 2000, Skeletal growth rates of Upper Cretaceous rudist bivalves: implications for carbonate production and organism-environment feedbacks: Geological Society, London, Special Publications, v. 178, no. 1, p. 21–32, doi:10.1144/GSL.SP.2000.178.01.03.
- Vail, P. R., R. G. Todd, and J. B. Sangree, 1977, Seismic stratigraphy and global changes of sea

- level: part 5. Chronostratigraphic significance of seismic reflections: section 2. Application of seismic reflection configuration to stratigraphic interpretation, *in* J. B. S. P. R. Vail, R. G. Tod, ed., *Seismic Stratigraphy--Applications to Hydrocarbon Exploration: AAPG Memoir 26*: p. 99–116, doi:10.1306/M26490C3.
- Vergés, J., M. Fernández, and A. Martínez, 2002, The Pyrenean orogen: pre-, syn-, and post-collisional evolution: *Journal of the Virtual Explorer*, v. 8, p. 55–74, doi:10.3809/jvirtex.2002.00058.
- Vicens, E., G. López, and A. Obrador, 1998, Facies succession, biostratigraphy and rudist faunas of Coniacian to Santonian platform deposits in the Sant Corneli anticline (Southern Central Pyrenees): *Geobios*, v. 31, p. 403–427, doi:10.1016/S0016-6995(98)80089-2.
- Van Wagoner, J. C., R. M. Mitchum, K. M. Campion, and V. D. Rahmanian, 1990, Siliciclastic Sequence Stratigraphy in Well Logs, Cores, and Outcrops: Concepts for High-Resolution Correlation of Time and Facies, *in* *Siliciclastic Sequence Stratigraphy in Well Logs, Cores, and Outcrops: Concepts for High-Resolution Correlation of Time and Facies: AAPG Methods in Exploration Series 7*: p. 1–55, doi:0-89181-657-7.
- Van Wagoner, J. C., H. W. Posamentier, R. M. Mitchum, P. R. Vail, J. F. Sarg, T. S. Loutit, and J. Hardenbol, 1988, An overview of the fundamentals of sequence stratigraphy and key definitions, *in* *Sea-Level Changes - An Integrated Approach*, SEPM Special Publication: SEPM (Society for Sedimentary Geology), p. 39–45, doi:10.2110/pec.88.01.0039.
- Wentworth, C. K., 1922, A scale of grade and class term for sifting sediments: *The Journal of Geology*, v. 30, no. 5, p. 377–392, doi:10.2307/30063207.
- Yancey, T. E., 1991, Controls on carbonate and siliciclastic sediment deposition on a mixed carbonate–siliciclastic shelf (Pennsylvanian Eastern Shelf of north Texas): p. 263–272.



## 5 ADVANCES IN UNDERSTANDING THE INTERNAL AND OUTCROP-SCALE GEOMETRIES OF SHOAL AND BUILD-UP BODIES WITHIN UPPER CRETACEOUS CARBONATE PLATFORMS

Jonathan Lavi<sup>1</sup>, Cathy Hollis<sup>1</sup>, Thomas Seers<sup>1\*</sup>, Ian Billing<sup>2+</sup>, Christoph Lehmann<sup>2</sup>, James Gardner<sup>2</sup>, Anna Matthews<sup>2</sup>, Katherine Tutton<sup>2</sup>, Stefan Schröder<sup>1</sup>

Contact: [jonathan.lavi@manchester.ac.uk](mailto:jonathan.lavi@manchester.ac.uk)

<sup>1</sup>School of Earth, Atmospheric and Environmental Sciences, The University of Manchester, Manchester, M13 9PL, UK

<sup>2</sup>BP Exploration, Chertsey Road, Sunbury-On-Thames, Middlesex TW16 7LN.

\*Now at Texas A&M University, Education City Student Center, Doha, Qatar

+Now at School of Science, University of Derby, Kedleston Road, Derby DE22 1GB, UK

### 5.1 Abstract

Carbonate platforms show complex internal facies architecture caused by sub-seismic scale depositional elements such as grainstone-packstone shoal and margin clinoforms, and biogenic build-ups. While their mode of formation is well documented on a qualitative basis, the quantitative aspect of their size and internal structure, as well as relationships of these to their location on the platform, are still poorly understood. Such geobodies frequently lead to reservoir heterogeneity and are often difficult to assess with traditional seismic interpretations and well-correlation. Using digital outcrop modelling techniques, shoal and margin clinoforms and build-up bodies from several outcrops of the Upper Cretaceous carbonate platforms of the Tremp Basin in the south-central Pyrenees were quantified. Widths and lengths of these depositional elements are interpreted, and their interior geometries are quantified. By comparing the data and interpretations against similar examples, variability across other geological systems is assessed. It becomes obvious that the dimensions and interior geometry of shoal bodies, margin clinoforms, and build-ups are inherently controlled by their position on the platform and the underlying topography, as well as by the carbonate factory. Thus, a comprehensive understanding of the broad platform geometry and carbonate systems is essential for predicting the location, size and internal structure of sub-seismic scale geobodies. While general observations can be applied to geological examples of different ages and settings, the complexities of each basin and platform must be considered when making interpretations on depositional element scale. Consequently, geometrical rules and relationships vary for every carbonate platform.

## 5.2 Introduction

### 5.2.1 Rationale and aims

Within carbonate platforms, complex facies heterogeneity often results from the presence of small-scale depositional geobodies such as biogenic mounds, shoal bodies and other grain aggregations. Since such geobodies may ultimately result in variability in rock physical properties and reservoir connectivity, it is important for hydrocarbon production to understand both their dimensions and the controls on their distribution in the subsurface. Seismic data allow quantification of the size and distribution of only the largest bodies in the subsurface. Although borehole logs and core are theoretically of high vertical resolution, they only provide a 1D transect of the sediment, leaving the understanding of distribution and scale of small-scale geobodies poorly constrained. To determine the dimensions of smaller geobodies, it is therefore necessary to study outcrops in order to gain significant insight on lateral continuity, which can be transferred as statistical databases into subsurface datasets (e.g. Bryant et al., 2000; Grammer et al., 2004).

The platform-scale exposure of Upper Cretaceous strata in the Tresp area in the South-Central Pyrenees allowed studying the platform architecture and scale of depositional environments (cf. Chapter 3). The exposure of a variety of geobodies provides an excellent opportunity to investigate their architecture in a regional context and by considering the control mechanisms on basin-scale evolution. That allows description of shape, size and distribution of the geobodies.

Small-scale geobodies have been widely described qualitatively in the past. Only in recent years, with the development and widespread availability of outcrop digitalisation workflows, precise quantification of such elements became common. Many studies focused on geobodies in siliciclastic settings, e.g. by investigating sedimentary architecture of deltaic or fluvial systems (e.g. Enge et al., 2010; Moore et al., 2012; Graham et al., 2015). An increasing number of carbonate systems have also been studied (e.g. Kerans and Kempter, 2002; Adams et al., 2005, 2011; Grélaud et al., 2010; Koehrer et al., 2011). Nevertheless, the current understanding of small-scale heterogeneities within carbonate systems is far from comprehensive, and many of the studies do not place the presented geobodies in the regional context of the carbonate platform they reside in. This is partly the result of the difficulty of studying the 3-dimensional architecture of geological elements from 2D outcrop and seismic data, and 1D well data. Another reason is the limited applicability of modern analogues to ancient in-situ carbonate build-ups due to the inherent difference of the carbonate producers. While skeletal carbonates may not vary significantly over time, due to the main control on their formation residing in

hydrodynamic processes, equally little quantitative geometrical data is published on such geobodies. This paper contributes towards this by focusing on the following objectives:

- Capture and quantify the geometries and facies of a variety of geobodies within the Turonian –Santonian carbonate platforms of the Tresp Basin in the South-Central Pyrenees
- Investigate any patterns within their geometrical properties and compare these to patterns recognised within examples from modern and ancient carbonate systems
- Use these data to improve understanding of shape, size and distribution of such sub-seismic scale geobodies, and establish possible relationships that can be transferred onto subsurface examples

### 5.2.2 Sedimentology of Shoal and Build-up Geobodies

Three principle geobody types are investigated in this work: packstone-grainstone shoals and sigmoidal-bedded clinofolds, and biogenic build-ups, with rudists often being the dominant bioclast producers and framework-building organisms. The term carbonate shoal is generally used to describe depositional elements with an internal structure similar to the submarine dunes or sand waves as defined by Allen (1980), and constituting predominantly either of bioclastic or ooidal/peloidal material (e.g. Rankey and Reeder, 2011). The mechanisms of formation and sedimentological characteristics of such shoal bodies were previously studied in great detail in the modern grainstone shoals of the of the Great Bahama Bank (e.g. Ginsburg, 1956; Ball, 1967; Hine, 1977). On carbonate ramps, these bodies form at the shoreline or further seaward, in the high-energy zone above fair-weather wave base. On rimmed shelves, they are found rimming the platform edge or topographic elevations on the platform top, such as islands or reefs. In both settings, the shoal bodies are formed preferentially where wave energy is locally increased by a change in seafloor topography (Harris, 2009a). Based on formation mechanism and their geometry, shoal bodies are classified as either marine sand belts or tidal-bar belts (Ball, 1967). The former are the result of combined tidal and storm currents aggregating grains, and are elongated perpendicularly to the current direction, and the latter controlled solely by tidal currents, forming narrow, current-parallel bars (Hine, 1977). The orientation of these bodies depends on the seafloor topography and wave energy, and may vary throughout the platform (Harris, 2009a).

The internal structure of modern Bahaman shoal bodies was the topic of numerous studies (e.g. Bebout et al., 2009; Harris, 2009a; Rankey and Reeder, 2011; Harris et al., 2015). The main components of shoal bodies include longitudinal tidal sand ridges, transverse shoulder bars, parabolic bars, and intermediate sand flats, with each shoal body displaying a unique combination of a number of these elements (Rankey and Reeder, 2011). Furthermore,

variations in thickness and vertical stacking patterns are observed between and within shoal bodies (Harris, 2009a). It has been previously shown that grain size and height of individual shoal bars are positively correlated with wider facies belts (Rankey and Reeder, 2011).

The geometries of sigmoidally- or oblique-bedded packstone and grainstone clinofolds were studied by numerous authors (e.g. Bosellini, 1984; H. Droste, 2010; H.J. Droste, 2010; Adams et al., 2011). The term clinofold refers to the sigmoidally dipping bedding surface, and the term clinofold is used to describe a rock volume bound by such sigmoidal surfaces (Rich, 1951). Systematic quantification of such bedforms was however done predominantly in clastic settings (e.g. Anell and Midtkandal, 2015; Patruno et al., 2015). Key characteristics for the quantification are the height (relief) and length of a clinofold, the average and maximum angle, as well as the thickness of the produced clinofolds. In the three-dimensional study of these, the trajectory of the progradation also becomes important in determining sediment transport direction and rate (Anell and Midtkandal, 2015).

One of the concepts used to interpret the formation of depositional elements consisting of seaward-dipping, meso-scale (100s m to few km) sigmoidal bedforms is the Infralittoral Prograding Wedge (Hernández-Molina et al., 2000). Infralittoral prograding wedges (IPW) are observed in both siliciclastic settings (Mitchell et al., 2012; Ortega-Sánchez et al., 2014) and carbonate settings (Pomar et al., 2015; Andrieu et al., 2017). They are interpreted to form when periods of high water energy mobilise sediment from the upper shoreface, which is then resedimented seawards when current energy decreases (Hernández-Molina et al., 2000). In strike, they are typically on the scale of several 10s of kilometres, but can extend across 100s of kilometres along the length of the continental shelf. In dip, they reach between few 100s of metres to few kilometres, and the bedding angles of the internal surfaces are typically between 1.5° and 15°. Thicknesses are observed between 0.5 metres and several 10s of metres (Pomar et al., 2015).

Biogenic build-ups may be classified with a variety of terms, depending on their shape, location on the carbonate platform, and the dominating organism contributing to their formation (Riding, 2002). The build-ups were previously differentiated into bioherms and biostromes based on their morphological characteristics (Cumings, 1932), whereas more recently, they are divided into skeletal reefs and reef mounds, on the basis of their genetic origin (Tucker and Wright, 1990). Skeletal reefs are defined to pose a wave resistant structure that is formed by in-situ frame builders. By contrast, mounds lack a prominent framework, and are formed through trapping and binding of bioclasts and mud by organisms, and by biogenic production of large amounts of skeletal material. Biogenic build-ups are known to occur in a variety of settings, from shallow to deep marine, and can form various geometries, such as fringes, patches,

barriers, knolls and atolls (Tucker and Wright, 1990; Riding, 2002). The spatial distribution of build-ups across platforms may vary widely among basins and organisms, as demonstrated by a number of case studies (Aconcha et al., 2008; Amour et al., 2012; Janson and Madriz, 2012). In recent sequence stratigraphic interpretations, carbonate build-ups are often attributed with specific phases of sequence development, and thus are being used in correlations and in facies prediction (e.g. Pomar and Ward, 1994).

For rudist build-ups, Ross and Skelton (1993) have differentiated a variety of bodies depending on their morphology and position on the platform; steep margin complexes, low-angle open shelf margin complexes, inner shelf basin prograding margin complexes, isolated build-ups and inner shelf and platform biostromes. Sanders (1998) presented typical shallowing up patterns in coral-rudist build-ups topped by rudist biostromes. From the establishment phase of the build-up, starting with a layer of bioclastic limestones, the build-up grades into massive coral-rudist boundstones, followed by dense frameworks of rudist limestones dominated by a single species, and capped by bioclastic limestones from migrating sand bodies. The internal architecture of rudist build-ups is often complex, with facies distribution depending on the dominant current directions (e.g. Loucks and Kerans, 2003; Aconcha et al., 2008).

### **5.2.3 Dimensions of Shoal and Build-up Geobodies**

In carbonate platforms, sedimentary architecture can be described on a variety of different scales (Figure 5.1). These include:

- 1) The platform scale architecture, in which gross depositional environments and facies belts are quantified,
- 2) The lateral scale of depositional elements such as shoal bodies and complexes, such as those described by Harris (2009a) and Rankey and Reeder (2001), or biogenic build-ups (e.g. Ross and Skelton, 1993), and
- 3) The scale of internal architecture and bedding characteristics of these depositional elements, such as of sand bars, grainstone clinofolds, sigmoids or individual elements of a composite reef.

The platform-scale architectures of the Turonian-Coniacian platforms in the study area were previously established in Chapter 3. In this paper, the depositional element scale and internal architecture of the geobodies will be investigated with consideration of the regional context.

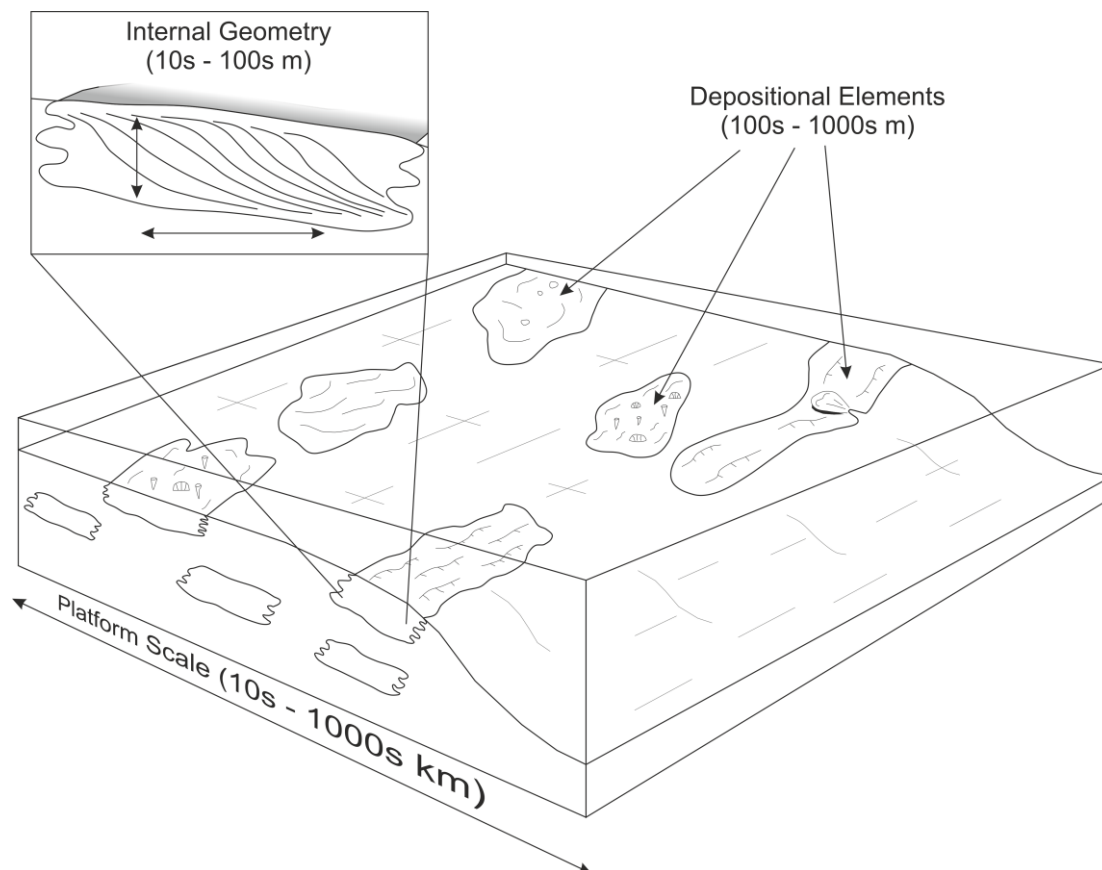


**Figure 5.1: Conceptual sketch of the different architectural elements and their scales within carbonate platforms. This paper focuses on defining the scales of depositional elements and their internal geometry. The depicted internal geometry is for illustration purposes only. For clinofolds, internal geometries include widths, heights, angles and bed thicknesses. For bedded/mounded geometries, these would include thickness, width and length of the feature, as well as slope angles. The platform scale architecture was previously discussed in Chapter 3.**

Few studies present comprehensive quantitative data on sedimentary architecture in a three-dimensional framework. Often, geometries are given with an estimated range (e.g. 10s to 100s metres). Typically, quantitative data is limited to two dimensions, commonly thickness and dip-width. In some cases, a minimum value for the strike-parallel length of geobodies is presented, as this often exceeds the width by an order of magnitude and is therefore difficult to assess in most outcrops. However, some publications provide direct thickness, width, and length of depositional elements (cf. Tables 1 & 2), with some studies also describing their internal geometry in detail (e.g. Kerans, 2002; Aconcha et al., 2008; Grélaud et al., 2010; Adams et al., 2011).

Modern analogues can often be used to quantify widths and lengths of geobodies, and provide an understanding of the internal geometry and shape of a variety of ancient sedimentary structures, including shoal bodies and reefs (Harris, 2009b). However, there are fundamental dissimilarities between modern and ancient examples. These include the nature of exposure, with modern analogues often quantified precisely in lateral extent, for example via satellite images, but lacking the vertical component which is available in outcrop exposure of ancient

deposits. Moreover, there are fundamental variations between carbonate producing organisms between modern and ancient examples. Lastly, diagenetic and compaction history of ancient deposits must be considered when comparing thickness and petrophysical properties to modern sediments.

Previous authors established distinct relationships between various parameters for carbonate shoal bodies in both modern and ancient examples. These parameters include lateral extent, thickness, grain composition, or sequence stratigraphic position and stacking patterns, and location on the platform. Koehrer et al. (2011) showed a positive correlation between the thickness and dip-extent of ramp ooidal-peloidal grainstone shoals in the Triassic Muschelkalk of Oman (Khuff Formation). In recent examples, Harris et al., (2011) have shown relationships between the form of ooid shoals and area they occupy, with smaller sand bars tending to be rounded, while larger ones (>1km) are generally elongated. Furthermore, different bodies within the same geological system may show highly variable connectivity between bars (P.M. Harris et al., 2011). Moreover, it was shown that grain size and the height of shoal bars are greater in wider facies belts (Rankey and Reeder, 2011). In the Permian Basin of Texas Kerans and Harris (2010) have shown how the dip-extent, thickness and composition of grainstone bodies varies in response to the changing physiography of the shelf during a transition from ramp to rimmed shelf. In the initial ramp system, grainstones form as ramp-crest bars, parallel to the strike of the shelf. They exhibit a thickness of 2-10 m, and widths of 0.1-2 km and consist of fine-medium grained fusulinid-ooid grainstones. In the transitional ramp-rim stage, the margin experienced higher relief and wave energy, and formed 0.5-5 km wide, <2m thick wave- and tide-dominated sand bars with medium-coarse intraclastic-ooidal grainstones. When the platform evolved into a reef-rimmed shelf, wave dominated grainstone bars formed only 0.1-0.5 km wide bodies. Early cementation led to a variety of grains sourced from lagoonal mudstones, shoal complexes and outer shelf packstones. Kerans and Harris (2010) were further able to show how variations of accommodation occurring on a sequence-scale affected the vertical and lateral stacking of these grainstone bodies. This is most evident in the Permian ramp systems, where TSTs exhibit narrow (<2 km) tide-dominated grainstones, whereas HST show potentially wider (<5 km) seaward-prograding and wave-dominated sheet sands from the foreshore-upper shoreface environment. In the later shelf-rimmed systems, the steep gradient of the margin resulted in high wave energy concentrating in a narrow zone. This limited progradation, leading to predominantly vertical stacking of grainstone beds.

**Table 5.1: Geometrical data of grainstone shoals throughout geological time, collected from a variety of literature sources. Values in *italics* were calculated on the basis of several data points from the respective sources. To reduce sample bias, average values were calculated from publications where several data points were presented (presented in brackets). The column “Geometry” is filled with the appropriate term from the classification of Jung and Aigner (2012), based on the descriptions of the geobody in the respective publication. + denotes entries were plotted in a width vs. length diagram (Figure 5.14), \* denotes entries were plotted in a width vs. thickness diagram (Figure 5.15).**

Age	Type	Locality	Geometry	Source	Platform Type	Systems Tract	Width [m] Min-Max (Avg)	Length [m] Min-Max (Avg)	Thickness [m] Min-Max (Avg)	Reference
Quaternary	Ooid Grainstone Shoal	Lily Bank, Great Bahama Bank	Bar	Modern	Isolated Platform	HST	(4000)	(24000)	<3.6	Handford (1988)+ *
Quaternary	Ooid Grainstone Shoal	Miami Limestone, Florida, USA	Bar	Outcrop	Isolated Platform	Unknown	(1600)	(32000)	<9.1	Halley et al. (1977)+ *
Quaternary	Ooid Grainstone Shoal	Cat Cay, Great Bahama Bank	Bar	Modern	Isolated Platform	HST	2000-3000	(35000)		Handford (1988)+ *
Quaternary	Ooid Grainstone Shoal	Fish Cay, Great Bahama Bank	Bar	Modern	Isolated Platform	HST	7000-9000	(35000)		Rankley and Reeder (2011)+ *
Quaternary	Ooid Grainstone Shoal	Schooners Cay, Little Bahama Bank	Bar	Modern	Isolated Platform	HST	(16000)	(60000)		Rankley and Reeder (2011)+ *
Quaternary	Ooid Grainstone Shoal	Exuma, Great Bahama Bank	Bar/Sheet	Modern	Isolated Platform	Unknown	<17000 (12000)	(62000)		Harris et al. (2011) and sources therein
Quaternary	Ooid Grainstone Shoal	Tongue of the Ocean, Great Bahama Bank	Bar/Sheet	Modern	Isolated Platform	Unknown	<27000 (20000)	(155000)		Harris et al. (2011) and sources therein
Quaternary	Ooid Grainstone Shoal	Various modern ooid shoals, Great Bahama Bank	Bar	Outcrop	Isolated Platform	HST	2400-4300	6200-10200	0.9-3.3	Qi et al. (2007)+ *
Albian	Carbonate allochem grainstone Shoals	Devils River/Salmon Peak, 18 HFS, Mavericks Intrashelf Basin, Texas, USA	Bar	Outcrop/Model	Ramp	HST	(9250)	>8000	10-35 (23)	Sitgreaves (2015)+ *
Mid Albian	Ooid Grainstone Shoal	Callahan Carbonate-Sand Complex, Fredericksburg Limestone, Mavericks Intrashelf Basin, Texas, USA	Sheet	Outcrop	Ramp	Unknown	>6440	>8050	(18.29)	Boutte (1969)*
Late Albian-Early Turonian	Rudist Rudstone Shoal	Natih Sequence II, Jabel Shams, Bab Basin, Oman	Bar	Outcrop	Ramp	HST	(100)	?	<10	Adams et al. (2011)*
Late Albian-Early Turonian	Rudist Grainstone Shoal	Natih Sequence I/5, Jabel Madmar, Bab Basin, Oman	Bar	Outcrop	Ramp	HST	>600	?	3-10 (4.5)	Grélaud et al. (2010)+ *
Lower Aptian	Bioclastic Grainstone (Inner Ramp)	Shur'alba, Jebel Akhdar, Oman	Bar	Outcrop	(Inner) Epeiric ramp	HST	5000-30000	?	1-4 (1.74)	Borgomano et al. (2002)*
Lower Aptian	Bioclastic Grainstone (Outer Ramp)	Shur'alba, Jebel Akhdar, Oman	Bar	Outcrop	(Outer) Epeiric ramp	HST	3000-10000	?	1-5 (2.39)	Borgomano et al. (2002)*
Upper Muschelkalk	Ooids and bioclast grainstone shoal	Germanic Basin, Southwest Germany	Sheet/Bar	Outcrop	Ramp	HST	5000-15000	10000-25000	0.7-3.5 (2)	Aigner et al. (2007)+ *
Lower Triassic	Oolitic Grainstones	Upper Khuff Formation, Jebel Akhdar, Oman	Sheet/Bar	Outcrop	Epeiric ramp	HST	1400 - >8000	?	0.4-6 (1.71)	Koehler et al. (2011)*
Lower Jurassic	Skeletal and Ooidal-Peloidal Grainstone	Djebel Bou Dahar, Morocco	Bar	Outcrop	Rimmed Platform	Unknown	350-420	?	0.09-3.83 (1.96)	Verwer et al. (2009)+ *
Permian	Ooid Grainstone Shoal	Grayburg Formation, Delaware Mountain Group, Texas, USA	Bar?	Outcrop	Ramp	HST	>1200	>1000	<4.3	Barnaby and Ward (2007)*
Permian	Fusulinid-Ooid Grainstone Shoal	San Andres Formation (G1-9HFS), Guadalupe Mountains, Texas, USA	Bar	Outcrop	Ramp	TST and HST	100-2000	?	2-10	Kerans and Harris (2010) *
Permian	Mixed Intraclastic-Oolitic Grainstone Shoal	Grayburg (G10-12HFS) and Queen Formations (G13-14HFS), Guadalupe Mountains, Texas, USA	Bar	Outcrop	Ramp - Rimmed Shelf	TST and HST	500-5000	?	<2	Kerans and Harris (2010) *
Permian	Oolitic-intraclastic Grainstone Shoal	Upper Yates (G24-26HFS) and Tansill Formations (G27-28HFS), Guadalupe Mountains, Texas, USA	Bar?	Outcrop	Rimmed Shelf	HST	100-500	?	1.5-4.5	Kerans and Harris (2010) *
Carboniferous	Ooid Grainstone Shoal	St. Louis Limestone, Meramecian, Hugoton embayment, SW Kansas, USA	Sheet/Bar	Model	Ramp	HST	(9000)	(9000)	0.9-3.3 (2.1)	Qi et al. (2007)+ *
Carboniferous	Skeletal and ooidal Grainstone shoal	St. Louis Limestone, Damme Field, Hugoton embayment / Anadarko Basin, SW Kansas, USA	Bar	Outcrop	Ramp	Unknown	(16000)	(16000)	(5.5)	Handford (1988)+ *



**Table 5.2: Geometrical data of biogenic build-ups in Cretaceous times, collected from a variety of literature sources. Values in *italics* were calculated on the basis of several data points from the respective sources. To reduce sample bias, average values were calculated from publications where several data points were presented (presented in brackets). The column “Geometry” is filled with the appropriate term from the classification of Jung and Aigner (2012), based on the descriptions of the geobody in the respective publication. + denotes entries were plotted in a width vs. length diagram (Figure 5.16), \* denotes entries were plotted in a width vs. thickness diagram (Figure 5.17).**

Age	Type	Locality	Geometry	Source	Platform Type	Systems Tract	Width Min-Max (Avg)	Length Min-Max (Avg)	Thickness Min-Max (Avg)	Reference
Campanian-Maastrichtian	Hippuritids, Vaccinites and Coral Floatstone Patch Reef	Merfeg Formation, Tunisia	Bar	Outcrop	?	Unknown	(500)	(5000)	1-10 (5.5)	Negra et al. (1995)+*
Albian-Turonian	Caprinid and Radiolitid Reef	Beit Oren, Judea Limestone, Israel	Bar/Bow	Outcrop/Wells	Rimmed Shelf?	Unknown	1000-2000	>9000	(25)	Bein (1976)+
Albian-Turonian	Reef of mainly Radiolitids, with few Chondrodonts and Caprinids	Nahal Ha'mearot, Judea Limestone, Israel	Bar/Bow	Outcrop/Wells	Rimmed Shelf?	Unknown	(300)	>1300	>130	Bein (1976); Ross (1992)+
Albian-Turonian	Undefined Rudist Reef	Helez, Judea Limestone, Israel	Bar/Bow	Outcrop/Wells	Rimmed Shelf?	Unknown	(1000)	<13000	(300)	Bein (1976)+
Albian	Hippuritid, Caprinid and Coral Patch Reefs (Bafflestone)	Upper Mural Limestone, Bisbee Group, Chihuahua Trough, Arizona, USA	Mound	Outcrop	Ramp	Unknown	120	270	20-60	Roybal (1981)+*
Albian	Caprinid, Requinid, Radiolitid and Chondrodont Biostromes	Pecos River, Lewis Canyon, Mavericks Intraself Basin, Texas, USA	Mound	Outcrop	Ramp	Unknown	41.11-114.83 (80.15)	41.11-114.83 (80.15)	0.85-2.27 (1.53)	Purkis et al. (2012)+*
Late Albian	Chondrodont- Radiolitid Floatstone Patch Reef	Devils River Formation, Mavericks Intraself Basin, Texas, USA	Mound	Outcrop	Ramp	TST	30-1000	30-1000	1-5	Kerans (2002)+*
Upper Albian	Caprinid Bafflestone Reef	Salmon Peak Formation, Mavericks Intraself Basin, Texas, USA	Mound/ Bar	Outcrop	Ramp	HST	30-700	30-700	0.5-2	Kerans (2002)+*
Mid Albian	Caprinid, Toucasid and Radiolitid Bioherms and Biostromes	Edwards Formation, Mavericks Intraself Basin, Texas, USA	Mound	Outcrop	Ramp	Unknown	13-20 (14.75)	13-20 (14.75)	1-3.5 (2)	Mukherjee et al. (2012)+*
Mid Albian	Caprinid Floatstone Patch Reef	Edwards Formation, Mavericks Intraself Basin, Texas, USA	Mound	Outcrop	Ramp	HST	10-30 (20)	17-51 (34)	2-7 (4.5)	Janson et al. (2015)+*
Lower Albian	Caprinid Bafflestone Patch Reefs	Lower Glen Rose Formation, Red Bluff Creek, Mavericks Intraself Basin, Texas, USA	Mound	Outcrop	Ramp	HST	5-25 (15)	7.5-42.5 (21.5)	3-10 (6.33)	Janson et al. (2015)+*
Lower Albian	Requinid-Caprinid Bafflestone Patch Reefs	Lower Glen Rose Formation, Mavericks Intraself Basin, Texas, USA	Mound	Ground Penetrating Radar	Ramp	HST	350-970 (576)	500-2170 (1035)	<21.33	Locks and Kerans (2003)+*
Aptian to Upper Albian	Coral and lithocodium Boundstone Reefs	Al Hassanat FM, Wadi El Assy, Oman	Bar/Bow	Outcrop	Epeiric Platform	LST	200	500-700	70	Immenhauser et al. (2002)+*
Early-Mid Aptian	Rudist Patch Reefs	Upper Shu'aba -Al Huwauash, Oman	Mound	Seismic	Epeiric Platform	Unknown	1000-4000	1000-4000	?	Mijnsen et al. (2003) +

#### 5.2.4 Study Area

The study area is located in the Tremp Basin (Figure 5.2), in the South-Central Pyrenees, Catalonia, within the upper of the three thrust sheets that formed during the convergence of the European and Iberian Plates during the Alpine Orogeny. The upper thrust sheet preserved a succession of the Upper Cretaceous, as part of a largely continuous Mesozoic section. The Upper Cretaceous strata unconformably overlie the Aptian/Albian and form a series of carbonate platform sequences with only limited structural deformation. The carbonate platforms were established on the shelf of the narrow foreland basin that formed between the Iberian and European plates (Plaziat, 1981), forming platforms on the scale of 60-100 km (Chapter 3). A general proximal-distal trend from south to north is observed throughout the platforms, with slight variations through time (Chapter 3). Each platform sequence represents a third-order sea-level cycle (Simó, 1993). The stratigraphy, evolution and depositional controls affecting the basin and each platform are discussed in detail in Chapter 3. Three platforms are investigated in this study.

The Congost Platform is mid-Turonian to early Coniacian in age. Internally, this platform is further divided into two sequences (Congost A and Congost B). The platform interior of the Congost A shows coral and rudist floatstones, rudstones and wackestones with intercalations of bioclastic grainstones, that are interpreted as a shallow-water platform top lagoon (lithofacies CGA1, Chapter 3). The Congost A Sequence has a steeply dipping platform margin (up to 20°), defined by large (10s of metres) scale clinofolds of skeletal packstones and grainstones (Lithofacies CGA2, Chapter 3). These bodies largely comprise highly fragmented and well-sorted bioclasts originating from the diverse fauna of the platform top, which included rudist and corals and various benthic foraminifera, amongst others. The younger Congost B sequence comprises coralgal boundstones (Lithofacies CGB2, Chapter 3) with an aggradational-progradational architecture and a steep slope angle (up to 30°), basinward of lagoonal rudist and coral boundstones interbedded with occasional beds of grainstones and packstones (Lithofacies CGB1, Chapter 3). The Congost B is restricted to the northernmost (basinward) part of the study area and correlates landward to a sequence boundary, and is therefore interpreted as a lowstand wedge (Booler and Tucker, 2002; and Chapter 3, this study). Both phases show a similar slope sediment composed of nodular marly limestones with small shell fragments, pelagic organisms and occasional glauconite grains (Lithofacies RE1, Chapter 3).

The Sant Corneli Platform is of mid-Coniacian age, and represents a distally steepened ramp. The geobodies investigated within the Sant Corneli Platform are found in the nearshore-inner ramp transitional lithofacies association (Chapter 3). They form cross-bedded, quartz bearing bioclastic grainstones and packstones intercalating into poorly consolidated and partially cross-stratified sandstones (Lithofacies NIT1 and NIT 2, Chapter 3). These are well exposed along the

East-West transect of the southern Montsec Range, where they have been previously mapped in detail (Institut Cartogràfic i Geològic de Catalunya, 2015). Further basinwards, the deposits are characterised by lagoonal and inner ramp bioclastic nodular wackestones, as well as horizons of in-situ rudist build-ups and small clusters of rudist-coral associations, and occasional intercalations of coarser bioclastic grainstones and packstones (Chapter 3). Laterally, these pass into finer grained slope sediments characterised by occasional bioclasts and common echinoids, and further into fine-grained pelagic calcareous marls and resedimented margin limestones (Chapter 3).

The Bastus Platform is of Late Coniacian to Santonian age, and forms a flat-topped platform (<0.1°) with a gentle slope (<1°, Chapter 3). The proximal environments are dominated by deltaic sandstones with occasional bioclastic material. The principal geobodies in this platform occur in the platform interior, where intercalations of bioclast bearing sandstones and quartz bearing grainstones and packstones, lagoonal patch reefs and peloidal grainstone shoals form thin lenticular units within the surrounding nodular wackestones. At the platform margin, the principal geobodies are composite rudist and coral build-ups with bedded apron facies of bioclastic packstones and grainstones, as well as quartz bearing grainstones and packstones forming platform margin shoals. The slope sediments show nodular or platy marly wackestones with fine-grained skeletal material and common large benthic foraminifera. The basin is characterised by bedded, fine grained pelagic mudstones and packstones with planktonic foraminifera, sponge spicules and fine shell fragments, as well as intercalations of resedimented platform margin limestones (Chapter 3).

The platform margin geobodies within the Congost A Sequence (Gallinove North/South localities), Congost B (Congost d'Erinyá locality) and Bastus Platforms (Montagut Gully and Carreu River localities) were quantified using digital outcrop modelling techniques, captured either via lidar scanning or via photogrammetry. The platform interior geobodies in the Sant Corneli and Bastus Platforms (both in the south of the Montsec Range) were quantified using digital mapping techniques (Figure 5.2).

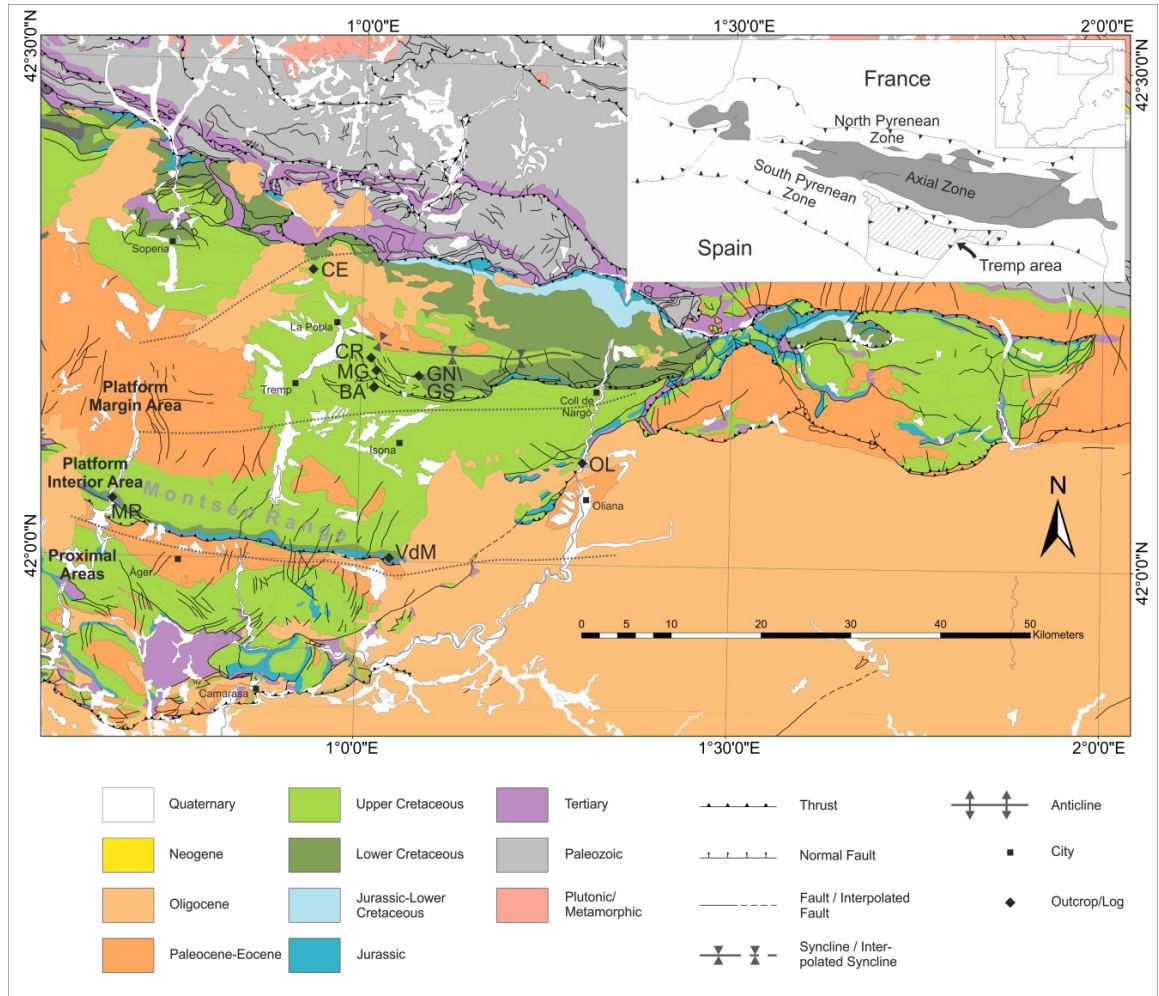


Figure 5.2: Geological Map of the study area within the Tremp Basin (Modified from Institut Cartogràfic i Geològic de Catalunya, 2015). Marked with dotted lines are the approximate boundaries of different platform areas (Proximal, Interior, and Margin). BA = Collades de Basturs; CE = Congost d'Erinyà; CR = Carreu River; MG = Montagut Gully; MR = Mont Rebei; OL = Oliana; GN/GS= Gallinove North/Gallinove South.

## 5.3 Methods and Materials

### 5.3.1 Fieldwork and Lithofacies Analysis

Sedimentary logs were recorded across outcrops at a scale of 1:50 using traditional methods (cf. Appendix B.2), noting lithology, depositional texture after Dunham (1962) and Embry and Klovan (1971), fossil and grain assemblages, sedimentary structures and grain sizes. Facies of interest were sampled and thin sections prepared. Thin sections were described in order to allow interpreting depositional environments and processes (cf. Appendix C.2). Logs and samples were georeferenced and photo-panels and facies maps of individual outcrops were produced to inform the digital outcrop models. Palaeocurrent/bedding orientation data was not collected systematically (except for the grainstone shoal bodies of the Carreu River outcrop) due to inaccessibility of vertical cliff faces.

### 5.3.2 Digital Outcrop Data Acquisition and Processing

#### Lidar Data Acquisition and Processing

Lidar point clouds were acquired at Montagut Gully and Gallinove using a RIEGL LMS-Z420i scanner. Overlapping high-resolution scans were merged and georeferenced to a point cloud from aerial lidar of the area (Instituto Geográfico Nacional and Centro Nacional de Información Geográfica, 2011) using the Iterative Closest Point (ICP) algorithm of CloudCompare 2.6.2. The resulting point cloud shows a resolution <15 cm throughout. Removal of noise and unnecessary areas (vegetation and scree slope) is made within RiSCAN Pro, followed by meshing and colouring using Virtual Reality Geological Studio (2016).

#### Photogrammetry Data Acquisition and Processing

A series of 2000-3000 images for digital outcrop model construction were collected using a Nikon D100 digital SLR camera and 50 mm set focal length lens. A point cloud was constructed from these images with the VisualSFM and bundler software packages (Wu, 2011; Wu et al., 2011), which matches pairs of images using reference points. Features are then identified in 3D space using triangulation to construct at first a rough, then a dense 3D point cloud. The point clouds were then cleaned of noise and undesired areas (vegetation, slopes) using Meshlab 1.3.3 (2014). Next, they were meshed using a Poisson surface reconstruction (Kazhdan et al., 2006), and textured using a subset of the original images for visualisation purposes. The point clouds were scaled and georeferenced to freely available aerial lidar point-clouds of the area (Instituto Geográfico Nacional and Centro Nacional de Información Geográfica, 2011) using the Iterative Closest Point (ICP) algorithm built into CloudCompare 2.6.2.

Bedding surfaces were extracted from the digital outcrop models using a modified approach of that developed by Seers (2015). The desired elements were traced on the source images and the corresponding pixels projected onto the point cloud using the camera position previously defined during the construction of the model. This method has the advantage of picking elements smaller than the point cloud resolution. The extracted elements are represented by polylines, which can be imported into the digital outcrop model at a later stage for quantification.

### 5.3.3 Digital Outcrop Model (DOM) Construction and Geobody Picking

Outcrop point clouds and bedding surface point clouds were imported into Virtual Reality Geological Studio (2016). Using the remove-dip function of the software, the DOMs were aligned to a horizontal stratigraphic surface to remove the effect of tectonic tilt from any measurements. Lithofacies and geobodies were then defined using the top and bottom surface of a rock unit of one lithofacies through the “map geobody” tool. Facies boundaries defined in the field through logs and outcrop photographs, or via the tracing of bedding surfaces in the

photogrammetry workflow were the basis for these picks. For each geobody, a set of measurements was made to define lateral extent, minimum, maximum and average thickness, as well as slope inclination where applicable. Sigmoidal geobodies were quantified based on the parameters defined in the following section.

#### 5.3.4 Quantification Scheme for Sigmoidal Geometries

Sigmoidal bedforms were quantified using a modified variation of the measurement scheme presented by Anell and Midtkandal (2015; Figure 5.3). The following elements were quantified:

- Slope relief
- Maximum foreset thickness
- Edge-to-Toe distance (ETT)
- Overall slope angle
- Maximum slope angle

In the Carreu River outcrop, this scheme proved impractical for the exposed bedforms, and was modified by defining a clinothem through two sigmoidal proximal and distal bounding surfaces Figure 5.4. These surfaces were chosen so that the toplap point (B) of the distal surface was directly above the downlap point (A) of the proximal surface. The slope of the bounding surfaces was defined, both through an overall foreset angle  $\beta$  and through the maximum foreset angle  $\alpha$ . The ratio of these two angles allowed classification of a slope as either near-linear ( $\alpha \approx \beta$ ), or sigmoidal ( $\alpha > \beta$ ).

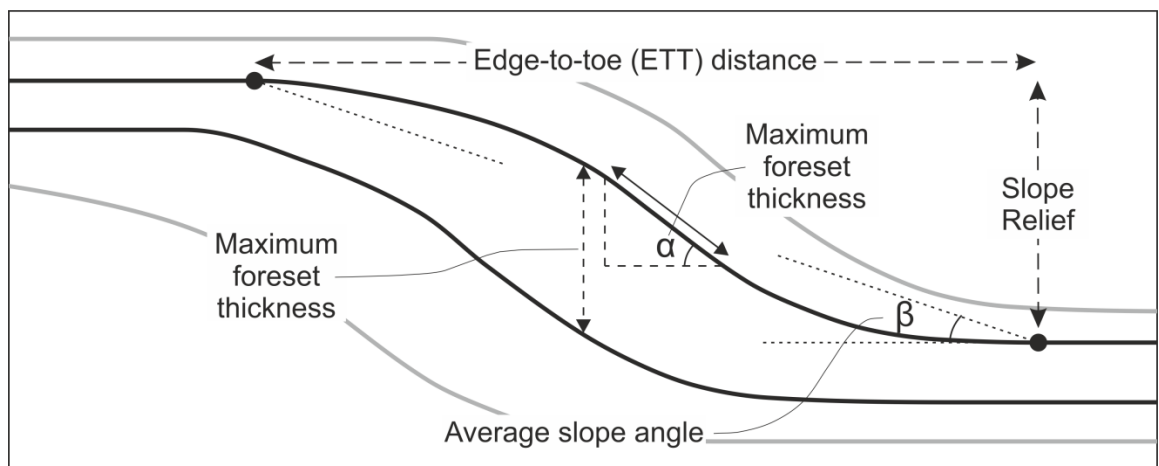
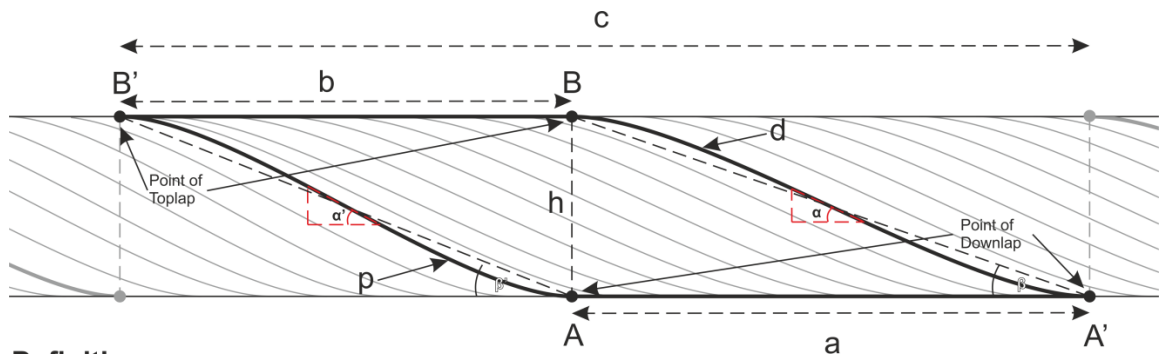


Figure 5.3: Schematic concept of the quantification parameters for clinofolds, modified from the scheme established by Anell and Midtkandal (2015).



**Definitions:**

**d:** distal bounding surface

**p:** proximal bounding surface

**h:** clinothem height (equivalent to unit thickness)

**a:** distal limb length (equivalent to Edge-to-Toe distance)

**b:** proximal limb length

**c:** total clinothem length

**A; A':** point of downlap for the proximal and distal bounding surface, respectively

**B; B':** point of toplap for the distal and proximal bounding surface, respectively

$\alpha; \alpha'$ : maximum distal and proximal foreset angle, respectively

$\beta; \beta'$ : overall distal and proximal foreset angle, respectively.  $\beta = \arctan(h/a)$ ;  $\beta' = \arctan(h/b)$

Figure 5.4: Quantification concept and parameters for the clinoforms of the Bastus Platform margin grainstone shoals.

### 5.3.5 Mapping Regional-Scale Depositional Elements

Acquisition of dimensions of the 100s to 1000s metre long geobodies exposed along the southern side of the Montsec mountain range was made using geological maps of the study area (Institut Cartogràfic i Geològic de Catalunya, 2002, 2003, 2007). The maps were imported into Google Earth, where they were georeferenced using their bounding GPS coordinates. In Google Earth, measurements of geobodies were made using the ruler tool based on several criteria (Figure 5.5):

- If the along strike (usually east-west) terminations of a geobody were exposed, the direct distance between the two was measured. Small faults were disregarded.
- If one termination was exposed, whereas the other was covered (usually by Quaternary sediments), the minimum length (from the edge of the body to the beginning of the cover) and the maximum length (from the edge of the body to the end of the cover) were determined. This was done while maintaining the approximate stratigraphic level and ensuring the strike direction of the measurement was maintained. From these values, the midrange value for each geobody was determined.
- Geobodies on either side of a Quaternary scree slope were interpreted to represent one continuous geobody – provided they are on a similar stratigraphic horizon- and so were measured from one termination to the other to give a maximum length.
- In exceptional cases, a combination of the described rules was used to determine maximum and minimum lengths of bodies.

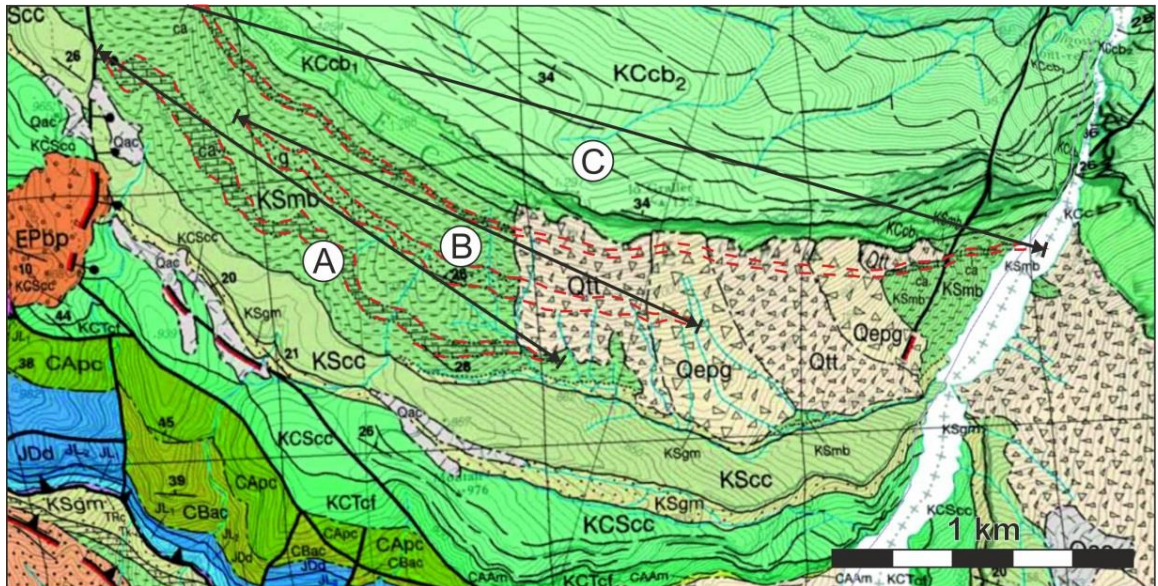


Figure 5.5: Annotated screenshot of a Google Earth view with an overlay of the geological maps by Institut Cartogràfic i Geològic de Catalunya (2007), showing three possible scenarios occurring during geobody measurement. Outlined with red dashed lines are geobodies and their interpolations under quaternary cover. A): the geobody is completely exposed. B): part of the geobody is covered and the extent is interpolated halfway into the overlying scree slope. C): the geobody is covered with quaternary deposits but continuity is interpreted through correlation with a similar body on the same stratigraphic level. Note that the western termination of the geobody depicted in C are not shown in this image.

## 5.4 Results

Shoal bodies, margin clinoforms and build-ups were quantified on depositional element scale and in regards to their internal architecture wherever possible. The depositional element scale represents the mappable exposure of the facies, and the internal scale is represented by the bedding architecture that is exposed in outcrop (cf. Figure 5.1). In some examples, only one of the scales was quantified due to exposure conditions.

### 5.4.1 Platform Margin Shoal and Clinoform Bodies

#### Platform Margin Fine Grained Bioclastic Grainstone and Packstone Clinoforms (Congost A Sequence, Turonian-Coniacian)

The outcrop of the Congost A Sequence at Gallinove shows a platform margin transect (Chapter 3). The sediments consist of fine-grained bioclastic grainstones and packstones forming large scale clinoforms (Figure 5.6). Grains are predominantly finely fragmented bivalve shells, uncommon peloids, rare small benthonic foraminifera and calcispheres and glauconite grains concentrated in discreet horizons. Confined by exposure, this lithofacies extended over at least 3.7 km in width and 19.4 km in length. The thickness increases from ca. 35 m in the south towards the north (basinwards), where it reaches up to 90 metres. At Gallinove, it reaches a maximum thickness of 42.7 metres, and the clinoforms show an average edge-to-toe distance of 64.0 metres, a maximum slope angle of 20.8° and an average angle of 9.5° (Table 5.3).



These strata are interpreted to have been formed in a fashion similar to an Infralittoral Prograding Wedge (IPW). These result from period increases in wave energy (storms), mobilising grains from the shallow shelf top and redepositing these in deeper waters, where hydrodynamic energy can no longer keep the allochems in suspension (Hernández-Molina et al., 2000). In the Congost A, bioclasts produced by the high-productivity organisms on the platform top were transported towards the margin, being sorted and broken down along the way. The formation of glauconite grains occurred in these deeper water settings during periods of low sedimentation rates, resulting in discreet enriched beds. These are further associated with occasional calcispheres implying proximity to marine conditions.



Figure 5.6: Outcrop photograph of the Congost A Sequence platform margin outcrop at Gallinove. Exposed here are the margin clinoforms formed by well-sorted bioclastic packstones and grainstones. White dashed lines mark stratigraphic contacts. Red dashed lines mark bedding surfaces in the clinoforms.

Table 5.3: Quantification results of the clinoforms within the platform margin outcrop of the Congost A Sequence at Gallinove. AVG = Average, STD DEV = Standard Deviation.

Body #	Max Foreset Thickness	Edge to toe (ETT)	Slope Relief	Max dip angle	Average slope angle (°)
1	11.4	63.6	6.8	16.8	6.1
2	2.8	64.4	11.6	21.7	10.2
3	9.2	65.4	11.5	20.7	10.0
4	11.9	62.6	13.0	24.0	11.7
<b>AVG</b>	<b>8.82</b>	<b>64.00</b>	<b>10.73</b>	<b>20.78</b>	<b>9.51</b>
<b>MEDIAN</b>	<b>10.32</b>	<b>63.99</b>	<b>11.56</b>	<b>21.21</b>	<b>10.09</b>
<b>STD DEV</b>	<b>3.63</b>	<b>1.06</b>	<b>2.33</b>	<b>2.60</b>	<b>2.06</b>
<b>VARIANCE</b>	<b>13.16</b>	<b>1.12</b>	<b>5.42</b>	<b>6.78</b>	<b>4.25</b>

### **Platform Margin Quartz-Bearing Grainstone and Packstone Shoals (Bastus Platform, Santonian)**

These lithofacies form clinothems that are several tens of metre wide and dipping towards the North-Northeast, with internal bedding on the scale of 10-40 centimetres (Figure 5.7). They are characterised by packstones in the bottomsets that grade upwards into grainstone at the topsets. Compositional variation along the topset-bottomset transect was found, showing decreased sorting and increase in mud contents towards the bottomset (Al Rahbi, 2015). The packstones are medium sorted and fine to medium grained, with common subrounded rudist fragments and angular monocrystalline quartz grains. The grainstones are well sorted and fine grained, and dominated by peloids, small benthic foraminifera, and well-rounded shell fragments. These lithofacies form units that intercalate into nodular wackestones with uncommon fine-grained shell fragments and benthic foraminifera and rare silt-grade quartz grains. In the Carreu-River outcrop, they also intercalate into beds representing platform-margin build-ups (cf. Figure 5.8 and Section 0).

On a regional scale, these two lithofacies were mapped around the Sant-Corneli Anticline. With respect to the south-north trending proximal to distal trend of the platform established in Chapter 3, they are situated at the platform margin, and extend across an area that is at least 2.4 km in width and 5.2 km in length. The nature of the exposure only allows minimum exposure to be defined.

In the Carreu River outcrop, which represents a strike-transect of the platform margin (Chapter 3), four distinct horizons show sigmoidal bedding surfaces (Figure 5.8). These horizons vary in thickness between 1 - 5.4 m. The average geometries of the clinofolds measured within each horizon are displayed in Table 5.4. For the complete data refer to Appendix E.2, Table E.2.2. The lengths of clinothems may vary between 41 and 78 metres, with individual clinofold surfaces spanning between 19.7 and 42 metres. Average slope angles are between 3.9° and 10.7°, and may reach up to 12.5°.

Based on the cross-bedding architecture and sedimentary composition, these beds are interpreted as tidal-dominated sandwaves. The observed scale of cross-stratification is suggested to be associated with these tidally-controlled bedforms, which deposit as bars that are elongated along the platform break (McCave, 1971; Nichols, 2009). These migrate in the direction of the dominant tidal current, producing various cross-stratification patterns depending on the relative intensity of the two opposing currents (Allen, 1980, 1982). In the case of the bedforms presented here, the reversing tidal currents are asymmetrical, and material transported unidirectionally. The enrichment quartz-grains in the bedding surfaces and of mud in the bottomsets is indicative of periodic reduction of tidal energy (Allen, 1980). The grains are

interpreted to originate from the platform top, with quartz and mud being introduced from the more proximal environments, whereas bioclasts are transported from the high-productivity platform interior foraminiferal wackestones and rudist build-ups and the composite margin build-ups (cf. Sections 5.4.3 and 5.4.4, as well as Chapter 4 for description).

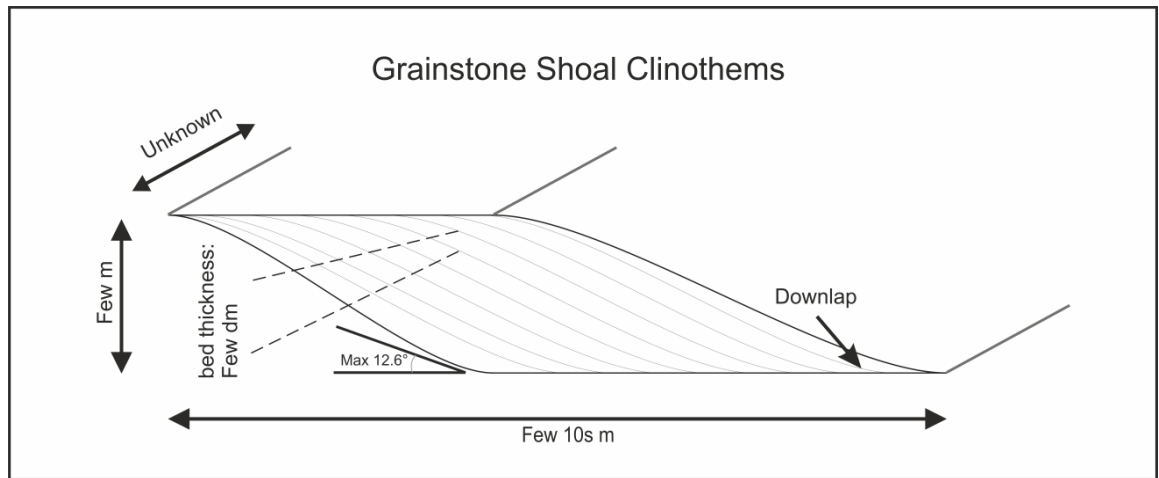


Figure 5.7: Conceptual diagram of the grainstone shoal clinothems of the Bastus Platform margin.

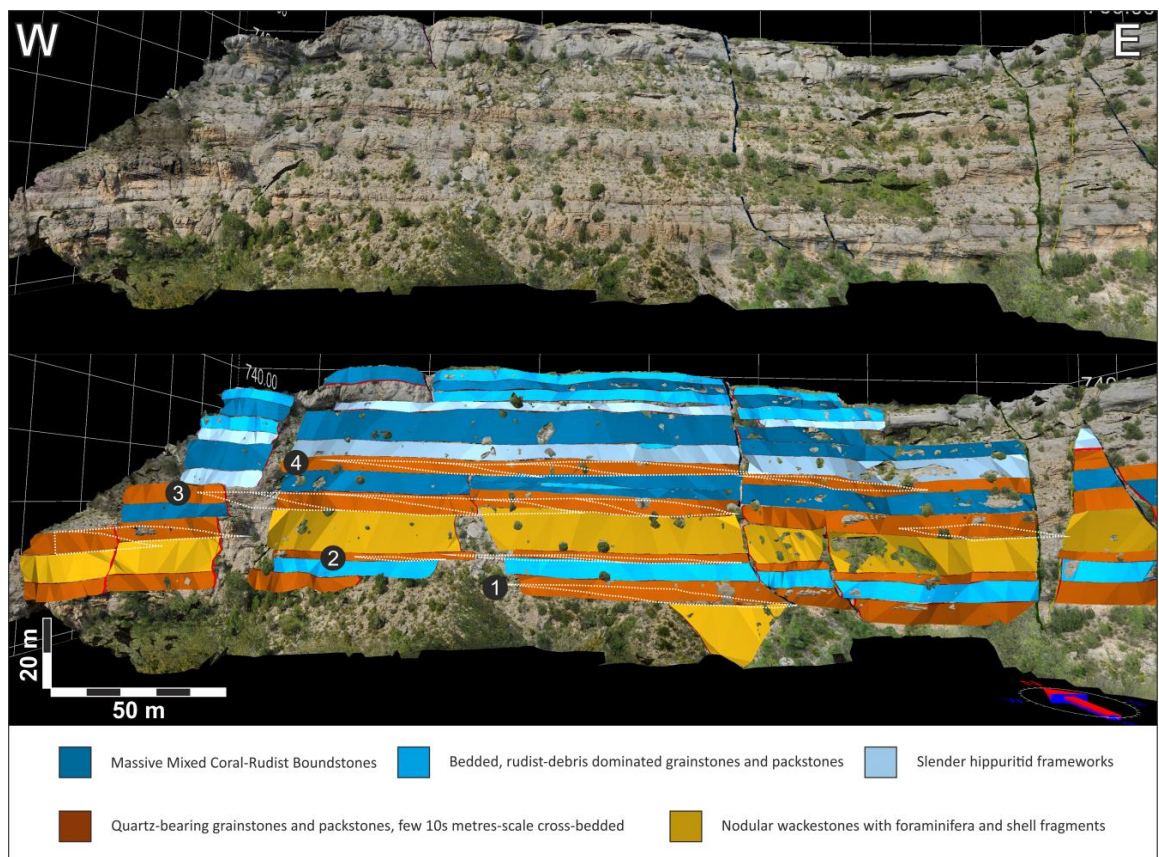


Figure 5.8: Digital outcrop model of the Carreu River outcrop, showing the Bastus Platform margin deposits. The bottom image shows the model overlain with colours representing the respective lithofacies. Outlined with dashed white lines are the measured geobodies. Numbers in black circles correspond to the grainstone shoal host unit numbers in Table 5.4.

**Table 5.4: Average geometrical parameters for each grainstone shoal host unit of the Bastus Platform margin, measured at the Carreu River outcrop.**

Host Unit	h - Height (m)	a - distal limb length (=Edge to Toe distance)	b – proximal limb length (m)	c – clinothem length (m)	Cross sectional area (m <sup>2</sup> )	Max dip angle – distal limb (°)	Average slope angle – distal limb (°)	Average slope angle – proximal limb (°)	n
Host Unit 1	3.57	35.50	42.51	78.01	143.65	8.46	5.74	4.80	1
Host Unit 2	1.47	19.71	21.77	41.48	27.51	5.23	4.32	3.94	3
Host Unit 3	4.20	26.00	23.45	49.39	106.73	12.51	9.46	10.75	8
Host Unit 4	3.33	30.32	28.96	59.27	98.51	8.52	6.35	6.63	4

#### 5.4.2 Platform Interior Shoal Bodies

##### Platform Interior Quartz-Bearing Bioclastic Grainstone Shoals (Sant Corneli Platform, Coniacian)

These geobodies are exposed along an E-W transect on the southern side of the Montsec Range. They comprise successions of limestone beds that intercalate into the surrounding cross-bedded sandstones. The limestone intercalations are internally bedded, occasionally showing metre-scale cross-bedding (Figure 5.9 and Log VMs, Appendix B). Depositional textures are grainstone to packstone, with coarse grained, rounded rudist fragments occasionally resulting in rudstone textures. Other components are peloids, miliolids, Lacazina and quartz grains, the latter occurring in discrete beds. Only for one body could the thickness be defined, where it was measured at >30 m in outcrop (Vilanova de Meià). An overview of the results of the width measurements is presented in Table 5.5. For the complete data refer to Appendix E.1, Table E.1.1. These bodies range between 0.29 and 13.49 kilometres in length, with an average of 3.82 kilometres.

The angular and coarse-grained sandstones surrounding the limestone intercalations indicate that the geobodies formed close to the source of siliciclastic input into the marine realm. Cross-bedding and coarse grain-sizes in both the limestone intercalations and the surrounding sandstones further imply that water-energy levels were high. The metre-scale cross-bedding observed in the limestone intercalations exhibit a consistent basinward (North) dip direction. This indicates that their formation was not due to tidal currents, which are interpreted to result in opposing cross-bedding between strata (Tucker, 2011). The close proximity to the palaeo-shoreline allows to conclude that these cross-bedded limestone intercalations formed following high-energy wave action in the nearshore environment, which resulted in bedforms similar in

internal structure to the submarine dunes described by Allen (1980). Strong wave action aggregated coarse rudist debris, possibly introduced from the platform interior, sorting and rounding the grains and forming the cross-bedded rudist rudstone beds.



Figure 5.9: Outcrop view showing the internal structure of the Sant Corneli Platform Interior shoals. Clearly visible is the sigmoidal internal bedding character, dipping towards the left side of the image (North, palaeo-seawards).

Table 5.5: Dimensions of the platform interior shoals of the Sant Corneli Platform (Lithofacies NIT1). Minimum and maximum lengths are measured from geological maps using the method described in Section 5.3.5.

Body Identifier	Minimum width [km] (exposed)	Midrange width [km] (calculated)	Maximum width [km] (calculated/exposed)	Comment
1			0.29	Completely exposed
2			0.68	Completely exposed
3			1.76	
4	0.61	1.17	1.78	
5			1.6	Completely exposed
6			1.84	
7	0.46	1.66	2.86	Completely exposed
8	N/A	N/A	10.05	Completely exposed
9	0.24	6.87	13.49	
10	2.11	?	?	No control on either termination
<b>AVG</b>	0.86	3.23	3.82	
<b>STDV</b>	0.74	2.58	4.38	

### Platform Interior Shoal Bodies (Bastus Platform, Santonian)

These geobodies consist of poorly sorted bioclast-rich sandstones and quartz-rich grainstones. Grain sizes vary from pebble to medium sand, and vary from angular to subangular. Most of the siliciclastic grains are monocrystalline quartz grains, although some polycrystalline quartz, feldspar and volcanic rock fragments also occur. Carbonate allochems are rounded rudist fragments, echinoids, peloids and small benthic foraminifera. Bedding is decimetre to metre scale, with commonly sharp bottom surfaces and either sharp or gradational top surfaces. Bioturbation (*Skolithos*, *Thalassinoides*) is common and some cross bedding is apparent. These bodies are interbedded into dark nodular wackestones with abundant foraminifera (cf. Logs Ola and OLb, Appendix B), which form the background sediment in the Bastus Platform interior, and

occasionally sharply overly and intercalate with platform interior rudist biostromes (cf. Section 4.4.5).

A total of 12 different shoal bodies were measured using the map-based technique outlined in Section 5.3.5 along the E-W transect on the south-side of the Montsec Range (Table 5.6). For the complete data refer to Appendix E.1, Table E.1.2. Out of those, minimum and maximum length was captured for 11 bodies. For the last, only a minimum exposure could be determined due to outcrop cover.

The presence of coarse and angular grains in this lithofacies implies that high water energies influenced deposition. The frequent intercalation of this lithofacies into the surrounding fine-grained sediment with sharp lower boundaries, as well as the presence escape-structures (Skolithos), indicate that deposition occurred in periodic, sudden events. Because of the mixing of carbonate and siliciclastic grains, as well as the poor sorting and rounding of grains, these depositional elements are therefore interpreted to represent reworked sediments that formed during periodic introduction of siliciclastic grains from the shore into the platform interior under high water energy events, during which bioclasts were integrated into the grain association. The platform interior carbonate factory, represented by the foraminiferal nodular wackestones and the rudist biostromes, ceases productivity at the introduction of the siliciclastics, but quickly resumes production after, as evident by the frequent intercalation of these two facies. Similar successions and reactions of the carbonate systems to siliciclastic introduction were previously described and associated to flash flooding in the modern Red Sea (Friedman, 1988).

**Table 5.6: Dimensions of the platform interior shoals of the Bastus Platform (Lithofacies P11). Minimum and maximum lengths are measured from geological maps using the method described in the methods section.**

Body #	Length (km, Measured)			Comment
	Minimum	Midrange	Maximum	
1	0.13	0.2	0.33	
2	0.11	0.36	0.47	
3	0.27	0.46	0.73	
4	0.49	0.65	0.93	
5	0.58	0.65	1.14	
6	0.48	0.69	1.17	
7	0.43	0.93	1.23	
8	0.7	1.27	1.79	
9	0.5	1.79	1.88	
10	1.17	1.85	1.97	
11	1.67	2.1	2.53	
12	0.24		N/A	Quaternary cover too extensive to provide realistic interpretation
<b>AVG</b>	0.56	0.89	1.25	
<b>STDV</b>	0.43	0.55	0.59	

### 5.4.3 Platform Margin Build-ups

#### Platform Margin Coralgall Boundstones (Congost B Platform, Turonian)

The outcrop at Congost d'Erinyá shows a transect through the platform margin of the Congost B sequence (Chapter 3). It shows sigmoidally bedded boundstones with in-situ corals and abundant encrusting red algae. On the palaeo-landward (South) side of the outcrop, bedded coral-and rudist floatstones and rudstones with in-situ specimen, as well as beds of bioclastic grainstones and packstones are exposed. The part of the depositional element that displays sigmoidal features measures a width of ca. 150-200 metres (Figure 5.10). The exact width is difficult to constrain, as part of the landward half of the depositional element is not exposed. The average thickness of the unit is 74 metres. The internal sigmoidal bedding surfaces allow quantifying 13 individual clinothems, all of which contain both aggradational and progradational components (Figure 5.10, Table 5.7). On average, the clinothems show a width of 110 m, height of 23 m, maximum foreset thickness of 7 m, an edge to toe distance of 85.9 metres, a slope relief of 19.5 metres, a maximum dip angle of 27.7° and an average slope angle of 15.9°. The standard deviation and variance of the dataset are high, and no linear trend can be determined from the dataset (Table 5.7).

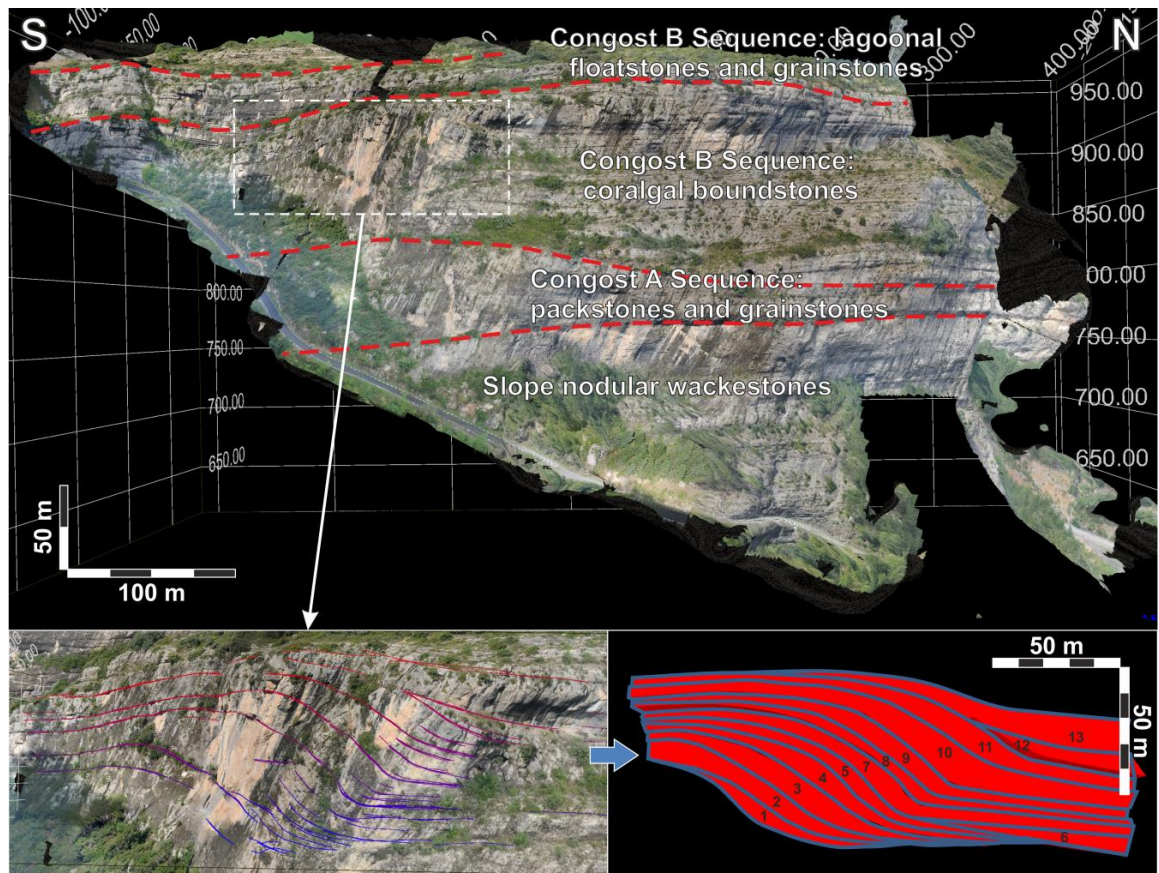


Figure 5.10: The digital outcrop model produced for the Congost B Sequence exposure at Congost d'Erinyá, representing the platform margin. Top: overview of the DOM. Red dashed lines mark lithofacies association boundaries. Bottom left: zoomed view of the sigmoidal structures in the coralgall boundstone lithofacies. Lines represent picked bedding surfaces. Bottom right: view of interpreted and extracted geobodies within the coralgall boundstone unit. Numbers correspond to the body numbers in Table 5.7.

These depositional elements are interpreted as platform margin build-ups. This is due to their internal sigmoidal structure, which represents the angle of the slope break, as well as the palaeo-landward presence of shallow-water platform top rudstones, floatstones and grainstones, and the palaeo-seaward downlapping onto platform slope nodular wackestones with a pelagic fauna. It was previously discussed in Chapter 3 that the change from the packstone-grainstone clinof orm-dominated margin of the Congost A platform to the coralg al boundstone dominated margin of the Congost B may have been associated with a change in oceanic conditions that followed a significant sea-level drop between the two platform phases. This will have possibly restricted the growth of the rudist-coral communities of the platform top, reducing the amount of sediment exported off-platform, and so enabled the growth of coralg al communities at the margin.

**Table 5.7: Results of the measurements of sigmoids within the build-up unit of the Congost B sequence platform margin at Congost d'Erinyá.**

Body #	Max Foreset Thickness	Edge-to-toe distance (ETT)	Slope Relief	Max dip angle	Average slope angle (°)
1	5.7	81.6	18.2	32.0	12.6
2	7.1	94.4	23.1	32.1	13.8
3	8.2	103.8	25.9	29.5	14.0
4	7.9	97.5	25.3	36.2	14.5
5	5.5	102.9	28.7	42.5	15.6
6	6.7	52.7	1.8	2.0	2.0
7	7.0	77.6	23.7	31.1	17.0
8	3.4	94.8	24.3	31.9	14.4
9	6.0	103.2	24.0	30.6	13.1
10	10.9	107.6	21.7	32.4	11.4
11	7.9	113.1	22.0	27.9	11.0
12	4.8	39.1	7.3	13.5	10.6
13	9.4	48.2	7.1	18.1	8.4
<b>AVG</b>	7.0	85.9	19.5	27.7	12.2
<b>MEDIAN</b>	7.0	94.8	23.1	31.1	13.1
<b>STD DEV</b>	1.9	23.5	8.1	10.2	3.7
<b>VARIANCE</b>	3.6	554.4	66.0	103.4	13.4

### **Platform Margin Composite Rudist-Coral Build-Ups (Bastus Platform, Santonian)**

Exposed at Collades de Basturs, Montagut Gully and Carreu River, are successions interpreted to represent the margin of the Bastus Platform (cf. Chapter 3). These are represented by an association of autochthonous and bioclastic lithofacies that intercalate into fine-grained nodular wackestones of the upper slope (Figure 5.12). Boundstones of mixed rudists and corals with a muddy and bioclastic matrix form internally structureless units. These are interpreted to pose seaward-facing, wave-resistant build-ups bioherms. Dense framestones formed of colonies of elongated and thin hippuritid rudists are common up-dip of the bioherms, and are interpreted



to represent biostromes in the protected back-margin environment. Both these facies are often found overlying a distinct sheet-like association of corals, rudists and sponges, which are interpreted to represent the initial colonisation of the seafloor. Bedded bioclastic packstones formed of rudist debris, peloids and small benthic foraminifera are found onlapping the downdip side of the mixed-rudist-coral bioherms, and overlying the biostromes. These packstones are interpreted as reefal debris aprons shedding onto the slope, and forming behind the margin.

This lithofacies association forms combined units (“composite build-ups”) that are recognisable on map-scale. Map data and correlations imply extents of at least 2.4 km in width (cf. Chapter 3, and geological maps), and of at least 3.4 km in length (geological maps and Sanders and Pons 2001). Continuous lateral extents exposed in outcrop are smaller, however. In the Montagut Gully, the platform margin exposure of the rudist-coral lithofacies shows minimum widths of the individual beds of at least 240 metres along dip. The exposed strike section at Carreu shows at least 250 metres in lateral continuity. The sections of Collades de Basturs and Carreu River, show the lateral extent (strike) of all lithofacies within this association to reach at least 3.4 km (outcrop limit). Vertically, successive beds of rudist-coral bioherms, hippuritid biostromes and bioclastic grainstones are interpreted to represent a single depositional element that comprises individual build-up generations. These may reach between 37 and 73 metres thickness (average: 57.2, n=5; Chapter 4).

The interior architecture of the composite build-ups in dip-section is presented in the digital outcrop model in Figure 5.11, and conceptually in Figure 5.12. Lateral limitations on exposure and coverage in the dip-section at Montagut Gully (cf. Figure 5.11) pose a constraint on defining the extent of some facies. The dense hippuritid biostromes are observed to have an extent in dip of greater than few 100s metres, whereas the massive coral-rudist bioherms are limited to few 10s metres. Measurements of maximum unit thickness and minimum unit width of each lithofacies are presented in Table 5.8. For the complete data refer to Appendix E.2, Table E.2.1. Note that a large amount of these beds are truncated by coverage and could not be correlated throughout the outcrop.

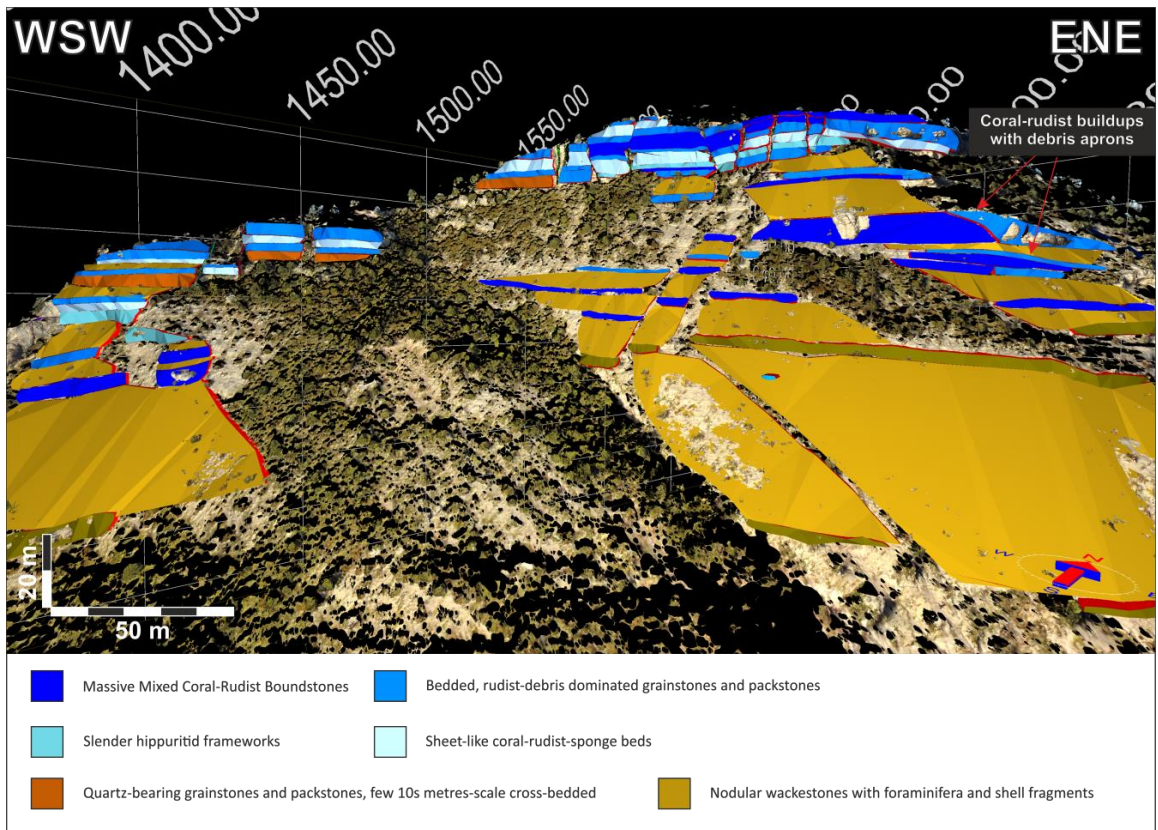


Figure 5.11: Digital outcrop model of the Montagut Gully outcrop, showing the Bastus Platform margin deposits. The model is overlain with colours representing the respective lithofacies. Highlighted in the top-right part of the figure are bedded rudist-debris grainstone and packstone beds onlapping onto the massive coral-rudist boundstones.

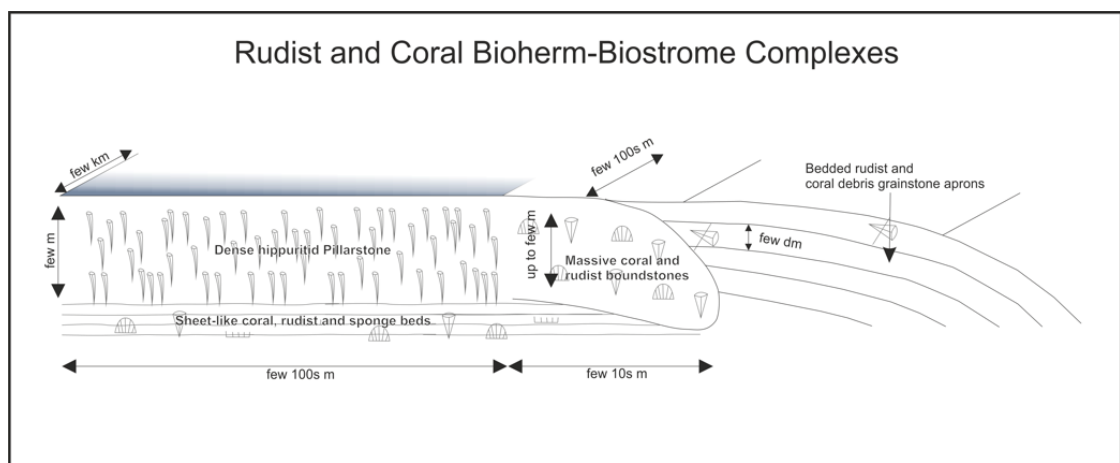


Figure 5.12: Conceptual sketch of the build-ups formed at the Bastus Platform Margin. For the description of individual elements refer to text.

**Table 5.8: Measured thicknesses and widths of individual lithofacies of the Bastus platform margin at Montagut Gully and Carreu River.**

Lithofacies association	Maximum Thickness (m)				Minimum Width (m)			
	Lowest Value	Highest Value	Avg Value	n	Lowest Value	Highest Value	Avg Value	n
Massive mixed coral-rudist boundstones	1.0	10.7	4.2	14	12.7	96.8	50.0	10
Sheet-like coral, rudist and sponge beds	2.7	3.6	3.2	2	40.6	73.5	57.0	2
Slender hippuritid frameworks	3.2	6.1	4.4	5	24.6	243.5	109.1	3

#### 5.4.4 Platform Interior Build-ups

##### Platform Interior Rudist Build-ups (Bastus Platform, Santonian)

These geobodies are exposed along the East-West transect on the southern side of the Montsec Range. They are found bedded into the dark foraminiferal wackestones that are interpreted to form the lagoonal background sediment. They are internally planar bedded on the scale of several decimetres to few metres. They consist predominantly of rudistid rudstones and floatstones with a matrix of dark micrite (Figure 5.13). The rudist association often consists of only few species and rare corals, and in some horizons is monospecific. They are commonly loosely bound and show no obvious clustering, but in the monospecific beds they present a uniform growth direction and form dense frameworks. Accessory grains in the matrix are fine-grained monocrystalline quartz, as well as small and large benthic foraminifera. Occasionally, beds of well-sorted, fine-grained grainstones with peloids and rudist shell fragments and other bioclasts intercalate into these. The build-ups are commonly sharply overlain by coarse sandstones with rudist-debris and quartz-rich grainstone. Four build-ups were measured using the map-based technique outlined in Section 5.3.5 (Table 5.9). For the complete data refer to Appendix E.1, Table E.1.3. Multiple successive beds of this lithology compose a depositional element. In previous cross-sections and sequence stratigraphic correlations (Chapter 4), these bodies were measured to show thicknesses between 25 and 50 metres, which represent intervals of several successive beds of this lithofacies, commonly intercalated with coarse sandstone/grainstone beds or nodular foraminiferal wackestones.

Due to the low-diversity or monospecific rudist associations, as well as the occasional formation of biostrome-like frameworks, these beds are interpreted to represent platform interior patch-reefs that occur sporadically within the lagoonal foraminiferal nodular wackestones. These will have formed in an opportunistic development fashion, as proposed for this type of biostrome by Sanders (1996), and periodically terminated by influx of siliciclastic and reworked bioclastic material, represented by the coarse sandstones and grainstones. Moreover, it is suggested that such build-ups lack topographic relief due to the limited thickness of less than few metres, and a

tabular shape in plan-view, with lateral extents of up to several hundreds of metres (Masse and Philip, 1981).



Figure 5.13: Left: Outcrop view of the Bastus Platform interior build-ups. Note massive sandstone bed at the bottom left of the image. Red lines on the measuring pole are 10 cm apart. Right: detail view of the build-ups. Note nodular nature and abundant very large rudist shells.

Table 5.9: Dimensions of the platform interior rudist build-ups of the Bastus platform (Lithofacies PI3 and PI3). Minimum and maximum lengths are measured from geological maps using the method described in Section 5.3.5, and midrange lengths calculated from these.

Body#	Length (km, Measured)		
	Minimum	Midrange	Maximum
1	1.29	1.58	1.87
2	0.72	1.08	1.99
3	NA	NA	2.00
4	0.6	1.45	2.7
5	2.1	2.36	4.1
<b>AVG</b>	0.57	1.62	2.53
<b>STDV</b>	0.46	0.47	0.84

## 5.5 Discussion

The results present the geobody dimensions for a range of genetically related bodies within the different carbonate platforms. Because of the evident differences between geobody sizes varying on their position on the platform, they will continue to be discussed separately here, focussing upon the scale of the depositional elements first, followed by the internal geometry.

### 5.5.1 Platform Margin Shoal and Clinoform Bodies

#### Depositional Element Scale

In the area of the Sant Corneli Anticline, the Congost Platform Sequence A margin clinoforms (strike extent >19.4 km) are notably longer than the Bastus Platform margin shoals (>5.2 km) along strike (Table 5.10). Similarly, the Congost A Sequence platform margin clinoforms are wider (> 3.7 km) and thicker (up to 90 m thick), than the Bastus Platform margin shoals (>2.4 km and up to 5.9 m thick).

The larger width and thickness of the Congost A Platform margin clinoforms compared to the Bastus Platform shoals are interpreted to be the result of their different modes of formation and interactions with the surrounding facies; The packstone-grainstone clinoforms of the Congost A are interpreted to have formed as infralittoral prograding wedges, that resulted from deposition of large amounts of fine bioclasts on the platform slope, mobilised from the platform top in high-energy events. The progradation formed continuous vertical successions of packstones and grainstones over a wide area and extensive length of the margin, which is characteristic for IPW (Pomar et al., 2015).

The shoals of the Bastus Platform margin are often observed over- and underlying both the platform margin composite build-ups, and the slope nodular wackestones in vertical section (Figure 5.8). In outcrop (Carreu River) and in map data these are observed in the same stratigraphic horizon as the build-ups (Institut Cartogràfic i Geològic de Catalunya, 2010). It is therefore interpreted that these are juxtaposed with the composite build-ups in a zone that represents the platform margin area (Chapter 3, cf. Sections 0 & 0) and thus form bodies that are narrower and thinner than those of the Congost A. It is described that sandwaves and subaqueous dunes similar to those interpreted into the deposits packstone-grainstone shoals of the Bastus Platform form bars elongated along the strike of the margin (Allen, 1980; Nichols, 2009). Comparable sedimentary bodies from the modern Bahama Bank also show limited lateral extent and complex internal architecture, due to the influence of tidal channels and the topography of the surrounding reefs and islands (Rankey and Reeder, 2011). In the Bastus Platform margin, the juxtaposition with platform margin build-ups and slope nodular wackestones implies that the margin shoals were limited in their extent in dip by these neighbouring facies. It is therefore suggested that while the IPW of the Congost A showed extensive width and length, and a substantial total thickness caused by continuous sedimentation via a single process, the shoal bodies of the Bastus Platform margin are narrower, shorter, limited in thickness and vertically interbedded with the neighbouring facies of the platform margin build-ups and the upper slope nodular wackestones.

**Table 5.10: Summary data for the depositional element and internal geometry of the Congost A and Bastus Platform margin shoal bodies.**

Platform	Lithofacies	Depositional Element			Internal Geometry (Average Values)				
		Width [km]	Length [km]	Max thickness [m]	Geometry Type	Length	Foreset Thickness	Height (Relief)	Maximum Angle
Congost A Sequence	Large-scale cross-bedded packstones and grainstones	>3.7 km (Map)	>19.4 km (Map)	90 m (Cross-section)	Clinoforms	64 m	8.8 m	10.7 m	20.8°
Bastus Margin	Quartz-bearing grainstones and packstones	>2.4 km (Map)	>5.2 km (Map)	1.8 - 5.9 m (Outcrop)	Clinothems	41-78 m	3.5 m	3.5 m	10.5°

### Internal Geometry

The internal geometry of the platform margin packstone-grainstone bodies in the Congost A Platform and the Bastus Platform vary significantly (Table 5.10). In the Congost A platform margin, large-scale and high-relief (>64 m wide, >10 m relief and >8.8 m thick) clinoforms are observed, whereas in the Bastus platform margin, clinoforms are shorter, thinner, show less relief, and are limited to the thickness of the host depositional elements (<26.5 m wide, and <3.5m relief and thickness). This variability internal geometry is also likely to be closely linked to the formation mechanism and grain composition. The large-scale progradational nature of the margin in the in the Congost A Sequence (cf. Chapter 3) have formed a much steeper relief and thicker sediment packages, whereas lower margin angles, aggradation, and frequent intercalation with margin build-up facies in the Bastus Platform formed clinoforms of a much smaller scale.

The shorter clinoform length of the Bastus Platform Margin shoals indicates a smaller volume of sediment than in those of the Congost A Sequence. Furthermore, in the Bastus Margin, the topsets of the clinoforms show lower amounts of micrite and higher contents of peloids and rounded grains than in the Congost A Sequence. This implies long and frequent reworking of grains under current action in the Bastus, whereas the Congost A Sequence clinoforms formed by large sediment volumes being deposited on the platform break, and did not experience much reworking. These characteristics are the direct result of the different depositional processes – infralittoral prograding wedges in the Congost A and tidal sandwaves in the Bastus Platform - that formed these two bedforms.

Booler (1994) previously compared the clinoform bodies formed by the bioclastic packstones and grainstones of the Congost A Sequence platform at Gallinove to data gathered by Kenter (1990) and to those described in the Triassic of the Dolomites by Bosellini (1984). It was

concluded that the high angle (<20°) of the clinoforms is the result of slope declivity, which is a function of the large amount of sand grade grains in the sediment, as opposed to mud (Kenter, 1990; Booler, 1994). The sigmoidal shape of the clinoforms results from the mud component travelling further down slope while the sand-grade grains are deposited on the flank (Bosellini, 1984; Booler, 1994). It was further concluded that the clinoforms at the margin of the Congost A Sequence prograded during stable relative sea level, onto a substratum which was sloping at ca. 0.6°. Subsequently, the Congost Platform prograded and increased in thickness basinwards (cf. Chapter 3), due to sediment filling the available accommodation space (Bosellini, 1984; Booler, 1994).

On the basis of their depositional element size, internal geometry and grain composition, the Bastus Platform Margin shoals are considered to resemble modern grainstone shoals on the Great Bahama Bank (e.g. Rankey and Reeder, 2011). These develop on the seaward side of rimmed shelves or other elevations on the platform top, where wave energy is increased due to the change in topography (Harris, 2009a). However, in the Bastus Platform, the margin-oblique dip of the clinoforms (towards NNE) implies that contour currents were the main control on their formation. Despite this difference in interpreted formation mode, the sedimentary characteristics, depositional element scale and internal geometry are very similar.

### **5.5.2 Platform Interior Shoal Bodies**

The platform interior shoal bodies of the Sant Corneli Platform are larger than those found in the Bastus Platform interior (Table 5.11). Furthermore, the platform interior shoal bodies of the two platforms vary in host lithology, internal structure and sediment composition. On the Sant Corneli platform, the shoals show metre-scale cross bedding and comprise predominantly rudist shell fragments with a high degree of rounding and sorting. The shoals are surrounded by coarse-grained, cross-bedded sandstones. These features are consistent with deposition in a high-energy environment under consistent wave-agitation. On the Bastus Platform, the shoals show occasional decimetre-scale cross bedding, comprise fine grained, well sorted peloidal grainstones or coarse grained, moderately sorted and poorly rounded grainstones with abundant quartz. They are predominantly tabular and are surrounded by fine-grained foraminiferal wackestones. This suggests deposition under periodic surges of water energy in a generally low-energy environment, leading to reworking of bioclasts and introduction of siliciclastic grains in distinct horizons.

**Table 5.11: Summary data for depositional element geometry of the Sant Corneli and Bastus Platform interior shoal bodies.**

Platform	Lithofacies	Internal Structure	Host lithology	Depositional Element Maximum Length (Strike)			Depositional element thickness [m]	Internal bed thickness [m]
				Smallest Value	Largest Value	Average Value		
Sant Corneli Platform	Moderately sorted coarse grained grainstones to packstones, with rounded rudist fragments	Sigmoidal Cross-Bedded to Tabular	Coarse grained shallow marine sandstones	0.29	13.49	3.82	Measured: >30 m,	0.2-2.4 ( $\phi=0.71$ ), n=37)
Bastus Platform	Poorly sorted bioclast-rich sandstones and quartz-rich grainstones with rounded rudist fragments	Tabular	Fine grained foraminiferal nodular wackestones	0.33	3.02	1.33	Unknown	0.09-3.47 ( $\phi=0.93$ ), n=62

### 5.5.3 Platform Margin Build-Ups

#### Depositional Element Scale

The Congost B platform margin build-ups formed as part of a lowstand wedge that established during relative sea-level fall. They mark a pronounced change from the packstone/grainstone shoal dominated margin of the Congost A to a coralgal build-up dominated margin. The mechanism behind this change is interpreted in the change in oceanic conditions that followed the sea-level drop, and favoured coralgal growth over the previous rudist dominated community. The Bastus Platform Margin build-ups form in juxtaposition with the platform margin shoals at the sea-level highstands (Chapter 4). Both the underlying topography and the organism association may have a significant influence on the shape and size of these elements.

The platform margin build-ups of the Congost B Platform and the Bastus Platform vary greatly in their maximum width (Table 5.12): while the coralgal build-ups of the Congost B platform only show up to 200 m in width, the composite build-ups of the Bastus Platform possibly stretch over more than 2.4 km in width. The length of the Congost B margin build-ups could not be defined in outcrop. Immenhauser et al. (2001) have described Coral-Lithocodium bodies from the Aptian-Upper Albian of Oman, showing similar values for width, thickness and internal sigmoidal inclination. They measure length values between 500 and 700 metres. These lengths are interpreted to apply to the coralgal build-ups of the Congost B Platform margin investigated here. Subsequently, these build-ups had an elongate to lenticular plan-view geometry. Arguably, the continuity in length is possibly dictated by structural elements along the margin, such as



gullies or palaeohighs, for example caused by margin collapse, mass transport or faulting. Alternatively, continuity could be caused by hydrodynamic elements such as tidal channels. Furthermore, a natural limit of the size of the geobody may be dictated by the carbonate factory. Therefore, it must be noted that a possible maximum length and plan-view geometry of these bodies remains somewhat unknown. The continuity in width is possibly governed by the steep pre-existing margin topography, which proves more suitable for encrusting organisms than substrate dwelling ones.

**Table 5.12: Summary Data for the depositional element geometry of the Congost B and Bastus Platform margin build-ups. Interpretation/comparison data sources are noted in parentheses.**

Platform / Area	Lithofacies / Structure	Max width [km]	Interpreted Max Length [km]	Max thickness [m]
Congost B Margin Coralline Build-ups	Coralgal build-ups, sigmoids	0.2 km ( <i>Digital Outcrop Model</i> )	0.5-0.7 km ( <i>via comparing to Immenhauser et al., 2001</i> )	74 m ( <i>Digital Outcrop Model</i> )
Bastus Margin Build-ups	Composite rudist-coral build-ups, tabular, includes lithofacies PM1-4	>2.4 km ( <i>Sequence stratigraphic interpretation, Chapter 4, and geological maps</i> )	>3.4 km ( <i>Geological map</i> )	37 - 73 m intervals ( $\phi=57.2$ ; Chapter 4)

In contrast to the build-ups of the Congost B Sequence margin, the Bastus Platform margin build-ups are interpreted to have been much wider due to the lower inclination of the margin, allowing them to extend over a larger area. The width of the platform-margin facies belt in which these bodies may occur is estimated to be in the range of ~3.5—6.5 km (Chapter 3). It is evident from the vertical intercalations of build-ups and platform margin shoal lithofacies that the two were juxtaposed along the margin. Therefore, the build-ups were possibly confined in width and length to accommodate both geobodies in the margin zone. Pomar et al., (2005) previously interpreted the facies relationships in the Carreu River outcrop to represent the platform having switched completely between rudist-dominated carbonate production and foraminiferal-shoal based production over time. However, due to the frequent intercalation between build-up, shoal and slope lithofacies, as well as their lateral relationships observed in this study (Chapter 4), it is interpreted here that these lithofacies coexisted across the platform and do not represent two different factories. This interpretation is critical for defining the plan-view geometry of the depositional elements produced by these facies. As both bodies also intercalate with slope nodular wackestones, it is implied that both may have at some point assumed the basinward position, and juxtaposition at the margin is assumed both in dip and in strike, leading to interpreting the bodies to have limited extent in strike. Therefore, the plan-view geometry may have been in the shape of an elongated ellipsoid to a bar.

In order to establish the plan-view geometry and lateral extents of the Bastus Platform Margin rudist build-ups, it is helpful to compare with others presented in the literature. In examples

from the Aptian-Albian of Oman, rudist build-ups are commonly circular to ellipsoid in shape (Mijnssen et al., 2003; Aconcha et al., 2008). Since these build-ups are only slightly older than those described in this study, and were deposited in a similar platform position, they might well be considered analogous, particularly since they are of a similar width and lengths (1-4 km). However, the build-ups on the Bastus Platform are formed by stacking of several generations of build-up, each under 10 metres in thickness, and amounting to 37-73 metres in total, whilst the build-ups in Oman were interpreted to represent a single generation.

The thicknesses of the build-up depositional elements varies between the Bastus Platform Margin (37-73 m, avg = 57.2, n=4) and the Congost B Platform Margin (up to 73 m). The thickness may vary in the build-ups of the Bastus Platform margin because of the juxtaposition with shoal bodies and slope wackestones, as well as the lateral migration of these facies, as observed in outcrop. The Congost B Sequence platform margin build-ups however represent the entire thickness of the platform margin at that time. Nevertheless, the single measurement in this platform may significantly contribute to sampling bias. It must further be considered that productivity and the behaviour of relative sea level have had a control on the thickness of these platform margin build-ups. The Congost B platform margin build-ups represent a continuous progradational to aggradational trend, whereas the Bastus Platform margin build-ups were possibly terminated by relative sea-level variations, due to the fact that they are commonly interrupted by slope nodular wackestones (cf. section 5.4.3 and Chapter 4).

### **Internal Geometry**

The internal geometries of the Congost B Sequence platform margin build-ups and the Bastus Platform margin build-ups are inherently different (Table 5.13, Figure 5.10 and Figure 5.12). The Congost B Sequence coralgall boundstones form sigmoidal bodies similar to a clinothem with a progradational-aggradational trend. Conceptually, these can be compared to the “sigmoid” units defined by Pomar & Ward (1994), who interpreted each body as a parasequence or sequence stratigraphic systems tract. The main organisms are corals and red algae, and the encrusting and binding characteristics of these allowed the relatively steep slopes to form. In contrast, the Bastus Platform margin is dominated by a mixture of rudists and corals, which were less able to form a rigid framework. Subsequently, the slopes in this example are of much shallower relief. As it has been previously proposed by Skelton (1993), rudist formations establish in the substrate and topography that is suitable for their colonisation, rather than being the driving force behind the establishment of topography and platform-wide geometries. This would imply that the underlying topography of both platform margins was the dominant control on defining which organism communities could establish there. Subsequently, the underlying topography of the Congost B Sequence margin is interpreted to have been steep,

allowing only corallgal boundstones to develop, whereas that of the Bastus Platform margin was shallow, supporting a mix of corals and rudists.

**Table 5.13: Summary data for the internal geometry of the Congost B and Bastus Platform margin build-ups.**

Platform / Area	Lithofacies and Internal Geometry / Lithofacies	Max width [km]	Max Length [km]	Thickness [m]
Congost B Margin Coralline Build-ups	Corallgal Sigmoids	Confined to the depositional element measurements; <200 m wide, and interpreted to be 500-700 m long (cf. Immenhauser et al., 2001)		ø=7 m (Measured)
Bastus Margin Build-ups	Mixed Coral-Rudist Margin Bioherms	Few 10s metres	<3.8 km (same extent as depositional element)	1 - 10.7 m
	Backreef Rudist Biostromes	Few 100s of metres	<3.4 km (same extent as depositional element)	3.2 - 6.1 m

The sigmoids of the Congost B Sequence platform margin show an increase in slope angle from 12° up to 17°, followed by a decrease to 8°. This trend of progradation to aggradation and back to progradation (Figure 5.10) can be interpreted as the result of intermittent generation of accommodation space, forcing the build-ups to aggrade instead of step out basinwards. Although this development is observable qualitatively on the outcrop face, there is no quantitative trend observable in the gathered clinofom data. This is possibly the result of the geological system being too variable on this small scale, unlike with the sigmoids interpreted by Pomar & Ward (1994).

The internal architecture of the Bastus Platform margin build-ups is interpreted to have a basinward and a landward component. Facing the basin are mixed coral-rudist bioherms, which form a barrier protecting the fragile rudist biostromes forming in the protected backreef environments. This is common for many similar build-ups (e.g. Aconcha et al., 2008). In shallowing upwards successions, this architecture results in a recognisable vertical sedimentary pattern; slope nodular wackestones are followed by coral-rudist boundstones, which are successively overlain by rudist framestones (Chapter 4). The successions are frequently intercalated and capped with bioclastic grainstones of reefal debris and reworked grains. Such stacking patterns may facilitate recognition of such build-ups from core and wireline log data.

#### 5.5.4 Platform Interior Build-Ups

##### Depositional Element Scale

The maximum length of these geobodies was found to lie between 1.9 and 4.1 km (Table 5.14), a similar range to the platform margin build-ups of the Bastus Platform. However, both geobodies show principal differences in internal structure, as elaborated in the next section. The width of these bodies could not be defined due to outcrop conditions. The plan view geometry

of similar rudist biostromes is generally interpreted to be lenticular to slightly elongate (e.g. Aconcha et al., 2008, Mukherjee et al., 2012).

The mechanism controlling the establishment of these platform interior build-ups is difficult to define. In order to produce a sequence stratigraphic correlation of the Bastus Platform (Chapter 4), it was necessary to define typical stacking patterns. This was due to an absence of key surfaces for correlation. In the defined stacking patterns, the platform interior build-ups were placed at the bottom of sequences. This was necessary in order to ensure equal amounts of sequences in all sections throughout the basin. However, stratigraphic forward modelling was unable to assign them to a specific systems tract, or reproduce any other regularity in their occurrence (Chapter 4). It is therefore difficult to interpret their sequence stratigraphic position and whether there is an underlying control on their formation throughout the platform interior, such as preferential establishment on existing topography or within or at the rims of smaller depressions within the platform interior. Ross & Skelton (1993) proposed opportunistic establishment of similar monospecific rudist biostromes. As stratigraphic forward modelling was not able to tie their occurrence to sequence-scale mechanisms, it is proposed that these are not directly relative sea-level controlled, but are subject to self-organisation of the biological system (e.g. Burgess and Wright, 2003).

### Internal Geometry

The platform interior build-ups of the Bastus Platform are internally planar bedded. This is interpreted to be the result of several successive generations of rudist build-ups amalgamating into one depositional element. Individual beds are only 1.1 metres thick on average. Compared to the lateral extent of the depositional elements of few kilometres, these are very thin. This uniform and planar internal architecture is most likely governed by the low inclination of the seafloor in the Bastus platform interior, which was presumably less than 0.1° (Chapter 3). [Table 5.14: Summary data for the depositional element geometry of the Bastus Platform interior build-ups.](#)

Platform	Lithofacies	Internal Structure	Host lithology	Depositional Element Maximum Length (Strike)			Depositional element thickness [m]	Internal bed thickness [m]
				Smallest Value	Largest Value	Average Value		
<b>Bastus Platform</b>	Rudist bafflestones and rudstones with in-situ rudists and very coarse rudist debris. Micritic matrix with abundant benthic foraminifera	Tabular, bedded	Fine grained foraminiferal nodular wackestones	1.99 km	4.1 km	2.70 km	<b>25-50 m</b> (amalgamation of several generations)	0.08-4.77 m ( $\phi=1.10$ ), n=35

### 5.5.5 Implications for Assessment and Prediction of Geobody Geometries

Investigating the geometries of depositional elements and their internal structure contributes towards providing usable analogue data for subsurface modelling of complex carbonate platforms. It is of particular interest to establish whether there are set relationships between width, length, thickness, and what control do texture, components, carbonate producers, sequence stratigraphic position as well as the location in respect to the platform margin, and topography of the respective platform have on the geometrical properties of the depositional elements and their internal structure.

A comprehensive review of geometrical data presented in the literature was made (Table 5.1, Table 5.2). The majority of this literature data on shoal bodies originates from the modern Bahama Banks (e.g. P. Harris et al., 2011; Rankey and Reeder, 2011), and on build-ups from the Mavericks Intrashelf Basin, Texas (e.g. Kerans, 2002; Loucks and Kerans, 2003; Mukherjee et al., 2012; Janson et al., 2015). As a result, there is some selection bias when comparing the collected data and investigating for potential geometrical trends. For shoal bodies, a potential positive correlation between width and length is observed in the data (length = 5.38 \* width,  $R^2 = 0.66$ , Figure 5.14), while a relationship between thickness and either length or width is not present (Figure 5.15). For biogenic build-ups, a potential positive correlation between width and length is observed (length = 1.46 \* width,  $R^2 = 0.76$ , Figure 5.16), whereas no clear relationship between thickness and either width or length is apparent (Figure 5.17).

Widths and lengths of shoal bodies, clinoforms, and build-ups measured in this study fit well within the literature data. The results of this study demonstrate that shoal bodies, clinoforms and build-ups vary both on the depositional element scale and in their interior geometry depending on the depositional mechanism, the nature of the host platform, the specific position on the platform, and the main carbonate producing organism. The shoal bodies of the Bastus and Sant Corneli Platform interiors and those of the Bastus Platform Margin are on average 14.2-18 km shorter and 1.3-3.5 km narrower than the infralittoral prograding wedge of the of the Congost Platform. Similarly, the platform interior biostromal build-ups, and the backreef biostromal component (lithofacies PM4) of the platform margin composite build-ups of the Bastus Platform are an order of magnitude larger than the barrier forming bioherms (lithofacies PM1) at the platform margin. This indicates that the size and location of geobodies is essentially governed by the configuration of the basin/platform, depositional mechanism as well as by the organism producing the geometries.

Although the concept of geobody architectures being tied to their position on the respective platform has been previously discussed (e.g. Pomar et al., 2012), quantitative studies regarding exact geobody sizes and geometrical trends of specific platforms or organisms are still rare.

While the variations between types of geobodies and between platforms are high, both the outcrop data gathered in this study and literature data suggest that within individual platforms and basins there are trends in geobody measurements. The literature demonstrates this principle when comparing shoal bodies or build-ups within individual localities or basins (Figure 5.14 and Figure 5.16, Tables 5.1 and 5.2). Specifically, this becomes evident in the length-width relationships of Aptian-Albian rudist build-ups in the Mavericks Intrashelf Basin, USA (Kerans, 2002; Loucks and Kerans, 2003; Mukherjee et al., 2012; Janson et al., 2015), where build-ups are shown to have a width-length ratio of 1.5-2.5. Similarly, a relationship is observed between width-thickness of ooidal-bioclastic grainstone shoals of the Triassic Khuff Formation in Oman (Koehrer et al., 2011), where the thickness-width ratio of shoal bodies was found to be 1:3000. This review further expands upon the work of Kerans and Harris (2010), who have shown variations in grainstone shoal sizes and thicknesses in the Permian Basin of Texas occurring as a reaction to the transition of the initial ramp system to a rimmed shelf. The comparison between geological eras across several basins in this study highlights the importance of acknowledging the platform setting when investigating different platforms and geobodies.

The collected literature data provides an insight on preferential relationships between thickness and plan-view dimensions. There is an apparent preferential thickness of shoal bodies of <5 metres (Figure 5.15). However, it must be considered that inconsistencies in data reporting may skew these statistics; not all authors differentiate whether they refer to the cumulative thickness of grainstone/packstone beds that comprise a shoal unit, or to the thickness of individual beds within it. For the rudist build-ups of the Albian Mavericks Intrashelf Basin, the literature data implies that the thickness of these bodies generally does not exceed 5 metres (Figure 5.17). As with the shoal bodies, a clear definition of whether the measurement represents an interval or single generations of a build-up is not made in every case.

It is of particular interest to be able to define whether specific sediment compositions, textures, or organisms can be used to derive the geometrical properties of a geobody, as this would facilitate their recognition from well and core data. The literature data does not allow defining whether the type of grains affects the extent or thickness of a shoal body (Figure 5.14 and Figure 5.15), or whether specific organisms produce a typical extent or thickness of build-up (Figure 5.16 and Figure 5.17). The results of this study show that the platform interior shoal bodies of the Sant Corneli have on average a 2.5 km greater length than those of the Bastus Platform (Table 5.11). Internally, these bodies differ in both their composition and the surrounding sediment they are found in. The Sant Corneli platform interior shoals consist of predominantly coarse grained, well sorted and rounded rudist fragments, and are internally cross-bedded on metre scale, and encased in coarse- to medium-grained, poorly-consolidated sandstones. The platform interior shoals of the Bastus Platform are a combination of bedded,

poorly sorted, quartz and angular bioclastic bearing grainstones and packstones or sandstones, as well as bedded and well sorted, fine grained peloidal grainstones. They are found interbedded into nodular, micritic wackestones with common rudist fragments. These observations imply that the former were formed under higher energy conditions than the latter. Subsequently, the texture, which is ultimately controlled by the energy of the depositional environment, shows a possible relationship to the length of the geobodies. It must be noted that this is observed here in low angled ramps (Sant Corneli Platform) and rimmed shelves (Bastus Platform). In carbonate ramps, the dissipation of wave energy along a specific transect of the ramp may be the limiting factor on this dimension.

The concept that different carbonate producing organisms tend to generate specific geometries of build-ups has been previously discussed (e.g. Ross and Skelton, 1993; Gili et al., 1995; Skelton et al., 1997; Sanders, 1998). Substrate-dwelling, monospecific rudist biostromes are known to generally form low-topography, thin (<few m) and generally extensive bodies (up to few km; e.g. Ross & Skelton 1993). Mixed bioherms of rudists-coral communities are considered to form more prominent topography (<10 m), and be slightly limited in dip-direction (few 10s. m; e.g. Bover-Arnal et al., 2015). Coralgall build-ups are commonly observed to form steeply dipping, laterally limited (<few 100s m) bodies (e.g. Immenhauser et al., 2002; Reolid et al., 2014). These differences are discussed to be the result of how organisms bind the sediment and construct the geobody framework, resulting in either higher resistance to wave action and more suitable to environments of higher water energy (Ross and Skelton, 1993), and thus their occurrence is essentially dictated by the platform profile which defines the water energy along it (Pomar et al., 2012).

The difference between organisms and the geometries they produce is clearly presented in this study. The rudist biostromes present in the platform interior of the Bastus Platform, and the biostrome component of the platform margin composite build-ups are an order of magnitude longer in dip than the mixed coral-rudist build-ups that pose the seaward part of the margin composite build-ups. Additionally, the coralgall build-ups of the Congost B Platform show a unique architecture, reaching potentially only few 100s metres in width and length, with steeply dipping bedding surfaces (up to 15°) and internal sigmoidal bodies.

For subsurface reservoir characterisation, it is of particular interest to define how the preferential sequence stratigraphic position of geobodies and whether predictions can be made regarding the systems tract in which a geobody resides and what geometry it may exhibit. The majority of the geobodies described in the literature are defined to occur in the highstand systems tracts of their respective sequences. For the Bastus Platform, a parallel study concluded that the composite rudist-coral margin build-ups occur in the late highstand (Chapter 4). The

platform interior rudist biostromes, however, could not be tied to a specific systems tract, and their development assumed not to be controlled by relative sea-level fluctuations. With this observation, it is important to acknowledge that the sequence stratigraphic frameworks used to interpret such carbonate deposits specifically define build-ups and shoals to occur in the highstands (Van Wagoner et al., 1988; Schlager, 2005). Therefore, this “preference” of the geobodies to occur here is in fact a bias resulting from the approach for interpretation generally used.

The effects of sequence-controlled accommodation on geobody dimensions have been shown by Kerans and Harris (2010); grainstone shoals established in the transgressive systems tract are generally wider and thinner than those of the highstand systems tracts. In the case of the geobodies investigated in this study, no similar observation could be made, due to the fact that either no detailed sequence stratigraphic framework is given (Congost and Sant Corneli Platform), or that the geobodies are either all concentrated in the same systems tract (Platform margin build-ups and shoal bodies of the Bastus Platform, late highstand), or their sequence stratigraphic context could not be determined (shoal bodies and build-ups of the Bastus Platform interior). This exhibits how detailed sequence stratigraphic frameworks are vital for predicting the presence of geobodies and attempting to interpolate their lateral dimensions from subsurface data.

The combination of these results highlights numerous factors to consider when trying to estimate geobody dimensions on the basis of limited data or when using outcrop data as an analogue to a subsurface example. It is important to consider the type of platform, the position of the geobody in relation to the margin, the position in a sequence stratigraphic context, as well as carbonate texture, grain associations and skeletal assemblages, as a direct result of the depositional environment. It was observed that there is a possible relationship between width and length of geobodies within a single geological setting. However, more studies are necessary to be able to define broader, universal rules.



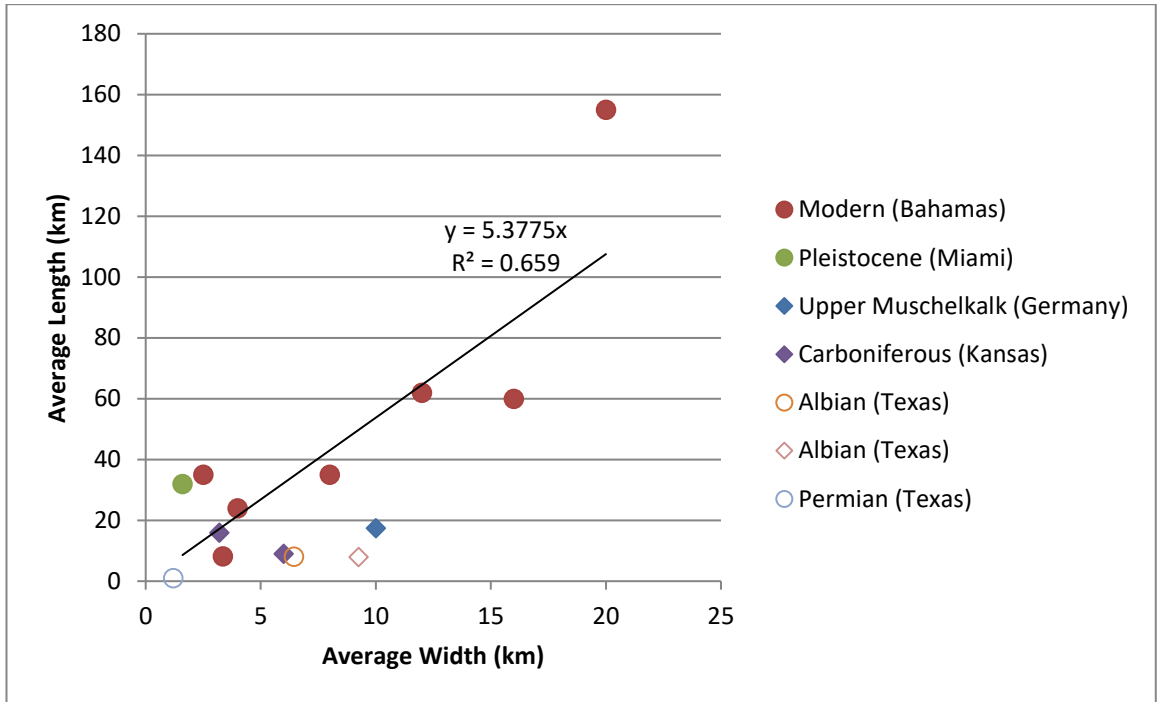


Figure 5.14: Cross plot of average width against average length of shoal bodies gathered from the literature. Data points denoted with circles indicate the majority of components are ooids, whereas data denoted with rhombs indicates bioclasts as the primary components. Data points with filled colours indicate that true average values were calculated and plotted, and data points left unfilled indicate that only a minimum estimate of either width or length was provided. In this case, the points were not included into defining the trend line and  $R^2$  value. Data sources are presented in Table 5.1.

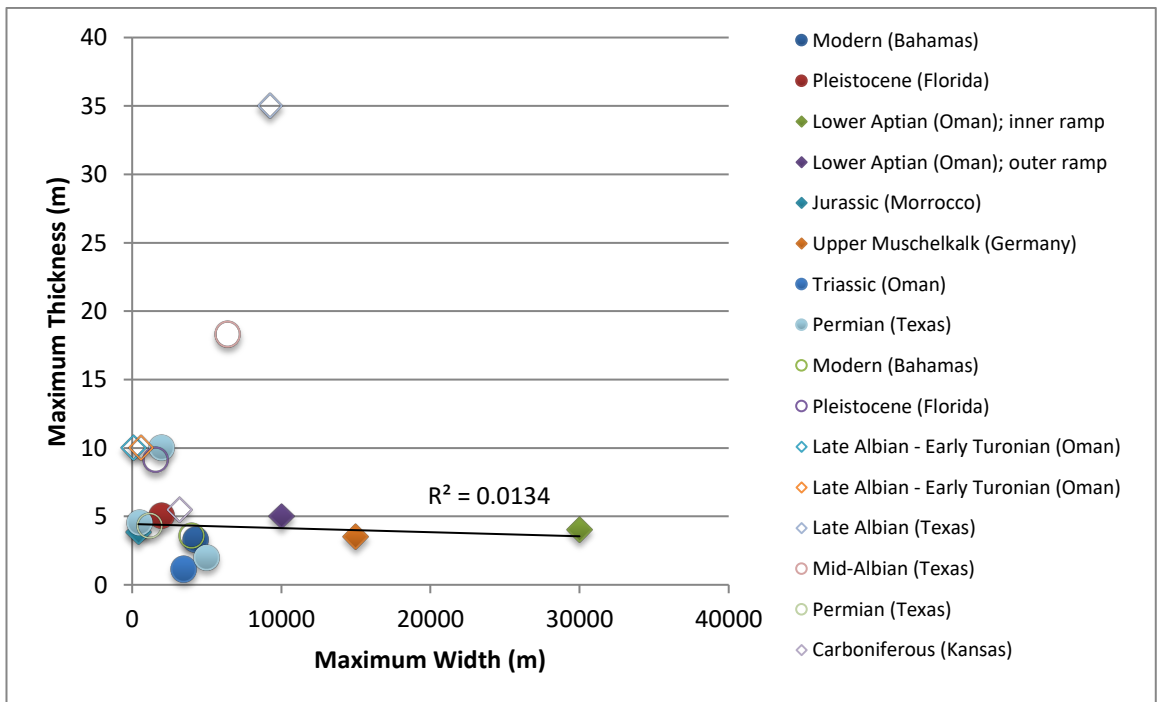


Figure 5.15: Cross plot of maximum width against maximum thickness of shoal bodies gathered from current literature. Data points denoted with circles indicate the majority of components are ooids, whereas data denoted with rhombs indicates bioclasts as the primary components. Data points with filled colours indicate that true maximum values were determined and plotted, and data points left unfilled indicate that only a minimum or average value of width was provided. The regression line applies exclusively to the data points where maximum width was provided (data points with filled colours). Data sources are presented in Table 5.1.

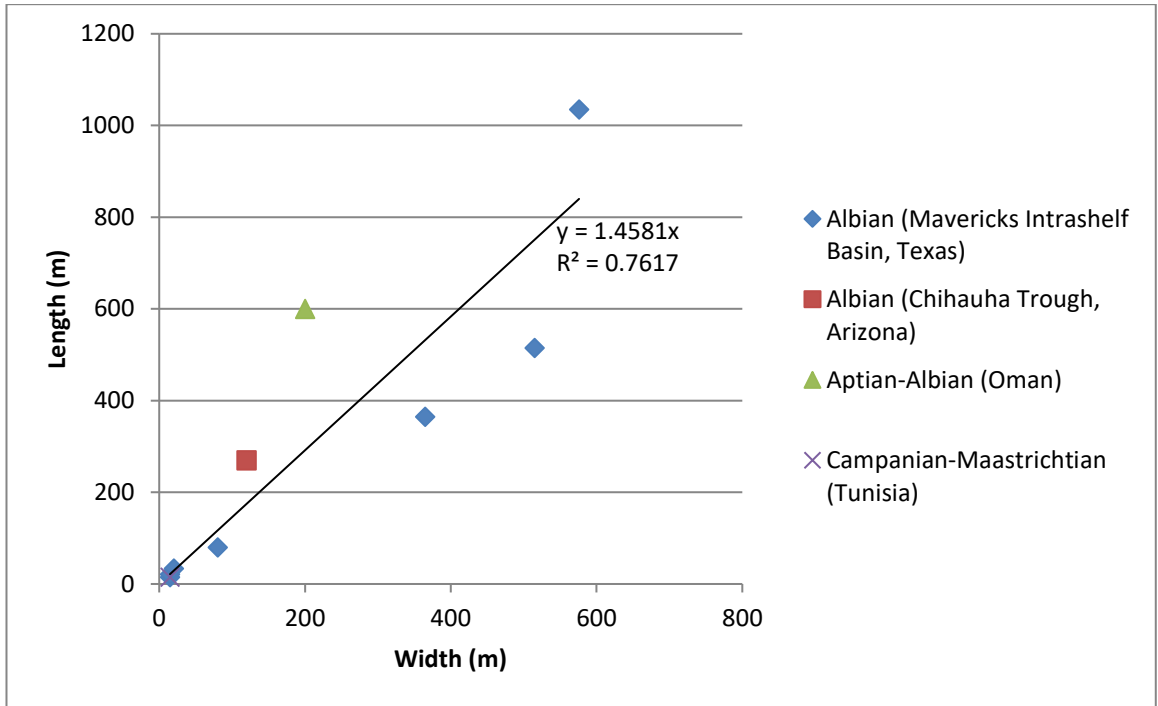


Figure 5.16: Cross plot of average width against average length of Cretaceous aged build-ups with dimensions smaller than 1.2 km gathered from literature data. Data sources are presented in Table 5.2. A positive correlation between width and length can be observed.

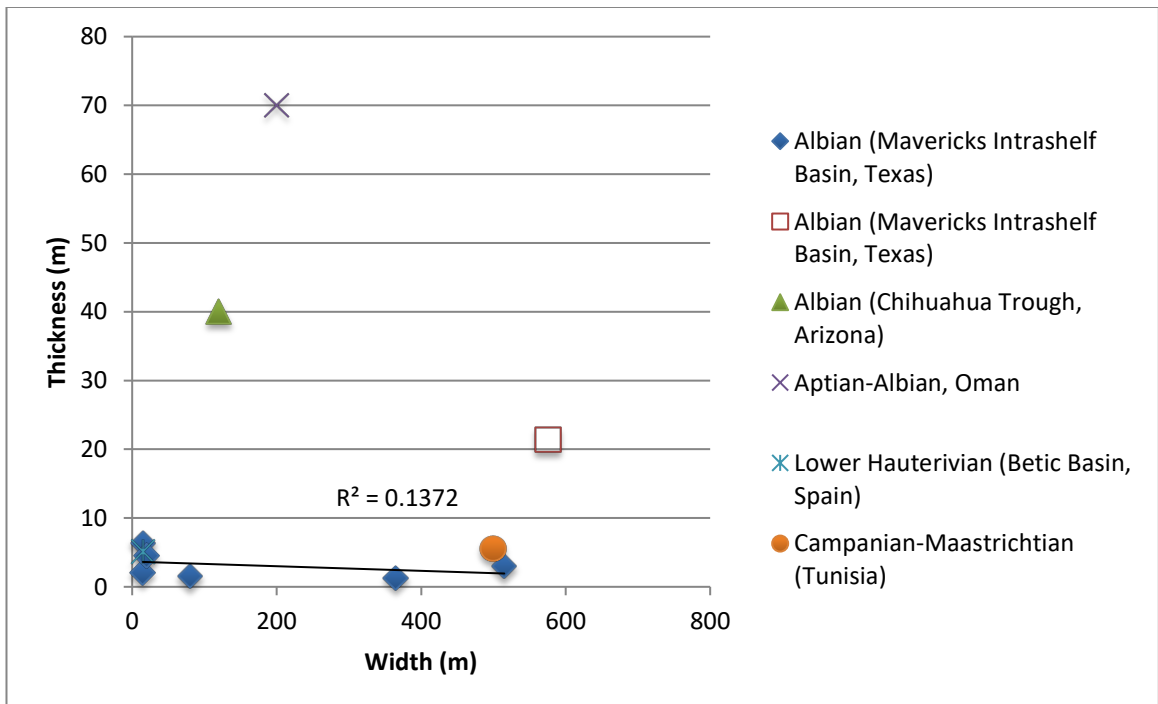


Figure 5.17: Cross plot of average width against average thickness from biogenic constructions from selected literature. The trend line applies only to the Albian dataset from the Mavericks Intrashelf Basin (blue rhombs). Data points with filled colours indicate that true average values were calculated and plotted, and data points left unfilled indicate that only a minimum or maximum estimate of their thickness was provided. Data sources are presented in Error! Reference source not found..

### 5.5.6 Limitations and Outlook

One of the key aspects not investigated in this study is the lateral distance between time-equivalent shoal bodies and build-ups and their temporal distribution and migration. The map-based approach for quantifying the platform interior shoal bodies and build-ups along the Montsec did not allow determination of whether geobodies are in the same stratigraphic horizon. The most viable approach to gaining such data would be a comprehensive field-study with a large number of logged sections across the Montsec exposure to allow geobody correlation. Alternative approaches were presented by Aconcha et al. (2008) where seismic geomorphology studies in the Mavericks Intrashelf Basin, allowing quantification of the plan-view distribution of rudist build-ups along the platform. Such data provide valuable input data for multiple point statistic (MPS) simulations for interpreting the lateral distribution of such depositional elements (e.g. Visser and Chessa, 2000; Jung et al., 2012), and are therefore of key importance for subsurface analogues.

The impact of variations in textures along clinoform surfaces and within clinothems on the flow properties has been previously discussed, particularly in clastic settings (Ainsworth et al., 1999; Dutton et al., 2000), with numerous authors applying flow modelling to address the effect on hydrocarbon production and advanced extraction via water injection and flooding (Jackson et al., 2009; Enge and Howell, 2010; Graham et al., 2015). These models depend on both a good control on clinoform geometry and of the textural composition and petrophysical properties of the sediments, and how the latter vary across the length clinoform. In this study, geometries of clinoforms in various geobodies were captured, providing a useful base for a fluid flow simulation in similar sediments. However, variations of petrophysical properties were only qualitatively constrained. A pilot study was made on a subset of samples from the platform margin shoals of the Bastus Platform (Al Rahbi, 2015) which were taken along a clinoform surface. It showed how sorting, rounding and foraminiferal and peloidal content decreased from topset to bottomset, whereas average grain size, quartz grains and micrite contents increased. For better control on how these clinoforms may affect fluid flow, more systematic and wide-scale study of composition and texture are suggested – similar to that presented by Lanfranchi et al. (2011).

Having demonstrated that the size and shape of geobodies is inherently governed by the platform geometry and producing organism, it would be of interest to investigate whether set relationships exist between these parameters. Particularly, identifying whether geobodies also increase in scale if the platform they reside in increases in scale but retains the same morphology. It can be postulated that where they are spatially limited by the available space, e.g. on the top of rimmed shelves, geobodies would be larger on larger platforms. However, if the geobodies are governed by the slope angle, i.e. on the margins of rimmed shelves or on

ramps, they might remain of the same size or even become narrower if the hydrodynamic zone they form in narrows. In case of ramps, an increase or decrease in angle is also expected to form narrower or wider geobodies, respectively.

Considering that comparability between geobody sizes is highly dependent on them having the same bounding parameters in regards to their host platform, there are a number of recommendations for drawing comparisons between geobodies from different settings. It is imperative to ensure that the broad platform architecture is comparable, as geobodies on rimmed shelves and on carbonate ramps are inherently different in shape (cf. Section 5.5.5). Next, a broad comparability between the scales of both geological systems should be given, as well as in the mode of geobody deposition. For build-ups, this means both carbonate factories consisting either of sediment-binding organisms or of substrate dwelling organisms. In the case of grain aggregations, comparability between depositional mechanism, energy regime and grain composition should be given.

Similarly to the above, it may prove useful to attempt to quantify how different associations of carbonate producing organisms result in different geometries. While it is generally accepted that coralgall communities, due to their sediment-binding nature, have a higher potential to create more topography than rudists, and knowledge of their interactions exists (Gili et al., 1995; Skelton et al. 1997, Sanders 1998), no quantitative study of the geometrical properties of the different build-ups were conducted to date. Studies similar to the one presented here may contribute towards a database that outlines what geometries can be expected from specific benthic communities.

The observation of how different organism communities result in specific geobody dimensions emphasises the importance of knowing acknowledging the principle constructing organism is in a specific setting. Furthermore, differentiation between individual generations of build-ups and vertical and lateral amalgamation of build-up phases is often not sufficiently clear in the literature, and this needs to be more clearly defined in future studies. It is particularly difficult to resolve the internal geometry of more complex bioconstructions such as the ones observed within the Bastus Platform margins. However, it is implied by the example of the Congost B margin build-ups that steeper margins dominated by coral and red algae are more likely to have an internal sigmoid-like structure, whereas low-topography margins may form a bioherm and backreef biostrome with a tabular internal structure.

In line with the acknowledgement of the control of the platform architecture and organism type on the size and shape of geobodies, it has also been proposed that the type of organism also directly defines the order of the sequence stratigraphic cycles they may form (e.g. Pomar et al. 2012). While this may apply for a single example with good exposure, the transferability of

these concepts onto other geological case studies still requires testing of the concept through a variety of studies on various platforms featuring different organism communities and different ages.

## 5.6 Conclusions

The results of this study pose a number of implications on the quantification and prediction of carbonate build up and shoal-body geometries:

- Build-ups and shoal bodies can vary both in scale and in their interior geometry, based on the nature of the platform they reside in. This is interpreted to include the scale and topography of the platform, as well as the position of the geobodies in question within the platform.
- For the investigated platforms, preferential ranges of width, length, thickness and internal geometry could be defined for distinct geobodies. However, preferential relationships between thickness and plan-view dimensions, such as previously shown by Koehrer et al. (2011) or Kerans and Harris (2010), could not be determined in this example.
- The presented data supports that specific sediment compositions, textures or organisms have the tendency to create preferential geometries. This is the result of the controlling sedimentary processes that are interpreted into these lithological properties.
- Particularly within build-ups, the present organism has a dominant control on the resulting architecture of the geobody. This previously established concept (Ross and Skelton, 1993; Gili et al., 1995) was clearly demonstrated by extracting geometries of the internally sigmoidal coralgall build-ups of the Congost B, and the landward-seaward differentiation of rudist and rudist/coral communities (respectively) within the platform margin build-ups of the Bastus Platform.
- Comparing the geometrical data of the build-ups investigated here with previously reported sizes from the literature has highlighted a number of issues. Inconsistent use of nomenclature and lack of clearly defined geometrical hierarchy makes direct comparison difficult in many cases. It was found that particular geobodies within individual basins have the tendency to exhibit specific sizes or specific width-length-thickness ratios (e.g. the rudist build-ups of the Mavericks Intrashelf Basin).
- However, due to the dependence of the geometries of geobodies on the broader platform framework and sequence stratigraphic framework, it is not possible to define overarching rules or relationships regarding the geometrical properties of geobodies.
- These new insights, together with the presented numerical data, provide a valuable addition to the understanding of geobody sizes, and are expected to facilitate

recognition and interpretation of geobodies and their dimensions in the subsurface where data is sparse.

- Improvements upon these results can be made both by further similar studies in other basins, to help constrain possible dimensional preferences of geobodies. Studying the spatial and temporal distribution of geobodies is further recommended in order to facilitate reservoir modelling and to serve as data-input for modelling approaches such as MPS.

## 5.7 References

- Aconcha, E., C. Kerans, and H. Zeng, 2008, Seismic Geomorphology Applied to Lower Glen Rose Patch Reefs in the Maverick Basin, Southwest Texas: Gulf Coast Association of Geological Societies Transactions, v. 58, p. 3–23.
- Adams, E. W., C. Grelaud, M. Pal, A. E. Csoma, O. S. Al Ja'aidi, and R. A. Hinai, 2011, Improving reservoir models of Cretaceous carbonates with digital outcrop modelling (Jabal Madmar, Oman): static modelling and simulating clinoforms: Petroleum Geoscience, v. 17, no. 3, p. 309–332, doi:10.1144/1354-079310-031.
- Adams, E. W., J. P. Grotzinger, W. a. Watters, S. Schröder, D. S. McCormick, and H. a. Al-Siyabi, 2005, Digital characterization of thrombolite-stromatolite reef distribution in a carbonate ramp system (terminal Proterozoic, Nama Group, Namibia): AAPG Bulletin, v. 89, no. 10, p. 1293–1318, doi:10.1306/06160505005.
- Aigner, T., S. Braun, D. Palermo, and W. Blendinger, 2007, 3D geological modelling of a carbonate shoal complex: reservoir analogue study using outcrop data: First Break, v. 25, no. 1110, p. 65–72, doi:10.3997/1365-2397.2007022.
- Ainsworth, R. B., M. Sanlung, and S. T. C. Duivenvoorden, 1999, Correlation techniques, perforation strategies, and recovery factors: An integrated 3-D reservoir modeling study, Sirikit Field, Thailand: AAPG Bulletin, v. 83, no. 10, p. 1535–1551.
- Allen, J. R. L., 1980, Sand waves: A model of origin and internal structure: Sedimentary Geology, v. 26, no. 4, p. 281–328, doi:10.1016/0037-0738(80)90022-6.
- Allen, J. R. L., 1982, Sedimentary Structures, Their Character and Physical Basis: 663 p.
- Amour, F., M. Mutti, N. Christ, A. Immenhauser, S. M. Agar, G. S. Benson, S. Tomás, R. Alway, and L. Kabiri, 2012, Capturing and modelling metre-scale spatial facies heterogeneity in a Jurassic ramp setting (Central High Atlas, Morocco): Sedimentology, v. 59, no. 4, p. 1158–1189, doi:10.1111/j.1365-3091.2011.01299.x.
- Andrieu, S., B. Brigaud, J. Barbarand, and E. Lasseur, 2017, Linking early diagenesis and sedimentary facies to sequence stratigraphy on a prograding oolitic wedge: The Bathonian of western France (Aquitaine Basin): Marine and Petroleum Geology, v. 81, p. 169–195, doi:10.1016/j.marpetgeo.2017.01.005.
- Anell, I., and I. Midtkandal, 2015, The quantifiable clinothem - types, shapes and geometric relationships in the Plio-Pleistocene Giant Foresets Formation, Taranaki Basin, New Zealand: Basin Research, p. 1–21, doi:10.1111/bre.12149.
- Ball, M. M., 1967, Carbonate Sand Bodies of Florida and the Bahamas: SEPM Journal of Sedimentary Research, v. Vol. 37, no. 2, p. 556–591, doi:10.1306/74D7171C-2B21-11D7-8648000102C1865D.
- Barnaby, R. J., and W. B. Ward, 2007, Outcrop Analog for Mixed Siliciclastic-Carbonate Ramp Reservoirs--Stratigraphic Hierarchy, Facies Architecture, and Geologic Heterogeneity: Grayburg Formation, Permian Basin, U.S.A.: Journal of Sedimentary Research, v. 77, no. 1, p. 34–58, doi:10.2110/jsr.2007.007.
- Bebout, D. G., R. P. Major, and P. M. Harris, 2009, Internal Geometry of a Modern Carbonate Grainstone Shoal - An Analog for Hydrocarbon Reservoir Heterogeneity: Search and Discovery Article, v. 60035.
- Bein, A., 1976, Rudistid fringing reefs of Cretaceous shallow carbonate platform of Israel: AAPG

- Bulletin, v. 60, no. 2, p. 258–272.
- Booler, J. P., 1994, Carbonate facies, sequences and associated diagenesis, Upper Cretaceous, Tremp Basin, Spanish Pyrenees: Durham University, 317 p.
- Booler, J., and M. E. Tucker, 2002, Distribution and geometry of facies and early diagenesis: the key to accommodation space variation and sequence stratigraphy: Upper Cretaceous Congost Carbonate platform, Spanish Pyrenees: *Sedimentary Geology*, v. 146, no. 3–4, p. 225–247, doi:10.1016/S0037-0738(01)00120-8.
- Borgomano, J., J. P. Masse, and S. Al Maskiry, 2002, The lower Aptian Shuaiba carbonate outcrops in Jebel Akhdar, northern Oman: Impact on static modeling for Shuaiba petroleum reservoirs: *AAPG Bulletin*, v. 86, no. 9, p. 1513–1529, doi:10.1306/61EEDCE2-173E-11D7-8645000102C1865D.
- Bosellini, A., 1984, Progradation geometries of carbonate platforms: examples from the Triassic of the Dolomites, northern Italy: *Sedimentology*, v. 31, no. 1, p. 1–24, doi:10.1111/j.1365-3091.1984.tb00720.x.
- Boutte, A. L., 1969, Callahan Carbonate-Sand Complex, West-Central Texas, *in* J. B. M. C. H. Moore Jr., A. L. Boutte, E. L. Marcantel, ed., *A Guidebook to the Depositional Environments and Depositional History, Lower Cretaceous Shallow Shelf Carbonate Sequence, West Central Texas*: Dallas, Texas, Dallas Geological Society, p. 40–74.
- Bover-Arnal, T., E. Pascual-Cebrian, P. W. Skelton, E. Gili, and R. Salas, 2015, Patterns in the distribution of Aptian rudists and corals within a sequence-stratigraphic framework (Maestrat Basin, E Spain): *Sedimentary Geology*, v. 321, p. 86–104, doi:10.1016/j.sedgeo.2015.03.008.
- Bryant, I. a. n., D. Carr, P. Cirilli, N. Drinkwater, D. McCormick, P. Tilke, and J. Thurmond, 2000, Use of 3D digital analogues as templates in reservoir modelling: *Petroleum Geoscience*, v. 6, no. 2, p. 195–201, doi:10.1144/petgeo.6.2.195.
- Burgess, P. M., and V. P. Wright, 2003, Numerical Forward Modeling of Carbonate Platform Dynamics: An Evaluation of Complexity and Completeness in Carbonate Strata: *Journal of Sedimentary Research*, v. 73, no. 5, p. 637–652, doi:10.1306/020503730637.
- Caers, J., and T. Zhang, 2004, Multiple-point geostatistics: a quantitative vehicle for integrating geologic analogs into multiple reservoir models, *in* G. M. Grammer, P. M. “Mitch” Harris, and G. P. Eberli, eds., *Integration of outcrop and modern analogs in reservoir modeling: AAPG Memoir 80*: p. 383–394.
- CloudCompare (version 2.6.2) [GPL software], 2016, Retrieved from <http://www.cloudcompare.org/>.
- Cumings, E. R., 1932, Reefs or Bioherms? *Geological Society of America Bulletin*, v. 43, no. 1, p. 331–352, doi:10.1130/GSAB-43-331.
- Droste, H., 2010, High-resolution seismic stratigraphy of the Shu’aiba and Natih formations in the Sultanate of Oman: implications for Cretaceous epeiric carbonate platform systems: *Geological Society, London, Special Publications*, v. 329, no. 1, p. 145–162, doi:10.1144/SP329.7.
- Droste, H. J., 2010, Sequence-stratigraphic framework of the Aptian Shu’aiba Formation in the Sultanate of Oman: Barremian - Aptian Stratigraphy and Hydrocarbon Habitat of the Eastern Arabian Plate, *GeoArabia Special Publication 4*, v. 1, no. 4, p. 229–283.
- Dunham, R., 1962, Classification of carbonate rocks according to depositional texture, *in* W. E. Ham, ed., *Classification of Carbonate Rocks: AAPG Memoir 1*: Tulsa, OK, AAPG, p. 108–121.
- Dutton, S. P., B. J. Willis, C. D. White, and J. P. Bhattacharya, 2000, Outcrop characterization of reservoir quality and interwell-scale cement distribution in a tide-influenced delta, *Frontier Formation, Wyoming, USA: Clay Minerals*, v. 35, no. 1, p. 95–95, doi:10.1180/000985500546756.
- Embry, A. F., and J. E. Klovan, 1971, A Late Devonian reef tract on northeastern Banks Island, NWT: *Bulletin of Canadian Petroleum Geology*, v. 19, no. 4, p. 730–781.
- Enge, H. D., and J. A. Howell, 2010, Impact of deltaic clinothems on reservoir performance: Dynamic studies of reservoir analogs from the Ferron Sandstone Member and Panther Tongue, Utah: *AAPG Bulletin*, v. 94, no. 2, p. 139–161, doi:10.1306/07060908112.
- Enge, H. D., J. A. Howell, and S. J. Buckley, 2010, Quantifying clinothem geometry in a forced-

- regressive river-dominated delta, Panther Tongue Member, Utah, USA: *Sedimentology*, v. 57, no. 7, p. 1750–1770, doi:10.1111/j.1365-3091.2010.01164.x.
- Friedman, G. M., 1988, Case Histories of Coexisting Reefs and Terrigenous Sediments: The Gulf of Elat (Red Sea), Java Sea, and Neogene Basin of the Negev, Israel, *in* L. J. Doyle, and H. H. Roberts, eds., *Developments in Sedimentology V42: Carbonate-Clastic Transitions*: p. 77–97, doi:10.1016/S0070-4571(08)70165-1.
- Gili, E., P. W. Skelton, E. Vicens, and A. Obrador, 1995, Corals to rudists—an environmentally induced assemblage succession: *Palaeogeography, Palaeoclimatology, Palaeoecology*, v. 119, no. 1–2, p. 127–136, doi:10.1016/0031-0182(95)00064-X.
- Ginsburg, R. N., 1956, Environmental relationships of grain size and constituent particles in some South Florida carbonate sediments: *Bulletin of the American Association of Petroleum Geologists*, v. 40, no. 10, p. 2384–2427, doi:10.1306/5CEAE598-16BB-11D7-8645000102C1865D.
- Google Earth (version 7.1.7.2602) [computer software], 2016, Retrieved from: <http://earth.google.com/>.
- Graham, G. H., M. D. Jackson, and G. J. Hampson, 2015, Three-dimensional modeling of clinoforms in shallow-marine reservoirs: Part 2. Impact on fluid flow and hydrocarbon recovery in fluvial-dominated deltaic reservoirs: *AAPG Bulletin*, v. 99, no. 6, p. 1049–1080, doi:10.1306/01191513191.
- Grammer, G. M., P. M. Harris, and G. P. Eberli, 2004, Integration of Outcrop and Modern Analogs in Reservoir Modeling: Overview with Examples from the Bahamas, *in* G. M. Grammer, P. M. Harris, and G. P. Eberli, eds., *Integration of Outcrop and Modern Analogs in Reservoir Modeling: AAPG Memoir 80*: p. 1–22, doi:10.1306/M80924C1.
- Grélaud, C., P. Razin, and P. Homewood, 2010, Channelized systems in an inner carbonate platform setting: differentiation between incisions and tidal channels (Natih Formation, Late Cretaceous, Oman): *Geological Society, London, Special Publications*, v. 329, no. 1, p. 163–186, doi:10.1144/SP329.8.
- Halley, R. B., E. A. Shinn, J. H. Hudson, and B. H. Lidz, 1977, Pleistocene Barrier Bar Seaward of Ooid Shoal Complex Near Miami, Florida: *AAPG Bulletin*, v. 61, no. 4, p. 519–526, doi:10.1306/C1EA3D7A-16C9-11D7-8645000102C1865D.
- Handford, C., 1988, Review of carbonate sand-belt deposition of ooid grainstones and application to Mississippian Reservoir, Damme Field, Southwestern Kansas: p. 1184–1199.
- Harris, P. M., 2009a, Depositional environments of carbonate platforms: *Search and Discovery*, v. Article #6, p. 31–60.
- Harris, P. M., 2009b, Heterogeneity within Carbonate Reservoirs-Guidelines from Modern Analogs: *Search and Discovery Article*, v. 60040.
- Harris, P., J. Kenter, T. Playton, and M. Andres, 2011, Enhancing Subsurface Reservoir Models—An Integrated MPS Approach Using Outcrop Analogs, Modern Analogs, and Forward Stratigraphic Models: *Search and Discovery*, v. 50418.
- Harris, P. M., S. J. Purkis, and J. Ellis, 2011, Analyzing Spatial Patterns in Modern Carbonate Sand Bodies From Great Bahama Bank: *Journal of Sedimentary Research*, v. 81, no. 3, p. 185–206, doi:10.2110/jsr.2011.21.
- Harris, P. M., S. J. Purkis, J. Ellis, P. K. Swart, and J. J. G. Reijmer, 2015, Mapping bathymetry and depositional facies on Great Bahama Bank: *Sedimentology*, v. 62, no. 2, p. 566–589, doi:10.1111/sed.12159.
- Hernández-Molina, F. J., L. M. Fernández-Salas, F. Lobo, L. Somoza, V. Díaz-del-Río, and J. M. Alveirinho Dias, 2000, The infralittoral prograding wedge: a new large-scale progradational sedimentary body in shallow marine environments: *Geo-Marine Letters*, v. 20, no. 2, p. 109–117, doi:10.1007/s003670000040.
- Hine, A. C., 1977, Lily Bank, Bahamas: History of an Active Oolite Sand Shoal: *Journal of Sedimentary Research*, v. 47, no. 4, p. 1554–1581, doi:10.1306/212F73B5-2B24-11D7-8648000102C1865D.
- Immenhauser, A., B. Van Der Kooij, A. Van Vliet, W. Schlager, and R. W. Scott, 2002, An ocean-facing Aptian-Albian carbonate margin, Oman: *Sedimentology*, v. 48, no. 6, p. 1187–1207, doi:10.1046/j.1365-3091.2001.00416.x.



- Institut Cartogràfic i Geològic de Catalunya, 2010, Mapa geològic de Catalunya (1:25 000) - Aramunt 252-2-2 (66-22).
- Institut Cartogràfic i Geològic de Catalunya, 2007, Mapa geològic de Catalunya (1:25 000) - Calladrons 289-1-2 (63-24) Sant Esteve de la Sarga 289-2-2 (64-24).
- Institut Cartogràfic i Geològic de Catalunya, 2003, Mapa geològic de Catalunya (1:25 000) - Llimiana 290-1-2 (65-24).
- Institut Cartogràfic i Geològic de Catalunya, 2002, Mapa geològic de Catalunya (1:25 000) - San Salvador de Toló 290-2-2 (66-24).
- Institut Cartogràfic i Geològic de Catalunya, 2015, Mapa geològic de Catalunya 1:50.000 (mgc50Mv01\_etr89).
- Instituto Geográfico Nacional, and Centro Nacional de Información Geográfica, 2011, VUELO FOTOGRAFÍCO DIGITAL con VUELO LIDAR.
- Jackson, M. D., G. J. Hampson, and R. P. Sech, 2009, Three-dimensional modeling of a shoreface-shelf parasequence reservoir analog: Part 2. geologic controls on fluid flow and hydrocarbon recovery: AAPG Bulletin, v. 93, no. 9, p. 1183–1208, doi:10.1306/05110908145.
- Janson, X., K. Lee, C. Zahm, and C. Kerans, 2015, Ground-penetrating radar imaging of Albian rudist buildups, central Texas: Interpretation, v. 3, no. 3, p. SY67-SY81, doi:10.1190/INT-2014-0273.1.
- Janson, X., and D. D. Madriz, 2012, Geomodelling of carbonate mounds using two-point and multipoint statistics: Geological Society, London, Special Publications, v. 370, no. 1, p. 229–246, doi:10.1144/SP370.5.
- Jung, A., and T. Aigner, 2012, Carbonate Geobodies: Hierarchical Classification and Database - A New Workflow for 3D Reservoir Modelling: Journal of Petroleum Geology, v. 35, no. 1, p. 49–65, doi:10.1111/j.1747-5457.2012.00518.x.
- Jung, A., T. Aigner, D. Palermo, S. Nardon, and M. Pontiggia, 2012, A new workflow for carbonate reservoir modelling based on MPS: shoal bodies in outcrop analogues (Triassic, SW Germany): Geological Society, London, Special Publications, v. 370, no. 1, p. 277–293, doi:10.1144/SP370.13.
- Kazhdan, M., M. Bolitho, and H. Hoppe, 2006, Poisson Surface Reconstruction, *in* Proceedings of the Fourth Eurographics Symposium on Geometry Processing: Eurographics Association, SGP '06, p. 61–70.
- Kenter, J. A. M., 1990, Carbonate platform flanks: slope angle and sediment fabric: Sedimentology, v. 37, no. 5, p. 777–794, doi:10.1111/j.1365-3091.1990.tb01825.x.
- Kerans, C., 2002, Styles of Rudist Buildup Development along the Northern Margin of the Maverick Basin, Pecos River Canyon, Southwest Texas: Gulf Coast Association of Geological Societies Transactions, v. 52, p. 501–516.
- Kerans, C., and P. M. Harris, 2010, Shelf Physiography and Accommodation as Controls on Permian Grainstone Bodies: Search and Discovery, v. Article #5.
- Kerans, C., and K. Kempter, 2002, Hierarchical Stratigraphic Analysis of a Carbonate Platform, Permian of the Guadalupe Mountains: American Association of Petroleum Geologists/Datapages Discovery Series, v. 5, p. 1986–1989.
- Koehrer, B., T. Aigner, and M. Poppelreiter, 2011, Field-scale geometries of Upper Khuff reservoir geobodies in an outcrop analogue (Oman Mountains, Sultanate of Oman): Petroleum Geoscience, v. 17, no. 1, p. 3–16, doi:10.1144/1354-079310-009.
- Lanfranchi, A., F. Berra, and F. Jadoul, 2011, Compositional changes in sigmoidal carbonate clinoforms (Late Tithonian, eastern Sardinia, Italy): insights from quantitative microfacies analyses: Sedimentology, v. 58, no. 7, p. 2039–2060, doi:10.1111/j.1365-3091.2011.01250.x.
- Loucks, R. G., and C. Kerans, 2003, Lower Cretaceous Glen Rose “Patch Reef” Reservoir in the Chittim Field, Maverick County, South Texas: Gulf Coast Association of Geological Societies Transactions, v. 53, p. 490–503.
- Masse, J., and J. Philip, 1981, European Fossil Reef Models: SEPM (Society for Sedimentary Geology), 399-426 p., doi:10.2110/pec.81.30.
- McCave, I. N., 1971, Sand waves in the North Sea off the coast of Holland: Marine Geology, v.

- 10, no. 3, p. 199–225, doi:10.1016/0025-3227(71)90063-6.
- Meshlab 1.3.3, 2014, 1.3.3: Visual Computing Lab - ISTI - CNR, Retrieved from <http://meshlab.sourceforge.net/>.
- Mijnssen, F. C. J., P. D. Oman, A. H. Davies, P. D. Oman, and K. Grondin, 2003, SPE 84285 Bringing Al Huwaisah's Volume to Value: no. Figure 2, p. 1–8.
- Mitchell, N. C., G. Masselink, J. M. Huthnance, L. M. Fernandez-Salas, and F. J. Lobo, 2012, Depths of Modern Coastal Sand Clinoforms: *Journal of Sedimentary Research*, v. 82, no. 7, p. 469–481, doi:10.2110/jsr.2012.40.
- Moore, J., A. Taylor, C. Johnson, B. D. Ritts, and R. Archer, 2012, Facies Analysis, Reservoir Characterization, and LIDAR Modeling of an Eocene Lacustrine Delta, Green River Formation, Southwest Uinta Basin, Utah, in O. W. Baganz, Y. Bartov, K. Bohacs, and D. Nummedal, eds., *Lacustrine sandstone reservoirs and hydrocarbon systems: AAPG Memoir 95*: p. 183 – 208, doi:10.1306/13291389M953449.
- Mukherjee, D., S. D. Khan, and C. Sullivan, 2012, Upper Albian rudist buildups of the Edwards Formation in central Texas: A GPR-assisted reservoir analog study: *Sedimentary Geology*, v. 247–248, no. March, p. 71–81, doi:10.1016/j.sedgeo.2011.12.015.
- Negra, M. H., B. H. Purser, and A. M'Rabet, 1995, Sedimentation, Diagenesis and Syntectonic Erosion of Upper Cretaceous Rudist Mounds in Central Tunisia: Special Publication International Association of Sedimentologists, v. 23, p. 401–419, doi:10.1002/9781444304114.ch14.
- Nichols, G., 2009, *Sedimentology and stratigraphy*: 419 p., doi:10.1017/CBO9781107415324.004.
- Ortega-Sánchez, M., F. J. Lobo, A. López-Ruiz, M. A. Losada, and L. M. Fernández-Salas, 2014, The influence of shelf-indenting canyons and infralittoral prograding wedges on coastal morphology: The Carchuna system in Southern Spain: *Marine Geology*, v. 347, p. 107–122, doi:10.1016/j.margeo.2013.11.006.
- Patruno, S., G. J. Hampson, and C. a-L. Jackson, 2015, Quantitative characterisation of deltaic and subaqueous clinoforms: *Earth-Science Reviews*, v. 142, p. 79–119, doi:10.1016/j.earscirev.2015.01.004.
- Plaziat, J.-C., 1981, Late Cretaceous to Late Eocene palaeogeographic evolution of Southwest Europe: *Palaeogeography, Palaeoclimatology, Palaeoecology*, v. 36, no. 3–4, p. 263–320, doi:10.1016/0031-0182(81)90110-3.
- Pomar, L., M. Aurell, B. Bádenas, M. Morsilli, and S. F. Al- Awwad, 2015, Depositional model for a prograding oolitic wedge, Upper Jurassic, Iberian basin: *Marine and Petroleum Geology*, v. 67, p. 556–582, doi:10.1016/j.marpetgeo.2015.05.025.
- Pomar, L., P. Bassant, M. Brandano, C. Ruchonnet, and X. Janson, 2012, Impact of carbonate producing biota on platform architecture: Insights from Miocene examples of the Mediterranean region: *Earth-Science Reviews*, v. 113, no. 3–4, p. 186–211, doi:10.1016/j.earscirev.2012.03.007.
- Pomar, L., E. Gili, A. Obrador, and W. C. Ward, 2005, Facies architecture and high-resolution sequence stratigraphy of an Upper Cretaceous platform margin succession, southern central Pyrenees, Spain: *Sedimentary Geology*, v. 175, no. 1–4, p. 339–365, doi:10.1016/j.sedgeo.2004.11.009.
- Pomar, L., and W. C. Ward, 1994, Response of a late Miocene Mediterranean reef platform to high-frequency eustasy: *Geology*, v. 22, no. 2, p. 131, doi:10.1130/0091-7613(1994)022<0131:ROALMM>2.3.CO;2.
- Purkis, S., B. Vlaswinkel, and N. Gracias, 2012, Vertical-To-Lateral Transitions Among Cretaceous Carbonate Facies--A Means To 3-D Framework Construction Via Markov Analysis: *Journal of Sedimentary Research*, v. 82, no. 4, p. 232–243, doi:10.2110/jsr.2012.23.
- Qi, L., T. R. Carr, and R. H. Goldstein, 2007, Geostatistical three-dimensional modeling of oolite shoals, St. Louis Limestone, southwest Kansas: *AAPG Bulletin*, v. 91, no. 1, p. 69–96, doi:10.1306/08090605167.
- Al Rahbi, B., 2015, Facies and rock property characterisation of clinoforms, Cretaceous carbonate platform, Spain: The University of Manchester.
- Rankey, E. C., and S. L. Reeder, 2011, Holocene Oolitic Marine Sand Complexes of the Bahamas:

- Journal of Sedimentary Research, v. 81, no. 2, p. 97–117, doi:10.2110/jsr.2011.10.
- Reolid, J., C. Betzler, J. C. Braga, J. M. Martín, S. Lindhorst, and J. J. G. Reijmer, 2014, Reef slope geometries and facies distribution: controlling factors (Messinian, SE Spain): *Facies*, v. 60, no. 3, p. 737–753, doi:10.1007/s10347-014-0406-4.
- Rich, J. L., 1951, Three Critical Environments of Deposition, and Criteria for Recognition of Rocks Deposited in each of them: *Geological Society of America Bulletin*, v. 62, no. 1, p. 1, doi:10.1130/0016-7606(1951)62[1:TCEODA]2.0.CO;2.
- Riding, R., 2002, Structure and composition of organic reefs and carbonate mud mounds: concepts and categories: *Earth-Science Reviews*, v. 58, no. 1–2, p. 163–231, doi:10.1016/S0012-8252(01)00089-7.
- RiSCAN Pro, 2015: RIEGL Laser Measurement Systems GmbH, <http://www.riegl.com/products/software-packages/riscan-pro/>.
- Ross, D. J., 1992, Sedimentology and depositional profile of a mid-Cretaceous shelf edge rudist reef complex, Nahal Ha'mearot, northwestern Israel: *Sedimentary Geology*, v. 79, no. 1–4, p. 161–172, doi:10.1016/0037-0738(92)90009-G.
- Ross, D., and P. Skelton, 1993, Rudist formations of the Cretaceous: a palaeoecological, sedimentological and stratigraphical review, in V. P. Wright, ed., *Sedimentology Review/1*: Oxford, UK, Blackwell Publishing Ltd., doi:10.1002/9781444304534.
- Roybal, G. H., 1981, Facies development in a Lower Cretaceous coral-rudist patch reef (Mural Limestone, southeast Arizona): *The Mountain Geologist*, v. 18, no. 3, p. 46–56.
- Sanders, D., 1996, Rudist biostromes on the margin of an isolated carbonate platform: The Upper Cretaceous of Montagna della Maiella, Italy: *Eclogae Geologicae Helvetiae*, v. 89, no. 2, p. 845–871.
- Sanders, D., 1998, Upper Cretaceous “Rudist” formations: *Geologisch-Palaeontologische Mitteilungen Innsbruck*, v. 23, p. 37–59.
- Schlager, W., 2005, Sequence stratigraphy of the T factory, in *Carbonate Sedimentology and Sequence Stratigraphy*: p. 105–146.
- Seers, T. D., 2015, Image Based Characterisation of Structural Heterogeneity within Clastic Reservoir Analogues: University of Manchester, 248 p.
- Simó, A., 1993, Cretaceous carbonate platforms and stratigraphic sequences; south-central Pyrenees; Spain., in J. Simo, R. W. Scott, and J.-P. Masse, eds., *Cretaceous carbonate platforms: AAPG Memoir 56*: Tulsa, OK, AAPG, p. 325–342, doi:10.1306/M56578C1.
- Sitgreaves, J. R., 2015, Shelf-to-Basin Architecture and Facies Variability of a Cretaceous Intraself Basin in the Northwest Gulf of Mexico: The University of Texas at Austin, 77 p.
- Skelton, P. W., E. Gili, B. R. Rosen, and F. X. Valldeperas, 1997, Corals and rudists in the Late Cretaceous: a critique of the hypothesis of competitive displacement: *Boletín de la Real Sociedad Española de Historia Natural. Sección Geológica*, v. 92, no. 1–4, p. 225–239.
- Tucker, M. E., 2011, *Sedimentary Rocks in the Field: A Practical Guide*: Wiley-Blackwell, 288 p.
- Tucker, M. E., and V. P. Wright, 1990, *Carbonate Sedimentology*: Oxford, UK, Blackwell Publishing Ltd., doi:10.1002/9781444314175.
- Verwer, K., G. Della Porta, O. Merino-Tomé, and J. A. M. Kenter, 2009, Controls and predictability of carbonate facies architecture in a Lower Jurassic three-dimensional barrier-shoal complex (Djebel Bou Dahar, High Atlas, Morocco): *Sedimentology*, v. 56, no. 6, p. 1801–1831, doi:10.1111/j.1365-3091.2009.01058.x.
- Virtual Reality Geological Studio, 2016: Retrieved from <http://www.vrgeoscience.com/>.
- Visser, C. a., and a. G. Chessa, 2000, Estimation of length distributions from outcrop datasets - application to the Upper Permian Cutler Formation, Utah: *Petroleum Geoscience*, v. 6, no. 1, p. 29–36, doi:10.1144/petgeo.6.1.29.
- Van Wagoner, J. C., H. W. Posamentier, R. M. Mitchum, P. R. Vail, J. F. Sarg, T. S. Loutit, and J. Hardenbol, 1988, An overview of the fundamentals of sequence stratigraphy and key definitions, in *Sea-Level Changes - An Integrated Approach*, SEPM Special Publication: SEPM (Society for Sedimentary Geology), p. 39–45, doi:10.2110/pec.88.01.0039.
- Wu, C., 2011, VisualSFM: A Visual Structure from Motion System: <<http://ccwu.me/vsfm/>>.
- Wu, C., S. Agarwal, B. Curless, and S. M. Seitz, 2011, Multicore Bundle Adjustment: CVPR.

## 6 SYNTHESIS

This chapter reviews the results of this thesis with respect to the aims and objectives presented in Chapter 1. It also makes an evaluation on the applicability of the studied carbonate platforms as analogues for Upper Cretaceous rudist-dominated hydrocarbon reservoirs on the Arabian Shelf. Lastly, an outlook on further work discusses areas for future studies and possibilities for integration in future projects.

### 6.1 Summary of Main Results and Implications

The three papers presented in this thesis investigated the geometry of carbonate deposits on several scales, and how these are affected by a variety of depositional processes. In Chapter 3, the previous chronostratigraphic scheme of Simó (1993) was updated with the time scale of Gradstein et al. (2012), implementing more recent correlations from the geological maps of the area and data from more recent bio and chemostratigraphic studies. Together with cross-sections of the Cenomanian-Santonian platforms of the area, this provides a better understanding of the platform architecture and development. It was concluded that the overall evolution of the Tresp Basin during compression and formation of a foreland basin has a substantial effect on the geometry and trends of successive carbonate platforms. This investigation allows describing platform geometry through time in response to changes in relative sea level, changes in tectonic regime and changes to sediment supply and carbonate factory. It was shown that on a platform scale, some variations in the sedimentary record could not be directly tied to relative sea-level variations, and other potential mechanisms for these were evaluated, including differential subsidence and localised faulting.

Chapter 4 investigated how large-scale platform architecture was controlled by changes in relative sea level within a rapidly subsiding basin. It was shown that global sea-level variations on a <0.5 My scale were most probably not the cause for sedimentary successions that in other platforms are commonly interpreted as 4<sup>th</sup> or 5<sup>th</sup> order sedimentary cycles. This highlighted the importance of basin-scale studies for correct sequence stratigraphic interpretations, as well how mechanisms other than sea-level fluctuations, such as temporal variations in carbonate productivity or tectonic tilting, may have been the driving forces behind so-called “sedimentary sequences”. This was supplemented with examples from stratigraphic forward models. These showed potential scenarios of different platform architectures, induced using variability in carbonate production rates or tectonic tilt.

In Chapter 5, a variety of smaller scale depositional elements (less than a few kilometres in diameter) and their internal geometry (less than a few 100 metres wide) were presented. This included biogenic build-ups, packstone and grainstone shoals and platform margin clinofolds. It

was concluded that their occurrence and position on the platform, as well as their internal geometry were highly dependent on the broad topography of the platform, as well as on the nature of the carbonate system at the time.

There are a number of reoccurring aspects recognised throughout this work that highlight the importance of studies spanning across platform top to basinal transects when investigating small-scale facies architecture in carbonate systems. Mainly, a variety of controls on platform evolution exists, and acknowledging these controls is important in predicting the basin-scale architecture of a platform. Particularly important are the controls of rising relative sea-level and differential subsidence in the investigated compressional regime, which lead to backstepping of the platform margins and differential development of thickness across platforms. The combination of tectonism, varying carbonate productivity and relative sea-level can produce distinct stratal geometries. This includes the general lack of transgressive systems tracts due to strong effect of subsidence, resulting in continuous relative sea-level rise, the absence of clearly defined sequence boundaries, and sequences transitioning from progradational to aggradational depositional modes, followed by backstepping. Furthermore, it is recognised that carbonate platforms have a tendency to inherit prior topography, and the presence of certain topographies may play an important role in the establishment of specific carbonate producers adapted to these conditions. This is evident in the Santonian Bastus Platform, which inherited the low-angle topography of the Coniacian Sant Corneli Platform. During the initial phase, it only shows quartz-bearing grainstone shoals at the margin, with platform-margin composite rudist and coral build-ups only establishing after ca. 1 My. Subsequently, it shows limited topography itself during the initial phases, but developed into a rimmed shelf with a gently dipping slope ( $<2^\circ$ ) later on. This implies that platform margin build-ups take a substantial amount of time to develop if a platform inherits previous low-angle topography.

The absence of key stratigraphic surfaces that are correlatable basin-wide, such as flooding or emergent surfaces, highlights the importance of large-scale studies when establishing a sequence stratigraphic interpretation. Sequence stratigraphic interpretations that were made by previous authors on the basis of single sections or restricted to only platform margin transects could not be carried over into the interpretations made during this study on the basis of basin-scale data. This is particularly important for subsurface reservoir characterisation, as further discussed in section 6.4. Characterisation is sometimes made on the scale of single hydrocarbon fields, based on well-data. The results presented here suggest that the basin-scale evolution of the host formations is imperative to the development of localised stratigraphic patterns and the small-scale elements associated with these.

## 6.2 Sequence Stratigraphy and Mixed Carbonate-Siliciclastic Systems

A key aspect of this study was the sequence stratigraphic interpretation of the Bastus Platform, including the attempt to attribute facies and geobodies to particular systems tracts. However, the common presence of siliciclastic material requires that the effect of siliciclastic input on the productivity of the carbonate platform and the resulting sequence stratigraphic patterns and geometries to be considered.

Mixed carbonate-siliciclastic systems are generally treated differently to “pure” carbonate systems, both in palaeo-environmental interpretations and sequence stratigraphic interpretations (Wilson, 1975; Hunt and Tucker, 1992; Handford and Loucks, 1993; Catuneanu et al., 2011). However, it has been suggested before that carbonate and siliciclastic systems each present the end-members of a continuum (Doyle and Roberts, 1988). Although some sequence stratigraphic models have been presented for mixed systems (Handford and Loucks, 1993; Catuneanu et al., 2011), there are few studies dedicated to this. The results of this study, summarised below, imply that a more detailed study of the spectrum between the pure siliciclastic and carbonate end members is necessary. Furthermore, it is likely that the interpretation of each mixed carbonate-clastic system on this spectrum to be regarded as unique to a certain extent.

In the platforms presented in this study, the Santonian Bastus Platform showed the highest amounts of siliciclastic material (<40% in the deltaic environment, and <10% in the platform interior). The siliciclastic influx is interpreted to have occurred in the form of sand and silt-grade quartz grains at minimal water depths (<10 m), occurring primarily at the top of the proposed 4<sup>th</sup> order cycles. The presence of siliciclastic material does not appear to have affected carbonate productivity. Overall, there was only periodic and local cessation of productivity in the platform interior resulting from the sudden influx of coarse grained siliciclastic material. After this, productivity quickly resumes. Similar sedimentary patterns were noted by Mount (1984) to occur in punctuated-style mixing of carbonate and siliciclastics in proximal areas. Transport of siliciclastic material did not reach far into the platform margin, and only a small amount of quartz grains is concentrated in the grain-dominated lithofacies of the platform margin due to gradual winnowing (<5%). Subsequently, there is little effect on carbonate productivity here or further basinwards. However, it behaved similarly to a “pure” carbonate system in regards to its reaction to environmental and relative sea-level changes, by showing keep-up of the platform margin during the rise of relative sea-level. Therefore, it was treated as such in the sequence stratigraphic interpretations, and the interpretation approach by Van Wagoner et al. (1988) was used.

The interpretation of the sedimentary patterns on the Bastus Platform shows key differences to the previous interpretation by Catuneanu et al. (2011). The Bastus Platform was there defined to consist of lower-mudrock and upper carbonate sequences. In the revised interpretation presented in Chapter 4, there may be clay in the bottom of the sequences, but the bulk of the siliciclastic material appears as silt to sand grade quartz grains at the top of the 4<sup>th</sup> order cycles, intermixed with carbonate sediments (cf. Chapter 3).

The recognition of different stacking patterns may be the result of the revised regional stratigraphy presented in Chapter 3. Catuneanu et al. (2011) base their interpretation of the sequences on the regional studies presented by Simó (1986, 1989, 1993), who interpreted the platform geometry and stacking patterns mainly on the margin deposits in the Sant Corneli area. At this locality, mudrocks (i.e. silty nodular wackestones) do indeed form the base of upward-shallowing sequences, grading into rudist build-up dominated carbonates at the top. The revised chronostratigraphic framework presented in Chapter 3, however, includes the platform interior deposits of the Montsec area and the deltaic deposits in the area of Camarasa following new bio- and lithostratigraphic correlations. This changes the previous concept of the platform by introducing the presence of the persistent deltaic system in the proximal parts. In these proximal and interior areas coarse siliciclastic beds are interpreted to occur at the top of the sequence. This highlights the necessity of regional correlations and interpretations to properly identify sequences in mixed settings.

### **6.3 Geometrical Quantification and Classification of Carbonate Geobodies**

Proper quantification and classification of depositional elements and their internal geometries in carbonate settings has been focus of many recent studies (e.g. Immenhauser et al., 2002; Loucks and Kerans, 2003; Adams et al., 2005; Janson et al., 2015). The results of this study have emphasised how carbonate shoal bodies, clinoform bodies, and build-ups can vary on both at the depositional element scale and within their interior geometry depending on a number of factors. The association of carbonate producers plays an important factor in the final shape of a build-up. This was shown in how monospecific rudist build-ups are likely to form thin-laterally extensive bioherms, whereas coral-rudist associations create depositional elements which are more likely to exhibit a bar shape. Most build-ups are either internally planar bedded, or structureless, whereas some margin coralgall build-ups were shown to display sigmoidal bedding. In shoal bodies and clinoforms, the size of the depositional element and internal geometry depended on the formation mechanism (hydrodynamic sorting vs. margin progradation), as well as the water depth, energy and rate of sediment production. These factors inherently vary based on the nature and topography of the platform, as well as on the

relative position of the geobody to the margin, which closely dictates local topography and energy levels. This information is fundamental to support interpretations and projections of geobody sizes in individual case studies and through subsurface data, and is sometimes not acknowledged in past studies. It is therefore recommended that future studies focus on first describing the geometry of the entire platform, as well as the position the investigated geobodies are found in. This would allow evaluation of the comparability between geological examples and may help to avoid application of inappropriate analogues to the subsurface.

Similarly, it is important to define the sedimentological character and geometry of geobodies in a consistent manner across studies in order to facilitate comparison between different geological examples. This is observed in Chapter 5, where some of the literature data collected on “shoal bodies” may have been described between the respective authors on different scales (depositional element/internal geometry) and were the result of different sedimentological processes (shelf progradation vs. hydrodynamic sorting). The nomenclature of Jung and Aigner (2012) is suggested here to form a good template for uniform reporting of depositional element geometry, and detailed description of interpreted formation mechanisms is encouraged. For biogenic build-ups, this also includes information on the main carbonate producing organisms, as different organisms were shown to create different geometries. For the quantification of clinoforms and clinothems, future authors are further encouraged to use a system such as the one proposed by Anell and Midtkandal (2015) where possible, in order to ensure comparability between data from different studies.

In this study, it was not possible to establish universal rules on the relationships between width, length and thickness of geobodies. A preferential relationship is possible within each of the platforms, but comparison with other studies shows geobodies may be vastly different in lateral extent and thickness between different platforms. This is inevitably the result of the dependency of geobody geometries on the geological framework. This implies that there are limitations to how accurately a relationship from one platform can be applied to another. However, relationships between sediment composition, texture or organism and the qualitative geometry of the resulting geobody were demonstrated in this study. For example, in the Santonian Bastus Platform, rudist formations characterised by a monospecific species association and in-situ growth of large amounts of specimen are likely to form low-topography bodies with large lateral extents (few kilometres), and limited thickness (<10 metres). This confirms the previous interpretations of such bodies by Ross and Skelton (1993). It is proposed that investigating such relationships between sedimentary features and geobody dimensions for a multitude of basins will facilitate interpreting geobodies in studies with limited data.



One of the aspects that were not investigated in detail in this study is how the presence of siliciclastics affects the size and positioning of carbonate build-ups. It was established that the platform interior build-ups were not under long-term effects following the periodic introduction of coarse grained quartz. In current literature, it is suggested that geobodies may establish in the vicinity of siliciclastics, but that the presence of terrigenous material may have a strong effect on the resulting build-up shape (Santisteban and Taberner, 1988), whereas established geobodies may pose an active role in channelizing the flow of siliciclastics around the topographic highs they create (McNeill et al., 2004). It is therefore recommended to further attempt to quantify the effects of siliciclastics on the spatial distribution and geometry of geobodies in future studies.

#### **6.4 Implication for Hydrocarbon Production and Exploration**

The results of this study provide a useful addition to our knowledge of carbonate platform growth and architecture on a basinal scale. This is of particular relevance to subsurface studies for hydrocarbon exploration and production where datasets are sparse and spatially restricted. The particular aspects touched by each chapter are presented and discussed in the following.

Chapter 3 demonstrates the relationship between regional platform architecture, and the role of prior platform shape and size on the growth of subsequent carbonate platforms. The results emphasise the importance of framing interpretations of stratal geometries and platform architecture within the framework of the wider basin, and may require sedimentological interpretations to be grounded in regional data rather than field-scale seismic data. Similar developments have been made in the study of the Aptian-Albian Shu'aiba and the Cenomanian Natih Formations in Oman, where re-evaluation of the regional geology allowed significantly improved predictability of facies (e.g. Grélaud et al., 2010; H. Droste, 2010; van Buchem et al., 2011). In this study, this is highlighted by using the knowledge of regional development to improve the interpretation of smaller-scale features, such as the differentiation between the Congost A and the Congost B lowstand wedge, with their platform architecture framing the lateral extent of the small-scale depositional elements within them.

The sequence stratigraphic study in Chapter 4 provides alternative methods of interpreting the controls on facies distribution in carbonate platforms, based on varying carbonate productivity or tectonic influence, rather than simply using relative sea-level as the sole controlling mechanism on the establishment of sedimentary stacking patterns. The plausibility of these alternative interpretations was tested using stratigraphic forward models and comparison with the known evolution of the basin. The knowledge gained from this study contributes towards applying stratigraphic forward models to various subsurface examples, and highlights other

potential interpretation approaches, which may lead to different interpolations of facies distributions and platform architectures.

In addition to the above, Chapter 4 showed how distinct surfaces, which are usually used in sequence stratigraphic interpretations, may not be preserved uniformly and correlatable across the entire platform. This is an important observation to subsurface studies, where such surfaces are often identified on the basis of limited data and may result in mis-correlation to neighbouring sections. As stratigraphic architecture is derived from sequence stratigraphic frameworks, these results emphasise how sequence stratigraphy should ideally be interpreted from a basin-wide transect, as opposed to the interpretations commonly only made on the scale of a single hydrocarbon field. Finally, Chapter 4 defines vertical sedimentary patterns that are associated with carbonate geobodies in the Bastus Platform. Comparable stacking patterns in core may allow recognition of the presence of similar depositional elements in subsurface examples, and potentially help predict their presence in similar small-scale, siliciclastics-influenced land attached platforms.

Chapter 5 describes the location of geobodies on these platforms. The geobodies are sub-seismic in scale and therefore their location, size and distribution can be difficult to predict in the subsurface. The results of Chapter 5 give upper limits to the size and the facies composition of biogenic build-ups and shoal clinoform geobodies. This data can be directly applied to subsurface examples, where identification of similar facies and stacking patterns can help interpreting the presence and possible size of geobodies. Data on the geometries of rudist build-ups is generally transferrable onto other rudist-bearing formations of the Cretaceous, whereas the shoal bodies are formed by organism-independent hydrodynamic processes, and can therefore be applied to a wider variety of other geological examples from various ages.

Furthermore, the composite platform margin build-ups of the Bastus platform, with the basinward bioherm component and the landward biostrome component, as well as other publications (e.g. Aconcha et al., 2008) show that internal structure of build-ups is dependent on the current direction and platform trajectory. The geometry of these build-ups and their internal components was quantified in Chapter 5, and similar rudist deposits are known as prolific hydrocarbon reservoirs throughout the world (Scott et al., 1993). Together with the geometrical data on geobody sizes and the knowledge of the regional platform setting, this can allow the heterogeneity of these build-up sections to be better captured in reservoir models. This improves assessment of how heterogeneity affects fluid flow in the subsurface, since many of the grain-dominated and rudist-rich facies commonly act as high-permeability layers, although in some cases diagenetic modification and cementation leads to them acting as baffles or barriers (e.g. Cross et al., 2010; Hollis, 2011).

Lastly, knowledge of the maximum sizes and shapes of these geobodies can be implemented as bounding parameters for multiple point statistics (MPS) based simulations of geobody distribution (e.g. Jung et al., 2012). Although there might be a large variation in the size of geobodies between different geological examples, use of analogues remains a proven approach in MPS based models to create different scenarios for interpreting subsurface heterogeneity.

## **6.5 Applicability of the Platforms of the Tresp Basin as Analogues for Middle Eastern Carbonate Systems**

### **6.5.1 Rationale and Aims**

Some of the major Mid- and Upper Cretaceous reservoir formations of the Arabian Shelf were dominated by large rudist-dominated carbonate systems (Scott et al., 1993). These systems often show a complex facies architecture, and due to their large size and limited amounts of outcrop they are difficult to characterise. The outcrops of the South-Central Pyrenees investigated in this work show rudist bearing strata of Upper Cretaceous age, which may be applicable as analogues for the rudist platforms of the Arabian Shelf. A detailed comparison of depositional setting, platform-scale and depositional element scale, and controlling mechanisms is important in order to define the applicability of the platforms of the Tresp Basin as analogous outcrops. Formations of particular interest are the Cenomanian-Turonian Mishrif Formation (in SE Iraq) and Natih (in Oman). This chapter aims to compare between the Pyrenean and Arabian Cretaceous carbonate platforms and to make an evaluation on the applicability of the former as analogues for the latter.

The vast majority of studies on carbonate platforms in the Arabian Shelf are specific to individual fields and reservoirs, and often limited to subsurface data (e.g. Droste, 2010; Mahdi et al., 2013). Outcrop analogues are therefore often used to supplement the understanding of the reservoir architecture, but direct outcrops of the respective facies in the Arabian Shield are limited to few areas in the region (Warrlich et al., 2010). The expansive size of the carbonate platforms that established here, reaching up to 2500 km in length and 1000 km in width, makes correlations across the basin difficult (van Buchem et al., 1996; Droste, 2010). Recent studies synthesise local knowledge of these systems and have proved significant in advancing the understanding of the large-scale platforms of this area (van Buchem et al., 2002; Sharland et al., 2004; van Buchem et al., 2011).

### **6.5.2 Cenomanian-Turonian Rudist Platforms of the Arabian Shelf**

During the Mid-Late Cretaceous, an epeiric carbonate platform dominated sedimentation on the Arabian Shelf (Droste and Steenwinkel, 2004). Following Triassic rifting, the north-eastern Arabian Peninsula was a passive margin during the Mid to Late Mesozoic (Searle et al., 2004;

Bordenave and Hegre, 2005). The area of the shelf is estimated to have been approximately 2500 by 1000 km from SE to NW (van Buchem et al., 1996; H.J. Droste, 2010). Several large intrashelf basins developed in this area in the late Permian, and some persisted through to Cenozoic times (Murriss, 1980; Burchette, 1993; Sharland et al., 2001). The control on these basins is poorly understood (van Buchem, Razin, et al., 2002; Razin et al., 2010). Most notably are the Kazhdumi Basin in modern SW Iran and the Bab Basin ranging from NW Oman over the western UAE to offshore Qatar (Frans S. P. van Buchem, Al-Husseini, et al., 2010). These intrashelf basins were frequently rimmed by carbonate deposits, with the ones relevant to this study being the Cenomanian-Turonian Mishrif (in the NW) and Natih (In the SE of the Arabian Peninsula).

Sedimentation is interpreted to be mostly controlled by relative sea-level fluctuations (Frans S. P. van Buchem, Al-Husseini, et al., 2010). However, a tectonic influence becomes apparent first in SW of Iran in the early Cenomanian, and later during the Turonian along the eastern Arabian Shelf margin, with the slow onset of compression and the transition towards an active margin (F. S. P. van Buchem et al., 2010).

Siliciclastic input varied substantially across the Arabian Shelf (Davies et al., 2002), and the development of the Burgan Delta in the area of Kuwait influenced the character of the Mishrif and Natih formation. Coarse siliciclastic material was introduced into the most proximal areas of the Mishrif, whereas fine-grained silt and clay material was transported onto the platform top of the Natih Formation, which was situated further from the source of siliciclastics, and substantially affecting carbonate deposition in this area (see below). The sedimentology, platform architecture and depositional elements of the Mishrif and Natih Formations are presented in the following, and summarised in Table 6.1.

**Table 6.1: Summary information of the Cretaceous Carbonate systems in the eastern Arabian Shelf and their geometry forming depositional elements.**

<b>Platform</b>	<b>Mishrif</b>	<b>Natih</b>
<b>Age (+Numerical)</b>	Middle Cenomanian to early Turonian (ca. 2.5 My; Sharland et al., 2004)	Late Albian –Mid-Turonian (ca. 9.5 My; van Buchem et al., 2002). 3 <sup>rd</sup> order cycles: Sq. I: ~2.3 My; Sq. II: ~2.4 My; Sq. III: ~3.3 My; Sq. IV: ~1.5 My
<b>Platform Shape</b>	Rudist rimmed shelf around intrashelf basin	Rudist rimmed shelf around intrashelf basin
<b>Slope Inclination</b>	?	<0.2° (Droste, 2010)
<b>Dominating geometries /Location</b>	Margin build-ups on palaeohighs	Progradational clinofolds
<b>Geometry forming process</b>	Carbonate production /progradation	Platform progradation (RSL?)
<b>Depositional element scale</b>	Build-ups: 2-9 km (Mahdi and Aqrabi, 2014)	Clinofolds: 10 m high, 100 m long, 1-5° slope angle (Adams et al., 2011)

<b>Sequence Stratigraphic Position</b>	Rudist biostromes at top of regressive sequences (3 <sup>rd</sup> order; Mahdi and Aqrawi, 2014)	Transgressive Systems Tract, Highstand Systems Tract, Forced Regressive Wedges (van Buchem et al., 1996; Grélaud, 2005; Homewood et al., 2008; Closson et al., 2009)
<b>Dominating Organism / Grain Type</b>	Rudist biostromes, platform interior biostromes and shoals. Margin rudist debris	Coarse rudist fragments and benthic foraminifera in fine grained micritic matrix.
<b>Siliciclastics</b>	Rare	Clay influx at the lowstands and transgressive systems tracts of each 3 <sup>rd</sup> order sequence

### **Mishrif Formation (Iraq)**

The Mishrif Formation is of Mid-Cenomanian to early Turonian age, and is a major carbonate hydrocarbon reservoir in southern Iraq (Aqrawi et al., 2010). Its upper boundary is a sharp contact to the overlying Khasib Formation, interpreted as the early-middle Turonian Unconformity. At the base, it gradationally overlies the Rumaila Formation (Mahdi and Aqrawi, 2014). The thickness of the Mishrif Formation is 350-400 metres in SE Iraq (Aqrawi et al., 1998), and becomes thinner until wedging out towards the W/SW (Mahdi and Aqrawi, 2014).

Previous studies of the sequence stratigraphy of the Mishrif Formation subdivide it into two long-term transgressive-regressive cycles, often referred to as Mishrif A and B (Reulet, 1982; Aqrawi et al., 1998). However, a more recent study subdivides it into three long-term transgressive-regressive cycles (3<sup>rd</sup> order; Mahdi et al., 2013); with the previous lower sequence now subdivided into two. These are separated by sequence boundaries, and show maximum flooding surfaces, both of which can be correlated across the basin (Mahdi et al., 2013). Each of these long-term regressive cycles is again subdivided into three medium-scale cycles (Mahdi and Aqrawi, 2014).

The 3<sup>rd</sup> order transgressive-regressive cycles are characterised by a deepening facies trend followed by a shallowing trend (Aqrawi et al., 1998; Aqrawi, 2010; Mahdi et al., 2013). At the base, these show deep- and shallow- shelf open marine facies and then grade upwards to bioclastic-rich limestones, followed by in-situ rudist biostromes, and capped by bioclastic shoal facies and inner shelf facies. These then follow a retrogradational trend, with the facies pattern occurring in the reverse order (Mahdi et al., 2013; Mahdi and Aqrawi, 2014).

A number of depositional models of the Mishrif Formation have been presented (e.g. Owen and Nasr, 1958; Reulet, 1982; Aqrawi et al., 1998; Sharland et al., 2001; Sadooni, 2005). Most recently, Mahdi and Aqrawi (2014) defined it as a carbonate platform rimmed around the margins of the intrashelf basins, with rudist congregations occupying the margin. Due to the study of the Mishrif Formation being limited to subsurface data, there is a distinct lack of knowledge regarding the small-scale facies distribution and the extent of depositional elements such as rudist patch reefs and shoal bodies. The presence of rudist biostromes in core and subsurface data is used to infer the position of the margin of the intrashelf basin (Aqrawi, 2010),

but the orientation of the platform margin towards the intrashelf basin is poorly understood (Mahdi and Aqrawi, 2014). The rudist build-ups formed a discontinuous rim around the intrashelf basin, passing laterally into shoals (Mahdi and Aqrawi, 2014). The rudist build-ups are interpreted to have selectively formed on paleo-highs. Mahdi and Aqrawi (2014) describe these to be 2-9 km in lateral extent, and are surrounded by fine-grained and mud-rich facies. Note that no indication was made on data source or samples size.

The depositional environments of the Mishrif Formation were described in detail by Mahdi et al., (2013) and Mahdi and Aqrawi (2014); From the most proximal areas, tidal flats pass into protected, open marine lagoonal environments with fine grained limestones and large benthic foraminifera. Occasional shoal bodies and rudist build-ups established within this shallow water platform top setting. The margin of the intrashelf basin is dominated by rudist biostromes, fringed landwards by shoals with rudist debris halos and back-shoals, and basinwards by rudist debris aprons. The upper slope shows shallow open marine facies under moderate energy conditions, with occasional mud mounds, and passes basinwards into deep marine facies. These show fine grained and mud-rich pelagic limestones with minor amounts of fine-grained material being introduced from shallower areas.

### **Natih Formation (Oman)**

The Natih Formation is part of the Wasia Group, and of Late Albian-Turonian age (van Buchem et al., 2010). It is subdivided into four 3<sup>rd</sup> order depositional sequences (van Buchem et al., 2011), which are in turn subdivided into seven informal members (A-G, from younger to older; Hughes Clarke, 1988; Scott, 1990). Sequence I encompasses the Natih G and F, is of late Albian age, and thus time-equivalent to the Safaniya Formation. Sequence II corresponds to the Natih E, is of early Cenomanian age, and equivalent to the Mauddud Formation and the upper Safaniya Formation in the Basin. Sequence III includes the Natih C and D, is of mid-Cenomanian age and equivalent to the Rumaila and Ahmadi Formations. Sequence IV encompasses the Natih A and B, is of upper Cenomanian to earliest Turonian age, and time-equivalent to the Mishrif Formation (Simmons and Hart, 1987; Smith et al., 1990; Kennedy and Simmons, 1991; Philip et al., 1995; van Buchem, Razin, et al., 2002; van Buchem et al., 2011). The sequences are separated by the regionally defined sequence boundaries, and show the corresponding maximum flooding surfaces recognised along the basin (K110; K120; K130 and K140, respectively. Sharland et al., 2001; van Buchem et al., 2011).

Spanning the Late Albian-Turonian, the Natih Formation shows the two modes of deposition that characterised the Lower and Upper Cretaceous of the Arabian Shelf (van Buchem et al., 2011). The lower Cretaceous is siliciclastic-influenced, whereas this component becomes less pronounced during the Upper Cretaceous (van Buchem et al., 2011). This development is

evident in the four sequences that comprise the Natih Formation. The transgressional component of Sequence I (Natih G and F) marks the backstepping of the siliciclastic systems in the area of Oman, with muddy carbonate ramps establishing (Droste and Steenwinkel, 2004; van Buchem et al., 2011). Following this, widespread rudist-carbonate platforms fringing organic-rich intrashelf basins developed during the Cenomanian-Turonian, with only minor amounts of siliciclastics occurring in the eastern Arabian Plate (van Buchem et al., 2011).

The base of Sequence II (earliest Middle Cenomanian; Natih E), locally shows siliciclastics at the base (Van Buchem et al. 2011), and is characterised by lagoonal facies marking the initial flooding phase (van Buchem, Razin, et al., 2002; van Buchem et al., 2011). During the transgressional phase, organic-rich intrashelf basins develop. Maximum water depths of 60 m are interpreted on the base of clinoform heights (van Buchem et al., 1996; H. Droste, 2010; Sharp et al., 2010) and faunal content (van Buchem et al., 2011). During the highstand, carbonate platforms with rudist dominated margins rim the intrashelf basins and prograde towards these (Burchette, 1993; van Buchem, Razin, et al., 2002; Homewood et al., 2008; Ghabeishavi et al., 2010; Razin et al., 2010; Sharp et al., 2010). The geometries of the prograding clinoforms were quantified in a number of previous studies (Droste and Steenwinkel, 2004; Grelaud et al., 2006; Grélaud et al., 2010; H. Droste, 2010; Adams et al., 2011). The top of the sequence shows an exposure surface following an estimated sea-level drop of 20-30 metres, with incised valley systems developing locally (Grelaud et al., 2006; Grélaud et al., 2010; Razin et al., 2010; Sharp et al., 2010).

Sequence III begins with a more shale rich succession (Middle Cenomanian) following the erosional contact (Grelaud et al., 2006; Grélaud et al., 2010). In the transgressive phase, low-relief carbonate ramps develop, with clay-input in discreet intervals occurring from proximal areas (H. Droste, 2010). These muddy carbonate ramps persist during the highstand (Natih D and C), although extensive carbonate platforms are known to have developed in SW Iran (Embry et al., 2010; Sharp et al., 2010).

Sequence III (Late Cenomanian-earliest Turonian sequence, equivalent to the Mishrif Formation of Iraq) again shows extensive carbonate deposition fringing localised intrashelf basins, represented by the Natih B (van Buchem et al., 2011). The intrashelf basins are interpreted as the possible results of amplification of regional subsidence variations, together with high-amplitude transgression (van Buchem et al., 2011). During the highstand, local tectonics led to an overprinting of relative sea-level in the area of Oman (Homewood et al., 2008). The Natih A then forms moderate energy platform top with rudist shoal facies (van Buchem, Razin, et al., 2002). In the northern Gulf, most of this sequence is missing due to tectonic uplift and erosion (van Buchem et al., 2011). The top of the sequence consists of a latest Cenomanian forced

regressive wedge. This is overlain by a thin transgressive backfill, with localised incised valley systems (van Buchem et al., 2011), and is capped by fault-controlled karst surfaces at the Cenomanian-Turonian boundary (Sharp et al., 2010).

Important in the Natih Formation is the variability of clinoform geometry, which has been found to be linked to sequence stratigraphic context (Grélaud, 2005; Closson et al., 2009); The transgressive systems tract is characterised by sigmoidal very low angle (0.1-0.3°), the highstand systems tract by sigmoidal low angle (0.5-1), and the forced regressive wedges by oblique high angle clinoforms (2-5°). Sub-horizontal clinoforms (<0.01°) are also described to occur in the TST and HST formed by the thin transgressive backfill below the termination of the Natih in the Cenomanian-Turonian boundary. These clinoforms are generally on a scale of 10-20 kilometres, reaching a thicknesses of ca. 50 metres (Droste and Steenwinkel, 2004). Smaller-scale clinoform structures of ca. 100 metres length, 10 metres thickness, and 1-5° slope angle are also known on the platform top (Adams et al., 2011).

### **6.5.3 Turonian-Santonian Rudist Platforms of the Tresp Basin**

The Tresp Basin features a largely continuous Mesozoic succession (Muñoz et al., 1986). Following rifting during the Triassic, the convergence of the Iberian and European Plate formed a narrow seaway between the Tethys and the Atlantic (Plaziat, 1981). A foreland basin developed here during the Upper Cretaceous, ahead of the impending Pyrenean Orogeny (Plaziat, 1981; Puigdefàbregas and Souquet, 1986; Vergés et al., 2002). A series of carbonate platforms were formed between Cenomanian and Maastrichtian, each representing a 3<sup>rd</sup> order sea-level cycle (Simó, 1993, and Chapter 3). Net global sea-level rise led to gradual back-stepping of each successive carbonate platform, and a general flattening of the shelf topography (Chapter 3).

Three carbonate platforms were studied in detail:

- The Turonian-Coniacian Congost Platform, showing a lower phase with a steep grainstone-clinoform dominated margin, and an upper phase with a steep corallgal boundstone margin
- The Coniacian Sant Corneli Platform, representing a distally steepened ramp with a complex platform interior facies mosaic
- The Santonian Bastus Platform, showing a grainstone shoal and rudist-build-up rimmed shelf and a low inclination slope (<1°), and a flat platform interior (<0.05°) with shoals and build-ups

The geometry forming depositional elements within each platform are discussed in Chapter 5, and are summarised in Table 6.2.



**Table 6.2: Summary information of the Upper Cretaceous Carbonate Platforms of the Tremp Basin in the South-Central Pyrenees and their geometry forming depositional elements.**

Platform	Congost A	Congost B	Sant Corneli	Bastus
<b>Age / Duration</b>	Mid Turonian (~1.6 My)	Late Turonian-Early Coniacian (~1.4 My)	Coniacian (~2.4 My)	Santonian (~3 My)
<b>Platform Shape (Ramp/Rimmed etc.)</b>	Rimmed Shelf	Rimmed Shelf	Distally steepened ramp?	Rimmed Shelf
<b>Platform Scale</b>	~60 km	<10 km?	~60 km	~60 km
<b>Slope Inclination</b>	<20°	<31°	1-2°?	<1°
<b>Dominating geometries /Location</b>	Platform Margin progradational clinofolds	Platform margin sigmoidal coralgall build-ups	Platform interior bioclastic shoals	Platform interior shoals and biostromes, platform margin composite build-ups and bioclastic shoals
<b>Geometry forming process</b>	Platform progradation; productivity	Build-up growth	Hydrodynamic sorting	Carbonate productivity; margin and interior build-ups, Hydrodynamic sorting; margin and interior shoals
<b>Depositional element scale</b>	Platform margin clinofolds (64 m wide, 10.7 m tall, <20.8° slope)	Platform margin coralgall build-ups (<200 m wide, <74 m thickness, <17° slope)	Platform interior shoals (avg. 3.8 x 0.7 km, <30 m thick units)	<ul style="list-style-type: none"> <li>Platform margin shoals: &gt;2.4 x 5.2 km depositional elements. Internally &lt;78 m wide and 3.5 m thick clinofolds (&lt;10.5°)</li> <li>Platform margin composite build-ups: &gt; 2.4 x 3.4 km, avg. 57 m thick units.</li> <li>Platform interior shoals: avg. 1.3 x 0.24 km, ca. 30 m thick units</li> <li>Platform interior build-ups: avg. 2.7 x 1.8 km, ca. 37 m thick units</li> </ul>
<b>Sequence Stratigraphic Position</b>	Late highstand	Lowstand wedge	?	Margin build-ups/shoals: Late highstand Interior build-ups: unknown Interior shoals: late highstand?
<b>Dominating Organism / Grain Type</b>	Fine to medium grained bioclasts	Corals and red algae	Coarse rudist debris	Margin build-ups: rudists and corals Interior build-ups: rudists Shoals: bioclasts and peloids
<b>Siliciclastics</b>	Trace amounts (<1%)	Trace amounts (<1%)	In platform interior shoals (<30%)	In deltaic environment (<40%), platform interior (<10%) and margin shoals (<5%)

#### 6.5.4 Discussion

The review of the relevant Cenomanian-Turonian carbonate systems of the Arabian Shelf is used below to compare these to the Cenomanian-Santonian platforms of the Tremp Basin. This discussion will evaluate similarities and differences between the platforms in time-scale, sequence stratigraphy, formation mechanism, geometry and sedimentology. This is done in

order to draw a conclusion on the applicability of the Tremp Basin carbonate platforms as outcrop analogues to the subsurface examples in the Arabian Shelf.

### **Time Scales, Sequence Stratigraphy and Regional Setting**

There are key differences in the stratigraphy of the Arabian Plate and the Pyrenean platforms. The platforms of the Tremp Basin each represent a 3<sup>rd</sup> order sea-level cycle (Chapter 4 and Simó, 1993), spanning ca. 2-3 My, the Mishrif Formation is subdivided into three (Mahdi and Aqrawi, 2014), and the Natih into three complete cycles in the Cenomanian and a truncated fourth cycle in the Turonian (Frans S. P. van Buchem, Al-Husseini, et al., 2010). Subsequently, the absolute time-spans on the Arabian Plate (2.5 - 9 My) are longer than in the Tremp basin (1.4 - 3 My). This implies more consistent depositional conditions on the Arabian shelf, leading to longer-lived platforms. The Arabian Plate was a passive margin throughout the period of deposition, although the onset of compression began closely after deposition of the Mishrif Formation (Sharland et al., 2004). In comparison, the carbonate platforms in the Tremp Basin record the transition from a passive margin to a foreland basin (Puigdefàbregas and Souquet, 1986; Vergés et al., 2002). Consequently, subsidence played a major role in generating accommodation space in the Tremp Basin, (Chapter 3), while global sea-level changes led to a lowstand wedge being deposited during the Turonian, and later successive backstepping of the platforms further landwards.

There are major differences in scale between the platforms of the Tremp Basin and those of the Arabian Shelf. While the former are estimated to have reached ca. 60 km in width, the scale of carbonate deposition on the Arabian Plate is estimated at few 1000s of kilometres. Similarly, the length is interpreted to be >2500 km, whereas the potential length of the Tremp Basin is an order of magnitude smaller. As the general topography of the platforms is interpreted to be comparably similar, showing flat tops and rimmed shelves, leading to a low-angle slope (<2 degrees), the effects on these different scales on the depositional system are possibly manifested in the width of facies belts, and in the resulting bedforms (see following section).

The role of syndepositional tectonics on the sediments of the Mishrif and Natih E, Particularly the driving mechanism behind the formation of the intrashelf basins, are not well understood (van Buchem et al., 2011). Sedimentation is interpreted to be mostly controlled by relative sea-level, although during the Turonian, influences of the Alpine-I compressional event are recognised in fault reactivation and inversion (F. S. P. van Buchem et al., 2010). The key observation in comparing the Arabian Shelf to the Tremp Basin is the advanced stage of compression taking place in the Pyrenees, whereas the Arabian Shelf is in a much earlier stage in the transition towards these conditions. Differential subsidence on the Arabian Shelf is concentrated in the intrashelf basins, whereas the Tremp Basin shows differential subsidence

on the margin and partially in the platform interior (Bastus Platform, Chapters 3 and 4). As a result, it is possible that the Bastus Platform showed higher lateral heterogeneity of facies and more abrupt facies transitions across the platform top when compared to the extensive lateral continuity in the Arabian Shelf.

### **Bedforms – Clinoforms and Shoal Bodies**

A key aspect of the comparison of both geological settings lies in the differences between the produced bedforms. In the Mishrif and Natih the best-described bedforms are large-scale (few 10s km long and up to 50 m thick), but low-angle ( $>2^\circ$ ) clinoforms. These are the result of slope progradation via basinward transport of bioclastic material on a low angle slope (Grélaud et al., 2010; Droste, 2010; Adams et al., 2011). The platform margin clinoforms of the Congost A platform are interpreted to have formed as infralittoral prograding wedges, which result in similar geometries due to basinward transport of grains by high energy events (Hernández-Molina et al., 2000). The fine-grained packstone and grainstone clinoforms are interpreted to prograde onto the slope, with sediment being sourced from the platform interior. However, the higher sedimentation rates and accommodation space generation at the Congost A margin led to much steeper ( $20^\circ$ ) and shorter (64 m) clinoforms (Chapter 5) than in the platforms of the Arabian Shelf. This highlights how the platform scale, topography and generation mechanism affect the dominant bedforms.

The few 100 metre-scale clinoforms described in the Natih Formation by Adams et al., (2011) can be compared to those of the Bastus Platform margin in terms of their mode of generation. Both are interpreted to have formed as high-energy shoal complexes, similarly to the grainstone shoals present in the modern Great Bahama Bank (cf. Chapter 5 and Allen, 1980; Harris, 2009; Rankey and Reeder, 2011).. However, the two examples show slight differences in scale and angle. The shoal bodies of the Natih are wider and lower-angle than those of the Bastus; the former show widths of few 100s metres, thicknesses of several metres and angles of  $1-5^\circ$ , and the latter widths of up to 78 metres, ca. 4 metres in thickness and angles of up to  $5-12^\circ$ .

The differences in slope angle and mud contents between the shoal complexes of the Bastus Platform and the various clinoforms of the Arabian Shield are interpreted as the result of different energy regimes, which are governed by the palaeogeographic setting. As the investigated sections of the Mishrif and Natih Formations deposit into intrashelf basins and are located away from the margin of the Arabian Shelf towards the Tethys (Frans S. P. van Buchem, Al-Husseini, et al., 2010), the energy levels here are possibly lower than those experienced by the margin of the Tresp Basin. While the Bastus Platform faces to a relatively enclosed seaway between the Atlantic and Tethys (Plaziat, 1981), there is still more connection to the open ocean and higher potential for hydrodynamic sorting and rounding at the margin. Furthermore,

the orientation of the clinoforms obliquely to the platform axis suggests the presence of margin-parallel currents (Chapter 5).

The differences in formation mechanism and energy regimes between the platform margin clinoforms also result in inherent differences in sedimentary texture and composition. The hydrodynamically formed clinoforms of the Santonian Bastus Platform margin feature good rounding and sorting, and their topsets lack mud (Chapter 5), whereas the shoal bodies described by Adams et al., (2011) are more mud-rich, implying overall lower energy conditions. The progradational clinoforms of the Arabian shelf potentially show large grain sizes and poor sorting, and are mud rich (Grelaud et al., 2006; Grélaud et al., 2010; Adams et al., 2011). The progradational clinoforms of the Congost A, however, show good sorting, but poor rounding and moderate amounts of micrite (Chapter 5). This implies that the grains have been subjected to increased mechanical abrasion and sorting during transport, which indicates that energy levels are possibly still higher than in the Arabian shelf.

### **Biogenic Build-ups**

A comparison of the build-ups in the Mishrif Formation of Iraq and the Bastus Platform in the Tremp Basin is made possible via presented literature data on the former. The platform margin sections of the Bastus Platform (Carreu, Montagut and Collades, respective 1:500 logs; Appendix) show well-organised and bedded facies, with sharp bedding planes and rapid facies transitions. The platform interior of the Bastus Platform shows both gradual transitions between lagoonal nodular wackestones and platform interior rudist biostromes, as well as sharply overlying reworked sandstones and quartz-rich bioclastic grainstones (Oliana section). In core, the platform interior deposits in Isona show disorganised floatstones and rudstones gradually passing into nodular wackestones and packstones with abundant planktonic foraminifera. These wackestones and float-rudstones are largely comparable to those described in the Mishrif Formation, which also show disorganised, rudist-debris rich bioclastic facies with gradual changes in bioclast frequency and size (Mahdi, 2013; Mahdi and Aqrawi, 2014).

In the Bastus, the platform interior build-ups are interpreted to have formed thin (up to few metres), loosely bound and disorganised rudist biostromes, with a low variety of species. As the sequence stratigraphic position of these could not be established during this study (Chapter 4), it is suggested that their establishment may have been opportunistic and their presence short-lived, as discussed by Ross and Skelton (1993). Laterally, they reach few km in strike (< 4.1 km), and while their width is not measured in the field, they are interpreted to be lenticular, with the width being ca. 1.5-2.5 times smaller than the length (Chapter 5). The main difference of the Mishrif Formation to the Tremp Basin lies in the absence of sharply interbedded sandstones and

quartz-rich grainstones, as seen in Oliana. This is interpreted to be the result of the more prevalent siliciclastic system in the Tremp Basin, as discussed in the following section.

The Pyrenean and Arabian platforms further show a key difference in rudist and coral fauna. This is likely the result of the stratigraphic difference, with major developments in rudist and coral communities occurring during this time. The recumbent rudists of the Mid-Cretaceous replaced by elevators following the OAE2 at the Cenomanian-Turonian Boundary (Ross and Skelton, 1993). During the Mishrif and Natih Formations, recumbent rudists are the most prolific forms on the Arabian Shelf. These have lower potential of forming elevations or distinct depositional elements (Ross and Skelton, 1993; Gili et al., 1995; Skelton et al., 1997; Sanders, 1998). Conversely, elevating rudists are the most common form in the Tremp Basin throughout the Upper Cretaceous. These have been shown to be able to form topography due to their higher tolerance to sediment influx, compared to recumbent variants (Ross and Skelton, 1993; Gili et al., 1995; Skelton et al., 1997; Sanders, 1998). Additionally, communities of corals and rudists are more common in the Tremp basin. The cohabitation with corals is interpreted to lead to more effective sediment binding, and results in steeper build-up morphologies, for example in the deposition of massive boundstones (platform margin build-ups of the Bastus Platform) as opposed to loosely arranged floatstones (Mishrif, Natih). In the Mishrif formation, only specific intervals show higher concentrations of corals, whereas in the remainder corals are rare. The Natih Formation behaves similarly, with corals only occurring as solitary, rare individuals.

### **Siliciclastic Contents and Effects on Carbonate Productivity and Geometries**

A noticeable difference between the Pyrenean platforms and the Mishrif and Natih Formations lies in the presence and nature of siliciclastics. It was established that a continuous influx of siliciclastics occurred into the Tremp basin, with increasing volume over the course of the Upper Cretaceous due to the rising hinterland (Chapter 3). Quartz grains are introduced into the in the Bastus Margin packstone-grainstone shoals through gradual winnowing, and are generally not present in high amounts in the in-situ producing facies, having little effect on productivity. In the platform interior, some rudist biostromes are sharply overlain by siliciclastic influx, but are quick to recover. Therefore, no long-lasting effect of the siliciclastic input on the carbonate factory is recognised (Chapters 3 and 5).

In the Mishrif and Natih formations, siliciclastics vary in contents and grain size. In the Mishrif Formation of Iraq, coarse grained siliciclastics are rare, and the presence of clay is limited (Mahdi et al., 2013; Mahdi and Aqrawi, 2014). Subsequently, little effect on carbonate productivity is given. The Natih is characterised by periodic influx during the base of sequences (van Buchem, Razin, et al., 2002). The siliciclastic material is largely clay and silt-grade, implying larger distance from the proximal siliciclastic system. Carbonate productivity is restricted during

the introduction of the siliciclastic material (van Buchem, Razin, et al., 2002). This regional difference is interpreted here to result from the location of both formations in the relation to the Burgan Delta in the area of modern Kuwait, which developed during the Albian (Davies et al., 2002). The closer distance of the Mishrif Formation of Iraq translates to coarse siliciclastic input, whereas the larger distance towards the Natih in Oman results in mostly fine-grained material being introduced.

For comparing between the Tremp Basin and the Mishrif and Natih formations, it is therefore important to examine the mechanism that leads to termination of biostromes and how quickly growth resumes, and what mechanism results in clinoformal bedforms. Poisoning of the carbonate producers occurs through clay influx in the Natih Formation over a period of ca. 0.7-1.7 My, with productivity only resuming in the highstands (van Buchem, Razin, et al., 2002), whereas such long-term cessation of productivity is not observed in the Tremp Basin throughout each platform cycle. This renders a comparison between the Tremp Basin and the Natih Formation fairly difficult, as the effects of siliciclastics on the carbonate production in the Natih Formation are more long-lasting than in the Tremp Basin.

In terms of sediment composition and growth style, the rudist build-ups of the Mishrif Formation are more comparable to the platform interior build-ups of the Sant Corneli and Bastus Platforms, rather than to those of the platform margin build-ups of these platforms. However, there is a major difference here in the presence and effect of siliciclastics on carbonate production. The Bastus Platform interior build-ups are often truncated and sharply overlain by siliciclastics and reworked bioclastic material, leading to a short-lived cessation of carbonate growth. Conversely, the build-ups of the Mishrif Formation are nearly quartz-free, and unaffected by siliciclastics. It is therefore suggested that in more siliciclastic-influenced systems such as the Bastus Platform, frequent intercalation of coarse grainstones and sandstones may lead to thinner individual rudist build-ups and build-up intervals. In turn, it is likely that fluid flow properties may be significantly different than in settings where siliciclastic intercalations are missing. Here, the alternations between build-ups and sandstones/grainstones possibly show higher contrasts in porosity and permeability. These are interpreted to be mostly planar, with uncommon sigmoidal bedding in the grain-dominated facies (Chapter 5). However, the development of long-lived rudist build-ups and prograding margin clinofolds in the Mishrif and Natih Formations results in sigmoidal bedforms, showing variations between bioclastic wackestones, packstones, floatstones and rudstones with various amounts and sizes of rudist debris (e.g. Adams et al., 2011). Therefore, it is likely that the longevity of the build-ups in the Arabian Shelf is responsible for the creation of more potential fluid-baffling clinofolds. As a result, it is proposed that the lithological contrasts and bedforms between the Mishrif and Natih Formation and the Tremp Basin are considerable, and that the

Tremp Basin should be used as an analogue for other, more –siliciclastic rich platforms of similar age.

### 6.5.5 Conclusions

A number of considerations must be made when using the Carbonate Platforms of the Tremp Basin as analogues for the Cenomanian-Turonian of the Arabian Shelf:

- The Arabian Shelf and the Tremp Basin vary largely in scale (1000s km vs. 100 km). However, the slope angles are interpreted to be similar between the Cenomanian-Turonian Natih and Mishrif Formations and the Coniacian Sant Corneli and Santonian Bastus Platform (1-2°). The Bastus platform is further interpreted to have exhibited a flat top (<0.1°), and thus presents a similar topography to that of the platforms forming around the intrashelf basins of the Cenomanian-Turonian Arabian Shelf, although of significantly smaller scale.
- The main control on sedimentation in the Arabian Shelf is interpreted to lie in relative sea level, although an increasing importance of local tectonics is recognised later in the Turonian. In the Tremp Basin, the foreland basin character is reflected in highly localised subsidence across the shelf, which may have potentially led to higher lateral variability of facies – although the differences in platform scales may also be considered a cause for this.
- The clinoforms forming at the margins of the intrashelf basins of the Natih Formation are inherently different to those forming at the margins of the Congost A or Bastus Platforms in the Tremp Basin. The clinoforms in the Natih have low angle (<5°) and large lateral extent (>100 m), and are formed by progradation of the margin. The clinoforms of the Congost A are also caused by progradation of the margin, but they exhibit a much higher angle (<20.8°), smaller bioclastic grain sizes, less micrite contents and far better sorting. This hints towards larger distance from the source of bioclasts, and possibly higher energy conditions during deposition. The Bastus Platform margin clinoforms, on the other hand, are formed by localised sorting and rounding of grains through frequent hydrodynamic agitation, similar to modern day grainstone shoals of the Great Bahama Bank. Subsequently they are smaller (<5 m) and shorter (<78 m), but steeper (<10.5°) than those of the Natih.
- The differences in both clinoforms and build-ups found at the margin of the different platforms are most likely the result of the differences in energy between the basins. The intrashelf basins of the Arabian Shelf are interpreted to have been <80 m deep (Van Buchem et al., 2011), but without connectivity to the open ocean these only displayed very low energy levels towards their margins, as evident in the organic rich mudstones

of the Natih B (Van Buchem et al., 2011). The Tremp Basin was facing a narrow straight between the Tethys and Atlantic, and therefore likely showed more hydrodynamic energy at the margin.

- Data on build-ups in the Cenomanian-Turonian of the Arabian Shelf largely limited to the subsurface. Subsurface studies from the Mishrif Formation of Iraq (Mahdi et al., 2013; Mahdi and Aqrabi, 2014) suggest that the build-ups formed here as loosely bound, poorly organised biostromes in a low energy environment. These are therefore most comparable to the platform interior build-ups of the Bastus Platform (maximum 4.1 by 2.8 km wide, and several rudist generations amalgamate to ca. 25-50 m thick units).
- Differences in the main carbonate producing organisms between the Tremp Basin (elevator rudists and corals) and the Arabian Shelf (recumbent rudists) are likely to have affected the shape and size of the produced build-ups, since these organisms have different potentials to produce a rigid framework and topography.
- The mode and effect of siliciclastic input on carbonate productivity varies between the Tremp Basin, the Mishrif Formation and the Natih Formation. While the Tremp Basin shows clay-free input of coarse quartz grains, which lead to periodic cessation of carbonate productivity, the Natih Formation is affected by fine-grained input of siliciclastics which had a negative effect on productivity during the lower parts of each 3<sup>rd</sup> order cycle. Meanwhile, the Mishrif Formation was largely free of siliciclastics.

## 6.6 Outlook

The presented study has investigated the basin evolution, sequence stratigraphy and geometrical characteristics of carbonate platforms on a platform scale, as well as the facies distribution and small-scale architecture of these in greater detail. In addition, the contribution towards these topics, several recommendations for further work can be made. These are focused on the areas of improving the knowledge of carbonate geobodies, as well as implementing the gathered data into future modelling studies.

In this study, most correlations with the relative sea-level history and sequence stratigraphic interpretations were made based on sedimentary surfaces and facies trends. One of the key ways to improve these correlations would be in supporting the dataset with detailed biostratigraphic and chemostratigraphic studies. Both can provide precise control on relative ages for better correlation between localities across the basin, and absolute ages for correlation with global sea-level fluctuations. This would improve understanding of how the individual platforms react to global sea-level changes and can help pinpoint the effects of local processes. Furthermore, a better constraint of absolute ages allows more precise determination of



sedimentation rates, thus improving the calibration of the stratigraphic forward modelling algorithms.

Detailed modal analysis studies can be used to help recognise and predict certain geobodies from core data. A pilot study made during this project showed that a lateral trend in modal composition exists in the small-scale grainstone shoal clinofolds of the Bastus Platform exposed in the Carreu River (Al Rahbi, 2015). Additionally, such studies were previously conducted by other authors (Lanfranchi et al., 2011). Hence, more systematic sampling and analysis would allow more such trends to be defined, both on small vertical scale and on a larger platform-wide scale and transfer them to other subsurface examples. Additionally, a quantification of the presence of siliciclastics across the platforms has been presented in Chapter 3. With a more in-depth study of the variation of sediment fabric and mineralogy along the platform, a contribution towards the prediction of petrophysical properties within similar mixed systems can be made, as previously demonstrated by Kleipool et al. (2015).

Recent advancements in quantitative stratigraphy allow discussion as to whether perceived sequences and order in strata are truly systematic, or merely coincidental (Burgess, 2016). This method defines the Markov Order Metric for a succession of strata, which quantifies the probability of a succession of strata to be systematically ordered or merely coincidental. For the interest of properly identifying stratigraphic patterns within the sedimentary logs recorded in this study, it is suggested for quantitative analysis as per Burgess (2016) to be conducted on the logged sections to optimise recognition of patterns and potentially refine interpretations. Notably, the Bastus Platform margin transect at the Carreu River section was analysed by Burgess (2016) based on the data presented by Pomar et al. (2005). It was concluded that the stratal pattern interpreted by Pomar et al. (2005) are likely to be coincidental, rather than cyclical. However, it must be noted that the interpretation of Pomar et al. (2005) was made on the platform margin sections only, and is not agreed with in this study, which incorporates the basinal and platform interior sections. Furthermore, this study does not agree with the interpretations of Pomar et al. (2005) regarding the substantial change in carbonate producing organism, and associates the facies changes with changes in water depths and the progradation/retrogradation of the margin. Considering these differences to previous interpretations of the cycles in the Carreu section, a reevaluation using the quantitative method of Burgess (2016) would prove useful in confirming the proposed sequence stratigraphic framework for the Bastus Platform and in recognising patterns in the older investigated platforms.

Stratigraphic forward modelling was successfully used to reconstruct some of the platform geometries observed in the field during this study (Chapter 4). This contributed to a definition of

the controls on platform development and architecture. The more the stratigraphic forward modelling algorithms are calibrated and refined using geological examples with an abundance of data, the better the modelling method be suited for predicting subsurface architecture where data is limited. It is therefore recommended for additional platforms to be modelled using this method, and previously modelled platforms to be revisited using the refined algorithms. Improvements to the modelling algorithm can further be made by including more precise simulation of differential subsidence across the platform and more realistic distribution of siliciclastic material, two major aspects of the platforms investigated in this study but not addressed with stratigraphic forward modelling. Such improved modelling methods may allow a reevaluation of the sequence stratigraphic interpretations made on the Bastus Platform, as well as allow testing such interpretations for other carbonate systems.

## 6.7 Conclusions

This study aimed to define the geometries and controls on facies distribution and sedimentary architecture on multiple scales. This is done to facilitate recognition of small-scale geobodies in the subsurface where sparse data, commonly from seismic lines and wireline logs, makes predicting these inherently difficult. As these geobodies may lead to variation in petrophysical and flow properties, their proper recognition and characterisation is imperative for integration into reservoir models for reducing reservoir risk.

The study area is located in the Tremp Basin of the South-Central Pyrenees, Spain. A succession of Cenomanian-Santonian carbonate platforms was studied. These are characterised by diverse, commonly rudist-dominated carbonate facies, with a marked increase of siliciclastic contents towards the younger platforms. Numerous outcrops along a proximal-basinal transect were investigated to establish the platform-scale sedimentology of the carbonate systems, with individual outcrops providing information on small-scale elements and processes.

The characterisation of facies distribution and sedimentary architecture was done via an integrated study. Field and map data, cross-sections, microfacies analysis and modal analysis provided a characterisation of the platform-scale sedimentology and geometry. Sequence stratigraphic interpretations were made and compared against stratigraphic forward models to investigate the controls on stratal patterns. Digital outcrop modelling was implemented to provide quantification of small-scale geobodies.

Three papers were presented, each addressing a specific aspect of characterisation of carbonate platform stratal patterns. The first paper deals with evolution on control on carbonate platform development and architecture in a foreland basin over the course of the Cenomanian-Santonian. The second paper investigated the sequence stratigraphic development of the

Santonian Bastus Platform, attempting to define the controls on sequence formation and testing this against stratigraphic forward models. The third paper addressed quantification of small-scale geobodies using digital outcrop techniques and whether their geometry can be interpreted in the subsurface.

The basin-scale study of the Santa Fe (Cenomanian), Pradina (Cenomanian-Turonian), Congost (Turonian-mid Coniacian), Sant Corneli (Coniacian), and Bastus (Santonian) Platforms provided insight on the development and reaction of the platforms to changes in relative sea-level, carbonate productivity, differential subsidence and tectonics. The margins of the platforms backstepped and their thickness increased successively following the subsidence of the basin and relative sea-level rise. A fault-controlled margin established in the Santa Fe Platform, followed by the Pradina Platform depositing as a pelagic drape following the Turonian OAE. The Congost Platform is divided into a lower part controlled by a margin of prograding fine grained packstone-grainstone clinofolds, and an upper part acting as a lowstand wedge with a steep ( $<30^\circ$ ) margin of corallgal boundstones. The Sant Corneli Platform follows as a distally steepened ramp. Lastly, the Bastus Platform develops a flat top ( $<0.1^\circ$ ) and a gentle slope ( $<1^\circ$ ). Additionally, the amount of siliciclastic input increased towards the end of the Cretaceous, but posed no discernible long-time effect on carbonate productivity overall.

The sequence stratigraphic reconstruction of the Bastus Platform proposed the separation into a lower and an upper sequence, subdivided into three and two smaller-scale sequences, respectively. The lower and upper sequences are separated by a flooding surface, which is followed by a marked backstepping of the platform margin rudist build-ups and an increase in clay contents on the slope. Stratigraphic forward models constructed as part of a parallel study at the Royal Holloway University of London were compared to this interpretation to investigate which possible controls may have led to this separation into a lower and upper sequence. It was concluded that models introducing oscillations of relative sea-level did not reproduce the observed stratal geometries, whereas the sequence development was successfully modelled using changes in carbonate productivity or abrupt tectonic tilting. These results highlight how common interpretations based on a relative sea-level control on sequence stratigraphic development can be improved by considering further controls on platform development.

Quantification of build-ups and shoal bodies within the Congost (Turonian-Coniacian), Sant Corneli (Coniacian) and Bastus (Santonian) Platforms was made using digital outcrop modelling and mapping techniques. It was shown that within each platform and depositional environment, geobodies show a specific range of geometry and width-length relationships, depending on the underlying topography, depositional process, carbonate producing organism and wave energy. Comparison with literature data allowed concluding that set width-length relationships of

geobodies may exist within a single platform, but are these are only transferrable if the target platforms present similar large-scale architecture, depositional environments, carbonate factories and facies. This highlights how evaluation of geobody dimensions is inherently tied to properly identifying the architecture, sequence stratigraphic development and carbonate factories of the host platform.

The combination of these studies provides insights on the interpretation of facies architecture and depositional geometries on several scales. Investigating the Cenomanian-Santonian series of carbonate platforms through time allows assessing how their geometry changes in reaction to variations in relative sea level, changes in carbonate factories, and differential tectonics across the basin. Forward modelling has displayed how mechanisms other than relative sea-level fluctuations may have been responsible for the formation of stratal patterns. These are important considerations for future sequence stratigraphic forward studies, particularly in data-poor scenarios, in order to improve interpretations and subsequently predictions of facies architecture. Similarly, the identification of these controls on the unique characteristics of the Bastus Platform allows to better address such irregularities in other studies, where they may impede sequence stratigraphic interpretations. These characteristics include the striking lack of transgressive systems tracts, differential development of thickness and difficulty in correlating surfaces between sections as a result. On the smallest scale, the quantification of shoal and build-up bodies showed that width-length relationships are most likely unique for each case study, depending on the scale and architecture of the platform. Therefore, caution is suggested in the selection of analogues, with an emphasis necessary on ensuring the gross platform scale and architecture, as well as carbonate producing organisms and controlling sedimentary processes are comparable between the two platforms.

The platforms of the Tresp basin were compared to those of the Cenomanian-Turonian Mishrif and Natih Formations of the Arabian Shelf. This was done in order to establish the applicability of the platforms in the Tresp Basin as potential analogues to those of the Cretaceous of the Arabian Shelf. Aspects of time scales, basin dimensions and depositional controls, carbonate factories, geobody dimensions, and depositional fabrics were compared. Key differences are found in the scale of the two basins (1000s km in the Arabian Shelf vs. 100 km in the Tresp Basin), as well as in the passive nature of the Arabian Shelf compared to the compressional nature of the Tresp Basin, which resulted in more expressed differential subsidence in the latter. Furthermore, key differences between the geobodies of each basin and platform are found in height and lateral extent, as well as grain composition. It was concluded that these are the direct results of the depositional mechanisms, water energy and underlying topography. Moreover, there are differences in the type of topography forming organisms (elevator rudists and corals in the Tresp basin, as opposed to recumbent rudists in the Arabian Shelf), and the

amount of siliciclastics showing much higher in the Tresp Basin than in the Natih or Mishrif Formations. Because of these differences, it is proposed that the carbonate platforms of the Tresp Basin cannot be used as a direct analogue for the Natih or Mishrif Formations. It is recommended to use the Tresp Basin Platforms as analogues for a more similar Upper Cretaceous platform showing smaller, more siliciclastic-rich, flat-topped characteristics than those of the Arabian Shelf.

Lastly, a number of suggestions for future work are made. These include improving the sequence stratigraphic correlations within the Bastus Platform through bio- and chemostratigraphic studies. This will also provide more precise insight on the variation of sedimentation rates over the life span of the platform, which can be used to better inform the stratigraphic forward models. More systematic sampling and modal analysis can be used to produce better characterisation of the geobodies observed in outcrop, which will help identify similar geobodies in the subsurface from core data. Furthermore, it was suggested to perform a statistical analysis of the stacking pattern in each locality following the method of Burgess (2016), which is expected to help in identifying true rhythmicity within the successions and thus improve the sequence stratigraphic correlation. Lastly, it is suggested to improve on the presented forward modelling approach by integrating a more precise simulation of differential subsidence across the platform and by refining the algorithm that simulates transport of siliciclastic material across the platform.

## 6.8 References

- Aconcha, E., C. Kerans, and H. Zeng, 2008, Seismic Geomorphology Applied to Lower Glen Rose Patch Reefs in the Maverick Basin, Southwest Texas: Gulf Coast Association of Geological Societies Transactions, v. 58, p. 3–23.
- Adams, E. W., C. Grelaud, M. Pal, A. E. Csoma, O. S. Al Ja'aidi, and R. A. Hinai, 2011, Improving reservoir models of Cretaceous carbonates with digital outcrop modelling (Jabal Madmar, Oman): static modelling and simulating clinoforms: Petroleum Geoscience, v. 17, no. 3, p. 309–332, doi:10.1144/1354-079310-031.
- Adams, E. W., J. P. Grotzinger, W. a. Watters, S. Schröder, D. S. McCormick, and H. a. Al-Siyabi, 2005, Digital characterization of thrombolite-stromatolite reef distribution in a carbonate ramp system (terminal Proterozoic, Nama Group, Namibia): AAPG Bulletin, v. 89, no. 10, p. 1293–1318, doi:10.1306/06160505005.
- Allen, J. R. L., 1980, Sand waves: A model of origin and internal structure: Sedimentary Geology, v. 26, no. 4, p. 281–328, doi:10.1016/0037-0738(80)90022-6.
- Anell, I., and I. Midtkandal, 2015, The quantifiable clinothem - types, shapes and geometric relationships in the Plio-Pleistocene Giant Foresets Formation, Taranaki Basin, New Zealand: Basin Research, p. 1–21, doi:10.1111/bre.12149.
- Aqrawi, A. A. M., 2010, Characterisation of the Mid-Cretaceous Mishrif Reservoir of the Southern Mesopotamian Basin, Iraq, *in* AAPG GEO Middle ...
- Aqrawi, A. A. M., J. C. Goff, a D. Horbury, and F. N. Sadooni, 2010, The Petroleum Geology of Iraq: Scientific Press, p. 424.
- Aqrawi, A. A. M., G. A. Thehni, G. H. Sherwani, and B. M. A. Kareem, 1998, Mid-cretaceous rudist-bearing carbonates of the Mishrif Formation: an important reservoir sequence in the Mesopotamian Basin, Iraq: Journal of Petroleum Geology, v. 21, no. 1, p. 57–82,

doi:10.1111/j.1747-5457.1998.tb00646.x.

- Bordenave, M. L., and J. A. Hegre, 2005, The influence of tectonics on the entrapment of oil in the Dezful Embayment, Zagros Foldbelt, Iran: *Journal of Petroleum Geology*, v. 28, no. 4, p. 339–368, doi:10.1111/j.1747-5457.2005.tb00087.x.
- van Buchem, F. S. P., D. Baghbani, et al., 2010, Barremian - Lower Albian sequence-stratigraphy of southwest Iran (Gadvan, Dariyan and Kazhdumi formations) and its comparison with Oman, Qatar and the United Arab Emirates: *GeoArabia Special Publication 4*, v. 2, p. 503–548.
- van Buchem, F. S. P., B. Pittet, et al., 2002, High-resolution Sequence Stratigraphic Architecture of Barremian / Aptian Carbonate Systems in Northern Oman and the United Arab Emirates (Kharaib and Shu'aiba Formations): *GeoArabia*, v. 7, no. 3, p. 461–500.
- van Buchem, F. S. P. et al., 1996, High resolution sequence stratigraphy of the Natih Formation (Cenomanian/Turonian) in northern Oman: distribution of source rocks and reservoir facies: *GeoArabia*, v. 1, no. 1, p. 65–91.
- van Buchem, F. S. P., M. I. Al-Husseini, F. Maurer, H. J. Droste, and L. A. Yose, 2010, Sequence-stratigraphic synthesis of the Barremian – Aptian of the eastern Arabian Plate and implications for the petroleum habitat: *GeoArabia Special Publication 1*, p. 9–48.
- van Buchem, F. S. P., D. Baghbani, L. Bulot, M. Caron, A. Hosseini, and B. Vincent, 2010, Sequence Stratigraphy of the Albian - Turonian Interval of Southwest Iran based on Outcrop and Subsurface Data, *in* EAGE 2nd Arabian Plate Geology Workshop: p. 24–27.
- van Buchem, F. S. P., P. Razin, P. W. Homewood, W. H. Oterdoom, and J. Philip, 2002, Stratigraphic organization of carbonate ramps and organic-rich intrashelf basins: Natih Formation (middle Cretaceous) of northern Oman: *AAPG Bulletin*, v. 86, no. 1, p. 21–53, doi:10.1306/61EEDA30-173E-11D7-8645000102C1865D.
- van Buchem, F. S. P., M. D. Simmons, H. J. Droste, and R. B. Davies, 2011, Late Aptian to Turonian stratigraphy of the eastern Arabian Plate - depositional sequences and lithostratigraphic nomenclature: *Petroleum Geoscience*, v. 17, no. 3, p. 211–222, doi:10.1144/1354-079310-061.
- Burchette, T. P., 1993, Mishrif Formation (Cenomanian-Turonian), Southern Arabian Gulf: Carbonate Platform Growth Along a Cratonic Basin Margin: Chapter 16, *in* J. Simo, R. W. Scott, and J.-P. Masse, eds., *Cretaceous carbonate platforms*: AAPG Memoir 56: Tulsa, OK, AAPG, p. 185–199.
- Burgess, P. M., 2016, Identifying Ordered Strata: Evidence, Methods, and Meaning: *Journal of Sedimentary Research*, v. 86, no. 3, p. 148–167, doi:10.2110/jsr.2016.10.
- Catuneanu, O., W. E. Galloway, C. G. S. C. Kendall, A. D. Miall, H. W. Posamentier, A. Strasser, and M. E. Tucker, 2011, Sequence Stratigraphy: Methodology and Nomenclature: *Newsletters on Stratigraphy*, v. 44, no. 3, p. 173–245, doi:10.1127/0078-0421/2011/0011.
- Closson, J., J.-Y. Chatellier, and A. Hargreaves, 2009, Carbonate Ramp Controlled by Alternate Fault Activity, Geological versus Seismic Expressions: *AAPG Search and Discovery*, v. Article #9.
- Cross, N., I. Goodall, C. Hollis, T. Burchette, H. Z. D. Al-Ajmi, I. G. Johnson, R. Mukherjee, M. Simmons, and R. Davies, 2010, Reservoir description of a mid-Cretaceous siliciclastic-carbonate ramp reservoir: Maudud Formation in the Raudhatain and Sabiriyah fields, North Kuwait: *GeoArabia*, v. 15, no. 2, p. 17–50.
- Davies, R. B., D. M. Casey, A. D. Horbury, P. R. Sharland, and M. D. Simmons, 2002, Early to mid-Cretaceous mixed carbonate-clastic shelfal systems: Examples, issues and models from the Arabian Plate: *GeoArabia*, v. 7, no. 3, p. 541–598.
- Doyle, L. J., and H. H. Roberts, 1988, *Developments in Sedimentology v42 - Carbonate – Clastic Transitions*: 1-304 p., doi:10.1016/S0070-4571(08)70162-6.
- Droste, H., 2010, High-resolution seismic stratigraphy of the Shu'aiba and Natih formations in the Sultanate of Oman: implications for Cretaceous epeiric carbonate platform systems: *Geological Society, London, Special Publications*, v. 329, no. 1, p. 145–162, doi:10.1144/SP329.7.
- Droste, H. J., 2010, Sequence-stratigraphic framework of the Aptian Shu'aiba Formation in the Sultanate of Oman: Barremian - Aptian Stratigraphy and Hydrocarbon Habitat of the

- Eastern Arabian Plate, *GeoArabia Special Publication 4*, v. 1, no. 4, p. 229–283.
- Droste, H., and M. Van Steenwinkel, 2004, *Stratal Geometries and Patterns of Platform Carbonates: The Cretaceous of Oman: Seismic imaging of carbonate reservoirs and systems: AAPG Memoir 81*, v. 81, p. 185–206.
- Embry, J. C., D. Hunt, I. Sharp, G. Casini, S. Homke, T. L. Scarrott, and M. R. Jamaledini, 2010, Constraints on regional-scale stratigraphic forward modelling in the Upper Sarvak Formation, Lurestan, Iran., *in* *Abstracts of the EAGE Second Arabian Plate Geology Workshop: Albian–Cenomanian–Turonian Carbonate–Siliciclastic Systems of the Arabian Plate*, Abu Dhabi, United Arab Emirates. *GeoArabia*, 15(1): p. 178.
- Ghabeishavi, A., H. Vaziri-Moghaddam, A. Taheri, and F. Taati, 2010, Microfacies and depositional environment of the Cenomanian of the Bangestan anticline, SW Iran: *Journal of Asian Earth Sciences*, v. 37, no. 3, p. 275–285, doi:10.1016/j.jseaes.2009.08.014.
- Gili, E., P. W. Skelton, E. Vicens, and A. Obrador, 1995, Corals to rudists—an environmentally induced assemblage succession: *Palaeogeography, Palaeoclimatology, Palaeoecology*, v. 119, no. 1–2, p. 127–136, doi:10.1016/0031-0182(95)00064-X.
- Gradstein, F. M., G. Ogg, and M. Schmitz, 2012, *The Geologic Time Scale 2012 2-Volume Set*: elsevier.
- Grélaud, C., 2005, *Enregistrement Stratigraphique des phases d’émersion sur Les Plates-Formes Carbonatees. Une étude intégrée à l’affleurement et en sismique de la plate-forme cénomaniennne d’Oman (Natih Fm).*: 285 p.
- Grélaud, C., P. Razin, and P. Homewood, 2010, Channelized systems in an inner carbonate platform setting: differentiation between incisions and tidal channels (Natih Formation, Late Cretaceous, Oman): *Geological Society, London, Special Publications*, v. 329, no. 1, p. 163–186, doi:10.1144/SP329.8.
- Grélaud, C., P. Razin, P. W. Homewood, and a. M. Schwab, 2006, Development of Incisions on a Periodically Emergent Carbonate Platform (Natih Formation, Late Cretaceous, Oman): *Journal of Sedimentary Research*, v. 76, no. 4, p. 647–669, doi:10.2110/jsr.2006.058.
- Handford, C., and R. G. Loucks, 1993, Carbonate Depositional Sequences and Systems Tracts—Responses of Carbonate Platforms to Relative Sea-Level Changes, *in* R. G. Loucks, and J. F. Sarg, eds., *Carbonate Sequence Stratigraphy: Recent Developments and Applications: AAPG*, p. 3–40, doi:10.1306/M57579C1.
- Harris, P. M., 2009, Depositional environments of carbonate platforms: *Search and Discovery*, v. Article #6, p. 31–60.
- Hernández-Molina, F. J., L. M. Fernández-Salas, F. Lobo, L. Somoza, V. Díaz-del-Río, and J. M. Alveirinho Dias, 2000, The infralittoral prograding wedge: a new large-scale progradational sedimentary body in shallow marine environments: *Geo-Marine Letters*, v. 20, no. 2, p. 109–117, doi:10.1007/s003670000040.
- Hollis, C., 2011, Diagenetic controls on reservoir properties of carbonate successions within the Albian-Turonian of the Arabian Plate: *Petroleum Geoscience*, v. 17, no. 3, p. 223–241, doi:10.1144/1354-079310-032.
- Homewood, P., P. Razin, C. Grélaud, H. Droste, V. Vahrenkamp, M. Mettraux, and J. Mattner, 2008, Outcrop sedimentology of the Natih Formation, northern Oman: A field guide to selected outcrops in the Adam Foothills and Al Jabal al Akhdar areas: *GeoArabia*, v. 13, no. 3, p. 39–120.
- Hughes Clarke, M. W., 1988, Stratigraphy and rock unit nomenclature in the oil-producing area of interior Oman: *Journal of Petroleum Geology*, v. 11, no. 1, p. 5–60, doi:10.1111/j.1747-5457.1988.tb00800.x.
- Hunt, D., and M. E. Tucker, 1992, Stranded parasequences and the forced regressive wedge systems tract: deposition during base-level fall: *Sedimentary Geology*, v. 81, no. 1–2, p. 1–9, doi:10.1016/0037-0738(92)90052-S.
- Immenhauser, A., B. Van Der Kooij, A. Van Vliet, W. Schlager, and R. W. Scott, 2002, An ocean-facing Aptian-Albian carbonate margin, Oman: *Sedimentology*, v. 48, no. 6, p. 1187–1207, doi:10.1046/j.1365-3091.2001.00416.x.
- Janson, X., K. Lee, C. Zahm, and C. Kerans, 2015, Ground-penetrating radar imaging of Albian rudist buildups, central Texas: *Interpretation*, v. 3, no. 3, p. SY67-SY81, doi:10.1190/INT-

2014-0273.1.

- Jung, A., and T. Aigner, 2012, Carbonate Geobodies: Hierarchical Classification and Database - A New Workflow for 3D Reservoir Modelling: *Journal of Petroleum Geology*, v. 35, no. 1, p. 49–65, doi:10.1111/j.1747-5457.2012.00518.x.
- Jung, A., T. Aigner, D. Palermo, S. Nardon, and M. Pontiggia, 2012, A new workflow for carbonate reservoir modelling based on MPS: shoal bodies in outcrop analogues (Triassic, SW Germany): *Geological Society, London, Special Publications*, v. 370, no. 1, p. 277–293, doi:10.1144/SP370.13.
- Kennedy, W., and M. Simmons, 1991, Mid-Cretaceous ammonites and associated microfossils from the Central Oman Mountains: *Newsletters on Stratigraphy*, v. 25, no. 3, p. 127–154.
- Kleipool, L. M., J. J. G. Reijmer, B. Bádenas, and M. Aurell, 2015, Variations in petrophysical properties along a mixed siliciclastic carbonate ramp (Upper Jurassic, Ricla, NE Spain): *Marine and Petroleum Geology*, v. 68, p. 158–177, doi:10.1016/j.marpetgeo.2015.08.017.
- Lanfranchi, A., F. Berra, and F. Jadoul, 2011, Compositional changes in sigmoidal carbonate clinoforms (Late Tithonian, eastern Sardinia, Italy): insights from quantitative microfacies analyses: *Sedimentology*, v. 58, no. 7, p. 2039–2060, doi:10.1111/j.1365-3091.2011.01250.x.
- Loucks, R. G., and C. Kerans, 2003, Lower Cretaceous Glen Rose “Patch Reef” Reservoir in the Chittim Field, Maverick County, South Texas: *Gulf Coast Association of Geological Societies Transactions*, v. 53, p. 490–503.
- Mahdi, T. A., 2013, Sequence stratigraphy and reservoir characterization of the Mishrif Formation ( Middle Cretaceous ), southern Iraq: no. May.
- Mahdi, T. A., and A. A. M. Aqrabi, 2014, Sequence stratigraphic analysis of the mid-cretaceous mishrif formation, southern Mesopotamian Basin, Iraq: *Journal of Petroleum Geology*, v. 37, no. 3, p. 287–312, doi:10.1111/jpg.12584.
- Mahdi, T. A., A. A. M. Aqrabi, A. D. Horbury, and G. H. Sherwani, 2013, Sedimentological characterization of the mid-Cretaceous Mishrif reservoir in southern Mesopotamian Basin, Iraq: *GeoArabia*, v. 18, no. 1, p. 139–174.
- McNeill, D. F., K. J. Cunningham, L. a Guertin, and F. S. Anselmetti, 2004, Depositional themes of mixed carbonate-siliciclastics in the South Florida Neogene; application to ancient deposits: Integration of outcrop and modern analogs in reservoir modeling: *AAPG Memoir* 80, p. 23–43.
- Mount, J. F., 1984, Mixing of siliciclastic and carbonate sediments in shallow shelf environments: *Geology*, v. 12, no. 7, p. 432, doi:10.1130/0091-7613(1984)12<432:MOSACS>2.0.CO;2.
- Muñoz, J. A., A. Martinez, and J. Verges, 1986, Thrust sequences in the eastern Spanish Pyrenees: *Journal of Structural Geology*, v. 8, no. 3–4, p. 399–405, doi:10.1016/0191-8141(86)90058-1.
- Murris, R. J., 1980, Middle East: stratigraphic evolution and oil habitat: *AAPG Bulletin*, v. 64, p. 597–618.
- Owen, R., and S. Nasr, 1958, Stratigraphy of the Kuwait-Basra Area, *in* L. G. Weeks, ed., *AAPG Special Publication 18: Habitat of Oil*: Tulsa, OK, AAPG, p. 1252–1278.
- Philip, J., J. Borgomano, and S. Al-Maskiry, 1995, Cenomanian-Early Turonian carbonate platform of northern Oman: stratigraphy and palaeo-environments: *Palaeogeography, Palaeoclimatology, Palaeoecology*, v. 119, no. 1–2, p. 77–92, doi:10.1016/0031-0182(95)00061-5.
- Plaziat, J.-C., 1981, Late Cretaceous to Late Eocene palaeogeographic evolution of Southwest Europe: *Palaeogeography, Palaeoclimatology, Palaeoecology*, v. 36, no. 3–4, p. 263–320, doi:10.1016/0031-0182(81)90110-3.
- Pomar, L., E. Gili, A. Obrador, and W. C. Ward, 2005, Facies architecture and high-resolution sequence stratigraphy of an Upper Cretaceous platform margin succession, southern central Pyrenees, Spain: *Sedimentary Geology*, v. 175, no. 1–4, p. 339–365, doi:10.1016/j.sedgeo.2004.11.009.
- Puigdefàbregas, C., and P. Souquet, 1986, Tecto-sedimentary cycles and depositional sequences of the Mesozoic and Tertiary from the Pyrenees: *Tectonophysics*, v. 129, no. 1–4, p. 173–203, doi:10.1016/0040-1951(86)90251-9.



- Al Rahbi, B., 2015, Facies and rock property characterisation of clinoforms, Cretaceous carbonate platform, Spain: The University of Manchester.
- Rankey, E. C., and S. L. Reeder, 2011, Holocene Oolitic Marine Sand Complexes of the Bahamas: *Journal of Sedimentary Research*, v. 81, no. 2, p. 97–117, doi:10.2110/jsr.2011.10.
- Razin, P., F. Taati, and F. S. P. van Buchem, 2010, Sequence stratigraphy of Cenomanian–Turonian carbonate platform margins (Sarvak Formation) in the High Zagros, SW Iran: an outcrop reference model for the Arabian Plate: Geological Society, London, Special Publications, v. 329, no. 1, p. 187–218, doi:10.1144/SP329.9.
- Reulet, J., 1982, Carbonate reservoir in a marine shelf sequence, Mishrif Formation, Cretaceous of the Middle East, *in* Exploration for carbonate petroleum reservoirs: New York, Wiley, p. 165–173.
- Ross, D., and P. Skelton, 1993, Rudist formations of the Cretaceous: a palaeoecological, sedimentological and stratigraphical review, *in* V. P. Wright, ed., *Sedimentology Review/1*: Oxford, UK, Blackwell Publishing Ltd., doi:10.1002/9781444304534.
- Sadooni, F. N., 2005, The nature and origin of Upper Cretaceous basin-margin rudist buildups of the Mesopotamian Basin, southern Iraq, with consideration of possible hydrocarbon stratigraphic entrapment: *Cretaceous Research*, v. 26, no. 2, p. 213–224, doi:10.1016/j.cretres.2004.11.016.
- Sanders, D., 1998, Upper Cretaceous “Rudist” formations: *Geologisch-Palaeontologische Mitteilungen Innsbruck*, v. 23, p. 37–59.
- Santisteban, G., and C. Taberner, 1988, Sedimentary Models of Siliciclastic Deposits and Coral Reefs Interrelation, *in* L. J. Doyle, and H. H. Roberts, eds., *Developments in Sedimentology V42: Carbonate-Clastic Transitions*: p. 35–76, doi:10.1016/S0070-4571(08)70164-X.
- Scott, R. W., 1990, Chronostratigraphy of the Cretaceous carbonate shelf, southeastern Arabia: Geological Society, London, Special Publications, v. 49, no. 1, p. 89–108, doi:10.1144/GSL.SP.1992.049.01.07.
- Scott, R. W., J. A. T. Simo, and J.-P. Masse, 1993, Economic Resources in Cretaceous Carbonate Platforms: An Overview, *in* J. Simo, R. W. Scott, and J.-P. Masse, eds., *Cretaceous carbonate platforms: AAPG Memoir 56*: Tulsa, OK, AAPG, p. 15–23.
- Searle, M. P., C. J. Warren, D. J. Waters, and R. R. Parrish, 2004, Structural evolution, metamorphism and restoration of the Arabian continental margin, Saih Hatat region, Oman Mountains: *Journal of Structural Geology*, v. 26, no. 3, p. 451–473, doi:10.1016/j.jsg.2003.08.005.
- Sharland, P. R., D. M. Archer, R. B. Casey, S. H. Davies, A. P. Hall, A. D. Heward, A. D. Horbury, and M. D. Simmons, 2001, Arabian plate sequence stratigraphy: *GeoArabia Special Publication 2*, p. 371.
- Sharland, P. R., D. M. Casey, R. B. Davies, M. D. Simmons, and O. E. Sutcliffe, 2004, Chrono-Sequence Stratigraphy of the Arabian Plate; Mesozoic and Cenozoic, Enclosure 1: *GeoArabia*, v. 9, no. 1, p. 199–214, doi:10.1007/BF00648031.
- Sharp, I., P. Gillespie, D. Morsalnezhad, C. Taberner, R. Karpuz, J. Vergés, A. Horbury, N. Pickard, J. Garland, and D. Hunt, 2010, Stratigraphic architecture and fracture-controlled dolomitization of the Cretaceous Khami and Bangestan groups: an outcrop case study, Zagros Mountains, Iran: Geological Society, London, Special Publications, v. 329, no. 1, p. 343–396, doi:10.1144/SP329.14.
- Simmons, M. D., and M. B. Hart, 1987, The biostratigraphy and microfacies of the Early to mid-Cretaceous carbonates of Wadi Mi’aidin, Central Oman Mountains, *in* E. Horwood, ed., *Micropalaeontology of carbonate environments*: Chichester, p. 176–207.
- Simó, A., 1986, Carbonate platform depositional sequences, Upper Cretaceous, south-central Pyrenees (Spain): *Tectonophysics*, v. 129, no. 1–4, p. 205–231, doi:10.1016/0040-1951(86)90252-0.
- Simó, A., 1989, Controls on Carbonate Platforms and Basin Development: *SEPM (Society for Sedimentary Geology)*, 365-378 p., doi:10.2110/pec.89.44.
- Simó, A., 1993, Cretaceous carbonate platforms and stratigraphic sequences; south-central Pyrenees; Spain., *in* J. Simo, R. W. Scott, and J.-P. Masse, eds., *Cretaceous carbonate platforms: AAPG Memoir 56*: Tulsa, OK, AAPG, p. 325–342, doi:10.1306/M56578C1.

- Skelton, P. W., E. Gili, B. R. Rosen, and F. X. Valdeperas, 1997, Corals and rudists in the Late Cretaceous: a critique of the hypothesis of competitive displacement: *Boletín de la Real Sociedad Española de Historia Natural. Sección Geológica*, v. 92, no. 1–4, p. 225–239.
- Smith, A. B., M. D. Simmons, and A. Racey, 1990, Cenomanian echinoids, larger foraminifera and calcareous algae from the Natih Formation, central Oman Mountains: *Cretaceous Research*, v. 11, no. 1, p. 29–69, doi:10.1016/S0195-6671(05)80041-2.
- Vergés, J., M. Fernández, and A. Martínez, 2002, The Pyrenean orogen: pre-, syn-, and post-collisional evolution: *Journal of the Virtual Explorer*, v. 8, p. 55–74, doi:10.3809/jvirtex.2002.00058.
- Van Wagoner, J. C., H. W. Posamentier, R. M. Mitchum, P. R. Vail, J. F. Sarg, T. S. Loutit, and J. Hardenbol, 1988, An overview of the fundamentals of sequence stratigraphy and key definitions, *in* *Sea-Level Changes - An Integrated Approach*, SEPM Special Publication: SEPM (Society for Sedimentary Geology), p. 39–45, doi:10.2110/pec.88.01.0039.
- Warrlich, G., H. Hillgärtner, N. Rameil, J. Gittins, T. Johnson, D. Alexander, B. Wassing, M. Van Steenwinkel, and H. Droste, 2010, Reservoir characterisation of data-poor fields with regional analogues : A case study from the Lower Shu ' aiba in the Sultanate of Oman: *Geoarabia*, p. 577–604.
- Wilson, J. L., 1975, *Carbonate Facies in Geologic History*: New York, NY, Springer New York, 472 p., doi:10.1007/978-1-4612-6383-8.

## APPENDICES

### Appendix A: Localities and Map Data

#### A.1 List of Localities

A list of localities investigated in this study is given in Table A.1.1. Note that the GPS coordinates given refer to the general outcrop location. Exact starting and ending points of recorded sedimentary logs are denoted in Section B.2. For reference, an indication of interpreted gross depositional environment is given. The respective interpretations are elaborated in the main body of the work.

**Table A.1.1: List of localities investigated in this study.**

Locality	Code	Stratigraphy	Northing	Easting	Gross Depositional Environment
Camarasa	CA	Bastus Platform	41°54'47.92"N	000°51'47.18"E	Proximal Environment
Vilanova de Meià	VM	Sant Corneli Platform	42°00'46.08"N	001°02'26.81"E	Proximal Environment
Mont Rebei	MR	Santa Fe, Pradina, Sant Corneli, Bastus and Terradets platforms	42°03'50.27"N	000°40'11.78"E	Platform Interior
Oliana	OL	Bastus Platform	42°07'50.29"N	001°18'39.66"E	Platform Interior
Borrell	BL	Congost and Sant Corneli Platform	42°09'56.17"N	001°03'52.98"E	Platform Interior
Collades de Basturs	BA	Bastus Platform	42°09'53.76"N	001°02'49.95"E	Platform Margin
Gallinove North	GN	Santa Fe, Pradina and Congost Platform	42°10'57.47"N	001°04'29.74"E	Platform Margin
Gallinove South	GS	Santa Fe, Pradina and Congost Platform	42°10'45.28"N	001°04'32.03"E	Platform Margin
Montagut Gully	MG, MGL	Bastus Platform, Sant Corneli Platform	42°11'14.92"N	001°02'11.81"E	Platform Margin
Carreu River	CR	Bastus Platform	42°11'46.64"N	001°01'24.65"E	Platform Margin
Congost d'Erinyà	CE	Congost and Sant Corneli Platforms	42°17'22.68"N	000°56'16.27"E	Platform Interior (Santa Fe, Pradina), Platform Margin (Congost), Slope (Sant Corneli)
Hortonedà	HO	Congost Platform	42°15'07.07"N	001°02'38.39"E	Platform Interior
Tamurcia	TT	Sant Corneli, Bastus and Terradets Platforms	42°17'54.84"N	000°50'08.42"E	Lower Slope

#### A.2 Cross-Section Data Points

The localities and the corresponding map sheets used to construct the cross sections presented in Chapters 3 and 4 are denoted in Table A.2.1. The method of constructing the cross section is elaborated in Chapter 2.

**Table A.2.1: Cross section data points**

Locality	Northing	Easting	Map Sheet
Camarasa	41°53'48.17"N	000°54'12.23"E	Camarasa Sheet 328-1-2 (65-26)
Figuerola de Meià	41°59'39.51"N	000°55'32.08"E	Figuerola de Meià Sheet 328-1-1 (65-25)
Montsec	42°04'24.98"N	000°39'42.27"E	Calladrons - Sant Esteve de la Sarga Sheets

Locality	Northing	Easting	Map Sheet
			289-1-2 (63-24) - 289-2-2 (64-24)
Isona	42°07'28.80"N	001°03'32.33"E	Isona Sheet 290-2-1 (66-23)
Collades de Basturs	42°10'16.74"N	001°01'53.91"E	Aramunt Sheet 252-2-2 (66-22)
Montagut	42°11'13.54"N	001°02'08.91"E	Aramunt Sheet 252-2-2 (66-22)
Carreu/Pessonada	42°12'32.53"N	001°02'21.87"E	Aramunt Fu Sheet II 252-2-2 (66-22)
Barranc d'Esplugafreda	42°15'18.78"N	000°44'41.50"E	Areny Sheet 251-2-1 (64-21)
Tamurica-1	42°16'32.26"N	000°45'09.59"E	Areny Sheet 251-2-1 (64-21)
Barranc de Mirales	42°18'22.68"N	000°45'24.24"E	Areny Sheet 251-2-1 (64-21)
Serra de Sant Grevas	42°19'10.81"N	000°45'24.51"E	Areny Sheet 251-2-1 (64-21)

## Appendix B: Field Logs and Well logs

### B.1 Sedimentary Log Key

All logs use a uniform notation for lithology, sedimentary structures, allochems and fossil assemblages (Figure 6.5.5.1).

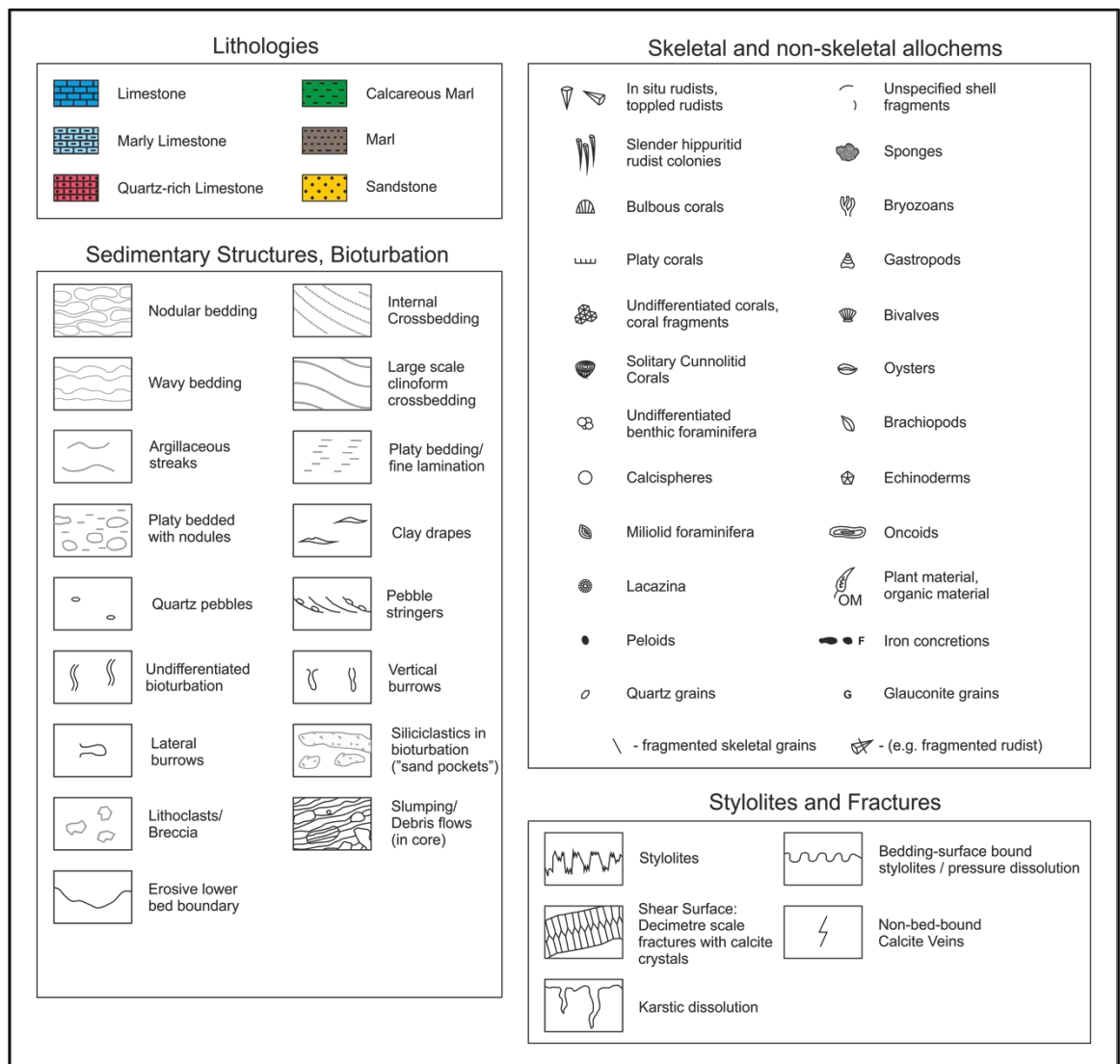


Figure 6.5.5.1: Sedimentary log key.

## B.2 Sedimentary Logs at 1:50 Scale

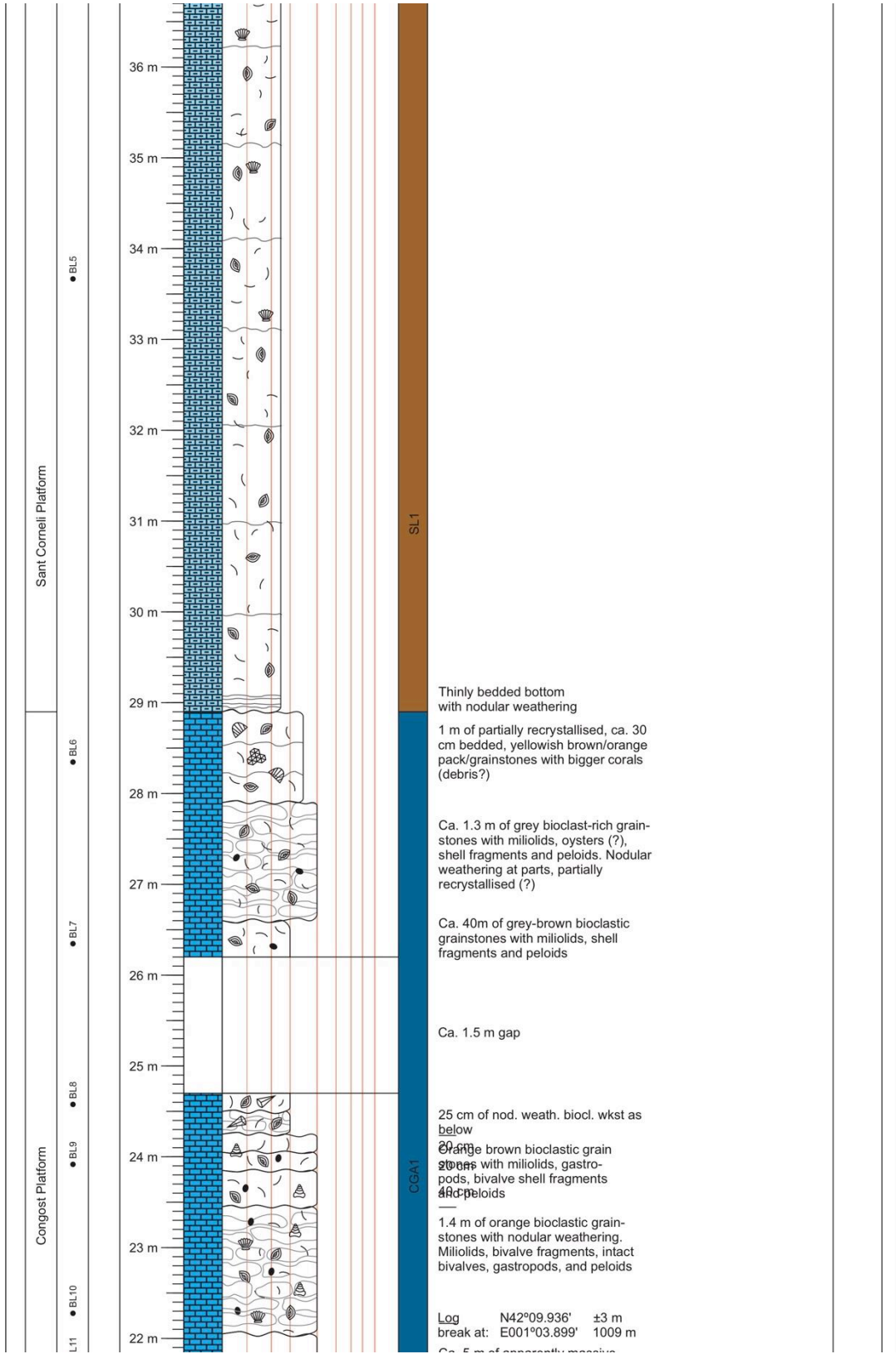
Digitalised log sections at a scale of 1:50 are presented in the following, with an overview given in [Table 6.5.5.1](#). The sedimentary logs are titled using a nomenclature consisting of the locality code (e.g. CA for Camarasa, c.f. Table A.1.1), and a lower case letter that is increased incrementally with each new log recorded at the same locality. For example, the locality Camarasa has two logs recorded: CAa and CAb. The methodology of sedimentary logging is described in Chapter 2. The origin of samples is denoted at the side of the log, and the sample nomenclature consists of the log code, followed by the number of the sample. For example, the sample with the code CAa2 is the second sample of the log CAa. A comprehensive list of samples, including specific GPS coordinates, lithology and size is given in 0.

**Table 6.5.5.1: List of logs at 1:50 scale**

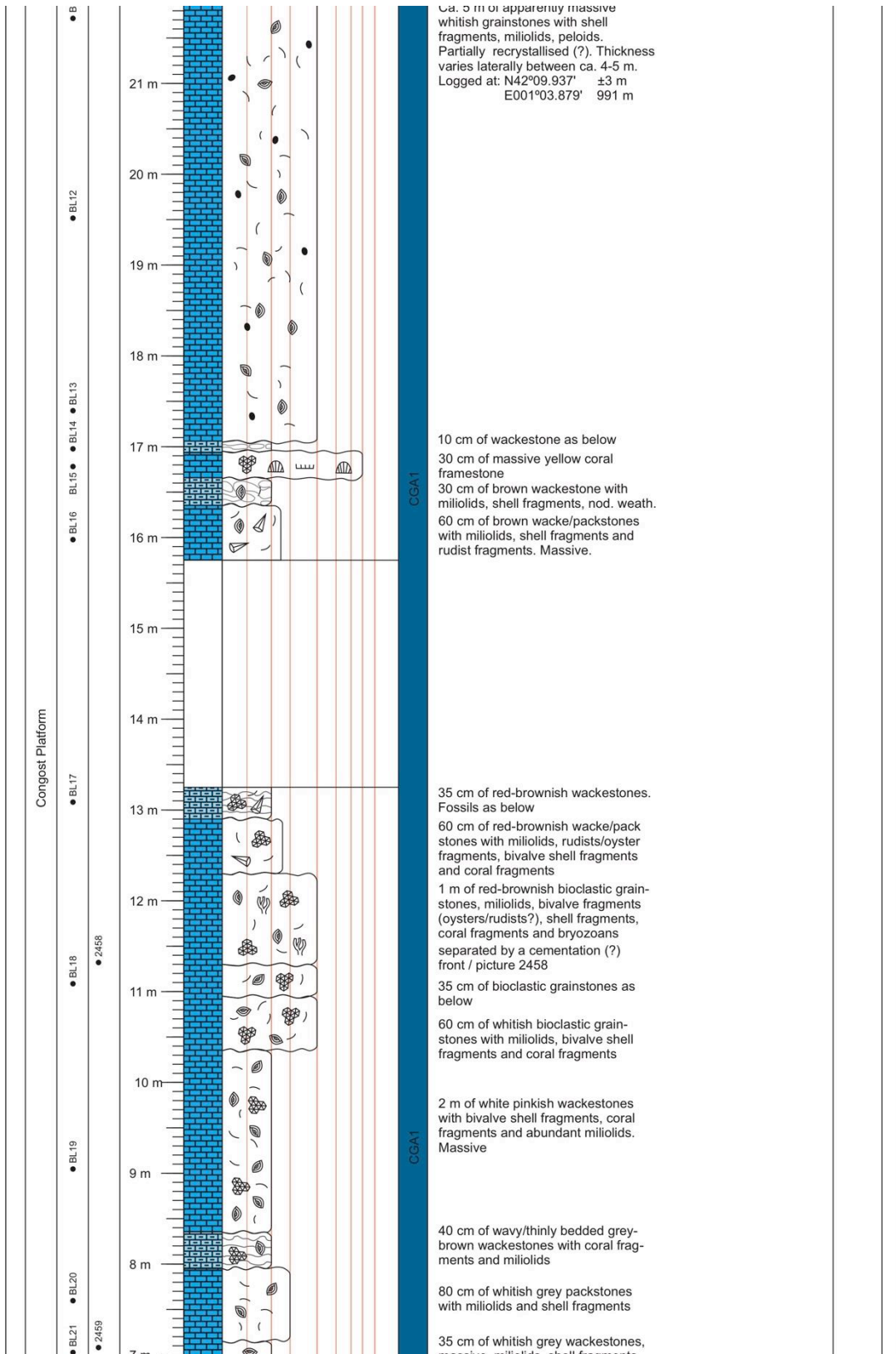
Code	Locality	Starting Point		Ending Point		Total Length [m]	Length of Gaps [m]	Net length [m]	Number of Samples [n]
		Northing	Easting	Northing	Easting				
BL	Borrell	42°09'57.0"N	001°03'51.7"E	42°19'55.5"N	001°03'53.9"E	48.2	4	44.2	24
CAa	Camarasa	41°54'52.5"N	000°51'52.1"E	41°54'56.5"N	000°51'57.2"E	23.25	0	23.25	2
CAb	Camarasa	41°54'46.8"N	000°51'44.7"E	41°54'46.1"N	000°51'42.7"E	13.6	0	13.6	3
CEa	Congost d'Erinyá	42°03'43.3"N	000°40'04.0"E	42°03'44.9"N	000°40'07.9"E	57.7	0	57.7	11
CEb	Congost d'Erinyá	42°17'16.6"N	000°56'12.8"E	42°17'12.63"N	000°56'11.6"E	71.5	3.5	68	18
CEd	Congost d'Erinyá	42°17'11.3"N	000°56'14.0"E	42°17'08.4"N	000°56'15.0"E	66.25	0	66.25	15
CRb	Carreu River	42°11'44.3"N	001°01'25.1"E	42°11'50.4"N	001°02'24.4"E	203.55	58.65	144.9	29
GNe	Gallinove North	42°10'59.4"N	001°04'23.3"E	42°10'00.0"N	001°04'23.4"E	16.85	0.5	16.35	11
GNd	Gallinove North	42°10'59.3"N	001°04'26.4"E	42°10'59.5"N	001°04'26.4"E	7.9	0	7.9	2
GNc	Gallinove North	42°10'59.9"N	001°04'27.7"E	42°10'59.9"N	001°04'27.6"E	8.35	0	8.35	4
GNb	Gallinove North	42°10'59.3"N	001°04'29.3"E	42°10'58.9"N	001°04'28.3"E	8	0	8	1
GNa	Gallinove North	42°10'57.7"N	001°04'29.4"E	42°10'57.7"N	001°04'29.4"E	4.6	0	4.6	2
GN	Gallinove North	42°10'57.4"N	001°04'30.1"E	42°10'57.2"N	001°04'30.7"E	9.8	0	9.8	5
GSc	Gallinove South	42°10'41.9"N	001°04'33.2"E	42°10'42.4"N	001°04'32.3"E	6.2	0	6.2	5
GSb	Gallinove South	42°10'43.6"N	001°04'33.0"E	42°10'43.6"N	001°04'33.0"E	3.75	0	3.75	4
GSa	Gallinove South	42°10'43.0"N	001°04'34.0"E	42°10'43.0"N	001°04'34.0"E	8.35	0	8.35	4
GS	Gallinove South	42°10'41.8"N	001°04'33.9"E	42°10'41.8"N	001°04'33.9"E	8.35	0	8.35	3
GSd	Gallinove South	42°10'43.0"N	001°04'33.2"E	42°10'43.0"N	001°04'33.2"E	7.3	0	7.3	4
HOa	Hortoneda	42°13'09.9"N	001°02'42.0"E	42°13'09.9"N	001°02'42.0"E	12.3	0	12.3	5
HOb	Hortoneda	42°15'09.5"N	001°02'38.5"E	42°15'10.9"N	001°02'39.7"E	21.25	0	21.25	13
HOc	Hortoneda	42°15'46.4"N	001°02'38.1"E	42°15'46.4"N	001°02'38.1"E	16	0	16	11
MG	Montagut Gully	42°11'07.90"N	001°02'12.0"E	42°11'10.4"N	001°02'08.2"E	56.75	16.7	40.05	26
MGa	Montagut Gully	42°11'15.2"N	001°02'17.7"E	42°11'16.1"N	001°02'12.8"E	34	0	34	14
MGb	Montagut Gully	42°11'16.5"N	001°02'12.9"E	42°11'17.0"N	001°02'12.8"E	19.4	5.5	13.9	7
MGc	Montagut Gully	42°11'16.8"N	001°02'12.5"E	42°11'17.5"N	001°02'11.8"E	19	0	19	13
MGd	Montagut Gully	42°11'16.1"N	001°02'09.7"E	42°11'16.4"N	001°02'09.7"E	10.5	0	10.5	8
MGe	Montagut Gully	42°11'18.8"N	001°02'19.1"E	42°11'19.4"N	001°02'18.8"E	18.6	0	18.6	2
MGf	Montagut Gully	42°11'17.8"N	001°02'15.6"E	42°11'18.0"N	001°02'13.6"E	42.15	0	42.15	12
MGg	Montagut Gully	42°11'11.3"N	001°02'10.6"E	42°11'12.7"N	001°02'08.3"E	72.5	3.2	69.3	14

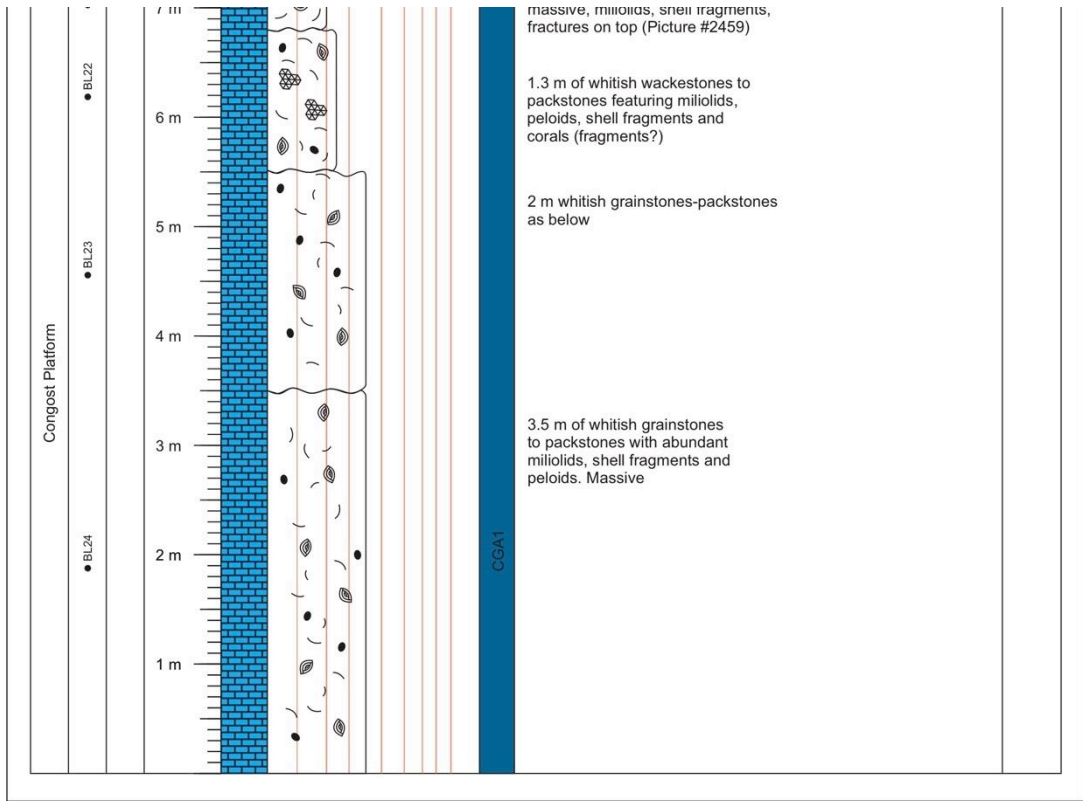
Code	Locality	Starting Point		Ending Point		Total Length [m]	Length of Gaps [m]	Net length [m]	Number of Samples [n]
		Northing	Easting	Northing	Easting				
MGh	Montagut Gully	42°11'06.9"N	001°01'57.2"E	42°11'16.5"N	001°01'54.1"E	96.45	0.5	95.95	16
MGL	Montagut Gully	42°10'49.7"N	001°02'22.0"E	42°10'50.6"N	001°02'22.1"E	17.1	0	17.1	19
MRa	Montagut Gully	42°03'43.3"N	000°40'04.0"E	42°03'44.9"N	000°40'07.9"E	44	0	44	10
MRb	Mont Rebei	42°03'15.2"N	000°40'43.1"E	42°03'15.2"N	000°40'43.1"E	12.5	1.35	11.15	8
MRc	Mont Rebei	42°03'49.9"N	000°40'09.9"E	42°03'49.9"N	000°40'09.9"E	15.45	0	15.45	3
MRd	Mont Rebei	42°03'43.3"N	000°40'04.0"E	42°03'44.9"N	000°40'07.9"E	46.4	0	46.4	15
MRe	Mont Rebei	42°03'43.3"N	000°40'04.0"E	42°11'44.9"N	000°40'07.9"E	21.9	2	19.9	12
MRf	Mont Rebei	42°03'43.3"N	000°40'04.0"E	42°03'44.9"N	000°40'07.9"E	23.3	5	18.3	3
OLa	Oliana	42°07'46.9"N	001°18'39.0"E	42°07'56.3"N	001°18'34.9"E	155.2	12.5	142.7	27
OLb	Oliana	42°07'44.7"N	001°18'37.9"E	42°07'43.9"N	001°18'36.4"E	12.5	0	12.5	3
TTa	Torre de Tamurcia	42°18'00.7"N	000°50'23.8"E	42°17'59.0"N	000°50'18.6"E	55.3	21.3	34	0
TTb	Torre de Tamurcia	42°17'57.8"N	000°50'11.9"E	42°17'51.4"N	000°50'01.7"E	136.9	28	108.9	0
VM	Vilanova de Meià	42°01'34.52"N	001°02'09.59"E	42°11'12.7"N	001°02'06.3"E	46	0	46	15



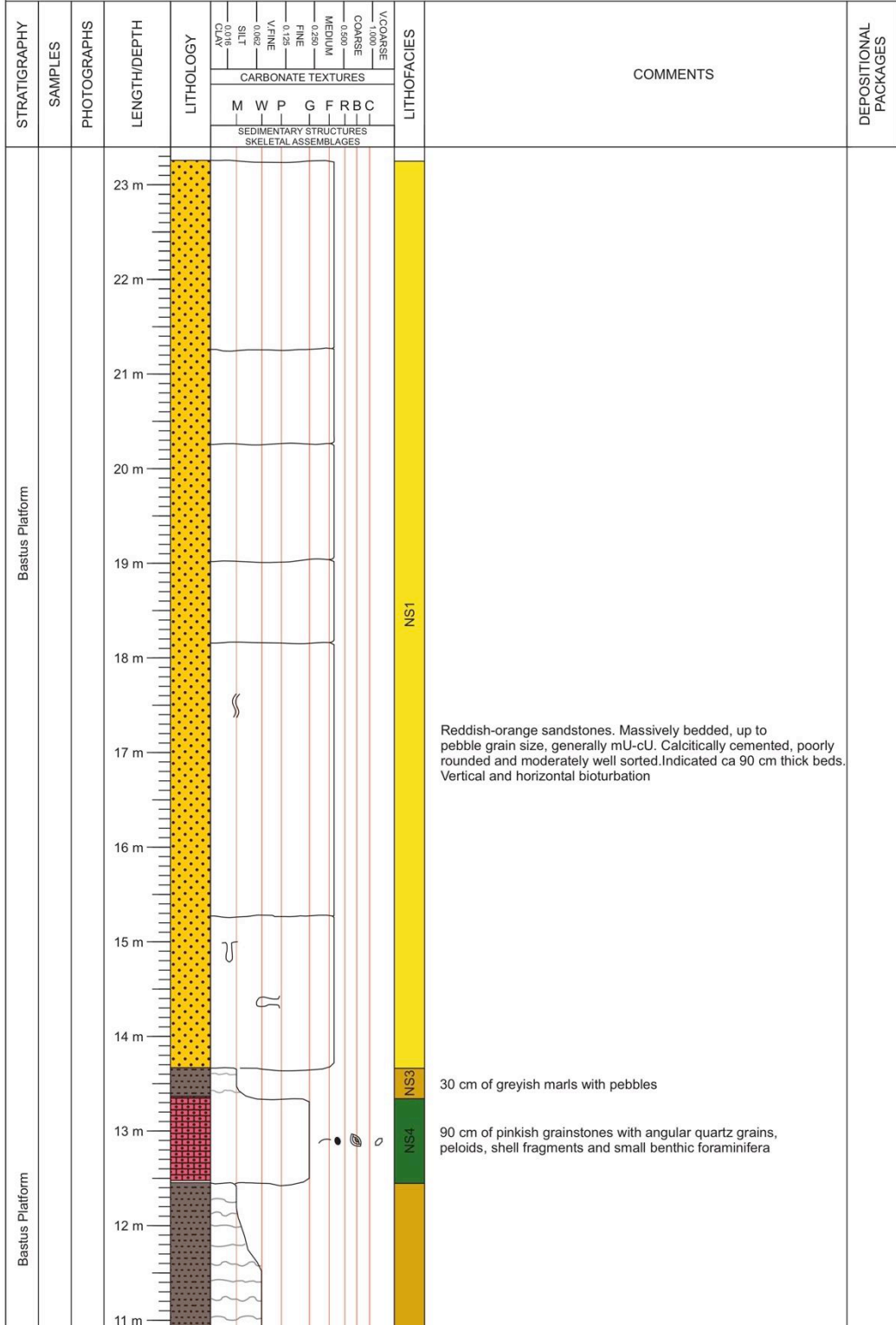


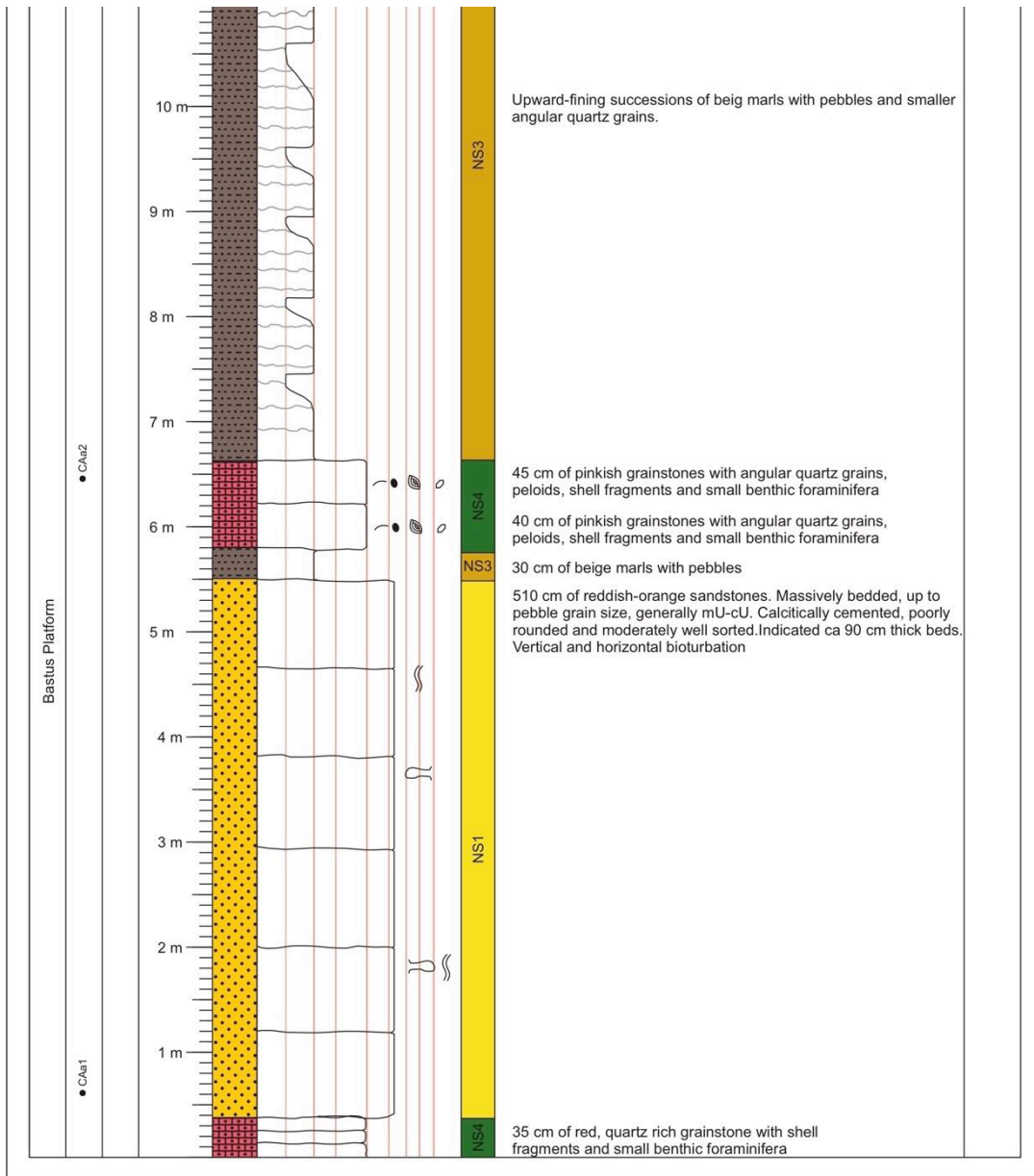






Camarasa A (CAa#) Starting 41°54'52.5"N (±3 m) Ending 41°54'56.5"N (±3 m)  
 (Logged 09/10/2015) Scale 1:50 point: 000°51'52.1"E Alt.: 438 m point: 000°51'57.2"E Alt.: 430 m



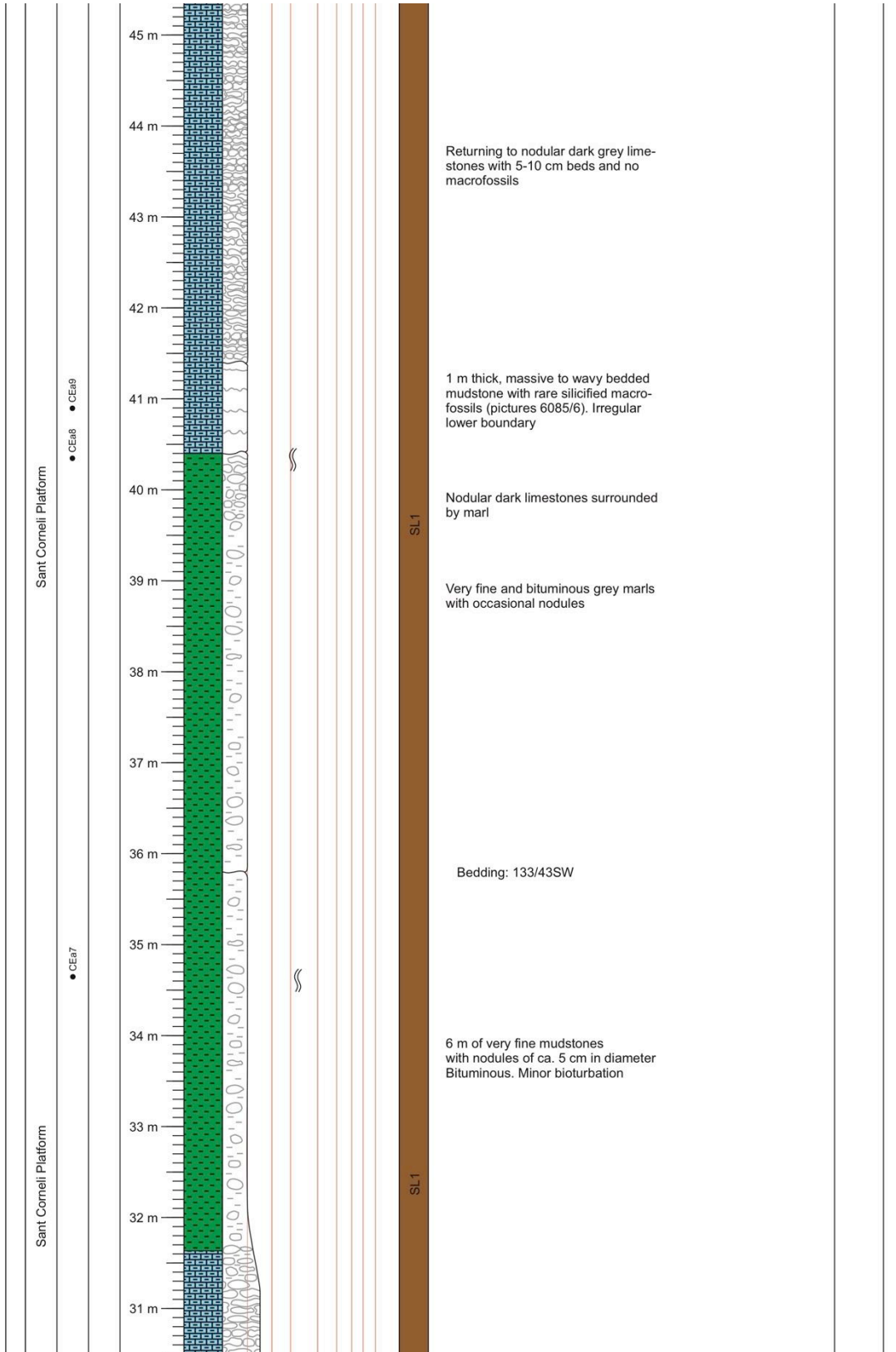


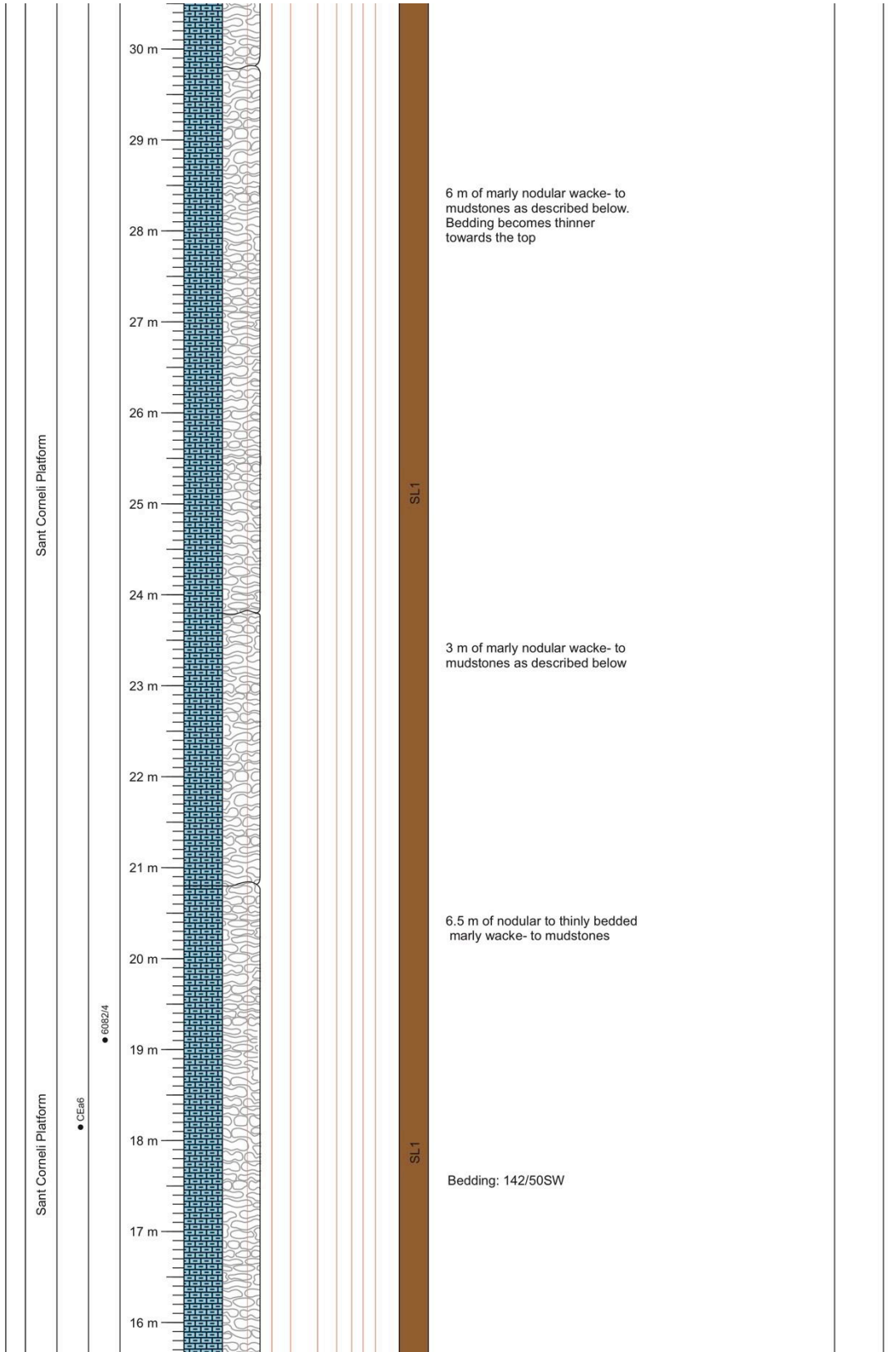
Camarasa B (CAb#) Starting 41°54'46.8"N (±3 m) Ending 41°54'46.1"N (±3 m)  
 (Logged 09/10/2015) Scale 1:50 point: 000°51'44.7"E Alt.: 453 m point: 000°51'42.7"E Alt.: 453 m

STRATIGRAPHY	SAMPLES	PHOTOGRAPHS	LENGTH/DEPTH	LITHOLOGY	LITHOFACIES		COMMENTS	DEPOSITIONAL PACKAGES
					CARBONATE TEXTURES			
					M	W P G F R B C		
					SEDIMENTARY STRUCTURES SKELETAL ASSEMBLAGES			
Bastus Platform	● CAb3		13 m			NS1	3 m of angular, moderately sorted and well cemented sandstones bedded on ca. 40 cm scale. Pebbles enriched on top surface	
			12 m				80 cm of sandstones as below with pebble stringers	
			11 m					
			10 m				140 cm of reddish, bedded sandstones. Angular, mostly well-sorted grains	
			9 m					
			8 m				160 cm of white-beige, poorly cemented and poorly sorted, angular sandstones	
			7 m				30 of well cemented and well sorted sandstone. Well sorted, angular grains	
			6 m				Beige, massive and poorly consolidated sandstones, cU-vcl. Occasional pebble stringers in cross-bedding, ripup clasts and clay drapes. Angular, poorly sorted grains	
			5 m					
			4 m					
Bastus Platform	● CAb1		3 m			NS2	250 cm alternation of reddish whitish, poorly consolidated sandstones interbedded with shales. Occasional concentrations of pebbles in bedding surfaces	
			2 m					
			1 m					

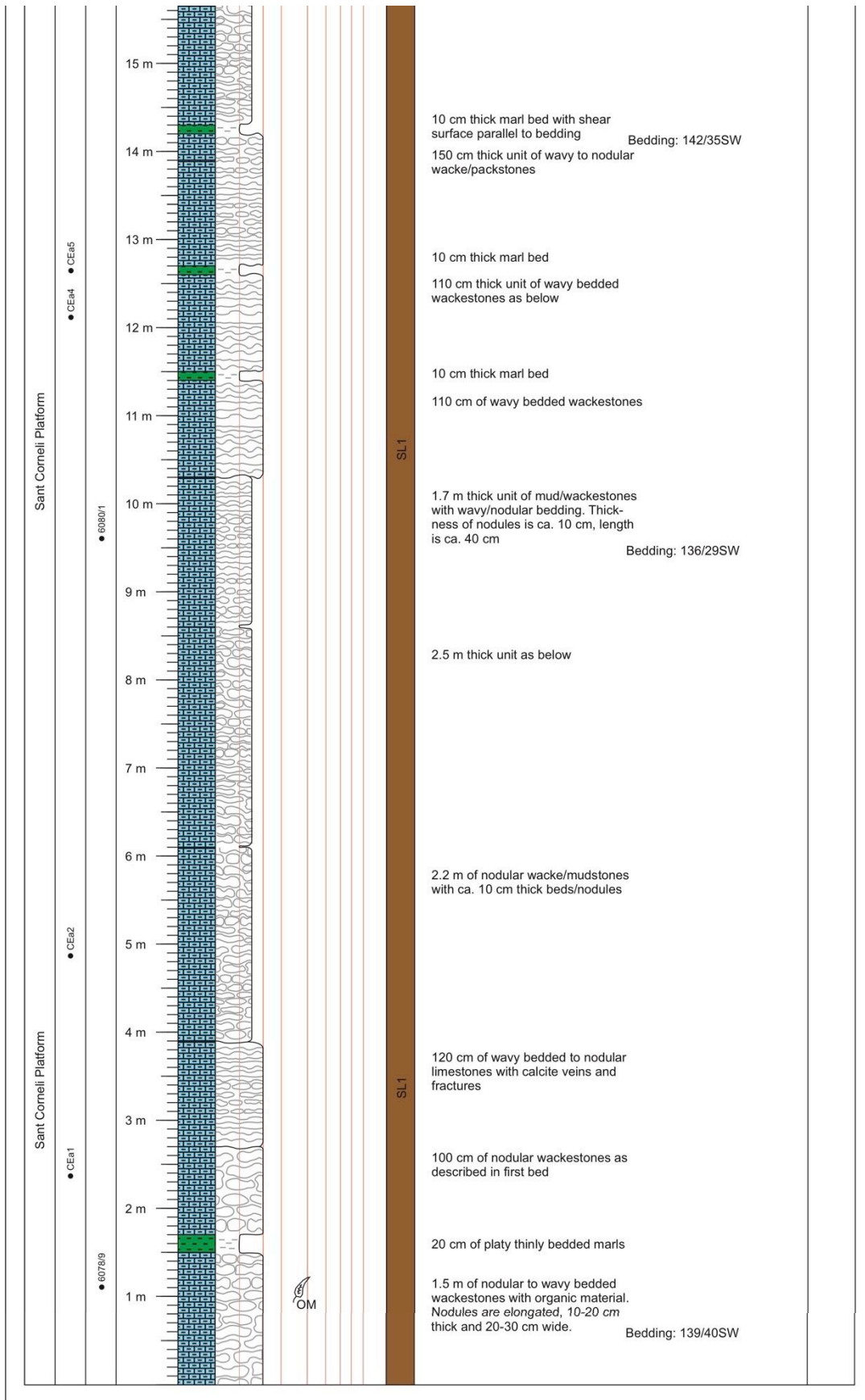
Congost d'Erinya A (CEa#) Starting 42°03'43.3"N (±10 m) Ending 42°03'44.9"N (±4 m)  
 (Logged 05/10/2014) Scale 1:50 point: 000°40'04.0"E Alt.: 541 m point: 000°40'07.9"E Alt.: 582 m

STRATIGRAPHY	SAMPLES	PHOTOGRAPHS	LENGTH/DEPTH	LITHOLOGY	LITHOFACIES										COMMENTS	DEPOSITIONAL PACKAGES
					CARBONATE TEXTURES											
					SEDIMENTARY STRUCTURES											
					SKELETAL ASSEMBLAGES											
					CLAY	SILT	V.FINE	FINE	MEDIUM	COARSE	V.COARSE					
					M	W	P	G	F	R	B	C				
Sant Corneli Platform	• CEa11		57 m												210 cm of wacke/packstones as below	
			56 m												40 cm of wacke/packstones as below 90 cm of wacke/packstones as below	
			55 m												180 cm of wacke/packstones as below	
			54 m													
			53 m												100 cm of wacke/packstones as below Bedding: 094/35SW	
			52 m													
			51 m													
			50 m													
			49 m													
			48 m												6 m of more wavy to nodular lime-stones. Rare iron concretions. Slickensides at bottom bed boundary	
Sant Corneli Platform	• CEa10	• 6087-90	47 m												Bedding: 142/28SW	
			46 m													

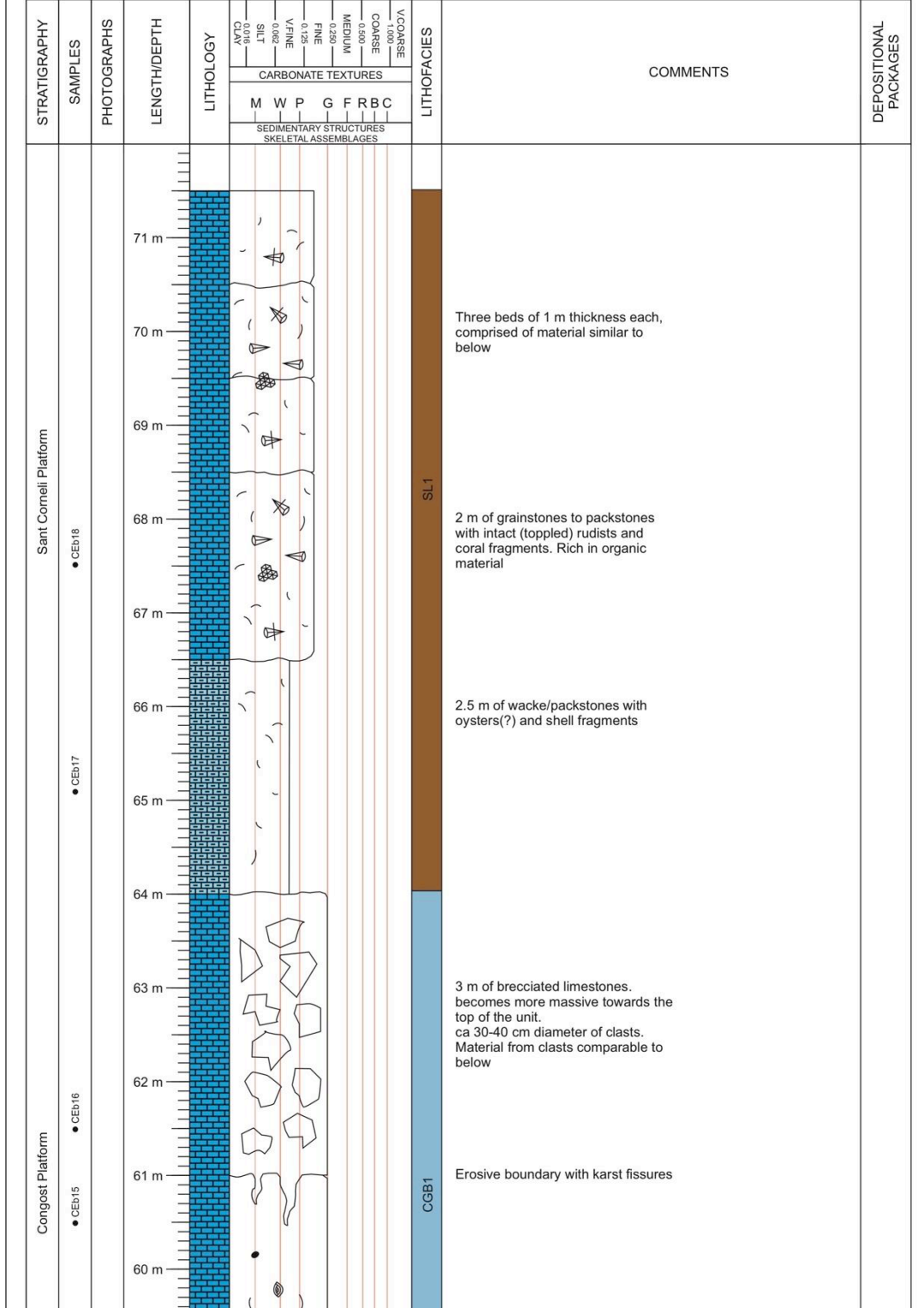


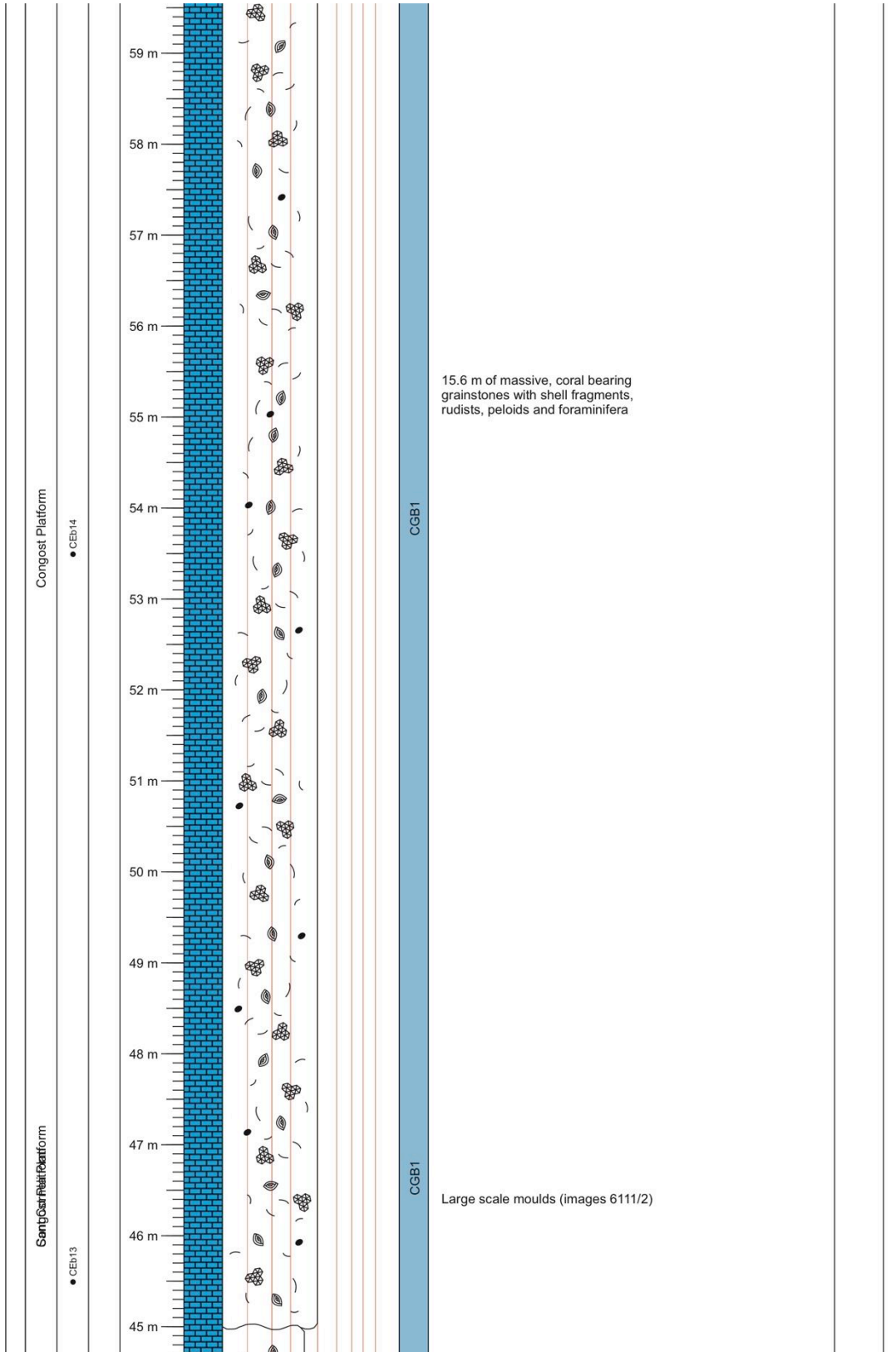






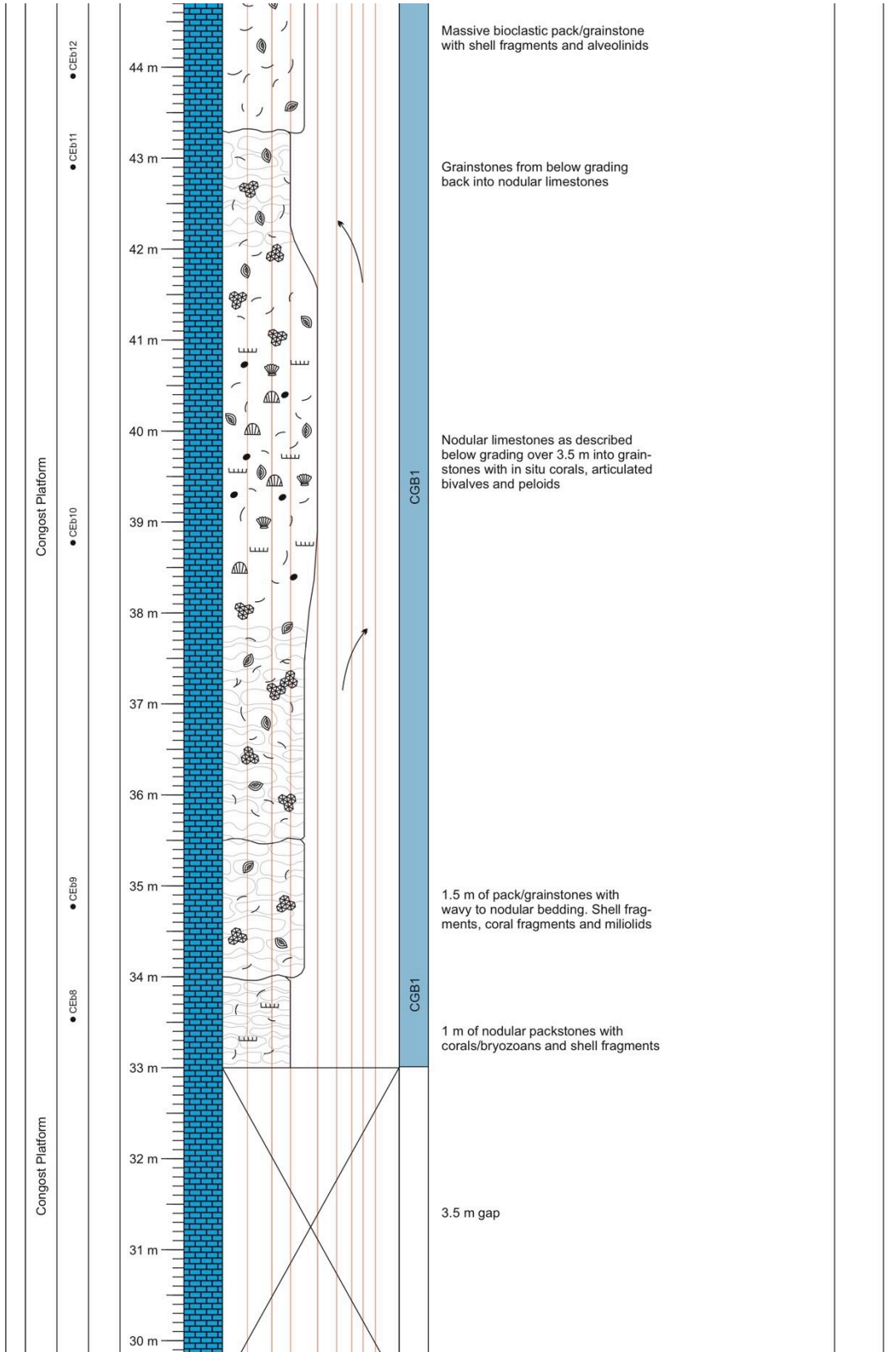
Congost d'Erinya B (CEb#) Starting 42°17'16.6"N (±4 m) Ending 42°17'12.63"N (±3 m)  
 (Logged 19/09/2014) Scale 1:50 point: 000°56'12.8"E Alt.: 666 m point: 000°56'11.6"E Alt.: 640 m

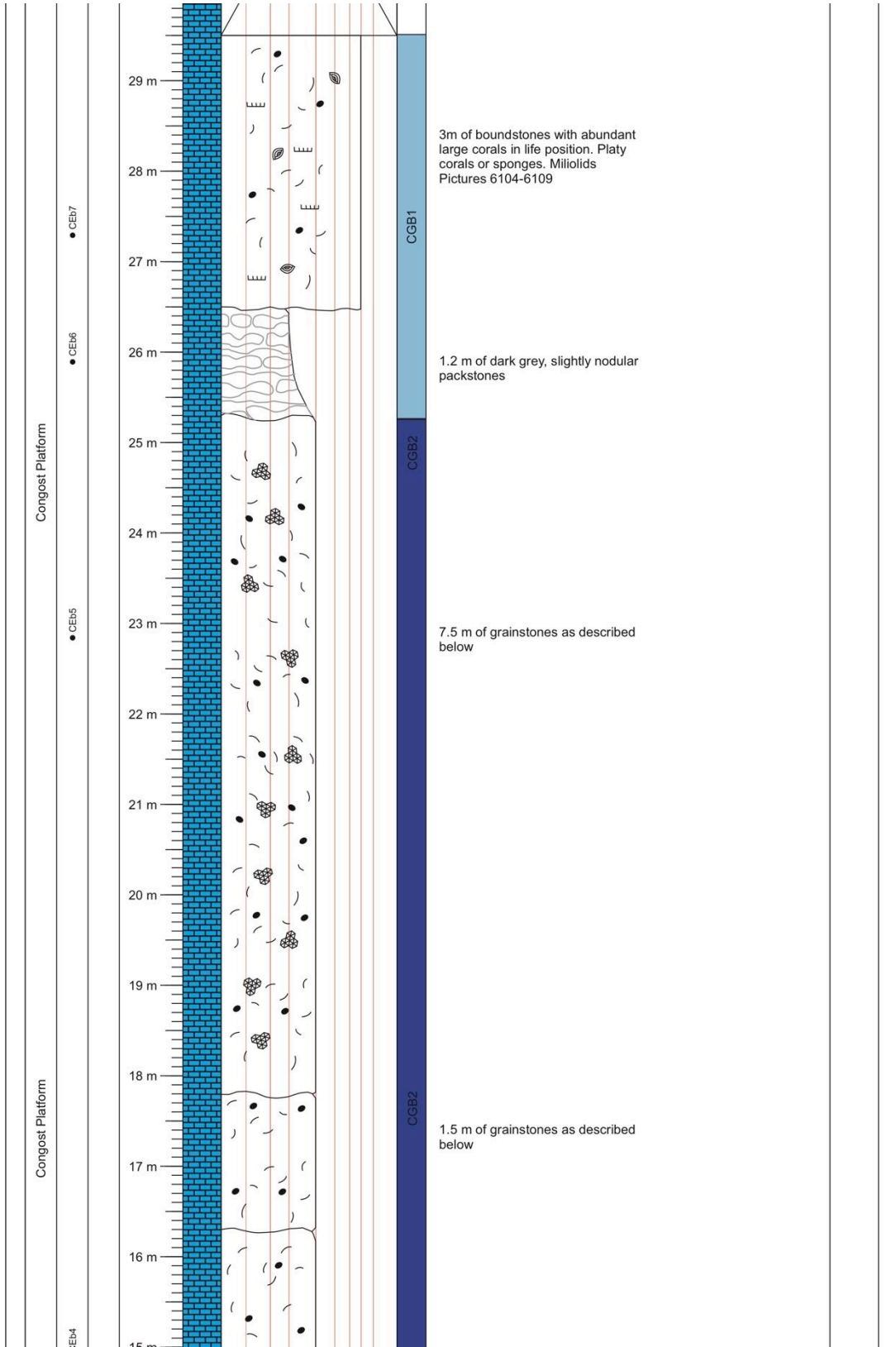


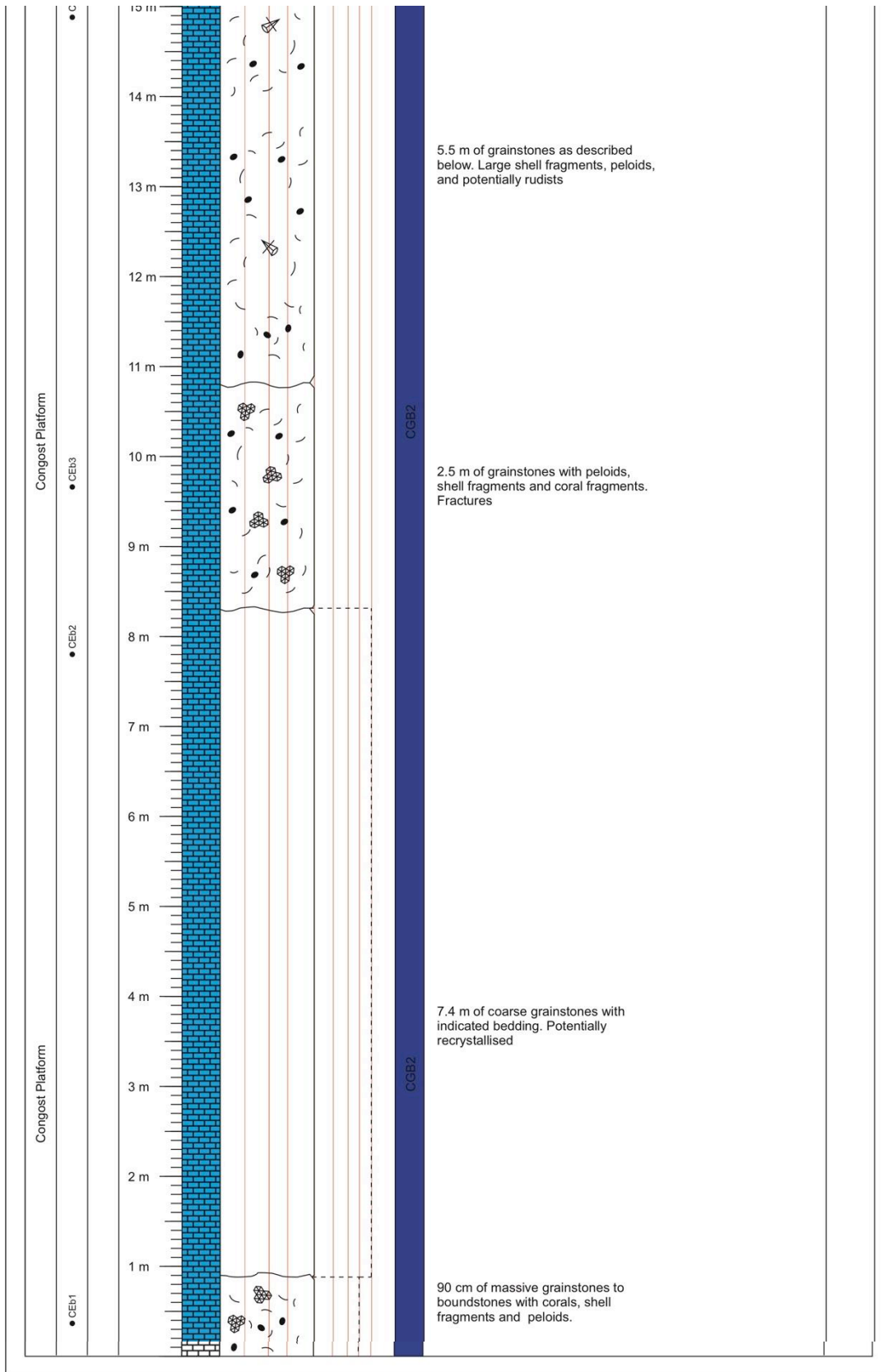


15,6 m of massive, coral bearing grainstones with shell fragments, rudists, peloids and foraminifera

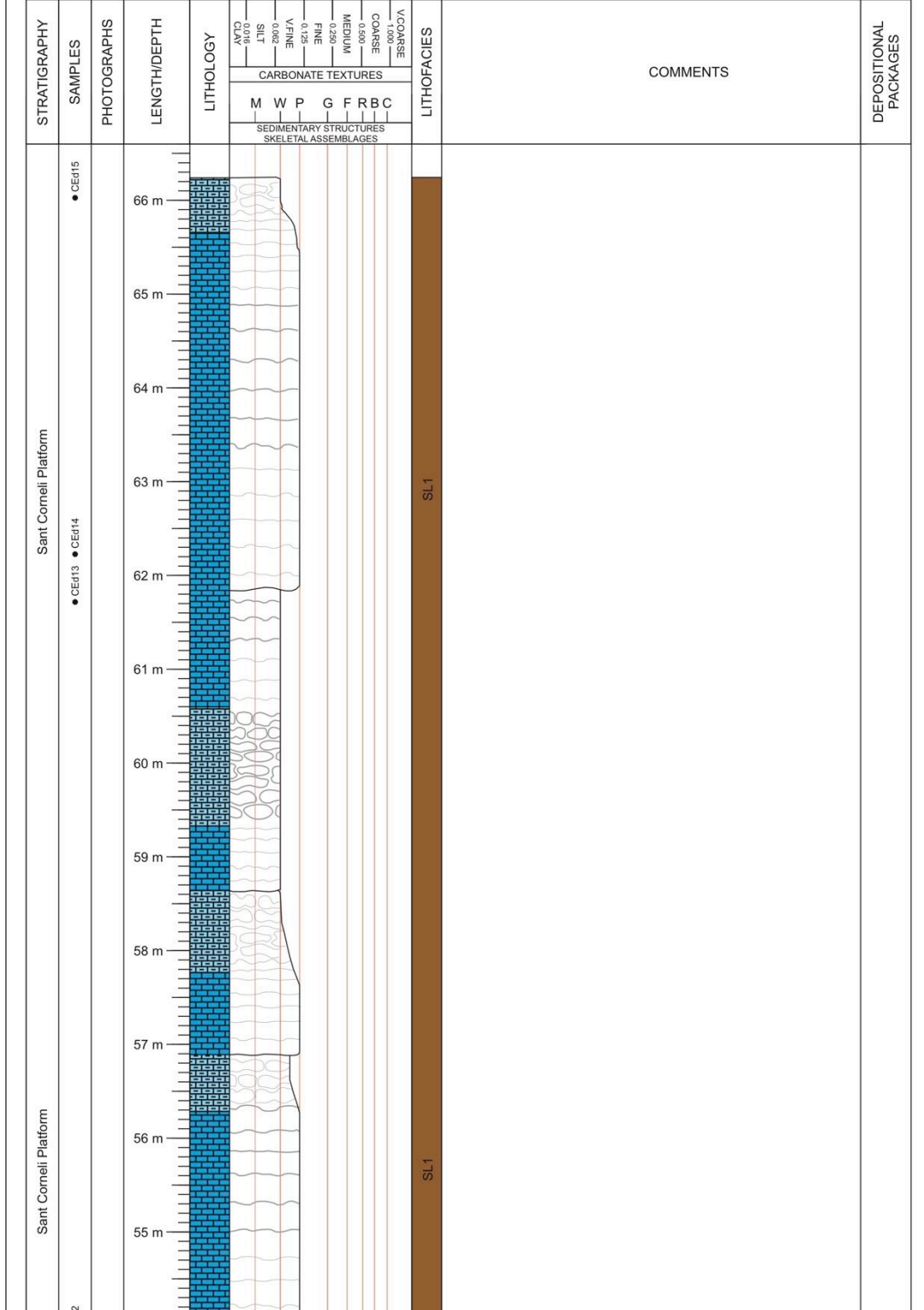
Large scale moulds (images 6111/2)

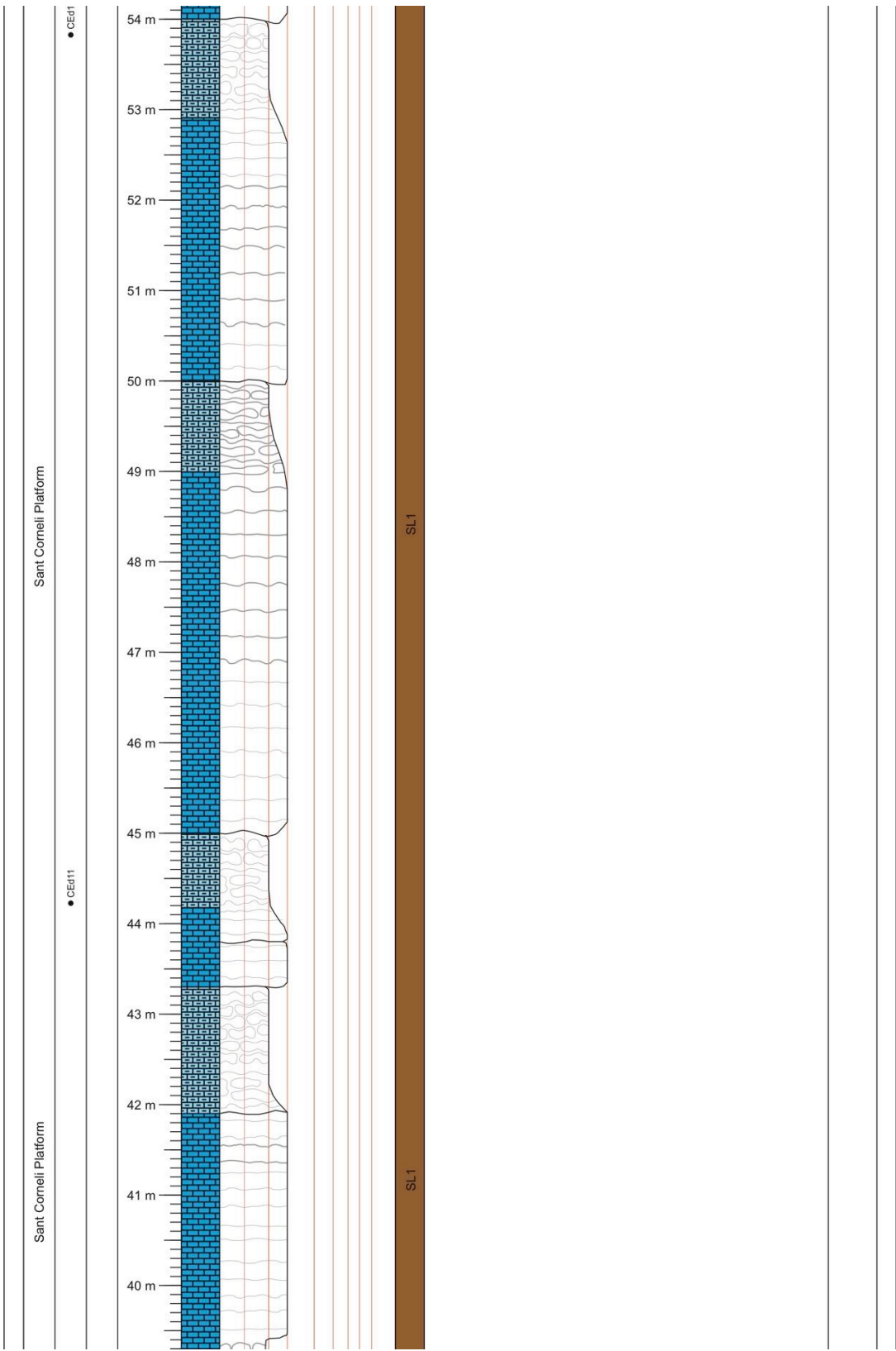




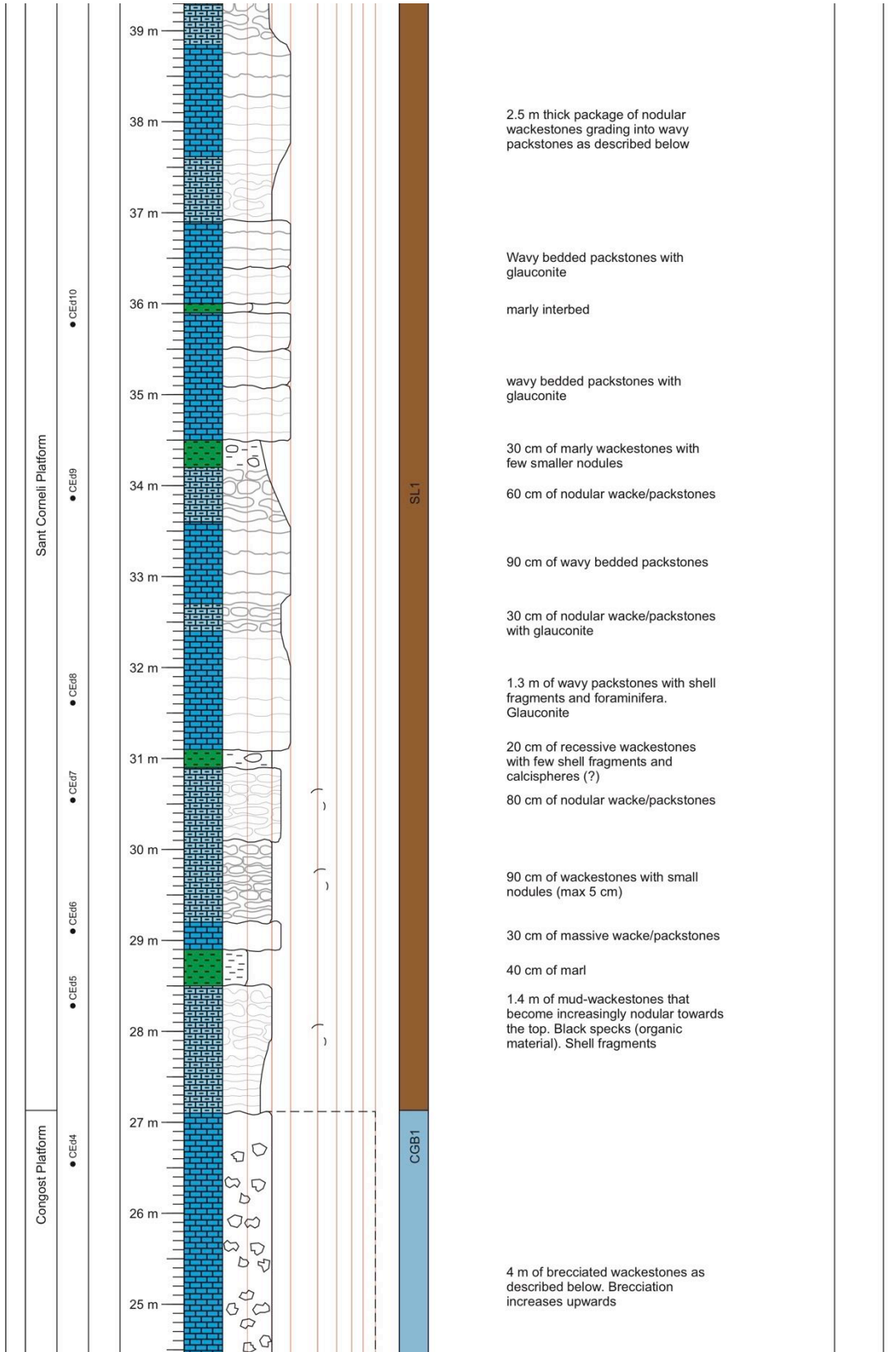


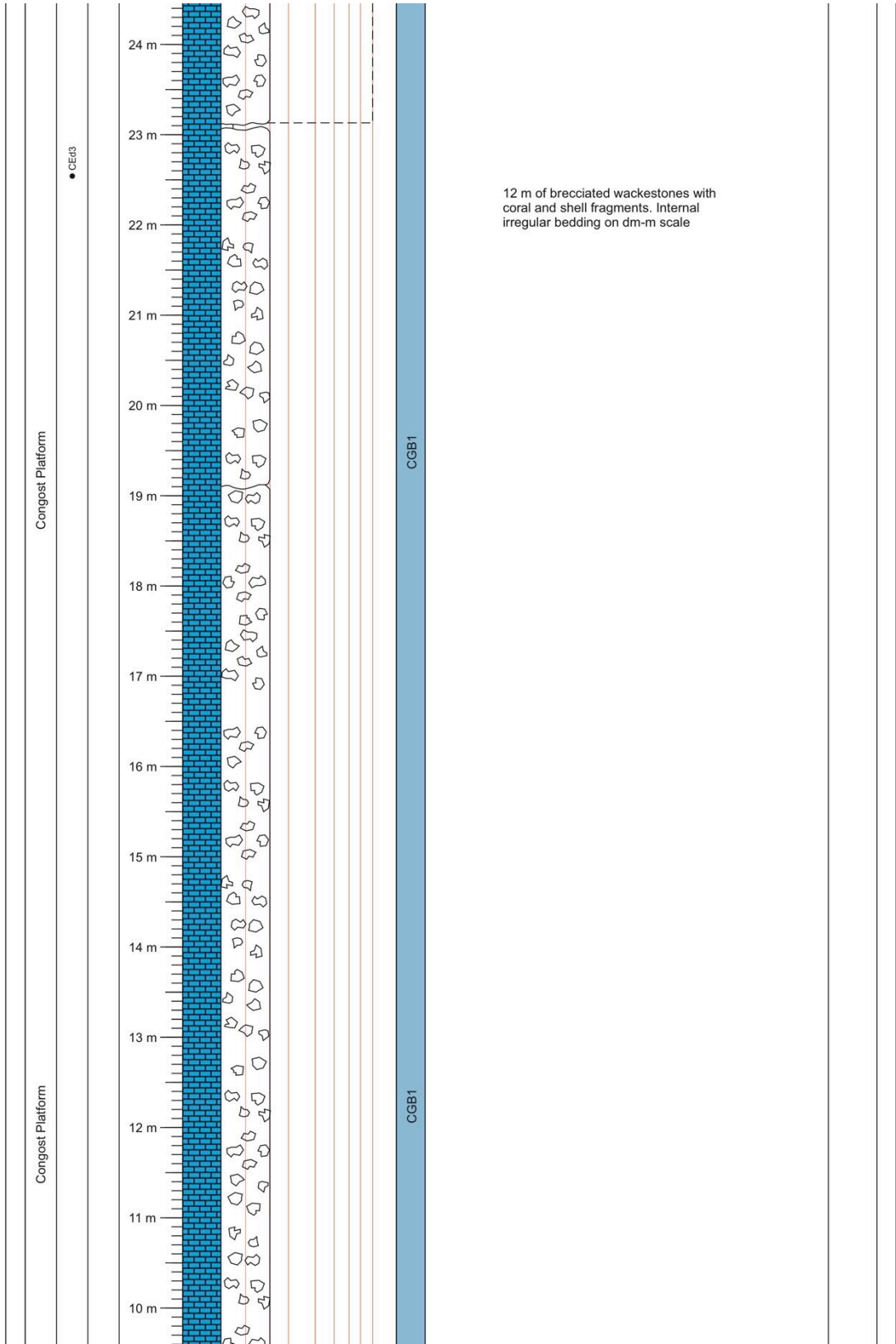
Congost d'Erinya D (CEd#) Starting 42°17'11.3"N (±4 m) Ending 42°17'08.4"N (±3 m)  
 (Logged 19/09/2014) Scale 1:50 point: 000°56'14.0"E Alt.: 666 m point: 000°56'15.0"E Alt.: 640 m

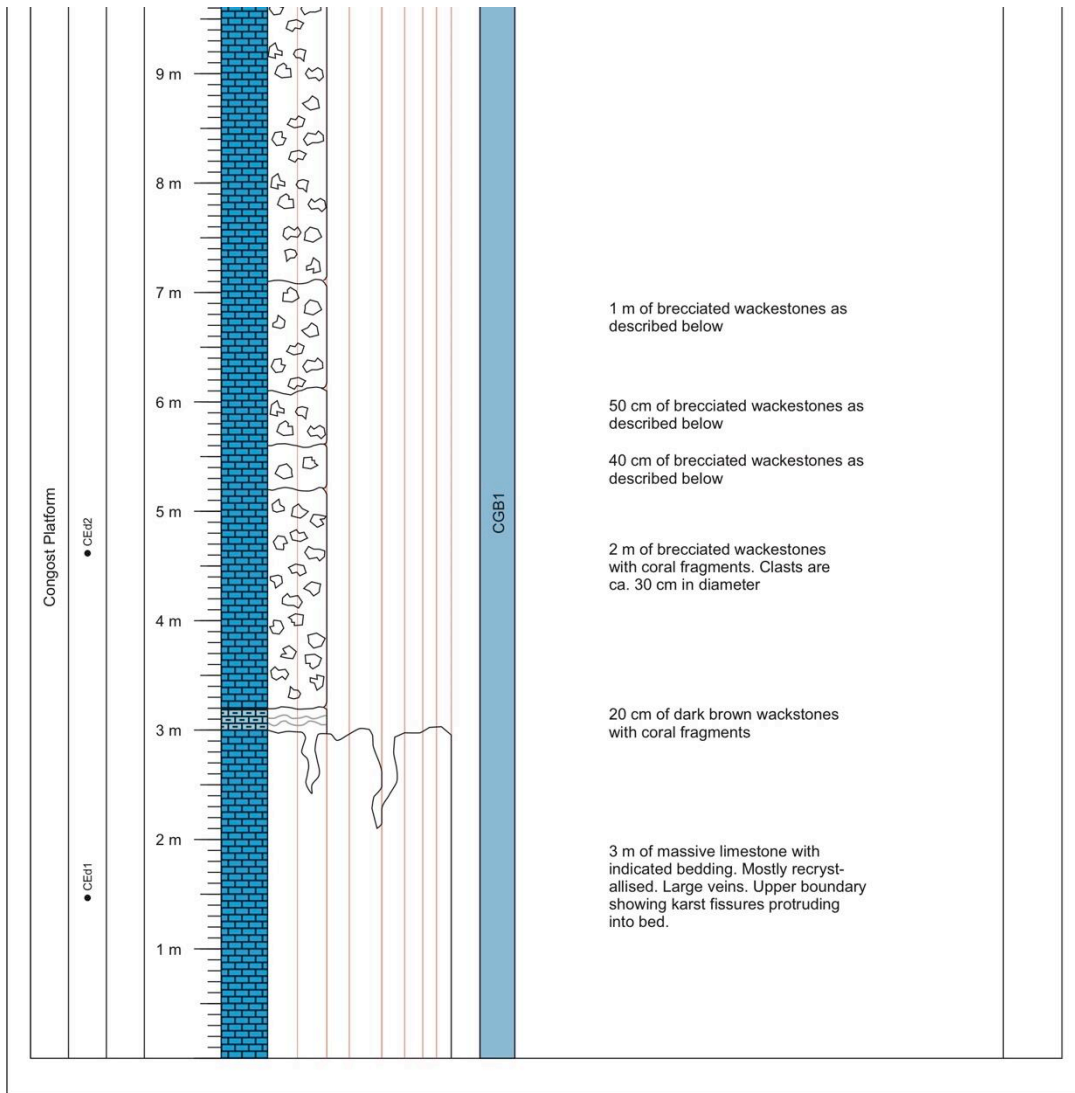




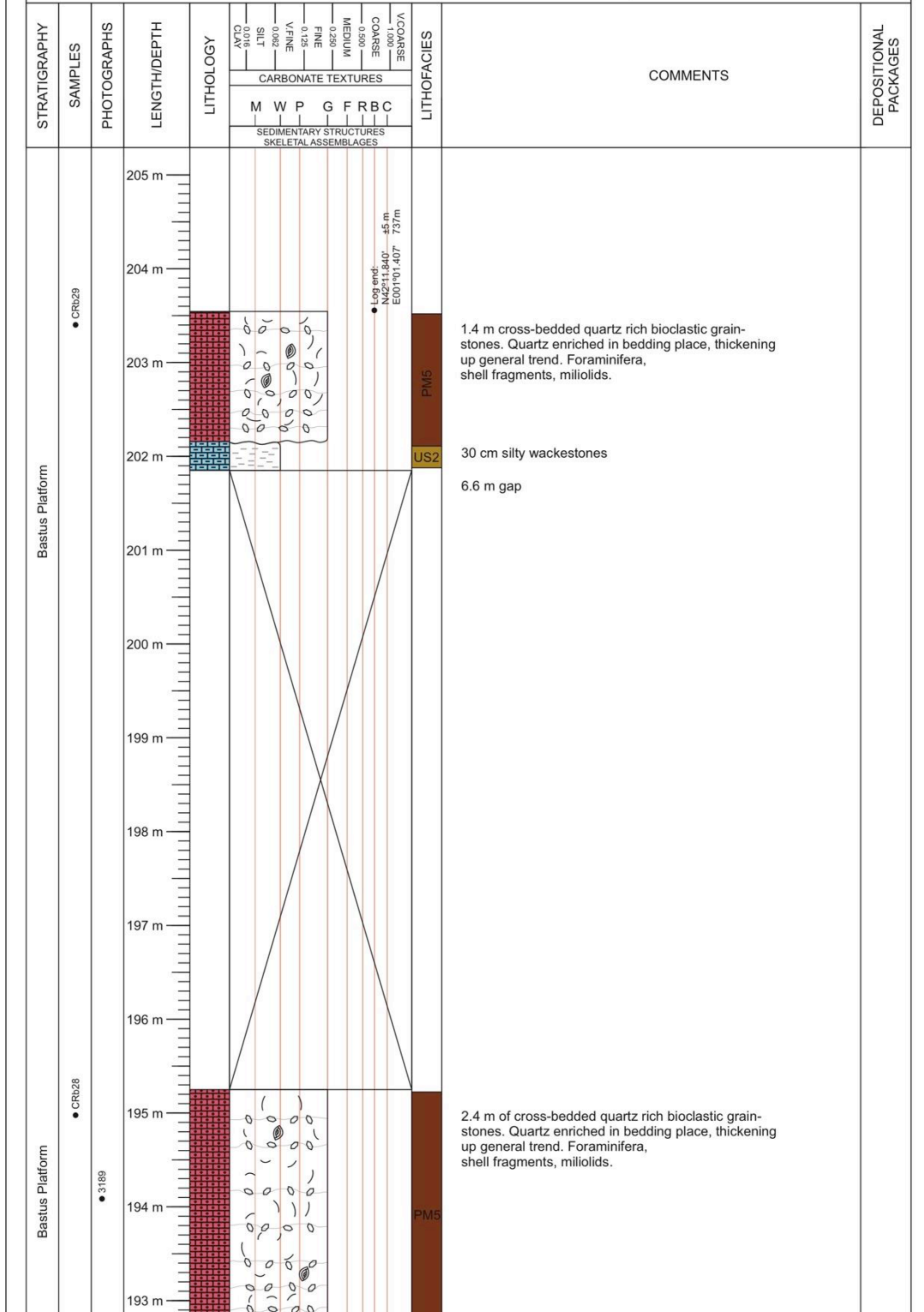


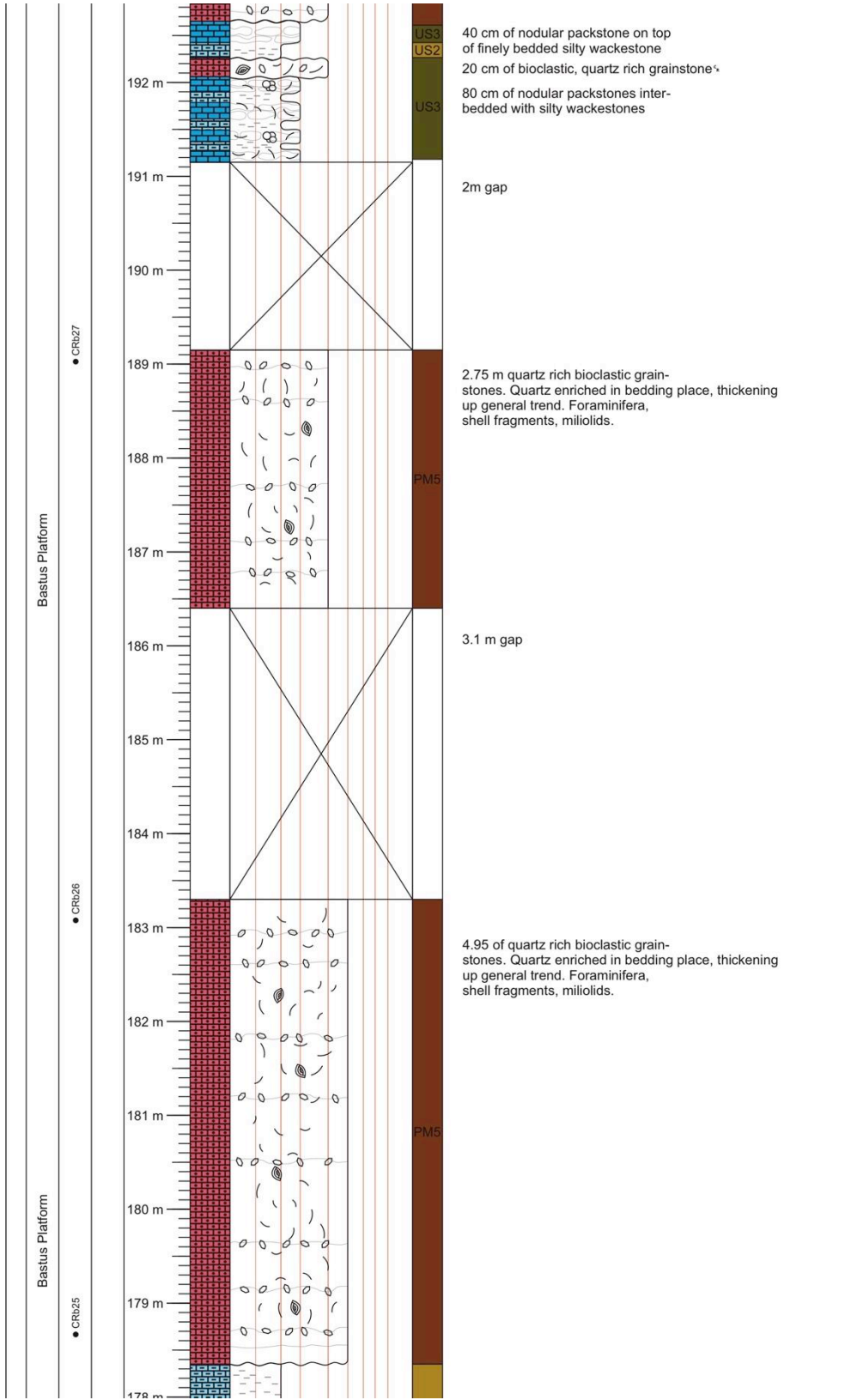


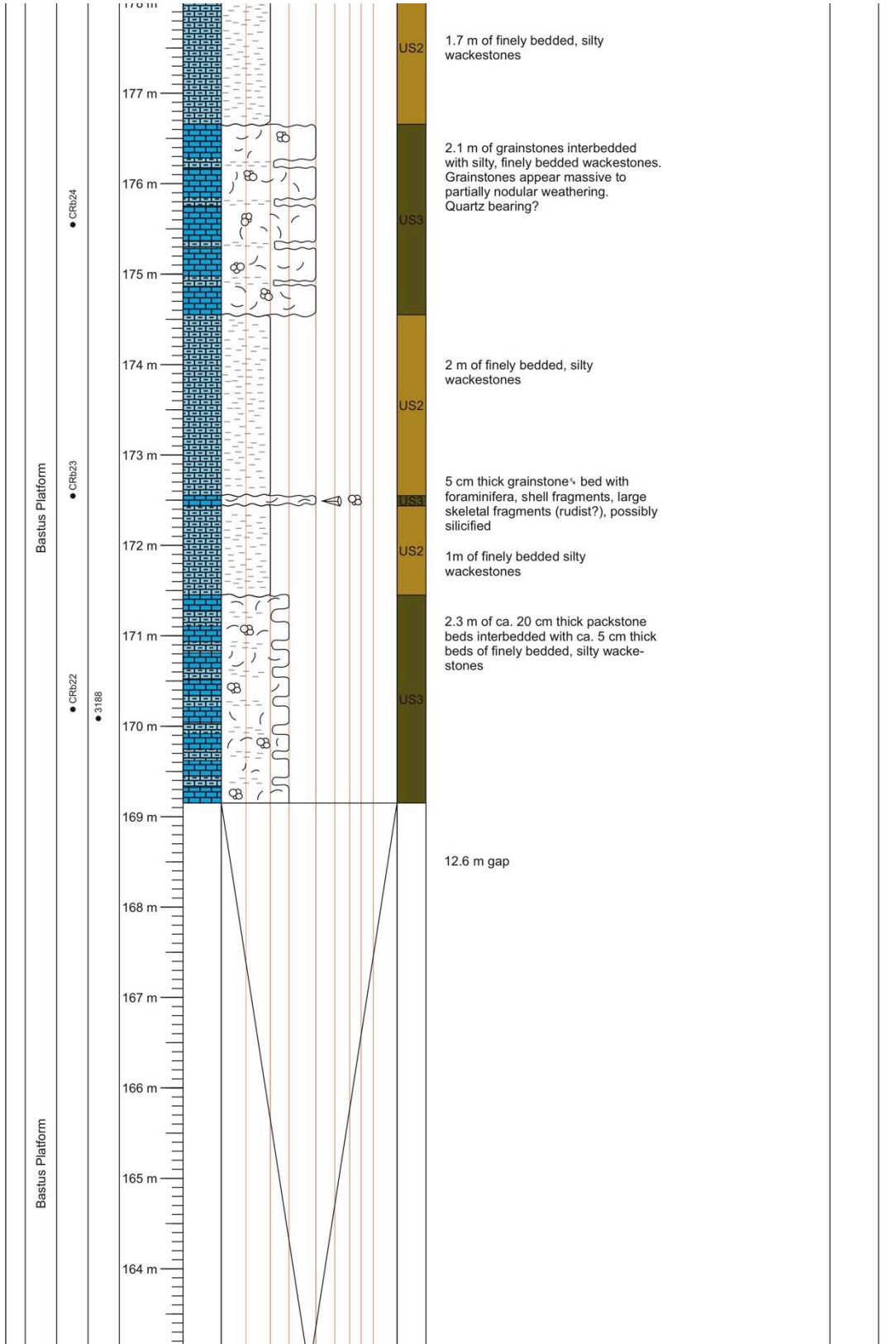


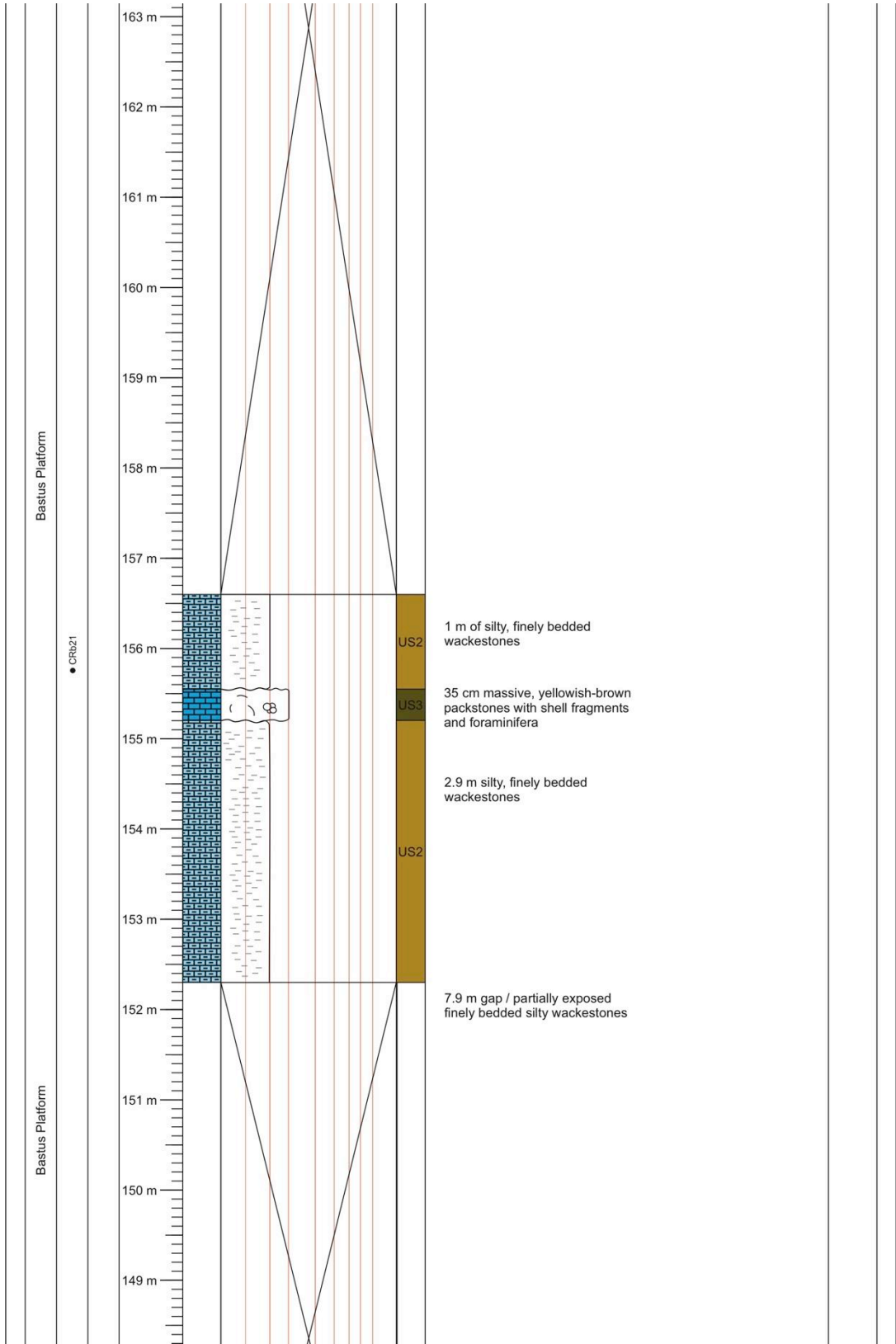


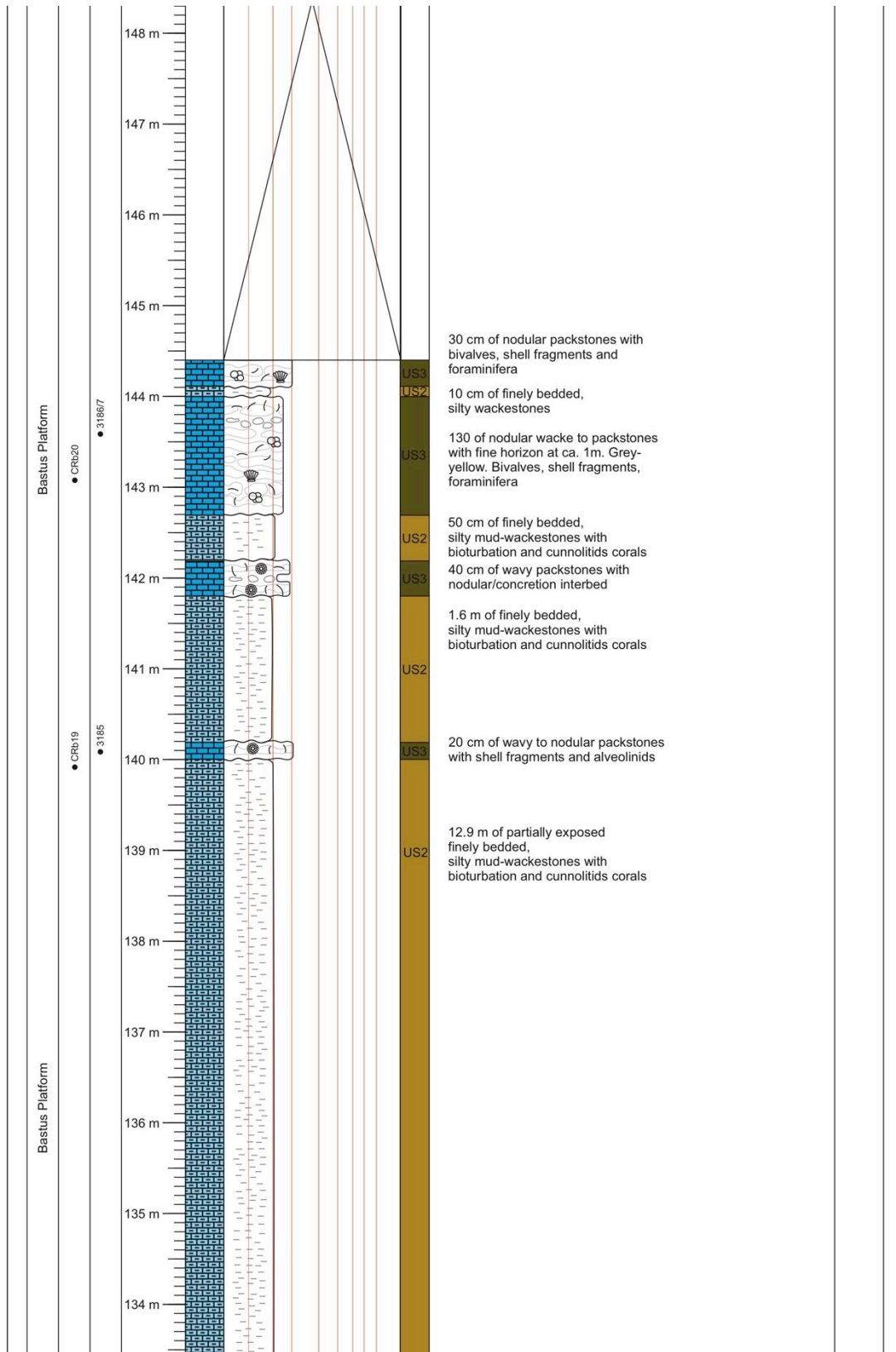
Carreu River B (CRb#) Starting 42°11'44.3"N (±6 m) Ending 42°11'50.4"N (±5 m)  
 (Logged 24/10/2013) Scale 1:50 point: 001°01'25.1"E Alt.: 655 m point: 001°02'24.4"E Alt.: 737 m



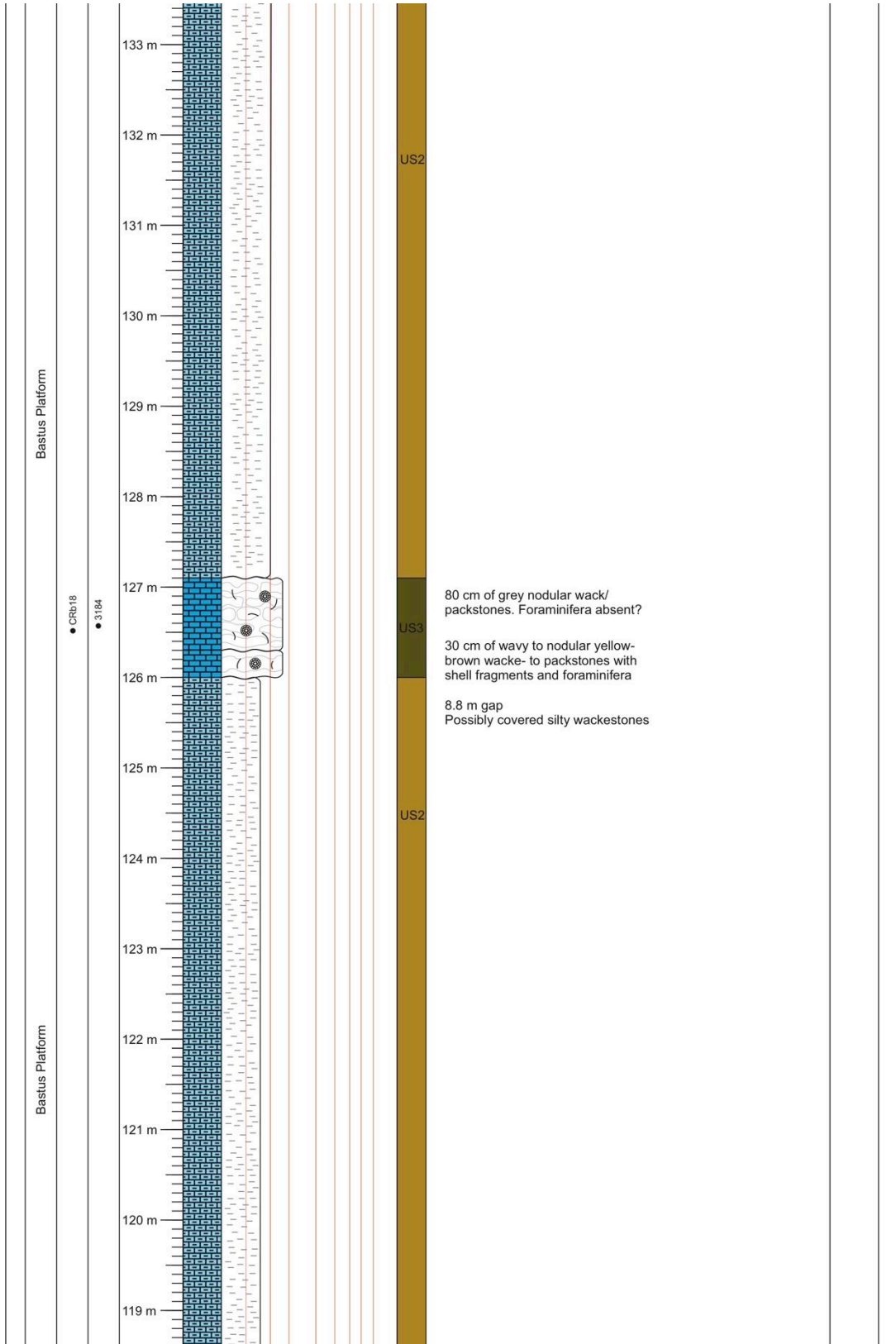


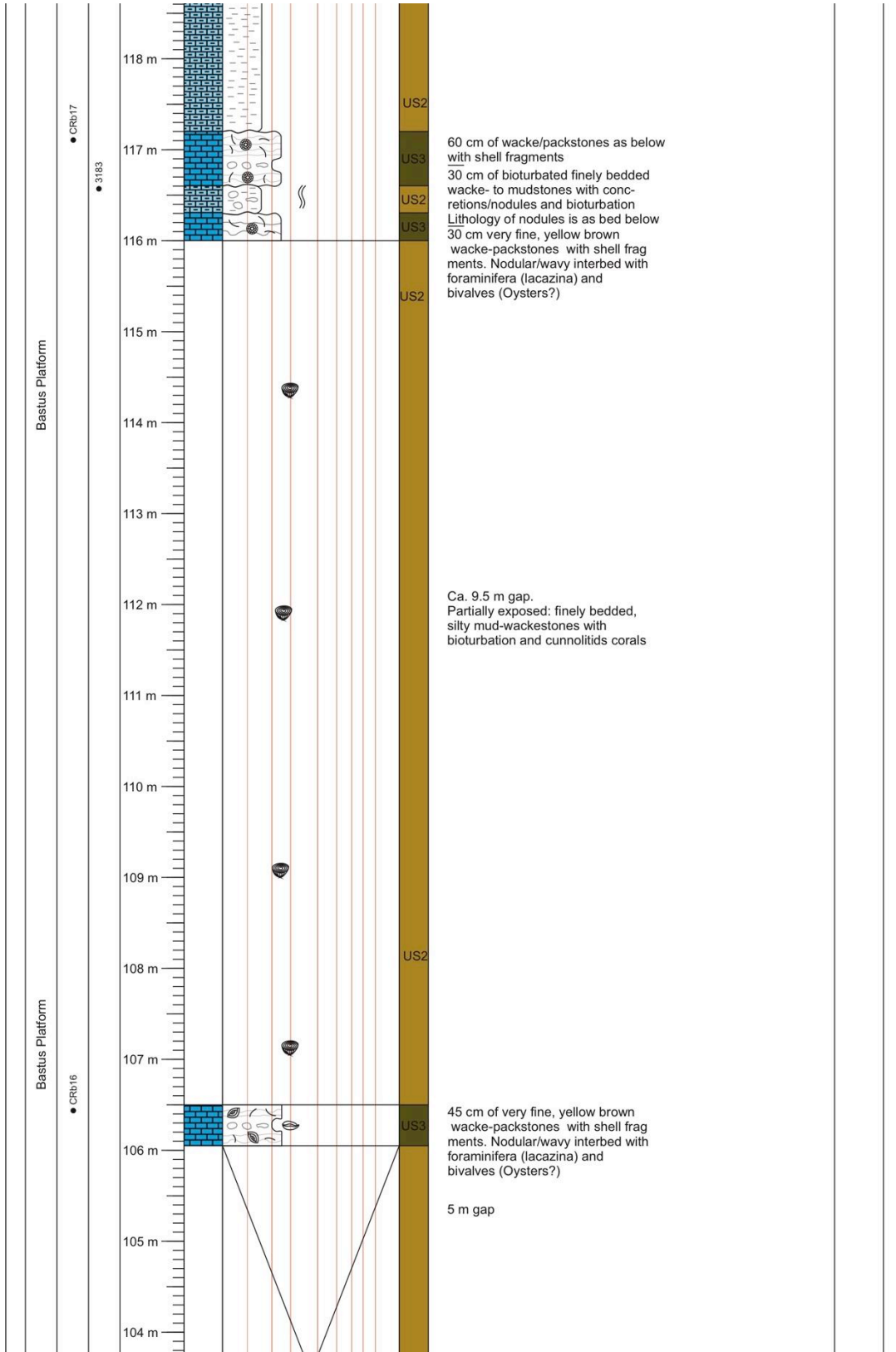


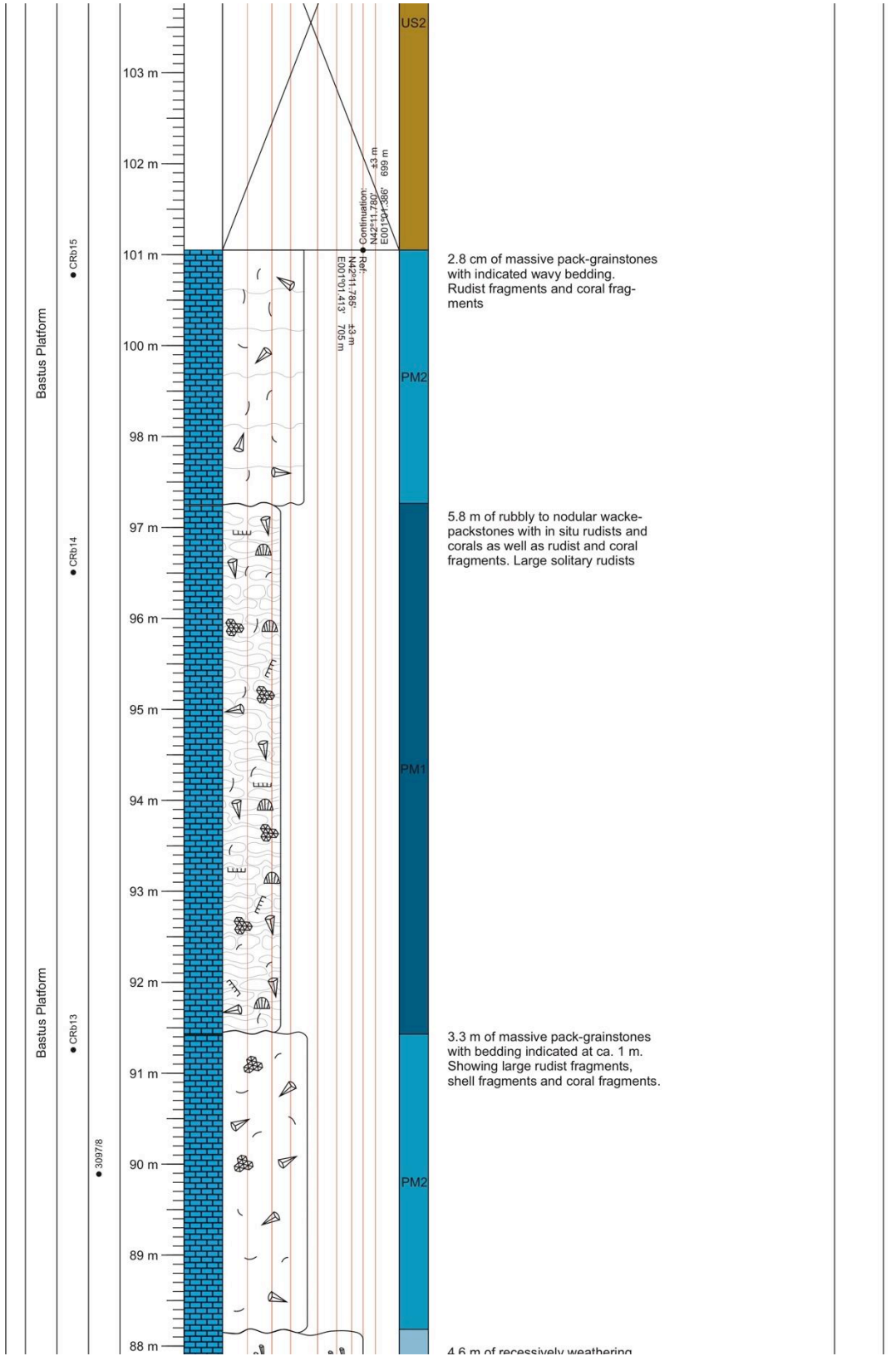


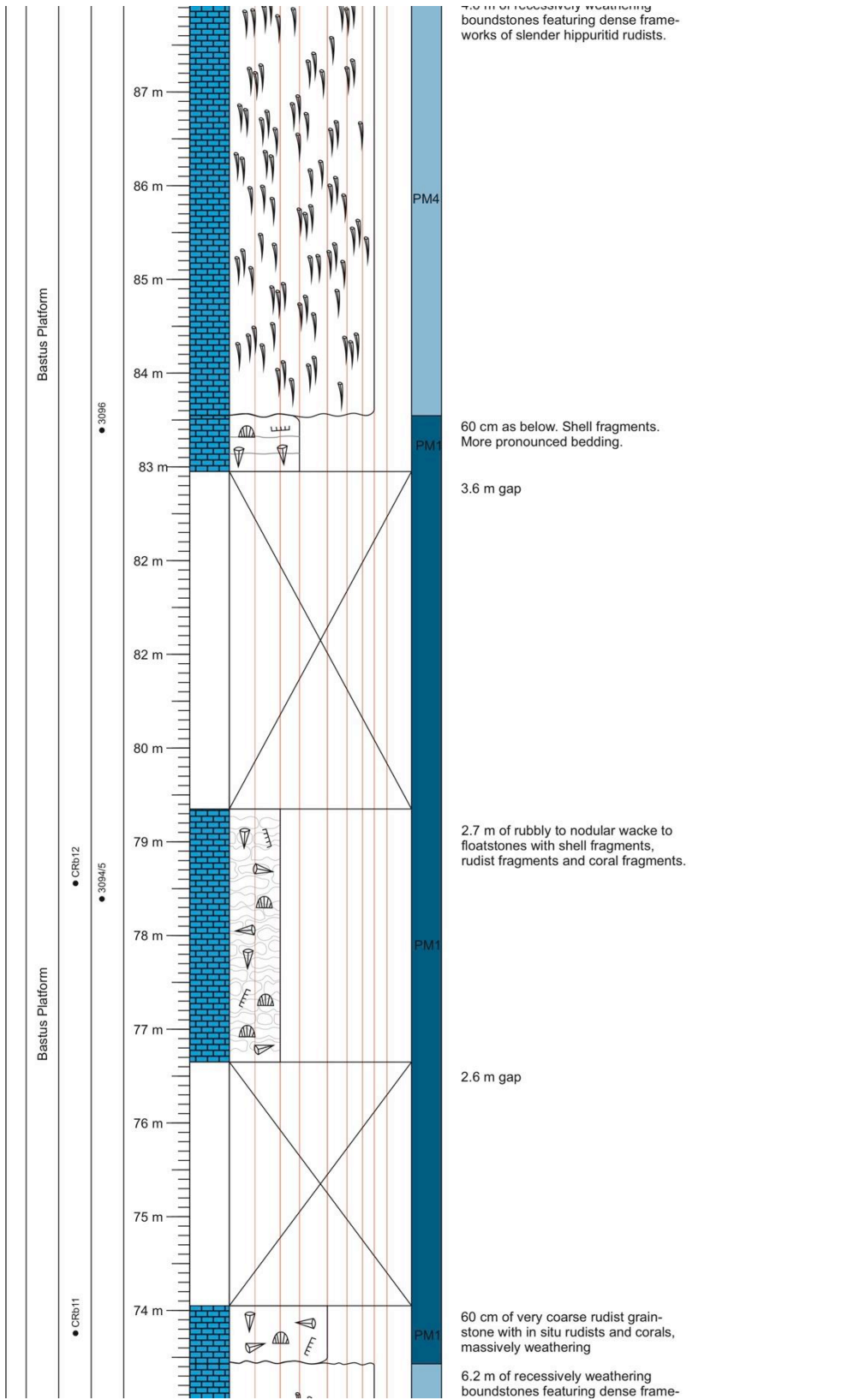


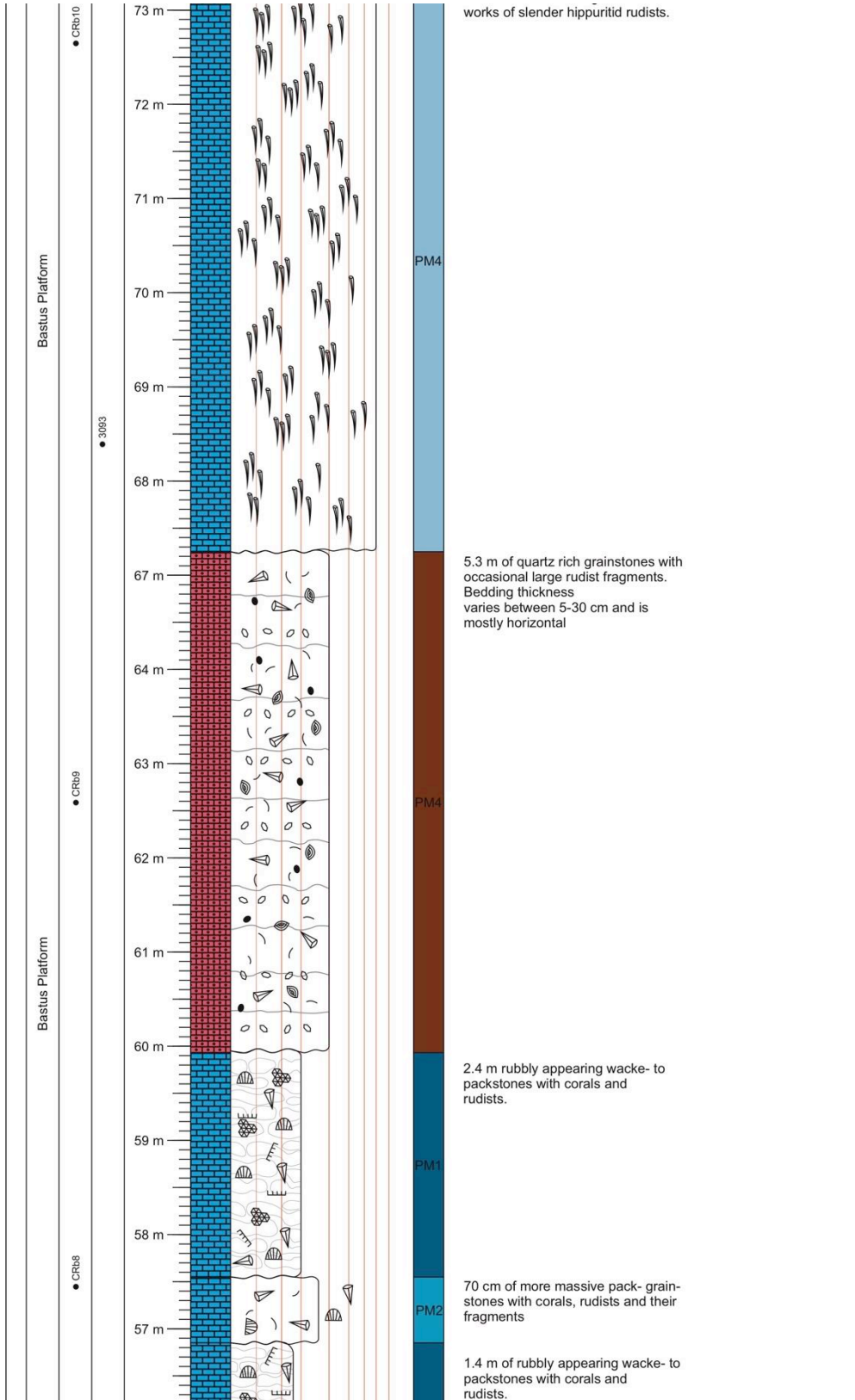


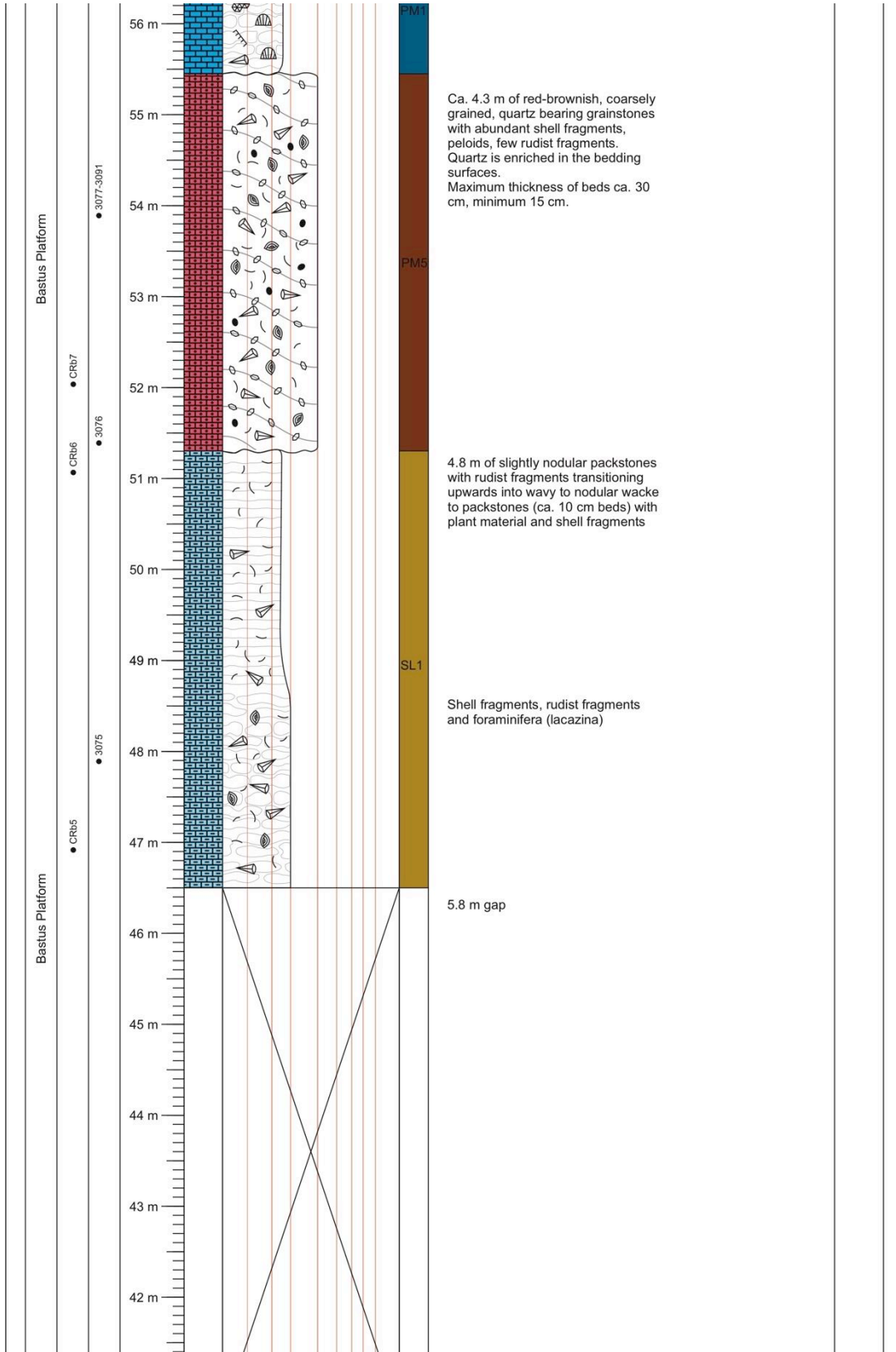


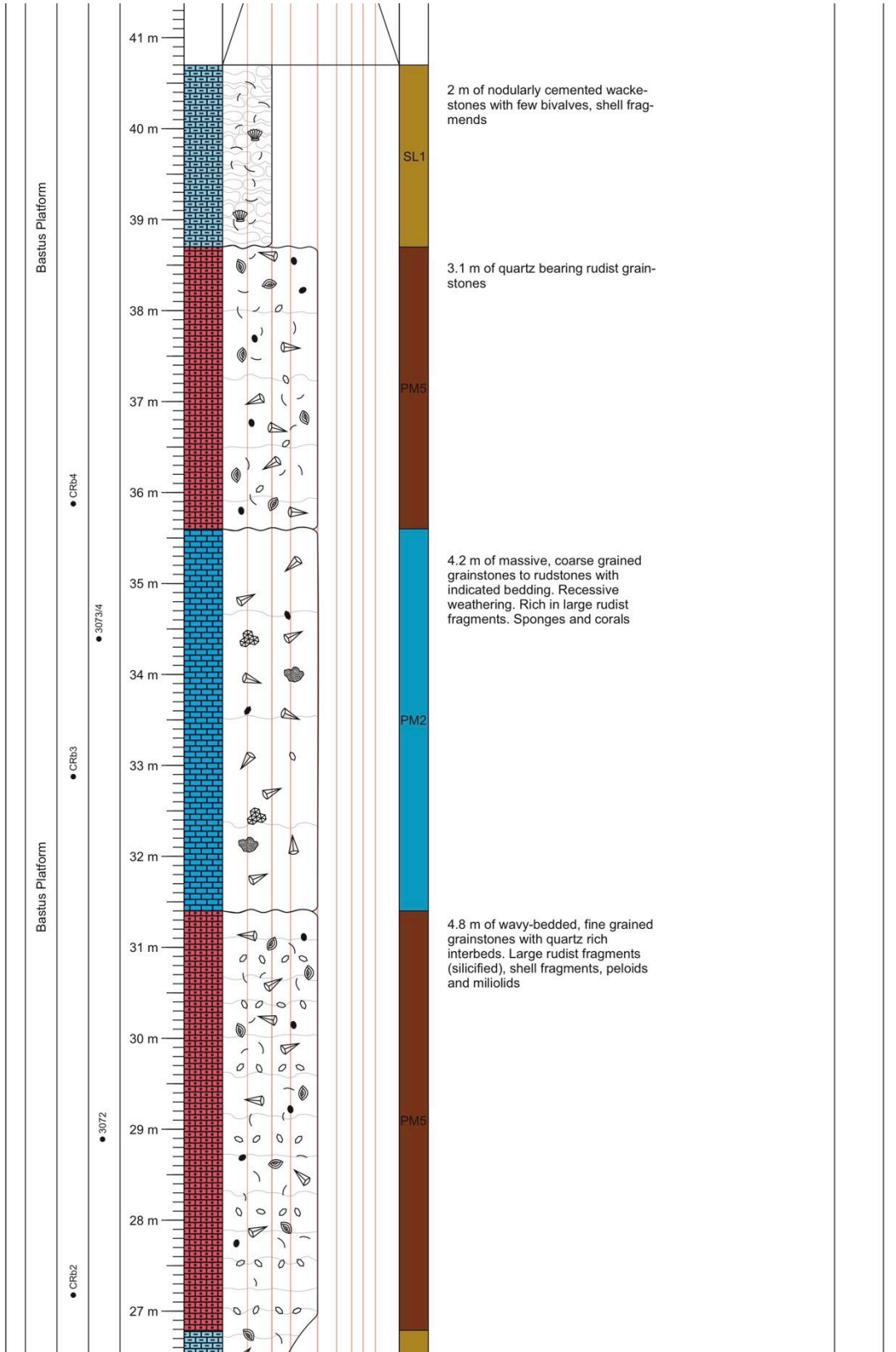








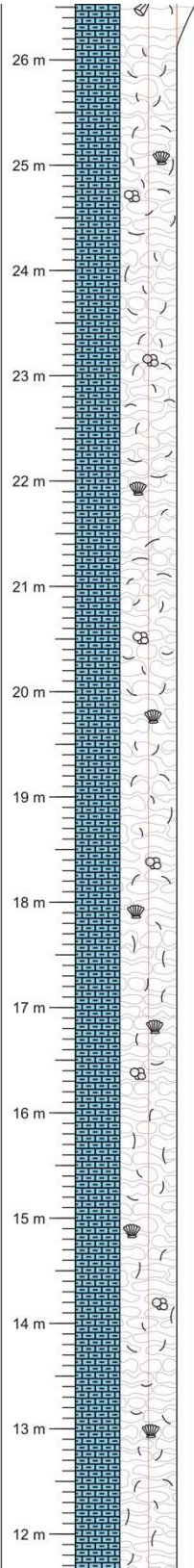




Bastus Platform

Bastus Platform

● CRb1

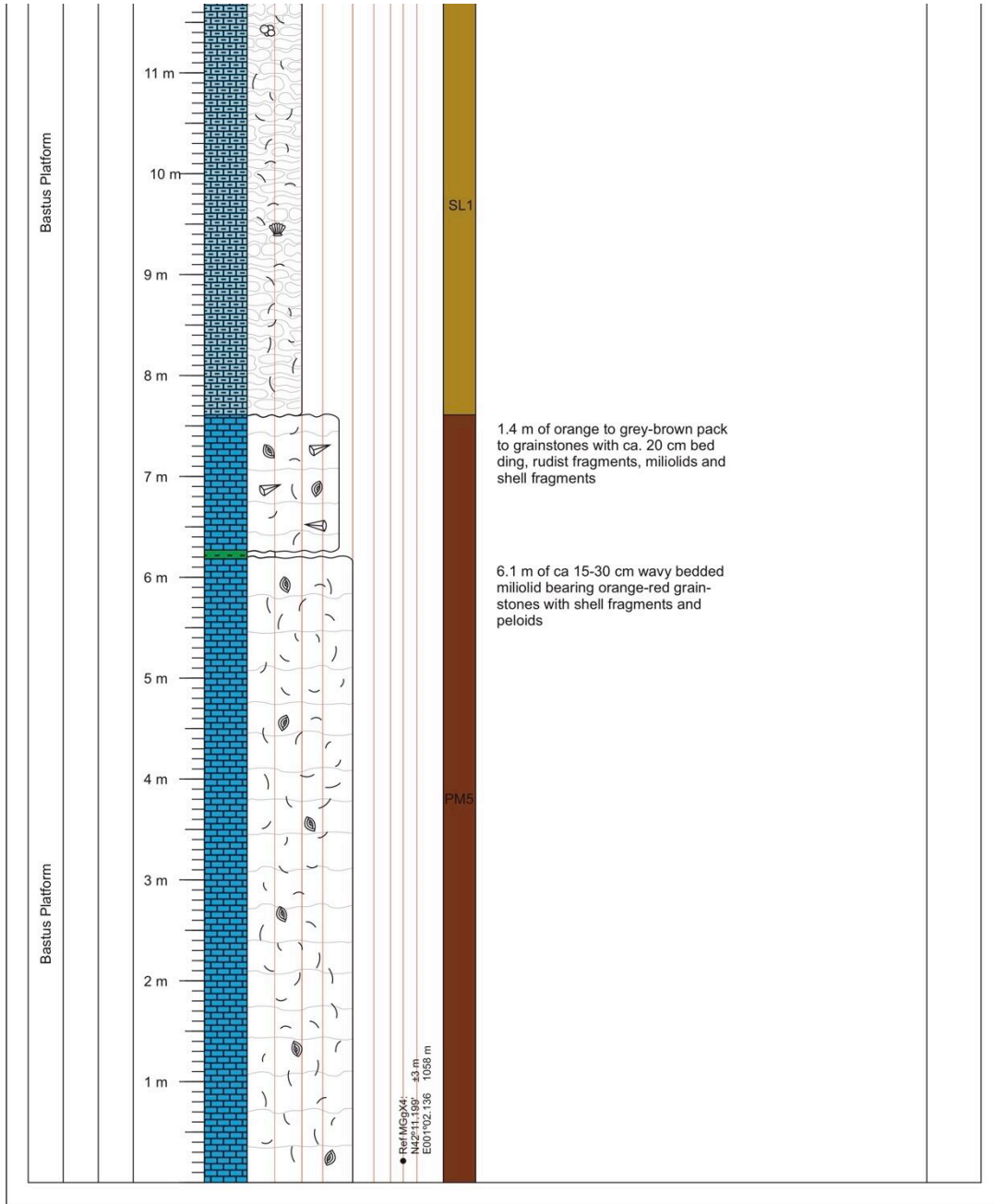


SL1

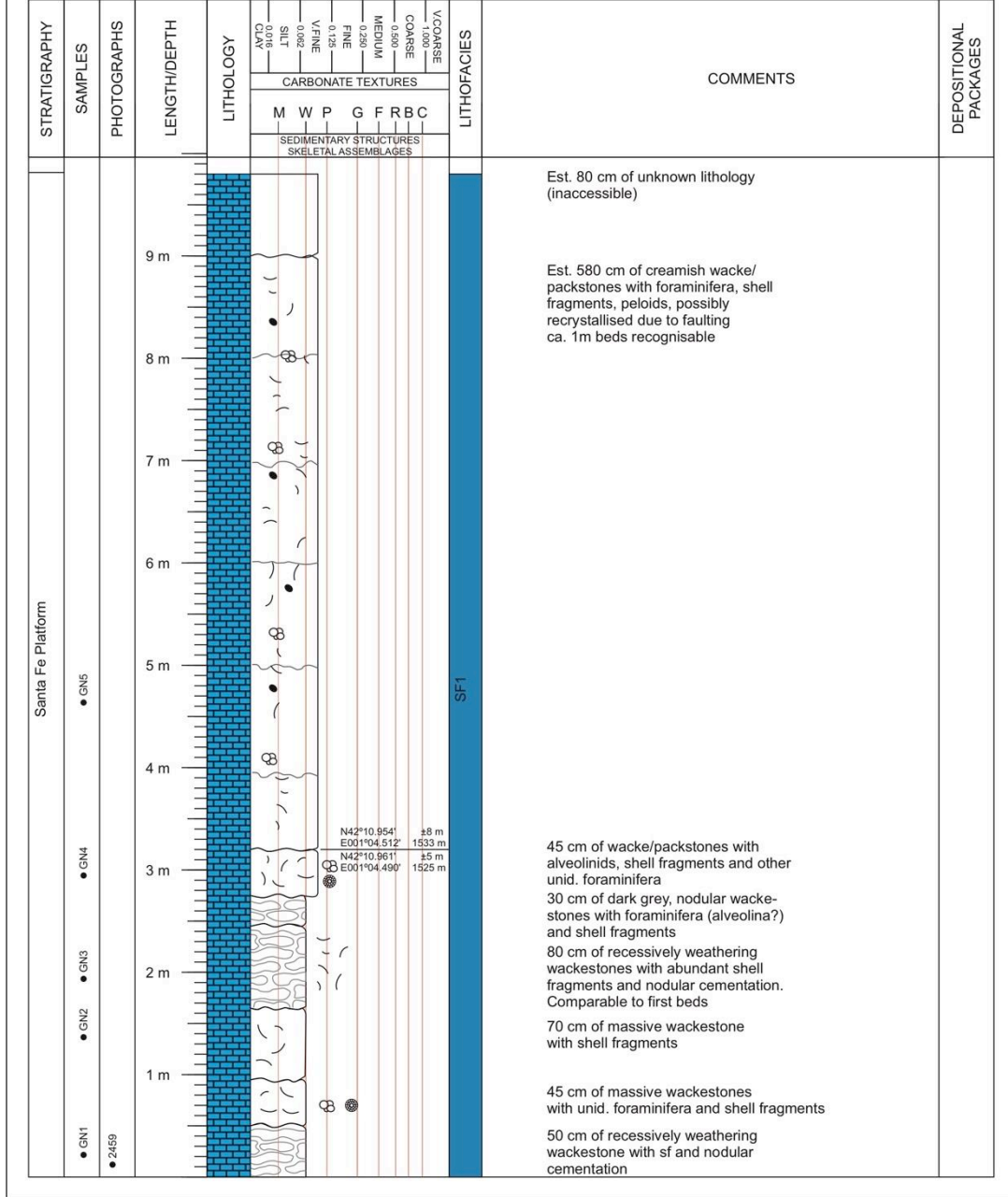
SL1

est. 19 m of nodular, grey brown wackestones, bottom part of the unit partially covered. Few shell fragments, foraminifera and rare bivalves





Gallinove North (GN#) Scale 1:50 Starting 42°10'57.4"N (±4 m) Ending 42°10'57.2"N (±8 m)  
 (Logged 26&28/10/2013) point: 001°04'30.1"E Alt.: 1515m point: 001°04'30.7"E Alt.: 1533m



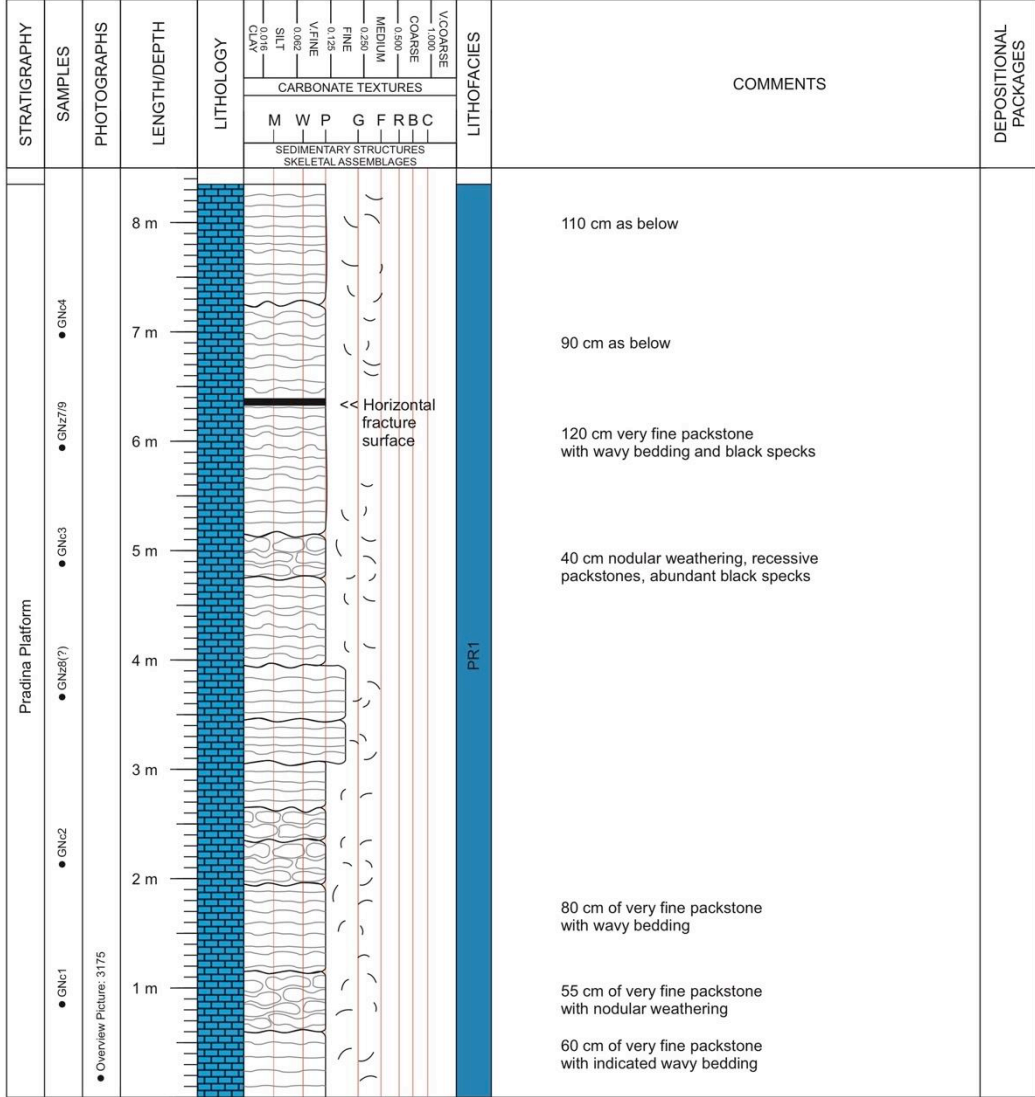
Gallinove North A (GNa#) Starting 42°10'57.7"N (±5 m) Ending 42°10'57.7"N (±5 m)  
 (Logged 26/10/2013) Scale 1:50 point: 001°04'29.4"E Alt.: 1525m point: 001°04'29.4"E Alt.: 1525m

STRATIGRAPHY	SAMPLES	PHOTOGRAPHS	LENGTH/DEPTH	LITHOLOGY	CARBONATE TEXTURES	SEDIMENTARY STRUCTURES	SKELETAL ASSEMBLAGES	LITHOFACIES	COMMENTS	DEPOSITIONAL PACKAGES
					M W P G F R B C					
Pradina Platform	● GNa1		0 m 1 m 2 m 3 m 4 m					PR1	Est. 4 m of wackestones with foraminifera and shell fragments Ca. 1m bedding apparent	
	● GNa2									

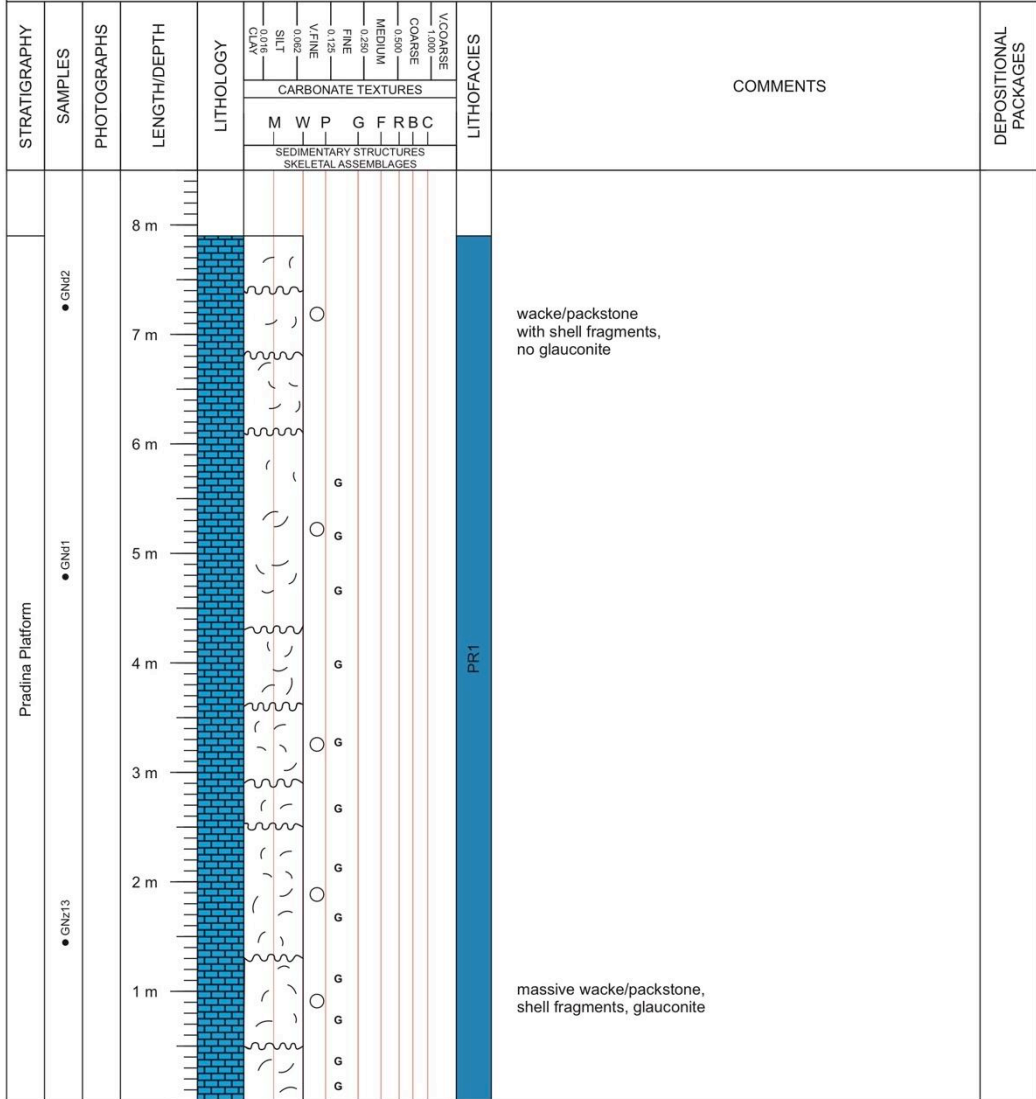
Gallinove North B (GNb#) Starting 42°10'59.3"N (±9 m) Ending 42°10'58.9"N (±9 m)  
 (Logged 26/10/2013) Scale 1:50 point: 001°04'29.3"E Alt.: 1520m point: 001°04'28.3"E Alt.: 1531 m

STRATIGRAPHY	SAMPLES	PHOTOGRAPHS	LENGTH/DEPTH	LITHOLOGY	CARBONATE TEXTURES										LITHOFACIES	COMMENTS	DEPOSITIONAL PACKAGES		
					SEDIMENTARY STRUCTURES														
					SKELETAL ASSEMBLAGES														
					M	W	P	G	F	R	B	C							
Congost Platform	● GNb1  ● GNb4		8 m														60 cm of very fine grained wacke/packstones		
			7 m															50 cm as below	
			6 m															40 cm of very fine grained wackestone	
			5 m															120 cm as below	
			4 m															90 cm of very fine grained wacke/packstone as below	
			3 m															70 cm as below	
			2 m															120 cm of cream-coloured, massive packstones/grainstones with shell fragments	
			1 m															80 cm as below	
																		90 cm as below bivalves	
																		80 cm of cream-coloured, massive packstones with shell fragments	

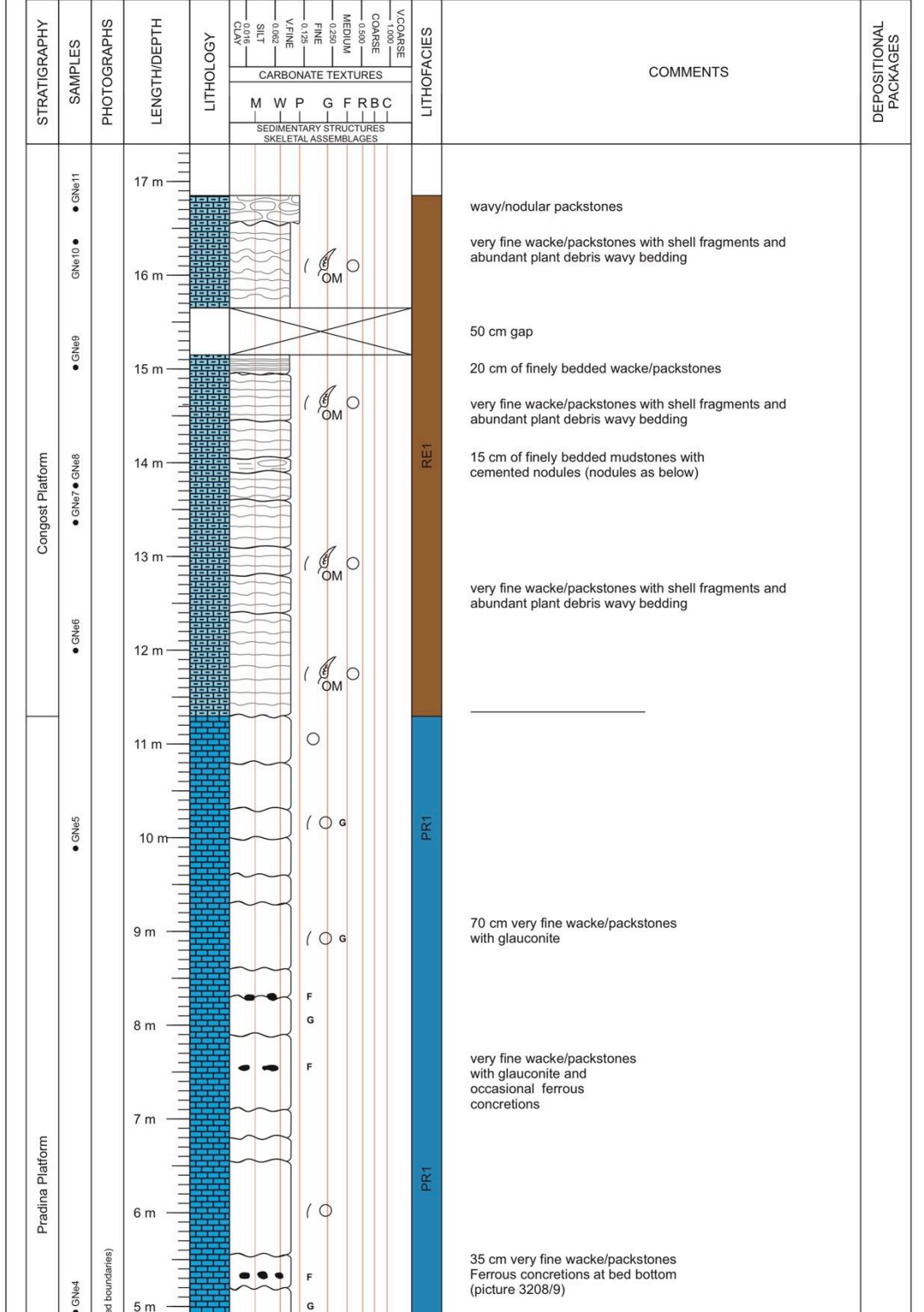
Gallinove North C (GNC#) Starting 42°10'59.9"N (±6 m) Ending 42°10'59.9"N (±7 m)  
 (Logged 26/10/2013) Scale 1:50 point: 001°04'27.7"E Alt.: 1566m point: 001°04'27.6"E Alt.: 1569m

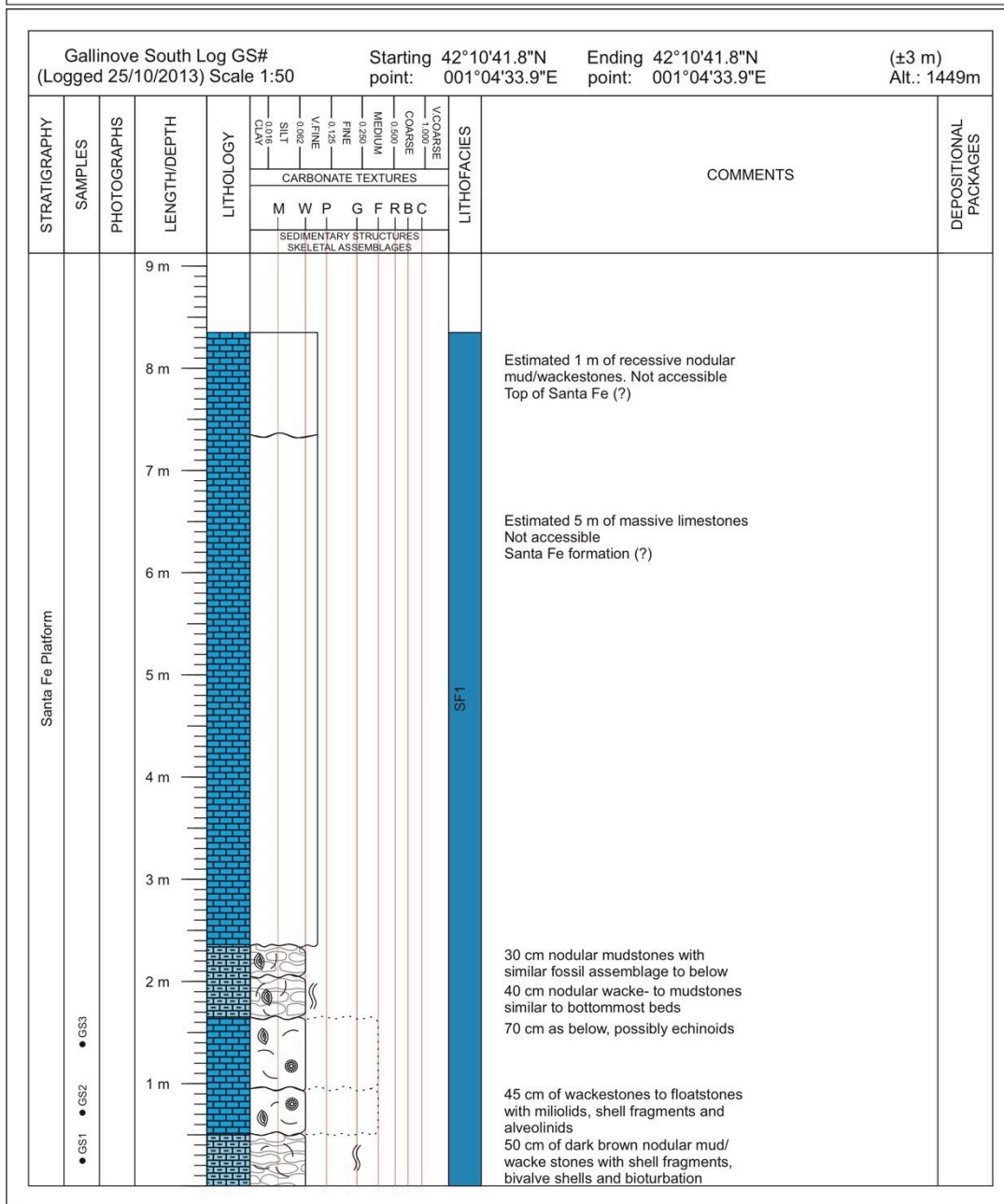
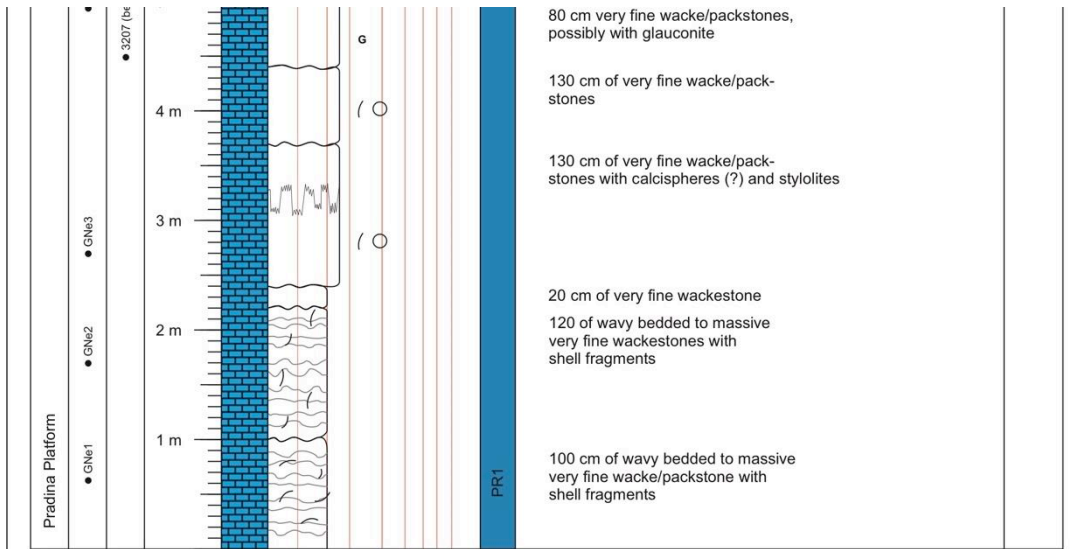


Gallinove North D (GNd#) Starting 42°10'59.3"N (±4 m) Ending 42°10'59.5"N (±6 m)  
 (Logged 28/10/2013) Scale 1:50 point: 001°04'26.4"E Alt.: 1512 m point: 001°04'26.4"E Alt.: 1515 m



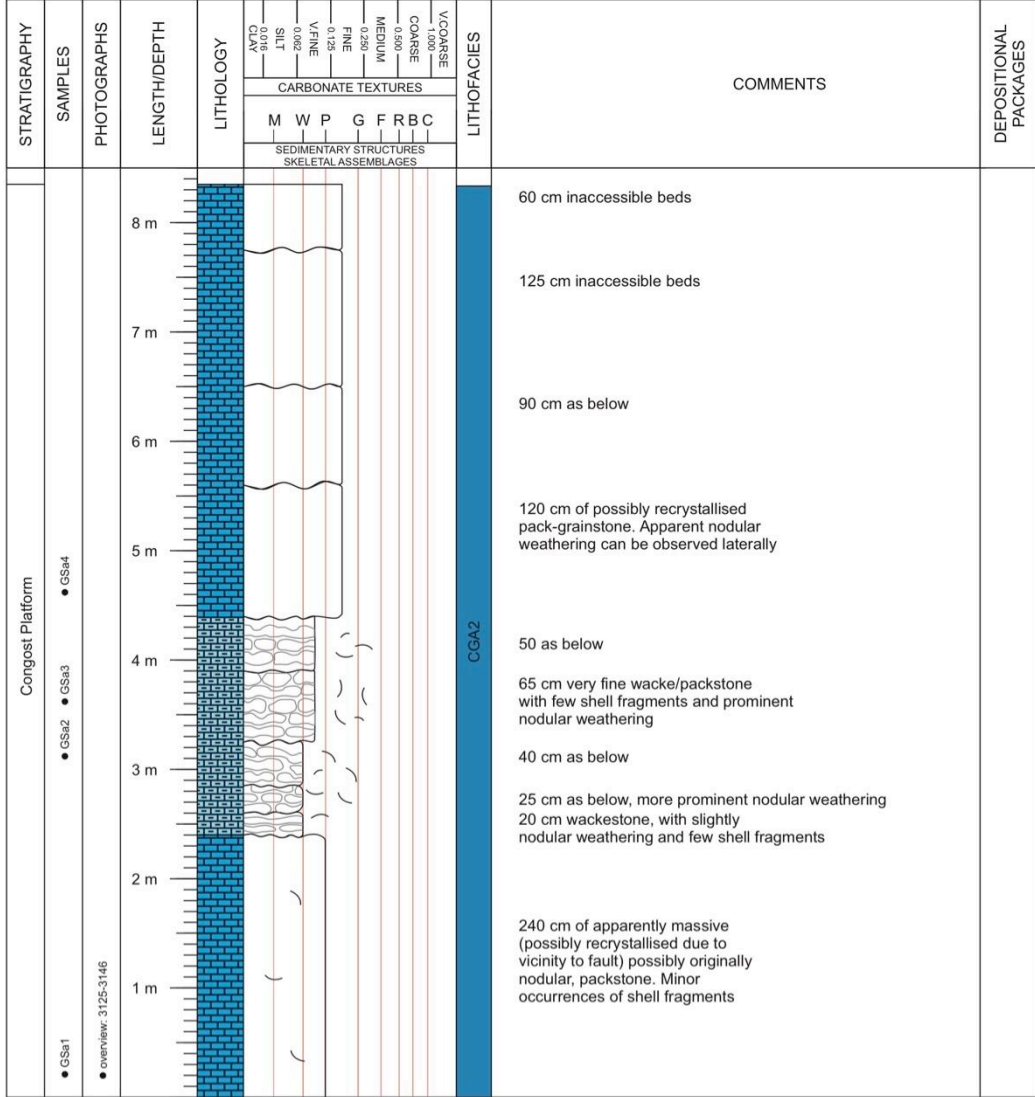
Gallinove North E (GNe#) Starting 42°10'59.4"N (±5 m) Ending 42°10'00.0"N (±6 m)  
 (Logged 28/10/2013) Scale 1:50 point: 001°04'23.3"E Alt.: 1505 m point: 001°04'23.4"E Alt.: 1514 m







Gallinove South A (GSA#) Starting 42°10'43.0"N (±7 m) Ending 42°10'43.0"N (±7 m)  
 (Logged 25/10/2013) Scale 1:50 point: 001°04'34.0"E Alt.: 1566 m point: 001°04'34.0"E Alt.:1566 m



Gallinove South B (GSb#) (Logged 25/10/2013) Scale 1:50		Starting point: 42°10'43.6"N 001°04'33.0"E	Ending point: 42°10'43.6"N 001°04'33.0"E	(±7 m) Alt.: 1499m			
STRATIGRAPHY	SAMPLES	PHOTOGRAPHS	LENGTH/DEPTH	LITHOLOGY	LITHOFACIES	COMMENTS	DEPOSITIONAL PACKAGES
				CLAY SILT V.FINE FINE MEDIUM COARSE V.COARSE 1:500 1:100			
				CARBONATE TEXTURES M W P G F R B C SEDIMENTARY STRUCTURES SKELETAL ASSEMBLAGES			
Congost Platform	GSb1 ● GSb2 ● GSb3 ● GSb4 ● ● Overview Pictures: 3147-3151		4 m 3 m 2 m 1 m		CGA2	60 cm as below  105 cm as below  1 m of very fine grained pack/grainstone with shell fragments and nodular to wavy indicated bedding  30 cm brown/grey vf. wacke/packstone 20 cm very fine, massive grain-packstone with bivalve shell fragments 60 cm brown/grey very fine wacke/packstone with nodular weathering	

Gallinove South C (GSc#) Starting point: 42°10'41.9"N Ending 42°10'42.4"N (±7 m)  
 (Logged 25/10/2013) Scale 1:50 001°04'33.2"E point: 001°04'32.3"E Alt.: 1482m

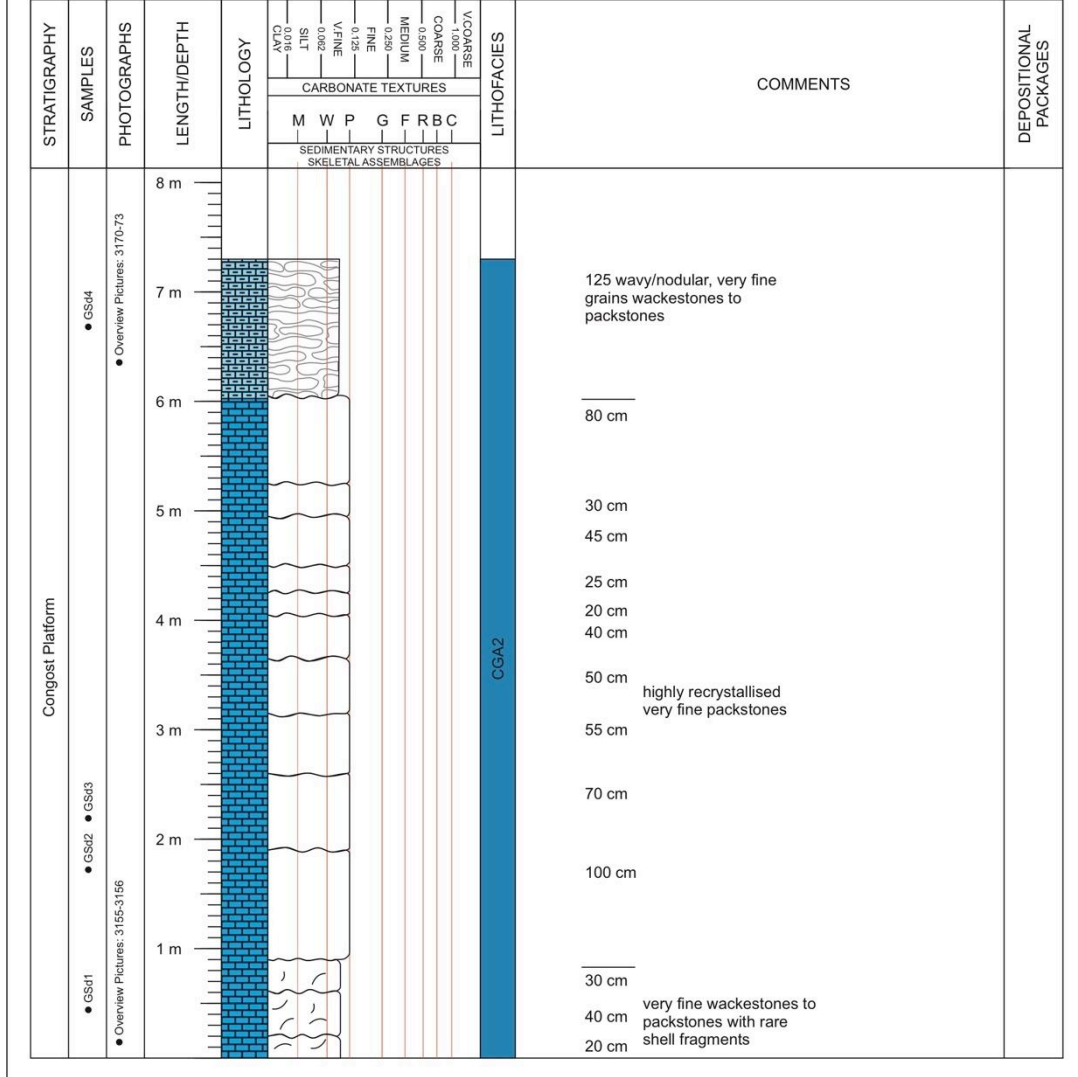
STRATIGRAPHY	SAMPLES	PHOTOGRAPHS	LENGTH/DEPTH	LITHOLOGY	LITHOFACIES	COMMENTS	DEPOSITIONAL PACKAGES	
Congost Platform	<ul style="list-style-type: none"> <li>● GSc1</li> <li>● GSc2</li> <li>● GSc3</li> <li>● GSc4</li> <li>● GSc5</li> </ul>	<ul style="list-style-type: none"> <li>● Overview Pictures: 3153-3154</li> </ul>		CARBONATE TEXTURES M W P G F R BC SEDIMENTARY STRUCTURES SKELETAL ASSEMBLAGES	V. COARSE COARSE MEDIUM FINE V. FINE SILT CLAY	RE1	<p>90 cm of massive to wavy bedded wacke/packstones. Very fine grained Lower boundary heavily bioturbated</p> <p>160 cm of bioturbated, finely bedded, plated., very fine grained wackestones with abundant carbonate concretions (Picture 3152)</p> <p>30 cm as below</p> <p>50 cm of dark grey very fine grained wackestone to packstones with nodular weathering</p> <p>50 cm of dark grey very fine grained pack- grainstone with nodular weathering, comparable to first bed</p> <p>70 cm of wavy bedded, very fine grained wackestones to packstones</p> <p>150 cm of dark grey, very fine grained pack- grainstone with nodular weathering</p>	

Gallinove South D (GSd#)  
(Logged 25/10/2013) Scale 1:50

Starting point: 42°10'43.0"N  
001°04'33.2"E

Ending point: 42°10'43.0"N  
001°04'33.2"E

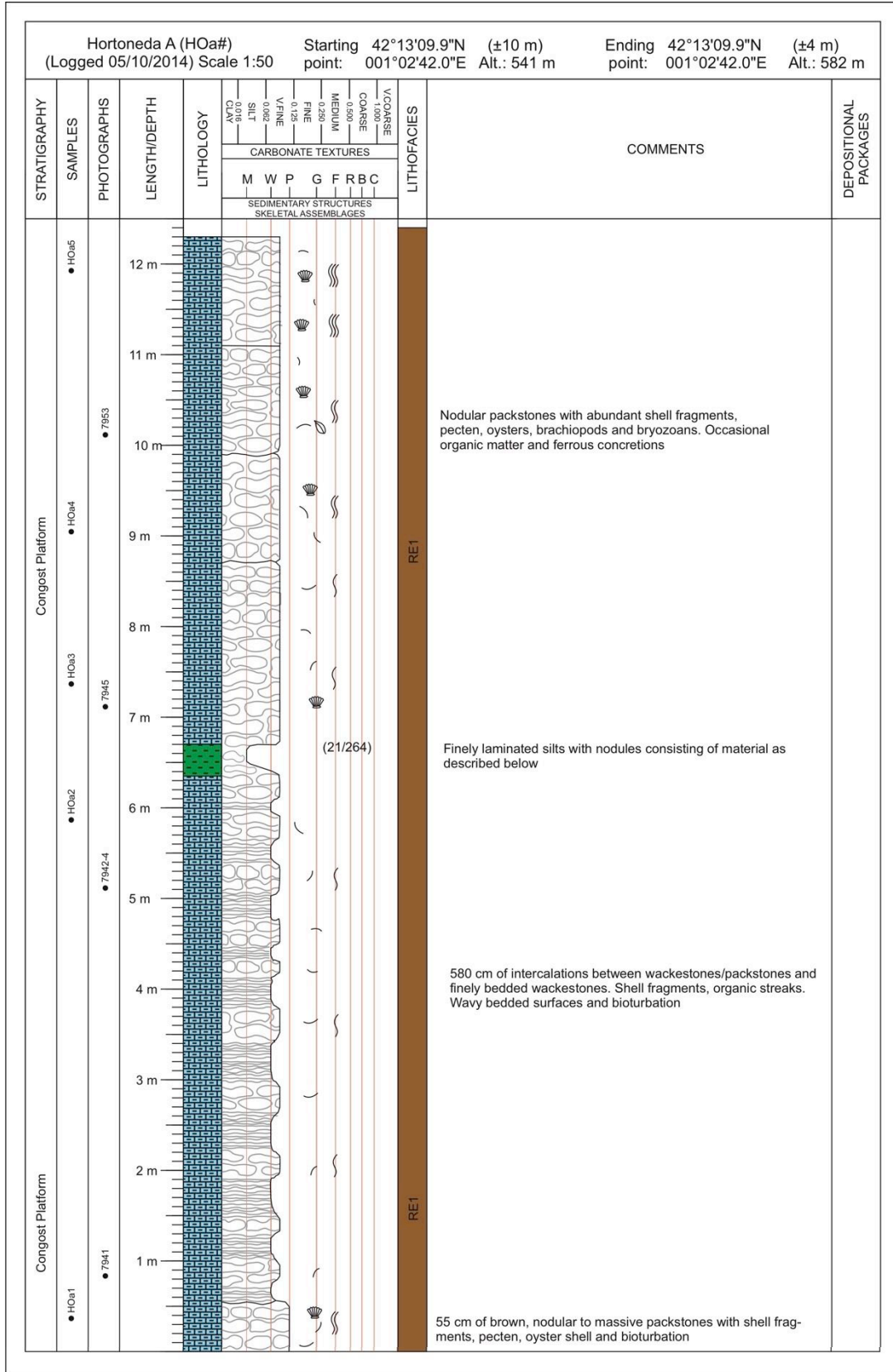
(±5 m)  
Alt.: 1479 m



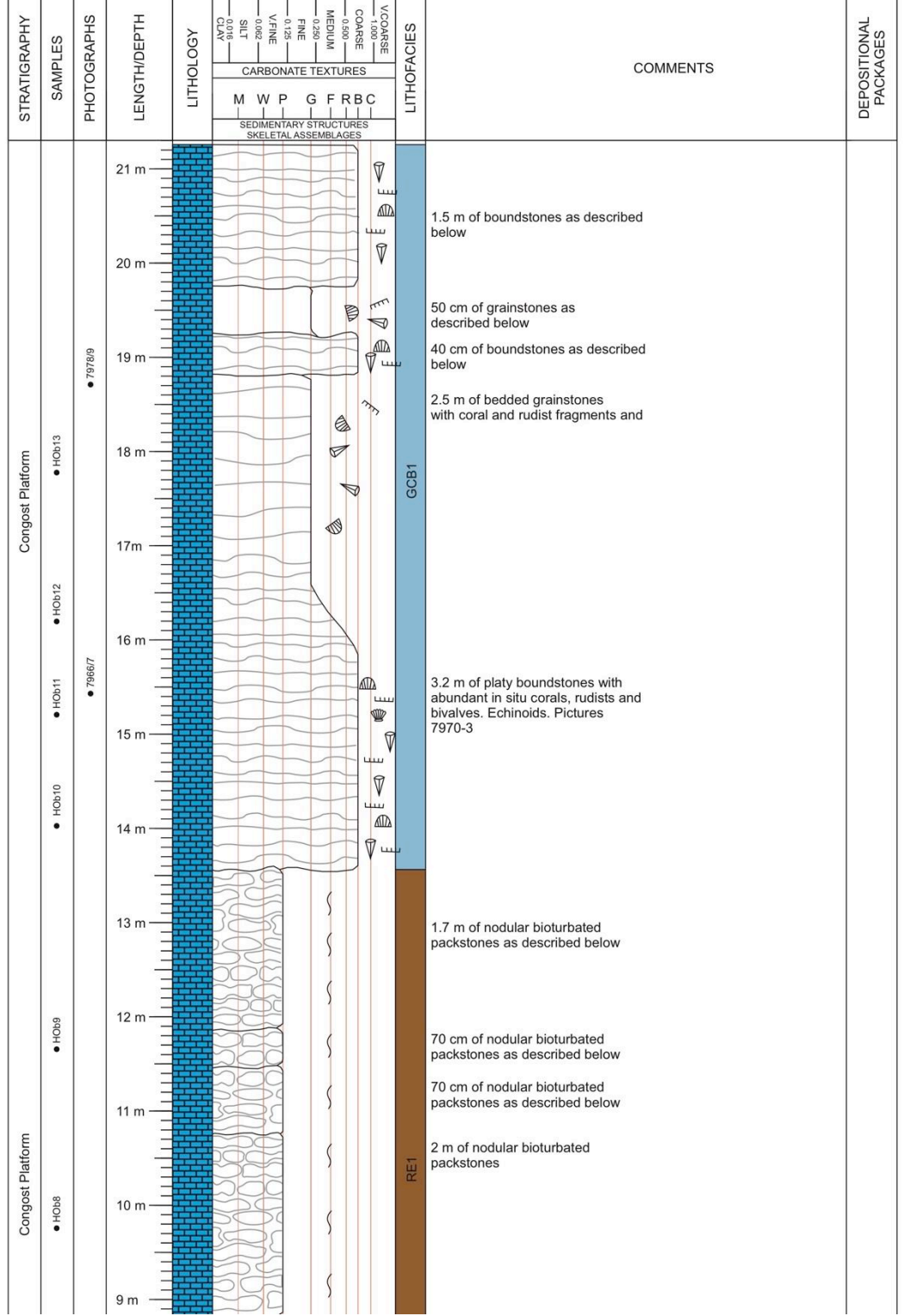
Hortonedada A (HOa#)  
(Logged 05/10/2014) Scale 1:50

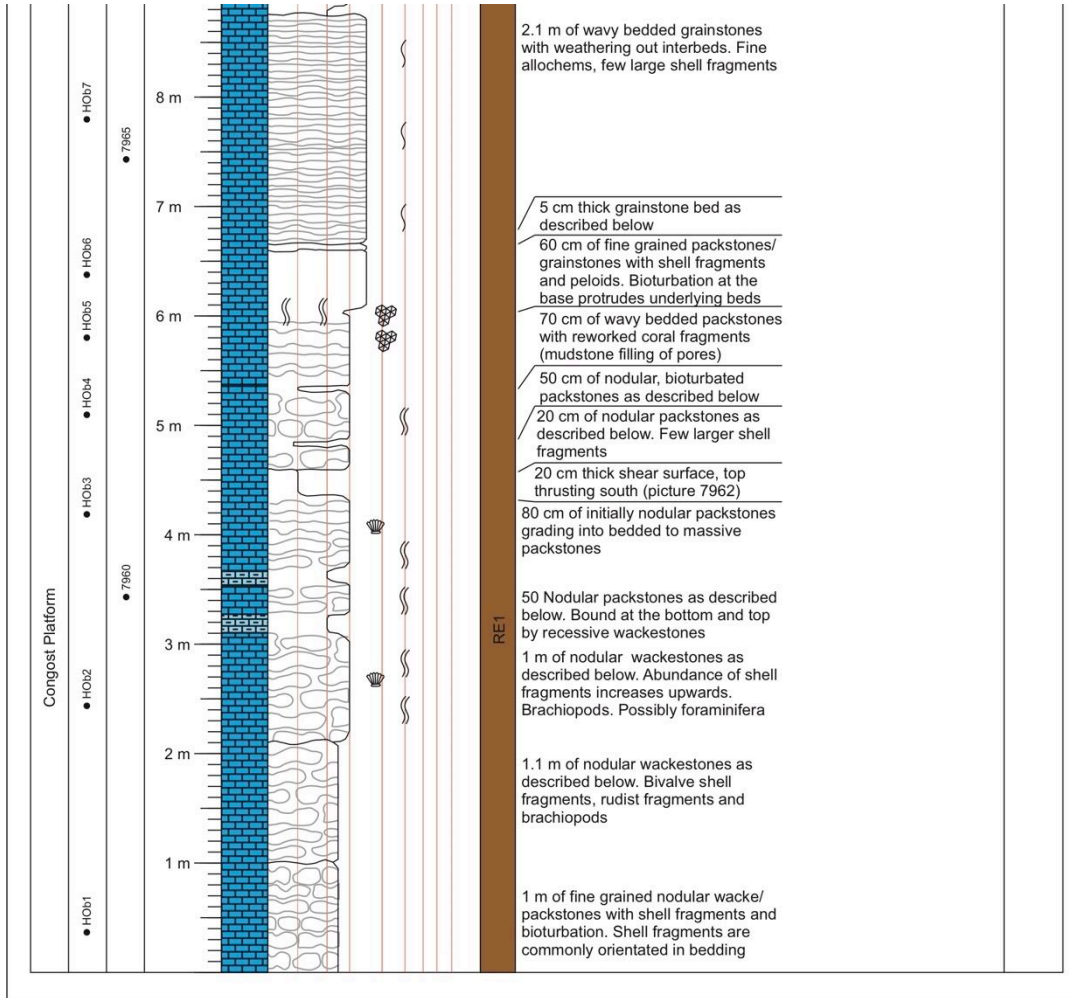
Starting point: 42°13'09.9"N (±10 m)  
001°02'42.0"E Alt.: 541 m

Ending point: 42°13'09.9"N (±4 m)  
001°02'42.0"E Alt.: 582 m

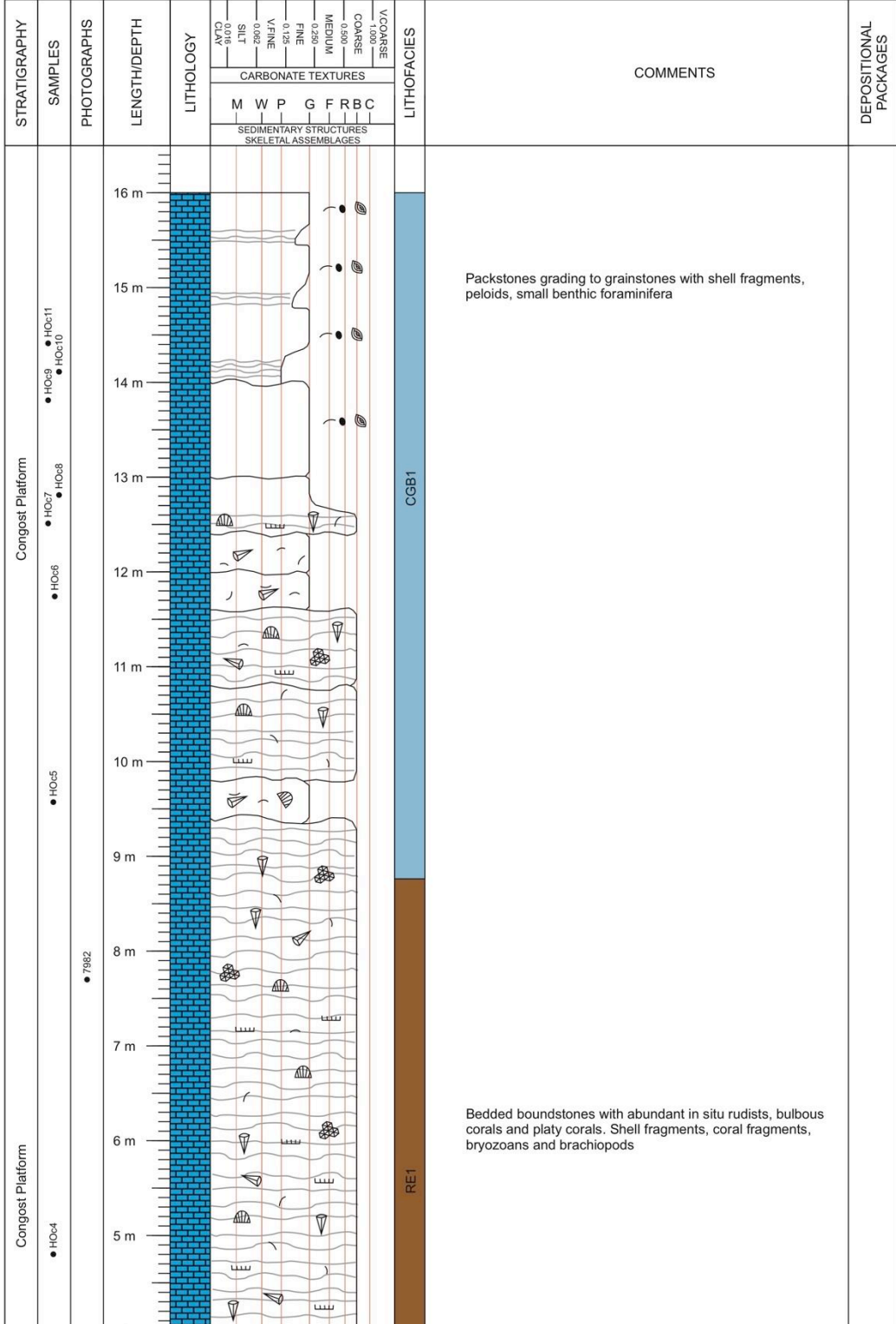


Hortoned B (HOb#) Starting point: 42°15'09.5"N (±10 m) 001°02'38.5"E Alt.: 541 m Ending point: 42°15'10.9"N (±4 m) 001°02'39.7"E Alt.: 582 m  
 (Logged 05/10/2014) Scale 1:50

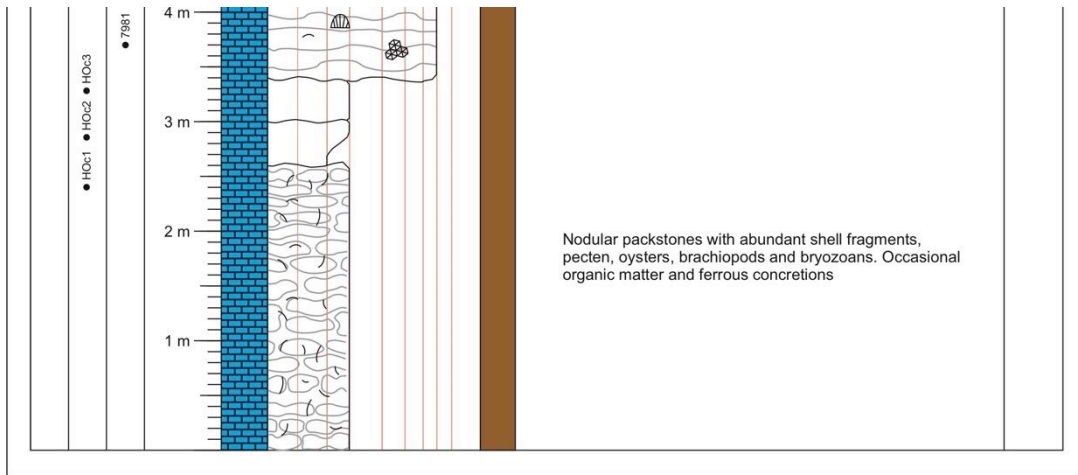




Hortonedá C (HOc#) Starting 42°15'46.4"N (±10 m) Ending 42°15'46.4"N (±4 m)  
 (Logged 05/10/2014) Scale 1:50 point: 001°02'38.1"E Alt.: 541 m point: 001°02'38.1"E Alt.: 582 m

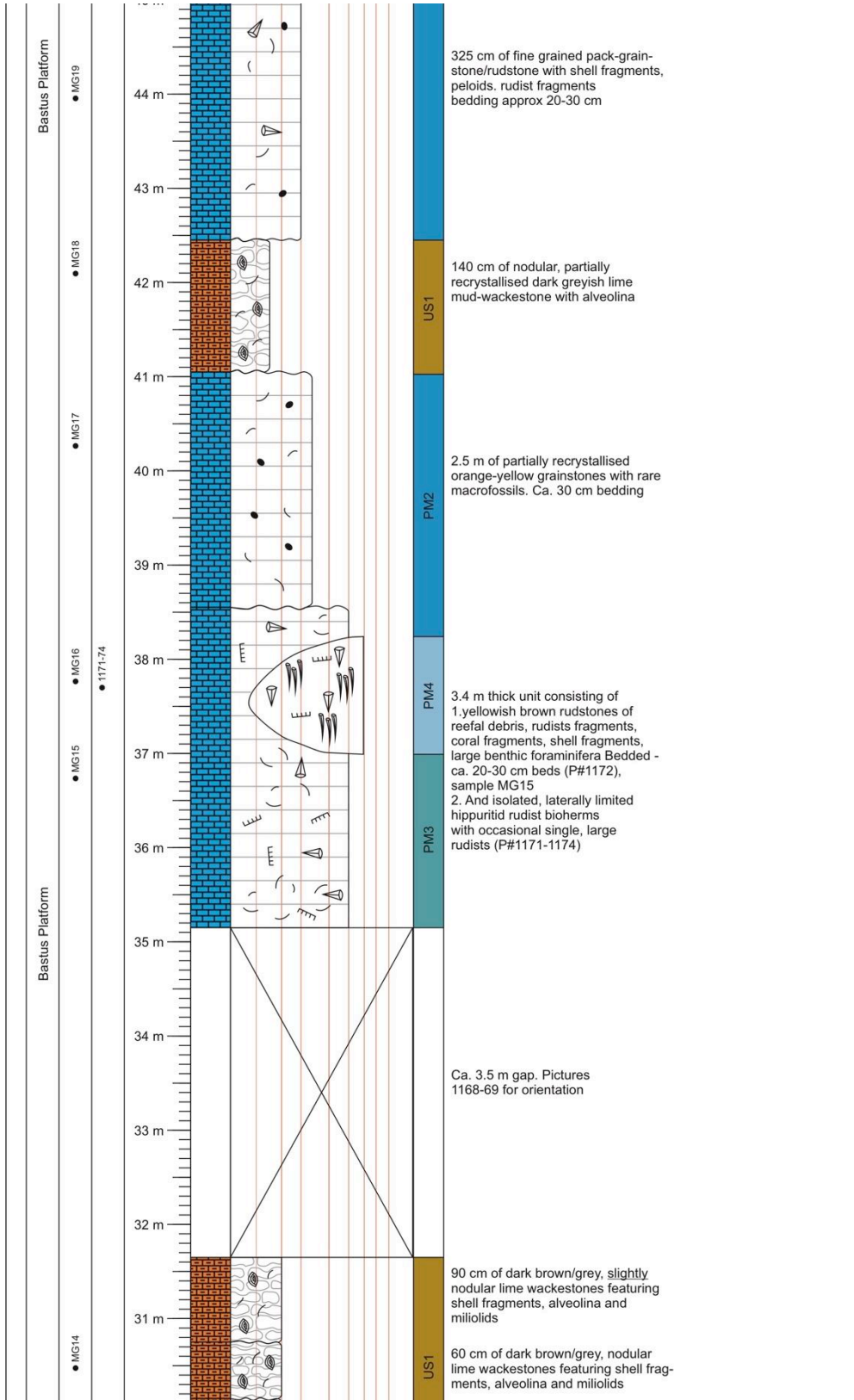


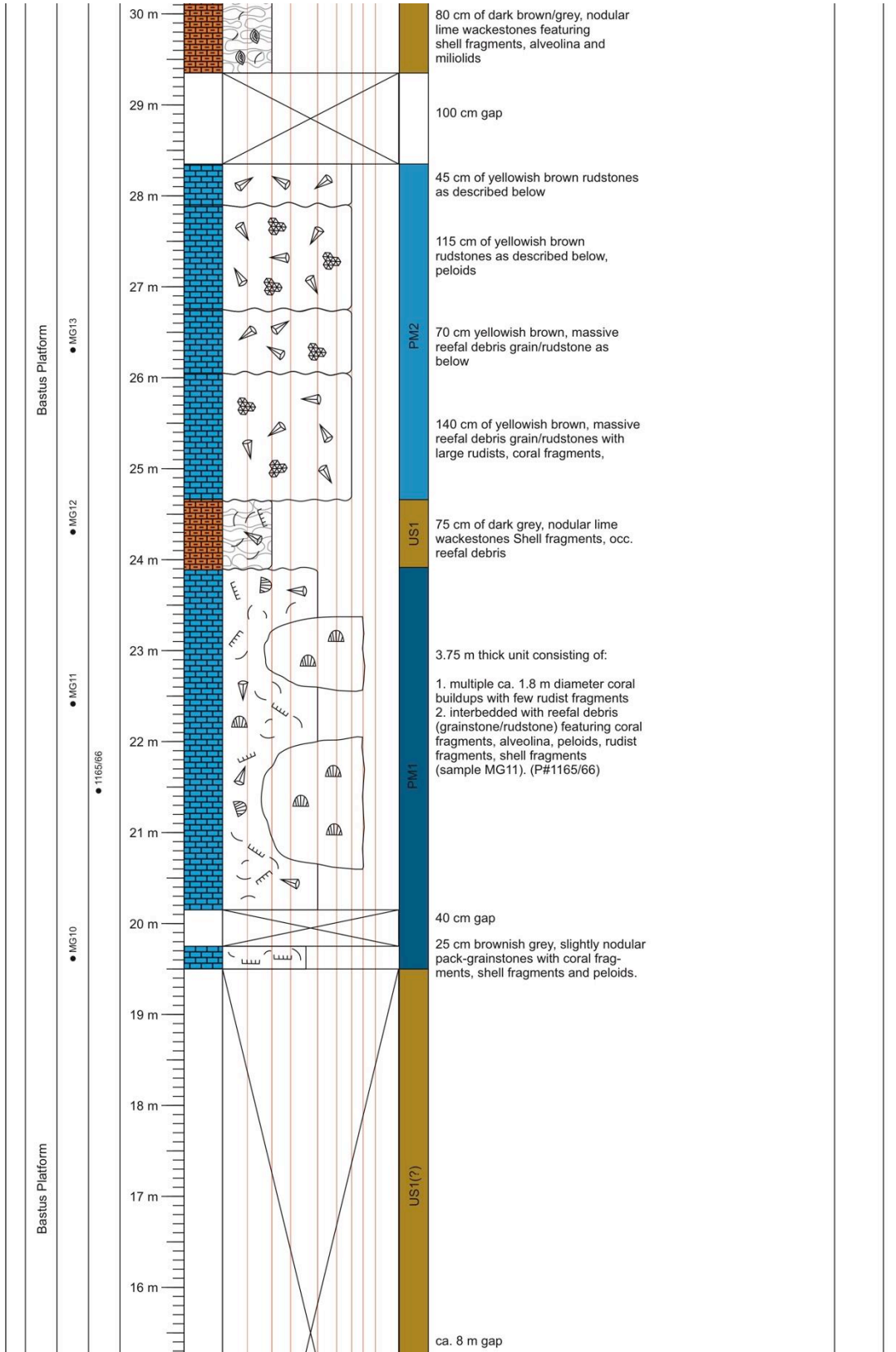


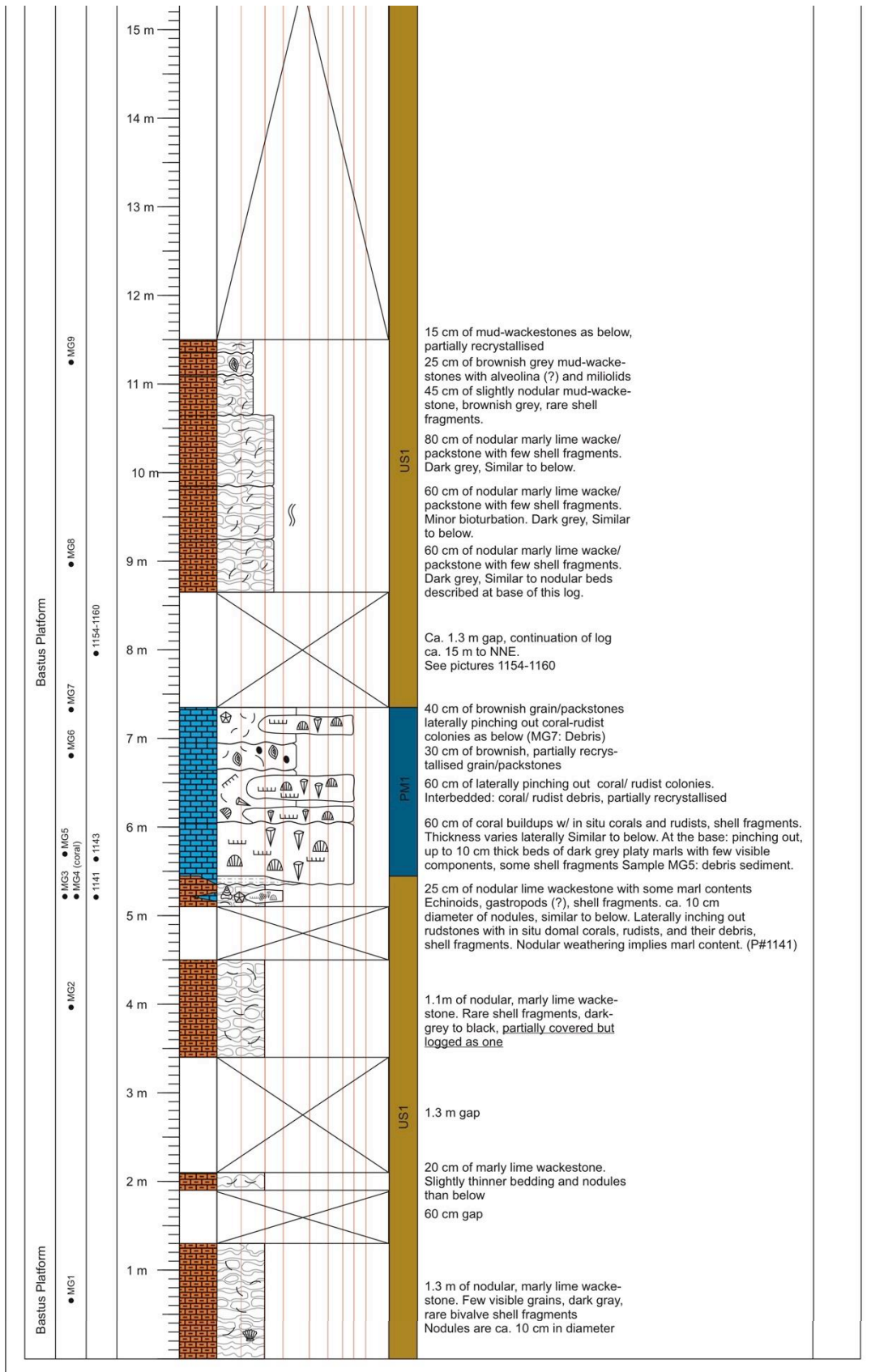


Montagut Gully (MG#) Starting 42°11'07.90"N (±3 m) Ending 42°11'10.40"N (±3 m)  
 (Logged 10/05/2013) Scale 1:50 point: 001°02'12.00"E Alt.: N/A point: 001°02'08.20"E Alt.: N/A

STRATIGRAPHY	SAMPLES	PHOTOGRAPHS	LENGTH/DEPTH	LITHOLOGY	LITHOFACIES	COMMENTS	DEPOSITIONAL PACKAGES
				(M) CO. 0.00 (W) SILT 0.00 (P) V.FINE 0.250 (G) FINE 0.125 (F) MEDIUM 0.250 (R) COARSE 0.500 (B) V.COARSE 1.000			
				CARBONATE TEXTURES M W P G F R B C			
				SEDIMENTARY STRUCTURES SKELETAL ASSEMBLAGES			
Bastus Platform	● MG26 ● MG25 ● MG24 ● MG23 ● MG22 ● MG21 ● MG20		57 m 56 m 55 m 54 m 53 m 52 m 51 m 50 m 49 m 48 m 47 m 46 m 45 m		PM2 PM4 PM2 PM2	60 cm of coral fragment rudstone  90 cm of yellowish brown grainstones with shell fragments, alveolina and peloids  80 cm as described below  135 cm of coral fragment rudstone. with shell fragments and very rare rudist fragments  150 cm of partially recrystallised peloidal grainstone  340 cm thick unit consisting of: 1. ca 40cm bedded reefal debris rudstone with coral fragments, shell fragments and rudist fragments. 2. ca. 2m in diameter hippuritid rudist bioherms with upright hippuritid rudists and occasional large single rudists  60 cm of yellowish brown grainstone with few corals (in situ?), shell fragments, large benthic foraminifera  155 cm of massive coral debris rudstone  40 cm of massive, orange, recrystallised (?) limestone with few visible shell & rudist fragments	

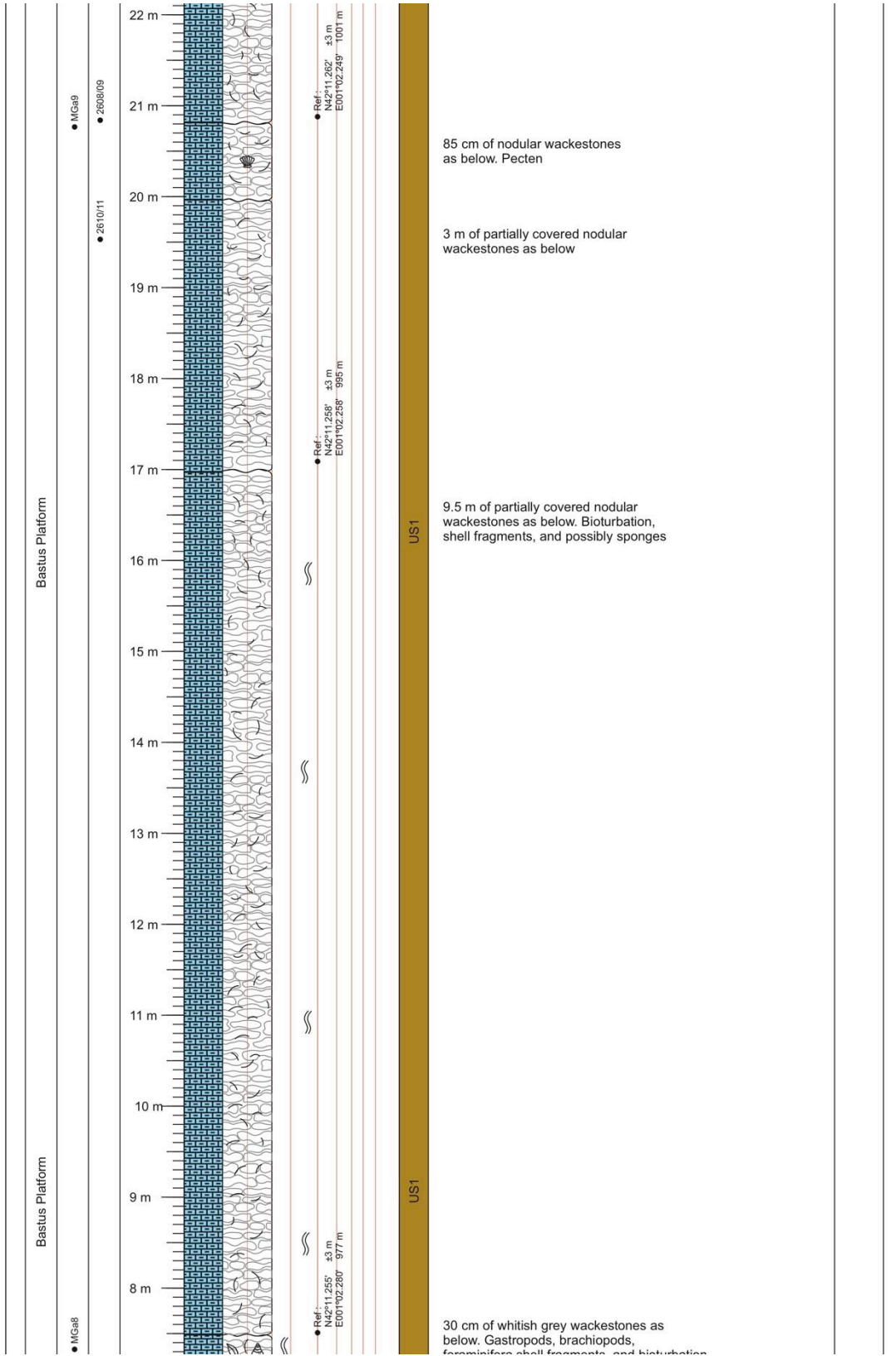


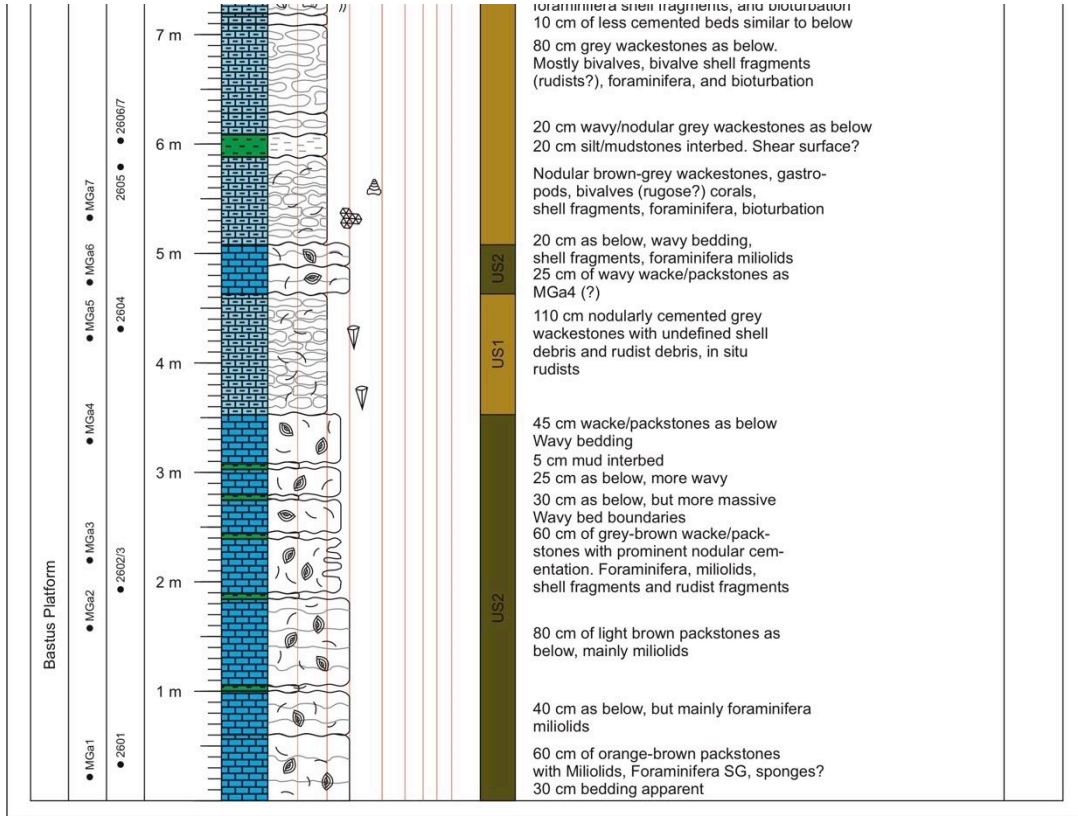




Montagut Gully A (MGa#) Starting 42°11'15.2"N (±3 m) Ending 42°11'16.1"N (±3 m)  
 (Logged 14/10/2013) Scale 1:50 point: 001°02'17.7"E Alt.: 965 m point: 001°02'12.8"E Alt.: 1023 m

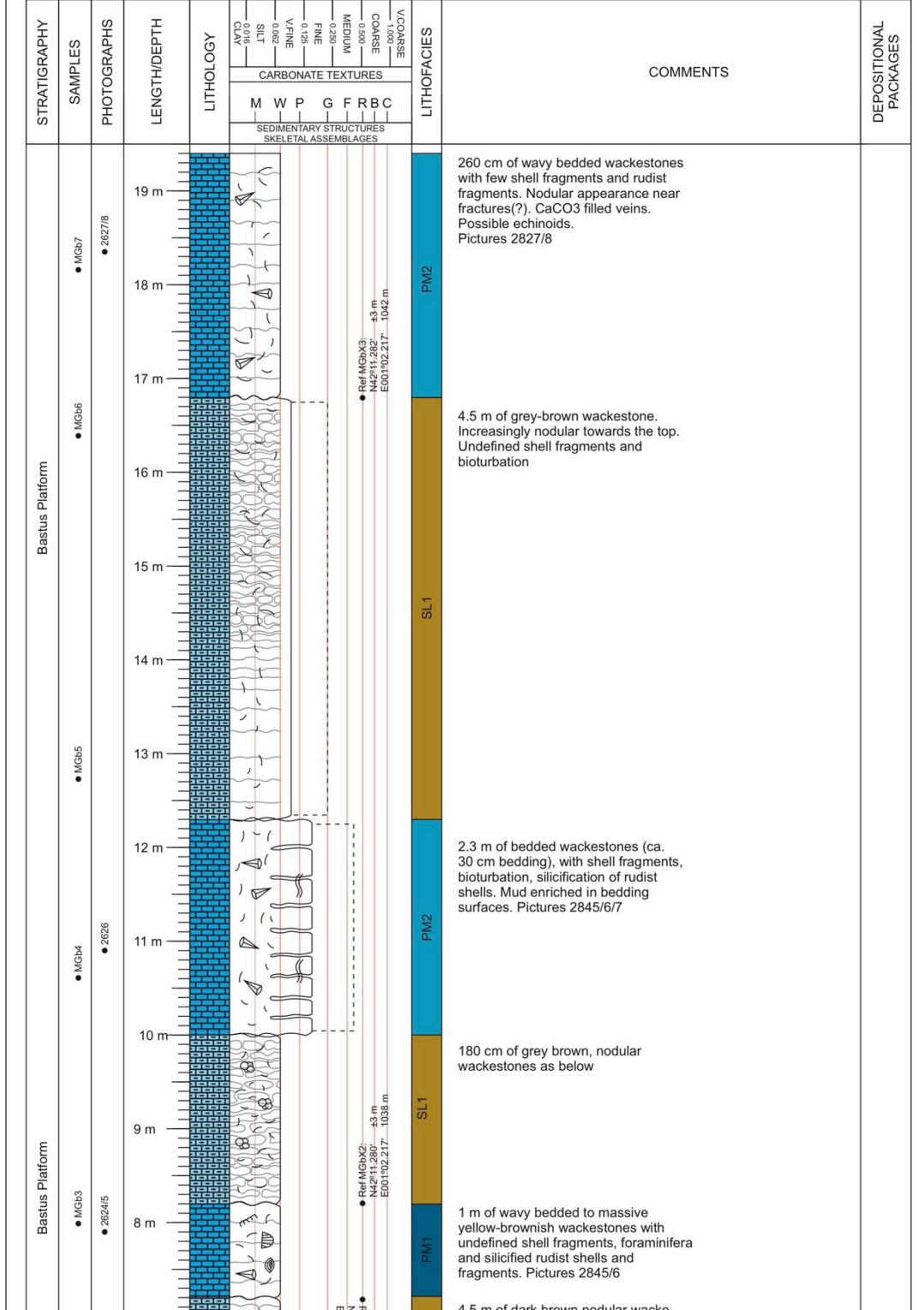
STRATIGRAPHY	SAMPLES	PHOTOGRAPHS	LENGTH/DEPTH	LITHOLOGY	SEDIMENTARY STRUCTURES SKELETAL ASSEMBLAGES	LITHOFACIES	COMMENTS	DEPOSITIONAL PACKAGES
Bastius Platform	● MGa10 ● MGa11 ● MGa12 ● MGa13 ● MGa14	● 2612/13 ● 2614/15 ● 2617/18 ● 2619	23 m to 34 m		Ref: N42°11'26.4" ±3 m E001°02'23.9" 1003 m Ref: N42°11'265" ±3 m E001°02'234" 1004 m Ref: N42°11'262" ±3 m E001°02'216" 1024 m Ref: N42°11'262" ±3 m E001°02'216" 1024 m Ref: N42°11'268" ±3 m E001°02'228" 1025 m	US1 US2 PM1	90 cm of yellow brown wacke/pack stones with shell debris, foraminifera and silicified coral skeletons (Picture 2620) 30 cm of massive/wavy light brown wackestones with rudist fragments and miliolids 60 cm of nodular cemented, whitish wackestones, with foraminifera, miliolids, sponges, in situ rudists and corals. Bioturbation 4.2 m of nodular cemented dark-brown wackestones with Corals (in situ?), gastropods, Bioturbation 65 cm of yellow-brown wacke/packstones with bivalve shell fragments 65 cm of nodular whitish grey wacke/packstones with shell fragments, gastropods and bivalves. Picture 2614/5 110 cm of nodular wacke/packstones with gastropods, bivalves and shell fragments. Unknown organism: 2613/2614 1 m of partially covered wackestones as below. Pecten 85 cm of nodular wackestones as below. Brachiopods 290 cm as below, partially covered	

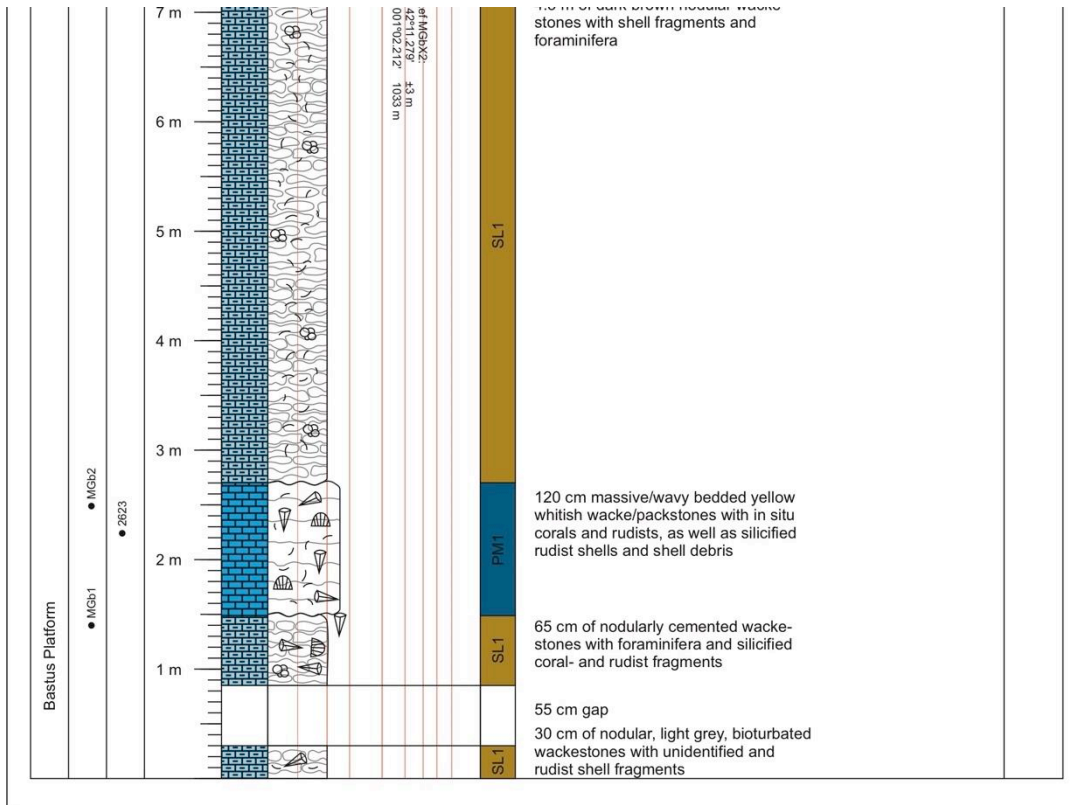




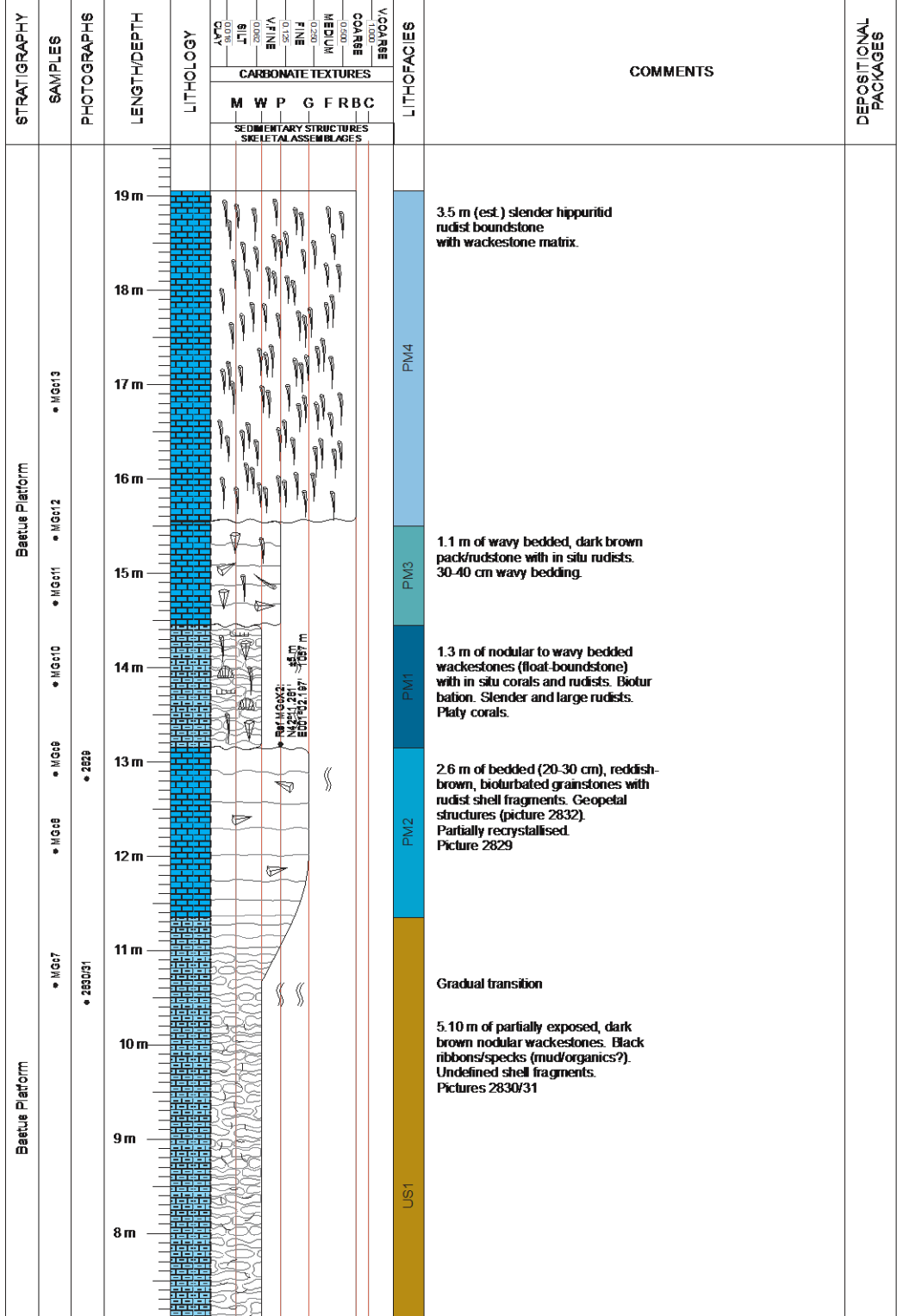


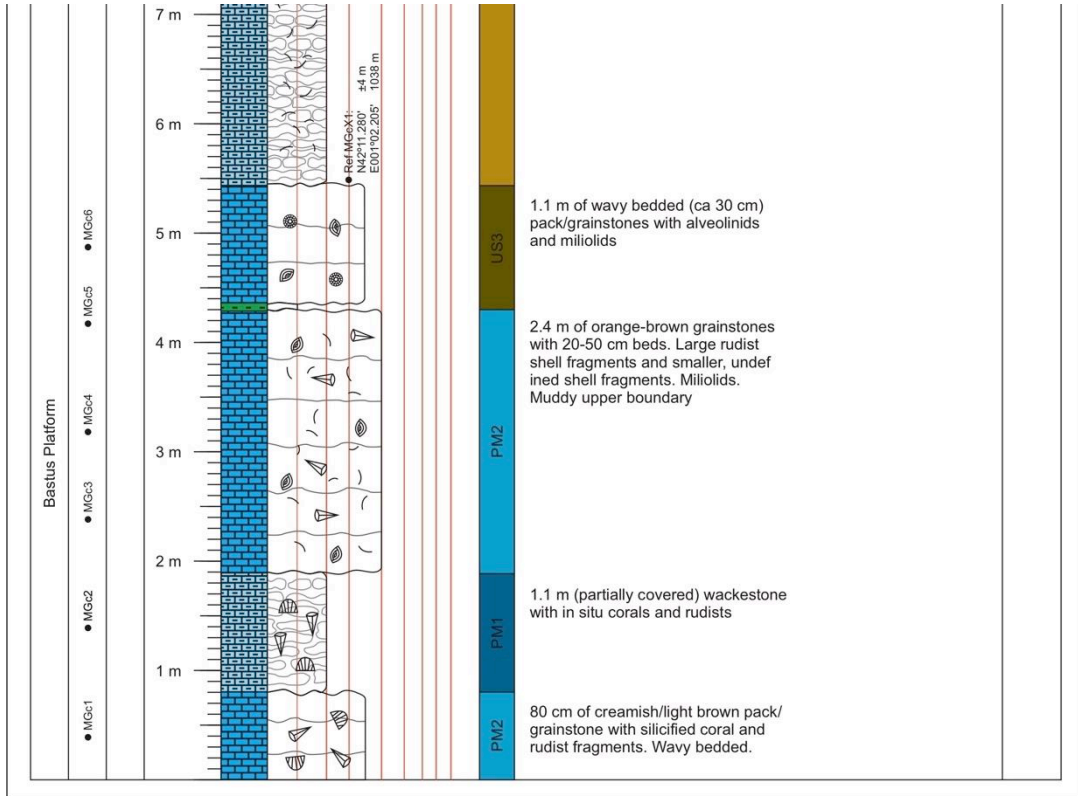
Montagut Gully B (MGB#) Starting 42°11'16.5"N (±3 m) Ending 42°11'17.0"N (±3 m)  
 (Logged 21/10/2013) Scale 1:50 point: 001°02'12.9"E Alt.: 1027 m point: 001°02'12.8"E Alt.: 1047 m



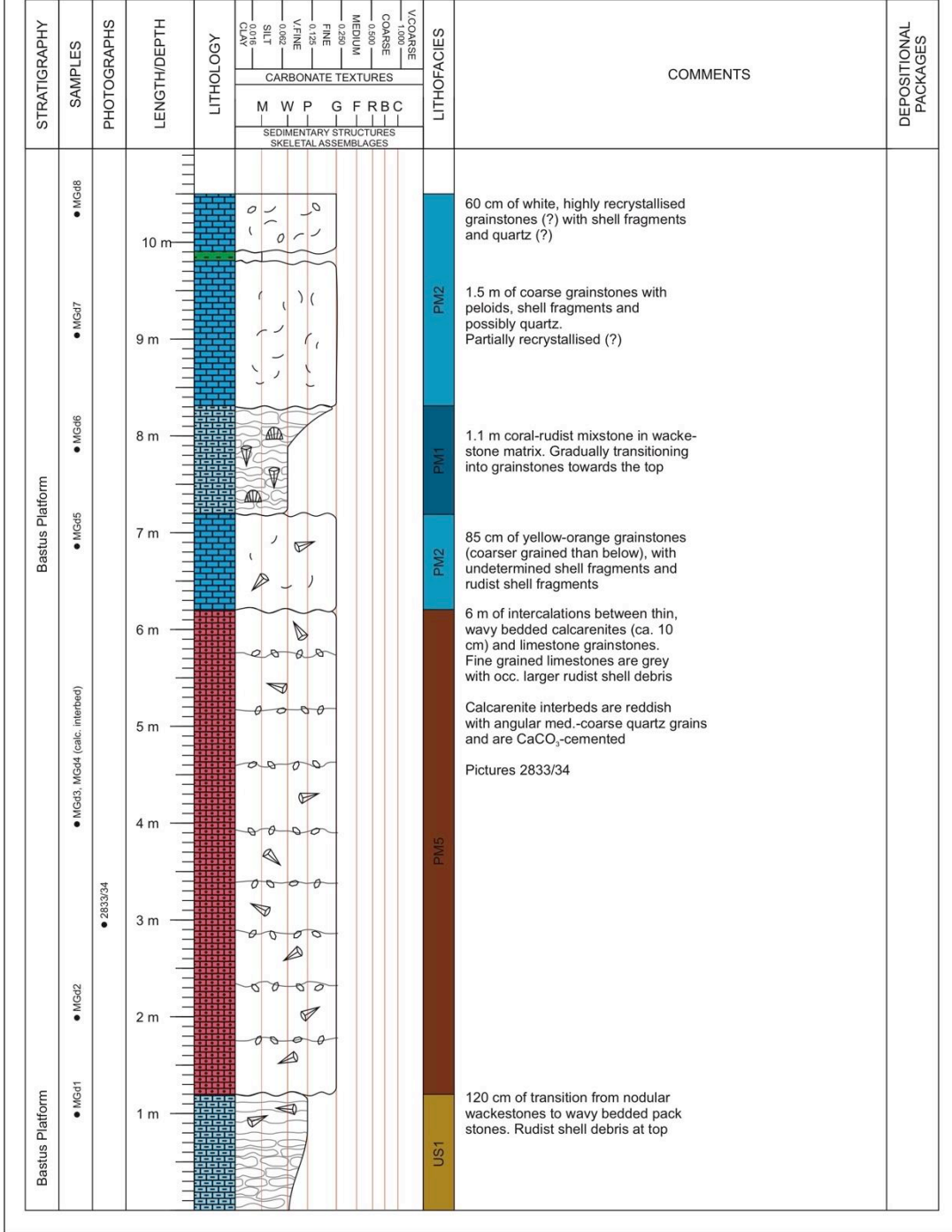


Montagut Gully C (MGc#) Starting 42°11'16.8"N (±3 m) Ending 42°11'17.5"N (±5 m)  
 (Logged 21/10/2013) Scale 1:50 point: 001°02'12.5"E Alt: 1040 m point: 001°02'11.8"E Alt: unknown

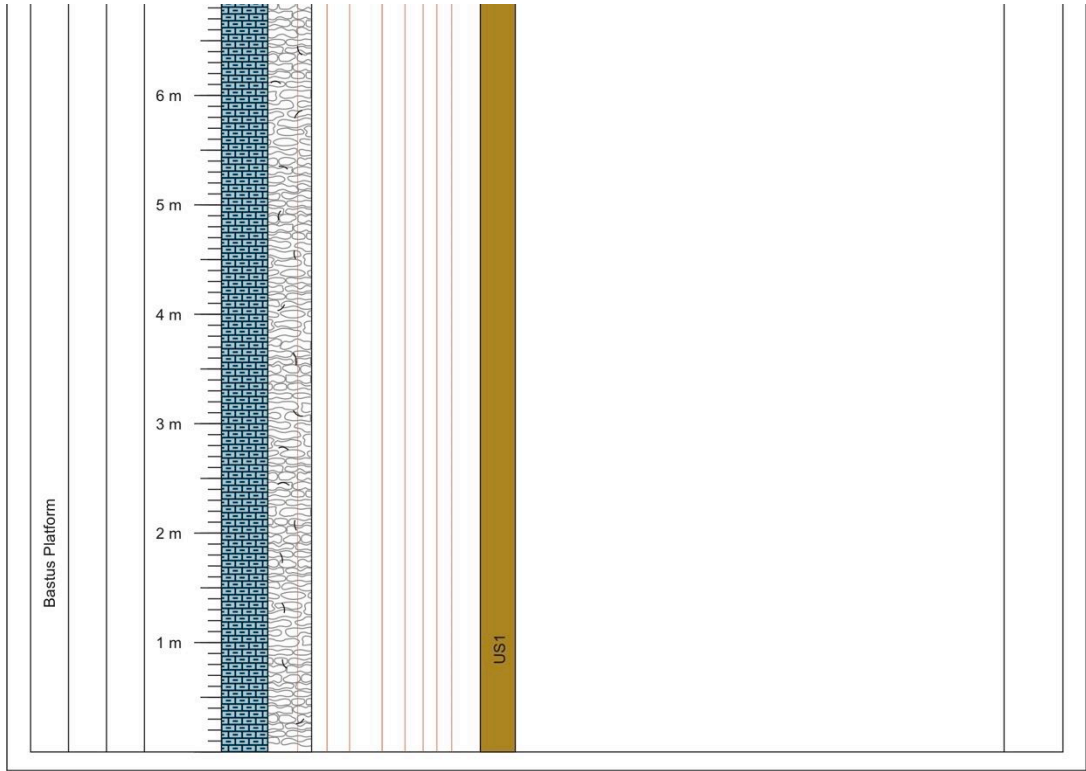




Montagut Gully D (MGd#) Starting 42°11'16.1"N (±3 m) Ending 42°11'16.4"N (±4 m)  
 (Logged 21/10/2013) Scale 1:50 point: 001°02'09.7"E Alt.: 1069 m point: 001°02'09.7"E Alt.: 1070 m





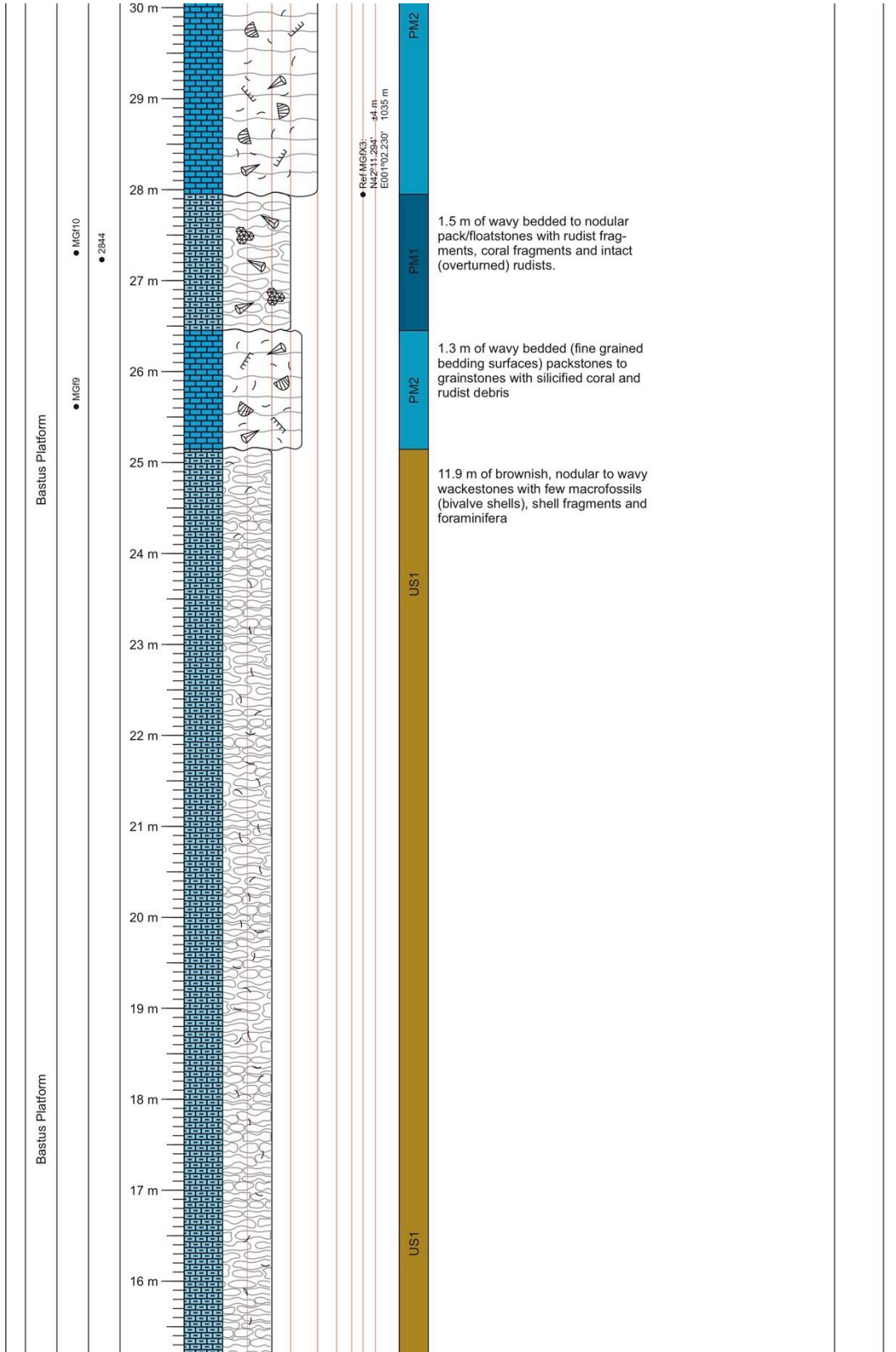


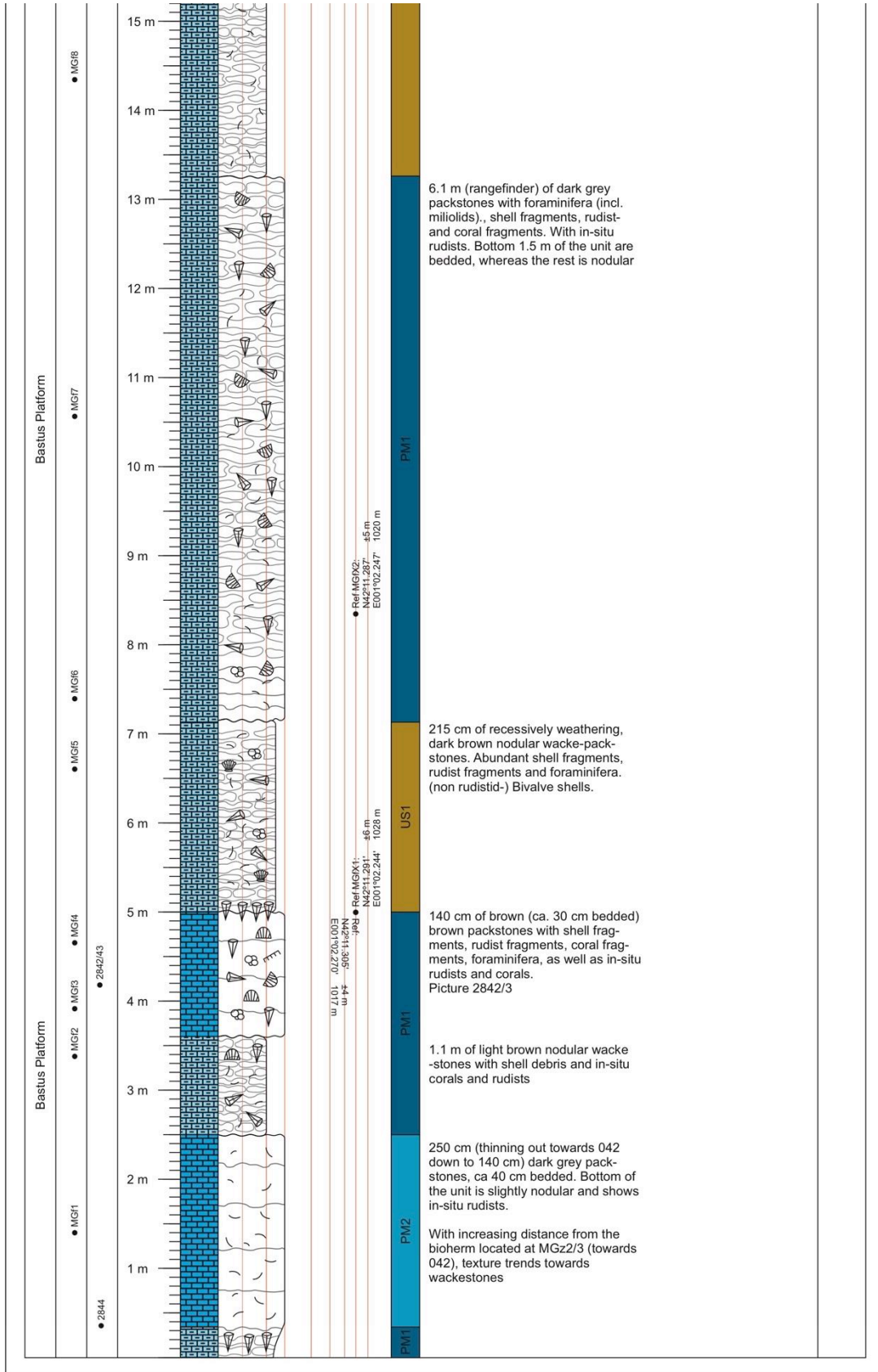
Montagut Gully F (MGF#) Starting 42°11'17.8"N (±4 m) Ending 42°11'18.0"N (±3 m)  
 (Logged 22/10/2013) Scale 1:50 point: 001°02'15.6"E Alt.: 1011 m point: 001°02'13.6"E Alt.: unknown

STRATIGRAPHY	SAMPLES	PHOTOGRAPHS	LENGTH/DEPTH	LITHOLOGY	CARBONATE TEXTURES	SEDIMENTARY STRUCTURES	SKELETAL ASSEMBLAGES	LITHOFACIES	COMMENTS	DEPOSITIONAL PACKAGES
Bastus Platform	● MGH12		42 m					PM2	50 cm of orange-brown, ca. 20-40 cm bedded bioclastic grainstones with sponge (?) fragments, rudist fragments	
			41 m					PM4	1.7 m of slender hippuritid dominated boundstone, with occasional larger, solitary rudists. Wackestone matrix.	
			40 m							
			39 m					PM3	2.7 m of wavy bedded / nodular weathering wacke/packstones with various in-situ rudists and corals (Equiv. to Sheetstone after Pomar et al. 2005?)	
			38 m							
Bastus Platform	● MGH11		37 m					PM2	2.8 m bedded, bioclastic pack/grain stones with silicified rudist and coral fragments. Equivalent to 2 beds below. Pinching out eastwards (?) Pictures 2845-49.	
	● 2845-2849		36 m							
			35 m							
			34 m					US1	3 m nodular, dark brown wackestone with shell fragments and foraminifera	
			33 m							
		32 m								
		31 m							3.5 m of bedded bioclastic grainstones, as 2 beds below. Coral and rudist fragments replaced by silica.	

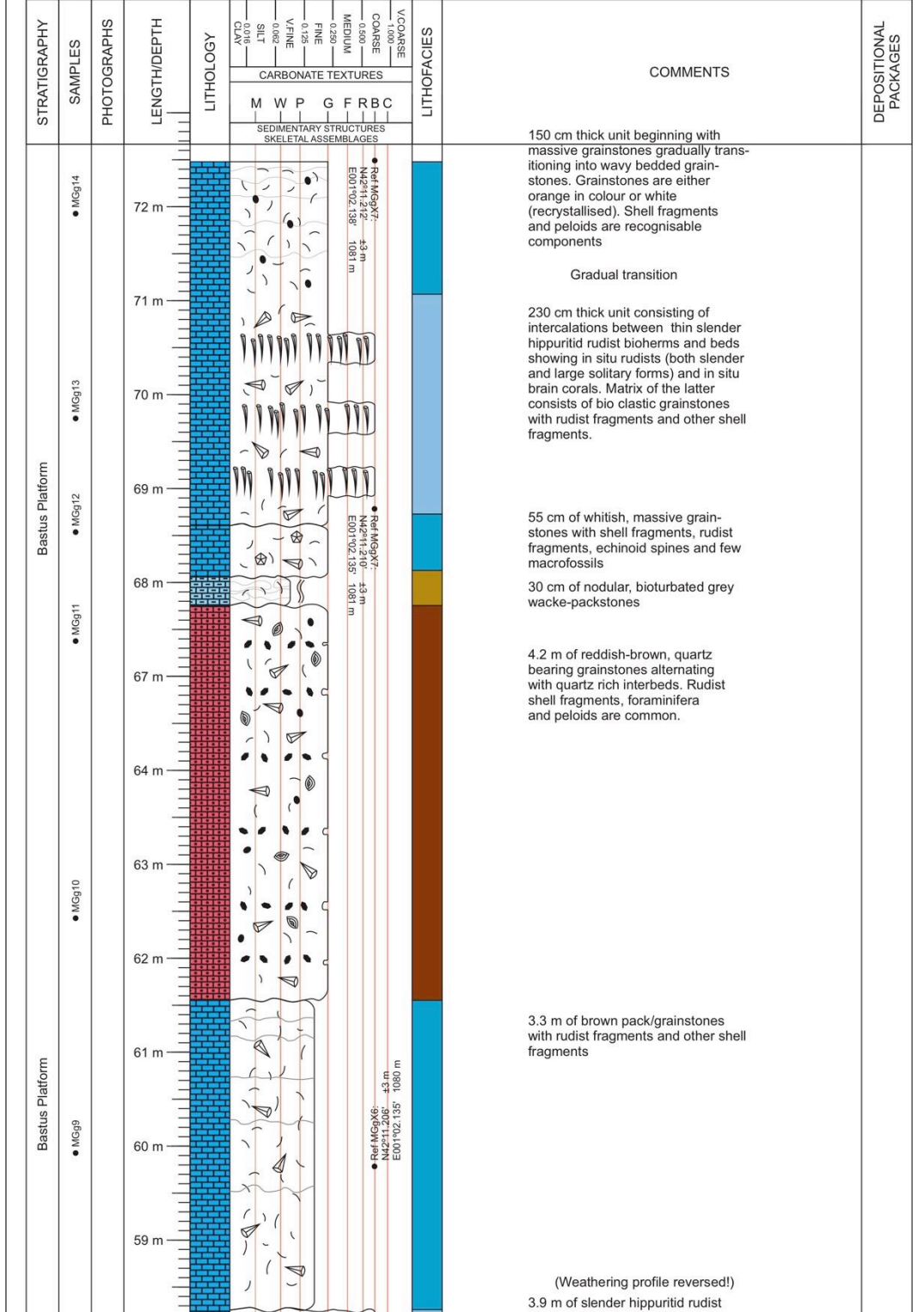
● Ref MGH4:  
 NE 1/4 Sec 20:  
 E00°10'2.220" 1044 m

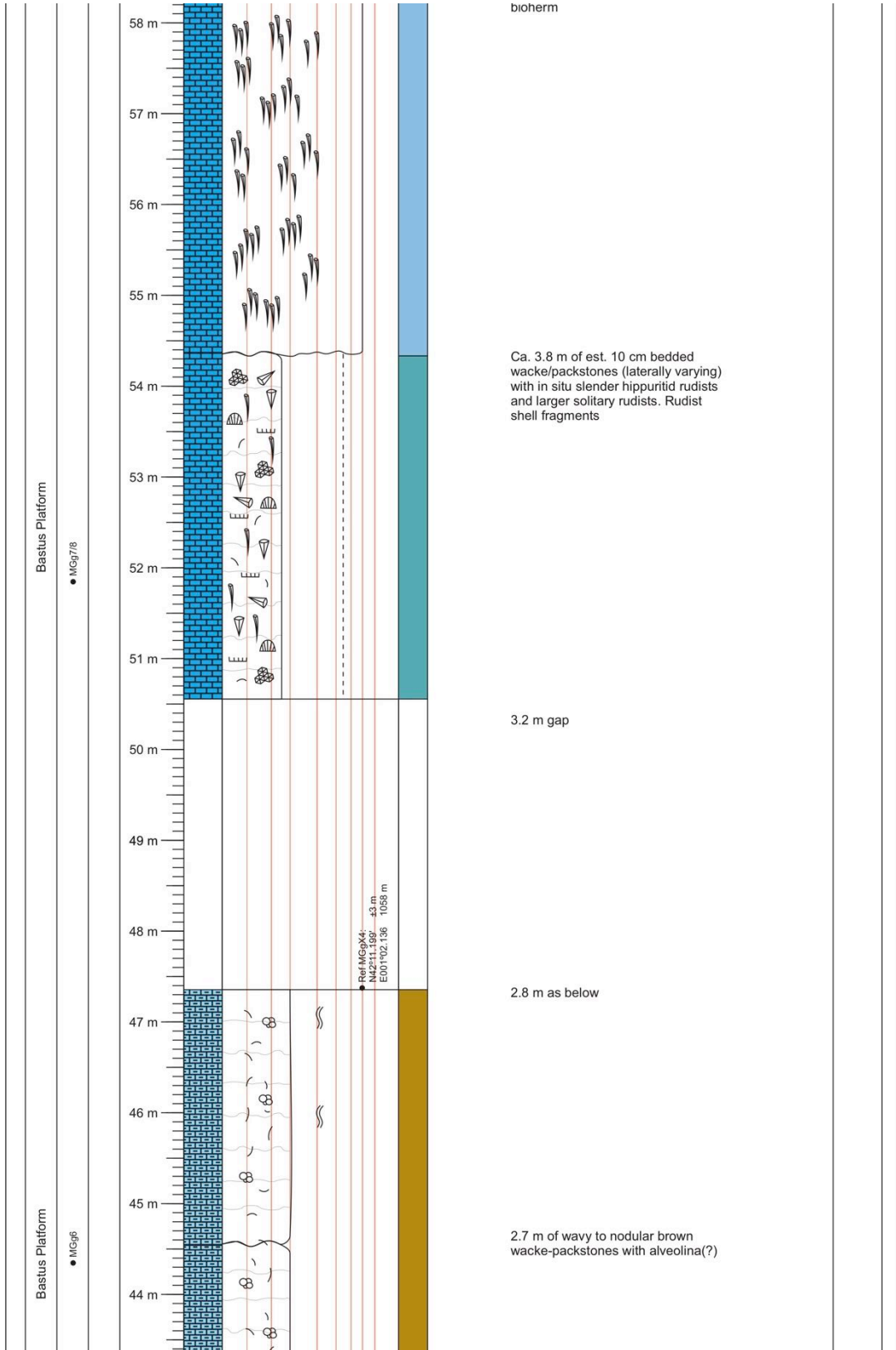






Montagut Gully G (MGg#) Starting 42°11'11.3"N (±3 m) Ending 42°11'12.7"N (±3 m)  
 (Logged 23/10/2013) Scale 1:50 point: 001°02'10.6"E Alt.: 1043 m point: 001°02'08.3"E Alt.: 1081 m





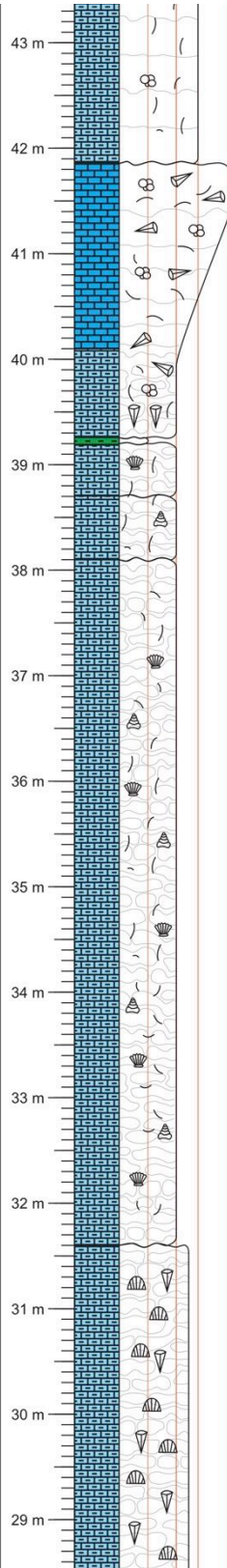
latform

Bastius Platform

● MGg5

● 2916/2917

● MGg4



● B4/MGg-3/4  
M2211.108' -44 m  
E001'02.154' 1056 m

● B4/MGg-3/4  
M2211.103' -44 m  
E001'02.145' 1064 m

11.5 m of partially covered beds as below

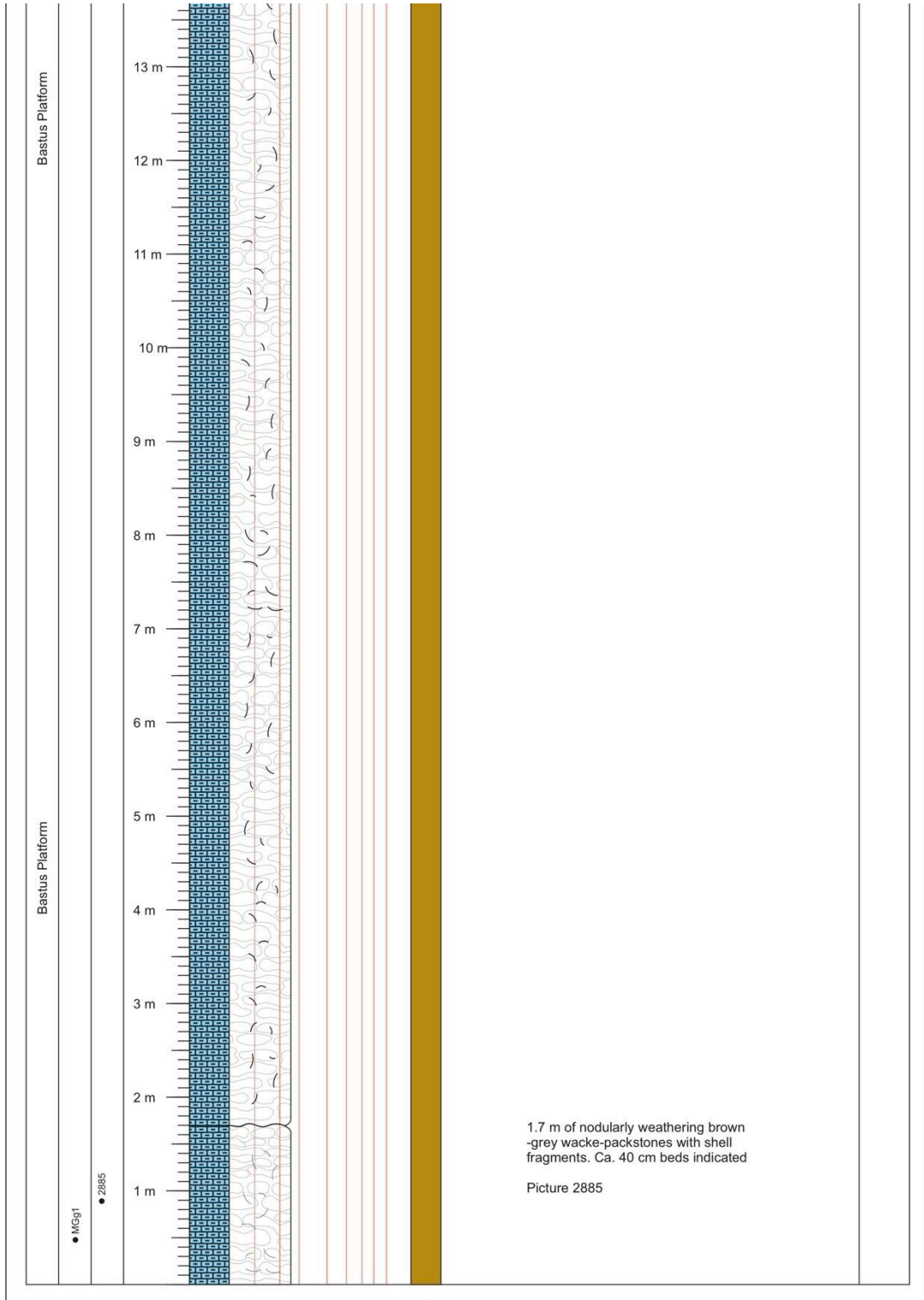
6.5 m of brown nodular to wavy wackestones with rare shell fragments and gastropods / bivalves

60 cm of nodular/wavy wackestones as below

50 cm of nodular/wavy wackestones as below

2.6 m transition from brown nodular wackestones over wavy grey-brown packstones to bedded orange grain-stones. Alveolina, bivalve shell fragments and rudist fragments are common throughout. In situ rudists observed at the bottom.

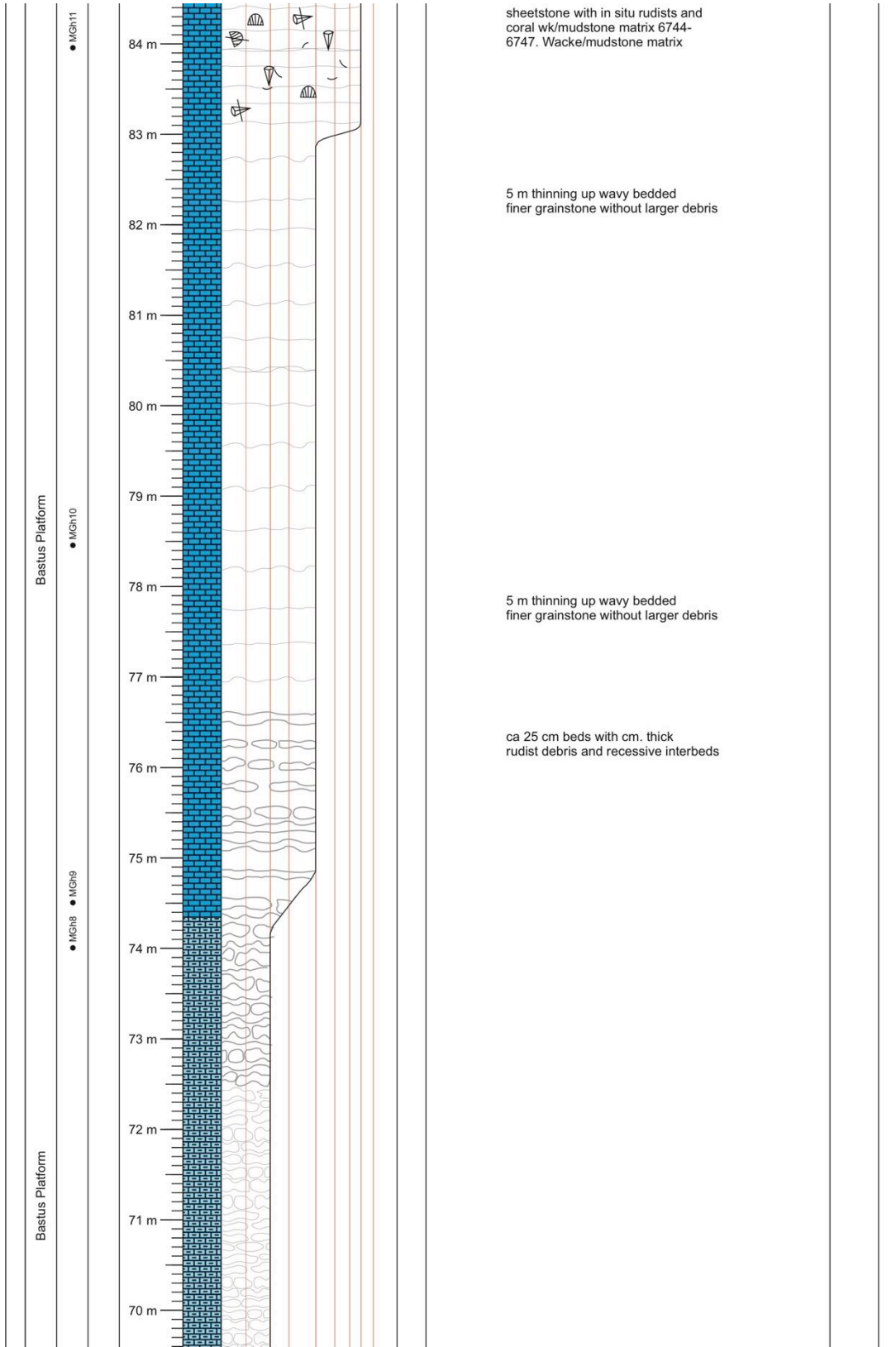


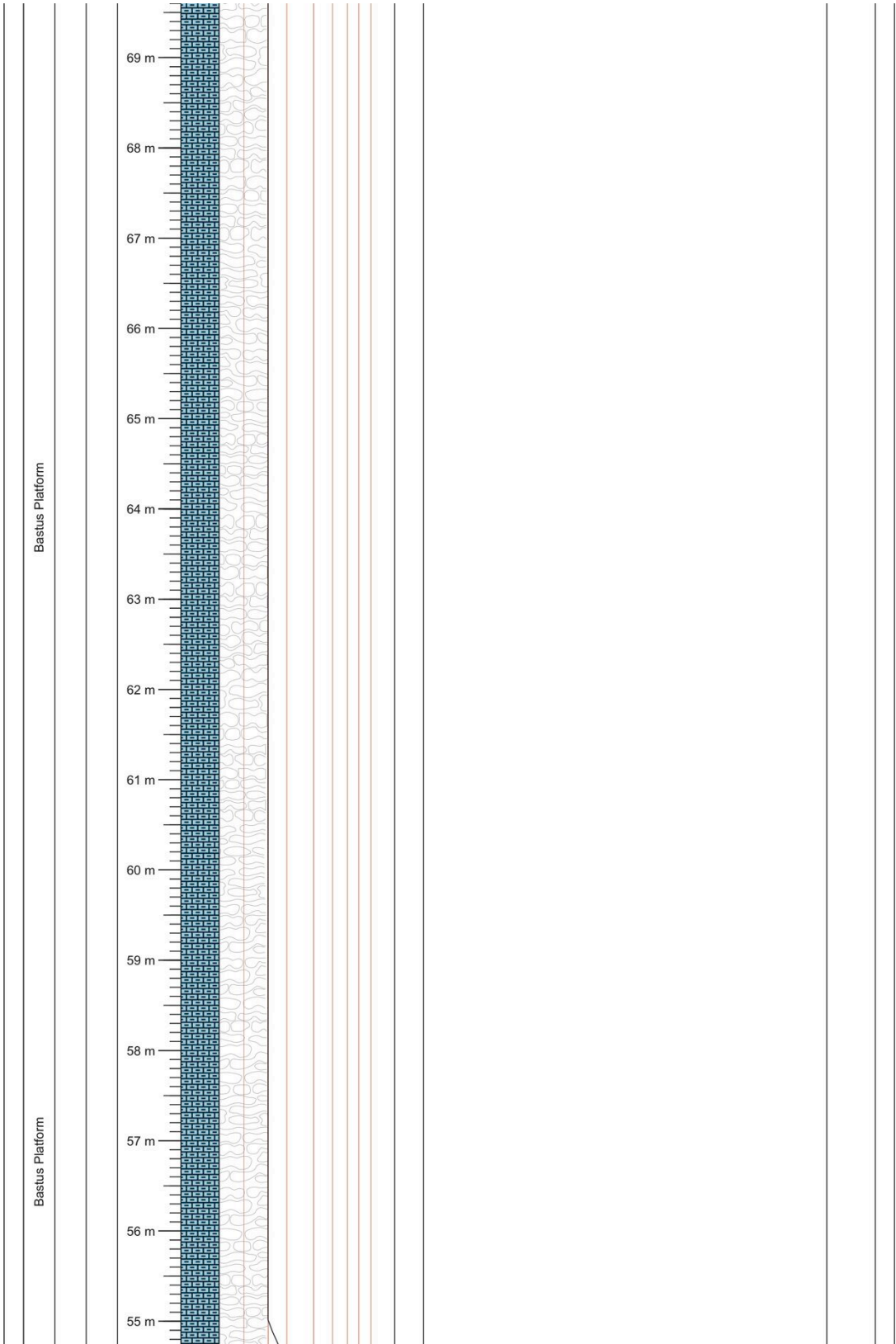


Montagut Gully H (MGh#) Starting 42°11'06.9"N (±3 m) Ending 42°11'16.5"N (±3 m)  
 (Logged 24/09/2014) Scale 1:50 point: 001°01'57.2"E Alt.: 1016 m point: 001°01'54.1"E Alt.: 1078 m

STRATIGRAPHY	SAMPLES	PHOTOGRAPHS	LENGTH/DEPTH	LITHOLOGY	CARBONATE TEXTURES							LITHOFACIES	COMMENTS	DEPOSITIONAL PACKAGES								
					M	W	P	G	F	R	B				C							
																SEDIMENTARY STRUCTURES						
																SKELETAL ASSEMBLAGES						
Bastus Platform	● MGh16		96 m									50 cm rudist bearing grainstones										
			95 m									150 cm of mix/sheetstone? with slightly wavy bedding										
	● MGh15		94 m									Rudist bearing grainstones with quartz. 40-10 cm beds. Silicified rudist debris. Wavy bedded. Orange to brown weathering										
			93 m																			
			92 m																			
	● MGh14		91 m									sheet/mixstone with flasery/wavy bedding. Silicified in situ corals and rudists. Grey weathering										
			90 m									Organ Pipes Partially silicified rudists on weathered surfaces Occasional larger individual rudists										
			89 m									3/4 m. Yellowish wacke/mudstone matrix Pictures until 6757										
	● MGh13		88 m																			
			87 m																			
	● MGh12		86 m																			
			85 m									Sheetstone transitioning into organ pipes. Pictures until 6750										

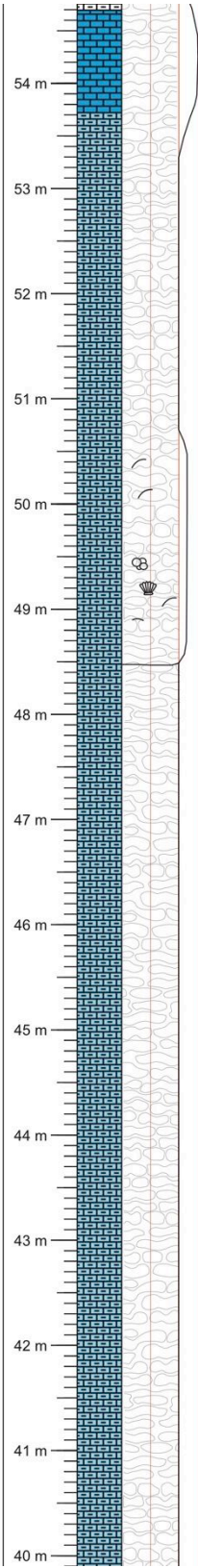






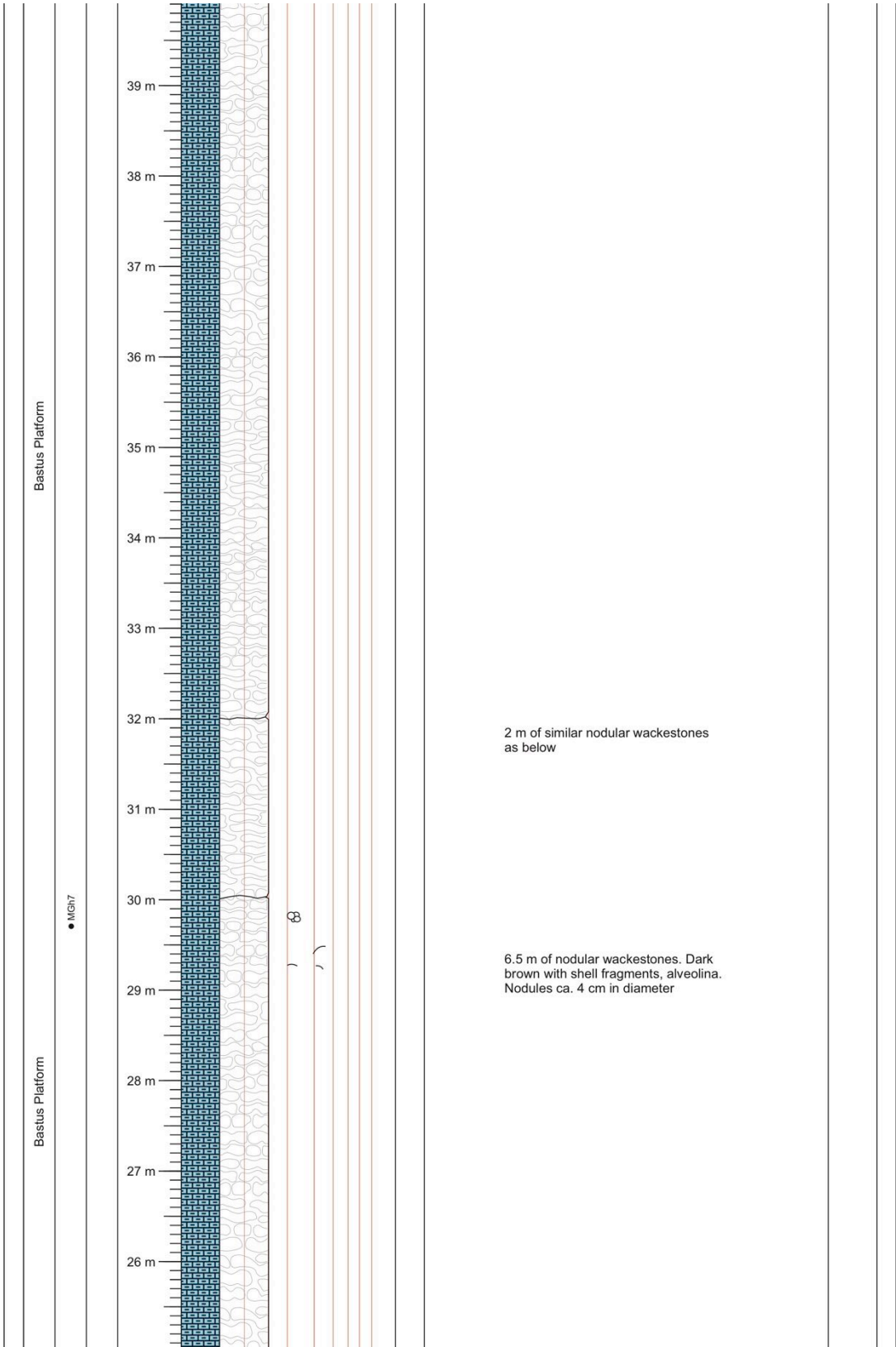
Bastus Platform

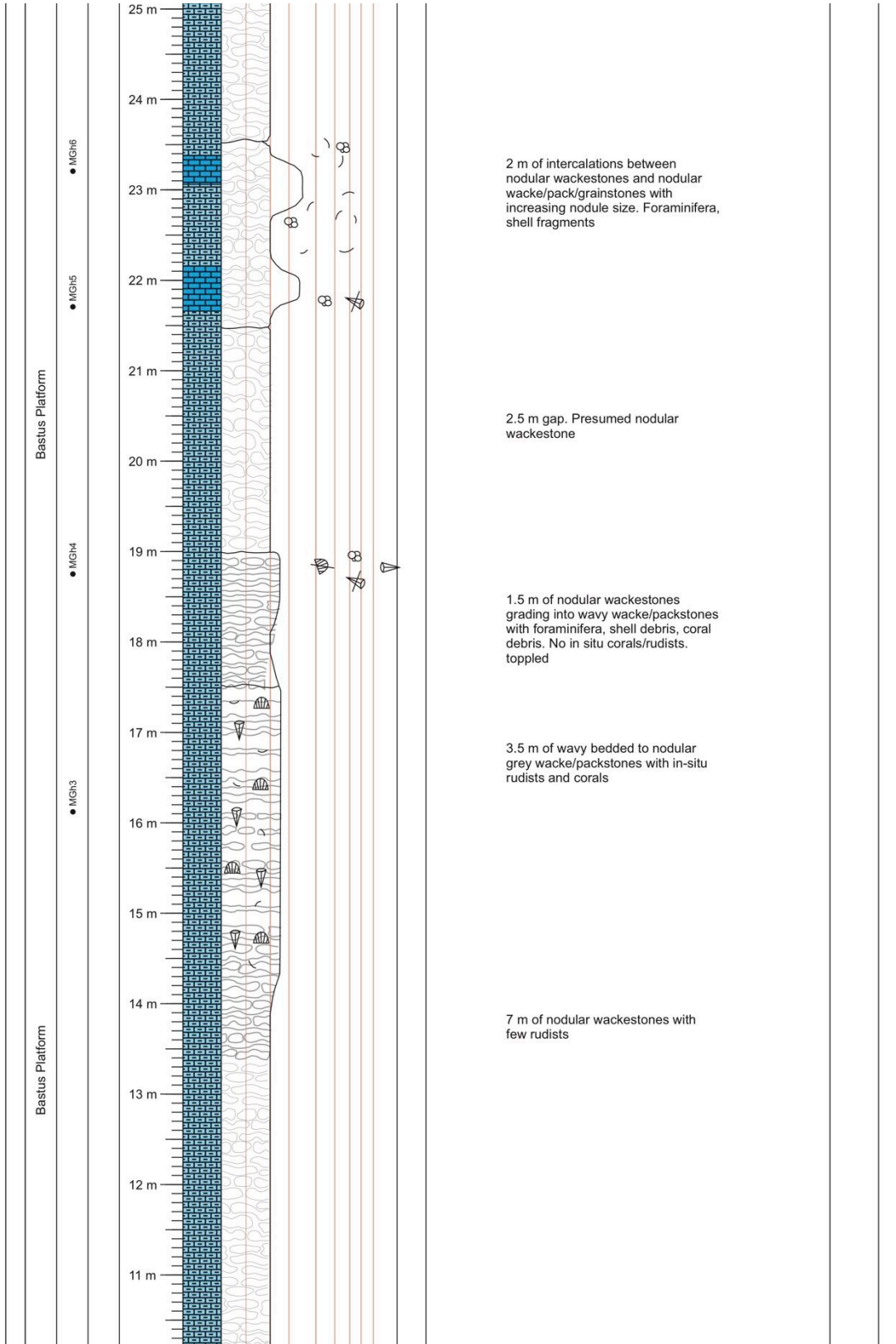
Bastus Platform

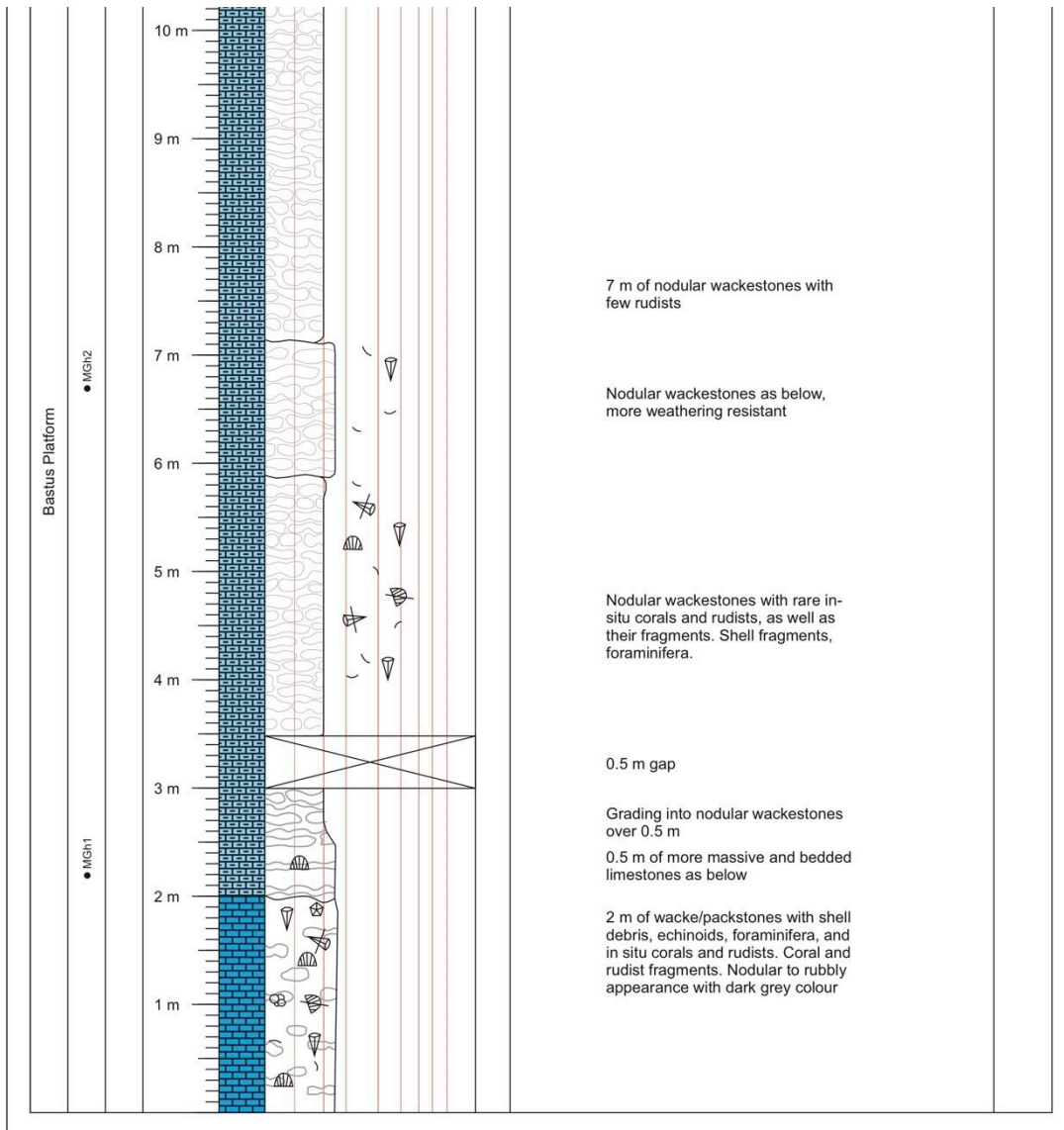


2 m of nodular wacke/packstones with bivalves, miliolids, foraminifera. Large nodules and more prominent bed. Dark brown

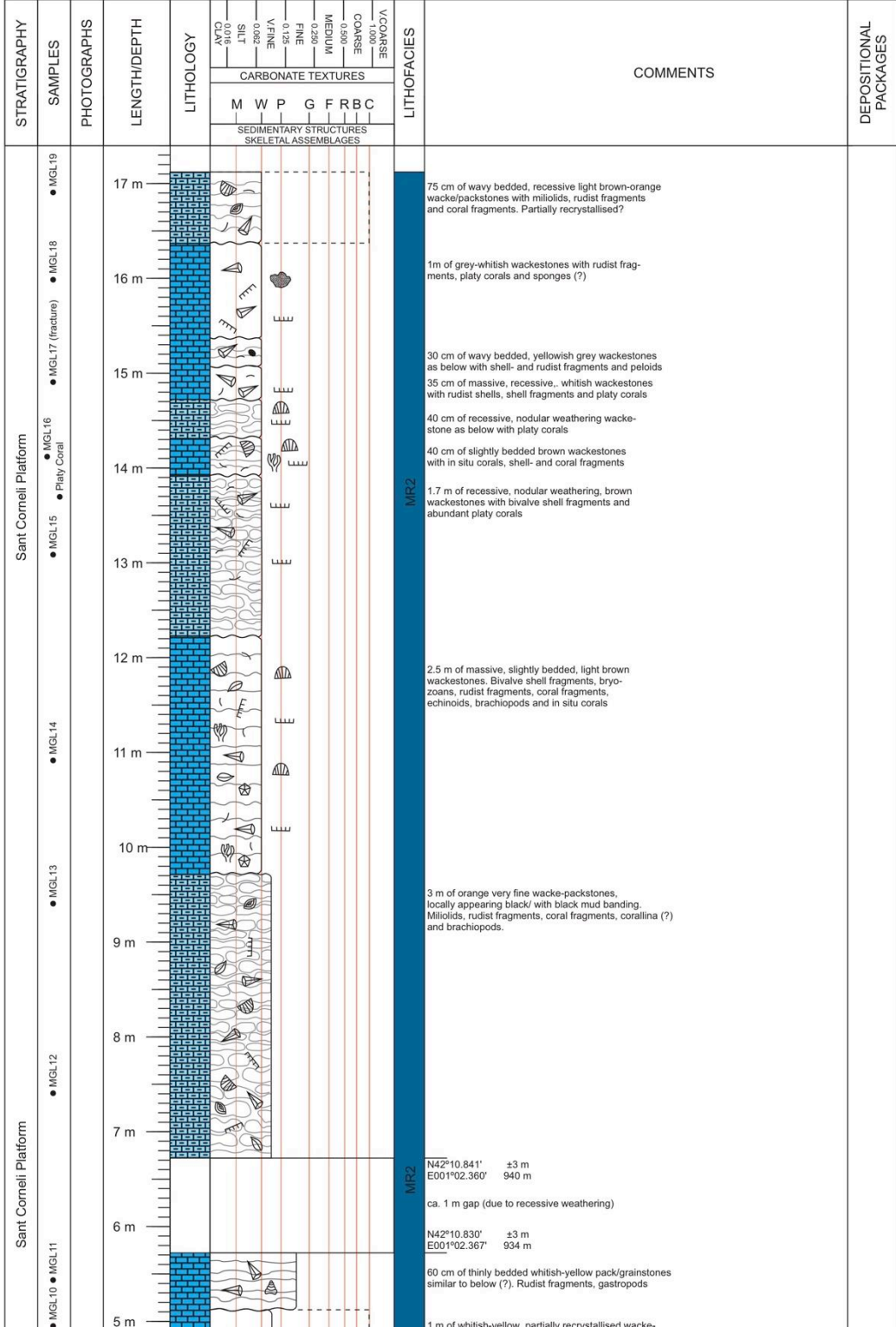
16.5 m of partially covered nodular wackestones as below

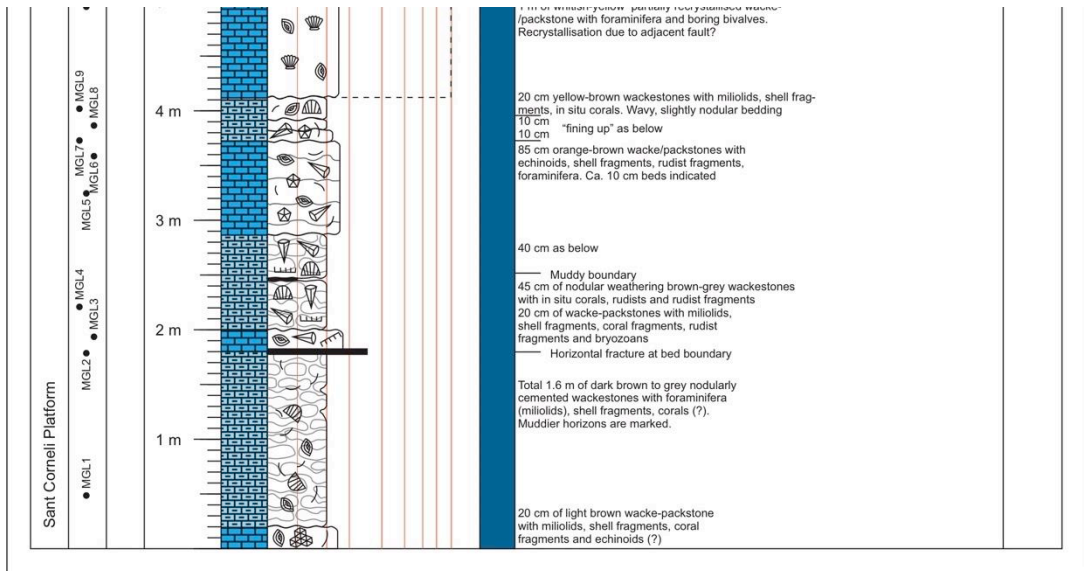






Montagut Gully Lagoon (MGL#) Starting 42°10'49.7"N (±3 m) Ending 42°10'50.6"N (±3 m)  
 (Logged 13/10/2013) Scale 1:50 point: 001°02'22.0"E Alt.: 936 m point: 001°02'22.1"E Alt.: 955 m







Mont Rebei A (MRa#)  
(Logged 04/10/2014) Scale 1:5

Starting point: 42°03'43.3"N (±10 m)  
000°40'04.0"E Alt.: 541 m

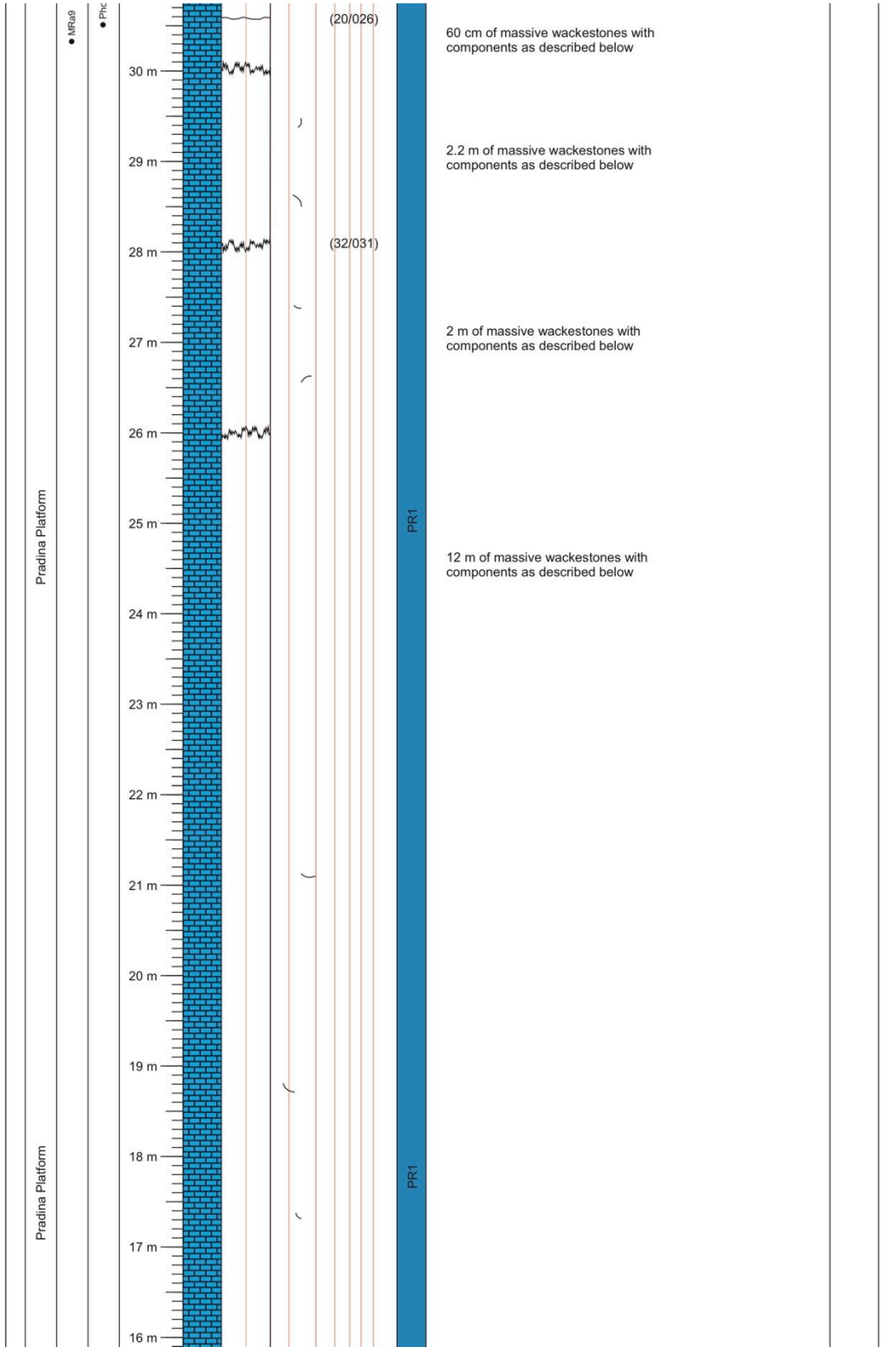
Ending point: 42°03'44.9"N (±4 m)  
000°40'07.9"E Alt.: 582 m

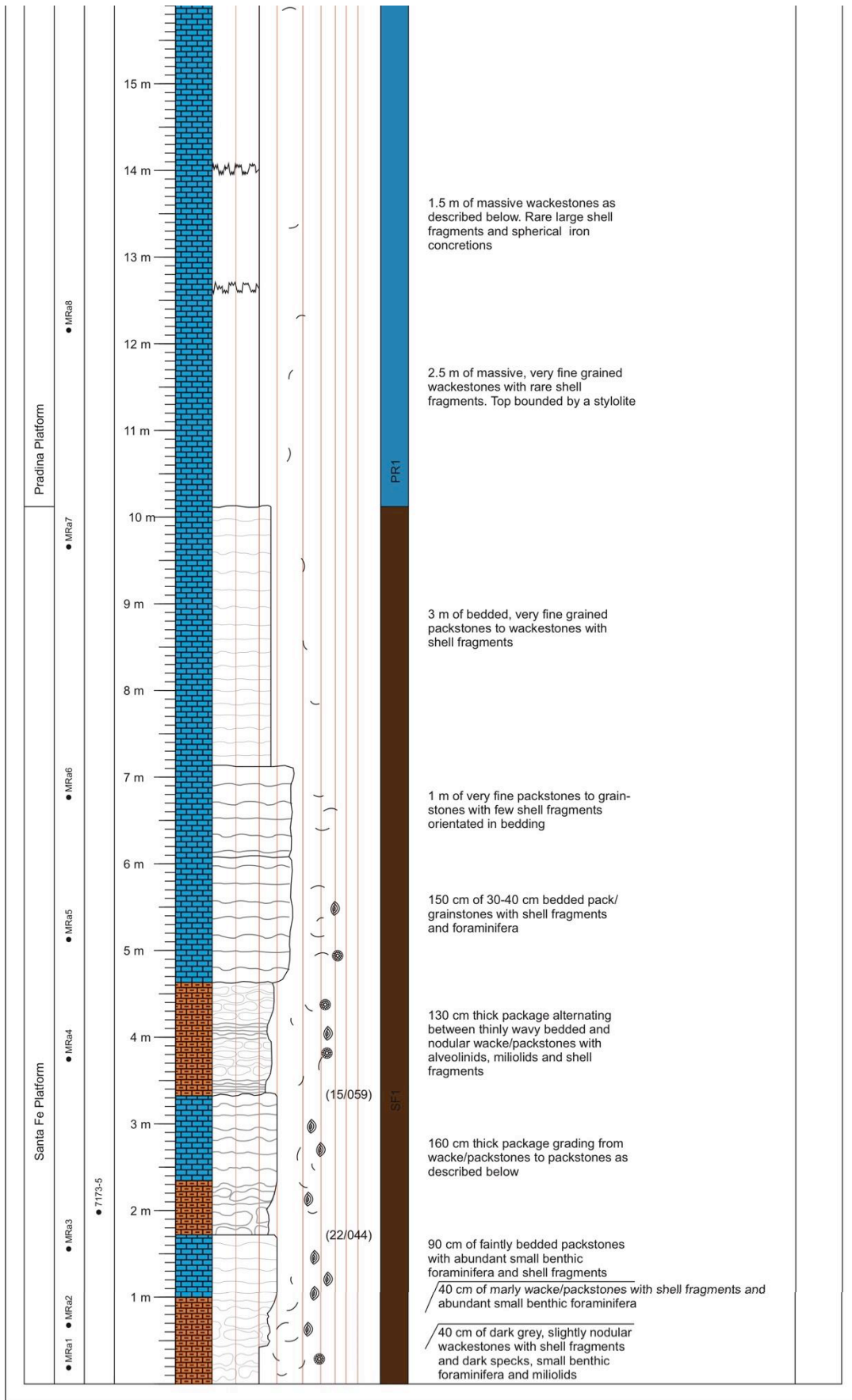
STRATIGRAPHY	SAMPLES	PHOTOGRAPHS	LENGTH/DEPTH	LITHOLOGY	CARBONATE TEXTURES							LITHOFACIES	COMMENTS	DEPOSITIONAL PACKAGES								
					M	W	P	G	F	R	B				C							
																SEDIMENTARY STRUCTURES						
																SKELETAL ASSEMBLAGES						
Pradina Platform	<ul style="list-style-type: none"> <li>MRa10</li> <li>7176/7</li> </ul>		44 m																			
			43 m																			
			42 m																			
			41 m																			
			40 m																			
			38 m																			
			37 m																			
			36 m																			
			35 m																			
			34 m																			
			33 m																			
			32 m																			
			31 m																			

13 m of massive wackestones with components as described below

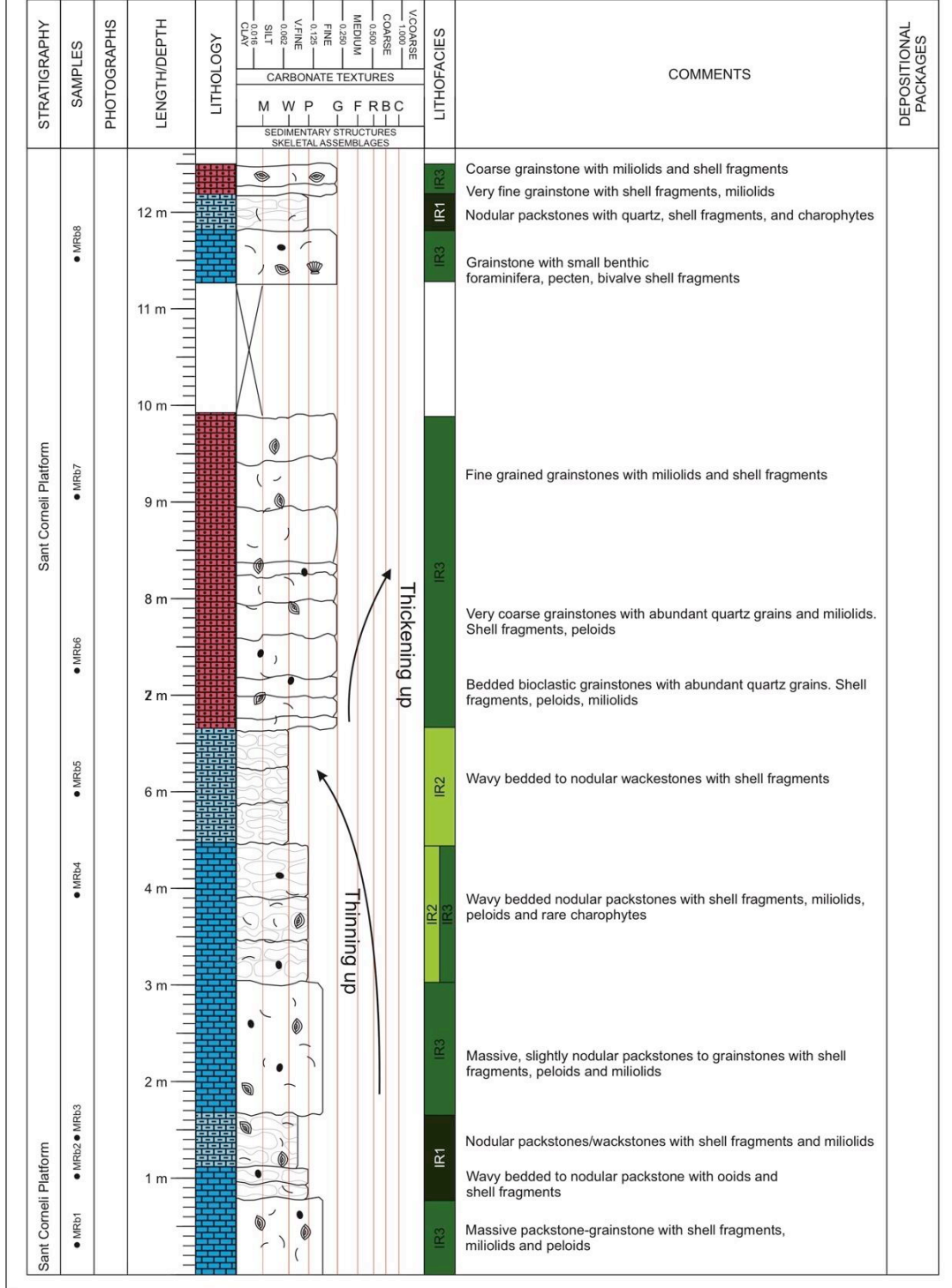
PR1

PR1





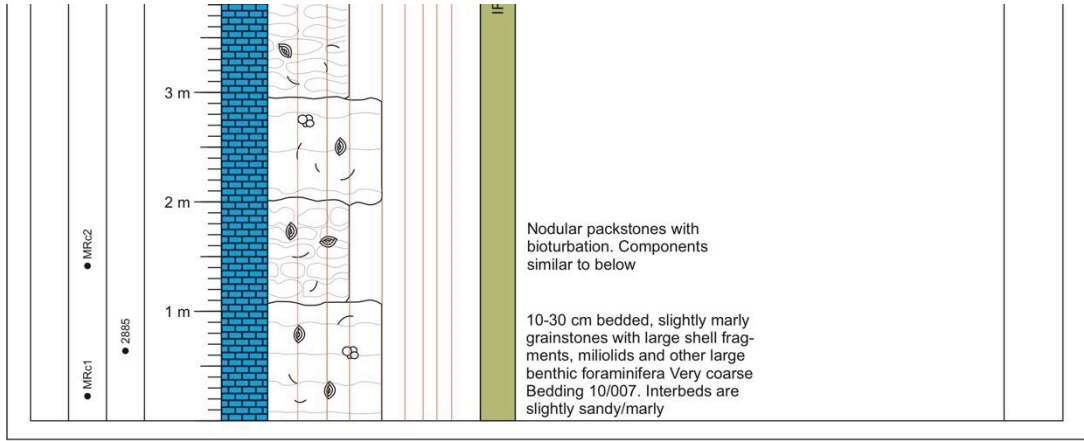
Mont Rebei B (MRb#) Starting 42°03'15.2"N (±2 m) Ending 42°03'15.2"N (±2 m)  
 (Logged 08/10/2014) Scale 1:50 point: 000°40'43.1"E Alt.: 717 m point: 000°40'43.1"E Alt.: 717 m



Mont Rebei C - Sketch-log (MRc#)  
(Logged 04/10/2014) Scale 1:50

Starting/ end 42°03'49.9"N (±4 m)  
point: 000°40'09.9"E Alt.: 608 m

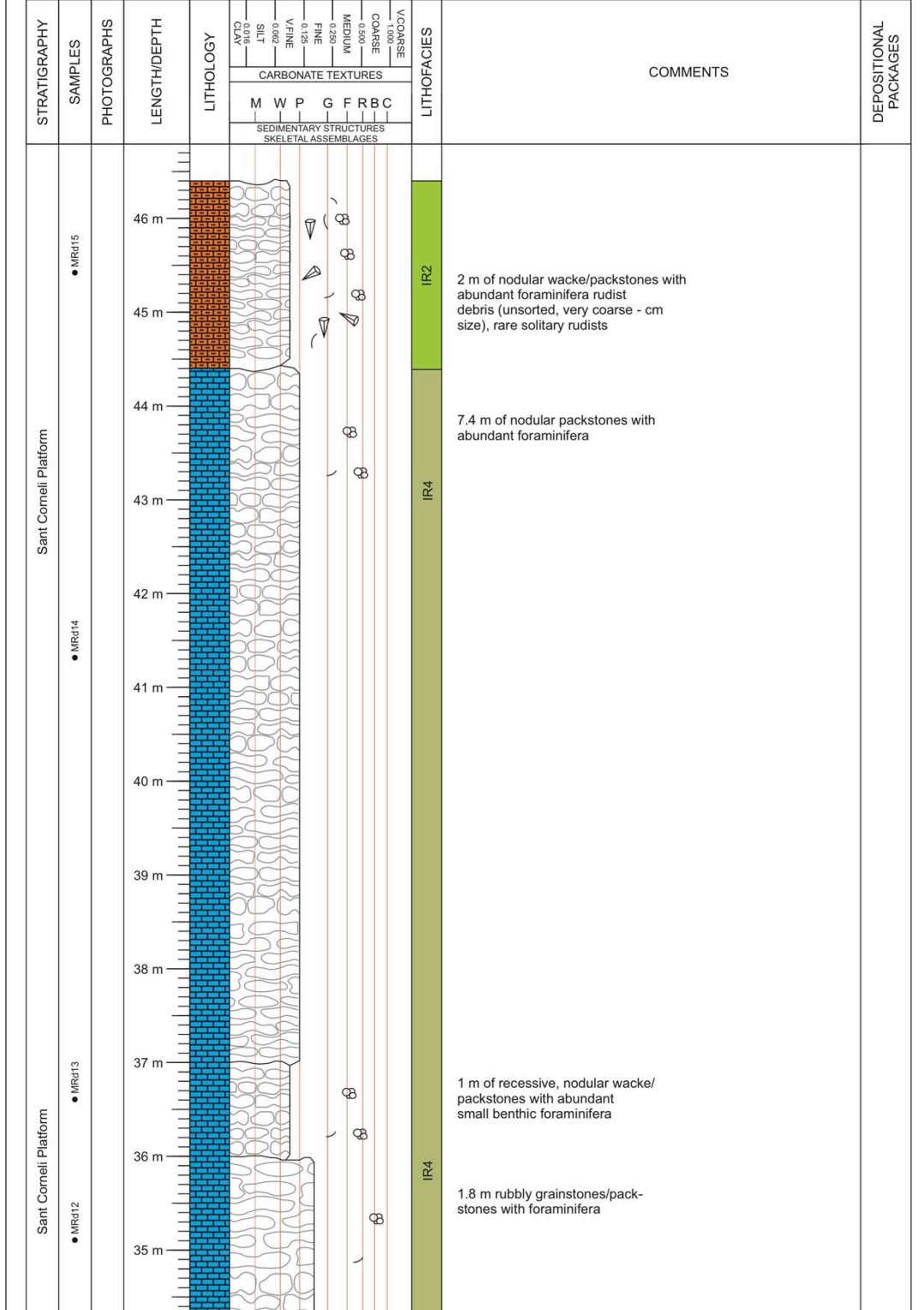
STRATIGRAPHY	SAMPLES	PHOTOGRAPHS	LENGTH/DEPTH	LITHOLOGY	LITHOFACIES	COMMENTS	DEPOSITIONAL PACKAGES																																																								
				<table border="1"> <tr> <td>CLAY</td> <td>0.00</td> <td></td> <td></td> <td></td> <td></td> <td></td> <td></td> </tr> <tr> <td>SILT</td> <td>0.062</td> <td></td> <td></td> <td></td> <td></td> <td></td> <td></td> </tr> <tr> <td>V.FINE</td> <td>0.125</td> <td></td> <td></td> <td></td> <td></td> <td></td> <td></td> </tr> <tr> <td>FINE</td> <td>0.250</td> <td></td> <td></td> <td></td> <td></td> <td></td> <td></td> </tr> <tr> <td>MEDIUM</td> <td>0.500</td> <td></td> <td></td> <td></td> <td></td> <td></td> <td></td> </tr> <tr> <td>COARSE</td> <td>1.000</td> <td></td> <td></td> <td></td> <td></td> <td></td> <td></td> </tr> <tr> <td>V.COARSE</td> <td>2.000</td> <td></td> <td></td> <td></td> <td></td> <td></td> <td></td> </tr> </table>	CLAY	0.00							SILT	0.062							V.FINE	0.125							FINE	0.250							MEDIUM	0.500							COARSE	1.000							V.COARSE	2.000									
CLAY	0.00																																																														
SILT	0.062																																																														
V.FINE	0.125																																																														
FINE	0.250																																																														
MEDIUM	0.500																																																														
COARSE	1.000																																																														
V.COARSE	2.000																																																														
				<table border="1"> <tr> <td colspan="7">CARBONATE TEXTURES</td> </tr> <tr> <td>M</td> <td>W</td> <td>P</td> <td>G</td> <td>F</td> <td>R</td> <td>B</td> </tr> <tr> <td colspan="7">SEDIMENTARY STRUCTURES</td> </tr> <tr> <td colspan="7">SKELETAL ASSEMBLAGES</td> </tr> </table>	CARBONATE TEXTURES							M	W	P	G	F	R	B	SEDIMENTARY STRUCTURES							SKELETAL ASSEMBLAGES																																					
CARBONATE TEXTURES																																																															
M	W	P	G	F	R	B																																																									
SEDIMENTARY STRUCTURES																																																															
SKELETAL ASSEMBLAGES																																																															
Sant Corneli Platform	● MRc3					<p>MRc3 taken at: 0307271 +-3m 4659574 571m</p>																																																									

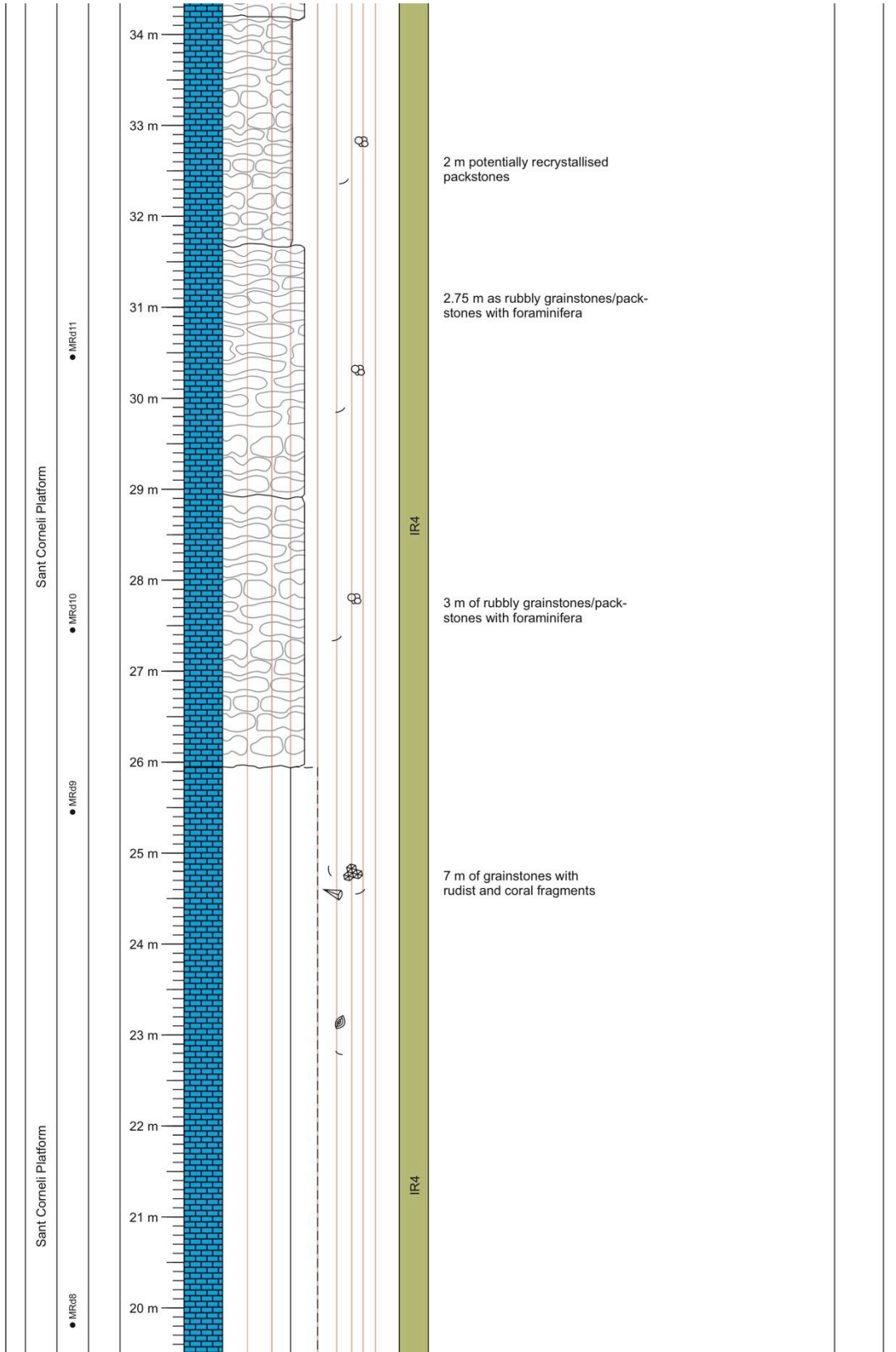


Mont Rebei D (MRd#)  
(Logged 04/10/2014) Scale 1:50

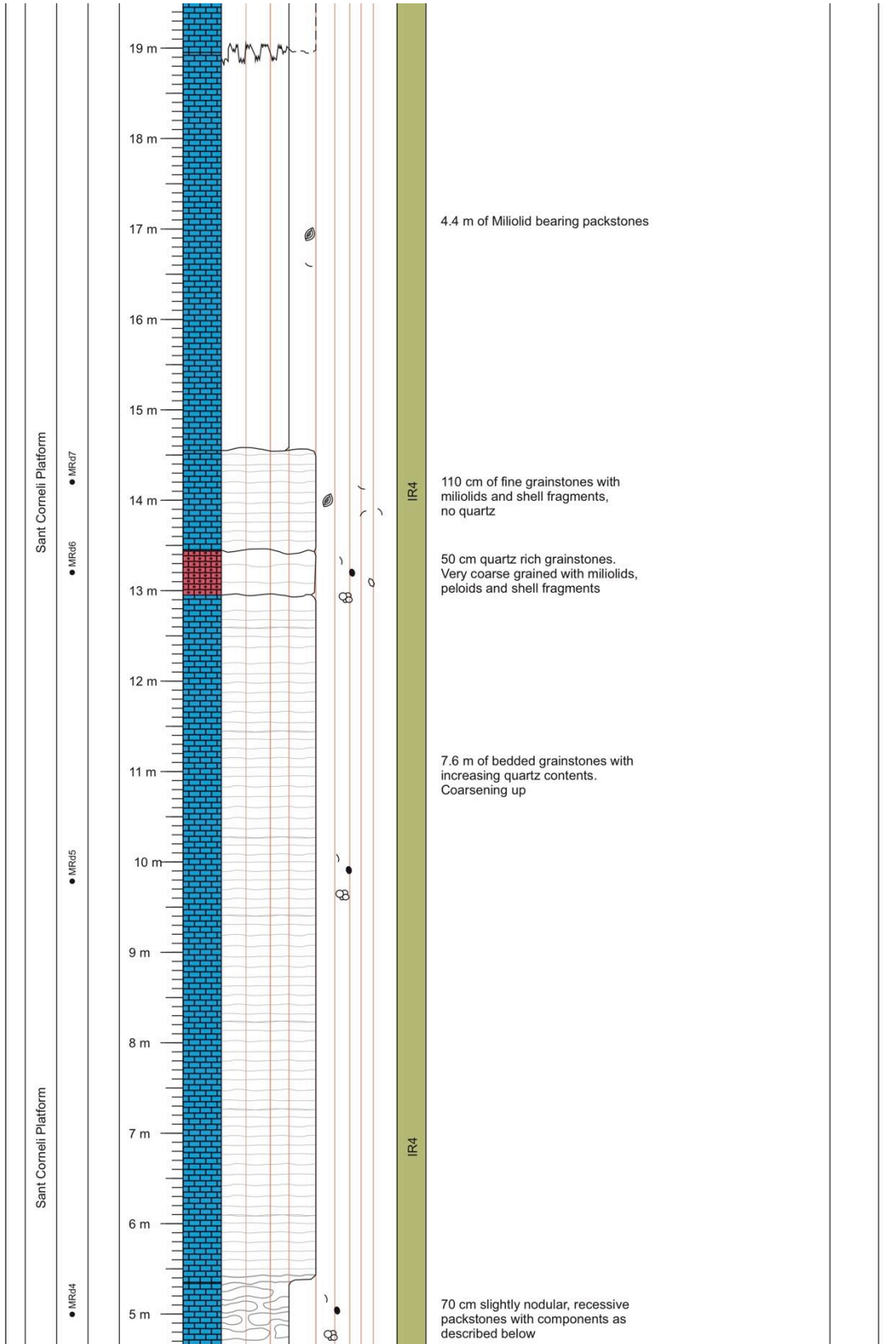
Starting point: 42°03'43.3"N (±10 m)  
000°40'04.0"E Alt.: 541 m

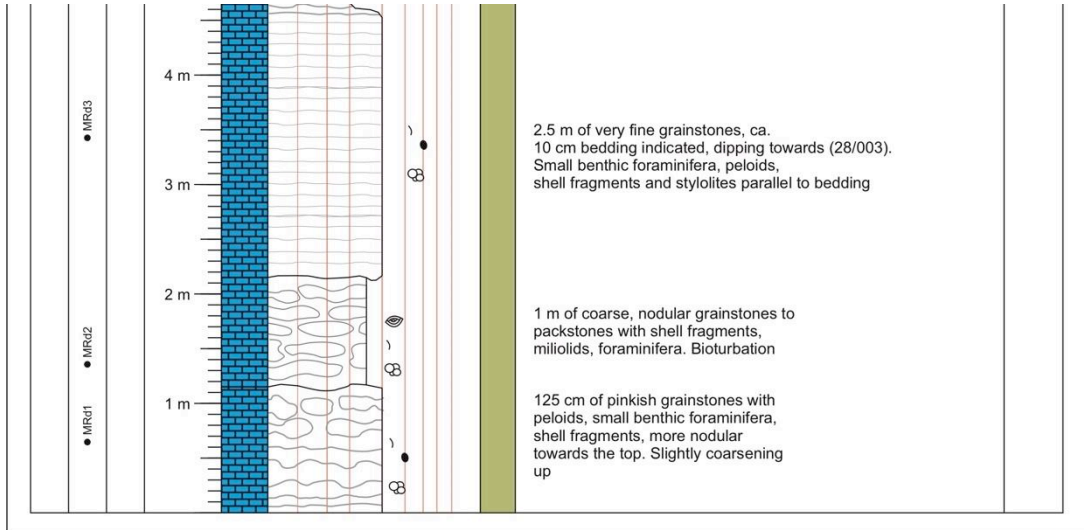
Ending point: 42°03'44.9"N (±4 m)  
000°40'07.9"E Alt.: 582 m





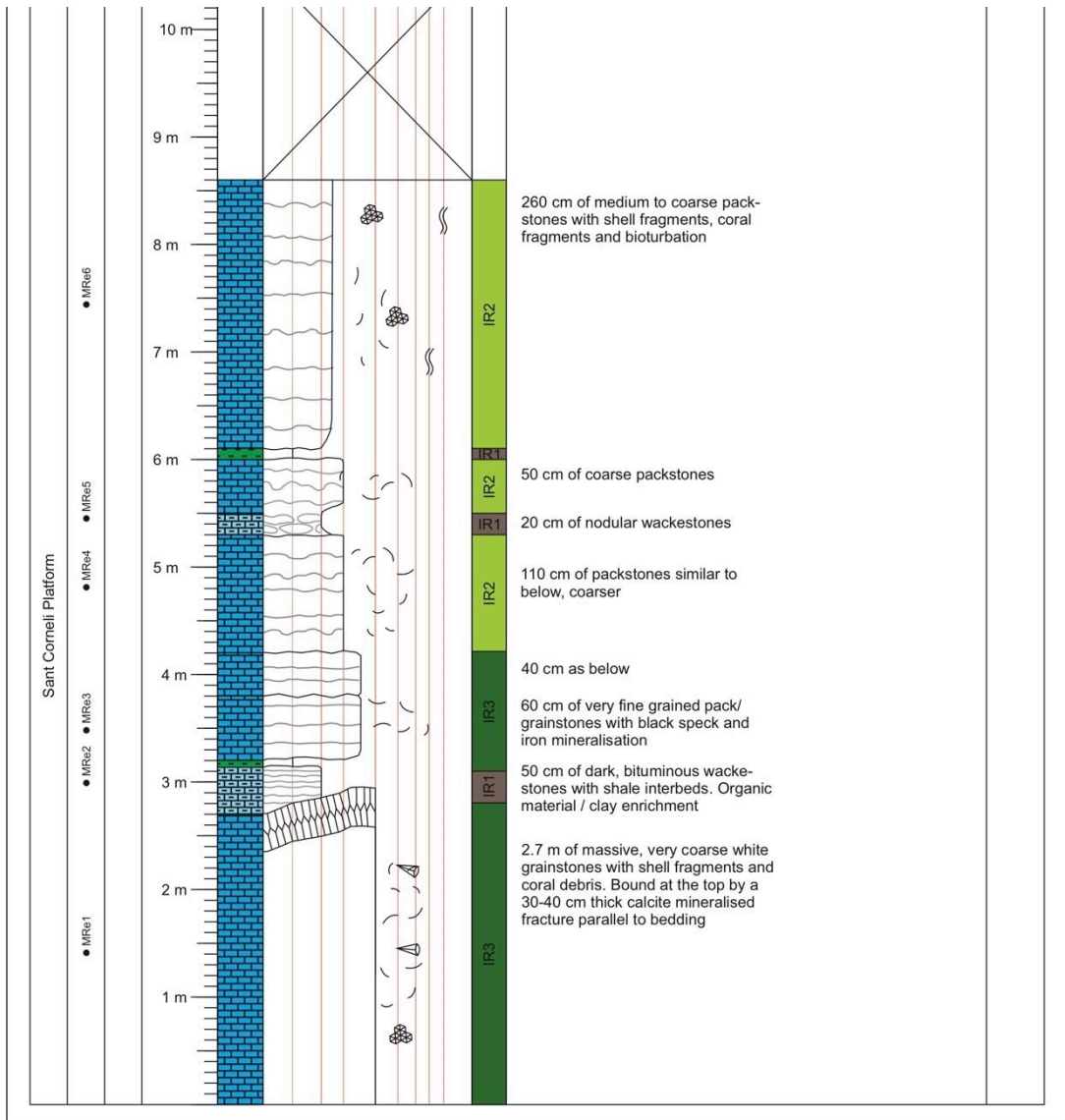






Mont Rebei E (MRe#) Starting 42°03'43.3"N (±10 m) Ending 42°11'44.9"N (±4 m)  
 (Logged 04/10/2014) Scale 1:50 point: 000°40'04.0"E Alt.: 541 m point: 000°40'07.9"E Alt.: 582 m

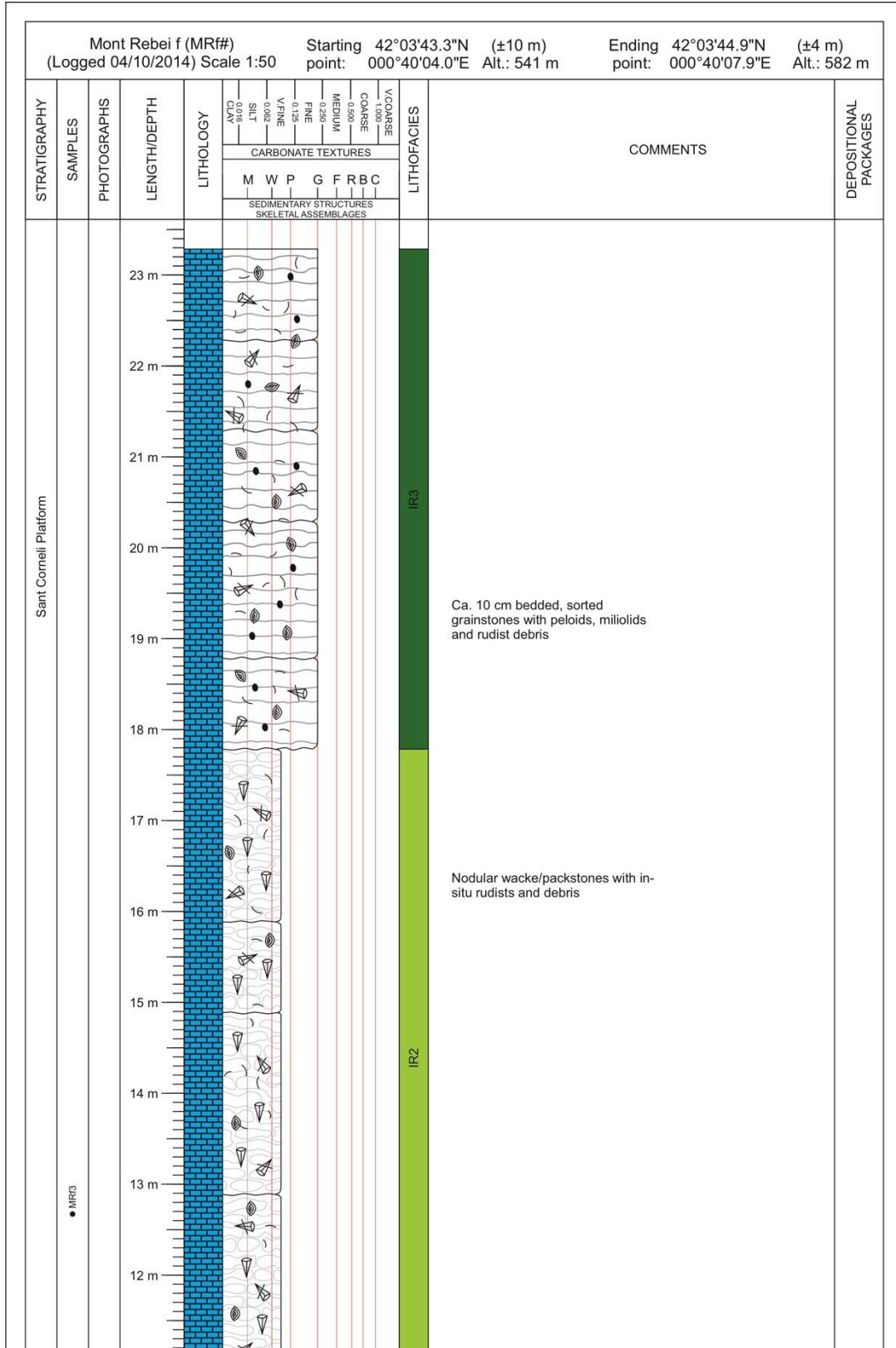
STRATIGRAPHY	SAMPLES	PHOTOGRAPHS	LENGTH/DEPTH	LITHOLOGY	CARBONATE TEXTURES	SEDIMENTARY STRUCTURES	SKELETAL ASSEMBLAGES	LITHOFACIES	COMMENTS	DEPOSITIONAL PACKAGES
					M W P G F R B C					
Sant Corneli Platform	● MRe12		22 m					IR3	1 metre of thinning up and fining up grainstones with shell fragments and miliolids	
			21 m					IR2	50 cm of grainstones with bedding thickness thinning up. Shell fragments and foraminifera	
			20 m					IR3	Nodular quartz bearing packstones with bioturbation	
	● MRe11		19 m					IR3	Coarse, quartz bearing grainstones with shell fragments and foraminifera Platy bedding in centre of the unit	
			18 m							
	● MRe10		17 m					IR2	60 cm of nodular wacke/packstones similar to below	
			16 m						2.7 m of nodular, bioturbated wackestones with shell fragments and bioturbation	
			15 m					IR3	50 cm of wavy bedded packstones to grainstones with miliolids/alveolids and shell fragments	
	● MRe9		14 m					IR3	25 cm of grainstones with abundant miliolids and other benthic foraminifera	
			13 m					IR1	25 cm of packstones with shell fragments, foraminifera and bioturbation	
	● MRe8		12 m					IR2	70 cm of fine grained grainstones with indicated bedding	
			11 m					IR2	10 cm of dark wackestones with charophytes (?)	
	● MRe7							IR2	50 cm of wacke/packstones similar to below. Wavy bedded, miliolid bearing	
Sant Corneli Platform								IR2	60 cm of wacke/packstones as described below	
								IR1	75 cm of light brown wacke/packstones with alveolids and organic material	
								IR2	20 cm of dark, bituminous wackestones	
								IR2	75 cm of packstones as described below	

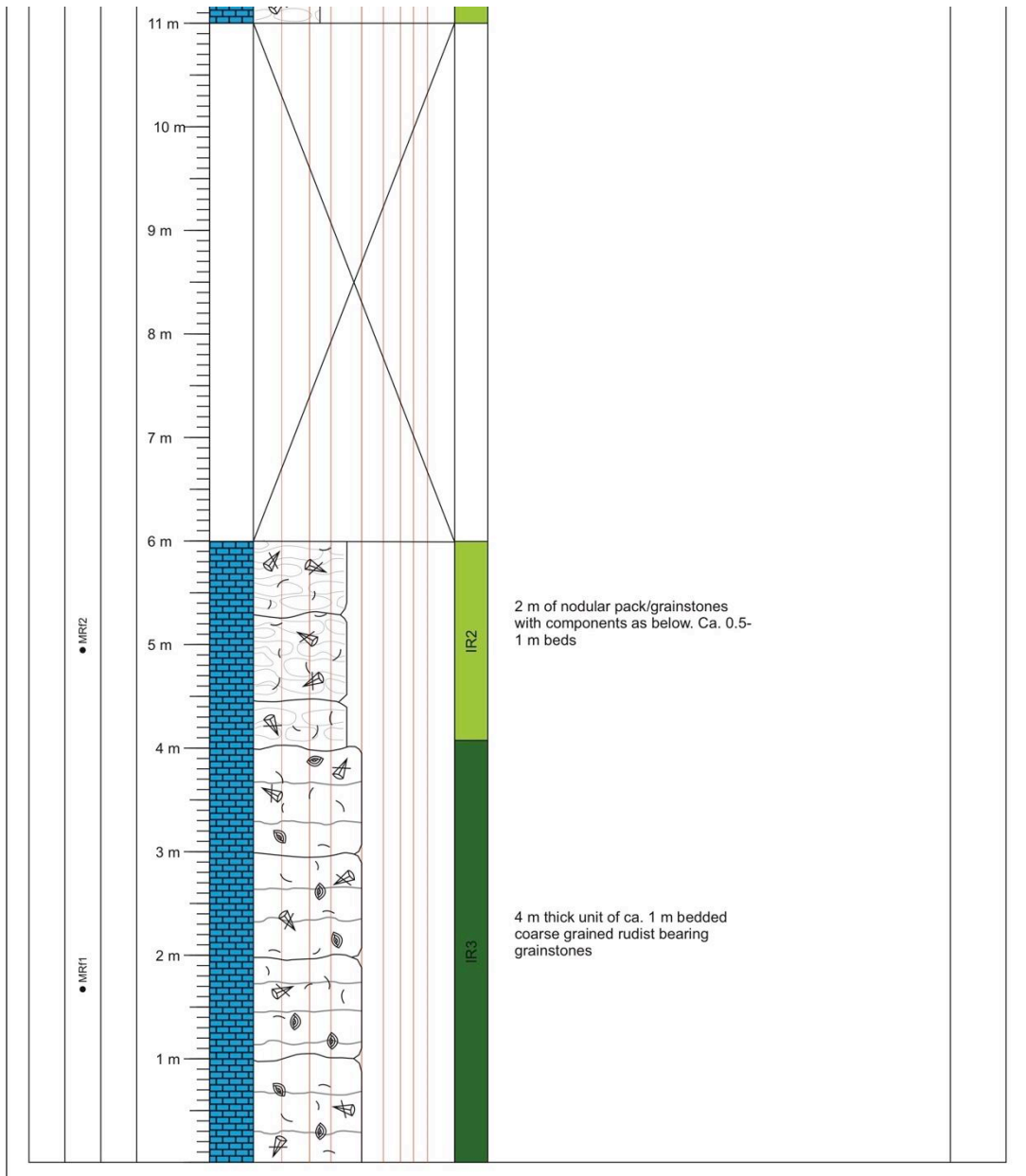


Mont Rebei f (MRf#)  
(Logged 04/10/2014) Scale 1:50

Starting point: 42°03'43.3"N (±10 m)  
000°40'04.0"E Alt.: 541 m

Ending point: 42°03'44.9"N (±4 m)  
000°40'07.9"E Alt.: 582 m

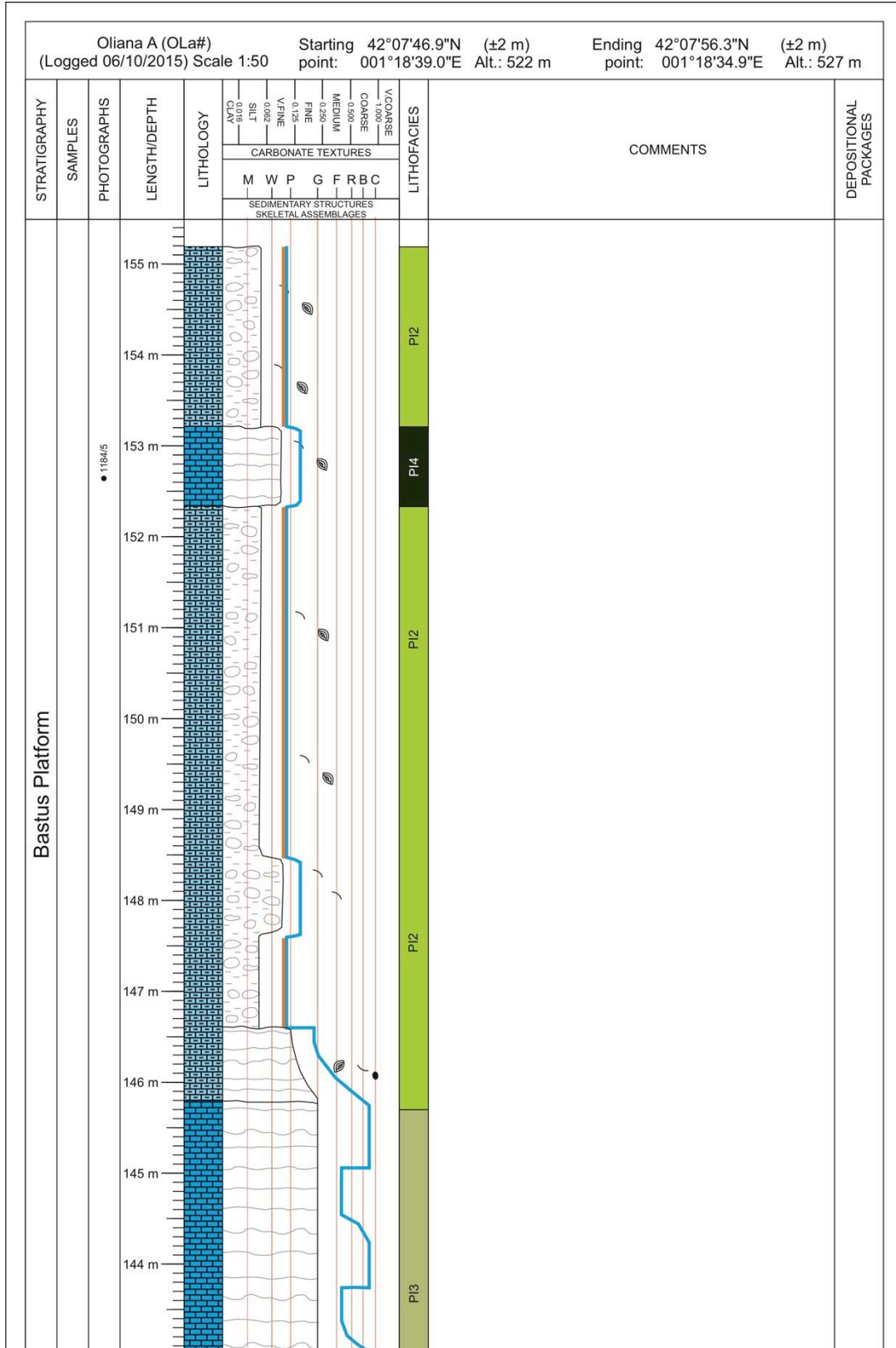




Oliana A (OLa#)  
 (Logged 06/10/2015) Scale 1:50

Starting point: 42°07'46.9"N (±2 m)  
 001°18'39.0"E Alt.: 522 m

Ending point: 42°07'56.3"N (±2 m)  
 001°18'34.9"E Alt.: 527 m



• OLa23 • OLa24

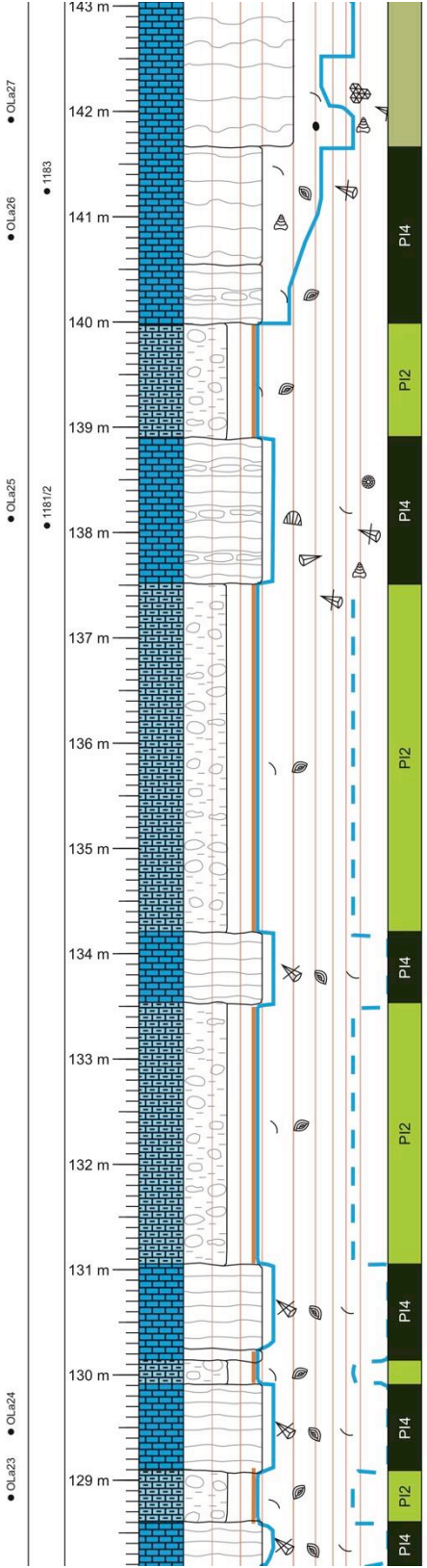
Bastus Platform

Bastus Platform

• OLa25

• OLa26

• OLa27



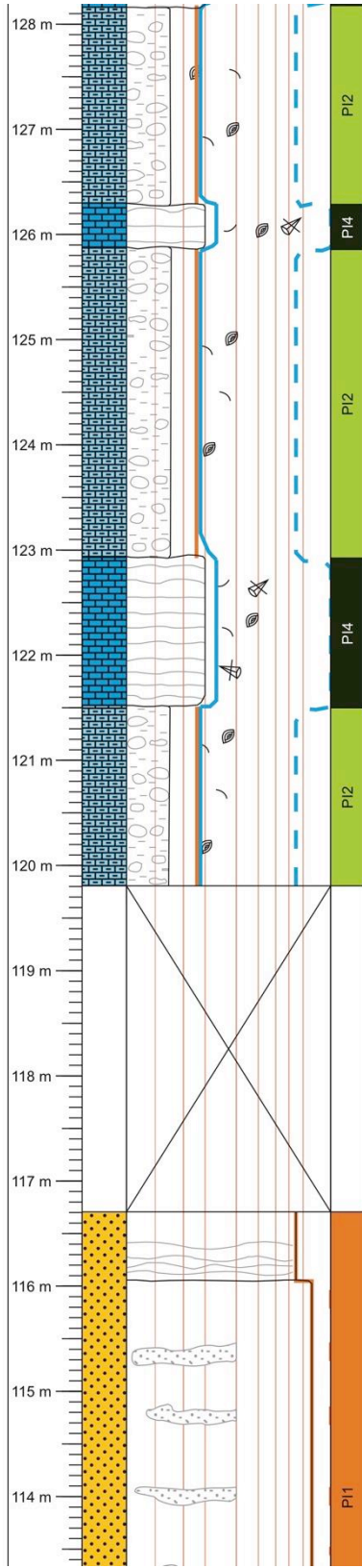


iform

Bastus Platform

Bastus Platform

• OLaz2

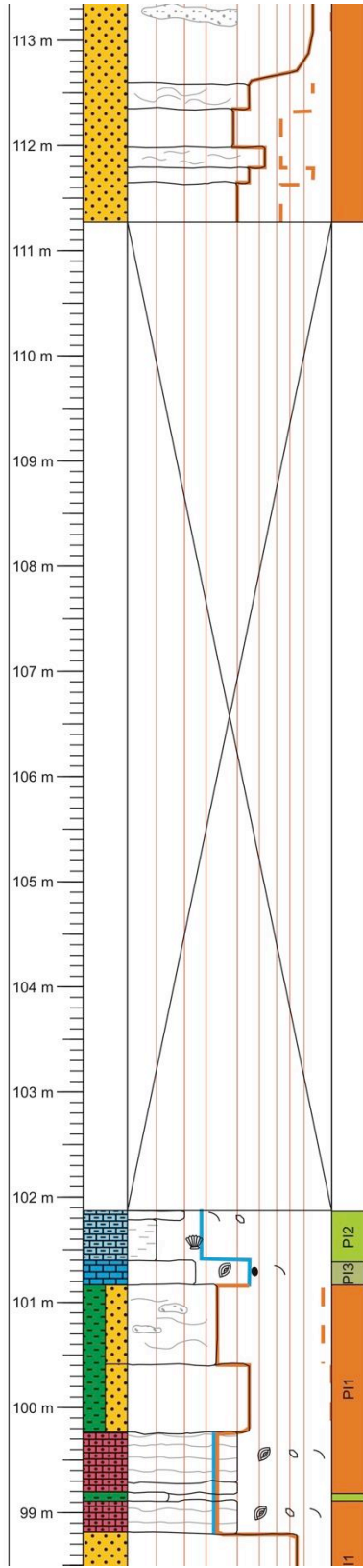


Platform

Bastus Platform

Bastus Plat

• OLa21



ius Platform

Bastus Platform

Bastus

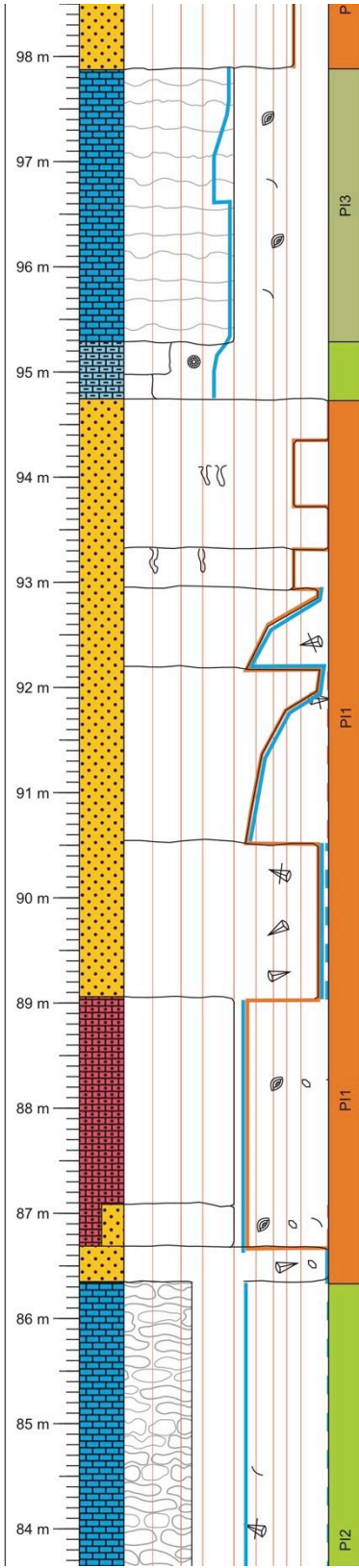
• Olat19

• Olat20

• 1178

• 1179

• 1180



Bastus Platform

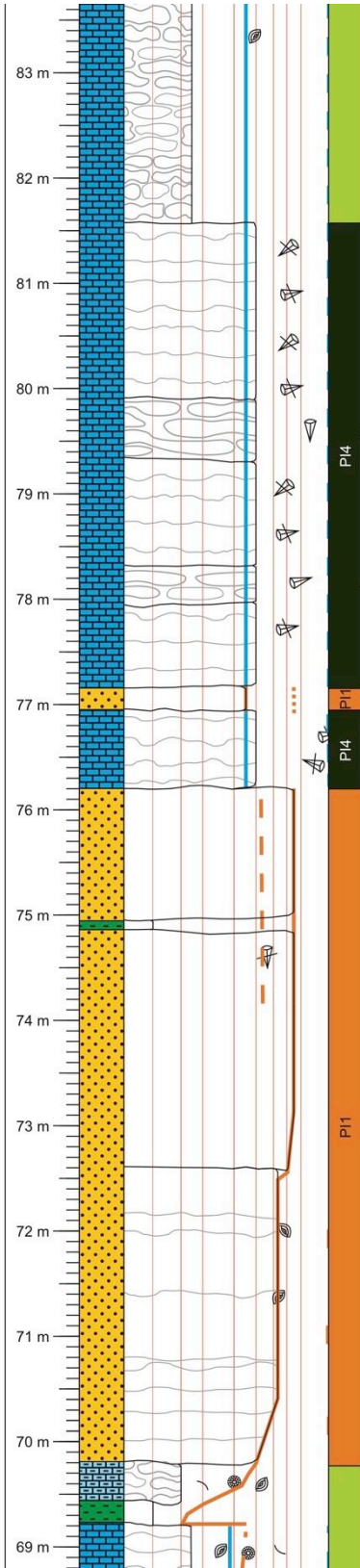
Bastus Platform

Bast

● OLat18

● 1175

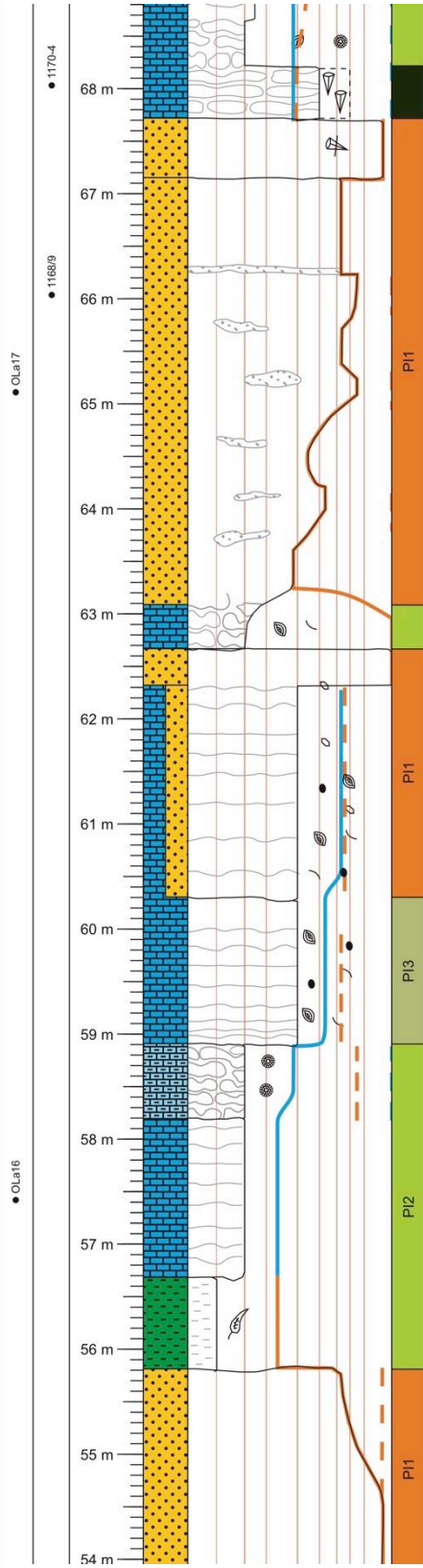
● 1176/7



Bastus Platform

Bastus Platform

E



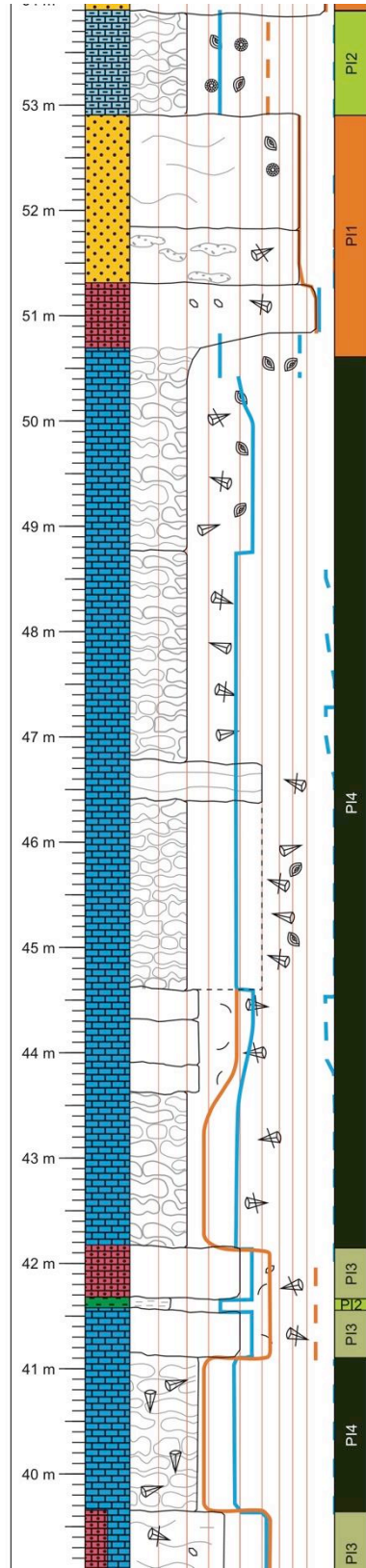
Bastus Platform

● OLa10 ● OLa11

Bastus Platform

● OLa12

● OLa13 ● OLa14 ● OLa15

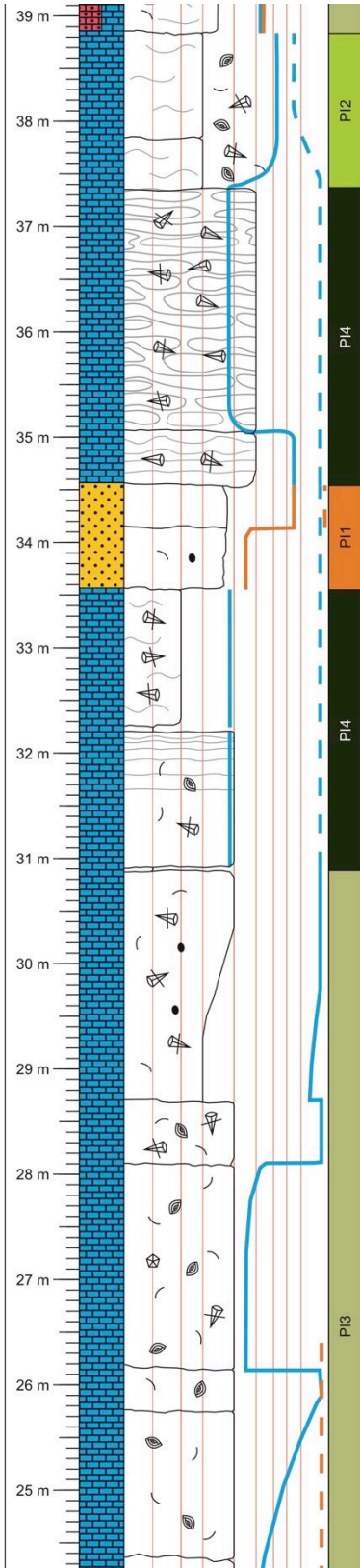


Bastus Platform

● Cl.a8

Bastus Platform

● Cl.a9



Bastus Platform

● OLa3 ● OLa4

● 1159/60 ● 1161-3

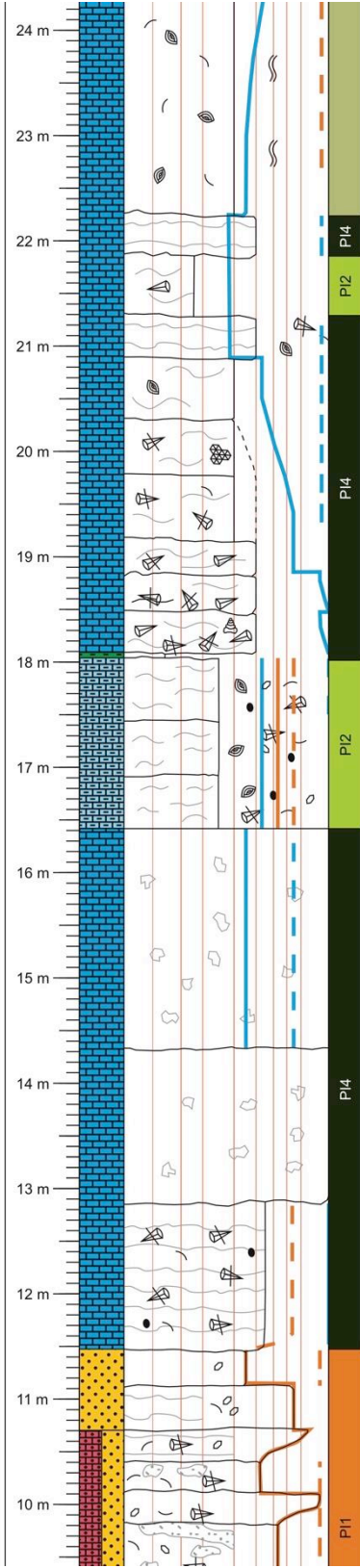
● 1164/5

● OLa5 ● 1166

● OLa6

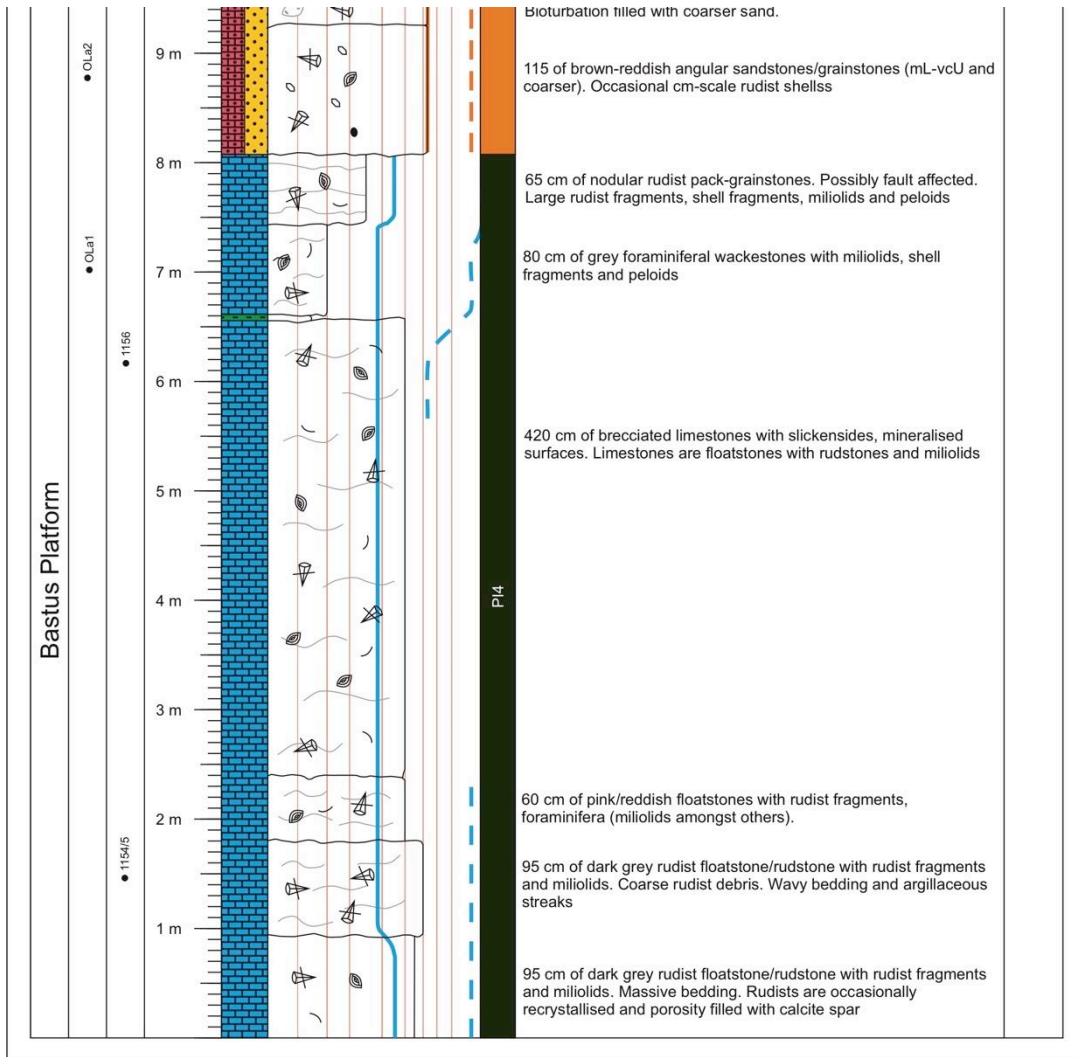
● OLa7

Bastus Platform



60 cm of sandstones/grainstones as below. Marginally finer grained.

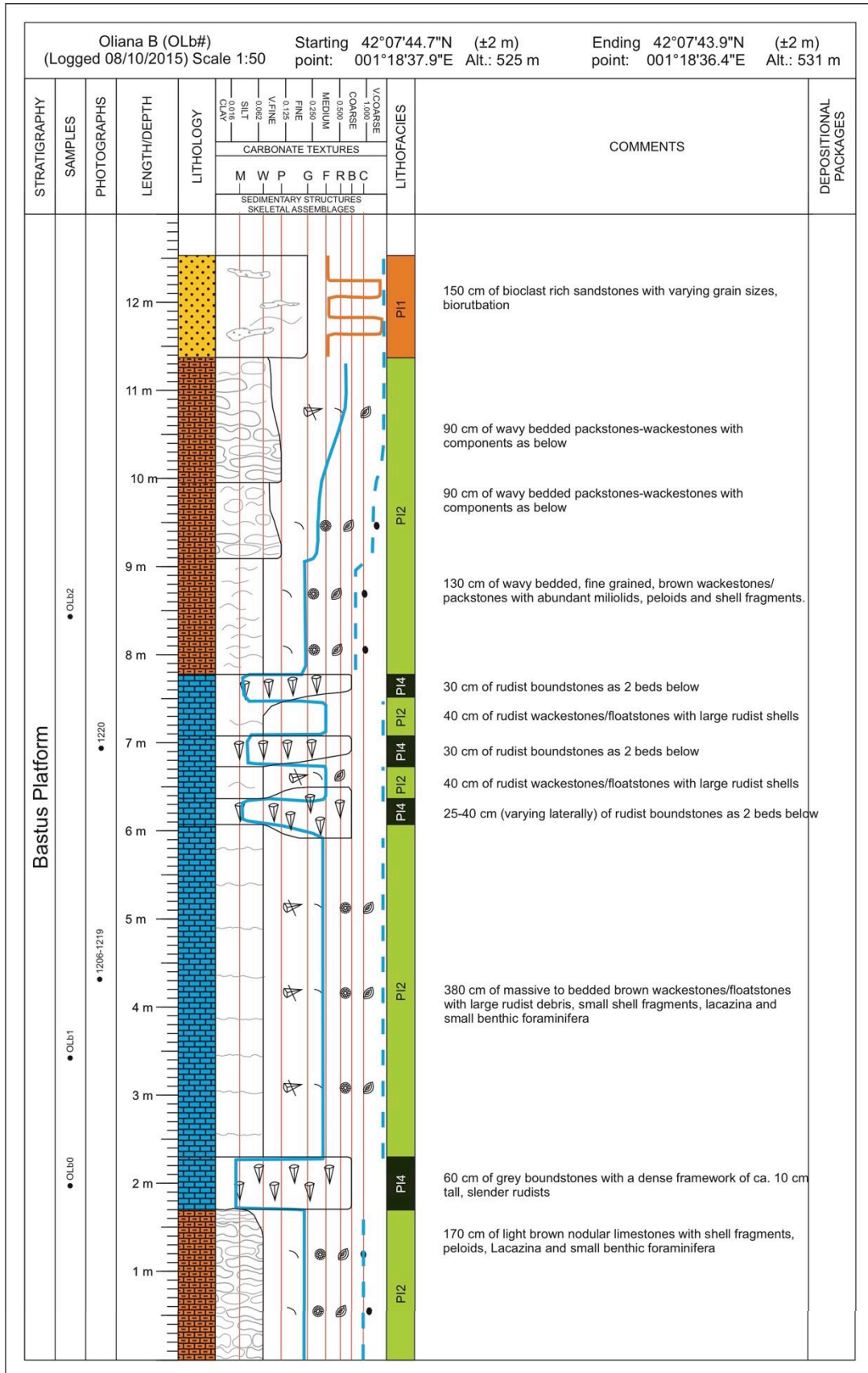




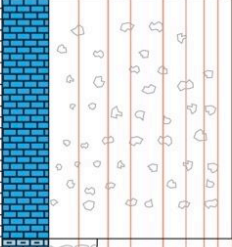
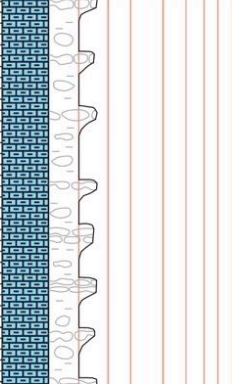
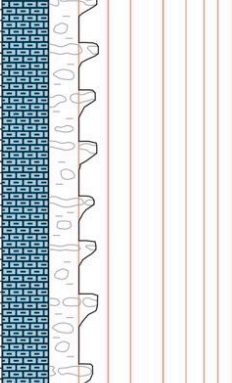
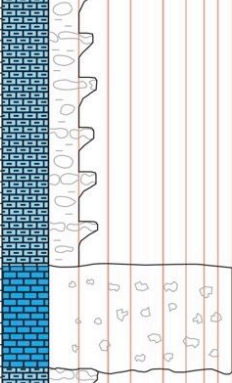
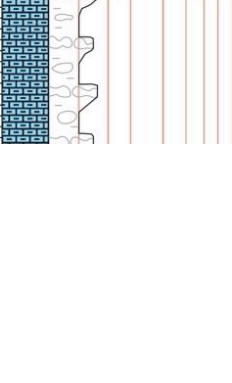

Oliana B (OLb#)  
(Logged 08/10/2015) Scale 1:50

Starting 42°07'44.7"N (±2 m)  
point: 001°18'37.9"E Alt.: 525 m

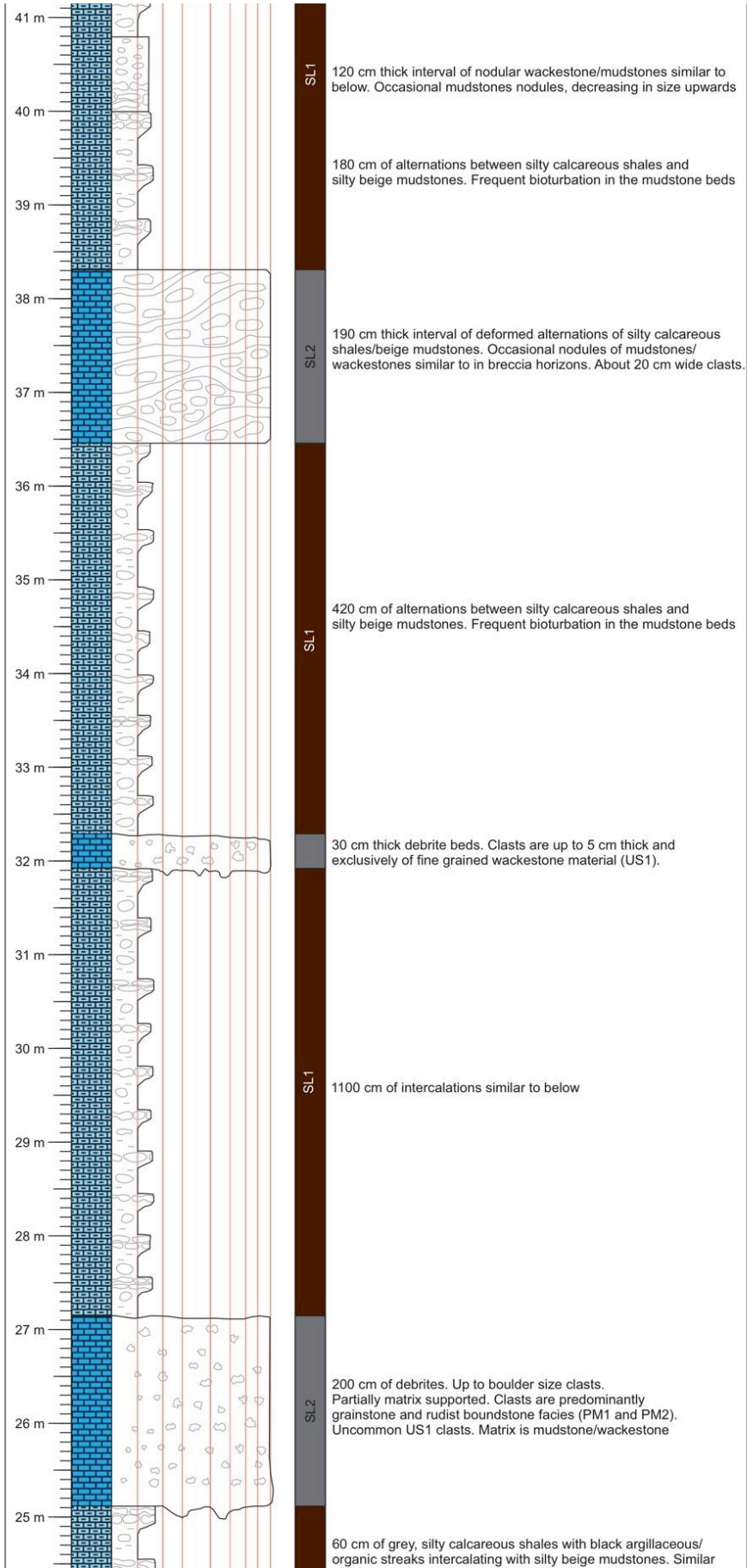
Ending 42°07'43.9"N (±2 m)  
point: 001°18'36.4"E Alt.: 531 m

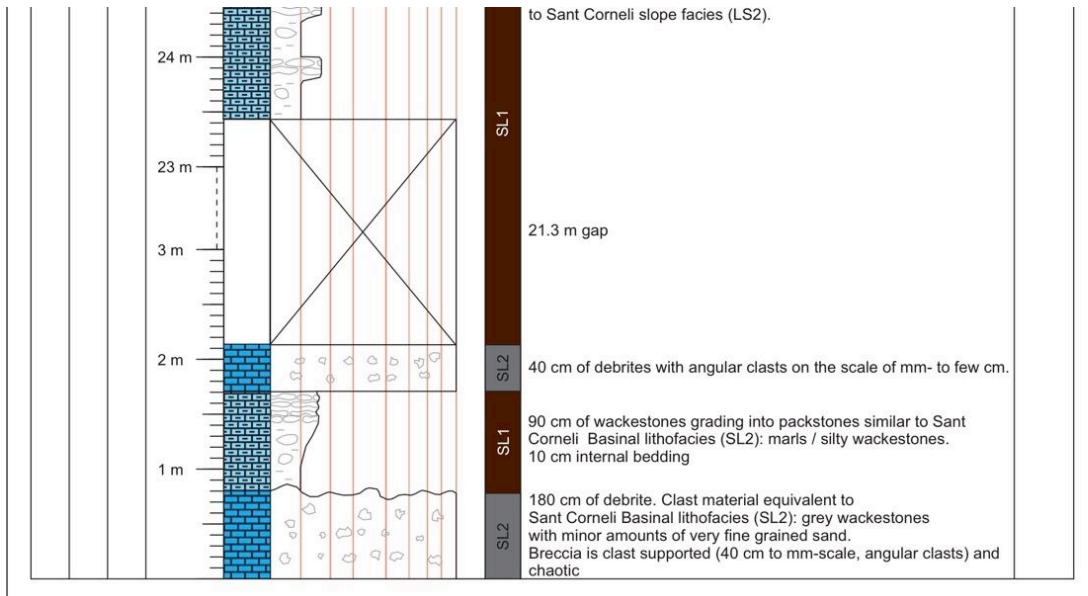


Torre de Tamurcia A (TTa#) Starting 42°18'00.7"N (±2 m) Ending 42°17'59.0"N (±3 m)  
 (Logged 17/10/2015) Scale 1:500 point: 000°50'23.8"E Alt.: 1099 m point: 000°50'18.6"E Alt.: 1088 m

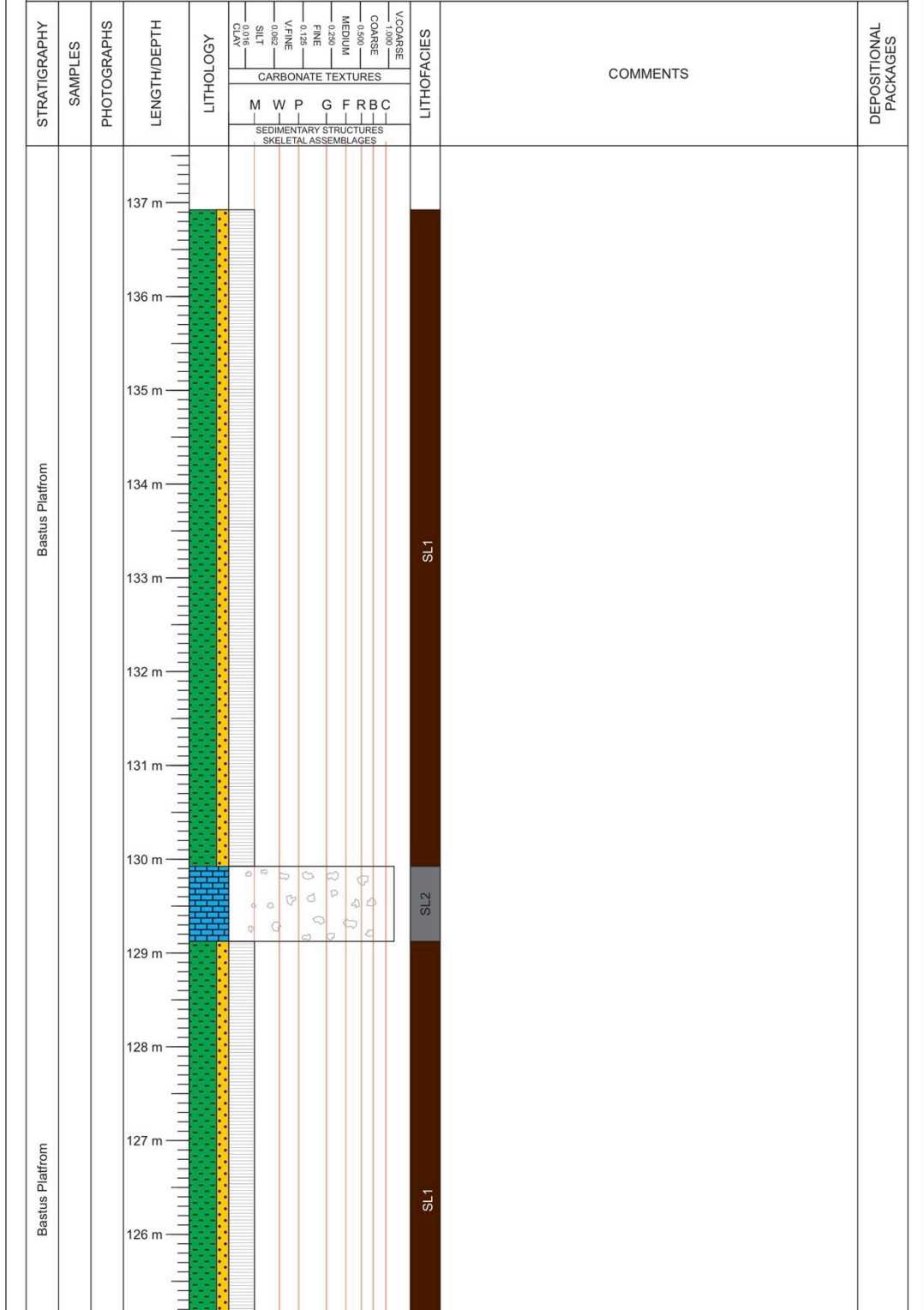
STRATIGRAPHY	SAMPLES	PHOTOGRAPHS	LENGTH/DEPTH	LITHOLOGY	LITHOFACIES	COMMENTS	DEPOSITIONAL PACKAGES		
Bastus Platfrom			55 m		VCOARSE 1.000- COARSE 0.500- MEDIUM 0.250- FINE 0.125- V/FINE 0.062- SILT 0.031- NPCL 0.015-	CARBONATE TEXTURES M W P G F R B C SEDIMENTARY STRUCTURES SKELETAL ASSEMBLAGES	SL2 SL1 SL2	260 cm thick debrite interval with sharp lower boundary. Deformation of matrix between clasts. Clasts are poorly sorted, and reach up to 1 metre in diameter. Clast material is predominantly wackestone (US1), but occasional clasts with rudist fragments (PM1) also occur.	
	Bastus Platfrom		54 m						
Bastus Platfrom			53 m						
	Bastus Platfrom		52 m						
Bastus Platfrom			51 m						
	Bastus Platfrom		50 m						
Bastus Platfrom			49 m						
	Bastus Platfrom		48 m						
Bastus Platfrom			47 m						
	Bastus Platfrom		46 m						
Bastus Platfrom			45 m						
	Bastus Platfrom		44 m						
Bastus Platfrom			43 m				80 cm thick debrite bed. Maximum 40 cm large, slightly rounded clasts. Clasts are exclusively of wackestone texture. Occasional glauconite grains in the matrix.		
	Bastus Platfrom		42 m				170 cm of alternations between silty calcareous shales and silty beige mudstones. Frequent bioturbation in the mudstone beds		

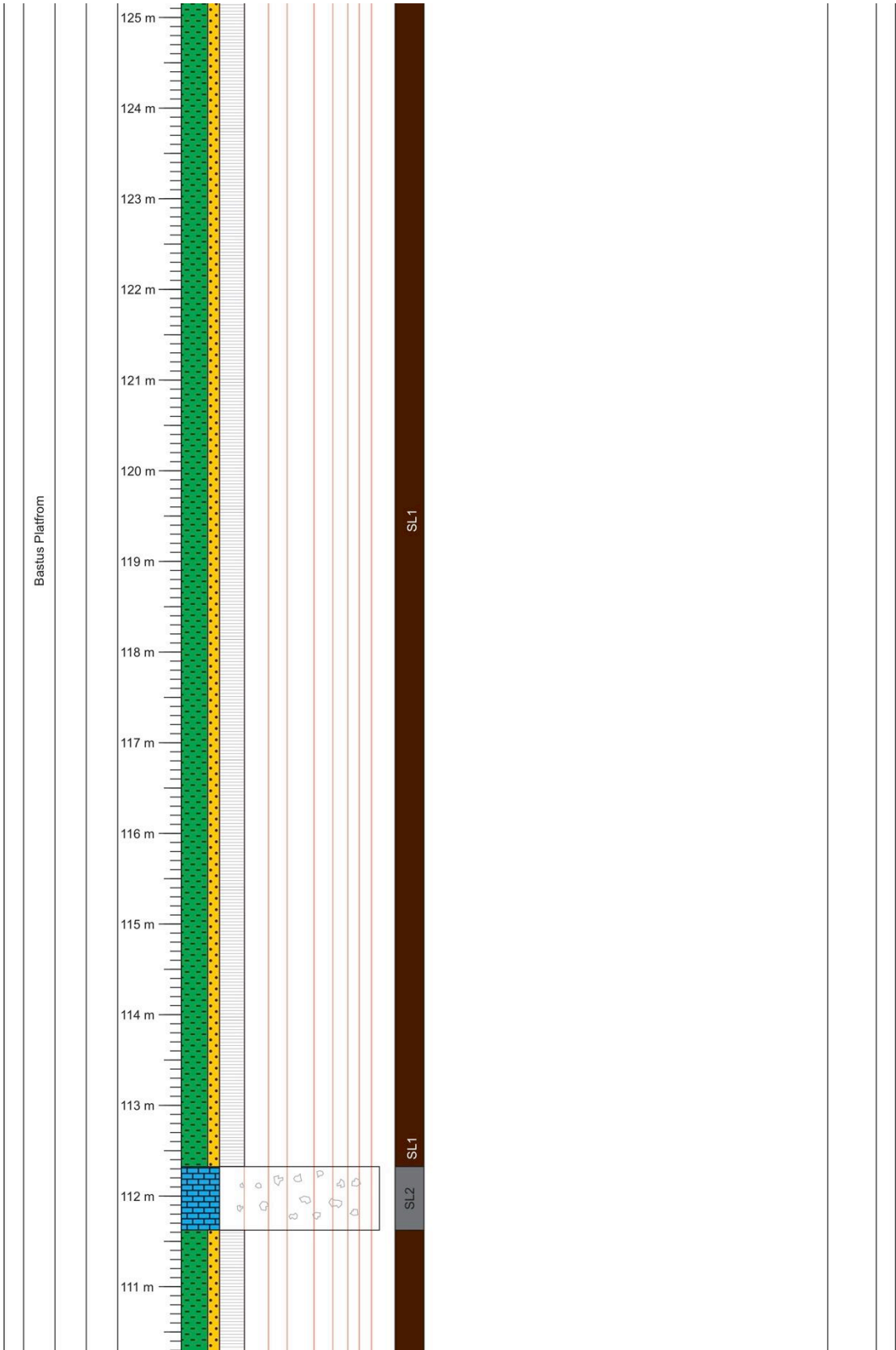
Bastus Platform

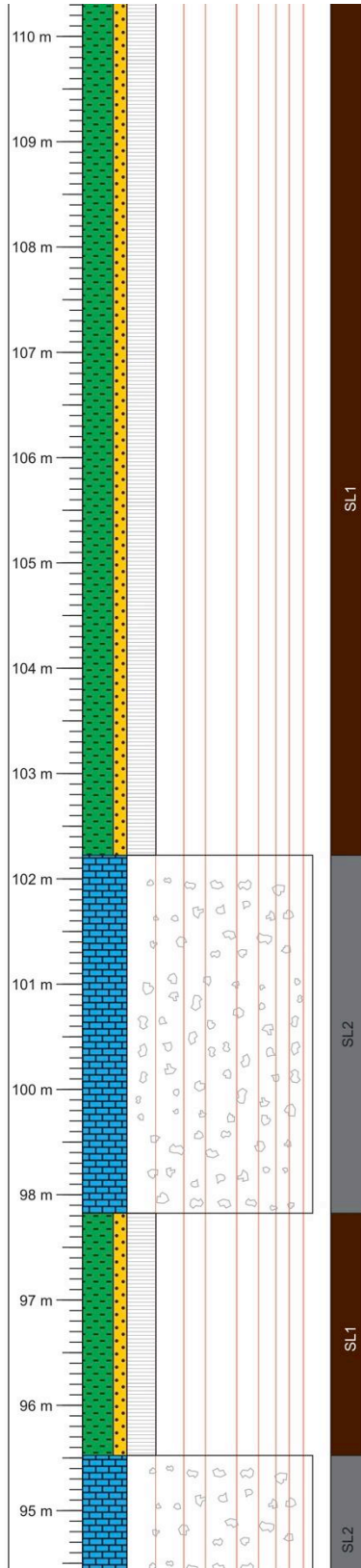




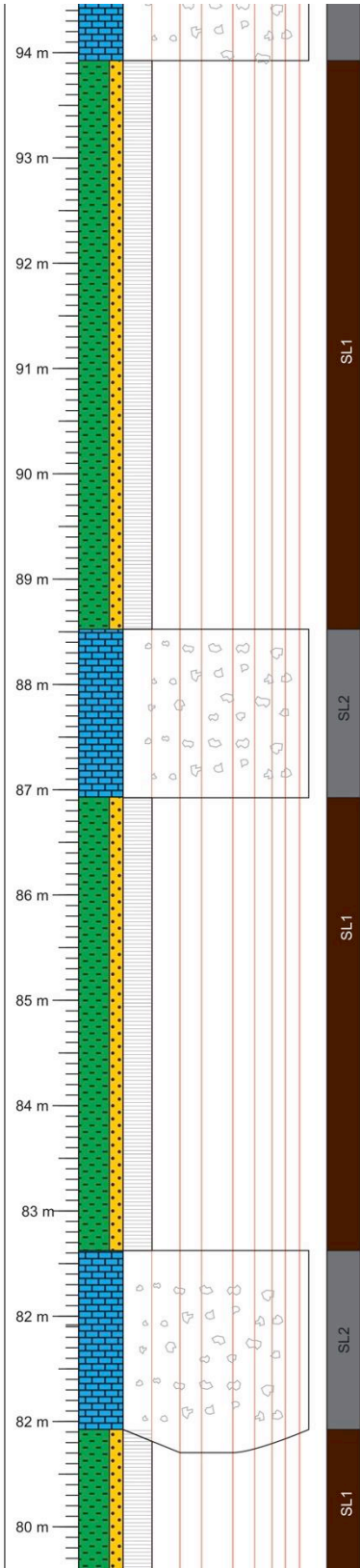
Torre de Tamurcia B (TTb#) Starting 42°17'57.8"N (±2 m) Ending 42°17'51.4"N (±3 m)  
 (Logged 17/10/2015) Scale 1:50 point: 000°50'11.9"E Alt.: 1070 m point: 000°50'01.7"E Alt.: 1049 m

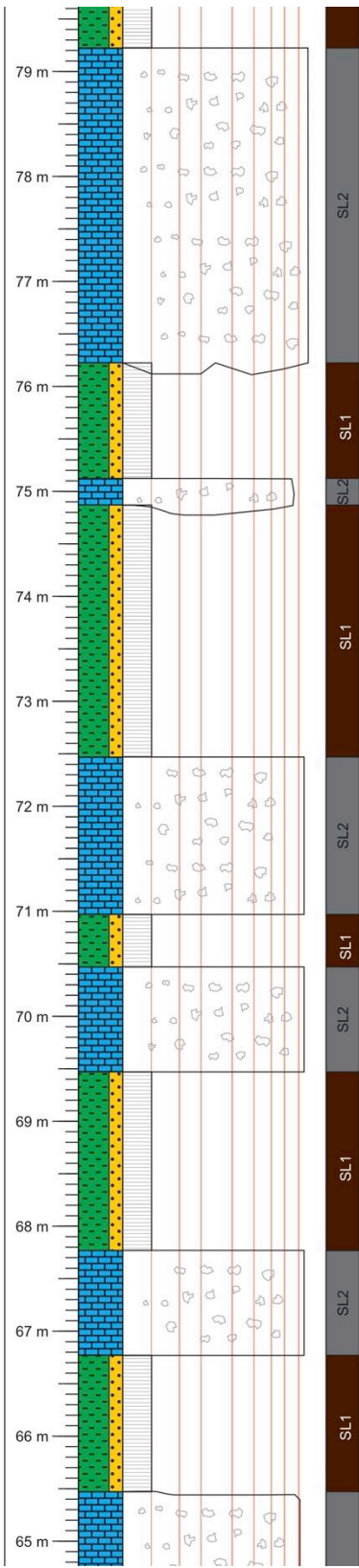


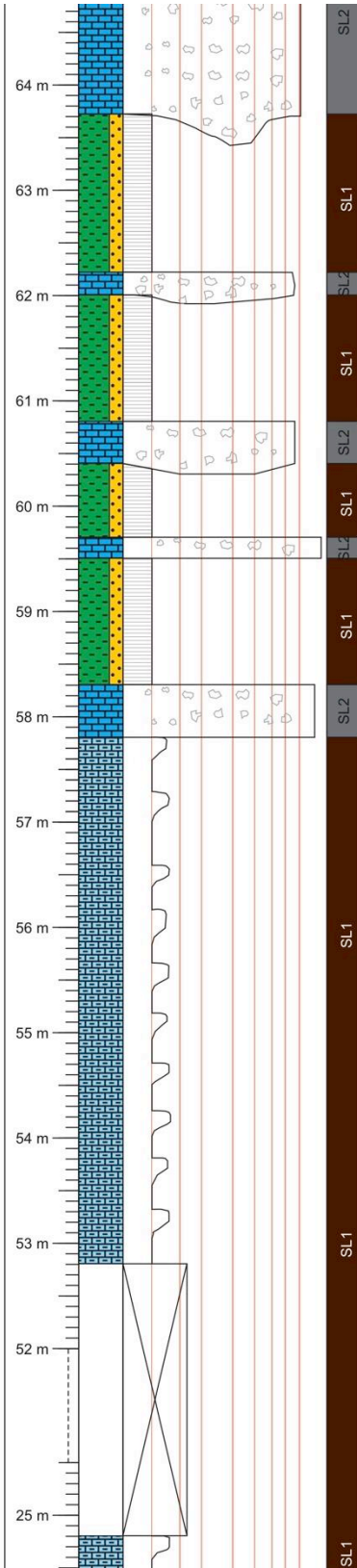




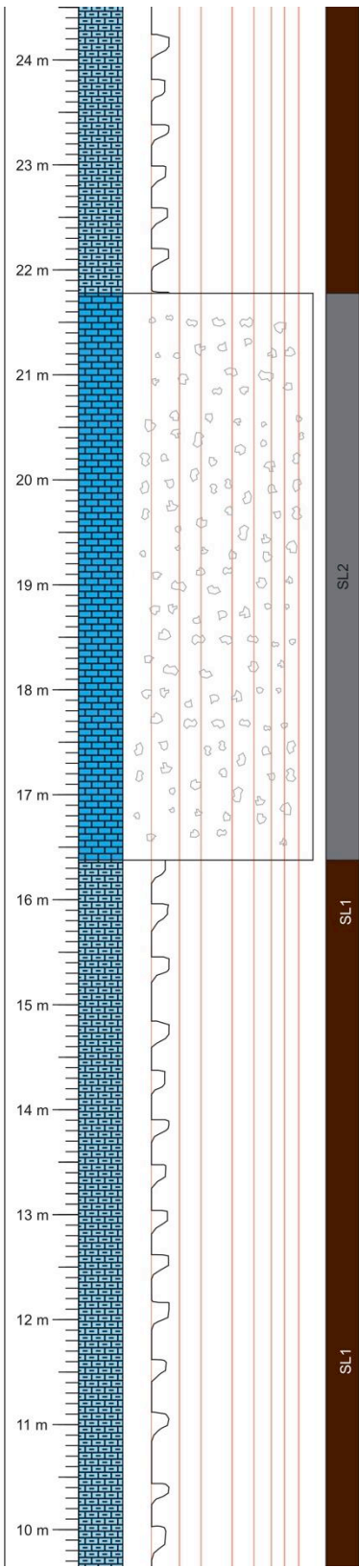


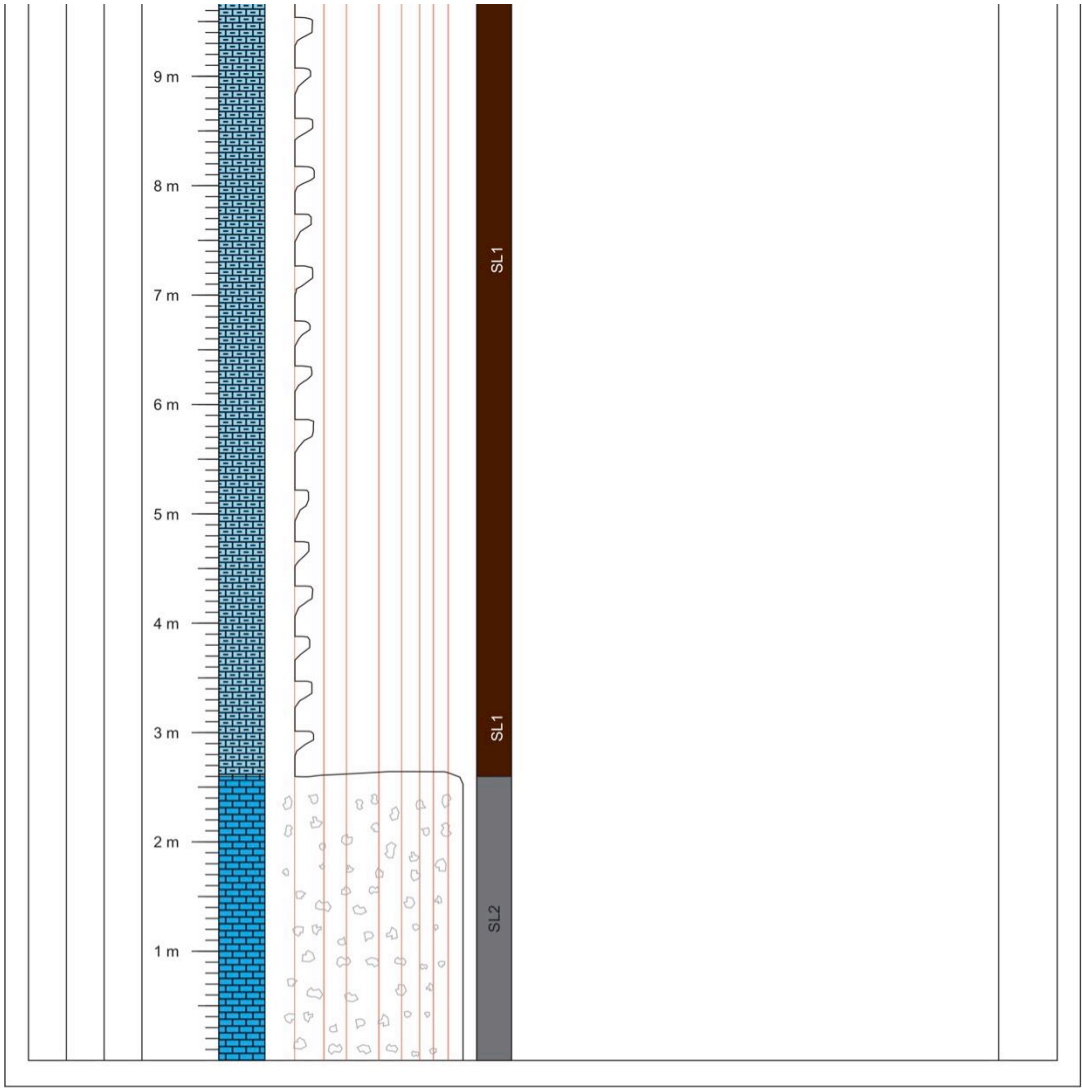




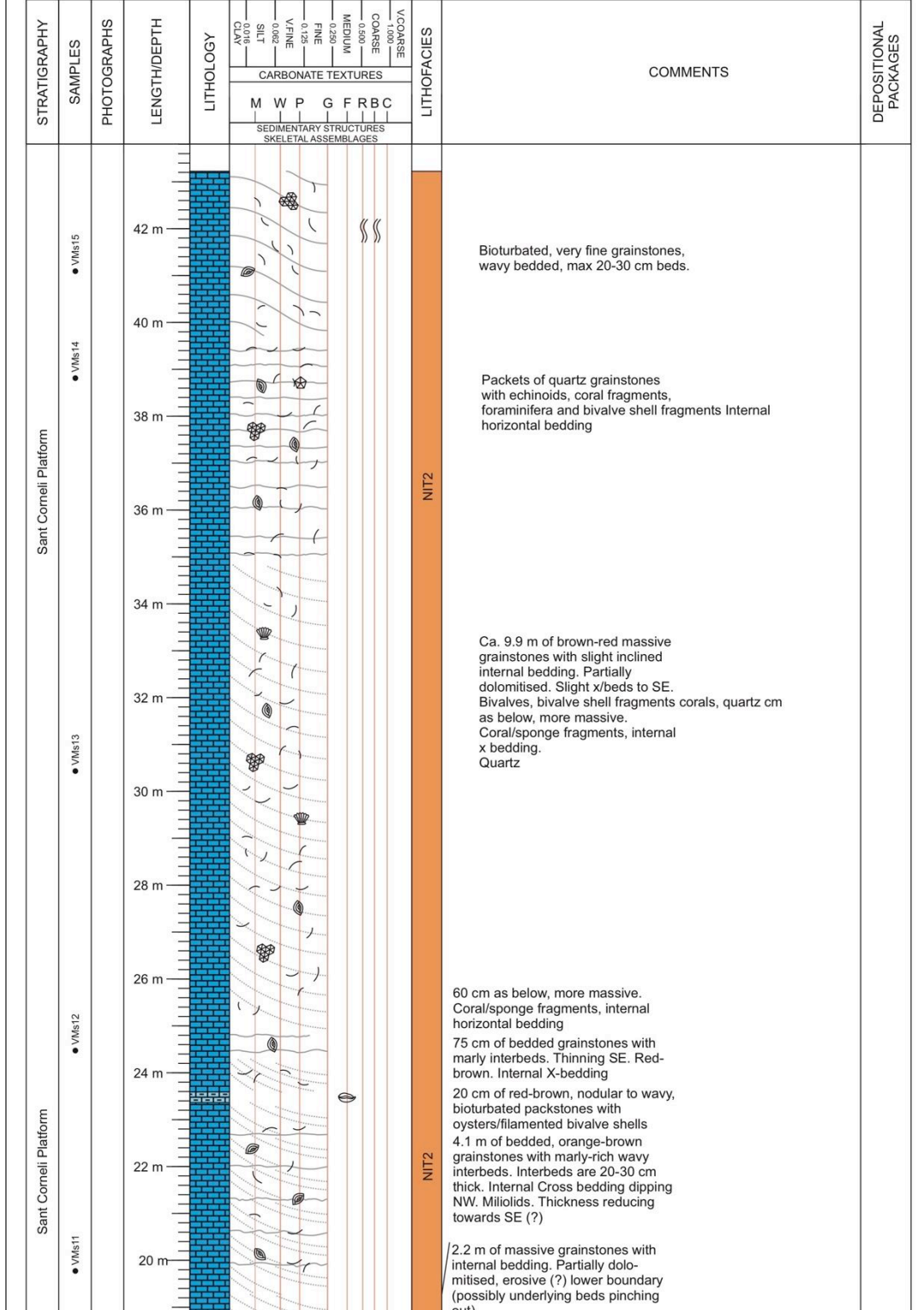


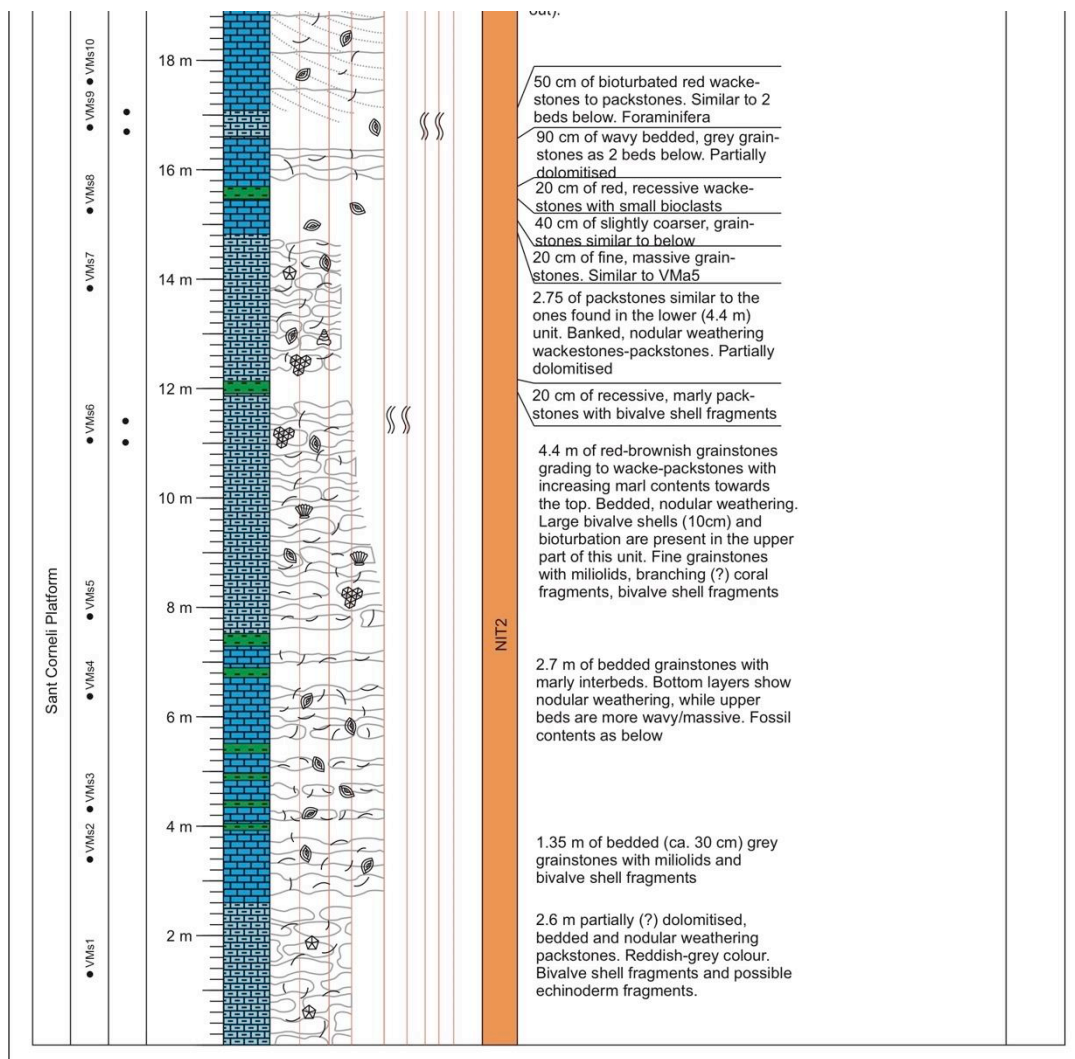
28 m gap





Vilanova de Meia S (VMs#) Starting 42°01'34.52"N (±20 m) Ending 42°11'12.7"N (±3 m)  
 (Logged 24/05/2014) Scale 1:50 point: 001°02'09.59"E Alt.: 977 m point: 001°02'06.3"E Alt.: 1081 m





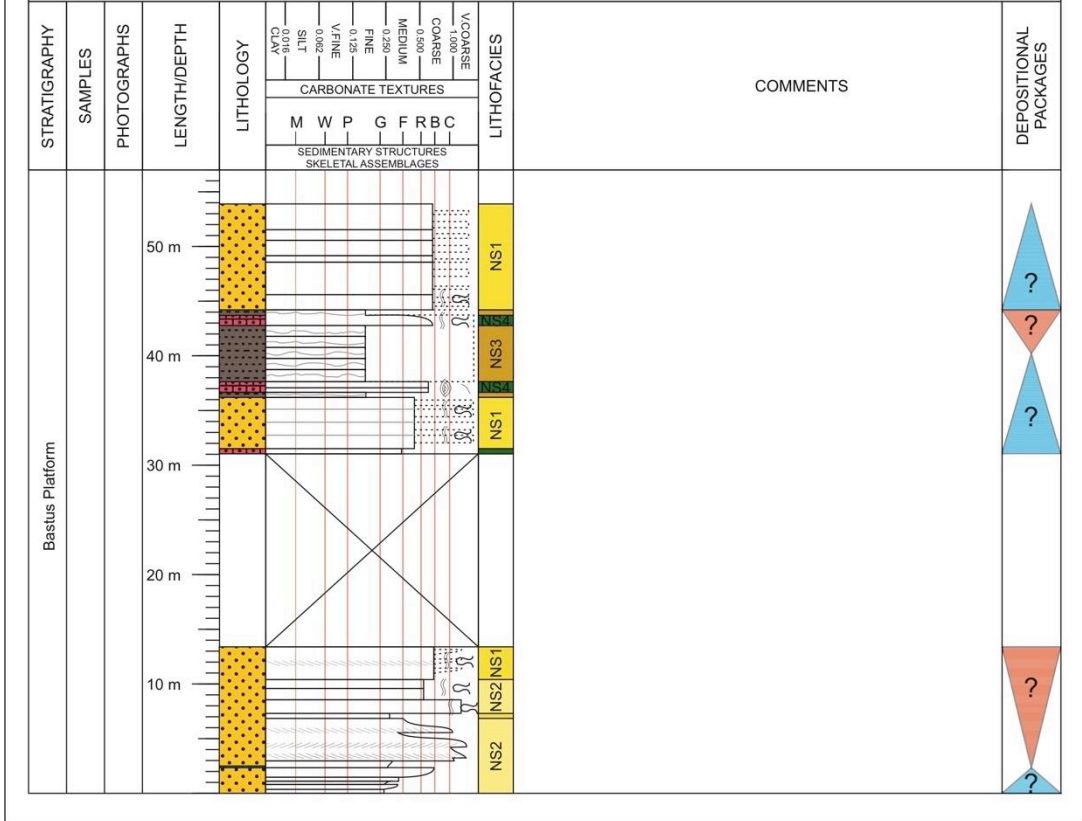
### B.3 Sedimentary Logs at 1:500 Scale

A subset of the sedimentary logs on 1:50 scale was redrawn at a scale of 1:500 (Table 6.5.5.2). These digitalised logs are presented in the following.

Table 6.5.5.2: List of composite sedimentary logs at 1:500 scale.

Log	Starting Point		Ending Point		Total Length [m]	Length of Gaps [m]	Net length [m]
	Northing	Easting	Northing	Easting			
Camarasa	42°54'46.8"N	000°51'44.7"E	42°54'56.5"N	000°51'57.2"E	54	18	36
Congost d'Erinyá	42°03'43.3"N	000°40'04.0"E	42°17'04.0"N	000°56'17.5"E	359	98	261
Oliana	42°07'44.7"N	001°18'37.9"E	42°07'56.3"N	001°18'34.9"E	153	12	141
Montagut Gully	42°11'06.9"N	001°01'57.2"E	42°11'16.5"N	001°01'54.1"E	96.45	0.5	95.95
Carreu River	42°11'44.3"N	001°01'25.1"E	42°11'50.4"N	001°02'24.4"E	203.55	58.65	144.9
Tamurcia	42°18'00.7"N	000°50'23.8"E	42°17'51.4"N	000°50'01.7"E	205.05	68	137.05

Camarasa A and B Composite Log Starting N42°54'46.8" (±3 m) Ending N42°54'56.5" (±3 m)  
 (Logged 24/10/2013) Scale 1:500 point: E000°51'44.7" Alt.: 453 m point: E000°51'57.2" Alt.: 453 m

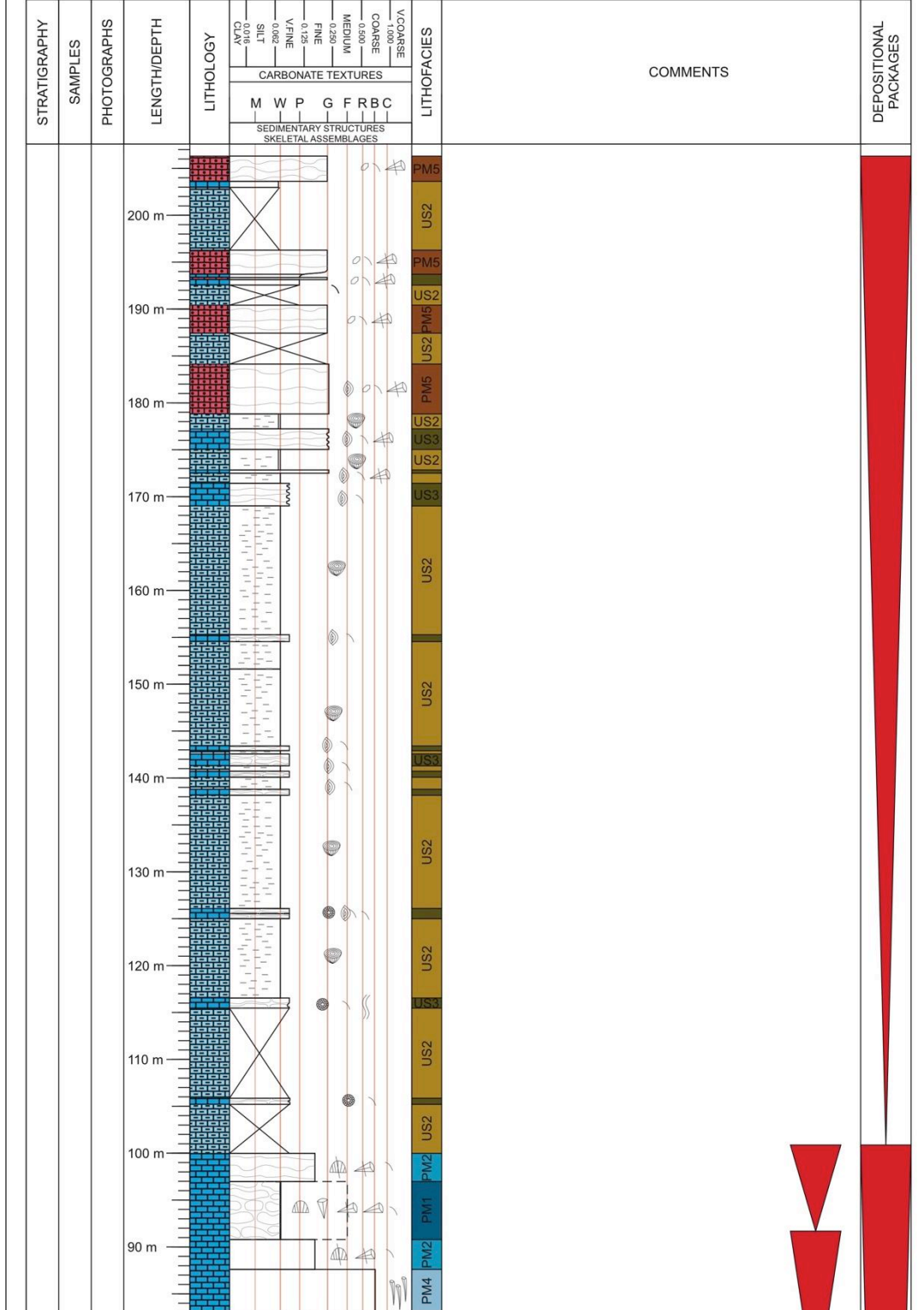


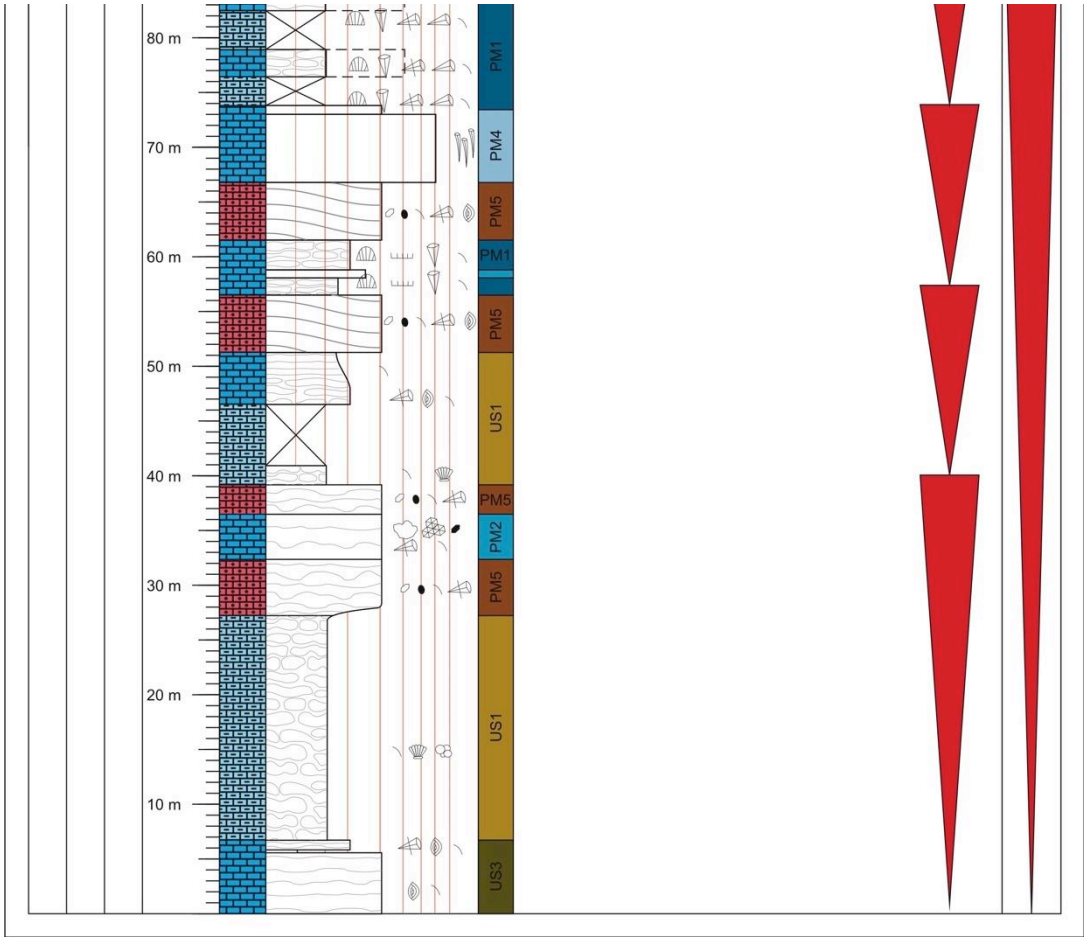


Carreu River B (CRb#)  
(Logged 24/10/2013) Scale 1:500

Starting N42°11.738' (±6 m)  
point: E001°01.418' Alt.: 655 m

Ending N42°11.840' (±5 m)  
point: E001°02.407' Alt.: 737 m

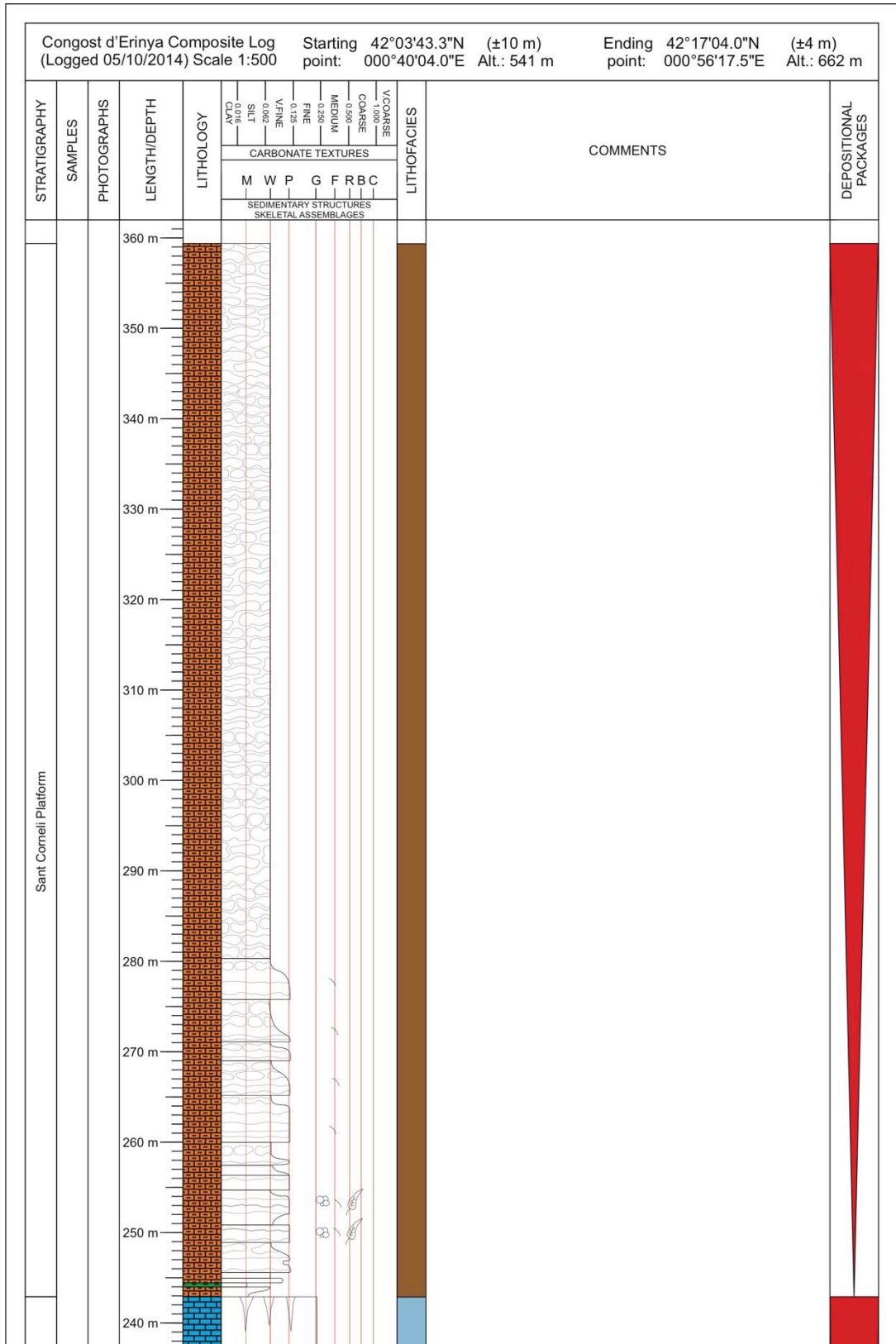


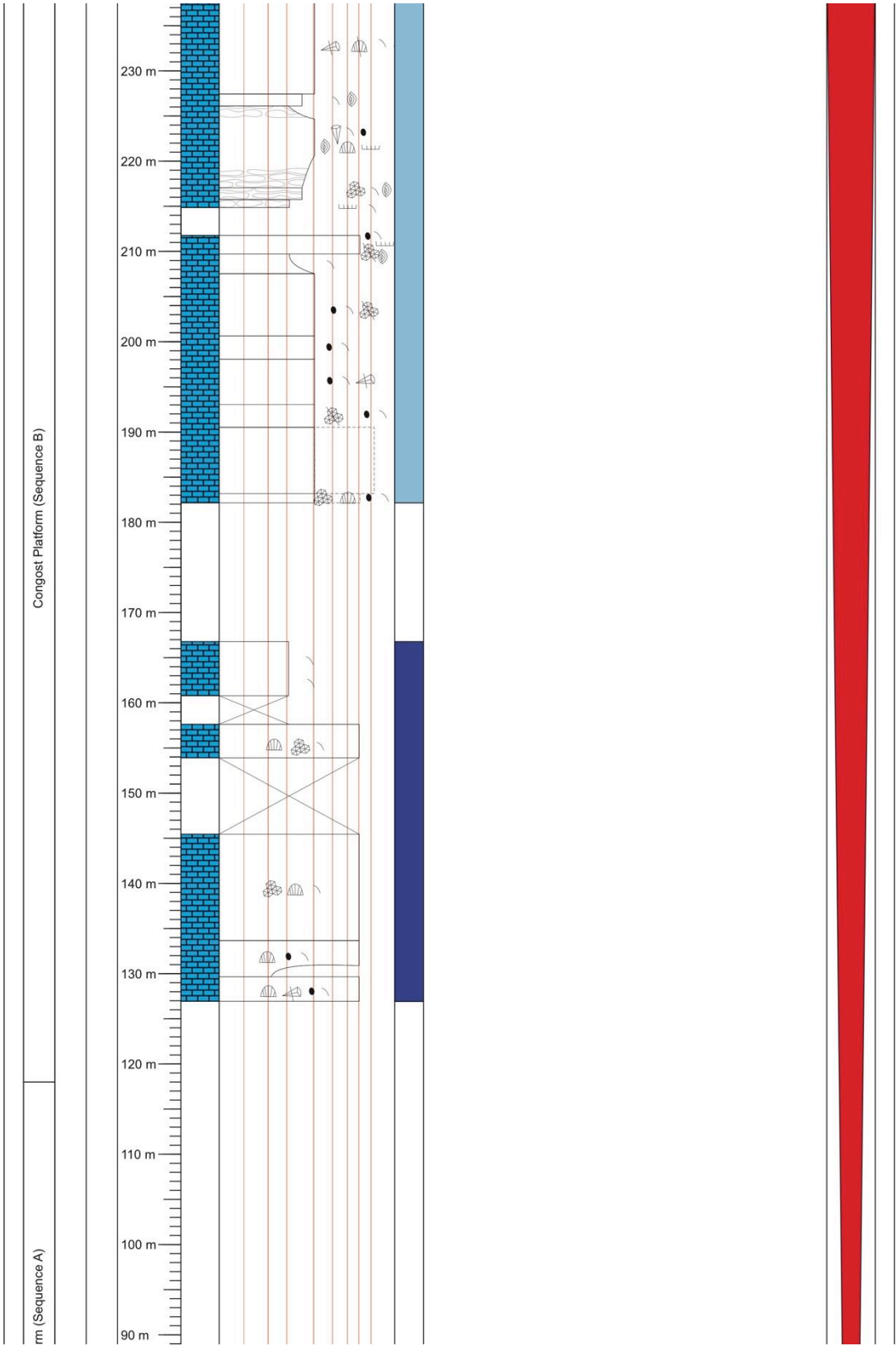


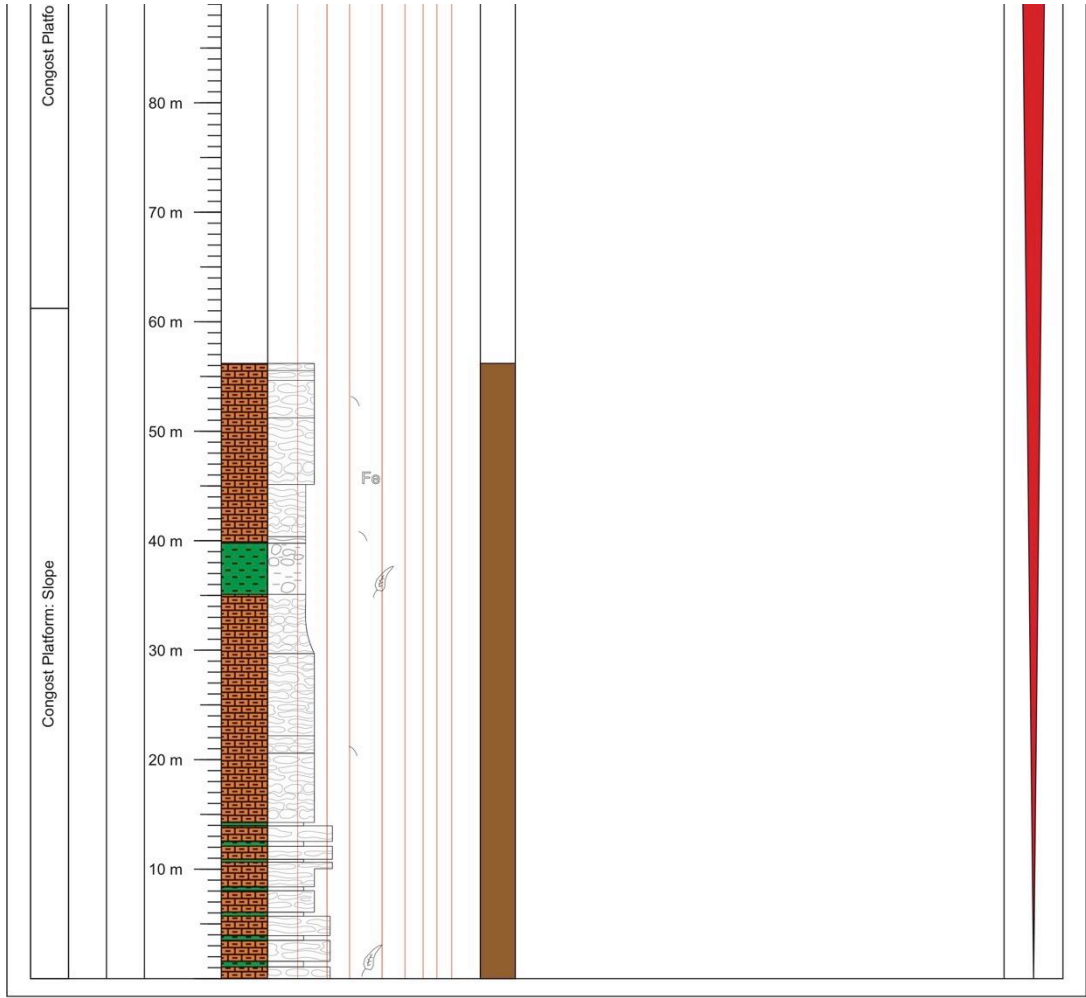
Congost d'Erinya Composite Log  
(Logged 05/10/2014) Scale 1:500

Starting point: 42°03'43.3"N (±10 m)  
000°40'04.0"E Alt.: 541 m

Ending point: 42°17'04.0"N (±4 m)  
000°56'17.5"E Alt.: 662 m



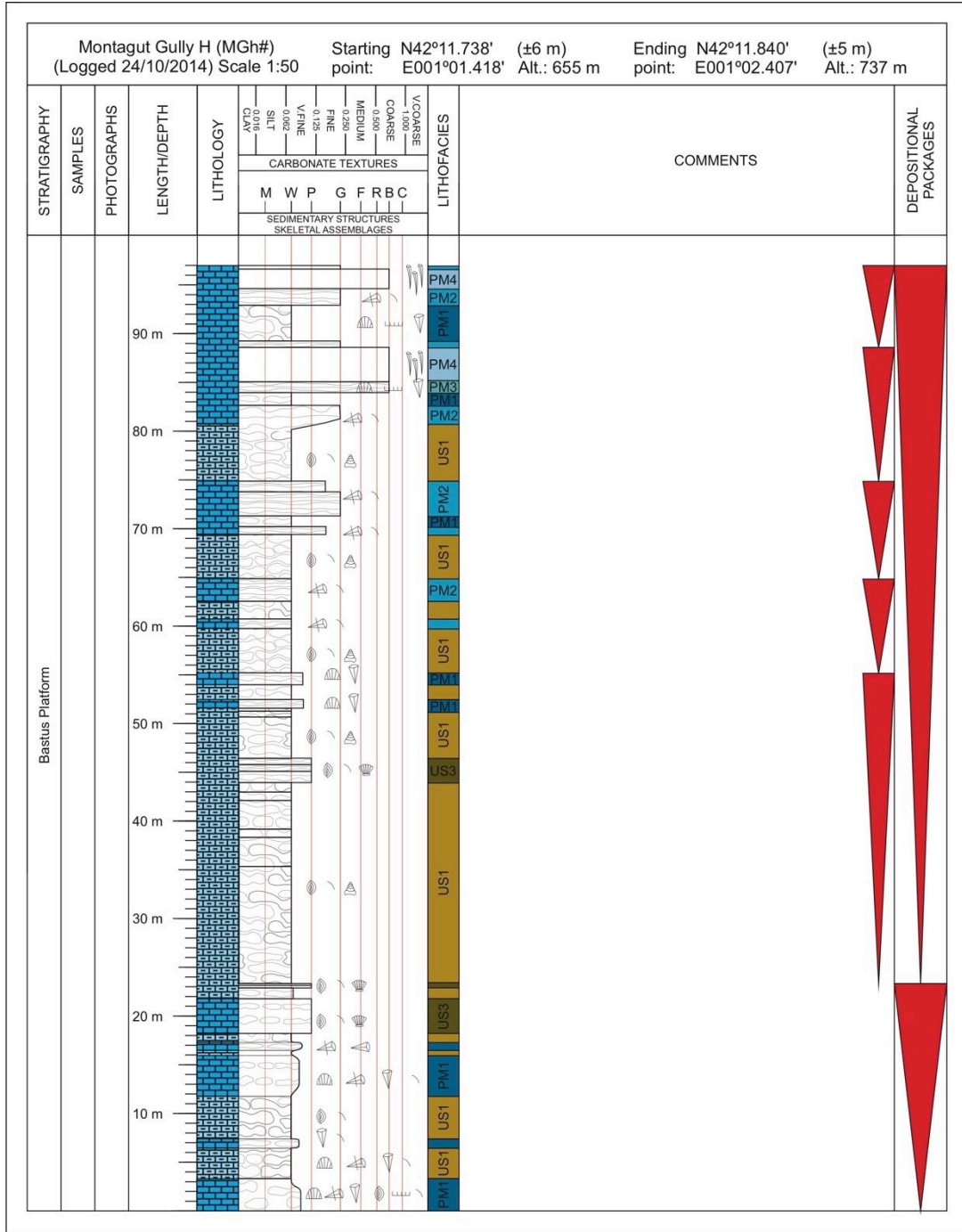




Montagut Gully H (MGh#)  
(Logged 24/10/2014) Scale 1:50

Starting point: N42°11.738' (±6 m)  
E001°01.418' Alt.: 655 m

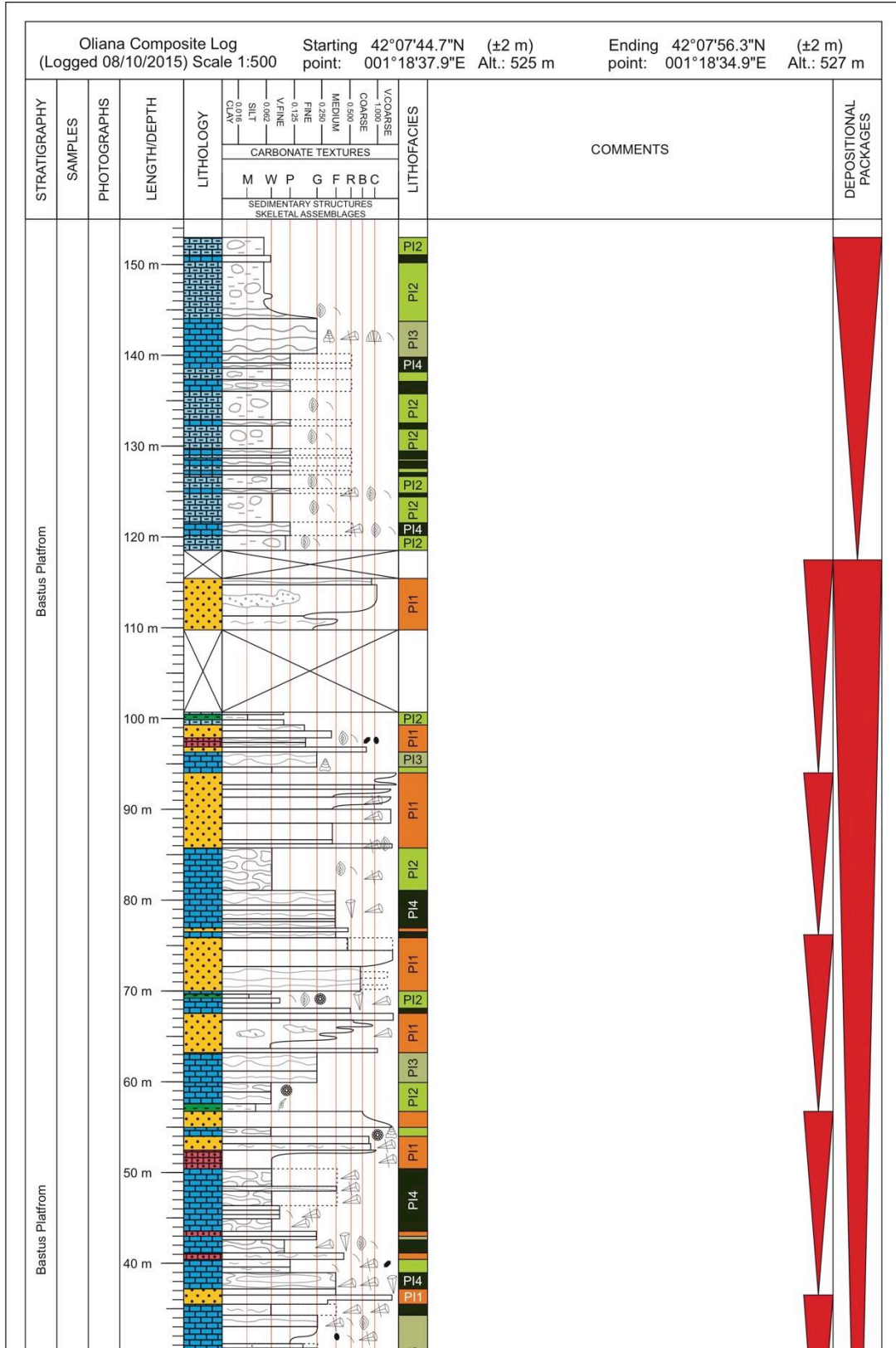
Ending point: N42°11.840' (±5 m)  
E001°02.407' Alt.: 737 m

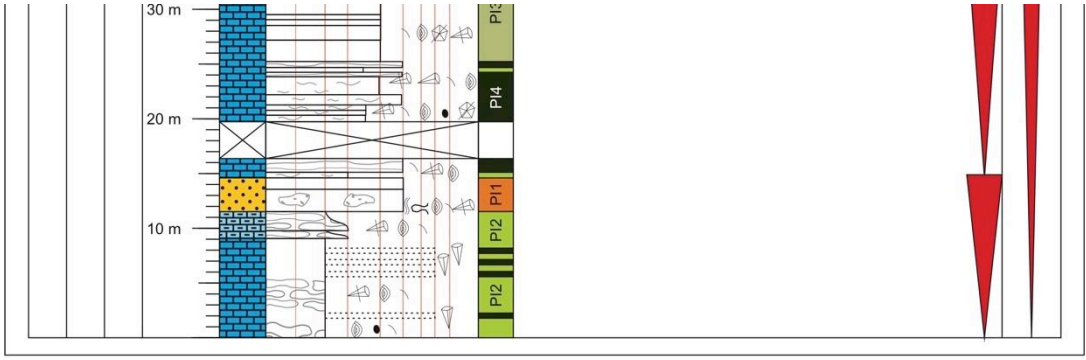


Oliana Composite Log  
(Logged 08/10/2015) Scale 1:500

Starting point: 42°07'44.7"N (±2 m)  
001°18'37.9"E Alt.: 525 m

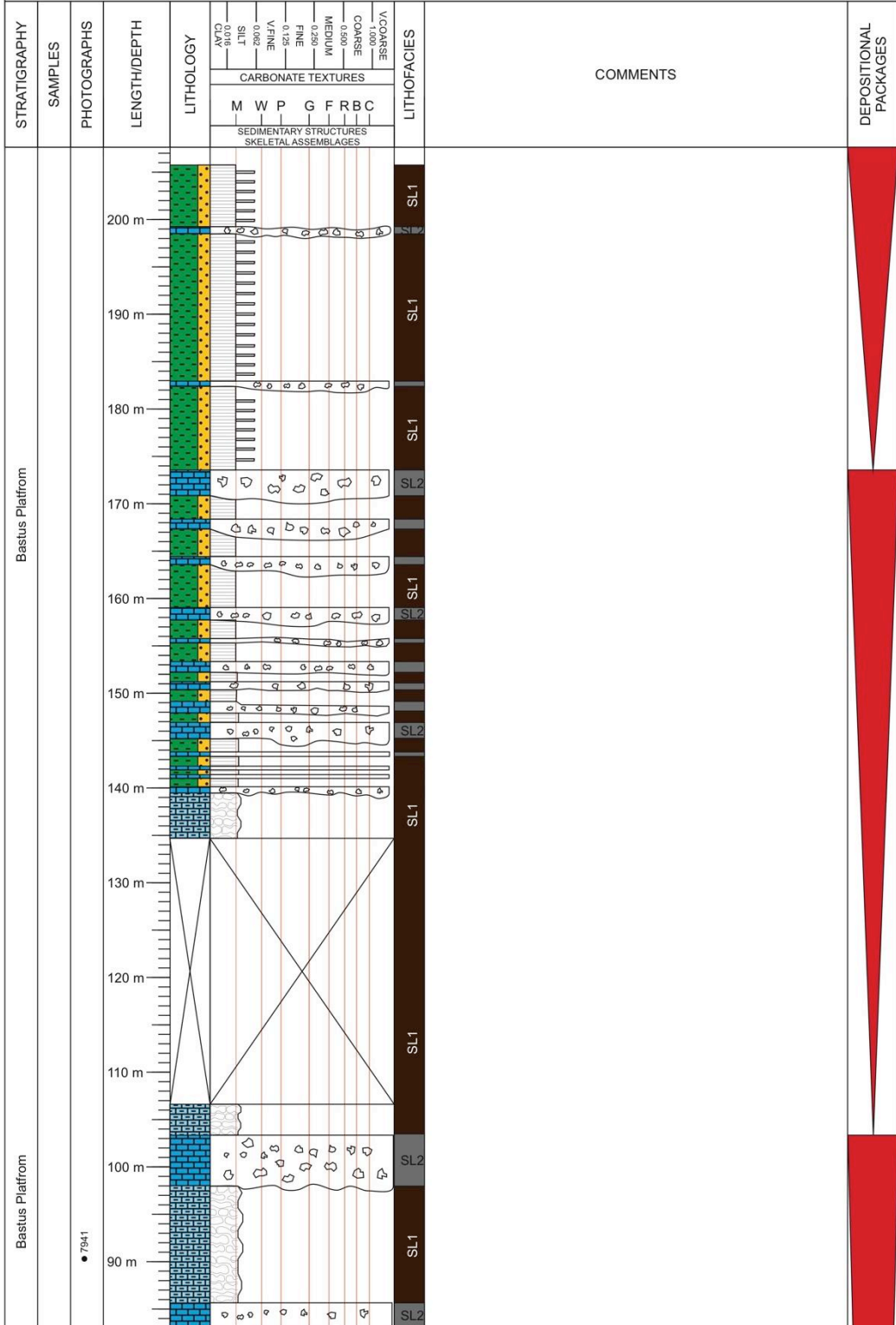
Ending point: 42°07'56.3"N (±2 m)  
001°18'34.9"E Alt.: 527 m

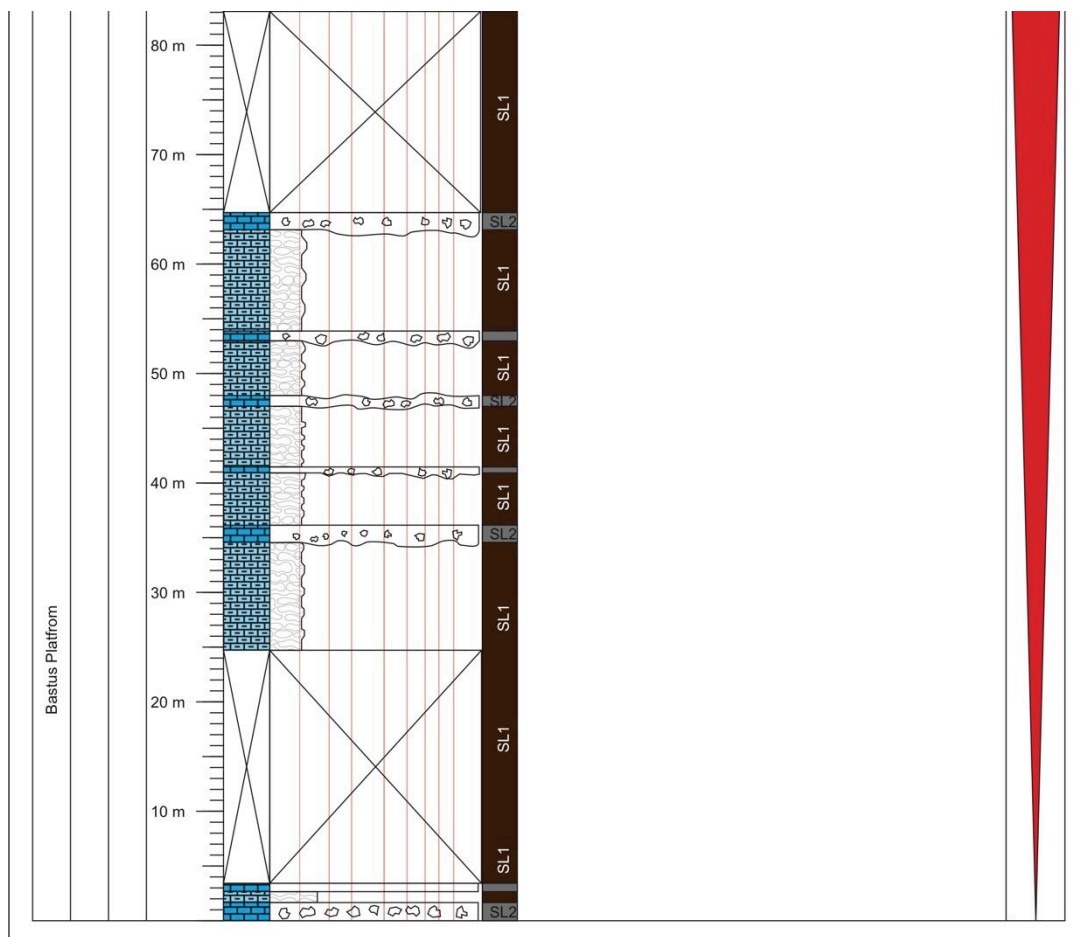






Torre de Tamurcia Composite Log Starting 42°18'00.7"N (±2 m) Ending 42°17'51.4"N (±3 m)  
 (Logged 17/10/2015) Scale 1:500 point: 000°50'23.8"E Alt.: 1099 m point: 000°50'01.7"E Alt.: 1049 m





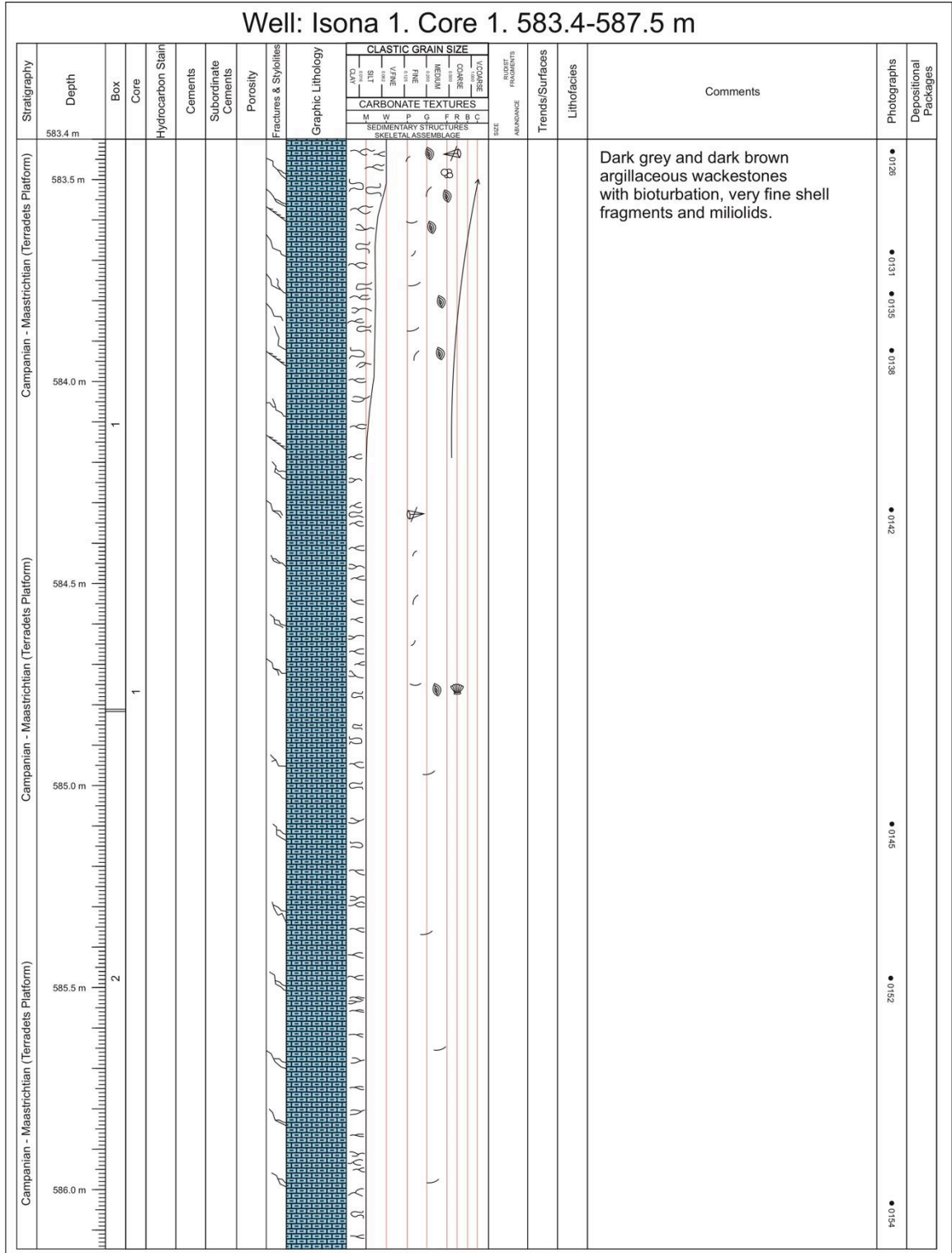
## B.4 Core Logs

Six cores from three wells were logged on a scale of 1:10 (Table 6.5.5.3), using the same key as with the sedimentary field logs (Figure 6.5.5.1). These digitalised logs are presented in the following.

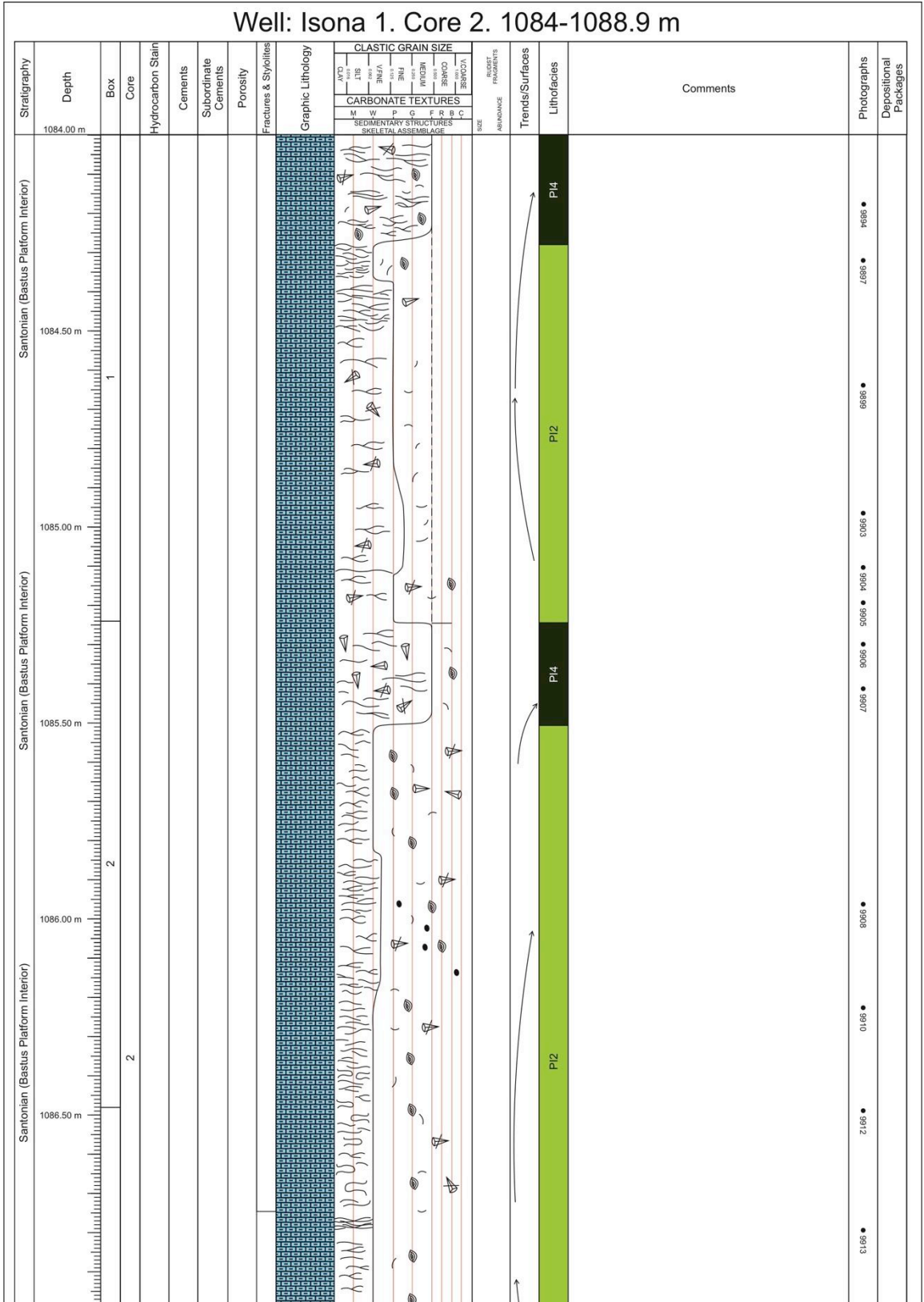
Table 6.5.5.3: List of core logs recorded on a scale of 1:10.

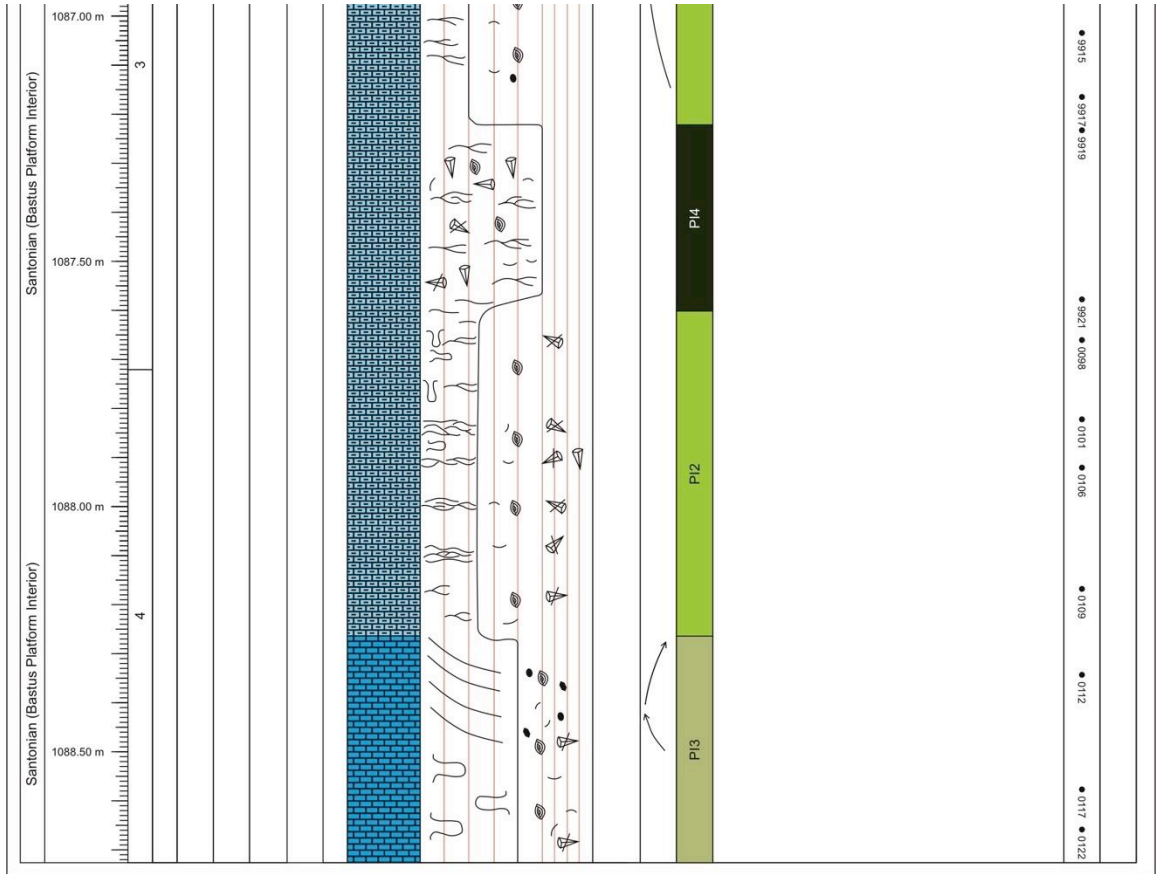
Well	Core	Stratigraphy	Platform	Possible LFA	Bottom Depth [m]	Top Depth [m]	Length [m]
Isona 1	1	Campanian-Maastrichtian	?	?	8	583.4	4.1
Isona 1	2	Upper Santonian	Bastus Platform	PI1-4	1088.9	1084	4.9
Sant Corneli 1	9	Turonian	Congost	RE1	2914.4	2910.5	3.9
Sant Corneli 1	10	Coniacian	Congost	CGA2	2945	2941.5	3.5
Tamurcia 1	1	Santonian/Campanian?	Sant Corneli/Bastus	LS1 (Bastus) SL1/SL2 (Sant Corneli)	?	?	1.7
Tamurcia 1	2	Lower Santonian	Sant Corneli?	SL1/SL2	1228	1223	5

# Well: Isona 1. Core 1. 583.4-587.5 m



# Well: Isona 1. Core 2. 1084-1088.9 m





Well: Sant Corneli 1. Core 9. 2910.5-2914.4 m. Overturned Turonian (Congost?)

Stratigraphy	Depth	Box	Core	Hydrocarbon Stain	Cements	Subordinate Cements	Porosity	Fractures & Stylolites	Graphic Lithology	CLASTIC GRAIN SIZE	CARBONATE TEXTURES	SEDIMENTARY STRUCTURES	SKELETAL ASSEMBLAGE	SIZE	ORIENTATION	FRAGMENT	Trends/Surfaces	Lithofacies	Comments	Photographs	Depositional Packages	
Turonian (Reguard Formation)	2910.50 m		9														RE1	Stylolitized, very fine grained wackepackstones with bioturbation. Presumably Reguard Formation				
	2911.00 m	1	9														RE1					
	2911.50 m																RE1		Fault breccia			
	2912.00 m	2	9														RE1					
	2912.50 m																RE1					
	2913.00 m	3	9																RE1	Fault breccia		
2913.50 m	4	9															RE1					
Turonian (Reguard Formation)	2913.50 m	5	9															RE1				
	2913.50 m	6	9															RE1				

Well: Sant Corneli 1. Core 10. 2941.5-2945.0 m. Overturned Coniacian (Congost?)

Stratigraphy	Depth	Box	Core	Hydrocarbon Stain	Cements	Subordinate Cements	Porosity	Fractures & Stylolites	Graphic Lithology	CLASTIC GRAIN SIZE		CARBONATE TEXTURES		SEDIMENTARY STRUCTURE	SKELETAL ASSEMBLAGE	TRENDS/SURFACES	Lithofacies	Comments	Photographs	Depositional Packages
										AVD	AVD	M	N							
Coniacian (Congost?)	2941.50 m		10													CGA2	Dark brown pack/grainstones, well sorted mU/mL grain size, occ. larger rudist shells. Little internal structures	8656 ●		
	2942.00 m		2	10												CGA2	Stratigraphic bottom ↓ Stratigraphic top	0956 ●		
Coniacian (Congost?)	2942.50 m		3	10												CGA2	Coraser (mU) pack/grainstones, well sorted, slightly angular	2966 ●		
	2943.00 m		4	10												CGA2	Pack/grainstones, mU	5966 ●		
	2943.50 m		5	10												CGA2	mU-cl pack/grainstones with quartz	4947 ●		
Coniacian (Congost?)	2944.00 m		6	10												CGA2	Cl - Cu as above, quartz and foraminifera	0966 ●		
	2944.50 m		7	10												CGA2	Cross-bedded (ca. 40 degrees to well) Cl/Cu grainstones/packstones	9566 ●		
	2945.00 m		9	10												CGA2	Up to Cl, down to ml, bioturbated, grainstone/packstones with common pyrite	4566 ●		

# Well: Tamurcia 1. Core 1.

Stratigraphy	Thickness (Depth Unknown)	Box	Core	Hydrocarbon Stain	Cements	Subordinate Cements	Porosity	Fractures & Stylolites	Graphic Lithology	CLASTIC GRAIN SIZE	CARBONATE TEXTURES	SEDIMENTARY STRUCTURES	SKELETAL ASSEMBLAGE	TRENDS/SURFACES	Lithofacies	Comments	Photographs	Depositional Packages
Coniacian? (Sant Corneli Platform)	40 cm	1	1											SL1		Possibly misplaced piece of core from Tamurcia-1 core 2 (judging by facies)	8900 ●	
	30 cm													SL1			8072 ●	
Santonian (Bastus Platform)	30 cm	2	1											SL1			8074 ●	
	20 cm	2	1											SL1		8076 ●		
	10 cm	2	1											SL1	Bioturbation. Depth relation unclear	8081 ●		
	0 cm	2	1											SL1	Slump breccia in black marl matrix intra-clasts consisting of material as below, 25 degree angle.	8086 ●		
	10 cm	7	1											SL1	Fine grained wackestones with rare shell fragments, bioturbation	8800 ●		
	10 cm	?	1											SL2	Slump breccia equivalent to top of piece 2, containing echinoderms. Rounded clasts, >vCU	8900 ●		



Well: Tamurcia 1. Core 2. 1223-1228. Sant Corneli Slope

Stratigraphy	Depth	Box	Core	Hydrocarbon Stain	Cements	Subordinate Cements	Porosity	Fractures & Stylolites	Graphic Lithology	CLASTIC GRAIN SIZE		CARBONATE TEXTURES		SEMI-PRESERVATION	SEDIMENTARY STRUCTURE	SKELETAL ASSEMBLAGE	TRENDS/SURFACES	Lithofacies	Comments	Photographs	Depositional Packages
										AVD	1/16	1/8	1/4								
Coniacian (Sant Corneli Slope?)	1223.00 m																				
	1223.50 m		3-4	2														SL2	Fine grained (mU) wacke/packstones with abundant miliolids, echinoids, rudist shells, peloids, bioturbation, medium sorting		
	1224.00 m																	SL2			
1224.50 m																					
Coniacian (Sant Corneli Slope?)	1225.00 m		6-8	2																	
	1225.50 m																				
	1226.00 m																				
Coniacian (Sant Corneli Slope?)	1226.50 m		9-11	2																	
	1227.00 m																				
	1227.50 m																				

## **Appendix C: Sample and Thin Section Data**

### **C.1 List of Samples**

A list of all samples collected during this study is found in the spreadsheet "*SampleList.xls*" on the enclosed CD. The methodology for sample naming is described in Chapter 2.

### **C.2 Thin Section Descriptions**

Descriptions of the thin sections made during this study are found in the spreadsheet "*SampleData.xls*" on the enclosed CD. The respective columns are A-W. The methodology of thin section description is described in Chapter 2.

### **C.3 Modal Analysis Data**

A top-tier breakdown of the modal composition and grain size statistics of the samples analysed for modal composition using point counting is found in the spreadsheet "*SampleData.xls*" on the enclosed CD. The respective columns are AH-AM (modal composition), and AN-AZ (grain size statistics).

### **C.4 XRD Data**

A summary of the mineralogical composition of the samples analysed using XRD is found in the spreadsheet "*SampleData.xls*", in columns X-AG, on the enclosed CD.

## Appendix D: Geobody Measurements

### D.1 Bastus/Sant Corneli Platform Interiors

Table 6.5.5.4: Detailed measurements on the exposure of lenticular sedimentary bodies in the south side of the Montsec Range, Sant Corneli Platform Cycle, platform interior. Facies codes refer to codes used in Chapter 3.

Body Identifier	Lithofacies	Minimum width [km] (exposed)	Midrange width [km] (calculated)	Maximum width [km] (calculated/exposed)	Comment
1	NIT2	-	0.29	-	Fully exposed
2	NIT2	-	0.68	-	Fully exposed
3	NIT2	-	1.76	-	Fully exposed
4	NIT2	0.61	1.17	1.78	
5	NIT2	-	-	1.6	Fully exposed
6	NIT2	-	-	1.84	Fully exposed
7	NIT2	0.46	1.66	2.86	No limitation on pinch out
8	NIT2	-	-	10.05	Fully exposed
9	NIT2	0.24	6.87	13.49	
10	NIT2	2.11	-	?	No limitation on pinch out
11	NIT2	-	-	0.43	Correlated into Body #9
12	NIT2	-	-	0.72	Correlated into Body #9
13	NIT2	-	-	1	Correlated into Body #7
14	NIT2	-	-	1.1	Correlated into Body #7
15	NIT2	-	-	2.4	Correlated into Body #9
16	NIT2	-	-	3.75	Correlated into Body #9
17	NIT2	-	-	4.84	Correlated into Body #9

Table 6.5.5.5: Detailed measurements on the exposure of lenticular sedimentary bodies in the south side of the Montsec Range, Bastus Platform Cycle, platform interior. Facies codes refer to codes used in Chapter 3.

Body Identifier	Lithofacies	Minimum width [km] (exposed)	Midrange width [km] (calculated)	Maximum width [km] (calculated/exposed)	Comment
1	PI1	0.13	0.2	0.33	
2	PI1	0.11	0.36	0.47	
3	PI1	0.27	0.46	0.73	
4	PI1	0.58	0.65	0.93	
5	PI1	0.49	0.65	1.14	
6	PI1	0.48	0.69	1.17	
7	PI1	0.43	0.93	1.36	
8	PI1	0.7	1.27	1.79	
9	PI1	0.5	1.79	2.29	
10	PI1	1.17	1.85	3.02	
11	PI1	1.67	2.1	3.77	
12	PI1	0.24	0.2	?	Quaternary cover too extensive to provide realistic interpretation
13	PI1	0.1		N/A	Correlated into Body #9
14	PI1	0.13		N/A	Correlated into Body #7

Table 6.5.5.6: Detailed measurements on the exposure of lenticular sedimentary bodies in the south side of the Montsec Range, Bastus Platform Cycle, platform interior. Facies codes refer to codes used in Chapter 3.

Body Identifier	Lithofacies	Minimum width [km] (exposed)	Midrange width [km] (calculated)	Maximum width [km] (calculated/exposed)	Comment
1	PI3 and PI4	1.29	1.58	1.87	
2	PI3 and PI4	0.72	1.08	1.99	
3	PI3 and PI4	2.00	-	2.00	Completely exposed
4	PI3 and PI4	0.6	1.45	2.7	
5	PI3 and PI4	2.1	2.36	4.1	
6	PI3 and PI4	0.16	-	N/A	Correlated into Body #2
7	PI3 and PI4	0.19	-	N/A	Correlated into Body #4
8	PI3 and PI4	0.57	-	N/A	Correlated into Body #4
9	PI3 and PI4	0.62	-	N/A	Correlated into Body #5

## D.2 Bastus Platform Margin Facies (Montagut Gully /Carreu Rover Localities)

Table 6.5.5.7: Individual measurements of width, length and thickness of lithofacies in the Bastus Platform margin made from digital outcrop models of the Montagut Gully and Carreu River localities. Facies codes refer to codes used in Chapter 3.

#	Facies	Maximum Width (m)	Thickness Width (m)	Thickness Length (m)	Maximum Thickness (m)	Minimum Thickness (m)	Average Thickness (m)	Locality/ Model
1	PM1			250	7.0	5.3	6.0	Carreu River
2	PM1			250	10.7	9.0	10.1	Carreu River
3	PM1			250	4.4	2.4	3.4	Carreu River
4	PM1		22.4		2.1			Montagut Gully
5	PM1		35.4		2.5			Montagut Gully
6	PM1		56.0		7.3			Montagut Gully
7	PM1		40.6		1.0			Montagut Gully
8	PM1		96.8		4.4			Montagut Gully
9	PM1		48.1		6.9			Montagut Gully
10	PM1		69.0		2.1			Montagut Gully
11	PM1		12.7		4.5			Montagut Gully
12	PM1	3.1			1.0			Montagut Gully
13	PM1		64.6		2.7			Montagut Gully
14	PM1		54.2		2.5			Montagut Gully
15	PM2			250	4.6	3.3	3.9	Carreu River
16	PM2			250	3.6	3.1	3.4	Carreu River
17	PM2			250	3.5	1.9	2.7	Carreu River
18	PM2		15.6		2.1			Montagut Gully
19	PM2		95.7		1.0			Montagut Gully
20	PM2		41.4		7.3			Montagut

#	Facies	Maximum Width (m)	Thickness Width (m)	Thickness Length (m)	Maximum Thickness (m)	Minimum Thickness (m)	Average Thickness (m)	Locality/ Model
								Gully
21	PM2		7.2		1.2			Montagut Gully
22	PM2		72.9		1.6			Montagut Gully
23	PM2		218.1		4.9			Montagut Gully
24	PM2		107.4		3.7			Montagut Gully
25	PM2		46.2		2.7			Montagut Gully
26	PM2		59.1		3.0			Montagut Gully
27	PM2		16.9		5.5			Montagut Gully
28	PM2		50.0		2.2			Montagut Gully
29	PM3		73.5		2.7			Montagut Gully
30	PM3		40.6		3.6			Montagut Gully
31	PM4			250	6.1	4.5	5.2	Carreu River
32	PM4			250	3.4	2.4	2.7	Carreu River
33	PM4		243.48		3.6			Montagut Gully
34	PM4		24.6		5.8			Montagut Gully
35	PM4		59.1		3.2			Montagut Gully
36	PM5			250	5.9	3.7	4.9	Carreu River
37	PM5			250	1.8	2.2	2.0	Carreu River
38	PM5			250	4.0	5.6	4.7	Carreu River
39	PM5			250	4.6	3.4	4.1	Carreu River
40	US1			250	11.0	9.4	10.1	Carreu River
41	US1		49.3		1.4			Montagut Gully
42	US1		30.1		1.9			Montagut Gully
43	US1		47.3		11.5			Montagut Gully
44	US1		135.8		34.1			Montagut Gully
45	US1		74.5		9.8			Montagut Gully
46	US1		9.7		2.3			Montagut Gully
47	US1		27.2		7.8			Montagut Gully
48	US1		12.7		3.3			Montagut Gully
49	US1		35.3		4.9			Montagut Gully
50	US1		44.7		8.2			Montagut Gully
51	US1		47.4		6.3			Montagut Gully
52	US1		69.9		5.1			Montagut

#	Facies	Maximum Width (m)	Thickness Width (m)	Thickness Length (m)	Maximum Thickness (m)	Minimum Thickness (m)	Average Thickness (m)	Locality/ Model
								Gully
53	US1		11.5		4.8			Montagut Gully
54	US1		63.7		6.5			Montagut Gully
55	US1		55.7		11.7			Montagut Gully
56	US1		18.3		9.9			Montagut Gully
57	US1		32.5		14.2			Montagut Gully
58	US1		78.0		27.1			Montagut Gully
59	US1		202.5		15.5			Montagut Gully
60	US3		225.9		2.4			Montagut Gully
61	US3		161.9		4.1			Montagut Gully
62	US3		116.3		2.7			Montagut Gully
63	US3		94.2		1.4			Montagut Gully
64	US3		35.2		2.3			Montagut Gully
65	US3		39.2		1.9			Montagut Gully
66	US3		24.3		3.9			Montagut Gully

Table 6.5.5.8: Results of the quantifications of clinothems formed by lithofacies PM5 (Quartz-bearing grainstones and packstones) at the Bastus Platform margin, measured on the digital outcrop model of the Carreu River outcrop.

Body #	Host Unit #	h: clinothem height	a: distal limb length	b: proximal limb length	c: total clinothem length	$\alpha$ : corrected max distal angle	$\beta$ : overall distal foreset angle	$\alpha/\beta$	$\alpha'$ : corrected max proximal foreset angle	$\beta'$ : overall proximal foreset angle	$\alpha'/\beta'$	Note
1	1	3.6	35.5	42.5	78.0	6.5	5.7	1.13	8.3	4.8	1.72	Possibly thicker
2	2	2.1	25.8	31.0	56.8	6.2	4.6	1.35	6.6	3.8	1.73	
3	2	1.1	12.6	13.9	26.4	7.0	4.8	1.44	5.4	4.4	1.23	
4	2	1.3	20.8	20.4	41.3	5.6	3.5	1.57	5.1	3.6	1.41	
5	3	4.2	41.0	23.0	64.0	10.3	5.9	1.74	16.1	10.5	1.54	
6	3	4.1	22.2	22.0	44.2	11.0	10.5	1.04	15.1	10.6	1.42	
7	3	4.2	26.3	19.6	45.9	12.2	9.0	1.35	21.2	12.0	1.76	
8	3	4.1	27.1	19.8	46.9	14.7	8.7	1.68	17.5	11.8	1.48	Tilted
9	3	3.8	21.4	17.6	39.0	12.7	10.1	1.25	13.7	12.3	1.12	
10	3	5.4	26.3	---	---	19.5	11.6	1.68	---	---	---	Tilted
11	3	4.2	22.4	15.0	37.4	12.2	10.6	1.15	21.1	15.5	1.36	
12	3	3.7	20.7	25.8	46.5	13.5	10.1	1.34	12.3	8.1	1.52	
13	3	4.0	26.7	44.6	71.3	12.3	8.5	1.44	8.2	5.1	1.60	
14	4	2.8	25.8	32.1	57.9	11.5	6.3	1.84	6.8	5.0	1.34	
15	4	3.3	29.5	28.5	58.0	10.5	6.4	1.64	10.6	6.6	1.60	
16	4	3.8	38.9	29.4	68.3	6.4	5.5	1.16	12.0	7.3	1.64	
17	4	3.4	27.1	25.8	52.9	7.3	7.2	1.01	10.7	7.6	1.42	
AVG		3.5	26.5	25.7	52.2	10.5	7.6	1.40	11.9	8.1	1.49	
MEDIAN		3.8	26.3	24.4	49.9	11.0	7.2	1.35	11.3	7.4	1.50	
STD DEV		1.1	6.8	8.6	13.4	3.6	2.4	0.25	5.0	3.5	0.18	
VARIANCE		1.2	45.8	73.1	178.8	13.0	5.7	0.06	25.4	12.4	0.03	